

Green Chemistry

Cutting-edge research for a greener sustainable future

www.rsc.org/greenchem

Volume 12 | Number 2 | February 2010 | Pages 181–352

Downloaded on 30 October 2010
Published on 01 February 2010 on <http://pubs.rsc.org> | doi:10.1039/C001636P



ISSN 1463-9262

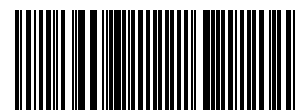
RSC Publishing

Goößen and Ohlmann
Catalysed synthesis of γ -lactones

Chen *et al.*
Platinum-nanoparticle-loaded bismuth
oxide

Rouden *et al.*
Decarboxylative aldol reactions

Subramaniam *et al.*
Oxidation of *p*-xylene to terephthalic
acid



1463-9262(2010)12:2;1-0

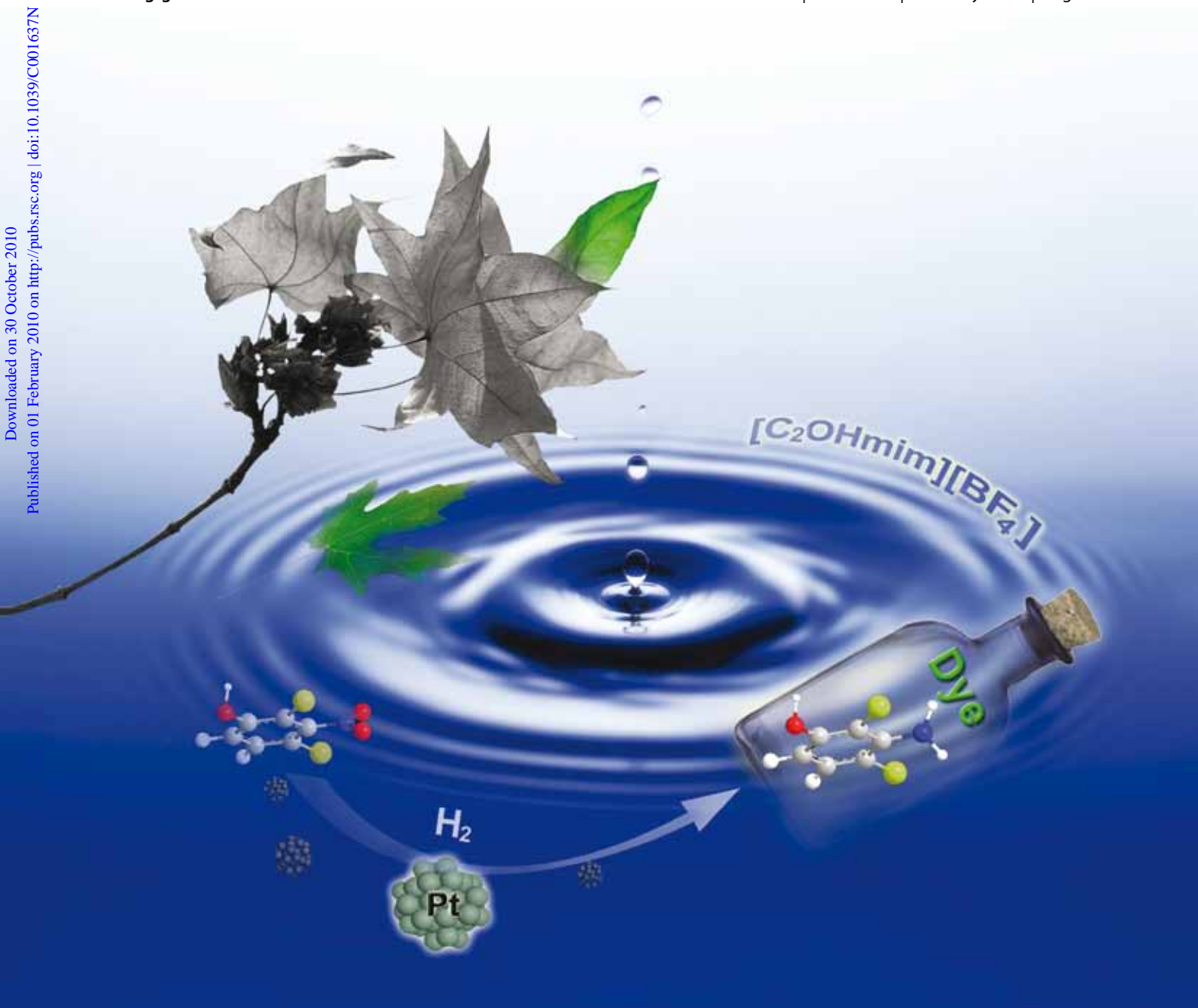
Green Chemistry

Cutting-edge research for a greener sustainable future

www.rsc.org/greenchem

Volume 12 | Number 2 | February 2010 | Pages 181–352

Downloaded on 30 October 2010
Published on 01 February 2010 on http://pubs.rsc.org | doi:10.1039/C001637N



ISSN 1463-9262

RSC Publishing

Kou *et al.*
Selective hydrogenation of aromatic
chloronitro compounds

Mack *et al.*
Enolates via solvent-free ball milling

Dai *et al.*
Oxidative lactonization of
1,2-benzenedimethanol

Wang *et al.*
Synthesis of tetraketones

Green Chemistry

Cutting-edge research for a greener sustainable future

www.rsc.org/greenchem

RSC Publishing is a not-for-profit publisher and a division of the Royal Society of Chemistry. Any surplus made is used to support charitable activities aimed at advancing the chemical sciences. Full details are available from www.rsc.org

IN THIS ISSUE

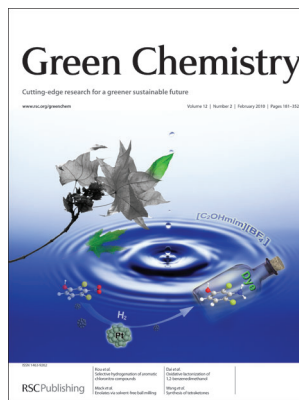
ISSN 1463-9262 CODEN GRCHFJ 12(2) 181–352 (2010)



Cover

See Gooßen *et al.*, pp. 197–200. The cover illustrates our direct silver-catalysed conversion of plant oil-derived oleic acid to γ -stearolactone, an additive for cosmetics.

Image reproduced by permission of Lukas J. Gooßen from *Green Chemistry*, 2010, **12**, 197.



Inside cover

See Kou *et al.*, pp. 228–233. A series of aromatic chloronitro compounds were converted to aromatic chloroamines by platinum nanoparticles coupling with alcohol-functionalized ILs.

Image reproduced by permission of Yuan Kou from *Green Chemistry*, 2010, **12**, 228.

COMMUNICATIONS

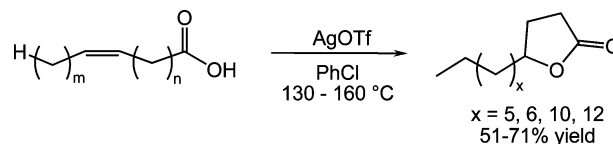
197



Silver triflate-catalysed synthesis of γ -lactones from fatty acids

Lukas J. Gooßen,* Dominik M. Ohlmann and Markus Dierker

An efficient catalytic tandem isomerization–lactonization protocol allows the direct preparation of γ -lactones from unsaturated fatty acids.

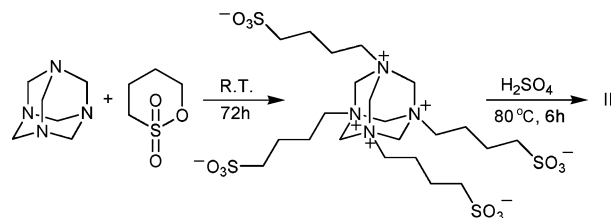


201

Synthesis of a novel multi $-\text{SO}_3\text{H}$ functionalized ionic liquid and its catalytic activities for biodiesel synthesis

Xuezheng Liang* and Jianguo Yang

A novel multi $-\text{SO}_3\text{H}$ functionalized strong Brønsted acidic ionic liquid has been prepared for the synthesis of biodiesel from rapeseed oil and methanol.



EDITORIAL STAFF

Editor

Sarah Ruthven

Deputy editor

Kathleen Too

Senior publishing editor

Elinor Richards

Publishing editorsMary Badcock, David Barden, David Parker,
Michael Townsend**Publishing assistants**

Anna Anderson, Jackie Cockrill

Publisher

Emma Wilson

For queries about submitted articles please contact Elinor Richards, Senior publishing editor, in the first instance. E-mail green@rsc.org

For pre-submission queries please contact Sarah Ruthven, Editor. E-mail green-rsc@rsc.org

Green Chemistry (print: ISSN 1463-9262; electronic ISSN 1463-9270) is published 12 times a year by the Royal Society of Chemistry, Thomas Graham House, Science Park, Milton Road, Cambridge, UK CB4 0WF.

All orders, with cheques made payable to the Royal Society of Chemistry, should be sent to RSC Distribution Services, c/o Portland Customer Services, Commerce Way, Colchester, Essex, UK CO2 8HP. Tel +44 (0)1206 226050; E-mail sales@rscdistribution.org

2010 Annual (print + electronic) subscription price: £1078; US\$2013. 2010 Annual (electronic) subscription price: £970; US\$1811. Customers in Canada will be subject to a surcharge to cover GST. Customers in the EU subscribing to the electronic version only will be charged VAT.

If you take an institutional subscription to any RSC journal you are entitled to free, site-wide web access to that journal. You can arrange access via Internet Protocol (IP) address at www.rsc.org/ip. Customers should make payments by cheque in sterling payable on a UK clearing bank or in US dollars payable on a US clearing bank. Periodicals postage paid at Rahway, NJ, USA and at additional mailing offices. Airfreight and mailing in the USA by Mercury Airfreight International Ltd., 365 Blair Road, Avenel, NJ 07001, USA.

US Postmaster: send address changes to Green Chemistry, c/o Mercury Airfreight International Ltd., 365 Blair Road, Avenel, NJ 07001. All despatches outside the UK by Consolidated Airfreight.

Advertisement sales: Tel +44 (0) 1223 432246; Fax +44 (0) 1223 426017; E-mail advertising@rsc.org

For marketing opportunities relating to this journal, contact marketing@rsc.org

Green Chemistry

Cutting-edge research for a greener sustainable future

www.rsc.org/greenchem

Green Chemistry focuses on cutting-edge research that attempts to reduce the environmental impact of the chemical enterprise by developing a technology base that is inherently non-toxic to living things and the environment.

EDITORIAL BOARD

Chair

Professor Martyn Poliakoff,
Nottingham, UK

Scientific Editor

Professor Walter Leitner,
RWTH-Aachen, Germany

Associate Editor

Professor C. J. Li,
McGill University, Canada

Members

Professor Paul Anastas,
Yale University, USA
Professor Joan Brennecke,
University of Notre Dame, USA
Dr Peter Dunn, Pfizer, UK
Professor Mike Green,
Newcastle University, UK

Professor Buxing Han,
Chinese Academy of Sciences,
China
Professor Shu Kobayashi,
University of Tokyo, Japan
Professor Steven Ley,
Cambridge, UK
Professor Tom Welton,
Imperial College, UK

ADVISORY BOARD

Tad Adschiri, Tohoku University, Japan
Yonas Chebude, Addis Ababa
University, Ethiopia

Cinzia Chiappe, University of Pisa,
Italy

James Clark, York University, UK

Avelino Corma, Universidad
Politecnica de Valencia, Spain

Robert H Crabtree, Yale University,
USA

Pierre Dixneuf, University of Rennes,
France

Alexey M. Egorov, Moscow State
University, Russia

Roald Hoffmann, Cornell University,
USA

Istvan Horvath, City University of
Hong Kong, Hong Kong
Graham Hutchings, Cardiff University,
UK

Philip Jessop, Queen's University,
Canada

Kyoko Nozaki, University of Tokyo,
Japan

Sang-Eon Park, Inha University,
Korea

Alvise Perosa, Universita Ca Foscari,
Italy

Colin Raston, University of Western
Australia, Australia

Robin Rogers, University of Alabama,
USA

Gadi Rothenberg, University of
Amsterdam, The Netherlands

Janet Scott, JLS Chem Consult Ltd, UK

Ken Seddon, Queen's University,
Belfast, UK

Roger Sheldon, Delft, The Netherlands

Christian Stevens, Ghent University,
Belgium

Barry M. Trost, Stanford University,
USA

Richard Wool, University of Delaware,
USA

INFORMATION FOR AUTHORS

Full details on how to submit material for publication in Green Chemistry are given in the Instructions for Authors (available from <http://www.rsc.org/authors>). Submissions should be made via the journal's homepage: <http://www.rsc.org/greenchem>.

Authors may reproduce/republish portions of their published contribution without seeking permission from the RSC, provided that any such republication is accompanied by an acknowledgement in the form: (Original Citation)—Reproduced by permission of The Royal Society of Chemistry.

This journal is © The Royal Society of Chemistry 2010. Apart from fair dealing for the purposes of research or private study for non-commercial purposes, or criticism or review, as permitted under the Copyright, Designs and

Patents Act 1988 and the Copyright and Related Rights Regulation 2003, this publication may only be reproduced, stored or transmitted, in any form or by any means, with the prior permission in writing of the Publishers or in the case of reprographic reproduction in accordance with the terms of licences issued by the Copyright Licensing Agency in the UK. US copyright law is applicable to users in the USA.

The Royal Society of Chemistry takes reasonable care in the preparation of this publication but does not accept liability for the consequences of any errors or omissions.

© The paper used in this publication meets the requirements of ANSI/NISO Z39.48-1992 (Permanence of Paper).

Royal Society of Chemistry: Registered Charity No. 207890.

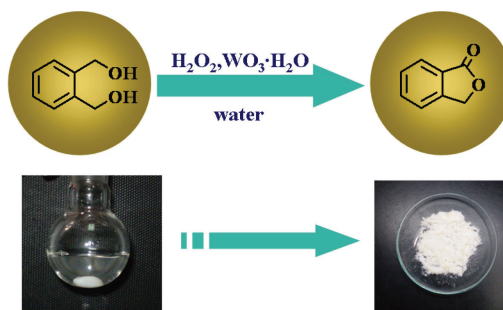
COMMUNICATIONS

205

A green process for the oxidative lactonization of 1,2-benzenedimethanol by tungstic acid with aqueous H₂O₂

Quan-Jing Zhu, Wei-Lin Dai* and Kang-Nian Fan

A new economic and green route to synthesize phthalide with high purity and good yield from 1,2-benzenedimethanol with a H₂O₂-tungstic acid catalytic system under organic solvent-free conditions is presented.

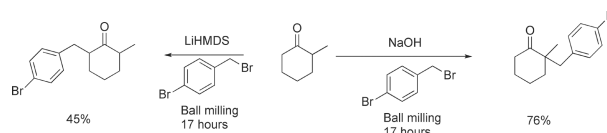


209

Making kinetic and thermodynamic enolates *via* solvent-free high speed ball milling

Daniel C. Waddell, Indre Thiel, Tammara D. Clark, S. Tyler Marcum and James Mack*

An investigation of the ability to selectively form products arising from a kinetic or a thermodynamic enolate under solvent-free high speed ball milling conditions.

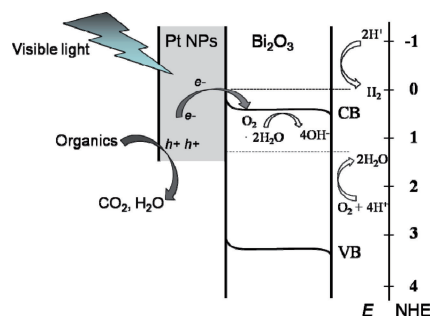


212

Platinum-nanoparticle-loaded bismuth oxide: an efficient plasmonic photocatalyst active under visible light

Renhong Li, Wenxing Chen,* Hisayoshi Kobayashi and Chunxia Ma

Employing a commercial semiconductor with a positive conduction band level, we investigated a new plasmonic photocatalyst, Pt/Bi₂O₃, with high photocatalytic activity for decomposition of environmental organic pollutants under visible light.

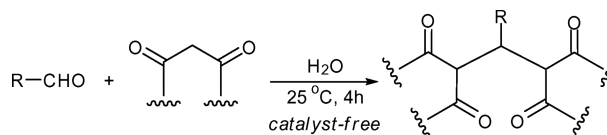


216

Synthesis of tetraketones in water and under catalyst-free conditions

Jian-Jun Yu, Li-Min Wang,* Jin-Qian Liu, Feng-Lou Guo, Ying Liu and Ning Jiao

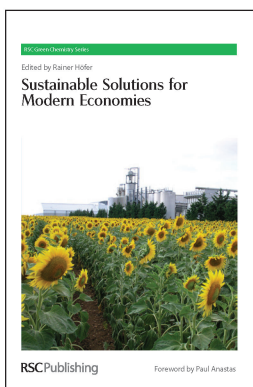
A greener improvement to the synthesis of tetraketones by the Knoevenagel condensation and Michael addition between aldehydes and cyclic-1,3-diketones was achieved using water as the solvent without catalyst.



Discover Green Chemistry with RSC Publishing

The RSC Green Chemistry book series is a timely and unique venture aimed at providing high level research books at the cutting edge of Green Chemistry

Series Editors James H Clark, University of York, UK | George A Kraus, Iowa State University, USA



Sustainable Solutions for Modern Economies

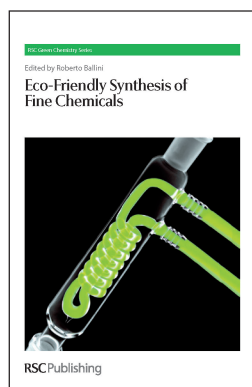
This fascinating book outlines the contribution of chemistry and renewable chemical or biological resources to the sustainability concept and potential resolution of the world's energy problems.

Hardback | ISBN 9781847559050 | 2009 | £90.00

Alternative Solvents for Green Chemistry

This book, appropriate for newcomers to the field, gives an overview of the many different kinds of solvents including alternative greener solvent choices.

Hardback | ISBN 9780854041633 | 2009 | £89.00



Eco-Friendly Synthesis of Fine Chemicals

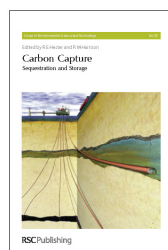
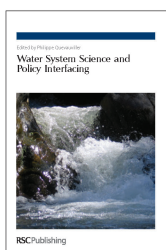
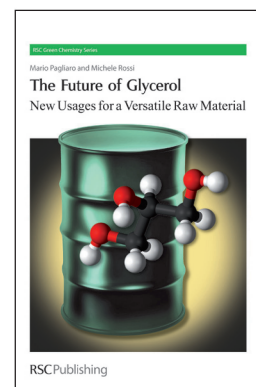
This book is devoted to the preparation of fine chemicals by new emerging approaches in the field of eco-friendly processes and procedures. A valid resource for researchers and industrialists as well as academia.

Hardback | ISBN 9781847559081 | 2009 | £99.95

The Future of Glycerol

This book depicts how practical limitations posed by glycerol chemistry are solved based on the understanding of the fundamental chemistry of glycerol.

Hardback | ISBN 9780854041244 | 2008 | £65.00



Also available from RSC Publishing...

Carbon Capture

Hardback | ISBN 9781847559173 | 2009 | £54.95

Water System Science and Policy Interfacing

Hardback | ISBN 9781847558619 | 2009 | £120.00

Visit the website to find out about the new RSC eBook Subject Collections! (Including an Environmental Sciences package)

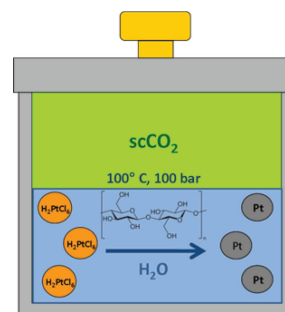
COMMUNICATIONS

220

Synthesis of platinum nanoparticles using cellulosic reducing agents

Karima Benaissi, Lee Johnson, Darren A. Walsh and Wim Thielemans*

The synthesis of platinum nanoparticle/cellulose nanocomposites using nanocrystalline cellulose from cotton in a water/supercritical carbon dioxide biphasic solvent system is described.

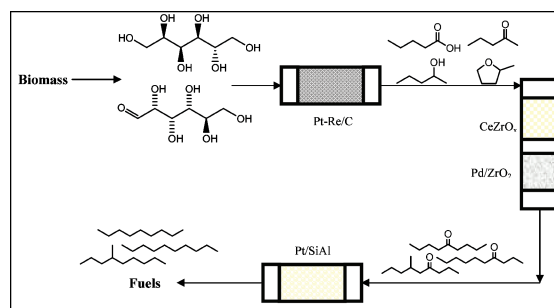


223

Dual-bed catalyst system for C–C coupling of biomass-derived oxygenated hydrocarbons to fuel-grade compounds

Elif I. Gürbüz, Edward L. Kunkes and James A. Dumesic*

Biomass-derived carbohydrates can be converted in a cascade system to fuel-grade alkanes having minimal branching, desirable for Diesel fuel. The overall process is streamlined by implementing a dual-bed catalyst system integrating two C–C coupling processes (ketonization and aldol condensation/hydrogenation) to upgrade light mono-functional species to higher molecular weight ketones.



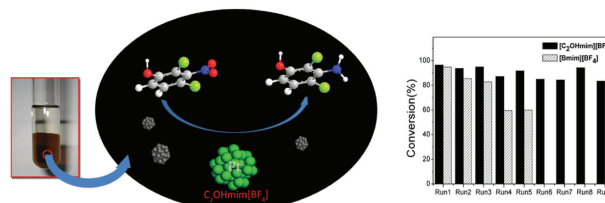
PAPERS

228

Highly selective hydrogenation of aromatic chloronitro compounds to aromatic chloroamines with ionic-liquid-like copolymer stabilized platinum nanocatalysts in ionic liquids

Xiao Yuan, Ning Yan, Chaoxian Xiao, Changning Li, Zhaofu Fei, Zhipeng Cai, Yuan Kou* and Paul J. Dyson*

The hydrogenation of 2,4-dichloro-3-nitrophenol to 4-dichloro-3-aminophenol may be achieved without the formation of dehalogenation by-products, using a Pt-based nanoparticle catalyst immobilized in a functionalized ionic liquid; the system can be recycled without depreciation in activity or selectivity.

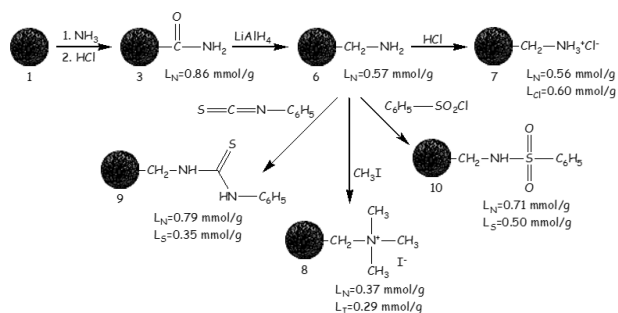


234

Access to a primary aminosporopollenin solid support from plant spores

Sylvain Barrier, Andreas Löbber, Alia J. Boasman, Andrew N. Boa, Mark Lorch, Stephen L. Atkin and Grahame Mackenzie*

Sporopollenin was converted into a primary amine form *via* a primary amide form, and the amine groups were further reacted.





International Symposia on Advancing the Chemical Sciences

A new generation of global conferences

REGISTER BY
1 MAY 2010
FOR REDUCED RATES

Register now to save on delegate fees

Book your delegate place now at the inaugural events in the International Symposia on Advancing the Chemical Sciences (ISACS) - a significant new global symposia series organised by the RSC. Early booking (by 1 May 2010) ensures reduced delegate fees and discounted room rates at the conference hotel.



Challenges in Organic Chemistry and Chemical Biology (ISACS1)

6-9 July 2010 • San Francisco, USA • www.rsc.org/isacs1

Speakers: Carolyn R Bertozzi, Stephen L Buchwald, Jason W Chin, Benjamin F Cravatt, Vy M Dong, Justin Du Bois, Ben L Feringa, Linda C Hsieh-Wilson, Christopher A Hunter, Eric N Jacobsen, David W C MacMillan, Keiji Maruoka, Takashi Ooi, Andreas Pfaltz, Peter H Seeberger, Erik J Sorensen, F Dean Toste, M Christina White.



Challenges in Physical Chemistry and Nanoscience (ISACS2)

13-16 July 2010 • Budapest, Hungary • www.rsc.org/isacs2

Speakers: Mike N R Ashfold, Mounqi G Bawendi, David C Clary, Jianguo G Hou, Tianquan Lian, Kopin Liu, Daniel M Neumark, Michel Orrit, Hongkun Park, Vahid Sandoghdar, Alec M Wodtke, Martin Wolf, Toshio Yanagida, Haw Yang, Xueming Yang.



Challenges in Inorganic and Materials Chemistry (ISACS3)

20-23 July 2010 • Hong Kong, China • www.rsc.org/isacs3

Speakers: Christopher J Chang, Chi-Ming Che, Christopher C Cummins, Makoto Fujita, Michael Grätzel, Hansjörg Grützmacher, Gregory L Hillhouse, Susumu Kitagawa, Jeffrey R Long, Tetsuro Murahashi, Daniel G Nocera, Philip P Power, Manfred Scheer, Jean-Marie Tarascon, Omar M Yaghi, Bing Xu, Vivian W W Yam, Peidong Yang.

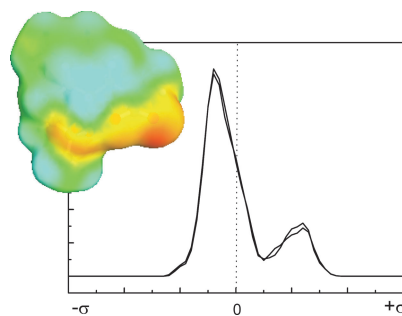
Join in – register today!

241

Screening of new solvents for artemisinin extraction process using *ab initio* methodology

Alexei A. Lapkin,* Martina Peters, Lasse Greiner, Smain Chemat, Kai Leonhard, Marcel A. Liauw and Walter Leitner

A calibrated COSMO-RS method gives much improved correlation with experimental data. A number of new solvents were identified for bio-extraction processes.

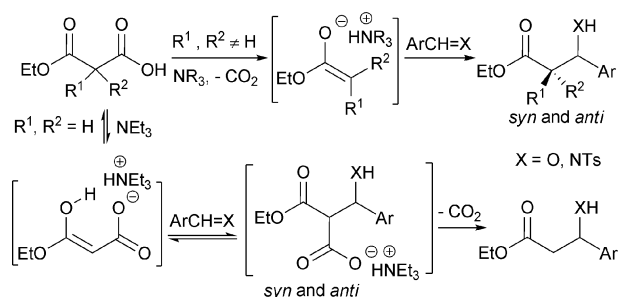


252

Environmentally benign metal-free decarboxylative aldol and Mannich reactions

Jérôme Baudoux, Pierre Lefebvre, Rémi Legay, Marie-Claire Lasne and Jacques Rouden*

Malonic acid half esters were used as the equivalent of ester carbanions for the practical one-step synthesis of β -hydroxy and β -amino esters from aryl aldehydes and arylimines *via* decarboxylative aldol and Mannich type reactions. Two mechanisms were unveiled depending on the substitution of the malonyl substrate.

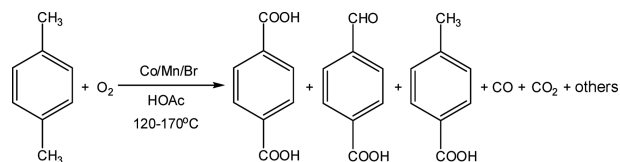


260

Liquid phase oxidation of *p*-xylene to terephthalic acid at medium-high temperatures: multiple benefits of CO₂-expanded liquids

Xiaobin Zuo, Fenghui Niu, Kirk Snavely, Bala Subramaniam* and Daryle H. Busch*

Compared with conventional Mid-Century process conditions, *p*-xylene oxidation in a CO₂-expanded reaction medium affords not only higher yield and purity of terephthalic acid, but also significantly less destructive conversion of solvent and product into CO and CO₂.

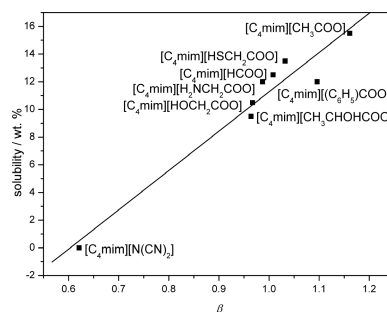


268

Effects of anionic structure and lithium salts addition on the dissolution of cellulose in 1-butyl-3-methylimidazolium-based ionic liquid solvent systems

Airong Xu, Jianji Wang* and Huiyong Wang

The anion structure of ILs and lithium salts added to the [C₄mim][CH₃COO] are found to significantly affect the solubility of the cellulose.





The European Sustainable Chemistry Award



Applications are invited

Applications are invited for the first Award, a prize of **€10,000**.

Individuals or teams of up to three persons who make significant contributions to sustainable development by applying green and sustainable chemistry are eligible.

The Award is designed to recognise innovation that delivers clear improvements in the sustainable production and use of chemicals and chemical products.

The prize will be presented during the 3rd EuCheMS Chemistry Congress on **29 August – 2 September 2010** in Nürnberg, Germany.

The online application form can be accessed at <http://www.euchems.org/ESCA/index.asp>

The deadline for receipt of completed applications is **1 March 2010**.

The Award has been launched by EuCheMS (the European Association for Chemical and Molecular Sciences), with the encouragement of the European Environment Agency (EEA) and the support of SusChem (European Platform for Sustainable Chemistry) and CEFIC (European Chemical Industry Association).

Sponsors

EuCheMS wishes to thank a number of organisations for their generous support for the Award and publishes a list of sponsoring organisations on the Award website.



ELSEVIER



NOVARTIS

EuCheMS (European Association for Chemical and Molecular Sciences) is a non-profit-making organisation, having 47 member societies which represent some 150,000 individual chemists in academia, industry and government in over 35 countries across Europe. Its object is to promote co-operation in Europe between non-profit-making scientific and technical societies in the field of chemistry and molecular sciences. EuCheMS provides a powerful single voice for chemists and the chemical sciences in Europe through its activities and development of policy.

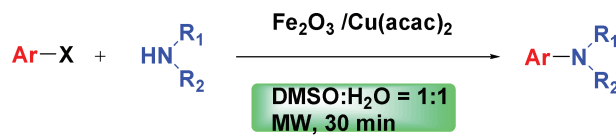
PAPERS

276

Ligand-free iron/copper cocatalyzed *N*-arylations of aryl halides with amines under microwave irradiation

Diliang Guo, He Huang, Yu Zhou, Jinyi Xu, Hualiang Jiang, Kaixian Chen and Hong Liu*

Ligand-free iron/copper cocatalyzed cross-coupling reactions of aryl halides with amines were carried out efficiently, which display broad substrate scope, and are convenient, rapid, low-cost and environmentally friendly.



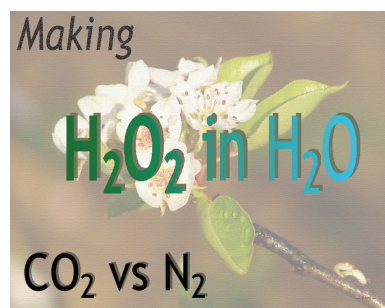
X = I, Br; R₁ or R₂ = H, alkyl, aryl

282

Direct synthesis of hydrogen peroxide in methanol and water using scCO₂ and N₂ as diluents

Teresa Moreno, Juan García-Serna* and María José Cocero

Hydrogen peroxide, H₂O₂, can be produced by direct synthesis over a commercial Pd/C catalyst using H₂O as solvent and CO₂ or N₂ as diluents. This is a breakthrough in H₂O₂ synthesis as it avoids the use of organic solvents.

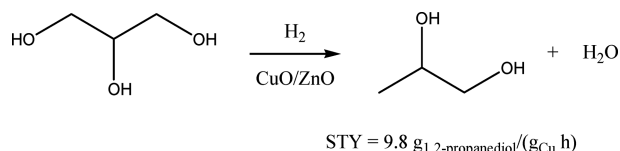


290

Hydrogenolysis of glycerol over a highly active CuO/ZnO catalyst prepared by an oxalate gel method: influence of solvent and reaction temperature on catalyst deactivation

Arne Bienholz, Frederick Schwab and Peter Claus*

A CuO/ZnO catalyst prepared by the oxalate gel method reveals a much higher activity in the hydrogenolysis of pure glycerol to 1,2-propanediol compared to a CuO/ZnO catalyst derived from a conventional coprecipitation method.

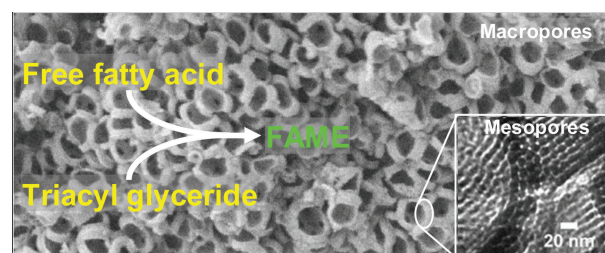


296

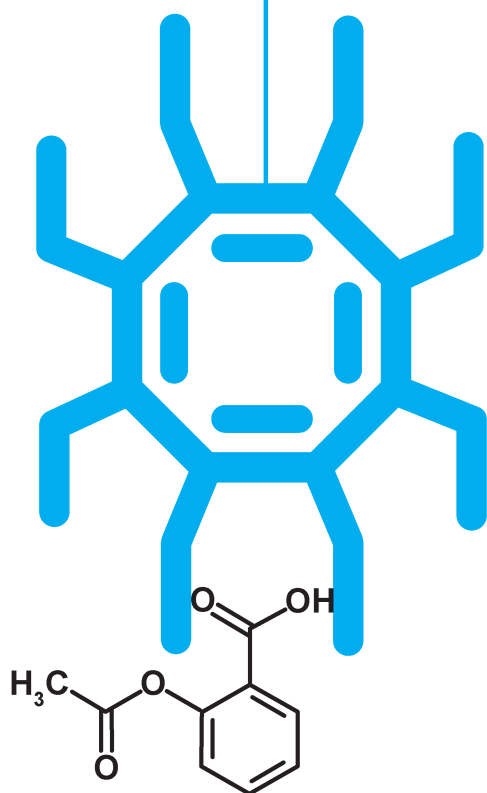
Hierarchical macroporous–mesoporous SBA-15 sulfonic acid catalysts for biodiesel synthesis

Jérémy Dhainaut, Jean-Philippe Dacquin, Adam F. Lee* and Karen Wilson*

Hierarchical macroporous–mesoporous SBA-15 sulfonic acid silicas have been synthesised *via* dual-templating routes employing liquid crystalline surfactants and polystyrene beads.



New adventures on the web



ChemSpider is a free online, structure centric community for chemists, providing fast access to millions of unique chemical entities, resources and information and the opportunity to collaborate with a world wide community of scientists. Rapidly becoming the richest single source of structure based chemistry information online, ChemSpider is a ground breaking initiative now supported by the RSC, the most innovative of chemical societies.

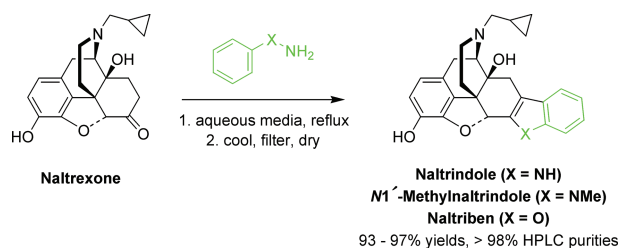
www.chemspider.com

304

Fischer indole synthesis in water: simple, efficient preparation of naltrindole, naltriben and analogs

Romain A. Duval and John R. Lever*

Mildly acidic aqueous conditions proved suitable for Fischer syntheses of naltriben, naltrindole and naltrindole analogs. Products were obtained by simple filtration in good to excellent yields and with high purities in the majority of cases.

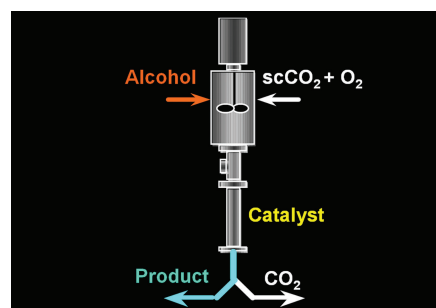


310

Continuous heterogeneous catalytic oxidation of primary and secondary alcohols in scCO₂

Adrian O. Chapman, Geoffrey R. Akien, Nicholas J. Arrowsmith, Peter Licence and Martyn Poliakoff*

Several secondary alcohols and 1-octanol were oxidised selectively with O₂ in continuous flow in supercritical CO₂ with, for the first time, the mass balance data for different reactor configurations.



316

Moringa stenopetala seed oil as a potential feedstock for biodiesel production in Ethiopia

Andinet Ejigu, Araya Asfaw, Nigist Asfaw and Peter Licence*

Oil recovered from the crushed seeds of the tree *Moringa stenopetala* are evaluated as a sustainable feedstock for biodiesel production in Ethiopia.

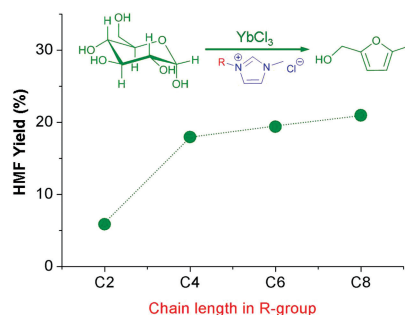


321

Direct conversion of glucose to 5-(hydroxymethyl)furfural in ionic liquids with lanthanide catalysts

Tim Ståhlberg, Mathilde Grau Sørensen and Anders Riisager*

The conversion of glucose to 5-(hydroxymethyl)furfural (HMF) in alkylimidazolium-based ionic liquids together with lanthanide catalysts is speeded up by the higher hydrophobicity of the imidazolium cation.



A new journal from RSC Publishing Launching mid 2010

Rapid communication of research
in medicinal chemistry

MedChemComm



Official journal of:



EFMC
European Federation
for Medicinal Chemistry

A new, peer-reviewed journal publishing medicinal chemistry research, including new studies related to biologically-active chemical or biochemical entities that can act as pharmacological agents with therapeutic potential or relevance.

The journal will publish monthly issues from mid 2010 and will contain a mix of vibrant and concise research and review articles. *MedChemComm* will complement the existing RSC Publishing portfolio of bioscience journals, providing authors in the field with a dedicated subject-specific publication.

From launch, the current issue of *MedChemComm* will be freely available to all readers via the website. Free institutional online access to all 2010/2011 content will be available following a simple registration process at www.rsc.org/medchemcomm_registration

Co-Editor-in-Chief: Dr Anthony Wood, Pfizer, UK

Co-Editor-in-Chief: Professor Gregory Verdine, Harvard University, USA

Sign up for free access today!

RSC Publishing

www.rsc.org/medchemcomm

Registered Charity Number 207890

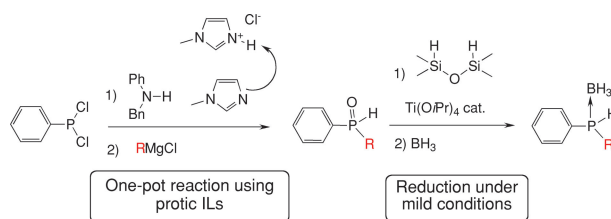
PAPERS

326

A straightforward synthesis of unsymmetrical secondary phosphine boranes

Christelle Petit, Alain Favre-Réguillon,* Gérard Mignani and Marc Lemaire*

An efficient and versatile one-pot synthesis of unsymmetrical secondary phosphine oxides has been developed using protic ionic liquids. The latter could be quantitatively reduced under mild conditions.



331

Microreactor with mesoporous silica support layer for lipase catalyzed enantioselective transesterification

Sho Kataoka, Yasutaka Takeuchi, Atsuhiko Harada, Mitsuhiro Yamada and Akira Endo*

Lipase PS was immobilized in mesoporous silica thin films inside a microreactor for use in the enantioselective transesterification of vinyl acetate with (±)-1-phenylethanol.

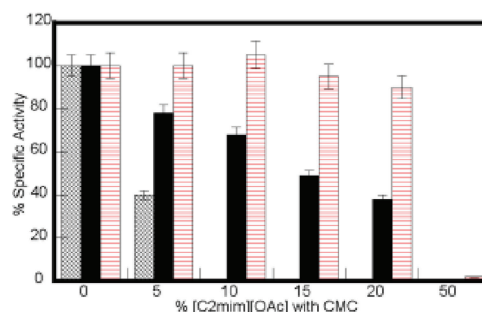


338

Ionic liquid tolerant hyperthermophilic cellulases for biomass pretreatment and hydrolysis

Supratim Datta, Bradley Holmes, Joshua I. Park, Zhiwei Chen, Dean C. Dibble, Masood Hadi, Harvey W. Blanch, Blake A. Simmons and Rajat Saprà*

Cellulases from hyperthermophilic bacteria (black filled) and archaea (horizontal red line) show significant tolerance to 15% (v/v) ionic liquid, [C2mim][OAc] (where [C2mim] = 1-ethyl-3-methylimidazolium), compared to *T. viride* cellulase (cross).

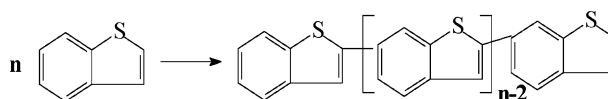


346

Ionic liquids based on imidazolium tetrafluoroborate for the removal of aromatic sulfur-containing compounds from hydrocarbon mixtures

Marya Nefedieva, Olga Lebedeva,* Dmitry Kultin, Leonid Kustov, Svetlana Borisenkova and Vladimir Krasovskiy

The redox reactions of BT and DBT to form new products led to decrease in concentration of these substances in ILs.



AUTHOR INDEX

- Akien, Geoffrey R., 310
 Arrowsmith, Nicholas J., 310
 Asfaw, Araya, 316
 Asfaw, Nigist, 316
 Atkin, Stephen L., 234
 Barrier, Sylvain, 234
 Baudoux, Jérôme, 252
 Benaissi, Karima, 220
 Bienholz, Arne, 290
 Blanch, Harvey W., 338
 Boa, Andrew N., 234
 Boasman, Alia J., 234
 Borisenkova, Svetlana, 346
 Busch, Daryle H., 260
 Cai, Zhipeng, 228
 Chapman, Adrian O., 310
 Chemat, Smain, 241
 Chen, Kaixian, 276
 Chen, Wenxing, 212
 Chen, Zhiwei, 338
 Clark, Tammara D., 209
 Claus, Peter, 290
 Cocero, María José, 282
 Dacquín, Jean-Philippe, 296
 Dai, Wei-Lin, 205
 Datta, Supratim, 338
 Dhainaut, Jérémy, 296
 Dibble, Dean C., 338
 Dierker, Markus, 197
 Dumesic, James A., 223
 Duval, Romain A., 304
 Dyson, Paul J., 228
 Ejigu, Andinet, 316
 Endo, Akira, 331
 Fan, Kang-Nian, 205
 Favre-Régouillon, Alain, 326
 Fei, Zhaofu, 228
 García-Serna, Juan, 282
 Gooßen, Lukas J., 197
 Greiner, Lasse, 241
 Guo, Diliang, 276
 Guo, Feng-Lou, 216
 Gürbüz, Elif I., 223
 Hadi, Masood, 338
 Harada, Atsuhiko, 331
 Holmes, Bradley, 338
 Huang, He, 276
 Jiang, Hualiang, 276
 Jiao, Ning, 216
 Johnson, Lee, 220
 Kataoka, Sho, 331
 Kobayashi, Hisayoshi, 212
 Kou, Yuan, 228
 Krasovskiy, Vladimir, 346
 Kultin, Dmitry, 346
 Kunkes, Edward L., 223
 Kustov, Leonid, 346
 Lapkin, Alexei A., 241
 Lasne, Marie-Claire, 252
 Lebedeva, Olga, 346
 Lee, Adam F., 296
 Lefebvre, Pierre, 252
 Legay, Rémi, 252
 Leitner, Walter, 241
 Lemaire, Marc, 326
 Leonhard, Kai, 241
 Lever, John R., 304
 Li, Changning, 228
 Li, Renhong, 212
 Liang, Xuezheng, 201
 Liauw, Marcel A., 241
 Licence, Peter, 310, 316
 Liu, Hong, 276
 Liu, Jin-Qian, 216
 Liu, Ying, 216
 Löbber, Andreas, 234
 Lorch, Mark, 234
 Ma, Chunxia, 212
 Mack, James, 209
 Mackenzie, Grahame, 234
 Marcum, S. Tyler, 209
 Mignani, Gérard, 326
 Moreno, Teresa, 282
 Nefedieva, Marya, 346
 Niu, Fenghui, 260
 Ohlmann, Dominik M., 197
 Park, Joshua I., 338
 Peters, Martina, 241
 Petit, Christelle, 326
 Poliakov, Martyn, 310
 Riisager, Anders, 321
 Rouden, Jacques, 252
 Sapra, Rajat, 338
 Schwab, Frederick, 290
 Simmons, Blake A., 338
 Snavely, Kirk, 260
 Sørensen, Mathilde Grau, 321
 Ståhlberg, Tim, 321
 Subramaniam, Bala, 260
 Takeuchi, Yasutaka, 331
 Thiel, Indre, 209
 Thielemans, Wim, 220
 Waddell, Daniel C., 209
 Walsh, Darren A., 220
 Wang, Huiyong, 268
 Wang, Jianji, 268
 Wang, Li-Min, 216
 Wilson, Karen, 296
 Xiao, Chaoxian, 228
 Xu, Airong, 268
 Xu, Jinyi, 276
 Yamada, Mitsuhiko, 331
 Yan, Ning, 228
 Yang, Jianguo, 201
 Yu, Jian-Jun, 216
 Yuan, Xiao, 228
 Zhou, Yu, 276
 Zhu, Quan-Jing, 205
 Zuo, Xiaobin, 260

FREE E-MAIL ALERTS AND RSS FEEDS

Contents lists in advance of publication are available on the web *via* www.rsc.org/greenchem – or take advantage of our free e-mail alerting service (www.rsc.org/ej_alert) to receive notification each time a new list becomes available.



Try our RSS feeds for up-to-the-minute news of the latest research. By setting up RSS feeds, preferably using feed reader software, you can be alerted to the latest Advance Articles published on the RSC web site. Visit www.rsc.org/publishing/technology/rss.asp for details.

ADVANCE ARTICLES AND ELECTRONIC JOURNAL

Free site-wide access to Advance Articles and the electronic form of this journal is provided with a full-rate institutional subscription. See www.rsc.org/ejs for more information.

* Indicates the author for correspondence: see article for details.



Electronic supplementary information (ESI) is available *via* the online article (see <http://www.rsc.org/esi> for general information about ESI).

Silver triflate-catalysed synthesis of γ -lactones from fatty acids†

Lukas J. Goossen,^{*a} Dominik M. Ohlmann^a and Markus Dierker^b

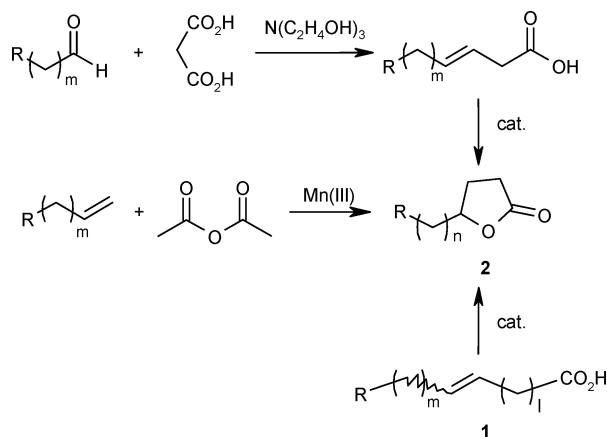
Received 17th August 2009, Accepted 21st November 2009

First published as an Advance Article on the web 16th December 2009

DOI: 10.1039/b916853b

A silver(I)-based catalytic system was found to efficiently promote the double-bond isomerization of unsaturated fatty acids and at the same time to mediate the intramolecular addition of the carboxylate group to the isomerized double bond under selective formation of five-ring lactones. The resulting one-step isomerization- γ -lactonization process allows the direct conversion of unsaturated fatty acids into the corresponding γ -lactones in good yields.

Aliphatic γ -lactones are widely present in plants, vegetables and fruits.¹ Due to their pleasant odor, they are also industrially important as ingredients in perfumes and as food additives.² Usually, γ -lactones are synthesized in multi-step sequences, e.g. via γ -hydroxycarboxylates, or from aldehydes and acrylates by reductive coupling using superstoichiometric amounts of SmI_2 .³ In a particularly expedient approach, aliphatic aldehydes are reacted with malonic acid in a special variant of the Knoevenagel condensation that leads to the formation of the 3-alkenoic acids instead of the expected α,β -unsaturated isomers.⁴ The 3-alkenoic acids are then cyclized to the corresponding lactones (Scheme 1).^{1,5,6} A variety of mediators for such intramolecular 5-*exo-trig* additions of carboxylate groups to C=C double bonds are known, among them iodine,⁷ salts of silver,⁸ thallium,⁹ and palladium,¹⁰ Brønsted acids,¹¹ and solid acid catalysts.¹²



Scheme 1 Traditional and new synthesis of γ -lactones.

^aFachbereich Chemie, Technische Universität Kaiserslautern, Erwin-Schrödinger-Straße 54, 67663 Kaiserslautern, Germany. E-mail: goossen@chemie.uni-kl.de; Fax: +49-631-3921

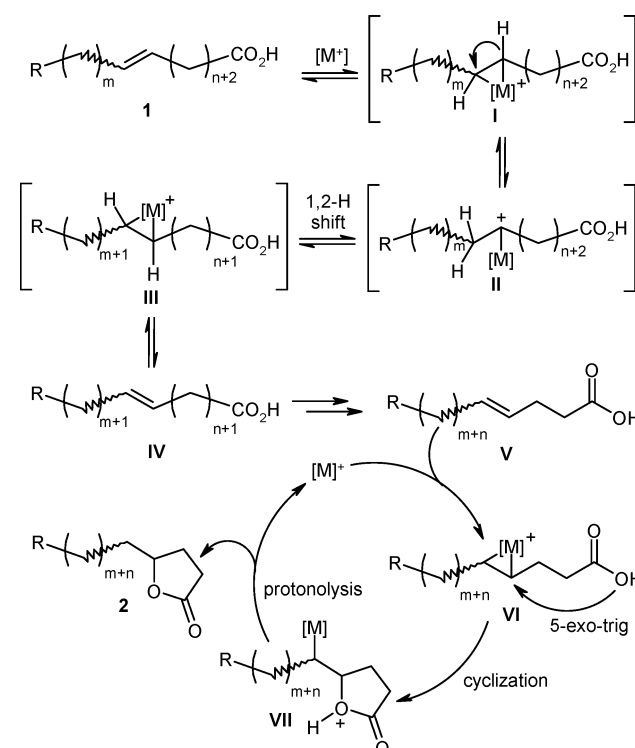
^bCare Chemicals Technology, Cognis GmbH, Henkelstraße 67, 40551 Düsseldorf, Germany

† Electronic supplementary information (ESI) available: Synthetic methods. See DOI: 10.1039/b916853b

This and related strategies are useful for the synthesis of short-chain lactones, where the aldehydes are readily available in large quantities. However, those aldehydes required to access longer-chain derivatives such as γ -stearolactone are rare and expensive. For the C_{18} -lactone, an expedient synthesis from 1-hexadecene derived from petrochemical sources by a free radical reaction mechanism has been described by Burger *et al.*¹³ Unfortunately, this process involves superstoichiometric amounts of the heavy metal manganese.

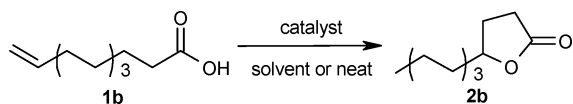
Arguably the most sustainable synthetic entry to aliphatic γ -lactones would instead start from long-chain unsaturated carboxylic acids derived directly from renewable fats and oils, which have the complete carbon skeleton in place as well as the correct oxidation state.

As shown in Scheme 2, one can imagine the possibility of shifting the double bond of such compounds toward the carboxylate group by several consecutive catalytic double-bond migration steps.



Scheme 2 Proposed mechanism of the tandem isomerization-lactonization.

This should take place via a Lewis or Brønsted acid-promoted carbocation formation (I),¹⁴ followed by a series of 1,2-H-shifts (II–III).^{11b} The 4-alkenoic acid isomer (V), activated by catalyst

Table 1 Optimization of catalyst and reaction conditions^a


Entry	Catalyst	Mol%	Solvent	T (°C)	Yield (%) ^b
1	TsOH	5	—	160	0
2	(PPh ₃) ₃ H ₂ (CO)Ru	5	—	160	0
3	(PPh ₃) ₃ (H)(Cl)Ru ^c	5	Toluene	110	0
4	AuCl ₃	5	—	160	0
5	AgBF ₄	5	—	160	0
6	PdCl ₂	5	—	160	0
7	Pd(dba) ₂	5	—	160	0
8	Bi(OTf) ₃	5	—	160	4
9	Cu(OTf) ₂	5	—	160	11
10	LiOTf	5	—	160	0
11	In(OTf) ₂	5	—	160	21
12	Cu ₂ (OTf) ₂ ·C ₆ H ₆	2.5	—	160	34
13	AgOTf	5	—	160	50
14	AgOTf	5	NMP	160	0
15	AgOTf	5	DMSO	160	0
16	AgOTf	5	Tetraglyme	160	0
17	AgOTf	5	1,2-Dichloroethane	85	0
18	AgOTf	5	Dowtherm A	160	50
19	AgOTf	5	PhCl	130	50
20	AgOTf	10	PhCl	130	80 (71) ^d

^a Reaction conditions: 1.0 mmol of acid **1b**, 2 mL of solvent (if used), 24 h. ^b Determined by GC using *n*-tetradecane as internal standard. ^c Generated *in situ* from (PPh₃)₃RuCl₂ and excess NaBH₄. ^d Isolated yield.

coordination to the C–C double bond (**VI**), would be removed from the resulting dynamic equilibrium of isomers by a fast *in situ* 5-*exo-trig* cyclization of the carboxylate group, giving the stable lactone ring of product **2**. Ideally, the overall process would lead to a quantitative formation of the desired γ -lactone in one step.

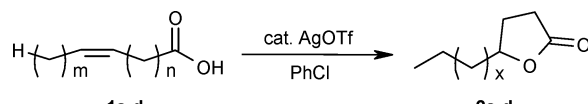
However, it has not been possible so far to selectively achieve isomerizing lactonizations in the absence of stoichiometric mediators: Previous attempts were plagued by side reactions, mainly di- and oligomerizations at the double bonds, or intermolecular additions of carboxylate groups to double bonds. Angelici *et al.* reported that when using Amberlyst-15 resin, these side reactions predominate for substrates that need to undergo a double-bond shift over five or more carbon atoms.¹² Isomerizing lactonizations of 9- or 10-alkenoic acids would require an even larger number of double-bond migration steps along the alkyl chain before the desired cyclization can take place, with the potential for side reactions over the entire course of the isomerization process. As a result, most known protocols starting from fatty acids involve the use of large quantities of corrosive and hazardous mediators, and their yields are low. For example, superstoichiometric amounts of sulfuric,¹⁵ methanesulfonic¹⁶ or even explosive perchloric acid¹⁷ are required to achieve the isomerizing cyclization of oleic acid (**1a**) to the γ -lactone **2a**. While only perchloric acid gave satisfactory yields, the use of this unstable, strongly oxidizing material at high temperatures on large scales represents a major health and safety hazard, precluding its application in chemical manufacturing.

We became interested in this transformation in the context of our research on the use of carboxylic acids as substrates in sustainable catalytic transformations.¹⁸ In order to establish

tandem isomerization–lactonization as a modern synthetic tool, a new process is vital in which only catalytic quantities of a non-toxic and easy-to-handle mediators are necessary. Our strategy to develop such a process was to focus the catalyst search on Lewis-acidic metal cations that have a marked affinity for carbon–carbon double bonds and a strong potential to effect isomerizations of olefinic carboxylic acid substrates, and at the same time to promote the addition of nucleophiles to multiple bonds. This way, we hoped to establish a rapid equilibration between all possible positional isomers, so that the selective trapping of one species by ring closure would lead selectively to a single product.

We chose the terminally unsaturated 10-undecenoic acid (**1b**) as a first model substrate and performed some preliminary experiments with neat reaction mixtures at 160 °C. We screened a broad range of Lewis and Brønsted acids as well as metal hydrides, with a focus on easily handled, commercially available catalyst precursors. Selected results are summarized in Table 1.

As expected, simple Brønsted acids (TsOH, HBF₄, F₃CCOOH) were inactive when only used in catalytic amounts (entry 1). Known isomerization catalysts, *i.e.* either preformed (entry 2) or *in situ*-generated ruthenium hydride complexes (entry 3), were similarly disappointing. Furthermore, the results obtained with simple Lewis acids (AuCl₃, AuI, CuF₂, AgBF₄, FeCl₂, FeCl₃) (entries 4 and 5) or Pd catalysts¹⁹ (entries 6 and 7) were unsatisfactory. In contrast, several metal triflates immediately afforded visible catalytic turnover in the absence of solvent (entries 8–13). Amongst them, the soft silver(i) triflate proved to be most effective and gave almost full conversion. However, only 50% yield was obtained due to oligomerization reactions.

Table 2 Substrate scope for the catalytic isomerization–lactonization^a


Entry	Acid	<i>m</i>	<i>n</i>	Mol% cat.	γ -Lactone	<i>x</i>	Yield (%)
1	1a	8	7	10	2a	12	51
2	1b	0	9	15	2b	5	72
3	1c	6	7	15	2c	10	57
4	1d	6	3	15	2d	6	66

^a Reaction conditions: 1.0 mmol of acid **1**, given amount of AgOTf, 2 mL of PhCl, 130 °C, 24 h. ^b Isolated yields. Products were characterized by means of ¹H-NMR and ¹³C-NMR.

In order to drive back these intermolecular processes in favor of the desired intramolecular lactonization, we sought for a suitable solvent (entries 14–19). Moderate yields were achieved when using the non-chlorinated solvent Dowtherm A at 160 °C (entry 18), but the best chemoselectivity was achieved with chlorobenzene at the lower temperature of 130 °C (its boiling point). Under these conditions and when stopping the reaction at incomplete conversion, the formation of unwanted and hard-to-separate oligomers was suppressed (entry 19).

The best results (80% yield determined by GC, entry 20) were finally obtained with a catalyst loading of 10 mol%, and γ -lactone **2b** was isolated in 71% yield after column chromatography (Table 2, entry 2). In contrast to other known procedures,^{15b} the catalytic process was highly regioselective: We never observed more than trace amounts of the thermodynamically only slightly disfavored¹⁴ six-ring lactone.

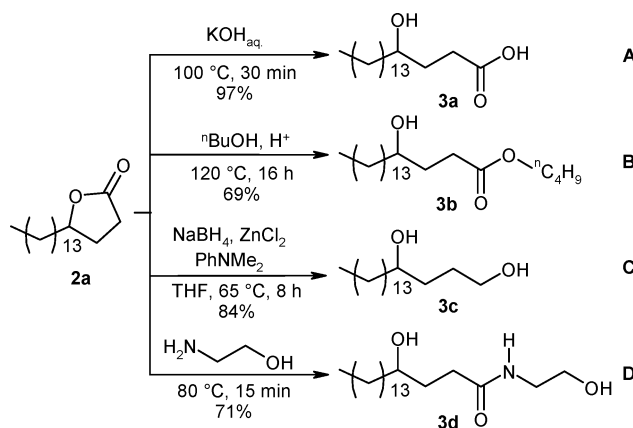
After having thus developed an effective protocol that allowed a double-bond isomerization over five chain positions, we next approached the even more challenging transformation of oleic acid (**1a**) to γ -stearolactone (**2a**). With its 33 possible double-bond isomers, this substrate can be seen as an ultimate benchmark for tandem isomerization–functionalization processes.²⁰ Under the optimized conditions we directly obtained **2a** in 33% yield. With a slightly higher catalyst loading of 15 mol%, **2a** was isolated in a remarkable 51% yield after column chromatography (Table 2, entry 1). Again, only traces of the six-ring lactone were detected, and the main side products resulted from oligomerization.

The product samples of this non-commercial long-chain lactone obtained with this protocol displayed interesting properties for applications in cosmetics. For the preparation of larger quantities of the γ -stearolactone required for further testing, we reduced the catalyst loading to 10% and increased the temperature to 160 °C by working at reflux in a 1:6 mixture of chlorobenzene and 1,2-dichlorobenzene. Moreover, we attempted to substitute the chromatographic purification by a more scalable process. Distillation proved not to be feasible as the lactone underwent thermal oligomerization. Instead, we found that the product could be obtained in high purity by fractional crystallization from ethanol (see ESI†). This way, we obtained γ -stearolactone on 180 g scale in a yield of 51%.

Using the same procedure, commercially available palmitoleic acid (**1c**) and *cis*-5-dodecenoic acid (**1d**) were also smoothly converted into the corresponding long-chain γ -lactones in

yields of 57% and 66%, respectively (Table 2, entries 3 and 4).

With such a viable synthetic entry into γ -stearolactone in place, we are currently exploring the properties of the material itself along with its use as a synthetic intermediate. Scheme 3 details successful derivatization reactions, giving access *e.g.* to long-chain γ -hydroxycarboxylates (**A**, **B**),^{21,22} γ -hydroxyalcohols (**C**),²³ or γ -hydroxyamides (**D**) useful as detergents,²⁴ as well as sphingolipid-like structures.²⁵ Saponification of **2a** with potassium hydroxide led to the formation of γ -hydroxystearic acid (**3a**) in nearly quantitative yield. The γ -hydroxyester **3b** was obtained in 69% yield from a transesterification with *n*-butanol. Reduction of **2a** with ZnCl₂/NaBH₄ furnished the long-chain 1,4-diol **3c** in 84% yield, and the stearamide **3d** was isolated in 71% yield after treating **2a** with ethanolamine.

**Scheme 3** Derivatization reactions of γ -stearolactone (**2a**).

Conclusions

Overall, an efficient catalytic tandem isomerization–lactonization protocol has been developed for the preparation of γ -lactones from renewable fatty acids. The products were obtained in good yields even in the rather extreme test cases of oleic and palmitoleic acid, where only one of the numerous possible double bond isomers could give rise to the desired γ -lactone. The products were shown to be useful starting points for further derivatizations.

Acknowledgements

We thank Cognis GmbH and NanoKat for financial support. D.M.O. thanks the Stiftung der Deutschen Wirtschaft for a scholarship.

Notes and references

- D. D. Zope, S. G. Patnekar and V. R. Kanetkar, *Flavour Fragrance J.*, 2006, **21**, 395 and references therein.
- (a) J.-A. Hislop, M. B. Hunt, S. Fielder and D. D. Rowan, *J. Agric. Food Chem.*, 2004, **52**, 7075 and references therein; (b) B. Schlutt, N. Moran, P. Schieberle and T. Hofmann, *J. Agric. Food Chem.*, 2007, **55**, 9634.
- S. Fukuzawa, A. Nakanishi, T. Fujinami and S. Sakai, *J. Chem. Soc., Perkin Trans. 1*, 1988, 1669.
- S. E. Boxer and R. P. Linstead, *J. Chem. Soc.*, 1931, 740.
- R. Fittig, *Chem. Ber.*, 1883, 373.
- R. P. Linstead, *J. Chem. Soc.*, 1932, 115.
- P. A. Bartlett and J. Myerson, *J. Am. Chem. Soc.*, 1978, **100**, 3950.
- C.-G. Yang, N. W. Reich, Z. Shi and C. He, *Org. Lett.*, 2005, **7**, 4553.
- H. M. C. Ferraz and C. M. R. Ribeiro, *Synth. Commun.*, 1992, **22**, 399.
- (a) R. C. Larock and T. R. Hightower, *J. Org. Chem.*, 1993, **58**, 5298; (b) U. Annby and M. Stenkula, *Tetrahedron Lett.*, 1993, **34**, 8545.
- (a) R. S. Mali and K. N. Babu, *Helv. Chim. Acta*, 2002, **85**, 3525; (b) M. F. Ansell and M. H. Palmer, *J. Chem. Soc.*, 1963, 2640; (c) L. Coulombel and E. Duñach, *Synth. Commun.*, 2005, **35**, 153.
- Y. Zhou, K. Woo and R. Angelici, *Appl. Catal., A*, 2007, **333**, 238.
- B. V. Burger, F.-C. Tien, M. Le Roux and W.-P. Mo, *J. Chem. Ecol.*, 1996, **22**, 739.
- T. A. Isbell and B. A. Plattner, *J. Am. Oil Chem. Soc.*, 1997, **74**, 153.
- (a) A. Granata, F. Sauriol and A. S. Perlin, *Can. J. Chem.*, 1994, **72**, 1684; (b) S. C. Cermak and T. A. Isbell, *J. Am. Oil Chem. Soc.*, 2000, **77**, 243.
- R. Stern and G. Hillion, *Fr. Pat.* 1987/2623499.
- J. S. Showell, D. Swern and W. R. Noble, *J. Org. Chem.*, 1968, **33**, 2697.
- (a) L. J. Gooßen, N. Rodríguez and K. Gooßen, *Angew. Chem., Int. Ed.*, 2008, **47**, 3100; (b) L. J. Gooßen and J. Paetzold, *Angew. Chem., Int. Ed.*, 2004, **43**, 1095; (c) L. J. Gooßen and A. Döhning, *Adv. Synth. Catal.*, 2003, **345**, 943; (d) L. J. Gooßen, J. Paetzold and L. Winkel, *Synlett*, 2002, 1721.
- for Pd-catalyzed isomerizations, see (a) Y. Wang, X. Dong and R. C. Larock, *J. Org. Chem.*, 2003, **68**, 3090; (b) C. Jiménez-Rodríguez, G. R. Eastham and D. J. Cole-Hamilton, *Inorg. Chem. Commun.*, 2005, **8**, 878.
- In catalytic isomerizing hydroborations, the formation of side products was substantially higher when using oleates compared to short-chain substrates: K. Y. Ghebreyessus and R. J. Angelici, *Organometallics*, 2006, **25**, 3040.
- P. W. Clutterbuck, *J. Chem. Soc.*, 1924, **125**, 2330.
- T. A. Isbell and B. A. Steiner, *J. Am. Oil Chem. Soc.*, 1998, **75**, 63.
- B. V. S. K. Rao and R. Subbarao, *J. Lipid Sci. Technol.*, 2006, **38**, 185.
- (a) J. K. Well, F. D. Smith and W. M. Linfield, *J. Am. Oil Chem. Soc.*, 1972, **49**, 383; (b) R. Lagerman, S. Clancy, D. Tanner, N. Johnston, B. Callian and F. Friedli, *J. Am. Oil Chem. Soc.*, 1994, **71**, 97.
- Y. Cai, C.-C. Ling and D. R. Bundle, *Org. Biomol. Chem.*, 2006, **4**, 1140.

Synthesis of a novel multi $-\text{SO}_3\text{H}$ functionalized ionic liquid and its catalytic activities for biodiesel synthesis

Xuezheng Liang^{*a,b} and Jianguo Yang^b

Received 11th June 2009, Accepted 2nd November 2009

First published as an Advance Article on the web 27th November 2009

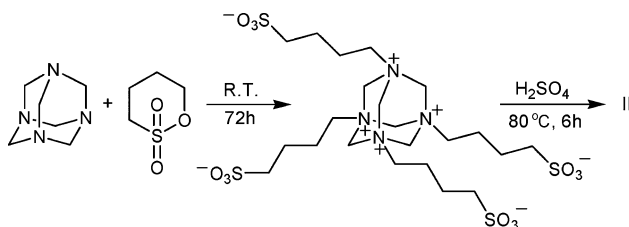
DOI: 10.1039/b922966n

A novel multi $-\text{SO}_3\text{H}$ functionalized strong Brønsted acidic ionic liquid has been prepared for the synthesis of biodiesel from rapeseed oil and methanol. The results showed that the novel catalyst was very efficient for the reaction, with excellent water and acid resistant ability. The catalyst could smoothly transform both the rapeseed oil and free fat acid to the biodiesel. Also the novel ionic liquid was insoluble in the organic phase, which made the recycling of the catalyst very convenient. Operational simplicity, low cost of catalyst used, high yields, wide applicability and reusability are the key features of this methodology. The novel catalyst therefore has great potential for use in green processes.

1. Introduction

Ionic liquids have received widespread attention as mediums for a variety of reactions because of their properties such as very low or practically no vapor pressure, remarkable solubility behavior and the possibility of varying their structure to manipulate parameters like density, solubility *etc.*^{1,2,3} Recently, alkane sulfonic acid group functionalized ionic liquids have been reported offering a new possibility for developing environmentally-friendly acidic catalysts due to a combination of the advantages of liquid acids and solid acids, *e.g.* uniform acid sites, stability in water and air, easy separation and reusability.⁴ In 2002, Cole *et al.*⁵ first published an article about sulfonic acid group functionalized ionic liquids with strong Brønsted acidity. The research and application of various $-\text{SO}_3\text{H}$ functionalized strong Brønsted acidic ionic liquids have received much attention for their potential application in replacing conventional homogeneous/heterogeneous acidic catalysts because they are flexible, nonvolatile, non-corrosive and immiscible with many organic solvents and could be used as dual solvents and catalysts.^{6–11} For example, $-\text{SO}_3\text{H}$ functionalized ionic liquids were applied to the esterification of aliphatic acids with olefins,¹² oligomerization of olefins,¹³ selective alkylation of *m*-cresol with *tert*-butanol,¹⁴ alkylation of *p*-cresol with *tert*-butanol¹⁵ and good results were achieved. Liu *et al.* investigated the structures of the $-\text{SO}_3\text{H}$ functionalized acidic ionic liquid 1-(3-sulfonic acid) propyl-3-methylimidazolium hydrogen sulfate ($[\text{C}_3\text{SO}_3\text{H-mim}]\text{HSO}_4$), and the results showed that when the cation and the anion

interacted near the functional group by double $\text{O-H}\cdots\text{O}$ hydrogen bonds, the ionic liquid was inclined to exist in a form of the zwitterion and H_2SO_4 .¹⁶ Here, we present a novel strong Brønsted acidic ionic liquid with four $-\text{SO}_3\text{H}$ groups. The ionic liquid was synthesized from hexamethylenetetramine and 1,4-butane sulfonate (Scheme 1). Biodiesel is a well-known renewable fuel¹⁷ as a replacement for the traditional mineral diesel fuel.¹⁸ Biodiesel is characterized by excellent properties as diesel engine fuels and thus can be used in compression-ignition (diesel) engines with little or no modifications.¹⁹ The novel ionic liquid was applied to the catalytic synthesis of biodiesel. The results showed that the catalyst was very efficient for the reaction with a yield over 98%. The novel ionic liquid had four SO_3H groups, which made the acidity of the catalyst extremely high. The high acidity resulted in a high activity for biodiesel synthesis. Also, the ionic liquid had high polarity with four positive charges, which made the recycling of the catalyst very convenient.



Scheme 1 The synthetic route to the novel catalyst.

2. Experimental

All organic reagents were commercial products of the highest purity available (>98%) and used for the reaction without further purification. Rapeseed oil was obtained from the Shanghai Oil Plant without further purification. The average molecular weight is 850.

2.1 Synthesis of the catalyst

2.1.1 Preparation of zwitterion. Hexamethylenetetramine and 4 M 1,4-butane sulfonate were mixed together without solvent and stirred magnetically for 72 h at room temperature (25 °C). Then, a white solid zwitterion was formed and the solid was washed repeatedly with ethyl ether. After being dried in vacuum (110 °C, 0.01 Torr), the white solid zwitterion was obtained in a good yield (>90%) and sufficient purity as assessed by a Varian DRX-400 NMR spectrometer. ¹H NMR (400 MHz,

^aInstitute of Applied Chemistry, Shaoxing University, Shaoxing, 312000, China. E-mail: xzliang@zscas.edu.cn

^bShanghai Key Laboratory of Green Chemistry and Chemical Process, Department of Chemistry, East China Normal University, Shanghai, 200062, China

D₂O, TMS): δ 1.423 (m, 2H), 1.584 (m, 2H), 2.593 (t, $J = 7.6$ Hz, 2H), 3.964 (t, $J = 7.6$ Hz, 2H), 8.463 (s, 2H). ¹³CNMR (100 MHz, D₂O, TMS): δ 21.180, 21.879, 50.368, 52.193, 79.999.

2.1.2 Preparation of –SO₃H-functionalized ionic liquid. 4 M sulfuric acid was added to the above obtained zwitterion and the mixture was stirred for 6 h at 80 °C to form the ionic liquid. The IL phase was then washed repeatedly with toluene and ether to remove non-ionic residues, and dried in vacuum (110 °C, 0.01 Torr). The product was formed quantitatively and in high purity as assessed by mass balance and ¹H NMR spectroscopies. ¹H NMR (400 MHz, D₂O, TMS): δ 1.323 (m, 2H), 1.483 (m, 2H), 2.503 (t, $J = 7.6$ Hz, 2H), 3.874 (t, $J = 7.6$ Hz, 2H), 8.263 (s, 2H).

2.2 The procedure for the synthesis of biodiesel

Typical procedure for the synthesis of biodiesel: rapeseed oil (5 g), methanol and the catalyst were mixed together in a three necked round bottomed flask equipped with a magnetic stirrer and a thermometer. The mixture was heated at 70 °C for the specified period. The process of the reaction was monitored by GC analysis of the small aliquots withdrawn at half an hour intervals. Here the ionic liquid had high polarity and was very easily separated from the organic phase. On completion, the reaction mixture formed two phases when switching off the magnetic stirrer for a while and the ionic liquid was recycled by centrifugation first. Because the presence of methanol made centrifugation of biodiesel and glycerol difficult, the excess methanol was distilled off under vacuum. After the reaction mixture was allowed to settle for >4 h, it formed two phases: the upper layer was biodiesel and the lower layer was glycerol. The biodiesel was collected for chromatographic analysis. Quantitative analysis of the extract solution was carried out on a temperature-programmed Shimadzu (GC-14B) gas chromatograph according to the method provide by Alcantara *et al.*²⁰ Here, other analysis methods such as NMR, glycerol titration and hydroxyl value were also used for the analysis, and the results showed that the GC analysis fits well with other methods with a difference within 1%. Furthermore, pure biodiesel was obtained under the optimal reaction conditions and the isolated yield also fits well with the GC analysis with a difference within 1%.

3. Results and discussion

3.1 The effect of the methanol amount on the reaction

The molar ratio of the rapeseed oil and methanol was investigated first (Table 1). The results showed that the yield increased with the amount of methanol and the peak value was achieved with methanol amount of 2.33 g. Increasing the amount of methanol is very useful for the reaction because it increases the collision probability of the reactants. However, too much methanol could cause a dilution effect and is not useful for the reaction for the yield changes little. So the optimal methanol amount was chosen as 2.33 g with a molar ratio of 12:1 (methanol to rapeseed oil).

Table 1 The effect of the methanol amount on the reaction

Methanol amount/g	Yield/% ^{a,b}
1.12	89.4
1.56	94.5
2.33	98.2
3.15	98.3
4.66	98.1

^a The reaction conditions: rapeseed oil 5 g, catalyst 2 mmol, 70 °C, 7 h.

^b The yield was calculated on a GC using an internal standard.

3.2 The effect of the reaction time on the reaction

Reaction time had a key effect on the reactions, so the effect of reaction time on the yield was investigated (Fig. 1). It can be seen from Fig. 1 that the catalyst was very efficient for the reaction with a yield over 98% after 7 h. For the traditional acid-catalyzed transesterification, a very long reaction time (>10 h) was needed to complete the reaction.²¹ The reaction took place quickly at first, and gradually reached equilibrium after 7 h. The yield changed little after 7 h, so 7 h was chosen as the optimal reaction time.

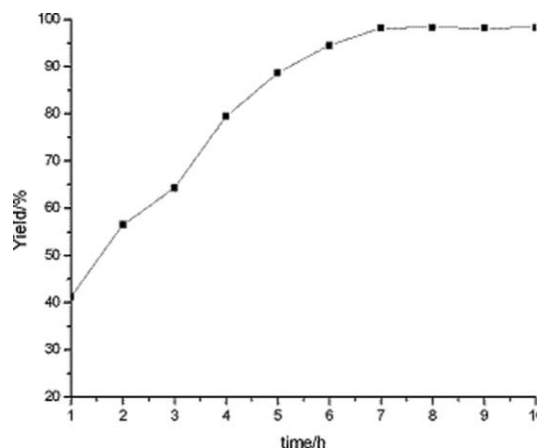


Fig. 1 The effect of reaction time on the yield. Reaction conditions: rapeseed oil 5 g, methanol 2.33 g, catalyst 2 mmol, 70 °C. The yield was calculated on a GC using an internal standard.

3.3 The effect of the catalyst amount on the reaction

The catalyst amount was also very important for the reaction (Table 2). There were not enough active sites for the reaction when the catalyst amount was low. The yields increased with the catalyst amount and the yield remained constant when the catalyst amount was 2 mmol. Increasing the catalyst amount further seemed to be meaningless for the yields improved little. Moreover, the reverse reaction could also be catalyzed by the catalyst because when too much catalyst was employed, the yield decreased slightly. So the optimal catalyst amount was chosen as 2 mmol.

3.4 The effect of water content in the rapeseed oil on the reaction

The water content in the oil affected the reaction greatly, so the effect of water content in the rapeseed oil on the reaction

Table 2 The effect of the catalyst amount on the reaction

The catalyst amount/mmol	Yield/% ^{a,b}
1.0	89.7
1.5	95.1
2.0	98.2
2.5	98.3
3.0	97.9

^a The reaction conditions: rapeseed oil 5 g, methanol 2.33 g, 70 °C, 7 h.

^b The yield was calculated on a GC using an internal standard.

Table 3 The effect of the water content on the reaction

Water content/%	Yield/% ^{a,b}
0.3	98.3
0.5	98.2
0.7	97.8
0.9	96.9
1.2	96.0
2.0	95.3

^a The reaction conditions: rapeseed oil 5 g, methanol 2.33 g, catalyst 2 mmol, 70 °C, 7 h. ^b The yield was calculated on a GC using an internal standard.

Table 4 The effect of the acidity on the reaction

Acidity/mgKOH g ⁻¹	Yield/% ^{a,b}
2	98.2
4	97.4
5	97.3
6	97.5
8	98.3

^a The reaction conditions: rapeseed oil 5 g, methanol 2.33 g, catalyst 2 mmol, 70 °C, 7 h. ^b The yield was calculated on a GC using an internal standard.

was investigated (Table 3). The results showed that the novel ionic liquid has good water resistant ability. The yields decreased slowly with increasing water content. According to research by Liu *et al.*,¹⁶ the ionic liquid should consist of a zwitterion and H₂SO₄. The H₂SO₄ has good water absorption ability, which causes the catalyst to have good water resistant ability. On the other hand, there were very little free zwitterion and H₂SO₄ in the ionic liquid, so the activity also decreased when the water content increased. The results indicate that the catalyst is a good choice for raw oil with a high water content; the catalyst could efficiently catalyze raw oil with a water content of 0.9%.

3.5 The effect of the acidity of the raw oil on the reaction

The effect of the acidity of the raw oil on the reaction was also investigated (Table 4). Acidic catalysts are good choices for raw oils with high acidity. The results showed that the novel catalyst was very efficient for rapeseed oil with high acidity. Both the rapeseed oil and the free fat acid could be transformed to biodiesel under these conditions. The catalyst had high activities not only for the transesterification of the rapeseed oil but also for the esterification of the free fat acid. The yields decreased little with the acidity and the transformation of the free fat acid

Table 5 A comparison of different catalysts

Catalyst	Catalyst amount/mmol	Reaction time/h	Yield/% ^{a,b}
Novel catalyst	2	7	98.2
[Et ₃ NH]Cl-AlCl ₃	5	9	98.5
[SO ₃ H-Bmim][HSO ₄]	3	9	96.5
H ₂ SO ₄	4	9	97.8
H ₃ PO ₄	4	12	88.7
Amberlyst-15	500 mg	18	87.5

^a The reaction conditions: rapeseed oil 5 g, methanol 2.33 g, 70 °C. ^b The yield was calculated on a GC using an internal standard.

to the corresponding product accounted for an increase in the yield when the acidity was 8.

3.6 Comparative study on the catalytic activities of different catalysts

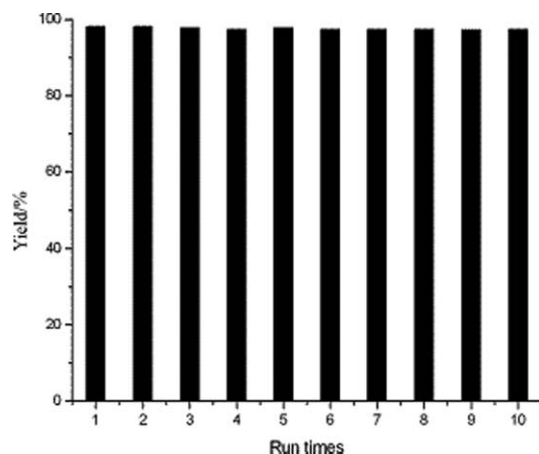
A comparative study on the catalytic activities of the novel catalyst with other catalysts was carried out (Table 5). From this study it can be concluded that the novel catalyst had much higher activity than the others. For the Lewis acid ionic liquid in our previous work,²² the catalytic amount was greater and a longer reaction time was needed. Furthermore, the catalyst was sensitive to water, which limited its application. As for the traditional single -SO₃H functionalized strong Brønsted acidic ionic liquid [SO₃H-Bmim][HSO₄], the catalyst was slightly soluble in the reaction mixture, which made purification of the product more difficult. After reaction, it was difficult to totally separate the ionic liquid from the reaction mixture. It was not only the glycerol phase, but also the biodiesel phase, that contained the catalyst, and the weight loss of the catalyst during the catalytic procedure was more than 8%. The novel ionic liquid had strong polarity, which made the catalyst insoluble in the organic phase. After reaction, the catalyst was easily separated from the organic phase without having to distill the excess methanol. Then, both the biodiesel and glycerol phases were analyzed by ICP. The results showed that no catalyst was dissolved in the biodiesel phase and little catalyst was dissolved in the glycerol phases. The weight loss of the novel catalyst during the catalytic procedure was below 0.2%. Traditional homogeneous catalysts such as H₂SO₄ and H₃PO₄ had relatively low activities. Also, traditional ionic exchange resins (Amberlyst-15, acidity 0.8 mmol g⁻¹) had much lower activity. The results showed that the novel catalyst should be one of the best choices for operational simplicity, being a user-friendly catalyst for scaling-up purposes.

3.7 The reuse of the catalyst

One property of the catalyst is reusability. After reactions, the catalyst was recovered by centrifugation and used without any disposal. The recovered activities of the novel ionic liquid were investigated carefully (Fig. 2). The yields remained unchanged even after the catalyst had been recycled ten times. Also the insolubility of the catalyst during the catalytic procedure made the workup process much easier.

Table 6 The quality of the refined biodiesel

Entry	Value
Density (15 °C)	0.88 g cm ⁻³
Viscosity (40 °C)	3.9 mm ² s ⁻¹
Flash point	138 °C
Sulfur content	3 mg kg ⁻¹
Water content	200 mg kg ⁻¹
Neutralization value	0.4 (KOH) mg g ⁻¹
Methanol content	0.05 %
Biodiesel content	>99.1 %
Monoglycerides content	0.4 %
Diglycerides content	0.2 %
Triglycerides content	0.1 %
Glycerol content	0.02 %

**Fig. 2** The reuse of the catalyst.

3.8 The quality of the refined product

After reactions, the biodiesel was collected and dried in vacuum for 5 h (110 °C, 0.01 Torr). The quality of the refined products was investigated carefully (Table 6). The results showed that the quality of the refined biodiesel achieved the standard of EN 14214, which further confirmed that the novel catalyst would be one of the best choices for the reaction.

4. Conclusion

In conclusion, a novel multi -SO₃H functionalized strong Brønsted acidic ionic liquid has been found to be highly efficient for the synthesis of biodiesel. Operational simplicity, excellent water and acid resistant ability, low cost of the catalyst used, high yields, insolubility in the organic phase, short reaction time, and applicability to large-scale reactions are the key features of this methodology. The novel catalyst therefore has great potential for green processes.

Notes and references

- 1 Y. Y. Jiang, G. N. Wang, Z. Zhou, Y. T. Wu, J. Geng and Z. B. Zhang, *Chem. Commun.*, 2008, 505.
- 2 D. Kuang, S. Uchida, R. Humphry-Baker, S. M. Zakeeruddin and M. Graetzel, *Angew. Chem., Int. Ed.*, 2008, **47**, 1923.
- 3 T. Singh and A. Kumar, *J. Phys. Chem. B*, 2008, **112**, 4079.
- 4 N. S. Gupta, G. L. Kad and J. Singh, *Catal. Commun.*, 2007, **8**, 1323.
- 5 A. C. Cole, J. L. Jensen, I. Ntai, K. L. T. Tran, K. J. Weaver, D. C. Forbes and J. H. Davis, *J. Am. Chem. Soc.*, 2002, **124**, 5962.
- 6 R. Sugimura, K. Qiao, D. Tomida and C. Yokoyama, *Catal. Commun.*, 2007, **8**, 770.
- 7 B. A. Da Silveira Neto, G. Ebeling, R. S. Goncalves, F. C. Gozzo, M. N. Eberlin and J. Dupont, *Synthesis*, 2004, 1155.
- 8 H. H. Wu, F. Yang, P. Cui, J. Tang and M. Y. He, *Tetrahedron Lett.*, 2004, **45**, 4963.
- 9 A. Kamal and G. Chouhan, *Adv. Synth. Catal.*, 2004, **346**, 579.
- 10 J. S. Yadav, B. V. S. Reddy and G. Kondaji, *Chem. Lett.*, 2003, **32**, 672.
- 11 A. Kamal and G. Chouhan, *Tetrahedron Lett.*, 2003, **44**, 3337.
- 12 Y. Gu, F. Shi and Y. Deng, *J. Mol. Catal. A: Chem.*, 2004, **212**, 71.
- 13 Y. Gu, F. Shi and Y. Deng, *Catal. Commun.*, 2003, **4**, 597.
- 14 X. Liu, M. Liu, X. Guo and J. Zhou, *Catal. Commun.*, 2008, **9**, 1.
- 15 X. Liu, J. Zhou, X. Guo, M. Liu, X. Ma, C. Song and C. Wang, *Ind. Eng. Chem. Res.*, 2008, **47**, 5298.
- 16 X. Liu, Z. Song and H. Wang, *Struct. Chem.*, 2009, **20**, 509.
- 17 R. Luque, L. Herrero-Davila, J. M. Campelo, J. H. Clark, J. M. Hidalgo, D. Luna, J. M. Marinasa and A. A. Romeroa, *Energy Environ. Sci.*, 2008, **1**, 542.
- 18 D. E. Lopez, J. G. Goodwin, D. A. Bruce and S. Furuta, *Appl. Catal., A*, 2008, **339**, 76.
- 19 I. N. Martyanov and A. Sayari, *Appl. Catal., A*, 2008, **339**, 45.
- 20 R. Alcantara, J. Amores, L. Canoira, E. Fidalgo, M. J. Franco and A. Navarro, *Biomass Bioenergy*, 2000, **18**, 515.
- 21 S. V. Ranganathan, S. L. Narasimhan and K. Muthukumar, *Biore-sour. Technol.*, 2008, **99**, 3975.
- 22 X. Liang, G. Gong, H. Wu and J. Yang, *Fuel*, 2009, **88**, 613.

A green process for the oxidative lactonization of 1,2-benzenedimethanol by tungstic acid with aqueous H₂O₂†

Quan-Jing Zhu, Wei-Lin Dai* and Kang-Nian Fan

Received 15th October 2009, Accepted 16th November 2009

First published as an Advance Article on the web 7th December 2009

DOI: 10.1039/b921334a

A new economic and green route to synthesize phthalide from 1,2-benzenedimethanol using aqueous hydrogen peroxide as the oxidant and tungstic acid as the catalyst under organic solvent-free conditions is presented. This process proceeds with advantages from the viewpoint of green chemistry, in which the only by-product of H₂O₂ is water and the catalyst can also be easily recovered. The desired product with high purity and good yield can be conveniently obtained when cooled after reaction.

At present, the development of environmentally friendly techniques in the field of oxidation of organic compounds has attracted much attention because the reagents used in stoichiometric amounts in these reactions are sometimes wasteful and toxic. Therefore, there is an urgent need to replace the classic oxidants with “clean” oxygen donors, such as H₂O₂. It is known that the oxidation of organic substrates using hydrogen peroxide as an oxidant has long been studied. Many useful reactions carried out with H₂O₂ have been developed, such as the oxidation of sulfides to sulfoxides and sulfones,¹ epoxidation of olefins and allylic alcohols² and the oxidative cleavage of carbon–carbon double bonds to aldehydes³ and acids.⁴ To date, the oxidation of diols to lactones with H₂O₂ has been rarely reported.

Lactones and their derivatives are ubiquitous in nature.⁵ Many substances containing the lactone ring show interesting biological activity.⁶ Lactones can also be used in the production of a variety of polymers.⁷ Although oxidation of alcohols has been widely used for the synthesis of lots of chemicals, the oxidation of diols to lactones usually requires fierce reaction conditions and specific oxidants. The reaction can be carried out under mild conditions in the presence of organic cooxidants which are not green oxidants, such as α,β -unsaturated ketones,⁸ PhBr,⁹ *N*-methylmorpholine *N*-oxide, or acetone. Mitsudome *et al.* recently obtained a high yield of lactones (99%) from diols using molecular oxygen as the oxidant and supported gold nanoparticles as the catalyst under mild conditions.¹⁰ However, the catalyst is expensive and cannot be easily synthesized. Among the diol oxidations to lactones, the oxidative lactonization of 1,2-benzenedimethanol to phthalide can be taken into account as a probe reaction, since phthalide and

its derivatives are commonly used in the manufacturing of dyes, pharmaceuticals,¹¹ bactericides and other useful products. The oxidation of 1,2-benzenedimethanol with aqueous H₂O₂ is an effective green process for the synthesis of phthalide, owing to the avoidance of waste or pollutant.

Phthalide is traditionally synthesized by reaction of phthalic anhydride, zinc and hydrochloric acid; reaction of phthalimide and sodium hydroxide; or hydrogenation of phthalic anhydride.¹² During these processes, serious environmental pollution is generated, a low yield of phthalide is obtained, or a high reaction temperature is required, which consumes a large amount of energy.

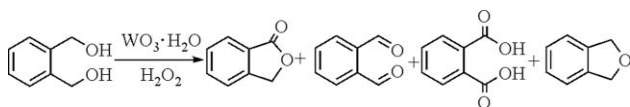
In the present work, the optimal reaction conditions are investigated in detail by using WO₃·H₂O as the catalyst and *tert*-butanol as the solvent, bearing in mind that the *tert*-butanol–H₂O₂ system is stable and has been used in a large number of oxidation reactions.¹³ In addition, analysis by GC is very convenient in the *tert*-butanol–H₂O₂ system. Then, under the optimized conditions, a green and novel approach to produce phthalide from 1,2-benzenedimethanol by catalytic oxidation with aqueous H₂O₂ without using organic solvents is presented because the reaction conditions are similar. In particular, aqueous hydrogen peroxide as an oxidant is environmentally clean, easy to handle and tungstic acid is an inexpensive catalyst. In this study, the catalyst can be easily removed by simple filtration after reaction because little H₂O₂ remains after reaction and it can be decomposed when heated at 90 °C, which leads to the deposit of WO₃·H₂O. The desired product phthalide can be easily obtained through cooling the reaction system because phthalide undergoes thermally reversible changes between the water-soluble and water-insoluble states from hot water to warm water at room temperature.

The activity test was performed at a set temperature for a given time with magnetic stirring in a closed 25 ml regular glass reactor using 50% aqueous H₂O₂ as the oxygen-donor and *t*-BuOH as the solvent. In a typical experiment, 0.0135 g of WO₃·H₂O (0.054 mmol) and 0.67 ml of 50 wt% aqueous H₂O₂ (11.1 mmol) were introduced into the regular glass reactor at 40 °C with vigorous stirring. Then, the reaction was started after the addition of 10 ml of *t*-BuOH and 0.690 g of 1,2-benzenedimethanol (5 mmol) into the mixture, which was left for 24 h or more. The conversion of H₂O₂ was measured by a standard iodimetric titration method. The quantitative analysis of the reaction products was performed by using a GC method and the identification of different products in the reaction mixture was determined by means of GC-MS on HP 6890GC/5973 MS, and ¹H NMR on DMX 500.

Department of Chemistry & Shanghai Key Laboratory of Molecular Catalysis and Innovative Material, Fudan University, Shanghai, 200433, P. R. China. E-mail: wldai@fudan.edu.cn; Fax: (+86-21) 55665572; Tel: (+86-21) 55664678

† Electronic supplementary information (ESI) available: Experimental section, ¹H-MNR and XRD data. See DOI: 10.1039/b921334a

According to the GC-MS analysis, the products of the catalytic oxidation of 1,2-benzenedimethanol, as shown in Scheme 1, comprise the main product phthalide and small amounts of by-product involving phthalaldehyde, phthalic acid and 1,3-dihydroisobenzofuran. Phthalaldehyde could be oxidized to phthalic acid. The catalytic performance and the optimization of the reaction conditions are based on the yield of phthalide.



Scheme 1 The oxidation products of 1,2-benzenedimethanol by H_2O_2 .

To elucidate the reaction process, the course of the conversion of 1,2-benzenedimethanol over time is tested, as shown in Fig. 1. It is suggested that the reaction proceeds rapidly at the first 6 h and then the reaction rate decreases slowly, which can be explained by the fact that the concentration of H_2O_2 and 1,2-benzenedimethanol decreases over time. Complete consumption of 1,2-benzenedimethanol is achieved when the reaction time reaches 12 h, whereas the yield of phthalide is only 72%. It is interesting to find that the yield of phthalide ascends with the prolonging of the reaction time. This phenomenon may be due to the mechanism of the oxidative lactonization of diols.¹⁴ The formation of phthalide proceeds *via* two steps: the initial chemoselective oxidation to 2-(hydroxymethyl)benzaldehyde, which is in equilibrium with 1,3-dihydroisobenzofuran-1-ol, and then the oxidation of 1,3-dihydroisobenzofuran-1-ol to phthalide. The phthalide would not be hydrolyzed upon continuing to elongate the reaction time under the present reaction conditions.

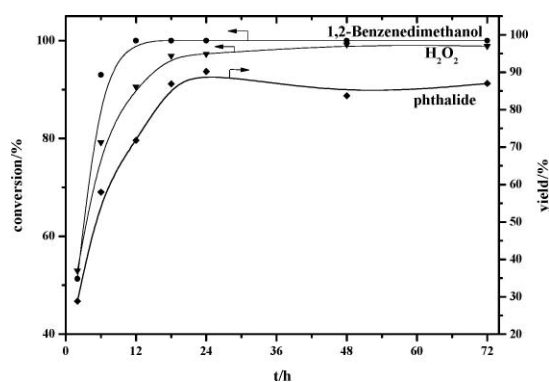
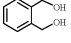


Fig. 1 Conversion of 1,2-benzenedimethanol and H_2O_2 and the yield of phthalide. (Reaction conditions: reaction temperature $80\text{ }^\circ\text{C}$, 1,2-benzenedimethanol 5 mmol, H_2O_2 11.1 mmol, $\text{WO}_3\cdot\text{H}_2\text{O}$ catalyst 0.054 mmol.)

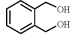
The reaction rate and the yield of products are dependant on the amount of H_2O_2 . Table 1 shows the catalytic performance of the oxidation of 1,2-benzenedimethanol with various molar ratios of H_2O_2 to 1,2-benzenedimethanol. As can be seen, the conversion of 1,2-benzenedimethanol ascends with an increase in the molar ratio of H_2O_2 to 1,2-benzenedimethanol when the ratio is lower than 2.2 : 1. Complete consumption of 1,2-benzenedimethanol and a 90% yield of phthalide can be achieved

Table 1 Catalytic performance of the oxidation of 1,2-benzenedimethanol with various molar ratios of H_2O_2 to substrate^a

H_2O_2 :substrate	Conversion (%)		Yield (%)
		H_2O_2	
1.5 : 1	79	98	57
2 : 1	94	98	85
2.2 : 1	100	97	90
3 : 1	100	86	84
4 : 1	100	87	86

^a Reaction conditions: reaction temperature $80\text{ }^\circ\text{C}$, 1,2-benzenedimethanol 5 mmol, $\text{WO}_3\cdot\text{H}_2\text{O}$ catalyst 0.054 mmol, reaction time 24 h, *t*-BuOH 10 ml.

Table 2 Catalytic performance of the oxidation of 1,2-benzenedimethanol over various temperatures^a

Entry	$T/^\circ\text{C}$	Conversion (%)		Yield (%)
			H_2O_2	
1	50	67	53	26
2	60	77	66	46
3	70	98	88	74
4	80	100	97	90

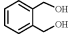
^a Reaction conditions: 1,2-benzenedimethanol 5 mmol, H_2O_2 11.1 mmol, $\text{WO}_3\cdot\text{H}_2\text{O}$ catalyst 0.054 mmol, reaction time 24 h, *t*-BuOH 10 ml.

when the ratio of H_2O_2 to 1,2-benzenedimethanol reaches 2.2 : 1. Although 100% 1,2-benzenedimethanol conversion could still be retained with further increasing the molar ratio, the yield of phthalide would decrease because of the over-oxidation, which may be a result of the further oxidation of the phthalide to phthalic acid. Considering both catalytic performance and H_2O_2 utility, the 2.2 : 1 molar ratio of the H_2O_2 to 1,2-benzenedimethanol is needed and is used in the following investigations.

It is known that the reaction temperature is essential to every reaction. As shown in Table 2, a higher temperature benefits the conversion of 1,2-benzenedimethanol and the formation of phthalide. Complete consumption cannot be achieved when the temperature is lower than $80\text{ }^\circ\text{C}$. Therefore, $80\text{ }^\circ\text{C}$ was chosen as the optimal reaction temperature because H_2O_2 would decompose at temperatures higher than $80\text{ }^\circ\text{C}$.

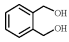
Independent experiments were carried out to obtain an insight into the effect of the amounts of catalysts on this reaction (see Table 3). As can be seen, there is a strong dependence of the conversion of 1,2-benzenedimethanol and the yield of phthalide on the dosage of the catalysts. The importance of the use of $\text{WO}_3\cdot\text{H}_2\text{O}$ was evident because the reactions gave much lower conversion of 1,2-benzenedimethanol and H_2O_2 , and lower yield of phthalide without any catalysts (Entry 1). In addition, it can be seen that the conversion of 1,2-benzenedimethanol increases with increasing catalyst dosage, the amounts of which range from 0 to 0.0135 g (0.054 mmol). The amount of catalyst influences the reaction rate and selectivity to the phthalide. However, when the amount is higher than 0.0135 g, the conversion of 1,2-benzenedimethanol and the yield of phthalide descends with an increase in the amount of catalyst. This is likely

Table 3 The effect of the amount of catalyst on the reaction^a

Entry	Amount of catalyst/g	Catalyst:substrate	Conversion (%)		
				H ₂ O ₂	Yield (%)
1	0	0	31	64	7
2	0.0051	0.004	94	98	65
3	0.0135	0.011	100	97	90
4	0.0249	0.020	96	98	71
5	0.1001	0.080	93	98	46

^a Reaction conditions: reaction temperature 80 °C, 1,2-benzenedimethanol 5 mmol, H₂O₂ 11.1 mmol, reaction time 24 h, *t*-BuOH 10 ml.

Table 4 The effect of volumes of *t*-BuOH on the oxidation of 1,2-benzenedimethanol^a

Volumes of <i>t</i> -BuOH/ml	Conversion (%)		
		H ₂ O ₂	Yield (%)
2	100	98	87
5	100	99	88
10	100	97	90
15	100	96	77
20	99	90	72

^a Reaction conditions: reaction temperature 80 °C, reaction time 24 h, 1,2-benzenedimethanol 5 mmol, H₂O₂ 11.1 mmol, WO₃·H₂O catalyst 0.054 mmol.

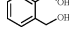
related to the consumption of H₂O₂ by the excess WO₃·H₂O, which decreases the utility of H₂O₂.

The reaction results as a function of the volumes of *t*-BuOH were also studied (see Table 4). It is obvious that there is an optimum volume of *tert*-butanol at which a maximum yield of phthalide is formed. The yield of phthalide increases from 72 to 90% with a decrease in the volume of *t*-BuOH from 20 to 10 ml. Such a phenomenon is not surprising when considering the fact that the concentration of active oxidizing species that depends on the concentration of H₂O₂ is required for the formation of phthalide. When the dosage of *t*-BuOH is lower than 10 ml, there is a negligible decrease in the yield of phthalide.

Solvent also has a crucial impact on the production of fine chemicals over homogeneous catalysts, and thus it was decided to study the solvent effect. Table 5 indicates that the maximum yield of phthalide is formed when the solvent is *tert*-butanol or water. Lower conversion of 1,2-benzenedimethanol was obtained in *n*-butanol and 2-propanol, as well as a lower yield of phthalide. It is interesting to find that the selectivity of phthalide in acetonitrile as a solvent was much lower than that in *tert*-butanol and water, although the conversion of 1,2-benzenedimethanol was a little lower than that in *tert*-butanol and water. The mechanism of the catalytic oxidation in these solvents is still under investigation.

Since the yield of phthalide in water is similar to that in *t*-BuOH (see Table 5), a novel process to separate phthalide from the reaction mixture was explored in water. As we know, phthalide is soluble in water when the oxidation is carried out at 80 °C but insoluble in water at room temperature. The catalyst can be easily removed when the excess H₂O₂ is decomposed at

Table 5 The effect of different solvents on the reaction^a

Solvents	Conversion (%)		
		H ₂ O ₂	Yield (%)
<i>n</i> -Butanol	86	99	26
2-Propanol	27	100	7
<i>tert</i> -Butanol	100	98	90
Water	100	96	89
Acetonitrile	93	100	18

^a Reaction conditions: reaction temperature 80 °C, reaction time 24 h, 1,2-benzenedimethanol 5 mmol, H₂O₂ 11.1 mmol, solvent 10 ml.

90 °C after the reaction. The product was separated out when the filtrate was cooled to room temperature and a 77.4% yield of the separated phthalide was obtained. The melting point of the powder obtained by this route was 70.0 to 73.8 °C (Sinopharm Chemical Reagent Co., Ltd, 71.0 to 75.0 °C). The GC purity of the as-prepared phthalide was higher than 99.5%, and it can be used directly in many fields. In addition, ¹H NMR spectroscopy and the XRD pattern of the product confirmed that the structure of the powder was that of phthalide (see Figure S1 and Figure S2, ESI†).

In summary, a new, economic and efficient route for the production of phthalide by catalytic oxidation of 1,2-benzenedimethanol with aqueous H₂O₂ has been developed using tungstic acid as a catalyst under organic solvent-free conditions. This process can be easily commercialized based on the following considerations. Firstly, the molar ratio of H₂O₂ to 1,2-benzenedimethanol is only 2.2:1, which is only 10% molar excess, thus the utilization efficiency of H₂O₂ is very high and this process is very economical. Secondly, the tungstic acid catalyst can be easily filtrated after reaction and the phthalide product can be removed from the reaction system after cooling the reaction mixture to room temperature. The used tungstic acid catalyst can be reused more than 6 times, thus leading to its great economical efficiency. Thirdly, the concentration of H₂O₂ is low due to the presence of water, therefore, it is safe to handle in industry. Finally, there is no need to use organic solvent in this transformation, so it is environmentally benign and low-cost. A further investigation of the present H₂O₂-tungstic acid catalytic system in many other significant transformations from α,ω -diols to lactones is currently under way.

Acknowledgements

Financially supported by the Major State Basic Resource Development Program (Grant No.2003CB615807), NSFC (Project 20973042, 20573024), and the Science and Technology Commission of Shanghai Municipality (08DZ2270500).

Notes and references

- 1 K. Sato, M. Hyodo, M. Aoki, X. Q. Zheng and R. Noyori, *Tetrahedron*, 2001, **57**, 2469.
- 2 (a) K. F. Lin, P. P. Pescarmona, K. Houthoofd, D. D. Liang, G. V. Tendeloo and P. A. Jacobs, *J. Catal.*, 2009, **263**, 75; (b) M. C. Capel-Sanchez, J. M. Campos-Martin and J. L. G. Fierro, *J. Catal.*, 2005, **234**, 488; (c) F. Somma, P. Canton and G. Strukul, *J. Catal.*, 2005, **229**, 490; (d) F. Somma and G. Strukul, *J. Catal.*, 2004, **227**, 344.

- 3 (a) J. F. Deng, X. H. Xu, H. Y. Chen and A. R. Jiang, *Tetrahedron*, 1992, **48**, 3503; (b) X. H. Xu, H. Y. Chen, J. F. Deng and A. R. Jiang, *Acta Chim. Sin.*, 1993, **51**, 399; (c) X. L. Yang, W. L. Dai, H. Chen, Y. Cao, H. X. Li, H. Y. He and K. N. Fan, *J. Catal.*, 2005, **229**, 259.
- 4 (a) H. Chen, W. L. Dai, X. L. Yang, R. H. Gao, Y. Cao, H. X. Li and K. N. Fan, *Appl. Catal., A*, 2006, **309**, 62; (b) C. Venturello and M. Ricci, *J. Org. Chem.*, 1986, **51**, 1599.
- 5 (a) M. Kataoka, K. Honda, K. Sakamoto and S. Shimizu, *Appl. Microbiol. Biotechnol.*, 2007, **75**, 257; (b) E. W. Debler, G. F. Kaufmann, R. N. Kirchdoerfer, J. M. Mee, K. D. Janda and I. A. Wilson, *J. Mol. Biol.*, 2007, **368**, 1392; (c) D. McDougald, S. A. Rice and S. Kjelleberg, *Anal. Bioanal. Chem.*, 2007, **387**, 445.
- 6 (a) K. H. Lee, H. Furukawa and E. S. Huang, *J. Med. Chem.*, 1972, **15**, 609; (b) S. M. Kupchan, M. A. Eakin and A. M. Thomas, *J. Med. Chem.*, 1971, **14**, 1147.
- 7 (a) A. C. Albertsson and I. K. Varma, *Biomacromolecules*, 2003, **4**, 1466; (b) H. Lee, F. Zeng, M. Dunne and C. Allen, *Biomacromolecules*, 2005, **6**, 3119; (c) Z. Z. Jiang, *Biomacromolecules*, 2008, **9**, 3246.
- 8 (a) Y. Ishii, K. Suzuki, T. Ikariya, M. Saburi and S. Yoshikawa, *J. Org. Chem.*, 1986, **51**, 2822; (b) Y. Ishii, K. Osakada, T. Ikariya, M. Saburi and S. Yoshikawa, *J. Org. Chem.*, 1986, **51**, 2034.
- 9 Y. Tamaru, Y. Yamada, K. Inoue, Y. Yamamoto and Z. Yoshida, *J. Org. Chem.*, 1983, **48**, 1286.
- 10 T. Mitsudome, A. Noujima, T. Mizugaki, K. Jitsukawa and K. Kaneda, *Green Chem.*, 2009, **11**, 793.
- 11 (a) J. E. Robinson and M. A. Brimble, *Chem. Commun.*, 2005, 1560; (b) M. A. Brimble and C. J. Bryant, *Chem. Commun.*, 2006, 4506.
- 12 (a) Y. X. Liu, T. F. Xing, Z. J. Wei, X. N. Li and W. Yan, *Catal. Commun.*, 2009, **10**, 2023; (b) Y. X. Liu, Z. J. Wei, J. Fu, Y. Gao and W. Yan, *Chin. J. Catal.*, 2008, **29**, 52.
- 13 (a) X. L. Yang, W. L. Dai, C. W. Guo, H. Chen, Y. Cao, H. X. Li, H. Y. He and K. N. Fan, *J. Catal.*, 2005, **234**, 438; (b) R. H. Gao, X. L. Yang, W. L. Dai, Y. Y. Le, H. X. Li and K. N. Fan, *J. Catal.*, 2008, **256**, 259; (c) R. H. Gao, W. L. Dai, Y. Y. Le, X. L. Yang, Y. Cao, H. X. Li and K. N. Fan, *Green Chem.*, 2007, **9**, 878; (d) Y. Ishii, T. Yoshida, K. Yamawaki and M. Ogawa, *J. Org. Chem.*, 1988, **53**, 5549.
- 14 T. Suzuki, K. Morita, M. Tsuchida and K. Hiroi, *Org. Lett.*, 2002, **4**, 2361.

Making kinetic and thermodynamic enolates *via* solvent-free high speed ball milling†

Daniel C. Waddell, Indre Thiel, Tammara D. Clark, S. Tyler Marcum and James Mack*

Received 12th May 2009, Accepted 17th November 2009

First published as an Advance Article on the web 8th December 2009

DOI: 10.1039/b922108p

We investigated the ability to selectively form products arising from a kinetic or a thermodynamic enolate under solvent-free high speed ball milling conditions. Using 2-methylcyclohexanone as the substrate and sodium hydroxide or lithium hexamethyldisilazide as the base, we were able to trap the thermodynamic or kinetic enolate in high selectivity. Although all the reagents were ball milled simultaneously, we observed no products resulting from aldol condensation.

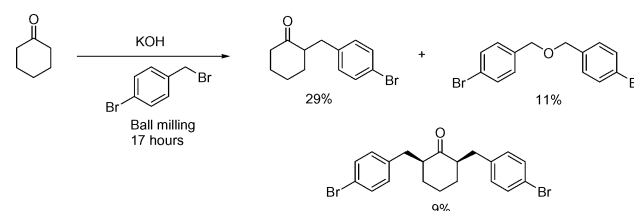
Environmental concerns about solvent-based chemistry have stimulated a renewed interest in the study of chemical reactions under solvent-free conditions.^{1–3} Traditionally, solvent-free reactions has been performed using a mortar and pestle, but recently high speed ball milling (HSBM) has shown to be a more attractive option. In the HSBM method, a ball bearing is placed inside a vessel that is shaken at high speeds. The high speed attained by the ball bearing has enough force to make an amorphous mixture of the reagents, subsequently facilitating a chemical reaction.^{4–6} The use of commercial ball mills have allowed these reactions to be scaled up to industrial levels, therefore understanding organic reactions using this methodology can significantly reduce solvent waste.^{7–16}

We have recently become interested in studying various organic reactions using this novel method. In addition to our work,^{17–20} various reports have shown solvent-free ball milling is a more environmentally benign alternative to traditional solution-based chemistry.^{21–28} Here, we report on our investigation of the formation of kinetic and thermodynamic enolates using high speed ball milling.

Enolates are one of the most important intermediates used for forming carbon–carbon bonds. The stereo- and regio-control of the products formed from enolates are an important aspect of organic synthesis. In solution, these reactions are conducted in a stepwise fashion whereby the base and ketone are first mixed together followed by addition of the electrophile. This is converse to the way most ball milled reactions are conducted. Typically, ball milled reactions are conducted in a sealed vessel in which all of the starting materials are added simultaneously. Creating enolates in this manner brings about the possibility of generating a complex mixture; most notably large amounts of aldol condensation products.²⁹ We started our study of

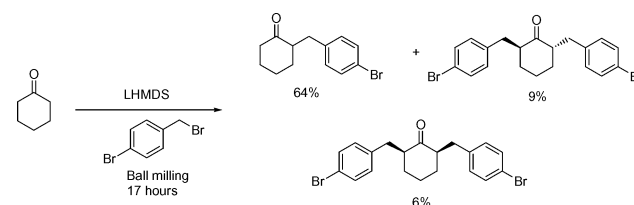
the formation of enolates under ball milling conditions using cyclohexanone and 2-methylcyclohexanone as the substrate, *p*-bromobenzyl bromide as the electrophile, and potassium hydroxide or lithium hexamethyldisilazide as the base.

Using a custom made 1/2" × 2" stainless steel vial, we added cyclohexanone, *p*-bromobenzyl bromide, potassium hydroxide and a 1/8" stainless steel ball bearing. The reaction was ball milled for an optimized time of 17 h in a Spex Certiprep Mixer/Mill 8000M. The reaction gave the monoalkylation product in 29%, the 2,6 dialkylated product in 9% (roughly 14 : 1 *cis* : *trans* ratio) and di-*p*-bromobenzyl ether in 11% yield. Under these conditions, we saw no evidence of the aldol condensation product nor did we observe the 2,2-di-*p*-bromobenzylcyclohexanone (Scheme 1).



Scheme 1 Formation of cyclohexanone enolate *via* HSBM using potassium hydroxide as base.

We next studied the formation of the cyclohexanone enolate using lithium hexamethyldisilazide (LiHMDS), a strong bulky base. We added cyclohexanone, LiHMDS and *p*-bromobenzyl bromide to a stainless steel vial with a 1/8" stainless steel ball and ball milled as above.³⁰ After isolation, we observed 64% of the monoaddition product, and 15% of the 2,6-dibenzylated product (roughly 2 : 3 *cis* : *trans* ratio). Under these conditions we did not observe *p*-bromobenzyl(hexamethyldisilyl)amine which would result from nucleophilic addition of LiHMDS with *p*-bromobenzylbromide (Scheme 2). It is important to note here that we observed a switch in stereochemistry for the disubstituted product when we changed the base from KOH to LiHMDS. We



Scheme 2 Formation of cyclohexanone enolate *via* HSBM using lithium hexamethyldisilazide as base.

University of Cincinnati, Cincinnati, OH, USA.

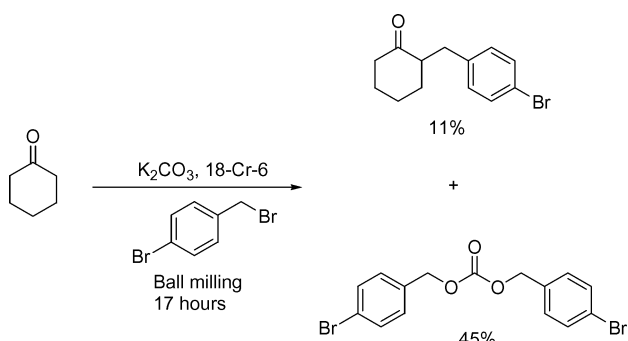
E-mail: james.mack@uc.edu; Fax: 01 513 556 9239;

Tel: 01 513 556 9249

† Electronic supplementary information (ESI) available: Experimental details and spectra. See DOI: 10.1039/b922108p

are currently investigating the nature of this stereochemical change.

One principle of green chemistry is to use safer chemicals when possible.³¹ Wang showed that bases are more reactive under solvent-free ball milling conditions than they are in solution.³² To this end, we substituted a more benign base, potassium carbonate, for LiHMDS. However, upon milling for 17 h we recovered unreacted starting materials. We added 18-crown-6 to see if that could increase the basicity; while we achieved 11% of the monoalkylation product, *p*-bromobenzyl carbonate was the major product formed in 45% yield (Scheme 3). Surprisingly, we did not observe any products resulting from aldol condensation regardless of the base that was used. However, if *p*-bromobenzyl bromide is not added to the reaction mixture we form the aldol product in moderate yield; this demonstrates the preference of enolate attack towards *p*-bromobenzyl bromide.

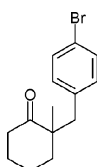
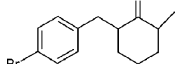
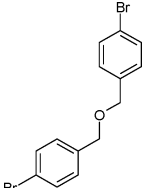


Scheme 3 Formation of cyclohexanone enolate *via* HSBM using potassium carbonate as base in the presence of 18-crown-6.

Because we obtain products resulting from formation of an enolate, we explored the possibility of preferentially forming the kinetic or thermodynamic enolate. In solution, the kinetic enolate is usually generated using low temperatures and a strong, bulky base. Conversely, the thermodynamic enolate is generated through the use of higher temperatures and a weaker base. House *et al.* showed that using lithium diisopropyl amide (LDA) with 2-methylcyclohexanone at $-50\text{ }^{\circ}\text{C}$ in 1,2-dimethoxyethane makes the kinetic enolate and upon addition of benzyl bromide reacts to make 2-methyl-6-*p*-bromobenzylcyclohexanone.^{33,34} 2-Methyl-2-benzylcyclohexanone, which is made from the thermodynamic enolate, can be synthesized under similar conditions using less than 1 equivalent of LDA. Additionally, the thermodynamic enolate can be achieved by using a less hindered, equilibrating base. Artuad *et al.* showed that using potassium hydroxide in 1,2-dimethoxyethane gives the thermodynamic enolate and provides 2-methyl-2-benzylcyclohexanone as the major product upon addition of benzyl bromide.³⁵ To further explore enolate chemistry in the ball mill we chose to examine the process when 2-methylcyclohexanone is used as the substrate.

In a stainless steel vial, 2-methylcyclohexanone, potassium hydroxide and *p*-bromobenzyl bromide were ball milled with a 1/8" stainless steel ball for 17 h. In this process the thermodynamically favoured 2-methyl-2-*p*-bromobenzylcyclohexanone was the major product but only formed in 24% yield. The product from the formation of the kinetic enolate was isolated in a 5% yield with the rest being unreacted starting material. We previously reported that the cation of the base and leaving

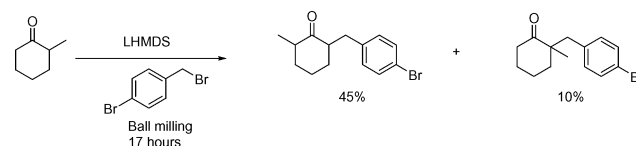
Table 1 The formation of the thermodynamic enolate as a function of the type of hydroxide used

Base			
NaOH	76%	1.8%	0%
CsF/LiOH	50%	9%	9%
KOH	29%	5%	8%
KOH ^a	9%	1%	90%
LiOH	0%	0%	0%

^a ball milled in the presence of 18-crown-6.

group plays an important role in the effectiveness of the reaction under ball milling conditions.¹⁷ Thus, we decided to explore the reaction using sodium hydroxide, lithium hydroxide and caesium hydroxide (prepared by ball milling a mixture of caesium fluoride and lithium hydroxide) (Table 1). Using lithium hydroxide as a base, we observed no reaction—only recovering unreacted starting materials. However, when we employed sodium hydroxide as the base, we were able to obtain the product resulting from formation of the thermodynamic enolate in a 76% yield. The product resulting from formation of the kinetic enolate was formed in less than 2% yield, with the rest of the mass accounted for as unreacted starting materials. We observed no dialkylation or products that resulted from aldol condensation in either of these reactions.

It has been postulated that ball milled reactions are high energy reactions such that thermodynamics should govern the system. If this is the case, the high energetics of the process along with the high concentrations of the reagents should favour thermodynamic enolate formation. To test this theory, we ball milled 2-methylcyclohexanone, LiHMDS and *p*-bromobenzyl bromide for 17 h to determine if under ball milling conditions we would be able to obtain the product which comes from formation of the kinetic enolate. At the conclusion of the reaction, we were able to isolate 2-methyl-6-*p*-bromobenzylcyclohexanone in a 45% yield and isolated the 2-methyl-2-*p*-bromobenzylcyclohexanone in a 10% yield with the rest recovered as unreacted starting materials (Scheme 4). This suggests that high speed ball milling conditions can provide products that are kinetically controlled. Additionally, when less than 1 equivalent of LiHMDS or sodium hydride was used, the thermodynamic product is formed preferentially. This shows that when less than one equivalent of a strong base is used equilibration of the 2-methylcyclohexanone and resulting enolate is fast compared to nucleophilic addition into *p*-bromobenzyl bromide. However, when one equivalent of LiHMDS is used the equilibration



Scheme 4 Generation of the kinetic enolate *via* HSBM conditions.

pathway is not available and nucleophilic addition occurs at the kinetic site. Surprisingly, when 1 equivalent of a strong base such as sodium amide or sodium hydride is used we observe a preference for formation of the thermodynamic enolate.

We wanted to determine if milling time played a large role in the selectivity that we observe. When the reactions were carried out for 15 min, 2 h and 4 h the overall yields were lower but the ratio of products were unchanged.

In conclusion, we report the first analysis of enolate chemistry under high speed ball milling conditions. We demonstrated that although ball milling is theoretically an extremely high energy process, ball milled reactions can be selective and can be driven by kinetics. We are currently investigating the stereochemical nature of the process to determine if chiral auxiliaries will add stereoselectivity under these novel reaction conditions. We have also studied other ketones such as acetophenone and pinacolone (3,3-dimethyl-2-butanone) with *p*-bromobenzylbromide and observed similar results to using cyclohexanone as the substrate. In addition, we reacted 2-methylcyclohexanone with benzyl chloride and benzyl bromide and observed the enolate product similarly to what is observed when *p*-bromobenzylbromide is used as the electrophile. We are currently undergoing a more complete substrate scope to examine the fundamental rules of the process. In addition to our more complete substrate scope we are in the process of developing a greener procedure for product isolation. Ball milling can be an excellent asset for the reduction of solvent waste and the generation of more environmentally benign reactions. However, in order to achieve these goals we must first understand the nuances of this process.

Acknowledgements

We would like to thank the National Science Foundation (CHE-0548150) for the financial support for this research. We would also like to thank the National Science foundation, iREU, The American Chemical Society and the Deutscher Akademischer Austausch Dienst for the financial support for Indre Thiel to conduct the research.

Notes and references

- 1 K. Tanaka and F. Toda, *Chem. Rev.*, 2000, **100**, 1025–1074.
- 2 G. Rothenberg, A. P. Downie, C. L. Raston and J. L. Scott, *J. Am. Chem. Soc.*, 2001, **123**, 8701–8708.
- 3 K. Tanaka and F. Toda, *Solvent-Free Organic Synthesis*, Wiley-VCH, Weinheim, Germany, 2003.
- 4 C. Suryanarayana, *Prog. Mater. Sci.*, 2001, **46**, 1–184.
- 5 L. Takacs, *Prog. Mater. Sci.*, 2002, **47**, 355–414.
- 6 B. Rodriguez, A. Bruckmann, T. Rantanen and C. Bolm, *Adv. Synth. Catal.*, 2007, **349**, 2213–2233.
- 7 V. V. Boldyrev, *J. Mater. Sci.*, 2004, **39**, 5117–5120.
- 8 G. Kaupp, *CrystEngComm*, 2003, **5**, 117–133.
- 9 G. Kaupp, *CrystEngComm*, 2006, **8**, 794–804.
- 10 M. A. Mikhailenko, T. P. Shakhshneider and V. V. Boldyrev, *J. Mater. Sci.*, 2004, **39**, 5435–5439.
- 11 H. Zoz, D. Ernst, T. Mizutani and H. Okouchi, *Adv. Powder Metall. Part. Mater.*, 1997, (part 11), 35–42.
- 12 H. Zoz, D. Ernst, R. Reichardt, T. Mizutani, M. Nishida and H. Okouchi, *Adv. Powder Metall. Part. Mater.*, 1998, (part 6), 69–79.
- 13 H. Zoz, D. Ernst, R. Reichardt, H. Ren, T. Mizutani, M. Nishida and H. Okouchi, *Mater. Manuf. Processes*, 1999, **14**, 861–874.
- 14 A. Bose, K. Ameyama, S. D. Torre, D. J. Viguera, D. Madan, T. S. Wei, P. Hightower and H. Zoz, *Adv. Powder Metall. Part. Mater.*, 2002, 1/175–171/190.
- 15 G. Kaupp, J. Schmeyer, M. R. Naimi-Jamal, H. Zoz and H. Ren, *Chem. Eng. Sci.*, 2002, **57**, 763–765.
- 16 H. Ren, H. Zoz, G. Kaupp and M. R. Naimi-Jamal, *Adv. Powder Metall. Part. Mater.*, 2003, 216–222.
- 17 P. Vogel, S. Figueira, S. Muthukrishnan and J. Mack, *Tetrahedron Lett.*, 2009, **50**, 55–56.
- 18 D. C. Waddell and J. Mack, *Green Chem.*, 2009, **11**, 79–82.
- 19 J. Mack, D. Fulmer, S. Stofel and N. Santos, *Green Chem.*, 2007, **9**, 1041–1043.
- 20 J. Mack and M. Shumba, *Green Chem.*, 2007, **9**, 328–330.
- 21 E. Colacino, P. Nun, F. M. Colacino, J. Martinez and F. Lamaty, *Tetrahedron*, 2008, **64**, 5569–5576.
- 22 Y.-W. Dong, G.-W. Wang and L. Wang, *Tetrahedron*, 2008, **64**, 10148–10154.
- 23 N. Giri, C. Bowen, J. S. Vyle and S. L. James, *Green Chem.*, 2008, **10**, 627–628.
- 24 G. Mugunthan and K. P. R. Kartha, *J. Carbohydr. Chem.*, 2008, **27**, 294–299.
- 25 P. R. Patil and K. P. R. Kartha, *J. Carbohydr. Chem.*, 2008, **27**, 279–293.
- 26 B. Icli, N. Christinat, J. Tonnemann, C. Schuttler, R. Scopelliti and K. Severin, *J. Am. Chem. Soc.*, 2009, **131**, 3154–3155.
- 27 S. Li, W. Yan and W.-x. Zhang, *Green Chem.*, 2009, **11**, 1618–1626.
- 28 J. Mokhtari, M. R. Naimi-Jamal, H. Hamzeali, M. G. Dekamin and G. Kaupp, *ChemSusChem*, 2009, **2**, 248–254.
- 29 B. Rodriguez, A. Bruckmann and C. Bolm, *Chem.–Eur. J.*, 2007, **13**, 4710–4722.
- 30 We ball milled these reaction under an open atmosphere with no decomposition of LiHMDS. Our investigation on the ability to ball mill hydroscopic reagents without precautions is a part of an account which will be available soon.
- 31 P. Anastas and J. Warner, *Green Chemistry: Theory and Practice*, Oxford Publishing, Oxford, UK, 1998.
- 32 Y.-W. Dong, G.-W. Wang and L. Wang, *Tetrahedron*, 2008, **64**, 10148–10154.
- 33 M. Gall and H. O. House, *Org. Synth.*, 1972, **52**, 121–130.
- 34 H. O. House, L. J. Czuba, M. Gall and H. D. Olmstead, *J. Org. Chem.*, 1969, **34**, 2324–2336.
- 35 I. Artaud, G. Torossian and P. Viout, *Tetrahedron*, 1985, **41**, 5031–5037.

Platinum-nanoparticle-loaded bismuth oxide: an efficient plasmonic photocatalyst active under visible light†

Renhong Li,^a Wenxing Chen,^{*a} Hisayoshi Kobayashi^b and Chunxia Ma^a

Received 21st August 2009, Accepted 20th November 2009

First published as an Advance Article on the web 5th January 2010

DOI: 10.1039/b917233e

Employing a commercial semiconductor with a positive conduction band level, we investigated a new plasmonic photocatalyst, Pt/Bi₂O₃, with high photocatalytic activity for decomposition of environmental organic pollutants under visible light.

Introduction

Heterogeneous photocatalysis has always been an urgent issue with regard to the important technological and societal benefits resulting from the removal of toxic organic pollutants in wastewater and in the purification of drinking water.¹ Not being able to use visible light, however, hinders the practical applications of most photocatalysts.² Modified photocatalysts, such as N-, C-, and S-doped TiO₂,³ have been much studied in order to extend the absorption edge into the visible light region, but such photocatalysts often suffer serious problems, for instance, their low quantum yields. In recent research, nano-sized Ag was employed, allowing the development of highly efficient and stable plasmonic photocatalysts due to its plasmon resonance (PR) in the visible region.⁴ Importantly, Huang *et al.* pointed out that the dipolar character of the surface plasmon state of Ag nanoparticles (NPs) was critical for enhancing the separation of plasmon-induced electron-hole pairs.⁴ In addition to Ag NPs, Au NPs can also be photoexcited under visible light illumination due to their PR. Tian *et al.* indicated that the photoexcitation of electrons from the Au NPs to the TiO₂ conduction band (CB), and the simultaneous transfer of compensatory electrons from the solution-phase electron mediator (Fe^{2+/3+}) to the Au NPs, resulted in the achievement of spatial charge separation in the Au/TiO₂ system.⁵ With regard to this, it should be noted that the potential of the Fe^{2+/3+} mediator is more positive (Fe³⁺ + e⁻ → Fe²⁺, +0.77 V *vs.* NHE) than that of the TiO₂ CB (-0.3 V *vs.* NHE) and that of the O₂ reduction potentials (single-electron reduction process: O₂ + e⁻ → O₂⁻; -0.56 V *vs.* NHE; or multi-electron reduction process: O₂ + 2H₂O + 4e⁻ → 4OH⁻; +0.40 V

vs. NHE), so that Fe^{2+/3+} pairs (rather than the CB level of TiO₂) give out electrons to the Au NPs.

Unlike Au or Ag, platinum is an important catalytic metal but usually shows no plasmonic activity. However, recent literature has demonstrated that Pt NPs can also be plasmon-excited by choosing an appropriate excitation wavelength.⁶ If this is true, after plasmon excitation, the holes generated on the surface of Pt NPs can be used for decomposing organic molecules so long as the electrons can be transferred successfully. Accordingly, with the aim of synthesizing a plasmonic photocatalyst active under visible light, we wanted to use a metal oxide with a positive CB level, where the transfer of plasmon-induced electrons can be achieved. Bismuth oxide (Bi₂O₃) is of this type.⁷ In the present study, density functional theory (DFT) calculations, together with the literature,^{7,8} show that Bi₂O₃ can serve as an electron carrier owing to its positive CB level (+0.4 V *vs.* NHE), which lies exactly in the potential range of the multi-electron reduction of O₂ (O₂ + 2H₂O + 4e⁻ → 4OH⁻; +0.40 V *vs.* NHE).

The above discussions so far led us to prepare a plasmonic photocatalyst by dispersing metallic Pt NPs onto Bi₂O₃ substrates. In addition, considering that home-made supports synthesized using various methods could lead to different particle sizes, crystal phases, morphologies, and thus different catalytic performance, the use of commercially available Bi₂O₃ is strongly desired for initial screening; catalyst optimization will be the subject of further research.

Results and discussion

Bi₂O₃ loaded with Pt NPs (denoted as Pt/Bi₂O₃) was prepared *via* a simple photoreduction method.⁹ The morphology of Pt/Bi₂O₃ was examined by TEM (JEM-2010, Fig. S1†) and FE-SEM (MIRA II-LMH, Fig. S1), its crystal structure by XRD (Rigaku D/Max-2550pc, Fig. S2), its surface area by BET (Micromeritics TriStar II) and its chemical composition by XPS (KRATOS AXIS ULTRA-DLD, Fig. S3). The photoactivity of Pt/Bi₂O₃ was initially evaluated by oxidative decomposition of aqueous acetaldehyde (AcH) under visible light illumination from a mercury lamp (λ > 400 nm).† In this case, Bi₂O₃ alone exhibits limited photoactivity. Intriguingly, its photoactivity increased significantly with increasing Pt content to a maximum at *ca.* 3.0 wt%, with the activity dropping gradually at higher Pt content. Fig. 1 illustrates that the rate of CO₂ evolution over Pt/Bi₂O₃ (10.37 μmol h⁻¹) was *ca.* 10-fold and 4-fold higher than that of bare Bi₂O₃ (1.01 μmol h⁻¹) and N-TiO₂ NPs (2.58 μmol h⁻¹) at room temperature (*ca.* 20 °C), respectively. To

^aKey Laboratory of Advanced Textile Materials and Manufacturing Technology, Ministry of Education of P. R. China, Zhejiang Sci-Tech University, Hangzhou, 310018, P. R. China. E-mail: wxchen@zstu.edu.cn; Fax: +86 571 86843251; Tel: +86 571 86843251

^bDepartment of Chemistry and Materials Technology, Kyoto Institute of Technology, Matsugasaki, Sakyo-ku, Kyoto, 606-8585, Japan. E-mail: kobayashi@chem.kit.ac.jp

† Electronic supplementary information (ESI) available: FE-SEM and TEM images; XRD data; XPS data; electron density contour map for Bi₂O₃. See DOI: 10.1039/b917233e

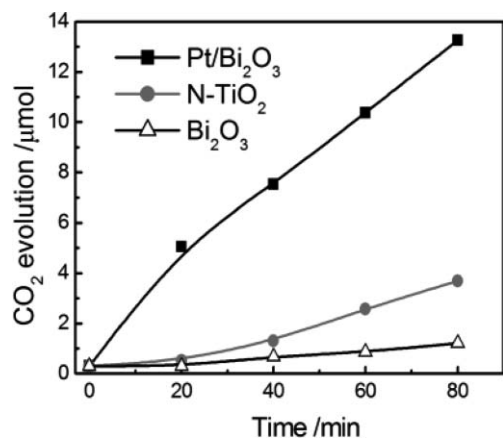


Fig. 1 Decomposition curves of acetaldehyde solution over Pt/Bi₂O₃, N-TiO₂ and Bi₂O₃ under visible light irradiation ($\lambda > 400$ nm) in the air.

clarify that the decomposition of AcH over Pt/Bi₂O₃ was not caused by regular photolysis or catalysis, we also carried out the experiments under visible light irradiation without catalysts (photolysis) and in the dark with the catalysts (catalysis). In the former experiment, no CO₂ evolution was detected, while the latter showed that a tiny quantity of CO₂ over Pt/Bi₂O₃ was generated within 20 min, with no further change during the subsequent period in the dark. These results fully confirmed that Pt/Bi₂O₃ acts as an active photocatalyst for the decomposition of AcH under visible light illumination.

The most notable application of the present photocatalyst is the photodecomposition of formaldehyde (FAD), another typical indoor air pollutant. As shown in Fig. 2, it is worth noting that the decomposition of FAD over Pt/Bi₂O₃ under visible light illumination proceeded with a rate (151.8 $\mu\text{mol h}^{-1}$) comparable to that of TiO₂ NPs (Degussa P25) driven by UV light (189.4 $\mu\text{mol h}^{-1}$), and was 34.4-fold higher than that of visible-light-irradiated N-TiO₂ (4.41 $\mu\text{mol h}^{-1}$). The oxidative ability of Pt/Bi₂O₃ is extremely high when we consider this is a visible-light-driven photocatalytic system.

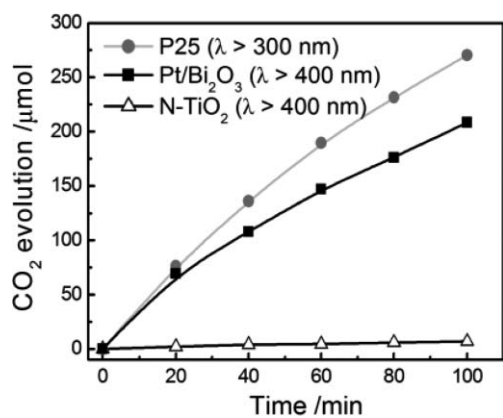


Fig. 2 Decomposition curves of formaldehyde solution over Pt/Bi₂O₃, P25 and N-TiO₂ under light irradiation in the air.

In addition to Pt/Bi₂O₃, Pt-loaded TiO₂ (Pt/TiO₂) and Pt-loaded CdS (Pt/CdS) were also prepared by photoreduction for comparison. As indicated in Fig. 3, when methanol was

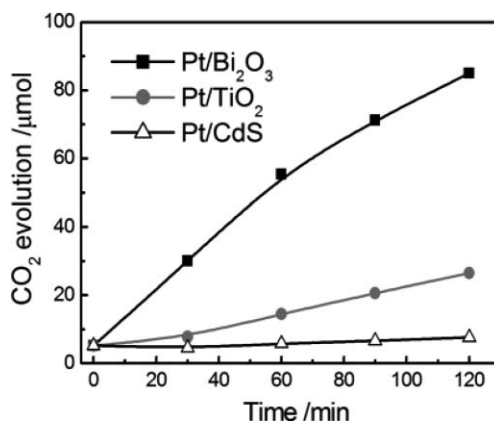


Fig. 3 Decomposition curves of methanol solution over Pt/Bi₂O₃, Pt/TiO₂ and Pt/CdS under visible light irradiation ($\lambda > 400$ nm) in the air.

selected as the target organic compound, the visible photoactivity of Pt/Bi₂O₃ was much higher than that of Pt/TiO₂ and Pt/CdS. It should be mentioned that although TiO₂ with a band gap of 3.2 eV can only be photoexcited by UV light, Pt/TiO₂ exhibits appreciable visible photoactivity (even higher than that of Pt-loaded CdS, whose band gap is only 2.4 eV). In order to determine the reusability and stability of Pt/Bi₂O₃, methanol was also chosen as the target compound, and the life-cycle tests are shown in Fig. S4†.

The band structures of Bi₂O₃ were evaluated through plane-wave-based DFT calculations. Fig. 4 shows the band structure and density of states (DOS) for Bi₂O₃, from which it is noteworthy that the Bi6p atomic orbitals are separated into two

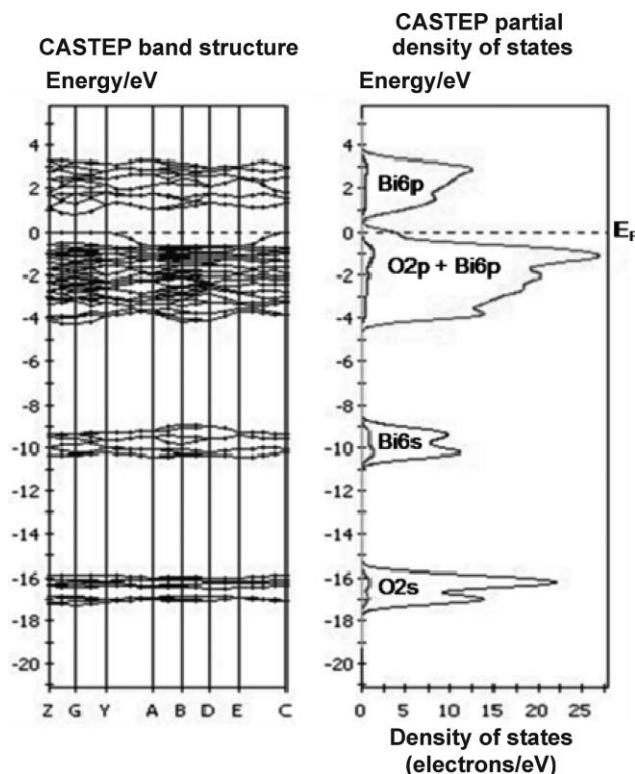


Fig. 4 Band dispersion and density of states for Bi₂O₃.

parts – an occupied part and an unoccupied part. The former hybridizes with the O2p band and partially contributes to the valence band (VB), whereas the latter is the main component for the CB. The presence of Bi6p electrons in the upper valence band provides p–p repulsion for the VB maximum, which results in a narrowing of the band gap. The electron density contour maps of the HOMO and LUMO levels related to photoexcitation are shown in Fig. S5†. Fig. 5 compares the UV/Vis absorption spectrum (Lambda 900, Perkin Elmer) of Pt/Bi₂O₃, Bi₂O₃ and N-TiO₂. N-TiO₂ exhibits a visible absorption shoulder due to the nitride at *ca.* 450 nm.¹⁰ In contrast to bare Bi₂O₃, a distinct feature of the UV/Vis absorption spectrum of Pt/Bi₂O₃ is its strong absorption in the visible region (up to 700 nm), comparable to that of the UV region. The spectrum is similar to that of the adsorption band of Ag NPs, as reported by Huang *et al.*⁴ Further, Ikeda *et al.* stated that nano-sized Pt can also absorb visible light owing to its PR.⁶ Thus the existence of the wide absorption band seems to be attributable to the surface plasmon state of Pt NPs.

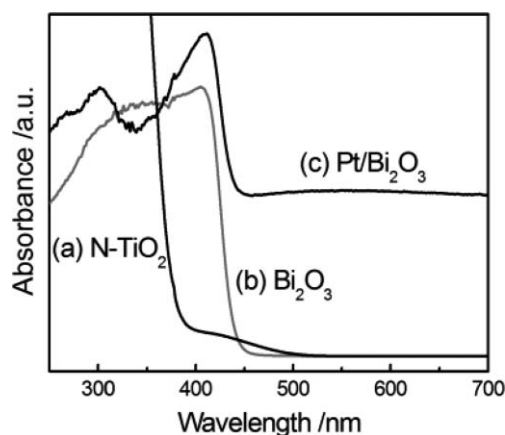


Fig. 5 UV/Vis absorption spectrum of (a) N-TiO₂, (b) Bi₂O₃ and (c) Pt/Bi₂O₃.

In view of the low surface areas of micron-sized powders, Bi₂O₃ scarcely has any BET specific surface area ($S_{\text{BET}} < 0.01 \text{ m}^2 \text{ g}^{-1}$) as compared to P25 ($S_{\text{BET}} = 48.7 \text{ m}^2 \text{ g}^{-1}$) and N-doped TiO₂ ($S_{\text{BET}} = 113.2 \text{ m}^2 \text{ g}^{-1}$), which results in a nearly complete lack of surface active sites where the decomposition of organics could take place. Moreover, although Bi₂O₃ has a direct band gap of 2.8 eV, which can be excited by visible light,⁷ the light-generated charge carriers in micron-sized semiconductor cannot efficiently transfer to the surface and tend to recombine in the bulk. As a result, in this work, Pt may play an important role in decomposition of organic molecules.

Generally, Pt has been recognized as a perfect electron scavenger that can greatly enhance the photoactivity of semiconductors by separating holes and electrons. However, it is hard to explain the visible photoactivity of Pt/Bi₂O₃ when one only considers the formation of Pt Schottky barriers on the surface of Bi₂O₃, because dyes with complicated conjugated structures cannot be decomposed by Pt/Bi₂O₃. For example, Pt/Bi₂O₃ showed very limited photoactivity for decomposition of methylene blue into CO₂ under visible light. If free holes can be generated in the deep VB level of Bi₂O₃ (3.13 V *vs.* NHE), their oxidative power should be strong enough to decompose both

aldehydes and dyes into CO₂. However, if holes are generated by Pt NPs, their oxidative ability (1.2 V *vs.* NHE) should efficiently decompose aldehydes but not dyes, because CH and CO are able to react with surface O atoms to form CO₂, with reaction barriers below 0.7 V (*vs.* NHE).⁶

Furthermore, considering that Pt/Bi₂O₃ shows much higher visible photoactivity than that of Pt/TiO₂ and Pt/CdS (neither of which have acceptable photoactivities), Pt must not be a co-catalyst that serves as a normal electron scavenger. The fact is, Pt NPs can be plasmon-photoexcited, and therefore the photoactivity of Pt/Bi₂O₃ and Pt/TiO₂ is most likely due to the direct participation of the plasmon-induced holes from Pt NPs. Since the CB levels of TiO₂ (−0.3 V *vs.* NHE) and CdS (−0.52 V *vs.* NHE) are much more negative than that of Bi₂O₃, once transferred to the negative CB, the plasmon-induced electrons cannot reduce O₂ by single-electron process (O₂ + e[−] → O₂[−]; −0.56 V *vs.* NHE), and would reduce O₂ by a multi-electron process (O₂ + 2H₂O + 4e[−] → 4OH[−]; +0.40 V *vs.* NHE) only with difficulty. Therefore, the plasmon-induced electrons tend to be trapped by Pt NPs again; this may be the reason that Pt/TiO₂ and Pt/CdS exhibit poor photocatalytic performance.

All of the results mentioned above seem to support the full picture of the plasmon-induced photocatalytic process – namely, absorbed photons on Pt NPs are efficiently separated into electrons and holes; the electrons transfer to the CB level of Bi₂O₃,^{4,5} and the holes diffuse to the surface of Pt NPs, where the decomposition of organic compounds occurs.¹¹ Since the multi-electron reduction process occurs at a potential of 0.4 V (O₂ + 2H₂O + 4e[−] → 4OH[−]) which is the same as that of the CB level of Bi₂O₃, the electrons in the Bi₂O₃ CB level can effectively transferred to the adsorbed O₂ rather than recombining with the holes. Consequently, the charge separation can be achieved by coupling Pt NPs with Bi₂O₃.

Conclusion

In summary, we have investigated a plasmonic photocatalyst, Pt/Bi₂O₃, which has the advantage of high visible-light photoactivity for decomposing organic pollutants in mild conditions. The positive CB level of Bi₂O₃, which is able to transfer plasmon-induced electrons from the Pt NPs, plays an important role in the unique catalytic properties of Pt/Bi₂O₃. Future work will focus on preparing Au/Bi₂O₃ and Ag/Bi₂O₃ plasmonic photocatalysts. We consider that these photocatalysts could have a wide range of practical purposes.

Experimental

Pt/Bi₂O₃ was prepared by a simple photoreduction method. An aqueous suspension containing commercial Bi₂O₃ powder (Analytical Grade, Hangzhou Huadong Medicine Group Co., Ltd) was sonicated for 2 h, followed by several rinses with Milli-Q water and ethyl alcohol, and subsequent drying at 80 °C for 12 h. The resulting powder (200 mg) was added to hexachloroplatinic acid (H₂PtCl₆·6H₂O) solution (0.1 g mL^{−1}, Sigma-Aldrich) and was then exposed to UV light ($\lambda > 300 \text{ nm}$) from a high pressure mercury lamp (input power 500 W, light intensity 598 $\mu\text{W cm}^{-2}$, Nanjing Xujiang, Ltd). After 1 h of irradiation, 10 mL methanol solution (10 vol%) was added as sacrificial reagent and the

suspension was exposed to further irradiation for 1.5 h after bubbling with pure N₂ for 15 min. The resulting sample was centrifuged, washed with Milli-Q water and ethyl alcohol to remove the impurities, and collected as a powder after drying at 60 °C for 12 h. Pt/TiO₂ and Pt/CdS were prepared in the same manner. N-TiO₂ (TS-S4230) for comparative analysis was obtained from Sumitomo Chemical (Japan). P25 TiO₂ powders were supplied by Degussa Co. Ltd. Other commercial chemicals were of the highest available grade and were used without further purification.

Decomposition of organics was carried out with 40 mg of the powdered catalyst suspended in 10 mL of aqueous organic solution in a Pyrex test tube (55 mL). Photocatalytic studies of all samples were carried out in a photochemical reactor (Nanjing Xujiang, Ltd), which was fitted with a cold quartz tube and an inner UV lamp. An optical filter (Shanghai Seagull Colored Optical Glass Co., Ltd) was adopted to provide visible light with $\lambda > 400$ nm. For photocatalysis experiments, the rate of agitation was set at 700 ± 10 rpm. Gas chromatography (Agilent 6890 with Agilent column 115-3133) was utilized for quantitative measurement of gaseous CO₂ generated as the organic substrate was oxidized. Gas volumes of 200 μ L were extracted from the test tubes using a microliter syringe at regular intervals.

Acknowledgements

We are grateful to Daisuke Toyoshima for the computer calculations, and Dr. Wangyang Lu and Dr. Yuyuan Yao for helpful discussions. This work was supported by the Program for Changjiang Scholars and Innovative Research Team in University (IRT 0654).

Notes and references

- 1 M. Fujihira, Y. Satoh and T. Osa, *Nature*, 1981, **293**, 206–208.
- 2 Z. H. Yuan and L. D. Zhang, *J. Mater. Chem.*, 2001, **11**, 1265–1268.
- 3 X. B. Chen and C. Burda, *J. Am. Chem. Soc.*, 2008, **130**, 5018.
- 4 P. Wang, B. B. Huang, X. Y. Qin, X. Y. Zhang, Y. Dai, J. Y. Wei and M. H. Whangbo, *Angew. Chem., Int. Ed.*, 2008, **47**, 7931–7933.
- 5 Y. Tian and T. Tatsuma, *J. Am. Chem. Soc.*, 2005, **127**, 7632–7637.
- 6 K. Ikeda, J. Sato, N. Fujimoto, N. Hayazawa, S. Kawata and K. Uosaki, *J. Phys. Chem. C*, 2009, **113**, 11816–11821.
- 7 S. Y. Chai, Y. J. Kim, M. H. Jung, A. K. Chakraborty, D. Jung and W. I. Lee, *J. Catal.*, 2009, **262**, 144–149.
- 8 C. H. Wang, C. L. Shao, Y. C. Liu and L. Zhang, *Scr. Mater.*, 2008, **59**, 332–335.
- 9 M. Harada and H. Einaga, *Langmuir*, 2006, **22**, 2371–2377.
- 10 H. G. Kim, P. H. Borse, W. Y. Choi and J. S. Lee, *Angew. Chem., Int. Ed.*, 2005, **44**, 4585–4589.
- 11 R. F. Howe and M. Gratzel, *J. Phys. Chem.*, 1987, **91**, 3906–3909.

Synthesis of tetraketones in water and under catalyst-free conditions†

Jian-Jun Yu, Li-Min Wang,* Jin-Qian Liu, Feng-Lou Guo, Ying Liu and Ning Jiao

Received 13th July 2009, Accepted 17th November 2009

First published as an Advance Article on the web 9th December 2009

DOI: 10.1039/b913816a

A simple, environmentally friendly, tandem Knoevenagel condensation and Michael addition procedure is reported. The reactions between cyclic-1,3-diketones and a variety of aldehydes were carried out in water to afford tetraketones (64–99%). In this green synthetic protocol, the solvent water itself catalysed the reaction by hydrogen bonding, thus avoiding the use of any other catalysts to make the work up procedure easier.

Introduction

Tetraketones (**I**), which have four carbonyl functionalities along with their tautomeric, that is, keto-enol-forms, have some tyrosinase inhibitory properties and some are even better than both the standards kojic acid and L-mimosine.¹ The dimeric intermediate (**I**) is a key intermediate for the preparation of heterocyclic three-ring systems—either xanthendione (**II**), acridindione (**III**),³ or 4*H*-1-benzopyran (**IV**) derivatives (Scheme 1).² Acridindione (**III**) derivatives have been used as electron donors and acceptors⁴ and in the photoinitiated polymerization of acrylates and methacrylates.⁵ They are also interesting because they have similar properties to those of 1,4-dihydropyridines, which are similar in structure to biologically important compounds such as NADH and NADPH.⁶ Recently they have been used as a new

class of laser dyes.³ 4*H*-1-Benzopyrans are an important class of naturally occurring compounds with biological activities.^{7,8}

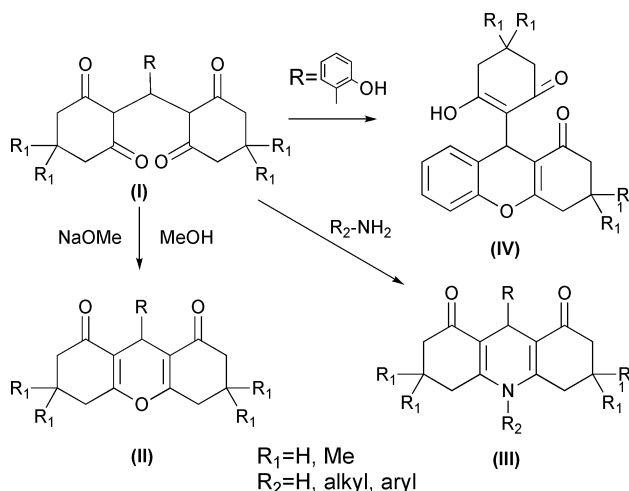
Tetraketones were synthesized through Knoevenagel condensations and Michael additions of aldehydes with cyclohexane-1,3-diones, dimedones or other types of 1,3-cyclic diketones. They were first reported by Merling in 1894 by synthesizing the cyclohexane-1,3-dione from resorcinol.⁹ Vorlander and Kalkow reported the practical synthesis of tetraketones in 1899.¹⁰ Several reports of the attempts to carry out an efficient synthesis of tetraketones have appeared in the literature. Many of these methods involve the use of NaOH,¹³ KOH,² piperidine^{1,11a,11c} and proline¹⁴ as catalyst, the use of cetyltrimethyl ammonium bromide (CTMAB) as surfactant,¹² and the use of aqueous organic solvent as cosolvent.^{1,2,3b,11}

In modern organic chemistry, the improvement of reaction efficiency, the avoidance of toxic reagents, the reduction of waste, and the responsible utilization of our resources have become critical objectives.^{14,15} By keeping these ideas in mind, a simple and green approach for the synthesis of tetraketones (**I**) has been developed. Pure water as solvent, catalyst free and room temperature conditions are enough to afford the tetraketones in nearly quantitative yields. Most important of all, the purification procedure is just followed by filtration, washing and drying and the water can be reused for the next cycle, so the waste can be reduced effectively.

Results and discussion

First, the reaction conditions were optimized in the reaction of benzaldehyde and dimedone (Table 1). By comparing the reaction yields of Entries 1 to 5 in Table 1, it was found that 4 h was enough for this reaction. Room temperature gave excellent yields. However, the high temperature decreased the yields (Entries 4, 6 and 7, Table 1). Ethanol and aqueous ethanol were the solvents used mainly for this reaction, however, it is exciting to find that water can also afford the product in good yield even better than ethanol (Entries 4, 8 and 9, Table 1). This may be because the polarity of water is higher than that of ethanol and the effect of ethanol in this reaction is just to increase the solubility of the substrates. Among the various reaction conditions used in Table 1, those indicated in Entry 4 were the most promising conditions.

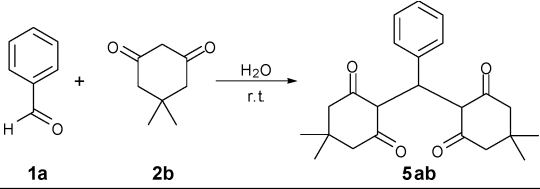
With the optimal conditions in hand, the range of the substrates was checked. First, the Knoevenagel condensation and Michael addition reaction were carried out by using a series of different aldehydes with cyclohexane-1,3-dione. The results are summarized in Table 2 (Entries 1–14). It was found that both electron-rich and electron-deficient aromatic aldehydes were suitable for this reaction. For benzaldehydes with



Scheme 1

Laboratory for Advanced Materials & Institute of Fine Chemicals, East China University of Science and Technology, 130 Meilong Road, Shanghai, 200237, China. E-mail: wanglimin@ecust.edu.cn

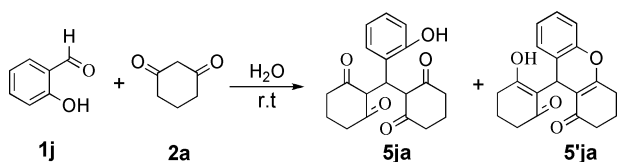
† Electronic supplementary information (ESI) available: Experimental and spectra. See DOI: 10.1039/b913816a

Table 1 Synthesis of tetraketones under various reaction conditions


Entry ^a	Time/h	T/°C	Solvent	Yield (%) ^b
1	0.5	rt	H ₂ O	64
2	1	rt	H ₂ O	72
3	2	rt	H ₂ O	88
4	4	rt	H ₂ O	96
5	6	rt	H ₂ O	94
6	4	40	H ₂ O	90
7	4	60	H ₂ O	86
8	4	80	H ₂ O	81
9	4	rt	Ethanol	80
10	4	rt	Ethanol/H ₂ O = 1:1 ^c	94

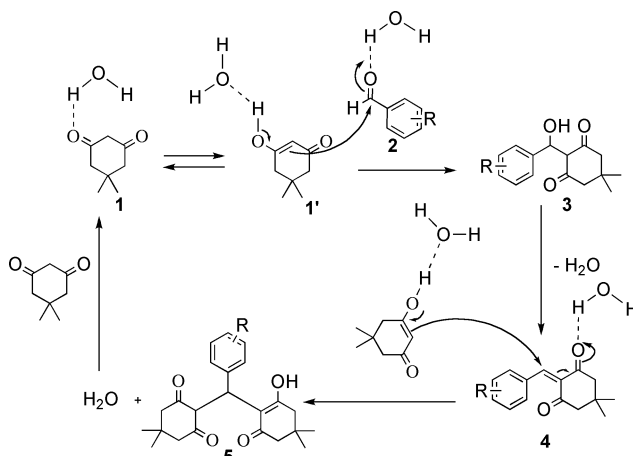
^a Reaction conditions: benzaldehyde (1 mmol), dimedone (2 mmol), and water (5 mL) at rt. ^b Isolated yield. ^c Aqueous solution of ethanol: ethanol (2.5 mL) and water (2.5 mL).

electron-donating groups such as 4-(dimethylamino) benzaldehyde, 4-methoxybenzaldehyde and piperonal, the desired products could be afforded in good yields (Entries 4, 5, 10, Table 2). However, all of the electron-deficient aromatic aldehydes investigated in this way could give excellent yields without obvious steric hindrance effects (Entries 1–3, 6–8, Table 2). A heterocyclic aromatic aldehyde such as 2-furaldehyde could also react with cyclohexane-1,3-dione to afford the tetraketone compound with a yield up to 98% (Entry 11, Table 2). Just as reported previously, when the 2-hydroxybenzaldehyde was used as starting material, the product was totally 2-(1-oxo-2,3,4,9-tetrahydro-1*H*-xanthen-9-yl) cyclohexane-1,3-dione (**5'ja**) instead of the tetraketone (**5ja**) (Scheme 2).

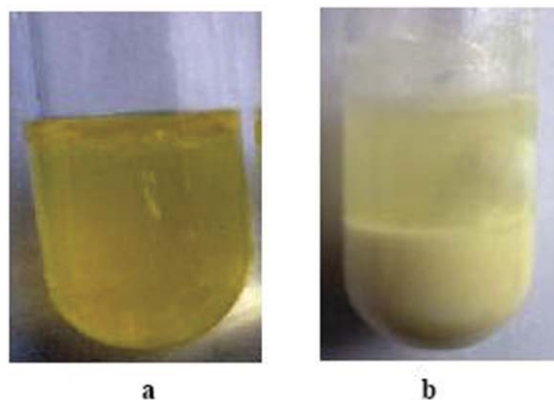
**Scheme 2** The Knoevenagel condensation, Michael addition and dehydration reaction of salicylaldehyde and 1,3-cyclohexanedione.

Besides cyclic-1,3-diketones (cyclohexane-1,3-dione and dimedone), heterocyclic-1,3-diones and cyclopent-1,3-diones were also investigated in these conditions. 4-Hydroxy-6-methylpyran-2-one, spirolactone and 2,2-tetramethylene-4,6-dioxo-1,3-dioxane were used to react with benzaldehyde and afforded the target products in good yields (Entries 16–18, Table 2). Cyclopent-1,3-dione was first reported to take part in this reaction and the yield was excellent (Entry 19, Table 2). More importantly, 1,3-indandione also gave a good result under these conditions (Entry 20, Table 2). However, under these conditions, dimethyl malonate and acetylacetone gave no reaction or just a Knoevenagel condensation product, respectively (Entry 21, 22 Table 2).

As well as its action as a solvent, water also helps in the enolization of **1** by making hydrogen bonds with the OH of **1'** and, thus, it increases the nucleophilic character of the methylene carbon (C-2) of **1**. Meanwhile, it also increases the electrophilic character of the carbonyl carbon of **2** by forming hydrogen bonds with the carbonyl oxygen of aldehyde **2**.^{15a} After the Knoevenagel condensation reaction, the intermediate **4** is afforded. By the nucleophilic attacking of **1'**, **4** is transformed to the tetraketone **5** (Scheme 3).

**Scheme 3** Plausible mechanism for the Knoevenagel condensation and Michael addition leading to tetraketones.

The reaction procedure is very simple (Fig. 1). After the benzaldehyde and 1,3-cyclohexanedione were added to water, a nearly homogeneous system was formed at the beginning of the reaction (Fig. 1(a)). After the reaction was completed, the product precipitated (Fig. 1(b)). The product could be afforded after filtration, washing and drying.

**Fig. 1** The phenomenon of the reaction between benzaldehyde and 1,3-cyclohexanediones. (a) The homogeneous phase at the beginning of the reaction. (b) The product precipitated after reaction completion.

Conclusions

In summary, we report an effective, green and mild method for the synthesis of tetraketones. To the best of our knowledge, it is the first example of using water as a solvent without catalyst, surfactant or ionic liquid. This process provides an

Table 2 The synthesis of tetraketones **5** in water

Reaction scheme showing the synthesis of tetraketones **5** from R-CHO (**1**) and 1,3-cyclic diketones (**2**) in water at room temperature (rt).

Entry ^a	R-CHO (1)	1,3-cyclic diketones (2)	Time/h	Yield (%) ^b	Mp (lit.)/ ^c °C
1	4-Br-C ₆ H ₄ (1b)	2a	4	91	225–227 (240–241) ¹⁶
2	3-Br-C ₆ H ₄ (1c)	2a	4	96	206–208 (248–249) ¹⁷
3	2-Br-C ₆ H ₄ (1d)	2a	4	85	241–243 (199–200) ¹
4	4-MeO-C ₆ H ₄ (1e)	2a	4	93	190–191 (199–201) ¹
5	4-(NMe ₂)-C ₆ H ₄ (1f)	2a	4	70 ^c	142 (150) ^{11a}
6	4-NO ₂ -C ₆ H ₄ (1g)	2a	1/2	91	210–212 (218) ^{11a}
7	3-NO ₂ -C ₆ H ₄ (1h)	2a	1/2	99	204–205 (209–211) ¹
8	2-NO ₂ -C ₆ H ₄ (1i)	2a	4	90	204–206 (212–213) ^{11a}
9	2-OH-C ₆ H ₄ (1j)	2a	4	90 ^d	228–230 (234) ¹⁸
10	3,4-OCH ₂ O-C ₆ H ₃ (1k)	2a	4	80	204–206 (212) ^{11a}
11	2-Furyl (1l)	2a	4	98	142–144 (146) ^{11a}
12	H (1m)	2a	4	96	130–132 (134) ^{11a}
13	n-Pr (1n)	2a	4	64	97–98 (97–98) ^{11a}
14	C ₆ H ₅ (1a)	2a	4	94	207–208 (217–218) ¹
15	C ₆ H ₅ (1a)	2b	1/2	96	194–195 (190–192) ^{3b}
16	C ₆ H ₅ (1a)	2c	4	85	167–169 (176) ¹³
17	C ₆ H ₅ (1a)	2d	4	80	115–117
18	C ₆ H ₅ (1a)	2e	4	95	157–159
19	C ₆ H ₅ (1a)	2f	4	85	222–223
20	C ₆ H ₅ (1a)	2g	4	95	156–158 (162) ¹⁹
21	C ₆ H ₅ (1a)	2h	4	trace	/
22	C ₆ H ₅ (1a)	2i	4	trace	/

^a Reaction conditions: benzaldehyde (1 mmol), dimedone (2 mmol), and water (5 mL) at rt. ^b Isolated yield. ^c The product was recrystallized from ethanol. ^d The 4*H*-benzopyran derivative (**5'ja**) was afforded.

opportunity to avoid organic solvents and resource consumption compared to the traditional reaction system. The simplicity of the methodology, ease of the product isolation and mild conditions could make this process available on an industrial scale.

Experimental

General

Melting points were determined with an X-4 apparatus and were uncorrected. ¹H (400 MHz) and ¹³C (100 MHz) NMR spectra were recorded on a Bruker Avance 400 spectrometer in CDCl₃ using TMS as internal reference. Mass (EI) spectra were recorded on a Micromass GCTTM mass spectrometer. All chemicals used were reagent grade and were used as received without further purification.

Experimental procedure for the synthesis of compound **5a**

In a 20 mL flask was placed benzaldehyde (1 mmol/106 mg), cyclohexane-1,3-dione (2 mmol/224 mg) and water (5 mL). The resulting yellow solution was stirred at room temperature for 4 h (TLC monitored/R_f: 0.6 (CH₂Cl₂-EtOAc, 4:1), white precipitate was formed and the resultant precipitates were filtered, washed by cold water and dried in vacuum affording 2,2'-(phenylmethylene) dicyclohexane-1,3-dione (**5a**) as white solid. 0.294 g, yield: 94%. ¹H NMR (CDCl₃, 400 MHz): δ 1.99–2.09 (4H, m, H-5/H-5'), 2.35–2.52 (4H, m, H-4/H-4'), 2.54–2.70 (4H, m, H-6/H-6'), 5.48 (1H, s, H-7), 7.12 (2H, d, *J* = 8.0 Hz, H-2/H-6), 7.18 (1H, t, *J* = 7.2 Hz, H-4), 7.27 (2H, t, *J* = 7.8 Hz, H-3/H-5), 12.36 (2H, br s, -OH); ¹³C NMR (CDCl₃, 100 MHz): δ 20.1 (C-5/C-5'), 32.9 (C-4/C-4'), 33.0 (C-7), 33.5 (C-6/C-6'), 116.4 (C-2/C-2'), 125.8 (C-4), 126.5 (C-2/C-6), 128.1 (C-3/C-5), 137.8 (C-1), 190.7 (-COH), 192.1 (CO); EIMS: *m/z* 312.1 (M⁺, 45).

Experimental procedure for the synthesis of compound 5fa

In a 20 mL flask was placed 4-(dimethylamino) benzaldehyde (1 mmol/149 mg), cyclohexane-1,3-dione (2 mmol/224 mg) and water (5 mL). The red solution was stirred at room temperature for 4 h (TLC monitored/ R_f : 0.3 (CH_2Cl_2 -EtOAc, 4:1), red precipitate was formed and the resultant precipitates were filtered to afford the raw product. Recrystallization from ethanol afforded the pure product 2,2'-(4-(dimethylamino) phenyl)methylene)dicyclohexane-1,3-dione (**5fa**) 0.246 g. Red solid; Yield: 94%. $^1\text{H NMR}$ (CDCl_3 , 400 MHz): δ 1.98-2.07 (4H, m, H-5/H-5'), 2.30-2.50 (4H, m, H-4/H-4'), 2.52-2.68 (4H, m, H-6/H-6'), 2.91 (6H, s, -N(CH₃)₂), 5.42 (1H, s, H-7), 6.67 (2H, d, $J = 8.8$ Hz, H-3/H-5), 6.96 (2H, d, $J = 8.4$ Hz, H-2/H-6), 12.38 (2H, br s, -OH); $^{13}\text{C NMR}$ (CDCl_3 , 100 MHz): δ 20.1 (C-5/C-5'), 32.0 (C-4/C-4'), 33.0 (C-7), 33.5 (C-6/C-6'), 40.7 (-N(CH₃)₂), 112.7 (C-2/C-2'), 116.8 (C-2/C-6), 125.5 (C-3/C-5), 127.2 (C-1), 148.8 (C-4), 190.8 (-COH), 191.9 (CO); EIMS: m/z 355.2 (M⁺, 10).

Experimental procedure for the synthesis of compound 5ja'

In a 20 mL flask was placed salicylaldehyde (1 mmol/122 mg), cyclohexane-1,3-dione (2 mmol/224 mg) and water (5 mL). The yellow solution was stirred at room temperature for 4 h (TLC monitored/ R_f : 0.45 (CH_2Cl_2 -EtOAc, 4:1). A creamy white solid was formed and the resultant precipitates were filtered, washed by cold water and dried in vacuum affording 2-(1-oxo-2,3,4,9-tetrahydro-1H-xanthen-9-yl) cyclohexane-1,3-dione (**5ja'**) as creamy white solid. 0.278 g, yield: 90%. $^1\text{H NMR}$ (CDCl_3 , 400 MHz): δ 1.71-2.82 (12H, m, 6CH₂), 4.65 (1H, s, CH), 7.00-7.05 (3H, m, ArH), 7.13-7.20 (1H, m, ArH), 10.85 (b, 1H, OH); $^{13}\text{C NMR}$ (CDCl_3 , 100 MHz): δ 20.7, 20.8, 25.8, 25.9, 27.7, 37.1, 112.4, 115.7, 124.7, 126.2, 127.3, 128.9, 150.0, 167.1, 196.5; EIMS: m/z 310.2 (M⁺, 34).

Acknowledgements

This work was financially supported by the Natural Science Foundation of China (NO. 20672035).

References

- 1 K. M. Khan, G. M. Maharvi, M. T. H. Khan, A. J. Shaikh, S. Perveen, S. Begun and M. I. Choudhary, *Bioorg. Med. Chem.*, 2006, **14**, 344.
- 2 B. A. Marco, T. A. Manuel, P. M. Itzia, M. M. Francisco, E. Georgina, M. Elies and E. Enrique, *J. Chem. Crystallogr.*, 1999, **29**, 759.
- 3 (a) P. Shanmugasundaram, K. J. Prabahar and V. T. Ramakrishnan, *J. Heterocycl. Chem.*, 1993, **30**, 1003; (b) N. Srividya, P. Ramamurthy, P. Shanmugasundaram and V. T. Ramakrishnan, *J. Org. Chem.*, 1996, **61**, 5083.
- 4 (a) H. J. Timpe, S. Ulrich and S. Ali, *J. Photochem. Photobiol., A*, 1991, **61**, 77; (b) H. J. Timpe, S. Ulrich and J. P. Fouassier, *J. Photochem. Photobiol., A*, 1993, **73**, 139; (c) S. Ulrich, H. J. Timpe, J. P. Fouassier and F. M. Savary, *J. Photochem. Photobiol., A*, 1993, **74**, 165.
- 5 H. J. Timpe, S. Ulrich, C. Decker and J. P. Fouassier, *Macromolecules*, 1993, **26**, 4560.
- 6 F. T. McNamara, J. W. Niefert, J. F. Ambrose and E. S. Huysen, *J. Org. Chem.*, 1977, **42**, 988.
- 7 G. P. Ellis, Ed. *Chromenes, Chromanones and Chromones*, Wiley, New York, 1977.
- 8 (a) I. Yavari, M. A. Abbasinejad, A. Alizadeh and Z. Hossaini, *Tetrahedron*, 2003, **59**, 1289; (b) I. Yavari, H. Djahaniani and F. Nasiri, *Tetrahedron*, 2003, **59**, 9409; (c) H. Miao and Z. Yang, *Org. Lett.*, 2000, **2**, 1765; (d) P. Kumar and M. S. Bodas, *Org. Lett.*, 2000, **2**, 3821.
- 9 Merling, *Annalen.*, 1894, **278**, 28.
- 10 Vorlander and Kalkow, *Justus Liebigs Annalen der Chemie.*, 1899, **309**, 380.
- 11 (a) F. E. King and D. G. I. Felton, *J. Chem. Soc.*, 1948, **13**, 1371; (b) H. Stetter, *Angew. Chem.*, 1955, **67**, 769; (c) E. C. Horning and M. G. Horning, *J. Org. Chem.*, 1946, **11**, 95.
- 12 Z. J. Ren, W. G. Cao, W. Q. Tong and X. P. Jing, *Synth. Commun.*, 2002, **32**, 1947.
- 13 G. Cravotto, A. Demetri, G. M. Nano, G. Palmisano, A. Penoni and S. Tagliapietra, *Eur. J. Org. Chem.*, 2003, 4438.
- 14 D. B. Ramachary and M. Kishor, *J. Org. Chem.*, 2007, **72**, 5056.
- 15 (a) L. D. S. Yadav, S. Singh and V. K. Rai, *Green Chem.*, 2009, **11**, 878-882; (b) W. Leitner, *Green Chem.*, 2009, **11**, 603.
- 16 N. G. Kozlov, K. N. Gusak and A. V. Tkachev, *Chem. Heterocycl. Compd.*, 2007, **43**, 740.
- 17 K. N. Gusak, A. B. Tereshko, N. G. Kozlov and N. I. Shakailo, *Russ. J. Gen. Chem.*, 2000, **70**, 1893.
- 18 N. G. Kozlov, K. N. Gusak and Russ, *J. Org. Chem.*, 1999, **35**, 402.
- 19 L. B. Rosine, L. Claude and J. G. Jean, *J. Med. Chem.*, 1975, **18**, 85.

Synthesis of platinum nanoparticles using cellulosic reducing agents

Karima Benaissi, Lee Johnson, Darren A. Walsh and Wim Thielemans*

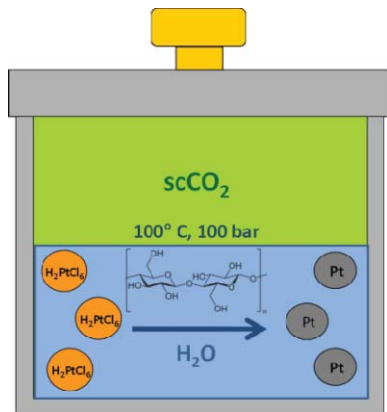
Received 6th July 2009, Accepted 21st November 2009

First published as an Advance Article on the web 16th December 2009

DOI: 10.1039/b913218j

Platinum nanoparticles were formed by reduction of H_2PtCl_6 using nanocrystalline cellulose from cotton as the reducing agent.

Biomass-derived cellulosic materials are currently attracting a great deal of attention for the development of alternative energy resources and the production of chemical feedstocks.^{1–3} Cellulose-based nanotechnology is also an active area of research; cellulose has a nanofibrillar structure, can be functionalised, and can form stable nanostructured architectures by self-assembly.^{4–6} Nanocrystalline cellulose whiskers can be extracted from native biomass resources using very simple, green processes and applications of these materials include uses in nanocomposites,⁷ dialysis membranes,⁸ and electrochemical devices.^{9–11} Cellulose can also be used for the synthesis of metal nanostructures, as functional groups on the nanocrystalline surface can reduce metal ions, offering a very simple, green route to metal nanoparticles.^{7,12,13}



Scheme 1 Schematic of the reaction in which H_2PtCl_6 is reduced by cellulose nanowhiskers in aqueous medium in contact with scCO_2 .

The synthesis of noble metal nanoparticles is extremely important for the catalyst industry. Platinum, in particular, is especially useful for myriad industrial catalytic applications, and a large number of reports describe the synthesis of platinum nanoparticles using a wide variety of methods.^{14–17} While a number of researchers have described the synthesis of various metal nanoparticles using renewable carbohydrate- and cellulose-based materials,^{18–21} the synthesis of Pt nanoparticles

using renewable, cellulose-based reducing agents appears difficult.^{7,22} A small number of reports describe the formation of platinum/cellulose nanocomposites.^{7,23,24} However, in those cases, a chemical reducing agent was added to the system to reduce the platinum precursor in the presence of the cellulose, which acted as a structure-directing agent. Therefore, the development of methods for synthesising platinum nanoparticles using renewable reagents remains an important goal with significant industrial consequences.

In the development of new chemical processes, application of the 12 principles of green chemistry can impart significant benefits in terms of environmental impact and cost.^{25,26} In particular, the choice of supercritical fluids (SCFs) as replacements for traditional solvents has proven beneficial in a number of chemical processes.^{27–29} Amongst SCFs, supercritical carbon dioxide (scCO_2) is an especially green alternative to traditional solvents due to its availability, non-toxicity and non flammability. Biphasic systems, incorporating scCO_2 in contact with a water phase, have also become extremely useful for chemical processing.³⁰ In this communication, we describe the use of an scCO_2 /water system for the synthesis of platinum nanoparticles. H_2PtCl_6 was reduced to Pt in aqueous solution using suspended crystalline cellulose nanofibrils from cotton as a reducing agent. In this system, the reactants and products are present in the aqueous phase and, interestingly, we show that the reaction only proceeds when the water is in contact with scCO_2 . This is the first time that metallic Pt nanoparticles have been formed by direct reduction of a platinum species with plant cellulose, and this approach offers a very promising route to Pt nanoparticles using renewable reducing agents.

Cellulose nanowhiskers were extracted from cotton using the method previously described by Revol *et al.*³¹ The acid hydrolysis entails the hydrolysis of the amorphous sections of cellulose using 64 wt% sulfuric acid at 45 °C for 35 min. The sulfuric acid can be recycled after removal of hydrolysis products. This method yields cellulose nanowhiskers with average dimensions of $6 \times 6 \times 160$ nm containing *ca.* 10% of sulfate moieties at the surface. A home-built stainless-steel high pressure batch autoclave (internal volume 8.5 mL) was equipped with a magnetic stirrer bar and placed on a magnetic stirring plate. Five mL of an aqueous cellulose dispersion (1 wt%) and 25 mg of H_2PtCl_6 were added to the autoclave, and a band heater, thermocouple, and inlet and outlet tubes were connected. Prior to use, the autoclave was flushed with CO_2 , heated to the desired temperature and CO_2 was pumped into the reactor using a high pressure NWA PM-101 Pickel pump until the desired pressure was achieved.† The reaction mixture was stirred overnight to ensure completion of the reaction and the system was then depressurised by placing the autoclave in a dry ice-acetone

School of Chemistry and Division of Process and Environmental Engineering-Faculty of Engineering, The University of Nottingham, Nottingham, NG7 2RD, UK.
E-mail: wim.thielemans@nottingham.ac.uk; Fax: +44 115 9513562; Tel: +44 115 9513437

bath. To examine the phase behaviour of the mixture, reactions were also carried out, at the same reactant concentrations, in a variable-volume view cell at various temperatures and pressures. Fig. 1 shows the reaction mixture at ambient temperature and pressure, and at higher temperatures and pressures. After one hour at ambient temperature and pressure, the reaction mixture remained yellow, which is characteristic of H_2PtCl_6 in aqueous solution. After stirring the suspension for less than one minute at 80°C and 100 bar, the reaction mixture colour changed from yellow to black and a black precipitate formed, suggesting the rapid formation of metallic platinum. Upon increasing the reaction temperature to 100°C at 100 bar, the aqueous phase turned a darker colour, suggesting an increase in the rate of reaction at the higher temperature. After depressurising the reaction vessel at room temperature, the resulting residue was mixed with water (3 mL) and centrifuged for 2 min at 8000 rpm (4600 g). The supernatant was then decanted and the solid was dried in air at 70°C for one hour.

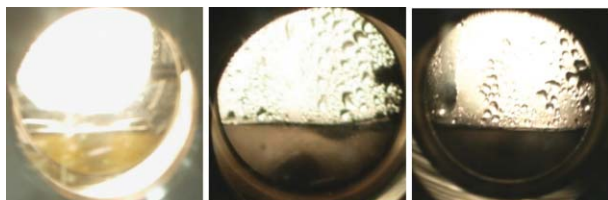


Fig. 1 Photographs of the reaction product after 1 hour at (left) ambient temperature and pressure, (middle) 80°C and 100 bar, and (right) 100°C and 100 bar.

Transmission electron microscopy was used to characterise the morphology of the reaction product, and Fig. 2 shows a typical TEM image obtained for the dried solid. Also shown is a TEM image of the bare cellulose for comparison. After the reaction, the cellulose nanowhiskers were decorated with nanoparticles. The majority of the particles were of approximately spherical geometry. Some clustering of the particles was evident, which made an accurate estimation of the average particle size difficult. However, the majority of the particles appear to be in the range 5–30 nm. Control reactions, in which cellulose nanofibrils and H_2PtCl_6 were mixed in water and heated at 100°C under air, were also carried out; the reaction mixture recovered was yellow, with no black precipitate being observed, indicating that metallic platinum was formed only when the scCO_2 was present. The formation of nanoparticles by reduction of H_2PtCl_6 with nanocrystalline cellulose using this method is significant because, as described previously, the

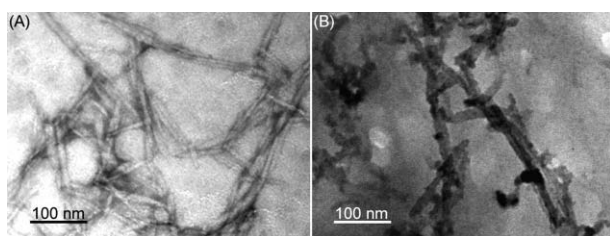


Fig. 2 TEM images of (A) bare cellulose nanowhiskers and (B) platinum nanoparticles formed by reduction of H_2PtCl_6 with cellulose nanofibrils. Bare cellulose was stained using 1 mM uranyl acetate to enhance the image contrast.

reduction of platinum salts by plant cellulose has been shown to be extremely difficult. For example, Evans reported difficulties in synthesising Pt nanoparticles using cellulose extracted from cotton as the reducing agent.²² However, in the same paper, the authors showed that Pd, Au and Ag metal nanoparticles could be easily synthesised using microbial cellulose as the reducing agent and attributed the difference in the reducing power of each material to structural differences between plant and bacterial cellulose.

The composition of the reaction product was analysed using powder X-ray diffraction (PXRD) with a $\text{Cu-K}\alpha$ source ($\lambda = 0.154\text{ nm}$) and by recording reflections (in diffraction mode) from 0 to 90° at 0.02° increments. Fig. 3 shows a typical diffractogram recorded for the solid recovered from the autoclave after 1 hour at 100°C and 100 bar. The peaks between 14° and 23° are due to crystalline cellulose,¹⁸ indicating that the cellulose within the reaction mixture retains its crystallinity during the reaction. The peaks at 39.8° , 46.2° and 67.3° are due to the Pt(111), Pt(200) and Pt(220) planes of pure fcc platinum, respectively.⁷ This clearly demonstrates the formation of metallic platinum during the reaction. The average Pt particle size, d , was estimated using the Scherrer formula ($d = 0.9\lambda/\beta\cos\theta$, where β is the full width at half-maximum peak height measured at the diffraction angle θ), which yielded a value of 21 nm. This is consistent with the size of platinum nanoparticles estimated using TEM.

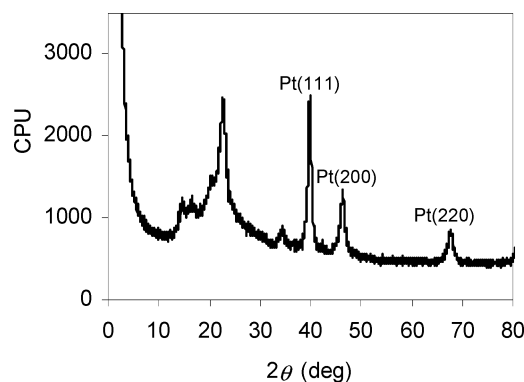


Fig. 3 PXRD diffractogram obtained for the Pt/cellulose product.

Compositional analysis of the product was also carried out using X-ray photoelectron spectroscopy (XPS). XPS spectra were recorded using an $\text{Al-K}\alpha$ X-ray source at a pass energy of 20 eV. Peaks were charge referenced using cellulose C 1s at 286.2 eV. Fig. 4A and 4B show typical XPS spectra of H_2PtCl_6 before the reaction and Pt after the reaction, respectively. Before the reaction, the $\text{Pt}4f_{7/2}$ and $\text{Pt}4f_{5/2}$ doublets of H_2PtCl_6 were visible at 78.5 and 74.8 eV, respectively (Fig. 4A). However, after the reaction, the $\text{Pt}4f_{7/2}$ and $\text{Pt}4f_{5/2}$ peaks had shifted to 71.2 eV and 74.4 eV, respectively, demonstrating the reduction of Pt(IV) to Pt(0).³²

In conclusion, for the first time we have synthesised platinum nanoparticles from H_2PtCl_6 using cellulose nanocrystals extracted from cotton as reducing agent. The addition of scCO_2 to the aqueous cellulose suspension allowed the rapid formation of Pt nanoparticles with an average size of 21 nm located on the cellulose nanowhiskers. While it is clear that none of the reagents enter the scCO_2 phase during the reaction, it is not

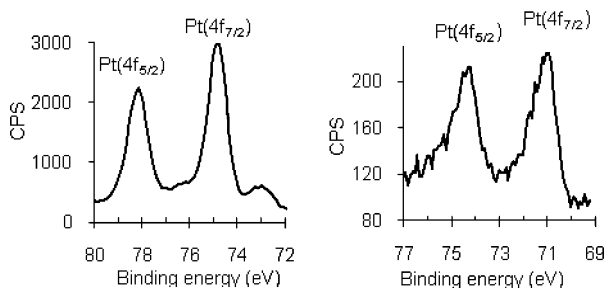


Fig. 4 XPS spectra of (left) H_2PtCl_6 and (right) platinum metal in the solid product showing the Pt4f regions. Peaks were charge referenced using cellulose C1s at 286.2 eV.

clear why an scCO_2 atmosphere above the reaction mixture is necessary for reaction to occur. To investigate this process, we carried out the reaction at pH 1.0 and pH 3.0 and, in each case, no reaction occurred. Therefore, it is not due to the drop in pH of the aqueous medium upon dissolution of CO_2 .

In addition, we carried out the reaction in water in contact with inert (N_2 and Ar) atmospheres and no reaction occurred, so it is not due to the inertness of the gas phase above the reaction mixture. Therefore, further work is required to establish the mechanism of platinum formation using our system and we are currently exploring the use of alternative supercritical fluids in order to identify whether our process is unique to scCO_2 . Nonetheless, our approach is a very useful method for the formation of platinum nanostructures using renewable, inexpensive reducing agents. The applications of the Pt/cellulose nanocomposites formed using this approach are also currently underway in our group, and we are investigating the applicability of our system to the synthesis of alternative nanomaterials using bioderived-reducing agents based on cellulose.

Acknowledgements

We thank the Engineering and Physical Sciences Research Council for funding this work through the DICE (Driving Innovation in Chemistry and Chemical Engineering) Project under the Science and Innovation Award (Grant Number EP/D501229/1). We also thank Dr. Ignacio J. Villar-Garcia for assistance with XPS measurements and Dr. Jaouad El Harfi for assistance with high-pressure experiments.

Notes and references

† **Safety note:** Experiments with scCO_2 involve high pressures and should only be carried out in equipment with the appropriate pressure rating and safety operating procedures.

1 J. B. Binder and R. T. Raines, *J. Am. Chem. Soc.*, 2009, **131**, 1979–1985.

- J. Ohlrogge, D. Allen, B. Berguson, D. DellaPenna, Y. Shachar-Hill and S. Stymne, *Science*, 2009, **324**, 1019–1020.
- O. J. Sanchez and C. A. Cardona, *Bioresour. Technol.*, 2008, **99**, 5270–5295.
- W. Thielemans, C. R. Warbey and D. A. Walsh, *Green Chem.*, 2009, **11**, 531–537.
- E. S. Medeiros, L. H. C. Mattoso, R. Bernardes-Filho, D. F. Wood and W. J. Orts, *Colloid Polym. Sci.*, 2008, **286**, 1265–1272.
- C. J. Grande, F. G. Torres, C. M. Gomez, O. P. Troncoso, J. Canet-Ferrer and J. Martinez-Pastor, *Mater. Sci. Eng. C*, 2009, **29**, 1098–1104.
- J. Cai, S. Kimura, M. Wada and S. Kuga, *Biomacromolecules*, 2009, **10**, 87–94.
- P. S. Liu, O. Chen, X. Liu, B. Yuan, S. S. Wu, J. Shen and S. C. Lin, *Biomacromolecules*, 2009, **10**, 2809–2816.
- M. J. Bonne, K. J. Edler, J. G. Buchanan, D. Wolverson, E. Psillakis, M. Helton, W. Thielemans and F. Marken, *J. Phys. Chem. C*, 2008, **112**, 2660–2666.
- M. J. Bonne, E. V. Milsom, M. Helton, W. Thielemans, S. Wilkins and F. Marken, *Electrochem. Commun.*, 2007, **9**, 1985–1990.
- K. Tsourounaki, M. J. Bonne, W. Thielemans, E. Psillakis, M. Helton, A. McKee and F. Marken, *Electroanalysis*, 2008, **20**, 2395–2402.
- W. Yang, Y. Ma, J. Tang and X. R. Yang, *Colloid Surf. A*, 2007, **302**, 628–633.
- H. Z. Huang and X. R. Yang, *Carbohydr. Res.*, 2004, **339**, 2627–2631.
- T. S. Ahmadi, Z. L. Wang, T. C. Green, A. Henglein and M. A. El Sayed, *Science*, 1996, **272**, 1924–1926.
- M. C. Orilall, F. Matsumoto, Q. Zhou, H. Sai, H. D. Abruna, F. J. DiSalvo and U. Wiesner, *J. Am. Chem. Soc.*, 2009, **131**, 9389–9395.
- Y. J. Song, R. M. Dorin, R. M. Garcia, Y. B. Jiang, H. Wang, P. Li, Y. Qiu, F. van Swol, J. E. Miller and J. A. Shelnett, *J. Am. Chem. Soc.*, 2008, **130**, 12602–12603.
- M. Q. Zhao and R. M. Crooks, *Adv. Mater.*, 1999, **11**, 217–220.
- Y. Shin, J. M. Blackwood, I. T. Bae, B. W. Arey and G. J. Exarhos, *Mater. Lett.*, 2007, **61**, 4297–4300.
- Y. Shin, I. T. Bae, B. W. Arey and G. J. Exarhos, *Mater. Lett.*, 2007, **61**, 3215–3217.
- P. Raveendran, J. Fu and S. L. Wallen, *Green Chem.*, 2006, **8**, 34–38.
- P. Raveendran, J. Fu and S. L. Wallen, *J. Am. Chem. Soc.*, 2003, **125**, 13940–13941.
- B. R. Evans, H. M. O'Neill, V. P. Malyvanh, I. Lee and J. Woodward, *Biosens. Bioelectron.*, 2003, **18**, 917–923.
- J. H. He, T. Kunitake and A. Nakao, *Chem. Commun.*, 2004, 410–411.
- J. H. He, T. Kunitake and A. Nakao, *Chem. Mater.*, 2003, **15**, 4401–4406.
- C. J. Murphy, *J. Mater. Chem.*, 2008, **18**, 2173–2176.
- Green Chemistry: Frontiers in Benign Chemical Synthesis*, ed. P. T. Anastas and T. C. Williamson, Oxford University Press, 1998.
- E. Reverchon, R. Adami, S. Cardea and G. Della Porta, *J. Supercrit. Fluids*, 2009, **47**, 484–492.
- D. Garcia-Rodriguez, A. M. Carro-Diaz and R. A. Lorenzo-Ferreira, *J. Sep. Sci.*, 2008, **31**, 1333–1345.
- H. R. Hobbs and N. R. Thomas, *Chem. Rev.*, 2007, **107**, 2786–2820.
- S. K. Karmee, C. Roosen, C. Kohlmann, S. Lutz, L. Greiner and W. Leitner, *Green Chem.*, 2009, **11**, 1052–1055.
- J. F. Revol, H. Bradford, J. Giasson, R. H. Marchessault and D. G. Gray, *Int. J. Biol. Macromol.*, 1992, **14**, 170–172.
- W. Yang, Y. Ma, J. Tang and X. R. Yang, *Colloid Surf. A*, 2007, **302**, 628–633.

Dual-bed catalyst system for C–C coupling of biomass-derived oxygenated hydrocarbons to fuel-grade compounds†

Elif I. Gürbüz, Edward L. Kunkes and James A. Dumesic*

Received 30th September 2009, Accepted 25th November 2009

First published as an Advance Article on the web 13th January 2010

DOI: 10.1039/b920369a

Mono-functional intermediates produced by catalytic conversion of sugars and polyols over Pt–Re/C catalysts (consisting of alcohols, ketones, carboxylic acids, and heterocyclic compounds) can be upgraded to fuel-grade compounds using two catalytic reactors operated in a cascade mode. The first reactor achieves C–C coupling of mono-functional intermediates using a dual-bed catalyst system, where the upstream catalyst bed ($\text{Ce}_1\text{Zr}_1\text{O}_x$) is employed to carry out ketonization of carboxylic acids, and the downstream catalyst bed (Pd/ZrO_2) is used to achieve aldol condensation/hydrogenation of alcohols and ketones. This second bed is not significantly inhibited by CO_2 and H_2O produced during ketonization. The high molecular weight ketones produced by C–C coupling reactions in the dual-bed catalyst system are subsequently converted to alkanes by hydrodeoxygenation (*i.e.*, dehydration/hydrogenation) over a $\text{Pt}/\text{SiO}_2\text{–Al}_2\text{O}_3$ catalyst. Using the aforementioned approach, an aqueous feed containing 60 wt% sorbitol was converted to a liquid stream of alkanes, 53% of which consisted of C_{7+} alkanes with minimal branching, desirable for Diesel fuel.

Utilization of biomass for the chemical industry and transportation sector is becoming of increasing importance in this era of diminishing fossil fuel resources and increasing accumulation of CO_2 in the atmosphere. Replacing petroleum in the transportation sector has been a challenge in terms of obtaining biomass-derived fuels with the requisite physical properties that allow for efficient storage, distribution and combustion. For instance, utilization of ethanol, the most common biomass-derived fuel, requires substantial changes to the internal combustion engine of a vehicle.¹ However, our group has recently explored reaction strategies in which biomass derived sugars and polyols can be converted to hydrocarbons that are identical to those obtained from petroleum,² allowing these bio-fuels to be used directly in current combustion engines. In particular, we showed that sugars and polyols can be converted first to mono-functional intermediates such as ketones, alcohols, heterocycles and carboxylic acids over a Pt–Re bi-metallic catalyst supported on carbon, followed by catalytic upgrading of these species (containing between

4 and 6 carbon atoms) to longer-chain alkanes appropriate for fuel applications. A similar process has been described by Blommel *et al.*³ in which the oxygen content of biomass derived carbohydrates is reduced by the use of H_2 generated *in situ* from aqueous-phase reforming to obtain mono-oxygenates such as alcohols, ketones and aldehydes.

A promising strategy for catalytic upgrading of mono-functional intermediates to produce liquid transportation fuels is to carry out C–C coupling of carboxylic acids by ketonization processes, forming higher molecular weight linear ketones plus CO_2 and H_2O ,⁴ followed by additional C–C coupling reactions of ketones and alcohols by aldol condensation/hydrogenation to produce heavier branched ketones.⁵ In the recent literature, aldol condensation has proven to be an effective means to produce large organic molecules by C–C bond coupling between carbonyl-containing furan compounds, such as 5-hydroxymethylfurfural and furfural. These molecules can then be converted to liquid alkanes by dehydration/hydrogenation over a bifunctional catalyst containing acid and metal sites.⁶ The ketonization processing must be carried out up-stream of aldol-condensation/hydrogenation reactions, because this latter processing step requires basic catalyst sites, and these sites are poisoned by carboxylic acids.^{7,8} Similar reaction conditions should allow the integration of these two processes in a single reactor. However, an important issue that must be addressed is the extent to which the catalyst employed for aldol-condensation/hydrogenation is inhibited by the CO_2 and water, by-products of ketonization reactions. In the present paper, we show that Pd/ZrO_2 catalysts are effective for aldol-condensation/hydrogenation in the presence of CO_2 and water, allowing for the integration of ketonization and aldol-condensation/hydrogenation processes for achieving C–C coupling of mono-functional intermediates in a single reactor, dual-bed catalyst system, thereby streamlining the overall catalytic upgrading process. The novelty of this process lies in the integration of two separate C–C coupling processes, such that an alkane stream suitable for Diesel fuel can be obtained in a two stage process, the latter being a dehydration/hydrogenation step to convert long-carbon chain ketones to alkanes, starting from biomass-derived mono-oxygenated streams. This combined process can be used for any oxygenate stream that contains carboxylic acids, carbonyl and alcohol species, and has potential for application in the emerging bio-refinery industry.

In our previous work, we studied a $\text{Pd}/\text{Ce}_1\text{Zr}_1\text{O}_x$ catalyst for the aldol condensation of 2-hexanone (a representative ketone) in the presence of CO_2 and water. These experiments showed a decrease by 90% and 40% in catalytic activity with the introduction into the feed stream of CO_2 and water, respectively,

Department of Chemical and Biological Engineering, University of Wisconsin-Madison, 1415 Engineering Drive, Madison, WI 53706, USA. E-mail: dumesic@engr.wisc.edu; Fax: 1 608 262 5434; Tel: 1 608 262 1095

† Electronic supplementary information (ESI) available: Catalyst preparation; reaction kinetics studies; acknowledgements. See DOI: 10.1039/b920369a

and we concluded that it would be difficult to integrate ketonization with aldol-condensation in a single reactor.⁷ In a more recent study, we investigated the extent of CO₂ inhibition on aldol condensation over catalysts prepared by depositing Pd on different compositions of ceria-zirconia mixed oxides (Ce_aZr_bO_x), including pure ceria and zirconia, and we found that Pd/ZrO₂ showed the best resistance towards CO₂ inhibition. In addition to this important feature, Pd/ZrO₂ also showed higher activity compared to Pd/Ce₁Zr₁O_x catalyst, as well as good resistance to water inhibition. The feasibility of a dual-bed catalyst system was studied using a mixture of a carboxylic acid and a ketone (20 mol% butanoic acid in 2-hexanone), and the integrated process showed high activity as well as selectivity to C–C coupling products.⁹ Following these promising results, the present study presents a detailed comparison of catalytic upgrading processes for a mixture of mono-functional intermediates obtained by conversion of an aqueous solution of 60 wt% sorbitol over a Pt–Re/C catalyst. Specifically, we compare the performance of two separate reactors for ketonization over Ce₁Zr₁O_x followed by aldol condensation/hydrogenation over 0.25 wt% Pd/ZrO₂, with removal of CO₂ and water between reactors, *versus* the performance of a dual-bed of these two catalysts in a single reactor.

A liquid stream of mono-functional intermediates was obtained by processing an aqueous solution containing 60 wt% sorbitol over a 10 wt% Pt–Re/C catalyst at 503 K and 18 bar, operating at a weight hourly space velocity (WHSV) equal to 0.6 h⁻¹ over the course of one month, during which the catalyst bed remained stable. The catalyst preparation and the experimental setup are described in the Electronic Supplementary Information,[†] and detailed characterization results can be found elsewhere.¹⁰ The carbon distribution among the gaseous phase, aqueous phase and organic phase (the latter denoted as inter-oil) is given in Table 1. The gas phase effluent contains about 39% of the carbon feed and consists of CO_x and light alkanes (C₁–C₆), and the aqueous phase (10% of the carbon feed) consists of higher oxygenates such as isosorbide. The carbon distribution in the inter-oil feed used for subsequent catalytic upgrading studies is shown in Table 1. (We note that the amount of C₄–C₆ alkanes in the inter-oil decreased to 1% from 8% due to evaporation during the time required to produce the inter-oil (*e.g.*, 1 month) to the time at which the inter-oil was used as a feed for catalytic upgrading studies.) For the cascade system of two reactors, the organic liquid product of the ketonization reactor was collected over a period of time and then used as the feed for the aldol condensation/hydrogenation reactor, whereas the inter-oil feed was supplied continuously to the dual-bed, single-reactor catalyst system. Preparation of Ce₁Zr₁O_x and Pd/ZrO₂ catalysts and the experimental set-up for the cascade and dual-bed systems are described in the Electronic Supplementary Information, and detailed characterization results can be found elsewhere.^{7,9} For both reactor systems, the effluent stream obtained from the aldol condensation/hydrogenation step consisted of a mixture of ketones and alkanes that could not be readily separated in the GC and GC-MS. Accordingly, these streams were subjected to dehydration/hydrogenation reaction over a 2 wt% Pt/SiO₂–Al₂O₃ catalyst (denoted as Pt/SiAl) to obtain a mixture of linear and branched alkanes only, which are well separated in the GC.

Table 1 Molar carbon distribution for the conversion of 60 wt% sorbitol solution over Pt–Re/C at 503 K and 18 bar with WHSV = 0.6 h⁻¹

Phases	Carbon distribution (%)
Organic (Inter-oil)	51
Gaseous	39
Aqueous	10
Species in the organic liquid (Inter-oil)	Carbon distribution in the organic liquid (Inter-oil) (%)
Alkanes	1
2-ketones	21
2-butanone	3
2-pentanone	7
2-hexanone	11
3-ketones	10
3-pentanone	3
3-hexanone	7
2° alcohols	15
2-butanol	3
2-pentanol	5
2-hexanol	7
3° alcohols	5
3-pentanol	2
3-hexanol	3
1° alcohols	1
1-butanol	1
Heterocyclics	30
Tetrahydrofuran (THF)	3
2-Methyl-THF	7
Tetrahydropyran (THP)	2
2-Methyl-THP	3
2,5-DiMethyl-THF	9
2-Ethyl-THF	6
Carboxylic Acids	17
Butanoic acid	9
Pentanoic acid	5
Hexanoic acid	3

Fig. 1 shows reaction pathways involved in ketonization, aldol condensation/hydrogenation and dehydration/hydrogenation for representative C₅ species. Acids combine in ketonization reactions to form linear ketones, CO₂ and water, whereas ketones and alcohols combine in aldol condensation/hydrogenation reactions to form branched ketones and water. Under our reaction conditions, secondary alcohols are equilibrated with the corresponding ketones through metal (Pd) catalyzed dehydrogenation reactions. The condensation of alcohols is thus initiated by dehydrogenation to form ketones. Similarly, primary alcohols can be condensed by the intermediate formation of aldehydes. When 2-ketones and/or secondary alcohols are combined, single methyl-branched ketones are obtained. When a 3-ketone/alcohol combines with a 2-ketone/alcohol, single ethyl branched ketones can be obtained. Finally, when 3-ketones or tertiary alcohols undergo self-coupling, multiple branching in the product ketone takes place. Ring opening reactions of heterocyclics can also take place over Pd/ZrO₂ to form aldehydes or ketones, depending on the structure of

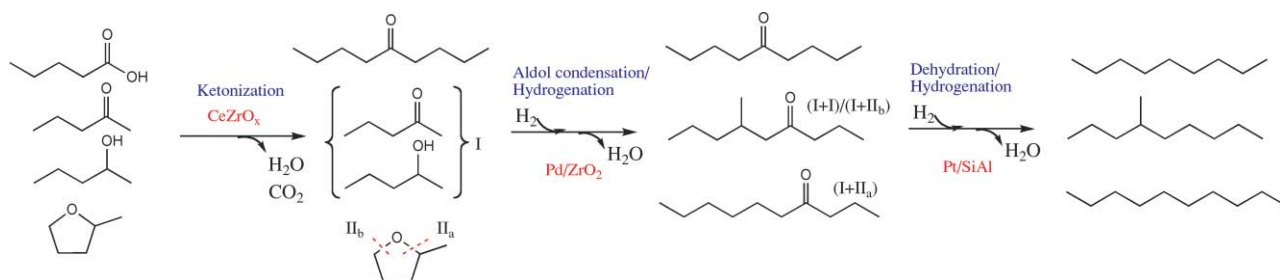


Fig. 1 Reaction pathways for ketonization, aldol condensation/hydrogenation and dehydration/hydrogenation for representative C₅ species. Species II_a and II_b are formed by ring-opening through C–O bond cleavages denoted in the figure.

the heterocyclic molecule and the location of C–C cleavage in the molecule. An aldehyde formed in this manner can couple with 2-ketones to form other linear ketones. In addition to coupling reactions, mono-functional species are also converted into alkanes over Pd/ZrO₂. As mentioned earlier, ketones are in equilibrium with the corresponding alcohols under our reaction conditions, and alkanes can be formed by α -scission over Pd sites and/or dehydration/hydrogenation of these alcohols over acid/metal sites. This latter pathway is important for Pd/ZrO₂ in view of the high concentration of acid sites for this catalyst,⁹ leading to the formation of alkanes especially at low space velocities. The distributions of carbon in the effluent streams from various reactors involved in the overall conversion of sorbitol to hydrocarbons are shown in Fig. 2A and 2B, starting from the conversion of the sorbitol solution over Pt–Re/C, followed by upgrading processes in the cascade

system (Fig. 2A) or the dual-bed catalyst system (Fig. 2B). Table 2 summarizes the values for overall conversion of mono-functional species and the overall yield of C₇₊ species, together with the selectivity values. In the cascade system, acids are completely converted to heavier linear ketones (C₇–C₁₁) in the ketonization reactor over Ce₁Zr₁O_x. Approximately 7% of the carbon leaves the ketonization reactor in the gaseous phase, and 20% and 40% of this gas stream consists of C₁–C₆ alkanes and CO_x respectively, with the remainder being present as mono-functional species. The liquid stream consists of heavy linear ketones and unreacted mono-functional species. This stream is then subjected to aldol condensation/hydrogenation over Pd/ZrO₂ in a separate reactor. The extent of alkane formation is more significant for this reactor, such that 19% of the carbon fed to the reactor leaves in the gas phase, 86% of this gas stream being present as light alkanes. In addition, 11% of the inlet

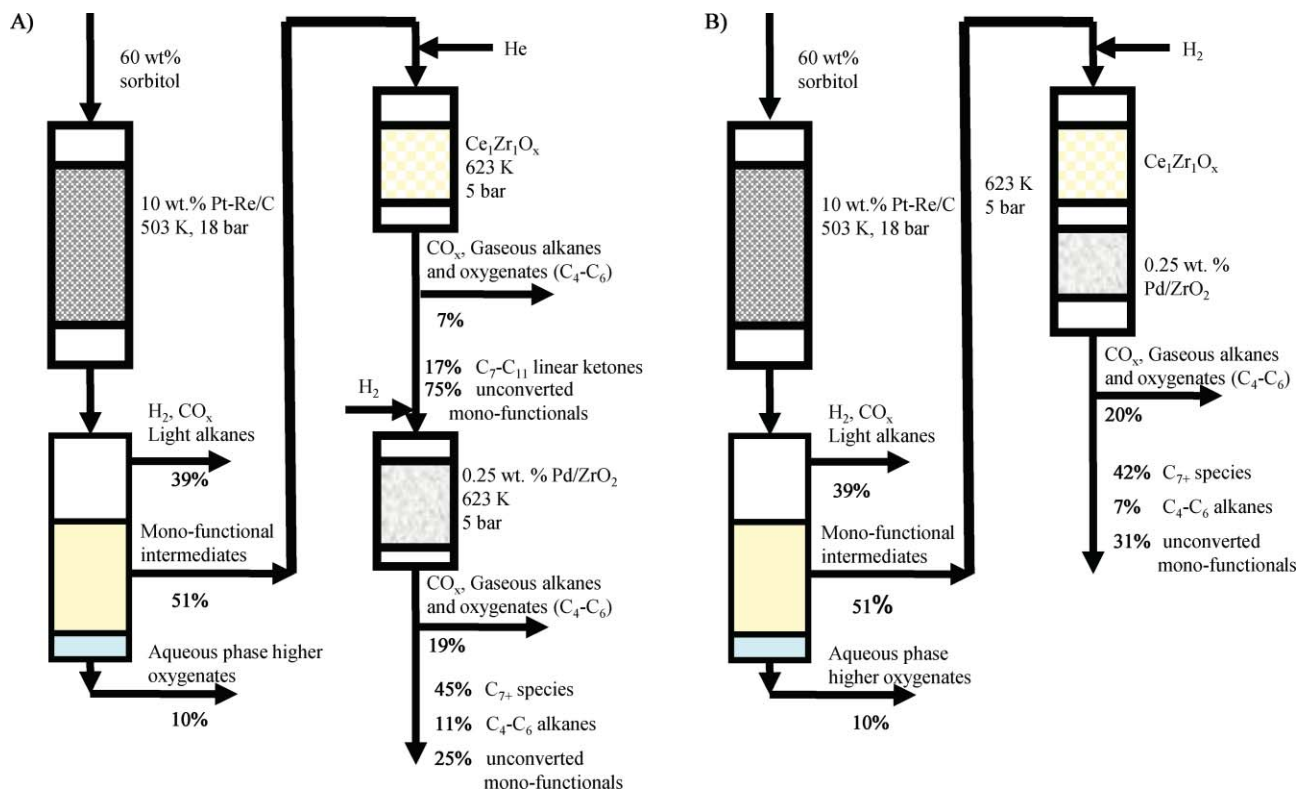


Fig. 2 Distribution of carbon for conversion of 60 wt% sorbitol solution over Pt–Re/C, ketonization of mono-functional intermediates over Ce₁Zr₁O_x (WHSV = 0.24 h⁻¹) followed by aldol condensation/hydrogenation over 0.25 wt% Pd/ZrO₂ (WHSV = 0.48 h⁻¹) A) in a cascade system and B) in a dual-bed catalyst system.

Table 2 Comparison of dual-bed catalyst system and cascade system for conversion of mono-functional compounds

	Dual-bed system	Cascade system
Overall conversion of mono-functional species (%)	66	71
Selectivity of C ₇₊ products (%)	61	55
Selectivity of light alkanes (%)	36	38
Loss of mono-functional species to gas phase (%)	3	7
Overall yield to C ₇₊ products (%)	42	42
Branched ketones/linear ketones	1.04	0.96

carbon exits in the liquid stream as C₄–C₆ alkanes. The product C₇₊ species consist of both ketones and alkanes. The overall yield to C₇₊ species based on the inter-oil feed is 42%, with 71% conversion of the mono-functional species. The reported selectivities are based on the difference between the amount of mono-functional species in the feed and amount present in the liquid effluent of the aldol condensation reactor. It is calculated that 7% of the mono-functional species is lost to the gas phase, 55% is converted to C₇₊ species, and 38% is converted into C₁–C₆ alkanes. In the dual-bed catalyst system, about 20% of the carbon feed leaves the reactor in the gas phase, only 14% of this gas stream being unconverted mono-functional intermediates. The remainder of the gas phase consists of C₁–C₆ alkanes (76%) and CO_x (10%). In addition, 7% of the inlet carbon leaves the reactor as C₄–C₆ alkanes in the liquid stream. The rest of the liquid stream consists of C₇₊ species and unconverted mono-functional species, corresponding to 42% and 31% of the inlet carbon, respectively. The overall yield for the dual-bed system is 42%, with 66% conversion of mono-functional species. Selectivity values and loss of mono-functional species to the gas phase are calculated the same way as in the cascade system, and these values are shown in Table 2. It is apparent from the data in Table 2 that the performance of the two reactor systems is essentially the same. The dual-bed, single reactor system is thus the preferred mode of catalytic upgrading, because the energy consumption as well as the reactor infrastructure associated with cooling and re-heating the products obtained from ketonization prior to the aldol condensation/hydrogenation step can be eliminated.

As mentioned earlier, both of the effluent streams from aldol condensation/hydrogenation were subjected to dehydration/hydrogenation reactions over Pt/SiAl. The catalyst preparation and experimental setup are described in the Electronic Supplementary Information.† In this way, linear alkanes and branched alkanes could be separated from each other and the corresponding ketones could be quantified. The ratios of branched to linear ketones for the two reactor configurations are shown in Table 2, and both ratios are approximately equal to 1. The concentration of linear ketones formed by ketonization is known from the effluent of the ketonization reactor of the cascade system. If the rest of the C₇₊ species in the final effluent were branched species formed by the condensation of ketones and alcohols, this ratio would be about 1.36. This comparison suggests that linear ketones are also formed during the aldol condensation step. For example, these linear ketones can be formed from the aldol condensation of 2-ketones with aldehydes generated by ring-opening reactions of heterocycles, as shown

Table 3 Carbon distribution among C₇₊ alkanes obtained from dehydration/hydrogenation over Pt/SiAl at 573 K, 28.5 bar, WHSV = 0.48 h⁻¹

Species	Carbon distribution (%)	
	Dual-bed system	Cascade system
C ₇	12	15
C ₈	17	17
C ₉	18	18
C ₁₀	18	18
C ₁₁	14	16
C ₁₂	12	9
C ₁₂₊	9	8

in Fig. 1. Ring-opening reactions of heterocyclic species have, in fact, been reported in the literature.¹¹ In addition, among the branched ketones or alkanes, only small amounts of single, ethyl-branched species are formed, showing that coupling of 2-ketones or alcohols are more favorable compared to coupling of 3-ketones/alcohols with 2-ketones/alcohols. Finally, the absence of species containing two branches indicates that coupling among 3-ketones/alcohols is not favorable. It is important to note that ketonization and aldol condensation reactions are unique routes to achieve C–C coupling, leading to reaction products that are valuable for Diesel fuel production, as the extent of branching in the high molecular weight alkanes is minimized and controlled, in contrast to acid-catalyzed coupling processes such as oligomerization of olefins.¹²

Dehydration/hydrogenation reactions are employed to convert the ketones obtained in the upgrading processes into fuel-grade alkanes. In this process, ketones are hydrogenated to corresponding alcohols, followed by dehydration on acid sites to form alkenes which are then hydrogenated to alkanes on metal sites. We have studied dehydration/hydrogenation reactions of simulated mixtures of mono-oxygenated species over Pt/SiAl at various temperatures and pressures to minimize the extent of C–C cleavage reactions while maintaining complete conversion of mono-oxygenated species to alkanes. The optimal conditions for operation are 573 K and 28.5 bar. Table 3 shows the distribution of C₇₊ alkanes in the liquid phase obtained over the Pt/SiAl catalyst at these reaction conditions for both reactor configurations. It is interesting to note that 10% of C₇₊ alkanes are present as branched cyclic alkanes for both reactor configurations, resulting from cyclization reactions of olefins¹³ produced from the dehydration of alcohols.

In summary, we demonstrate here that a dual-bed, single reactor catalyst system can be used to achieve effective C–C coupling processes to upgrade biomass-derived mono-functional species. In this dual-bed catalyst system, a Ce₁Zr₁O_x catalyst is used to achieve ketonization of carboxylic acids, followed by a Pd/ZrO₂ catalyst to carry out aldol condensation/hydrogenation reactions. Importantly, this Pd/ZrO₂ catalyst operates effectively in the presence of CO₂ and water formed during upstream ketonization reactions. This integration of two separate C–C coupling reactions in a single reactor is desirable for streamlining the overall process and reducing capital and operating costs. More generally, this single-reactor upgrading strategy can be applied to other biomass-derived oils that contain carboxylic acids, ketones and alcohols. The major difference of this work

compared to the work of Blommel *et al.*³ is the integrated C–C coupling route to utilize both acids and ketones/alcohols in the biomass-derived mono-functional stream to increase the amount of fuel-grade components in the final effluent. Finally, this strategy for achieving C–C coupling, combined with a dehydration/hydrogenation step, produces a mixture of linear and singly branched alkanes that is desirable for Diesel fuel applications.

Notes and references

- 1 B. West, K. Knoll, W. Clark, R. Graves, J. Orban, S. Przesmitzki and T. Theiss, *Effects of Intermediate Ethanol Blends on Legacy Vehicles and Small Non-Road Engines* National Renewable Energy Laboratory, 2008.
- 2 E. L. Kunkes, D. A. Simonetti, R. M. West, J. C. Serrano-Ruiz, C. A. Gaertner and J. A. Dumesic, *Science*, 2008, **322**, 417–421.
- 3 P. G. Blommel, G. R. Keenan, R. T. Rozmiarek and R. D. Cortright, *Int. Sugar J.*, 2008, **110**, 672–679.
- 4 O. Nagashima, S. Sato, R. Takahashi and T. Sodesawa, *J. Mol. Catal. A: Chem.*, 2005, **227**, 231.
- 5 A. A. Nikolopoulos, B. W. L. Jang and J. J. Spivey, *Appl. Catal., A*, 2005, **296**, 128–136.
- 6 J. N. Chheda and J. A. Dumesic, *Catal. Today*, 2007, **123**, 59–70.
- 7 E. L. Kunkes, E. I. Gurbuz and J. A. Dumesic, *J. Catal.*, 2009, **206**, 236–249.
- 8 R. M. West, E. L. Kunkes, D. A. Simonetti and J. A. Dumesic, *Catal. Today*, 2009, **147**, 115–125.
- 9 E. I. Gürbüz, E. L. Kunkes and J. A. Dumesic, *Appl. Catal. B: Environ.*, 2009, DOI: 10.1016/j.apcatb.2009.11.001.
- 10 E. L. Kunkes, D. A. Simonetti, J. A. Dumesic, W. D. Pyrz, L. E. Murillo, J. G. Chen and D. J. Buttrey, *J. Catal.*, 2008, **260**, 164–177.
- 11 K. Kreuzer and R. Kramer, *J. Catal.*, 1997, **167**, 391–399.
- 12 C. T. O'Connor and M. Kojima, *Catal. Today*, 1990, **6**, 329–349.
- 13 M. Guisnet, N. S. Gnep, D. Aittaleb and Y. J. Doyemet, *Appl. Catal. A*, 1995, **87**, 255–270.

Highly selective hydrogenation of aromatic chloronitro compounds to aromatic chloroamines with ionic-liquid-like copolymer stabilized platinum nanocatalysts in ionic liquids

Xiao Yuan,^a Ning Yan,^{a,b} Chaoxian Xiao,^a Changning Li,^a Zhaofu Fei,^b Zhipeng Cai,^a Yuan Kou^{*a} and Paul J. Dyson^{*b}

Received 29th July 2009, Accepted 17th November 2009

First published as an Advance Article on the web 18th January 2010

DOI: 10.1039/b915299g

Platinum nanoparticles (PtNPs stabilized by an ionic-liquid-like-copolymer (IP) immobilized in various ionic liquids (ILs)) effectively catalyze the selective hydrogenation of aromatic chloronitro compounds to aromatic chloroamines, a reaction of considerable commercial significance. The preparation of 2,4-dichloro-3-aminophenol (DAP) has been primarily studied due to its important industrial applications. DAP is usually prepared from 2,4-dichloro-3-nitrophenol (DNP) by reduction with hydrogen using Ni- or Pt-based catalysts. Compared to reactions in molecular (organic) solvents, the ILs system provides superior selectivity with functionalized ILs containing an alcohol group demonstrating the best recyclability, and ultimately achieving a turnover number of 2025 which is 750 fold higher than Raney nickel catalyst. A universal catalyst–ionic liquid system for the conversion of aromatic chloronitro compounds to aromatic chloroamines was also established. TEM, XPS, IR spectroscopy were used to characterize the morphology of the nanocatalysts allowing their structure to be correlated to their activity.

Introduction

Hydrogenation reactions catalyzed by transition metal nanoparticles (NPs) immobilized in ionic liquids (ILs) have been extensively explored in recent years.^{1–6} Nanoparticles composed of first row transition metals including Co⁷ and Ni,⁸ and second and third row transition metals including Ru,^{9–16} Rh,^{7,12,17–23} Ir,^{7,12,17,21,24–30} Pd,^{18,31–34} and Pt,^{18,35–37} have been successfully immobilized in ILs and evaluated in different hydrogenation reactions. NPs suspended in ILs have also been used as catalysts³⁸ and catalyst reservoirs^{39–41} in a range of other reactions. The advantage of these ‘soluble’ NP–ILs systems in catalysis corresponds to their high activity, selectivity and recyclability. In some cases the ILs themselves behave as effective NP stabilizers, as demonstrated by Dupont *et al.*, nevertheless it has been shown that additional stabilizers can further enhance catalytic performance in certain reactions.^{3,19} Polyvinyl pyrrolidone (PVP) is the most commonly used NP stabilizer, but due to its poor solubility in ILs is only of limited use. Two strategies have previously been used to overcome this limitation. First, an ‘IL-like’ copolymer formed from the copolymerization of the PVP monomer and a vinylimidazolium unit is highly IL soluble,¹⁹ and second, hydroxyl-functionalized ILs effectively

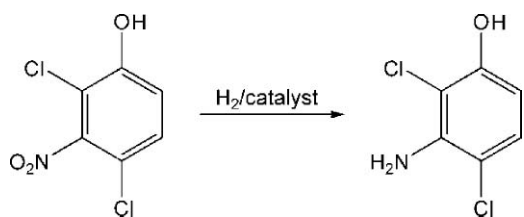
dissolve PVP.^{23,42–44} Both approaches were found to be highly effective, providing stable IL soluble NPs, which exhibit long lifetimes leading to high turnover numbers in hydrogenation reactions.

NP–IL systems also exhibit excellent regioselectivity in the hydrogenation of complex substrates and also inhibit side reactions such as dehalogenation. For example, o-chloroaniline may be obtained in quantitative yield from o-chloronitrobenzene using a NP–IL system, whereas considerable dehalogenation is observed in molecular solvents.³⁷ DFT calculations combined with IR spectroscopy showed that the exceptional selectivity arises from strong interactions between the IL cation and the nitro group of the substrate, thereby activating it selectively. Similarly, the selective hydrogenation of cinnamic aldehyde to cinnamyl alcohol has been demonstrated using a NP–IL system.⁴⁵

The selective hydrogenation of aromatic chloronitro compounds to aromatic chloroamines is a reaction of considerable commercial significance. Prins *et al.* published an alternative method⁵⁵ to reduce aromatic nitro compounds with hydrazine in the presence of an iron oxide catalyst and high selectivity was obtained. However, the disadvantage of this method is the danger of handling hydrazine. Notably, 2,4-dichloro-3-aminophenol (DAP) is a fine chemical with a high added-value usually prepared from 2,4-dichloro-3-nitrophenol (DNP) by reduction with hydrogen using Ni- or Pt-based catalysts (Scheme 1). The selective reduction of DNP to DAP is much more challenging than o-chloronitrobenzene, since it has four substituents attached to the aromatic ring, and there is a greater probability of dehalogenation side reactions taking place. Many patents and papers describe the preparation and use of DAP,^{46–48} nevertheless the catalytic efficiencies described tend to be poor.

^aPKU Green Chemistry Centre, Beijing National Laboratory for Molecular Sciences, College of Chemistry and Molecular Engineering, Peking University, Beijing, 100871, China. E-mail: yuankou@pku.edu.cn; Fax: +86 10 62751708; Tel: +86 10 62757792

^bInstitut des Sciences et Ingénierie Chimiques, Ecole Polytechnique Fédérale de Lausanne (EPFL), CH-1015, Lausanne, Switzerland. E-mail: paul.dyson@epfl.ch; Fax: +41 21 693 98 85; Tel: +41 21 693 98 54



Scheme 1 Catalytic synthesis of 2,4-dichloro-3-aminophenol *via* hydrogenation of 2,4-dichloro-3-nitrophenol. The synthesis is usually accompanied by significant dechlorination side-reactions.

For example, the turnover number (TON) of Raney Ni in ethanol is around 3 with a selectivity of 70%. Based on the promise shown by NP–IL systems in selective hydrogenation reactions, especially for selectivity towards nitro-groups, we decided to evaluate their application in the reduction of DAP to DNP. Herein we describe the outcome of this study which shows that a PtNP–IL system exhibits excellent selectivity toward the desired product. Moreover, using functionalized ILs a TON of 2025 with a selectivity of 100% was achieved. The same catalyst system may also be used to convert a range of aromatic chloronitro compounds to aromatic chloroamines.

Experimental

Synthesis of the copolymer and ILs

The ionic-liquid-like-copolymer (IP)¹⁹ and ILs [Bmim][PF₆], [Bmim][BF₄], [C₂OHmim][BF₄], were prepared according to literature methods.⁴⁹

Nanoparticle preparation

PtNPs were prepared using a published method.⁵⁰ In brief, NaOH (0.1 g, 2.5 × 10⁻³ mol) dispersed in ethylene glycol (5 mL) was added to H₂PtCl₆·6H₂O (0.1 g, 1.9 × 10⁻⁴ mol) in ethylene glycol (5 mL). The mixture was heated to 433 K for 3 h under argon affording a dark-brown solution.

Pt catalysts: The system was achieved by combining a 7.2 × 10⁻⁶ mol of the PtNP (0.38 mL ethylene glycol solution), IP or PVP (3.6 × 10⁻⁵ mol) with the appropriate solvent (5.0 mL).

Catalytic hydrogenation of aromatic chloronitro compounds

Hydrogenation of aromatic chloronitro compounds was performed at 363 K and 1.0 MPa of hydrogen in a stainless-steel autoclave (10 mL). Typically, the substrate (1.8 × 10⁻³ mol) and PtNP–IL solution (7.2 × 10⁻⁶ mol) were added in the autoclave, the autoclave charged with hydrogen, and then sealed and stirred for 2 h at 363 K. After reaction, diethyl ether (15 × 4 mL) was added to extract the products. The products were then analyzed on an Agilent 6820 gas chromatograph and Agilent 5975C/7890A GC-MS.

Characterization of the PtNPs

High-resolution transmission electron microscopy (HRTEM) measurements. HRTEM measurements were carried out on a Hitachi H-9000 electron microscope operated at 300 kV. The PtNPs were dispersed in methanol following their separation from the ILs by centrifugation. One drop of the solution was

placed onto a copper grid coated by a carbon film and dried under vacuum at 343 K for 24 h to remove any solvent, and used for HRTEM measurements. The average particle size of the PtNPs was determined from *ca.* 300 NPs.

X-ray photoelectron spectroscopy (XPS). XPS measurements were carried out using an Axis Ultra photoelectron spectrometer using an AlK α (1486.7 eV) X-ray source, with the pressure of the measuring chamber set at 5 × 10⁻⁹ Torr. The binding energy scales for the samples were referenced by setting the C 1 s binding energy of contamination carbon to 284.8 eV. Samples 1 and 2 (in Fig 4) were obtained by mixing the ILs with the fresh PtNPs and pretreated using a literature method,⁵⁰ and dripping the mixture on a piece of sheet copper. Samples 3 and 4 were made by centrifuging the PtNPs after reaction and fixing the PtNPs on a piece of sheet copper.

Fourier-transform infrared spectroscopy (FTIR). The samples were prepared by mixing DNP (0.005 g) with the appropriate solvent (0.10 mL). IR spectra of one drop of the solution dispersed on KBr windows were recorded on a Vector27 Bruker instrument with a resolution of 1.0 cm⁻¹.

IR-H₂S probe characterization of the catalysts. PtNP samples were prepared in the same way as Samples 1 and 2 for XPS measurement. The PtNP were placed into a flask under 0.1 MPa of H₂S and stirred for 1 h. An IR spectrum of one drop of the solution dispersed on CaF windows was recorded on a Vector27 Bruker instrument with a resolution of 1.0 cm⁻¹. An IR spectrum of the sample was obtained by subtracting the IR spectrum before H₂S adsorption.

Results and discussion

Hydrogenation of aromatic chloronitro compounds

PtNPs prepared according to a literature procedure were mixed with the IP or PVP in various solvents and evaluated as catalysts for the hydrogenation of DNP. For comparison purposes, Pt immobilized on activated carbon (Pt/AC) in methanol was evaluated in the same reaction. The results from these studies are summarized in Table 1.

The selectivity for DAP catalyzed by 5wt% Pt/AC was 88.7%, with extensive dehalogenation observed, giving 2-chloro-3-aminophenol (MAP) in significant quantities. Using the PtNP–methanol solution, DNP underwent quantitative conversion, but the selectivity for DAP was even lower. These results are not too dissimilar to those reported previously, notably that Raney Ni in ethanol catalyzes the hydrogenation of DNP with a selectivity of only 70.4% for the desired product.⁴⁶ Based on the low selectivity obtained in organic solvents the hydrogenation of DNP was assessed in ILs, including [Bmim][PF₆], [Bmim][BF₄] and [C₂OHmim][BF₄]. Under equivalent reaction conditions a dramatic improvement in selectivity was observed in all three ILs. Side (dehalogenation) reactions were suppressed and DAP was obtained in essentially quantitative yield.

It has previously been shown that dehalogenation is favored at high temperatures, usually occurring after reduction of the nitro-group,^{51,52} with the selectivity decreasing with reaction time and temperature. The reaction was therefore continued for 4, 8 and 12 hours (Table 1, entries 8, 9 and 10), albeit at a slightly reduced

Table 1 Hydrogenation of DNP^a

Entry	Catalyst	Solvent	Stabilizer	Reaction time (h)	Reaction temperature (K)	Conversion (%)	Selectivity (%)		
							DAP	MAP	other
1	Pt/AC(5wt.%)	CH ₃ OH	-	2	363	99.0	88.7	7.8	-
2	Pt	CH ₃ OH	PVP	2	363	100	66.0	1.9	30.0
3 ^b	Raney Ni	CH ₂ CH ₃ OH	-	-	313	-	70.4	-	-
4	Pt	[Bmim][PF ₆]	IP	2	363	95.8	99.9	<0.1	-
5	Pt	[Bmim][BF ₄]	IP	2	363	100	99.9	<0.1	-
6	Pt	[C ₂ OHmim][BF ₄]	IP	2	363	100	99.9	<0.1	-
7	Pt	[C ₂ OHmim][BF ₄]	PVP	2	363	100	99.9	<0.1	-
8	Pt	[Bmim][BF ₄]	IP	4	343	94.7	99.9	<0.1	-
9	Pt	[Bmim][BF ₄]	IP	8	343	100	99.9	<0.1	-
10	Pt	[Bmim][BF ₄]	IP	12	343	100	99.9	<0.1	-
11	Pt	[Bmim][BF ₄]	IP	4	303	6.5	99.9	<0.1	-
12	Pt	[Bmim][BF ₄]	IP	4	383	100	99.9	<0.1	-
13	Pt	[Bmim][BF ₄]	IP	4	423	100	98.1	1.7	-

^a Reaction conditions: solvent (5 mL), Pt (7.2×10^{-3} mmol), DNP (1.8×10^{-3} mol), H₂ (1.0 MPa), IP/PVP:Pt = 5:1. ^b From ref. 46. Reaction conditions: ethanol (900 mL), Ni (9.0 g), DNP (85 g), H₂ (2.0 MPa).

Table 2 Hydrogenation of various nitroarene substrates to their corresponding amines in [C₂OHmim][BF₄]

Entry	Substrate	Cat./Sub. ratio	Conversion (%)	Selectivity (%)
1	2,6-dichloro-4-nitrophenol	250	100	99.9
2	4-chloro-2-nitrophenol	250	100	99.0
3	1,4-dichloro-2-nitrobenzene	250	100	97.9
4	2,6-dichloro-3-nitrotoluene	250	100	100
5	2,4-dichloro-6-nitroaniline	250	100	98.0

Reaction conditions: [C₂OHmim][BF₄] (5 mL), Pt (7.2×10^{-3} mmol), substrate (1.8 mmol), H₂ (1.0 MPa) at 363 K, IP:Pt = 5:1.

temperature, showing that selectivity is essentially quantitative, merely with the conversion increasing. The effect of temperature was also explored, with the hydrogenation conducted at 303, 343, 383 and 423 K (Table 1, entries 11, 8, 12 and 13). The reaction was sluggish at 303 K (conversion < 10%), whereas at temperatures of 343 K and 383 K high conversions were observed with the selectivity for DAP being quantitative. The selectivity of DAP decreased slightly as the reaction temperature was increased further (to 423 K). Nevertheless, for the selective hydrogenation of DNP to DAP the PtNP-IL systems are superior, compared to catalysts operating in molecular solvent.

The IP protected PtNP in [C₂OHmim][BF₄] showed high conversion and perfect selectivity, so further substrates were evaluated using this system (see Table 2). Although the substrates contain different substituent groups, excellent selectivity to the corresponding aromatic chloroamines was achieved in all cases.

The improved selectivity observed for the hydrogenation of nitro groups in ILs was previously attributed to weak non-covalent interactions formed between the ILs and the nitro group, as evidenced by IR spectroscopy and corroborated by DFT calculations.³⁷ It is not unreasonable to assume that the reason for the exceptional selectivity observed here for the conversion of DNP to DAP (and other related substrates) is also due to hydrogen bonding between the ILs and nitro

group thereby preferentially activating this group. To verify this hypothesis IR spectra of DNP dissolved in both ILs and molecular solvents were recorded, see Fig 1. The asymmetric stretching vibration of the nitro (O=N=O) group of DNP in methanol is observed at 1552 cm⁻¹. In toluene the ν_{N=O} vibration is almost unchanged (1551 cm⁻¹), indicating that the change in polarity of the solvent has little influence on the strength of the N=O bonds. However, there is a significant red shift to 1547 ± 1 cm⁻¹ in the three ILs, implying that the N=O bonds are slightly weakened (and activated) in the ILs. The stretching vibration of the C-Cl bonds in DNP (Fig 1b) are identical in all five solvents indicating that the nature of solvent does not influence the C-Cl bond strength. Thus, the weak interaction between the nitro group in DNP and the ILs probably contributes to the higher selectivity for the reaction in these solvents.

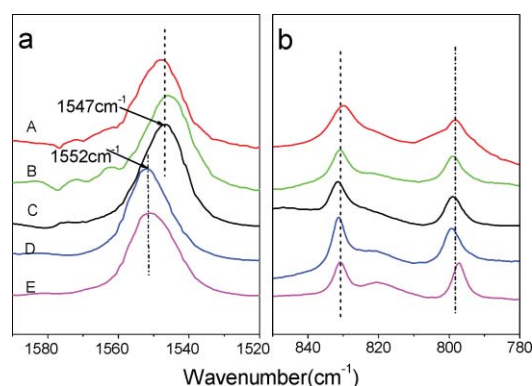


Fig. 1 IR spectra of (a) the asymmetric vibrations of the nitro groups and (b) the carbon-chlorine bond of DNP in (A) [Bmim][PF₆], (B) [Bmim][BF₄], (C) [C₂OHmim][BF₄], (D) methanol, and (E) toluene.

Catalyst recycling

The ability to reuse the PtNP-IL systems was also investigated. After catalysis, the product(s) were extracted into diethyl ether, and the remaining PtNP-IL solution was charged with reactants for a subsequent hydrogenation. The recyclability of

PtNP-[Bmim][BF₄] and PtNP-[C₂OHmim][BF₄] solutions in the hydrogenation of DNP are shown in Fig 2.

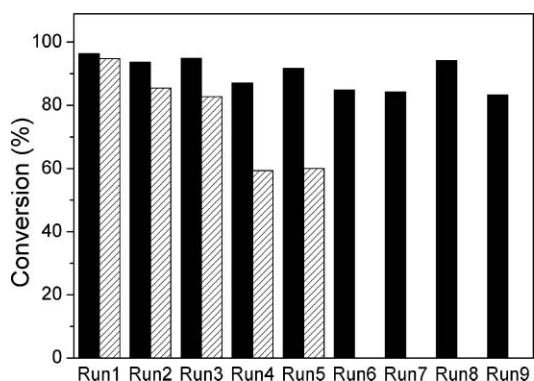


Fig. 2 Recycling of the Pt-[C₂OHmim][BF₄] (black) and Pt-[Bmim][BF₄] (grey) systems in the hydrogenation of DNP. Reaction condition: temperature 343 K; hydrogen pressure 1.0 MPa; reaction time 2 h; DNP 0.9 mmol; 3.6×10^{-3} mmol of PtNP (IP:Pt = 5:1) in IL (5 mL).

The selectivity of the reaction was maintained at 100% throughout the recycling for both systems, demonstrating the excellent control of the PtNP-IL systems with respect to selectivity. However, in case of the PtNP-[Bmim][BF₄] system the conversion steadily decreased during five runs, from *ca.* 95 to 60%. In comparison, the PtNP-[C₂OHmim][BF₄] system exhibits much better recycling characteristics and after 9 batches the conversion exceeds 80%, reaching a turnover number (TON) of 2025, which is 750 fold greater than the TON obtained using Raney Ni.⁴⁶

Characterization of the PtNPs by TEM and XPS

One of the main problems associated with NP catalysis is that NPs are kinetically stable and therefore tend to aggregate during reaction, thereby becoming less active. ILs have been shown to help stabilize NPs, and in certain studies it has been shown that ILs with functional groups such as hydroxyl or nitrile groups, may further enhance the stability of the NPs as they can form additional interactions with the NP surface. In the case of the PtNP-[Bmim][BF₄] system described herein, aggregation of the PtNP has been confirmed by TEM (Fig 3), presumably leading to the deterioration in catalytic activity during the recycling experiments. The PtNPs prepared in [Bmim][BF₄] have

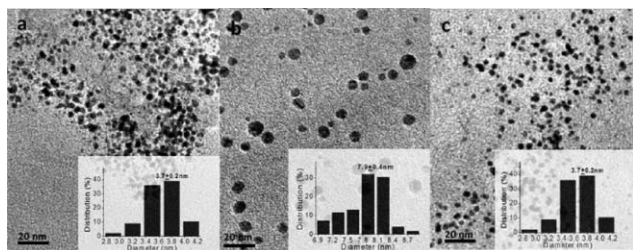


Fig. 3 TEM micrographs (scale bar = 20 nm) and size distribution of (a) PtNPs prepared in [Bmim][BF₄], (b) PtNPs after five catalytic cycles in [Bmim][BF₄] and (c) PtNPs after nine catalytic cycles in [C₂OHmim][BF₄].

an average particle size of 3.7 ± 0.2 nm, which after five catalytic cycles increases to 7.9 ± 0.4 nm. In [C₂OHmim][BF₄] aggregation of the PtNPs is scarcely observed; the average size of PtNPs prepared in [C₂OHmim][BF₄] is 3.7 ± 0.2 nm and after nine reaction cycles an average size of 3.8 ± 0.4 nm is observed.

XPS measurements (Fig 4) were carried on the PtNPs in an attempt to establish why the PtNPs immobilized in [C₂OHmim][BF₄] are more stable than those in [Bmim][BF₄]. The binding energy of the Pt 4f_{7/2} core-level in the PtNP-[Bmim][BF₄] system has a value of 72.2 eV, 0.5 eV higher than in the PtNP-[C₂OHmim][BF₄] system (71.7 eV). Although binding energies are sensitive to the average valency and size of the NP, the difference observed here cannot be attributed to these factors. The lower binding energy of the PtNPs in [C₂OHmim][BF₄] suggests that additional electron transfer from the IL to the PtNPs is evident. After five catalytic cycles the 4f_{7/2} core-level of PtNPs in [Bmim][BF₄] changes from 72.2 eV to 70.7 eV (C), a dramatic shift towards the metallic state of Pt, and in accord with the TEM analysis that shows PtNP aggregation (see below). In contrast, after nine cycles the 4f_{7/2} core-level value of the PtNPs in [C₂OHmim][BF₄] is 71.4 eV, almost the same value observed for the freshly prepared PtNPs. The constant binding energy for the PtNPs in [C₂OHmim][BF₄] provides additional evidence for the high stability of the PtNPs with respect to both their size and surface state. The XPS measurements, together with the TEM analysis, suggest that the hydroxyl groups in [C₂OHmim][BF₄] interact with the PtNPs helping to stabilize them. Indeed, alcohol functionalized ILs have been shown to be excellent media for the preparation of gold NPs.⁵³

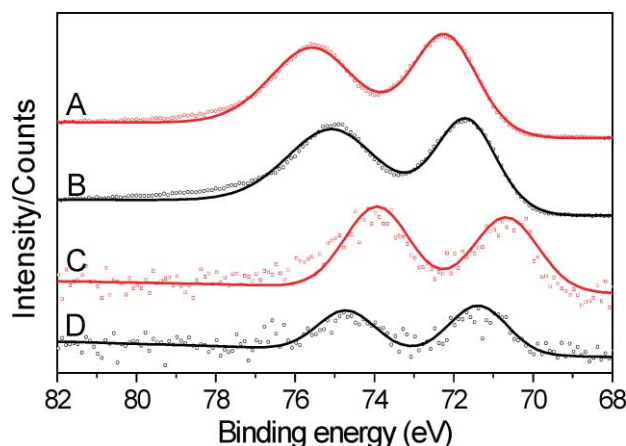


Fig. 4 Pt (4f) region of (a) Pt-[Bmim][BF₄] before catalysis, (b) Pt-[C₂OHmim][BF₄] before catalysis, (c) Pt-[Bmim][BF₄] after catalysis, (d) Pt-[C₂OHmim][BF₄] after catalysis.

Additional evidence for the interaction of OH groups with the surface of the PtNP is obtained from IR spectroscopy using H₂S as a probe molecule⁵⁴ (Fig 5).

In [C₂OHmim][BF₄], the antisymmetric and symmetric vibrations of H₂S were more overlapped than the case of Bmim[BF₄], probably due to the formation of hydrogen bonding between H₂S and OH groups. In Pt-Bmim[BF₄], the γ (SH) wavenumber for the symmetric and antisymmetric vibrations are 2588 cm⁻¹ and 2604 cm⁻¹ (A) respectively. In Pt-[C₂OHmim][BF₄] (B), however, both peaks display a blue shift to 2592 cm⁻¹ and 2607 cm⁻¹,

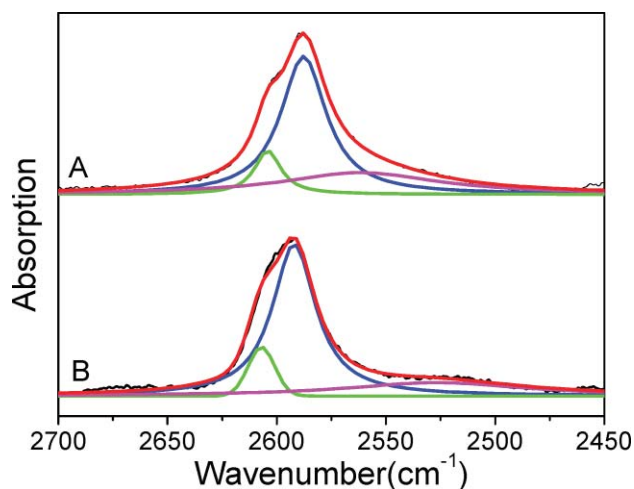


Fig. 5 IR spectra of H₂S adsorbed on PtNPs (raw data, black line), fitting of symmetric vibrations of H₂S (blue line), fitting for antisymmetric vibrations of H₂S (green line) after the adsorption of H₂S on (A) PtNP-[Bmim][BF₄] and (B) Pt-[C₂Omim][BF₄] (difference spectra: after H₂S adsorption minus spectrum without H₂S – pink line). The red line corresponds to the sum of the blue and green lines.

suggesting the OH groups in [C₂OHmim][BF₄] help to weaken the interaction of H₂S on the surface of the PtNPs. The H₂S-IR test gave further evidence for the presence of weak interactions between the PtNPs and OH groups in the IL. Moreover, the experiment indicates that the PtNPs in the hydroxyl group functionalized IL is poison resistant as it weakens the adsorption of poison (H₂S) molecule to the metal surface.

Conclusions

A highly effective PtNP-IL system has been established for the selective synthesis of aromatic chloroamines from aromatic chloronitro compounds. Compared to other catalytic systems employing NPs or heterogeneous catalysts operating in molecular organic solvents, the PtNP-IL systems described herein exhibit excellent selectivity to the desired product, and the hydroxyl-functionalized IL system, display excellent stability allowing extensive recycling and high turnover numbers. This system provides a further example of an IL-catalyst regime which offers environmental benefits in terms of eliminating organic solvents from the catalytic process, although on this laboratory scale, organic solvents were used to extract the product. Moreover, and importantly, based on experimental evidence the role of the ILs can be directly ascribed to the high selectivity obtained and the high catalyst stability.

Acknowledgements

This work was supported by the National Science Foundation of China (Project Nos 20773005, 20533010).

References

- 1 P. J. Dyson, *Appl. Organomet. Chem.*, 2002, **16**, 495.
- 2 D. Astruc, F. Lu and J. R. Aranzas, *Angew. Chem., Int. Ed.*, 2005, **44**, 7852.
- 3 P. Migowski and J. Dupont, *Chem.–Eur. J.*, 2007, **13**, 32.
- 4 V. I. Parvulescu and C. Hardacre, *Chem. Rev.*, 2007, **107**, 2615.

- 5 L. D. Pachón and G. Rothenberg, *Appl. Organomet. Chem.*, 2008, **22**, 288.
- 6 Y. L. Gua and G. X. Li, *Adv. Synth. Catal.*, 2009, **351**, 817.
- 7 E. Redel, J. Krämer, R. Thomann and C. Janiak, *J. Organomet. Chem.*, 2009, **694**, 1069.
- 8 P. Migowski, G. Machado, S. R. Teixeira, Maria. C. M. Alves, J. Morais, A. Traverse and J. Dupont, *Phys. Chem. Chem. Phys.*, 2007, **9**, 4814.
- 9 G. S. Fonseca, A. P. Umpierre, P. F. P. Fichtner, S. R. Teixeira and J. Dupont, *Chem. Eur. J.*, 2003, **9**, 3263.
- 10 E. T. Silveira, A. P. Umpierre, L. M. Rossi, G. Machado, J. Morais, G. V. Soares, I. J. R. Baumvol, S. R. Teixeira, P. F. P. Fichtner and J. Dupont, *Chem.–Eur. J.*, 2004, **10**, 3734.
- 11 L. M. Rossi, J. Dupont, G. Machado, P. F. P. Fichtner, C. Radtke, I. J. R. Baumvol and S. R. Teixeira, *J. Braz. Chem. Soc.*, 2004, **15**, 904.
- 12 G. S. Fonseca, E. T. Silveira, M. A. Gelesky and J. Dupont, *Adv. Synth. Catal.*, 2005, **347**, 847.
- 13 N. Yan, C. Zhao, C. Luo, P. J. Dyson, H. C. Liu and Y. Kou, *J. Am. Chem. Soc.*, 2006, **128**, 8714.
- 14 S. D. Miao, Z. M. Liu, B. X. Han, J. Huang, Z. Y. Sun, J. L. Zhang and T. Jiang, *Angew. Chem., Int. Ed.*, 2006, **45**, 266.
- 15 J. Wang, J. Feng, R. Qin, H. Fu, M. Yuan, H. Chen and X. Li, *Tetrahedron: Asymmetry*, 2007, **18**, 1643.
- 16 M. H. G. Precht, M. Scariot, J. D. Scholten, G. Machado, S. R. Teixeira and J. Dupont, *Inorg. Chem.*, 2008, **47**, 8995.
- 17 G. S. Fonseca, A. P. Umpierre, P. F. P. Fichtner, S. R. Teixeira and J. Dupont, *Chem. Eur. J.*, 2003, **9**, 3263.
- 18 X. D. Mu, D. G. Evans and Y. A. Kou, *Catal. Lett.*, 2004, **97**, 151.
- 19 X. D. Mu, J. Q. Meng, Z. C. Li and Y. Kou, *J. Am. Chem. Soc.*, 2005, **127**, 9694.
- 20 C. Zhao, H. Z. Wang, N. Yan, C. X. Xiao, X. D. Mu, P. J. Dyson and Y. Kou, *J. Catal.*, 2007, **250**, 33.
- 21 I. S. Park, M. S. Kwon, K. Y. Kang, J. S. Lee and J. Parka, *Adv. Synth. Catal.*, 2007, **349**, 2039.
- 22 M. J. Jacinto, P. K. Kiyohara, S. H. Masunaga, R. F. Jardim and L. M. Rossi, *Appl. Catal., A*, 2008, **38**, 52.
- 23 X. Yang, N. Yan, Z. Fei, R. M. C. Quesada, G. Laurency, L. K. Minsker, Y. Kou, Y. Li and P. J. Dyson, *Inorg. Chem.*, 2008, **47**, 7444.
- 24 J. Dupont, G. S. Fonseca, A. P. Umpierre, P. F. P. Fichtner and S. R. Teixeira, *J. Am. Chem. Soc.*, 2002, **124**, 4228.
- 25 G. S. Fonseca, J. D. Scholten and J. Dupont, *Synlett.*, 2004, 1525.
- 26 G. S. Fonseca, G. Machado, S. R. Teixeira, G. H. Fecher, J. Morais, M. C. M. Alves and J. Dupont, *J. Colloid. Interface. Sci.*, 2006, **301**, 193.
- 27 G. S. Fonseca, J. B. Domingos, F. Nome and J. Dupont, *J. Mol. Catal., A*, 2006, **248**, 10.
- 28 J. D. Scholten, G. Ebeling and J. Dupont, *Dalton Trans.*, 2007, 5554.
- 29 L. S. Ott, S. Campbell, K. R. Seddon and R. G. Finke, *Inorg. Chem.*, 2007, **46**, 10335.
- 30 Y. Zhu, C. Koh, A. T. Peng, A. Emi, W. Monalisa, L. K. J. Louis, N. S. Hosmane and J. A. Maguire, *Inorg. Chem.*, 2008, **47**, 5756.
- 31 J. Huang, T. Jiang, B. Han, H. Gao, Y. Chang, G. Zhao and W. Wu, *Chem. Commun.*, 2003, 1654.
- 32 J. Huang, T. Jiang, H. Gao, B. Han, Z. Liu, W. Wu, Y. Chang and G. Zhao, *Angew. Chem. Int. Ed.*, 2004, **43**, 1397.
- 33 J. Le Bras, D. K. Mukherjee, S. Gonzalez, M. Tristany, B. Ganchegui, M. Moreno-Manas, R. Pleixats, F. Henin and J. Muzart, *New J. Chem.*, 2004, **28**, 1550.
- 34 A. P. Umpierre, G. Machado, G. H. Fecher, J. Morais and J. Dupont, *Adv. Synth. Catal.*, 2005, **347**, 1404.
- 35 C. W. Scheeren, G. Machado, J. Dupont, P. F. P. Fichtner and S. R. Teixeira, *Inorg. Chem.*, 2003, **42**, 4738.
- 36 C. W. Scheeren, G. Machado, S. R. Teixeira, J. Morais, J. B. Domingos and J. Dupont, *J. Phys. Chem. B*, 2006, **110**, 13011.
- 37 C. X. Xiao, H. Z. Wang, X. D. Mu and Y. Kou, *J. Catal.*, 2007, **250**, 25.
- 38 T. J. Geldbach, D. B. Zhao, N. C. Castillo, G. Laurency, B. Weyershausen and P. J. Dyson, *J. Am. Chem. Soc.*, 2006, **128**, 9773.
- 39 D. B. Zhao, Z. F. Fei, T. J. Geldbach, R. Scopelliti and P. J. Dyson, *J. Am. Chem. Soc.*, 2004, **126**, 15876.
- 40 F. Fei, D. B. Zhao, D. Pieraccini, W. H. Ang, T. J. Geldbach, R. Scopelliti, C. Chiappe and P. J. Dyson, *Organometallics*, 2007, **26**, 1588.

- 41 Yang, Z. F. Fei, D. B. Zhao, W. H. Ang, Y. D. Li and P. J. Dyson, *Inorg. Chem.*, 2008, **47**, 3292.
- 42 M. Ruta, G. Laurency, P. J. Dyson and L. K. Minsker, *J. Phys. Chem., C*, 2008, **112**, 17814.
- 43 D. Dorjnamjin, M. Ariunaa and Y. K. Shim, *Int. J. Mol. Sci.*, 2008, **9**, 807.
- 44 N. Yan, X. Yang, Z. Fei, Y. Li, Y. Kou and P. J. Dyson, *Organometallics*, 2009, **28**, 937.
- 45 M. Zou, X. D. Mu, N. Yan and Y. Kou, *Chin. J. Catal.*, 2007, **28**, 5389.
- 46 US Pat., 4129414, 1978.
- 47 DE Pat., 10160815, 2003.
- 48 DE Pat., 102006020049, 2007.
- 49 L. C. Branco, J. N. Rosa, J. J. M. Ramos and C. A. M. Afonso, *Chem. Eur. J.*, 2002, **8**, 16.
- 50 Y. Wang, J. W. Ren, K. Deng, L. L. Gui and Y. Q. Tang, *Chem. Mater.*, 2000, **12**, 1622.
- 51 X. D. Wang, M. H. Liang, J. L. Zhang and Y. Wang, *Curr. Org. Chem.*, 2007, **11**, 299.
- 52 B. Coq, A. Tijani and F. Figueras, *J. Mol. Catal.*, 1991, **68**, 331.
- 53 L. Z. Ren, L. J. Meng and Q. H. Lu, *Chem. Lett.*, 2008, **37**, 106.
- 54 F. Maugé, A. Sahibed-Dine, M. Gaillard and M. Ziolek, *J. Catal.*, 2002, **207**, 353.
- 55 M. Benza, A. M. van der Kraanb and R. Prins, *Appl. Catal. A: General*, 1998, **172**, 149.

Access to a primary aminosporopollenin solid support from plant spores

Sylvain Barrier,^{a,b} Andreas Löbber,^a Alia J. Boasman,^a Andrew N. Boa,^a Mark Lorch,^a Stephen L. Atkin^{b,c} and Grahame Mackenzie^{*a,b}

Received 8th July 2009, Accepted 6th October 2009

First published as an Advance Article on the web 6th November 2009

DOI: 10.1039/b913215e

Sporopollenin, which is a naturally occurring and highly resilient organic polymer constituting the external shell of spores and pollen grains, has been converted into a primary amine form with a loading of 0.58 ± 0.04 mmol.g⁻¹ by reductive amination with ammonia and lithium aluminium hydride successively. The presence of the amine and precursor amide groups were established by combustion elemental analysis, ICP-OES, FTIR, solid-state NMR and reactivity of the primary amine group to salt formation and nucleophilic addition and substitution with phenyl isothiocyanate and benzene sulfonyl chloride, respectively. This relatively simple conversion has served to provide further information regarding the presence and reactivity of carboxylic acid functions on this relatively uncharted polymer and offers aminosporopollenin as a new material for potential solid-phase applications.

Introduction

The external shell of pollen grains and plant spores, namely the exine, is composed of sporopollenin which is an organic polymer exhibiting remarkable properties.^{1–3} Sporopollenins are renowned for their extraordinary physical, chemical and biological stability. For example, intact exines have been found in some sedimentary rocks, which are over 500 million years old, showing the resilience of sporopollenin to high temperatures and pressures, and acidic and basic conditions.²

The chemical structure of sporopollenins remains relatively mysterious due to their extraordinary inertness to non-oxidative chemical attacks.⁴ The sporopollenin extracted from the spores of club moss (*Lycopodium clavatum*) has, perhaps, been the most studied over the past century; it is commercially available and is probably one of the best understood.^{5–11} It resists strong acids and strong bases and does not dissolve into organic solvents. This is illustrated in particular by the harsh extraction protocols used to obtain exines devoid from other components of the spore, including proteins, lipids, nucleic acids and polysaccharides. Two especially evocative procedures are Erdtman's acetolysis,¹² which involves the use of a mixture of glacial acetic acid and concentrated sulfuric acid, and a sequential systematic isolation method using acetone, potassium hydroxide and phosphoric acid originally used by Zetzsche *et al.*,⁵ and later modified by others.^{11,13} Using such extractions, hollow uniform biodegradable resistant microcapsules were obtained in a green, sustainable and easy fashion from a natural renewable resource.

The remarkable stability of such exines could offer a wide range of applications, for instance for microencapsulation.^{14,15} It is of note that *Lycopodium clavatum* sporopollenin has been used as a solid support for various purposes (*e.g.* solid-phase synthesis, ion exchange, scavenging).^{13,16–26} It could advantageously replace artificial resins since the sporopollenin beads are monodispersed, composed of a renewable material, which is resistant to acids, bases and most organic solvents, and is commercially available in large quantities.

In spite of the chemistry performed during the previous studies of *Lycopodium clavatum* sporopollenin as a solid support, the chemical structure of sporopollenin is still poorly characterised due to its relative inertness.⁴ However, many features are commonly recognised: it contains only carbon, hydrogen and oxygen; it is virtually nitrogen-free; it has an aliphatic backbone and aromatic moieties. After extraction of the biopolymer from *Lycopodium clavatum* spores, some intrinsic functional groups have been observed by solid-state ¹³C NMR,^{9,11,27–29} namely, aliphatic carbons including methyls, oxygenated functions, olefinic and aromatic unsaturations, carboxylic acids and esters. Other investigations confirmed and completed the list of the features of sporopollenin: unsaturations,⁵ phenols,³⁰ carboxylic acids, ethers and hydroxyls.² A structure has even been proposed for sporopollenin: it could be considered as a lipidic copolymer of *para*-hydroxycinnamic acids (ferulic acid and *p*-coumaric acid) and fatty acids, whose linear hydrocarbon chains, mainly composed of 16 or 18 carbons, are highly cross-linked by ether and ester functions.⁴ However, this hypothesis has not been confirmed and most functional groups have not been quantified. Therefore, the derivatisation of sporopollenin with simple reagents can help to better understand the nature and in particular, the availability of such functional groups.

Polymers possessing primary amines have been much exploited as commercial insoluble supports.^{31–33} Examples of sporopollenin exhibiting a primary amine attached *via* a linker group have been described in the literature,^{13,17,18,23} which have

^aDepartment of Chemistry, University of Hull, Cottingham Road, Hull, HU6 7RX, United Kingdom. E-mail: g.mackenzie@hull.ac.uk; Tel: +44 1482 465479

^bSporomex Ltd., The Old Factory, Westgate Driffield, YO25 6TH, United Kingdom

^cThe Michael White Diabetes Centre, HS Brocklehurst Building, 220-236 Anlaby Road, Hull, HU3 2RW, United Kingdom

involved short ω -diamines. Shaw^{13,17} attached 1,3-diaminopropane to sporopollenin to yield a solid-phase support for peptide synthesis which involved a propyl chain as linker with an available primary amine. It was proposed by Shaw that anchoring to the sporopollenin involved a 'weakly basic function', which could form a hydrochloride salt but not be acylated. Although the type of function was not mentioned, the properties described might be more in character with a secondary amine, than an amide. Other research groups,^{18,23} whose work is based on Shaw's study, attached 1,2-diaminoethane to sporopollenin to yield an ion- or ligand-exchange medium. However, their interpretation of the anchoring attachment differed in that they considered both the terminal primary amine and the anchoring functional group to be modified by acylation. This hypothesis would rely on a surprisingly active hindered secondary amine.

None of the previous studies proposed the possibility of amide formation by reaction of an amine with sporopollenin or cross-linking of the diamines, which would have reduced the quantity of primary amines available for further attachment of ions, ligands or amino acids. To date no direct conversion of a functional group on sporopollenin into a primary amide and subsequent reduction to a primary amine has been reported.

This paper is aimed at better understanding the chemistry previously reported and offers a route to a new renewable primary amino solid support. We describe the direct amidation and subsequent amination of sporopollenin by simple reaction of ammonia followed by reduction. The use of ammonia avoids possible complications which might arise when using an amine and, since ammonia is a small molecule, provides maximum access to the available functional groups on sporopollenin. Also it is volatile and highly water soluble such that any unreacted ammonia would not contaminate the sporopollenin.

Results and discussion

Attachment of ammonia to sporopollenin

Sporopollenin (**1**), extracted by a modified protocol,¹¹ was found by combustion elemental analysis to contain carbon and hydrogen in the ratio of 5/8 (mol/mol) but no nitrogen was detected. It is notable that this ratio is highly reproducible and was first measured by Zetzsche *et al.*⁵ Treatment of **1** with concentrated aqueous ammonia at room temperature overnight gave a powder which was thoroughly washed with water and dried to constant mass. Elemental analysis revealed that the product had gained nitrogen which could not be removed by copious washing with water implying chemical attachment rather than physical attachment. The level of nitrogen attached was $0.46 \pm 0.05 \text{ mmol.g}^{-1}$. This showed that, using a simple direct treatment, ammonia could be attached to sporopollenin with a nitrogen loading in the same range as that of commercial amino-resins ($0.5\text{--}1 \text{ mmol.g}^{-1}$).^{31–33}

The level of nitrogen was found to increase with the time of treatment. After four days of reaction in ammonia, a loading of $0.70 \pm 0.09 \text{ mmol.g}^{-1}$ was assayed in the ammonia-treated sporopollenin (**2**).

Attempts to improve the loading further involved the use of a sealed tube at $120 \text{ }^\circ\text{C}$ and the nitrogen loading slightly

augmented from $0.63 \pm 0.09 \text{ mmol.g}^{-1}$ after one day, to $0.84 \pm 0.31 \text{ mmol.g}^{-1}$ after four days.

Addition of ammonium chloride as a catalyst showed an interesting increase, although moderate, of the nitrogen loading. When **1** was stirred overnight at high temperature in a sealed vessel with a small amount of ammonium chloride in concentrated ammonia, the level of nitrogen reached $1.37 \pm 0.48 \text{ mmol.g}^{-1}$ in the final product **2**, after filtration, copious washing and drying.

The sample of product **2** which was used in the rest of this study was obtained at $120 \text{ }^\circ\text{C}$ with addition of ammonium chloride and had a nitrogen content of $1.02 \pm 0.04 \text{ mmol.g}^{-1}$.

Resistance to acidic conditions

As part of a study to determine the nature of the attachment of ammonia to sporopollenin, **2** was stirred at room temperature in dilute hydrochloric acid. The level of nitrogen dropped slightly from $1.02 \pm 0.04 \text{ mmol.g}^{-1}$ to $0.86 \pm 0.13 \text{ mmol.g}^{-1}$, as detected by combustion elemental analysis. Between 7 and 24% of the nitrogen present in ammonia-treated sporopollenin (**2**) was thus removed by acidic treatment. This amount could correspond to that of an acid-labile covalent linkage, such as an imine derived from the carbonyl groups of sporopollenin; however, since imines are likely to be easily hydrolysed during the aqueous washings, it was thought that such functional groups would be unlikely and that the linkages cleaved by washing in acid were most probably of ionic nature. Such nitrogenous functions are thus interpreted as being ammonium salts formed on some acidic groups (*e.g.* carboxylic acids) of sporopollenin.

Nitrogen was still present in the acidified product **3** to a level of $0.86 \pm 0.13 \text{ mmol.g}^{-1}$. The stability of such nitrogen indicated that it was covalently bonded to sporopollenin. Functional groups hypothesised here could be amides derivatised from carboxylic acids and, less probably, imines stabilised by formation on conjugated ketones, but still less stable than amides.

Acidity and basicity of ammonia-treated sporopollenin **2**

Both *Lycopodium* sporopollenin (**1**) and ammonia-treated sporopollenin (**2**) were found to exhibit anionic acidic functions such as phenols and carboxylic acids. All of these functional groups were assayed by the amount of sodium ions adsorbed by **1** (respectively **2**) from a solution of sodium hydroxide to give a product **4** (respectively **5**) on the basis of its acting as an ion-exchange resin. The level of sodium determined by flame photometry, following its removal from **4** (respectively **5**) by treatment with hydrochloric acid, was $1.09 \pm 0.18 \text{ mmol.g}^{-1}$ (respectively $0.18 \pm 0.10 \text{ mmol.g}^{-1}$). Interestingly, the level of nitrogen in **5**, as detected by combustion elemental analysis, dropped to $0.91 \pm 0.03 \text{ mmol.g}^{-1}$ to match approximately that in **3**.

This was in agreement with the previous supposition that carboxylic acids were involved in the attachment of ammonia to sporopollenin. Indeed, the sodium loading on **1** is in keeping with that of nitrogen in **2**, indicating that the level of acidic functions in sporopollenin is the same as that of nitrogenous functional groups it can form with ammonia. The quantity of acidic groups left on **2**, as detected by sodium exchange, corresponds approximately to the difference of nitrogen loadings between **2** and **5** (or **2** and **3**), supporting the hypothesis that

10–20% of the nitrogenous functions of **2** are ammonium salts formed on carboxylic acids of sporopollenin. The presence of acidic functions not being involved in the attachment of ammonia, such as phenols, could explain the approximations.

In contrast, when **1** was treated with hydrochloric acid and successively washed with sodium hydroxide, no chloride ions were detected in the filtrate by addition of silver nitrate. Therefore, little or no chloride was adsorbed indicating that **1** did not contain cationic functional groups. In addition, similar treatment of product **3**, obtained by exposure of **2** to dilute hydrochloric acid at room temperature, failed to show any detectable chloride salt.

This indicated that the newly created nitrogenous functions on **2** were not strongly basic. Hence, they are very unlikely to be Schiff's bases which might have resisted the acidic treatment: reaction with ammonia did not form any imine stabilised by conjugation in sporopollenin. However, this result supports the hypothesis that most acid-resistant nitrogenous functions in **2** (and **3**) are amide groups.

Reduction of ammonia-treated sporopollenin **3**

In order to better characterise **3**, it was reduced with lithium aluminium hydride to give a product **6**, whose level of nitrogen was $0.57 \pm 0.04 \text{ mmol.g}^{-1}$ as measured by combustion elemental analysis. Contrary to the starting sporopollenin **3**, product **6** formed a chloride salt **7** when stirred with hydrochloric acid at room temperature, showing it to have basic character. Gravimetric assay of chloride ions released from **7** with sodium hydroxide showed it to contain $0.60 \pm 0.03 \text{ mmol.g}^{-1}$ chloride ions. This value was close to the loading of nitrogen measured by combustion elemental analysis ($0.56 \pm 0.05 \text{ mmol.g}^{-1}$). Therefore, virtually all of the nitrogenous functional groups appeared to have been reduced to give basic functional groups. These results are in keeping with a primary amide being converted to a primary amine. Interestingly, the level of primary amino groups in **3** is in the same range as that in commercial resins ($0.5\text{--}1 \text{ mmol.g}^{-1}$).^{31–33}

Spectroscopic data of ammonium-treated sporopollenin

In support of the foregoing chemical characterisation, compounds **1**, **2** and **6** were further studied by FTIR and solid-state NMR.

FTIR spectroscopy

The starting sporopollenin **1** and the ammonia-treated sporopollenin **2** had similar FTIR spectra (see Fig. 1) but differed in the range $1700\text{--}1600\text{cm}^{-1}$. The peak characteristic of carbonyl stretching shifted from 1705cm^{-1} in **1** to 1643cm^{-1} in **2**, which was consistent with the conversion of carboxylic acids to amides (amide I band).^{34–36} The amide II band, assigned to N–H deformation and C–N stretching, was also visible in the spectrum of **2** at 1602cm^{-1} , although its wave number was lower than expected.

In contrast, the reduction of **2** into product **6** strongly modified the FTIR spectrum (see Fig. 1). The broad peak around $3500\text{--}3400\text{cm}^{-1}$ in the spectrum of **2**, assigned to O–H and N–H stretchings,^{34–36} was reshaped in the spectrum

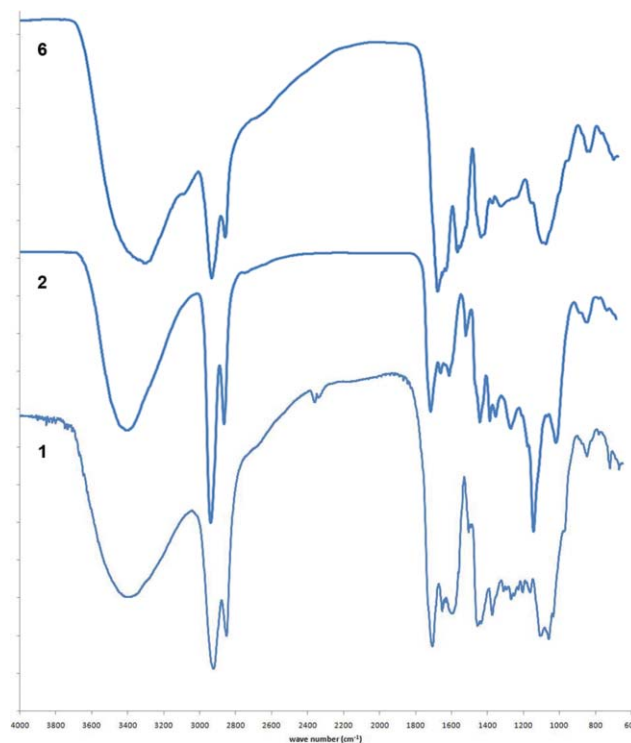


Fig. 1 FTIR spectra of **1** (original sporopollenin), **2** (ammonia-treated sporopollenin) and **6** (reduced ammonia-treated sporopollenin).

of **6** into three smaller bands: at $3550\text{--}3400\text{cm}^{-1}$ and $3450\text{--}3320\text{cm}^{-1}$ indicating respectively asymmetric and symmetric N–H stretching associated with non-bonded primary amines, and at $3300\text{--}3000\text{cm}^{-1}$ showing N–H stretchings associated with hydrogen-bonded primary amines. All signals in the range $1700\text{--}1600\text{cm}^{-1}$, characteristic of carbonyl stretchings, weakened drastically, which is consistent with the reduction of the carbonyl groups by lithium aluminium hydride. A shift of the peak around 1130cm^{-1} to 1070cm^{-1} , accounting for C–N stretching vibration, was interpreted as an increase in bond length. This could indicate conversion of an amide to a primary amine on the basis that C–N bonds are expected to be shorter in amides than in amines.

In conclusion, Fourier transform-infrared spectroscopic data support the hypothesis that the reaction of ammonia with sporopollenin yielded primary amides, which turned into primary amines after reduction with lithium aluminium hydride.

Solid-state NMR

Introduction of an ^{15}N label in ammonia-treated sporopollenin was made possible by the addition of ^{15}N -labelled ammonium chloride as a catalyst to the conversion of **1** into **2**. This enabled sporopollenin **2** to be analysed by solid-state ^{15}N NMR. Due to the low loading of the isotope, the background noise was relatively high but the spectrum (displayed in Fig. 2) distinctly showed two broad signals and one sharp signal. The peak at 0 ppm corresponds to unreacted ammonium chloride, whereas the peak at ca. 15 ppm is assigned to ammonium salts of acidic functional groups attached to **2**. The band at 73 ppm was interpreted as a covalent bond resonance since it was too high to be associated with a salt. Imines were not considered since they would not resonate at such a low frequency but would be

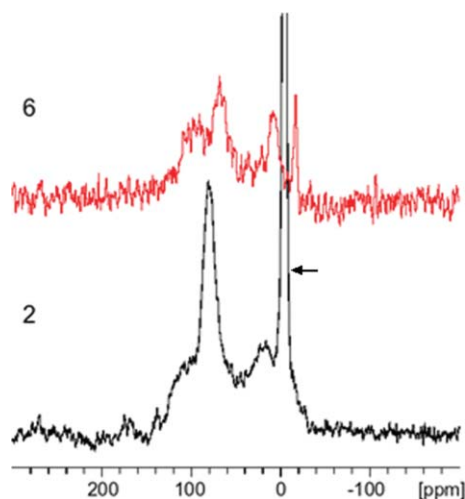


Fig. 2 ^{15}N NMR spectra of **2** (ammonia-treated sporopollenin) and **6** (reduced ammonia-treated sporopollenin). Note: the arrow indicates the peak corresponding to the signal of residual ammonium chloride.

expected to appear at 300–400 ppm.³⁷ However, the signal could correspond to an amide or an amine.

The proportion of ^{15}N isotope introduced into **2** was limited and therefore the overall quantity in the reduced product **6** was low. This gave a relatively broad and weak peak in the resulting spectrum of **6** (displayed in Fig. 2), with significant background noise. This peak could thus not be interpreted with certainty.

In conclusion, solid-state ^{15}N NMR, whilst not offering confirmation on its own, was at least supportive of the covalent attachment of functional groups containing nitrogen to **2** and **6**, but also consistent with a difference between the characteristics of the nitrogenous functional groups on the two compounds, indicating that a chemical conversion has taken place.

Additionally, solid-state ^{13}C NMR spectra (displayed in Fig. 3) of **1**, **2** and **6** were compared, following normalisation of the spectra at 128 ppm, interpreted as aromatic and olefinic resonance.^{34,38} This was done on the basis that all of such resonances would be expected to be reasonably consistent for the three derivatives. All three spectra showed very similar

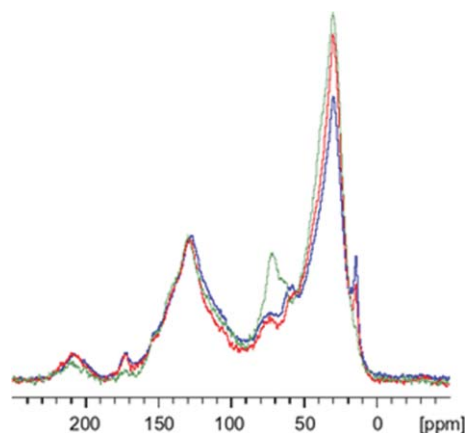


Fig. 3 ^{13}C CP MAS NMR spectra collected with 8 kHz sample spinning and 8K scans per spectra. Blue, **1** (original sporopollenin). Red, **2** (ammonia-treated sporopollenin). Green, **6** (reduced ammonia-treated sporopollenin).

contours. Treatment with ammonia did not significantly change the signals. This was expected since, if amide bonds were to form, their peak would be approximately at the same shift (173 ppm) as that of the initial carboxylic acid groups.^{34,38} In contrast, when **2** was reduced into **6**, the band assigned to the C=O of the carboxyl groups (173 ppm) decreased, as expected. The intensity of the peak at 73 ppm was largely augmented, which was interpreted as the formation of C–N bonds^{34,38} of primary amines in **6**.

In conclusion, interpretation of the solid-state ^{13}C NMR spectra of the series of compounds was in agreement with the functional group alterations assigned to **1**, **2** and **6**.

Further derivatisation of sporopollenin **6**

The availability of the nitrogenous functional groups present on product **6** was assessed with regard to three different reactions which are typical of primary amino groups.

Sporopollenin **6** was methylated with methyl iodide to yield a product **8**, following the conditions of Hoffmann's reaction. The level of nitrogen in **8** measured by combustion elemental analysis was $0.37 \pm 0.09 \text{ mmol.g}^{-1}$, whereas that of iodine determined by gravimetry after liberation in sodium hydroxide and precipitation with silver nitrate was $0.29 \pm 0.01 \text{ mmol.g}^{-1}$. This indicated that 80% of the nitrogenous groups of **6**, considered as primary amines, successfully formed quaternary ammonium iodides in **8**.

The reaction of **6** with phenyl isothiocyanate and benzene sulfonyl chloride yielded products **9** and **10**, respectively. The levels of sulfur in **9** and **10** were 0.35 mmol.g^{-1} and 0.50 mmol.g^{-1} , respectively, as determined by ICP-OES, and those of nitrogen 0.79 mmol.g^{-1} and 0.71 mmol.g^{-1} , respectively, as measured by combustion elemental analysis. The ratio of sulfur per nitrogen was therefore 44% in **9**, showing that 88% of the nitrogenous functional groups present in **6** had reacted covalently with phenyl isothiocyanate. Similarly, the results in **10** indicated that 70% of the nitrogenous groups of **6** had successfully formed covalent bonds with benzene sulfonyl chloride.

As primary amines react with isothiocyanates and sulfonyl chlorides by nucleophilic addition and substitution respectively, the success of such reactions confirmed the hypothesis of the nitrogenous functional groups present in **6** as being primary amino groups.

Experimental

Combustion elemental analysis

Combustion elemental analyses of sporopollenin and derivatives were performed on a Fisons instrument Carlo Erba EA 100 C H N S analyser. Each analysis reported is based on three repeats of the same samples. However, all of the errors identified on the nitrogenous derivative obtained were based on at least three repeats of the reaction, hence indicating the reproducibility of the reaction and not the analysis *per se*.

Flame atomic emission spectroscopy

Flame Atomic Emission Spectroscopy was carried out on a Corning 400 flame photometer fuelled with natural gas.

Inductively coupled plasma-optical emission spectrometry (ICP-OES)

Inductively Coupled Plasma-Optical Emission Spectrometry was performed on a Perkin Elmer Optima 5300DV Spectrometer.

NMR measurements

All NMR experiments were carried out (at 293 K) on a Bruker Avance II 500 MHz spectrometer using a 4 mm MAS probe operating at frequencies of 50.6747 MHz (^{15}N) and 125.7546 MHz (^{13}C). Spectra were externally referenced to tetramethylsilane at 0 ppm. Experiments were carried out at 8 kHz MAS speeds and spectra were acquired using cross polarization and TPPM decoupling during the acquisition period.

All NMR data was processed using 'Topspin' Version 1.3 (Bruker Instruments, Karlsruhe, Germany).

Extraction of sporopollenin 1

Spores (*Lycopodium clavatum* L., 250 g) were suspended in acetone (750 cm³) and stirred under reflux for 4 h. Particles were recovered by filtration, and dried overnight in open air.

The defatted spores were suspended in aqueous potassium hydroxide solution (6% wt., 750 mL) and stirred under reflux for 12 h, with filtration and refreshing of the alkaline solution after 6 h. Base-hydrolysed sporopollenin was recovered by filtration, and washed with hot water until the filtrate was neutral and with hot ethanol until the filtrate was uncoloured, and dried overnight in open air.

The previous product (100 g) was suspended in orthophosphoric acid (85% wt., 750 cm³) and stirred under reflux for 7 days. Acid-hydrolysed sporopollenin was recovered by filtration, washed with water (5 × 200 cm³), acetone (200 cm³), hydrochloric acid (2M, 200 cm³), aqueous sodium hydroxide (2M, 200 cm³), water (5 × 200 cm³), acetone (200 cm³) and ethanol (200 cm³), re-suspended in ethanol (750 cm³) and stirred under reflux for 2 h. It was finally recovered by filtration, washed with ethanol (200 cm³), and dried in an oven at 60 °C to a constant weight, to yield product **1** (mass recovery: 75 g).

The typical combustion elemental analysis of sporopollenin **1** was: %C 70.0, %H 8.0, %N 0.0.

Synthesis of 2 by reaction with ammonia

Sporopollenin **1** (0.5 g) was suspended in aqueous 0.88 ammonia (25 cm³) and stirred at room temperature for 4 days. It was recovered by filtration, washed with water (5 × 20 cm³), ethanol (2 × 20 cm³) and dichloromethane (20 cm³), and dried under vacuum over phosphorus pentoxide to a constant weight to yield product **2** (mass recovery: 0.5 g).

Alternatively, ammonium chloride (0.1 g) was added to ammonia before reaction, and/or the mixture was stirred at 120 °C in a sealed thick-walled tube.

The typical combustion elemental analysis of product **2** was: %C 69.9, %H 7.5, %N 1.4.

Synthesis of 3 by treatment of 2 in hydrochloric acid

Product **2** (0.5 g) was suspended in aqueous hydrochloric acid (2 mol.dm⁻³, 25 cm³) and stirred overnight at room temperature. The solid was recovered by filtration, washed with water (5 × 20 cm³), ethanol (2 × 20 cm³) and dichloromethane (20 cm³) and dried under vacuum over phosphorus pentoxide to a constant weight to yield **3** (mass recovery: 0.5 g).

The typical combustion elemental analysis of product **3** was: %C 70.1, %H 7.6, %N 1.2.

Synthesis of 4 by treatment of 1 in sodium hydroxide

Sporopollenin **1** (0.5 g) was suspended in aqueous sodium hydroxide (2 mol.dm⁻³, 25 cm³) and stirred overnight at room temperature. The solid was recovered by filtration, washed with water (5 × 20 cm³), ethanol (2 × 20 cm³) and dichloromethane (20 cm³) and dried under vacuum over phosphorus pentoxide to a constant weight to yield **4** (mass recovery: 0.5 g).

The typical combustion elemental analysis of product **4** was: %C 69.1, %H 7.4, %N 0.0.

Synthesis of 5 by treatment of 2 in sodium hydroxide

Sporopollenin **2** (0.5 g) was suspended in aqueous sodium hydroxide (2 mol.dm⁻³, 25 cm³) and stirred overnight at room temperature. The solid was recovered by filtration, washed with water (5 × 20 cm³), ethanol (2 × 20 cm³) and dichloromethane (20 cm³) and dried under vacuum over phosphorus pentoxide to a constant weight to yield **5** (mass recovery: 0.5 g).

The typical combustion elemental analysis of product **5** was: %C 69.1, %H 7.5, %N 1.3.

Synthesis of 6 by reduction of 3 with lithium aluminium hydride

Product **3** (0.5 g) was suspended in sodium dried 1,4-dioxane (20 cm³) and lithium aluminium hydride (1.0 g) was added. The mixture was stirred for 4 days under reflux in nitrogen. Excess reducing agent was quenched at 0 °C by successive addition of ethyl acetate (100 cm³), ethanol (50 cm³), water (100 cm³) and 2M sulfuric acid (200 cm³). Particles were recovered by filtration, washed with water (3 × 50 cm³), ethanol (3 × 30 cm³) and dichloromethane (2 × 30 cm³) and dried under vacuum over phosphorus pentoxide to a constant weight to yield **6** (mass recovery: 0.4 g).

The typical combustion elemental analysis of product **6** was: %C 59.3, %H 7.3, %N 0.8.

Synthesis of 7 by treatment of 6 in hydrochloric acid

Sporopollenin **6** (0.5 g) was suspended in aqueous hydrochloric acid (2 mol.dm⁻³, 25 cm³) and stirred overnight at room temperature. The solid was recovered by filtration, washed with water (5 × 20 cm³), ethanol (2 × 20 cm³) and dichloromethane (20 cm³) and dried under vacuum over phosphorus pentoxide to a constant weight to yield **7** (mass recovery: 0.5 g).

The typical combustion elemental analysis of product **7** was: %C 66.3, %H 7.8, %N 0.8.

Synthesis of **8** by Hoffman quaternisation of **6**

Product **6** (0.5 g) was suspended in acetonitrile (10 cm³) and methyl iodide (2 cm³) was added. The mixture stirred under reflux for 3 days. The solid was recovered by filtration, washed with acetonitrile (2 × 20 cm³), ethanol (2 × 20 cm³) and DCM (20 cm³) and dried under vacuum over phosphorus pentoxide to a constant weight to yield product **8** (mass recovery: 2.6 g).

The typical combustion elemental analysis of product **8** was: %C 54.9, %H 7.4, %N 0.7.

Synthesis of **9**

Product **6** (0.2 g) was suspended in dichloromethane (10 cm³). Phenyl isothiocyanate (2 cm³) was added and the mixture was stirred overnight at room temperature. The solid was recovered by filtration, washed with dichloromethane (3 × 10 cm³) and dried under vacuum over phosphorus pentoxide to a constant weight to yield product **9** (mass recovery: 0.8 g).

The combustion elemental analysis of product **9** was: %C 55.4, %H 7.8, %N 1.1. The level of sulfur determined by ICP-OES was 1.1%.

Synthesis of **10**

Product **6** (0.2 g) was suspended in chloroform (10 cm³). Benzene sulfonyl chloride (2 cm³) was added and the mixture was stirred overnight at room temperature. The solid was recovered by filtration, washed with dichloromethane (3 × 10 cm³) and dried under vacuum over phosphorus pentoxide to a constant weight to yield product **10** (mass recovery: 0.8 g).

The typical combustion elemental analysis of product **10** was: %C 55.4, %H 7.8, %N 1.0. The level of sulfur determined by ICP-OES was 1.6%.

Sodium assay

Dry product **4** or **5** (0.1 g, accurate to 1 mg) was stirred overnight in 2M hydrochloric acid (10 cm³) at room temperature, recovered by filtration and washed with water (3 × 10 cm³). Filtrate and aqueous washings were collected quantitatively, mixed and completed to 100 cm³ with distilled water.

The loading of sodium in the dry solid was calculated from the sodium concentration in the diluted filtrate, which was assessed by flame atomic emission spectroscopy against a calibration curve obtained with sodium chloride standard solutions.

Assay of chloride (or iodide) salts by gravimetric analysis

Dry (over phosphorous pentoxide) product **3**, **7** or **8** (0.1 g, accurate to 1 mg) was stirred overnight in 2M sodium hydroxide (10 cm³) at room temperature, recovered by filtration and washed with water (3 × 10 cm³).

Both filtrate and aqueous washings were collected quantitatively, mixed and acidified by 6M nitric acid (5 cm³). A 0.1M silver nitrate solution (5 cm³) was added to the mixture, which was immediately protected from light and set aside overnight. Silver chloride (or silver iodide) was coagulated by heating nearly to boiling point, with constant stirring, then cooled down for 1h, recovered by filtration in an oven-dry, pre-weighed funnel (10–16 µm-pored), washed with dilute nitric acid (3 × 10 cm³)

and dried at 120 °C away from light. The loading of chloride (or iodide) in the original sample was calculated from the weight of dry precipitate.

Conclusions

The combination of chemical and spectroscopic evidence is supportive of primary amide and primary amine functional groups forming from carboxylic acids present in the sporopollenin structure. This adds to the characterisation of this relatively unexplored natural polymer in respect of its carboxylic acid content or at least available carboxylic acid for derivatisation. Furthermore, this study demonstrates that it can be relatively easily converted into a solid-supported primary amine with a loading comparable to commercial synthetic polymers. The uniformity, reproducibility, availability and stability of such particles could put them in competition with commercial polymeric particles.

Acknowledgements

We thank Carol Kennedy, Bob Knight, and Lesley Galbraith for their technical assistance.

References

- 1 K. Faegri and J. Iversen, *Textbook of Pollen Analysis*, Blackwell, Oxford, UK, 1964.
- 2 G. Shaw, in *Phytochemical Phylogeny*, ed. J. B. Harborne, Academic Press, London, UK, 1970, pp. 31–35.
- 3 G. Shaw, in *Sporopollenin*, eds. J. Brooks P. R. Grant M. Muir P. Van Gijssel and G. Shaw, Academic Press, London & New York, 1971, pp. 305–348.
- 4 P. F. Van Bergen, P. Blokker, M. E. Collinson, J. S. Sinninghe Damsté and J. W. De Leeuw, in *The Evolution of Plant Physiology. From whole plants to ecosystems*, eds. A. R. Hemsley, and I. Poole, Elsevier Academic Press, London, UK, 2004, pp. 133–154.
- 5 F. Zetzsche and K. Huggler, *Liebig's Ann.*, 1928, **461**, 89–108.
- 6 G. Shaw and A. Yeadon, *Grana Palynol.*, 1964, **5**, 247–252.
- 7 J. Brooks and G. Shaw, *Nature*, 1968, **219**, 532–533.
- 8 J. Burczyk and J. Dworzanski, *Phytochemistry*, 1988, **27**, 2151–2153.
- 9 W. J. Guilford, D. M. Schneider, J. Labovitz and S. J. Opella, *Plant Physiol.*, 1988, **86**, 134–136.
- 10 A. R. Hemsley, W. G. Chaloner, A. C. Scott and C. J. Groombridge, *Ann. Bot.*, 1992, **69**, 545–549.
- 11 G. Shaw and D. C. Apperley, *Grana*, 1996, **35**, 125–127.
- 12 G. Erdtman, *Sven. Bot. Tidskr.*, 1960, **54**, 561–564.
- 13 G. Shaw, M. Sykes, R. W. Humble, G. Mackenzie, D. Marsden and E. Pehlivan, *React. Polym.*, 1988, **9**, 211–217.
- 14 S. L. Atkin, S. T. Beckett, and G. Mackenzie, Dosage form comprising an exine coating of sporopollenin or derivatized sporopollenin, patent WO 2005/000280, 2005.
- 15 S. L. Atkin, S. Barrier, S. T. Beckett, T. Brown, G. Mackenzie and L. Madden, *Coll. Symp. Ser.*, 2005, **7**, 307–311.
- 16 G. Mackenzie and G. Shaw, *Int. J. Pept. Protein Res.*, 1980, **15**, 298–300.
- 17 R. Adamson, S. Gregson and G. Shaw, *Int. J. Pept. Protein Res.*, 1983, **22**, 560–564.
- 18 E. Pehlivan and S. Yildiz, *Anal. Lett.*, 1988, **21**, 297–309.
- 19 E. Pehlivan, M. Ersoz, M. Pehlivan, S. Yildiz and H. J. Duncan, *J. Colloid Interface Sci.*, 1995, **170**, 320–325.
- 20 M. Ersoz, E. Pehlivan, H. J. Duncan, S. Yildiz and M. Pehlivan, *React. Polym.*, 1995, **24**, 195–202.
- 21 M. Ersoz, U. S. Vural, A. Okdan, E. Pehlivan and S. Yildiz, *J. Membr. Sci.*, 1995, **104**, 263–269.
- 22 M. Ersoz, U. S. Vural, M. Yigitoglu and M. Sezgin, *J. Colloid Interface Sci.*, 1996, **184**, 319–324.

- 23 A. A. Gürten, M. Uçan, M. I. Abdullah and A. Ayar, *J. Hazard. Mater.*, 2006, **B135**, 53–57.
- 24 N. Ünlü and M. Ersoz, *J. Hazard. Mater.*, 2006, **B136**, 272–280.
- 25 N. Ünlü and M. Ersoz, *Sep. Purif. Technol.*, 2007, **52**, 461–469.
- 26 F. Gode and E. Pehlivan, *Bioresour. Technol.*, 2007, **98**, 904–911.
- 27 A. R. Hemsley, *Courier Forschungsinst. Senckenberg*, 1992, **147**, 93–107.
- 28 A. R. Hemsley, P. J. Barrie, W. G. Chaloner and A. C. Scott, *Grana*, 1993, **Suppl. 1**, 2–11.
- 29 A. R. Hemsley, P. D. Jenkins, M. E. Collinson and B. Vincent, *Bot. J. Linn. Soc.*, 1996, **121**, 177–187.
- 30 K. Schulze Osthoff and R. Wiermann, *J. Plant Physiol.*, 1987, **131**, 5–15.
- 31 A. R. Mitchell, S. B. H. Kent, B. W. Erickson and R. B. Merrifield, *Tetrahedron Lett.*, 1976, **17**, 3795–3798.
- 32 A. R. Mitchell, B. W. Erickson, M. N. Ryabtsev, R. S. Hodges and R. B. Merrifield, *J. Am. Chem. Soc.*, 1976, **98**, 7357–7362.
- 33 J. T. Sparrow, *J. Org. Chem.*, 1976, **41**, 1350–1353.
- 34 J. B. Lambert, H. F. Shurvell, D. A. Lightner and R. G. Cooks, *Introduction to organic spectroscopy*, Macmillan Publishing Company, New York, 1987.
- 35 D. H. Williams and I. Fleming, in *Spectroscopic methods in organic chemistry*, McGraw-Hill Publishing Company Ltd., London, 1966, pp. 40–76.
- 36 R. M. Silverstein, C. G. Bassler and T. C. Morrill, *Spectrometric identification of organic compounds*, John Wiley & Sons, New York, 1974.
- 37 B. Kamiński, W. Schilf, T. Dziembowska, Z. Rozwadowski and A. Szady-Chełmieniecka, *Solid State Nucl. Magn. Reson.*, 2000, **16**, 285–289.
- 38 D. H. Williams and I. Fleming, in *Spectroscopic methods in organic chemistry*, McGraw-Hill Publishing Company Ltd., London, 1966, pp. 77–129.

Screening of new solvents for artemisinin extraction process using *ab initio* methodology†

Alexei A. Lapkin,^{*a} Martina Peters,^b Lasse Greiner,^b Smain Chemat,^c Kai Leonhard,^{d,e} Marcel A. Liauw^b and Walter Leitner^b

Received 23rd October 2009, Accepted 28th October 2009

First published as an Advance Article on the web 30th November 2009

DOI: 10.1039/b922001a

The solubility of artemisinin in a range of conventional and novel solvents was evaluated using the COSMO-RS approach, and verified experimentally as well as against literature data. The computational method was improved by calibrating against a limited set of experimental data, enhancing the accuracy of the calculations. The optimised method was shown to be in reasonable agreement with experimental data; however, lack of reliable experimental data is identified as an issue. Several novel solvents perceived as green alternatives to conventional solvents were targeted and shown to offer good solubility of artemisinin. Extraction from *Artemisia annua* by carbonate solvents was experimentally verified.

Introduction

Extraction of natural products is performed on a large scale for production of nutraceuticals, fragrances, biopharmaceuticals, bio-fuels and other products. With the increasing attention on renewable feedstocks as a basis for future chemicals' supply chains, there is a renewed interest in extraction due to the potential to obtain a wide variety of chemical synthons from sustainable sources.

Extraction processes are traditionally based on solid–liquid extraction. A solvent needs to penetrate the (usually pre-dried) plant material to dissolve the target components, allowing subsequent recovery. Steam distillation and hot water extraction allow the extraction of essential oils and some natural dyes. However, the vast majority of extraction processes utilise organic solvents, predominantly ethanol, hexane, or particular petroleum fractions, *e.g.*, petroleum ether (PE) 60/90. Only a small number of industrial extraction processes are currently using green solvents, mainly supercritical carbon dioxide *e.g.*, in the high-volume process of decaffeination of coffee or the extraction of rice bran oil.

Amongst the many natural product extraction processes, extraction of bio-pharmaceutical molecules is of particular importance due to the end-use demand. Thus, plants contribute to over half the library of small molecules of interest to

the pharmaceutical industry.¹ As an example, extraction of artemisinin (**1**)—the precursor to the current main antimalarial drugs—is currently its main source and is done predominantly *via* PE extraction.² This process is characterised by a relatively low overall yield, typically about 60% with respect to the dried plant content of artemisinin, which is largely due to the decomposition of artemisinin in hot extract solutions and the difficult recovery of artemisinin from the primary extracts. The difficult recovery is, in part, related to the presence of structurally similar co-metabolites and artemisinin degradation products, and also due to the presence of highly efficient solubility enhancers in the waxy and glycosidic fractions of the extract. There are significant health and safety risks associated with the large-scale use of solvents such as n-hexane and PE. These are due to the abnormally high toxicity of n-hexane among linear alkanes³ and the explosion risk through static discharge in the low dielectric constant solvents. The latter requires addition of polar additives, typically 5% v/v of ethyl acetate.

There is a considerable interest in developing cleaner extraction processes, or in attempting to reduce solvent use in natural product extraction. Supercritical fluids, with emphasis on supercritical carbon dioxide (scCO₂), have been shown to be effective extraction solvents for many natural products; scCO₂ is particularly attractive for biomedical applications due to the absence of any solvent residue. The main downside is the high capital investment due to the high pressures and temperatures required to attain efficient solvent strength. High investment costs can only be justified for either large enterprises with high-volume single component extraction, or multi-purpose facilities for high-value components.

Hydrofluorocarbons exhibit good solvation power at low pressures. Solvents such as 1,1,1,2-tetrafluoroethane R134a (trade names KLEA-134a, SOLKANE®134a)⁴ and iodotrifluoromethane⁵ have already found limited commercial use, even though these solvents are expensive. Further issues are potential in-use toxicity of iodotrifluoromethane^{6,7} (see discussion in ref. 2, also), very high global warming potential

^aSchool of Engineering, University of Warwick, Coventry, UK.
E-mail: a.lapkin@warwick.ac.uk; Fax: +44(0)2476 418922;
Tel: +44 (0)2476 151101

^bInstitut für Technische und Makromolekulare Chemie, RWTH Aachen University, Aachen, Germany

^cDepartment of Chemical Engineering, University of Bath, UK

^dChair of Technical Thermodynamics, RWTH Aachen University, Germany

^eEngineering Thermodynamics, Delft University of Technology, Delft, The Netherlands

† Electronic supplementary information (ESI) available: Structures of compounds 3–26 and Fig. S1 and S2. See DOI: 10.1039/b922001a

of tetrafluoroethane R134a and a rather complicated situation with patents covering its use for bio-extraction, which has been the issue of much consternation over the last five years. We have shown previously that extraction of artemisinin by R134a is a potentially highly efficient and economic method, assuming quantitative solvent recycling is designed into the process.²

Another class of interesting compounds are high boiling point solvents, such as ionic liquids, molten eutectics, carbonates, fluorinated solvents, *etc.* These are already known in commercial applications resulting in significant reductions in the release of volatile organic carbons (VOCs) through the substitution of low boiling solvents by higher boiling point solvents with considerably lower vapour pressures. However, the use of such solvents in extraction requires completely different processing approaches due to the generally high viscosity of these solvents and the need to use phase separation or extraction for recovery of the required molecules from the primary extracts. A recent life cycle assessment (LCA) study showed that downstream extraction is energetically less efficient than distillation, the latter being used in the case of low boiling point solvents.⁸ Therefore, we argue that high boiling point solvents should be applied only when their use offers a substantial functional benefit, offsetting any additional process 'costs' due to more complex and energy-intensive downstream separation.

Examples of additional functionalities from recent developments are: using a chiral solvent for performing stereoselective synthesis,⁹ exploiting stabilisation of metal nanoparticles in ionic liquids as an additional functionality,^{10,11} clean phase separation that may be attainable in aqueous biphasic catalysis, fluorosolvents, thermoresponsive solvents¹² or the new class of switchable solvents,¹³ *etc.* It has also been shown that ionic liquid solvents can potentially be applied to the extraction of bio-pharmaceuticals if the recovery step is designed such that simple partitioning with water results in effective phase separation.² For more detailed discussion of the topic of functional analysis of systems see an inspiring book, ref. 14; further discussion of metrics and functional approaches to analysis of chemical products and processes can be found elsewhere.^{15–17} Other solvents that attract interest as direct replacements for conventional organic solvents are ethyl lactate, diacetone alcohol, urea-based solvents and many others which present better biodegradability, lower toxicity and lower vapour pressure than conventional solvents.

With the introduction of a large number of new molecules as potential solvents, the problem of rapid evaluation of their usefulness in specific applications emerges. This can be done using time-consuming traditional laboratory methods, using novel high-throughput experimental methods, or by combining experimental measurements with initial pre-screening by computational tools. In this respect, the relatively recent method of calculating solvent performance using *ab initio* quantum chemical calculations combined with statistical thermodynamics (COSMO-RS)^{18–20} started to be used extensively in academia, and especially in industry.^{21–24} A recent review on solvent selection demonstrates the possible links between different molecular design tools and performance screening by COSMO-RS, thus expanding the potential molecular space for solvent screening even further.²⁵ There are, however, only a few reports on the applicability of COSMO-RS for solids solubility calculations, not expanding into the area of green solvents.^{19,26,27} It has recently

been highlighted that although the potential of COSMO-RS in property prediction and the design of solvent systems is very high, experience with applications of the method is thus far very limited.²⁸

In this study, we show a method for improving the accuracy of COSMO-RS predictions of the solubility of solids, which requires limited experimental data to fine-tune the model. A range of solvents was screened computationally for the specific application of extracting artemisinin as the precursor to current mainstream antimalarial drugs.

Experimental

Computational methodology

The initial molecular geometry of artemisinin, epiartemisinin and other molecules that were not available in the COSMOtherm database were set up in Spartan (v. 06, 08). Equilibrium conformer calculation and conformer distribution search were performed in Spartan (v. 06, 08) using the molecular mechanics (MMFF) and semi-empirical AM1 methods. Up to 10 lowest energy conformers were used for the molecules calculated in this study. Geometry optimisation and calculation of screening charge density for all conformers were done in Turbomole using BP-TZVP parameterisation. Consecutive calculations within COSMO-RS theory were performed in COSMOtherm (X_C21_0108 by COSMOlogic GmbH). The conformer treatment option was always employed.

The solubility is calculated according to eqn (1):²⁹

$$\log(x_i) = \log\left(\frac{Mw_i \rho_s}{Mw_s}\right) + \frac{1}{RT \ln(10)} \left(-\Delta_{i,s} + \min[0, \Delta G_{\text{fus},i}]\right) \quad (1)$$

where x_i is the mole fraction of solute i at the limit of its solubility, Mw_i and Mw_s are molecular weights of solute and solvent, ρ_s is the density of solvent, $\Delta_{i,s}$ is the difference between pseudo chemical potential of solute i in the solution and of pure i in the liquid state, $\Delta_{i,s} = \mu_{i,s} - \mu_{i,l}$, and $\Delta G_{\text{fus},i}$ is the free energy of fusion of solid i .

As noted in ref. 19, the problem of solubility calculation with COSMO-RS is the need to obtain a value of the Gibbs energy of fusion (ΔG_{fus}) of a substance of interest, which is the difference between the Gibbs energy of a pure solid and a pure liquid at a given temperature. Since this value cannot be measured directly, it can be estimated by a QSPR approach, as implemented in COSMOtherm. The QSPR estimate will introduce a considerable error, as will be shown below. Therefore, in this paper, we used a different method to estimate ΔG_{fus} .

Eqn (1) contains two unknowns: $\Delta_{i,s}$ and $\Delta G_{\text{fus},i}$. The $\Delta_{i,s}$ value can be found from a fine-grid liquid–liquid equilibrium (LLE) calculation in COSMOtherm. The resultant liquid phase chemical potential of a solute in the given solvent as a function of its molar fraction is shown in Fig. 1, calculated for ethanol and ethyl acetate. As expected, the graphs coincide at the point of pure artemisinin and epiartemisinin, see Fig. 1, $x = 1.0$. The difference between the chemical potentials of artemisinin and epiartemisinin in solution is more pronounced in the case of ethyl acetate, being *ca.* 1.353 kJ mol⁻¹ at artemisinin mole fraction $x_{\text{artemisinin}} = 0.033$, whereas the corresponding difference

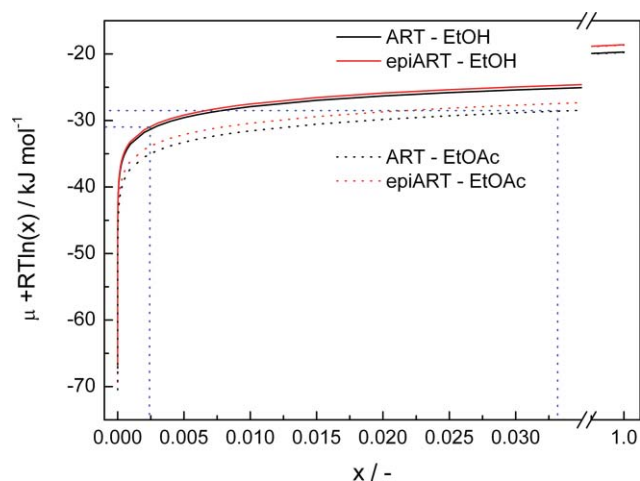


Fig. 1 Chemical potential of artemisinin in ethanol and ethyl acetate solutions at 294 K as a function of the molar fraction of artemisinin computed during LLE calculation with the fine-grid option in COSMOtherm. Vertical lines correspond to experimental solubility values for ethanol and ethyl acetate.

in the case of ethanol solution is only $0.451 \text{ kJ mol}^{-1}$ at $x_{\text{artemisinin}} = 0.0024$. The chemical potential of the solute at the experimentally verified value of its solubility limit concentration (x_i), at a given temperature, for compound i allows the value of $\Delta_{i,s}$ to be obtained.

Based on the calculated value of $\Delta_{i,s}$, the value of ΔG_{fus} can be readily obtained from eqn (1). Using this methodology and the literature data of solubility of artemisinin in ethanol and ethyl acetate given in Table 1, the estimated values for ΔG_{fus} were found to be 11.39 and 8.91 kJ mol^{-1} for the solubilities in ethanol and ethyl acetate, respectively. The value of ΔG_{fus} predicted by the COSMOtherm QSPR approach is 7.16 kJ mol^{-1} . The original experimental value of solubility in ethyl acetate used to determine the Gibbs fusion value (ref. 2) was later found

to be incorrect, in fact too high, which explains the difference between the estimated values of ΔG_{fus} based on ethanol and ethyl acetate experimental solubilities given above. Notably, the solubility of artemisinin in ethyl acetate calculated using $\Delta G_{\text{fus}} = 11.39$ coincides well with the more accurate experimental value, see Table 1. This illustrates the frequently encountered problem of low confidence in available experimental data and the potential for computational results to point out the likely erroneous experimental results.

For solubility calculations, an iterative procedure was used as implemented in COSMOtherm.

Extraction and solubility

Artemisia annua biomass was of East African and Argentinian origin. Artemisinin was kindly provided by Neem Biotech Ltd (Newport, Wales, UK). Exhaustive extraction was performed to determine the amount of artemisinin in the dry biomass. Extracts of *A. annua* were typically prepared using a ratio of 10 g of dry finely crushed biomass to 100 mL of solvent (ethyl acetate). Extractions were performed at $45 \text{ }^\circ\text{C}$ under reflux over 6 h. Extracts were filtered through filter paper, and later filtered using a $0.2 \text{ }\mu\text{m}$ Nylon filter prior to HPLC analysis. An HPLC instrument (Shimadzu Prominence) equipped with a UV-vis diode array (SPD-M20A, DAD) and in-line evaporative light scattering detector (ELSD, LTII, 350 kPa N_2 , nebulizer at $40 \text{ }^\circ\text{C}$) was used with Betasil C18 $5 \text{ }\mu\text{m}$ $250 \times 4.6 \text{ mm}$ at column flow-rate 1.0 mL min^{-1} and column temperature of $45 \text{ }^\circ\text{C}$ with acetonitrile : water 65 : 35% v/v. Analytical method development is described elsewhere.³⁰

Hexane/ethyl acetate (95 : 5 v/v) and carbonates extraction kinetics were measured using a 1 L glass double-jacketed stirred vessel (Büchi). Extraction was performed at $50 \text{ }^\circ\text{C}$ for 5 h with the ratio of biomass to solvent 1 : 6 (w : v). Samples of 1 mL were taken along the extraction experiment to follow artemisinin concentration in the solvents over time. At the

Table 1 Comparison of literature and calculated solubility of artemisinin in different conventional solvents

Solvent	T/K	Calculated solubility/ g L^{-1}		Experimental solubility/ g L^{-1}	Reference
		$\Delta G_{\text{fus}} = 11.39 \text{ kJ mol}^{-1}$	QSPR ^a		
Ethyl acetate	293	31.8	136.1	100	2
	293			34.5	34
Chloroform	293	280.1	396.8	304.0	34
Hexane	313	3.8/5.7 ^b	30.1	0.46	
	293	2.2	12.6	1.8	This study
Cyclohexane	293	2.2	15.0	2.0	34
Toluene	293	14.6	86.3	145.6	34
Acetonitrile	293	15.6	77.6	90.7	This study
				1.92	34
				157.7	This study
Acetone	293	36.7	149.0	25.7	34
Water @ pH 7.2	298 ^c	0.038	0.230	0.063	34
Methanol	203	8.7	45.1	7.7	35
Ethanol	294	11.8	55.0	12	2
				10.5 ^d	36

^a Value of ΔG_{fus} is estimated for each temperature by COSMOtherm using the QSPR approach. ^b The second value calculated using an estimated $\Delta G_{\text{fus}} (T = 313 \text{ K}) = 10.32 \text{ kJ mol}^{-1}$. ^c Temperature not specified in the original paper; presumed standard conditions; pH is not accounted for in the present calculation. ^d Calculated using the temperature dependence of solubility given in ref. 35: $\ln(x) = -123.96 + \frac{2041}{T/K} + 19.51 \cdot \ln(T/K)$ where coefficients are given for dry solutions of artemisinin in ethanol.

end of an experiment, the extract was evaporated to dryness, and the residue was re-dissolved in acetonitrile and analysed to determine the maximum amount of artemisinin extracted. In parallel, the remaining biomass was extracted twice with a fresh volume of ethyl acetate for three hours in each sequence. Then, the two extracts were combined, evaporated to dryness and the residue was re-dissolved in acetonitrile and analysed to determine the quantity of artemisinin not accessible for extraction. All samples were filtered using a 4 μm Nylon syringe filter before injection in HPLC.

In the case of solvents with high vapour pressure, the solubility of artemisinin was measured using a gravimetric method, using a set of thermostated vials at 293 K. The solvent (5 mL) was added to the vials and once the desired temperature was reached, excess artemisinin (considering the expected solubility) was added and the vials sealed. The suspension was stirred at 300–400 rpm with a magnetic stirrer for 6 h, which was considered sufficient to establish the equilibrium of the solute–solvent mixture. Samples of the solution were withdrawn rapidly using a micropipette to avoid any solvent loss or precipitation. The aliquots were filtered with pre-warmed 0.22 μm Nylon filters, solutions placed in vials brought to constant weights and transferred to a vacuum oven. Solutions were evaporated and vials were brought to constant weight. All weights were measured using a Sartorius microbalance with accuracy better than 0.05 mg. Experiments were performed in duplicate. Samples were also diluted and analysed using the HPLC instrument with a UV DAD detector set at 210 nm to verify the results of gravimetric measurements.

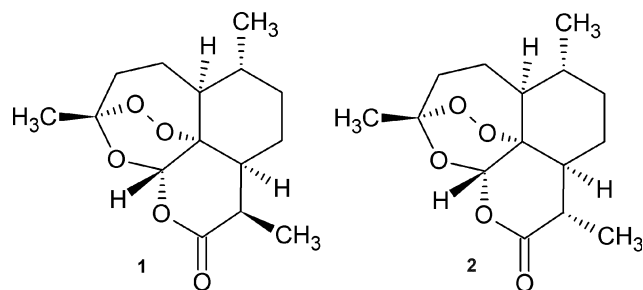
For the solvents with higher boiling points, the solubility of artemisinin was measured at 293 K in approximately 5 g of a given solvent. An excess of artemisinin was placed in a solvent in a sealed glass vial and gently stirred with a magnetic stirrer for 6 h, thermostated in a water bath. The suspension was allowed to settle and a sample was taken for analysis *via* a 0.5 μm Nylon syringe filter. The sample was injected into the HPLC instrument directly.

The structures of the compounds used as possible solvents are given in Scheme S1 in the ESI†. Carbonates (4–6, Scheme S1, ESI†) were kindly provided by Huntsman Chemicals. All other solvents were obtained from Fischer Chemicals. All solvents were used as received.

Results and discussion

Molecular geometry optimisation and calculation of screening charge densities

The initial geometry was built using the absolute conformation determined from single crystal diffraction³¹ and the earlier computational work³² as guidance. Two diastereoisomers of artemisinin are considered in the literature:³² artemisinin (1) and epiartemisinin (2), see Scheme 1. Both isomers are derivatised into arteether and artesunate APIs and it was shown that the pharmacokinetics of the resultant diastereomers of arteether is different, one being considerably slower than the other.³³ Although this was considered advantageous by the authors, the short life-time of the active artemisinin compound is believed to be an essential reason for malaria parasites being unable to develop tolerance towards artemisinin-based drugs



Scheme 1 Molecular structures of artemisinin and epiartemisinin

over significant periods of time. We therefore considered both diastereoisomers in our calculations.

The search for equilibrium conformers yielded two conformers for each of the two isomers. Thus, four structures were used for further geometry optimisation using density functional theory. The resultant molecular geometry could, in principle, be compared against experimental crystal diffraction data³¹ and the previous computational study.³² However, the geometry of a molecule in the liquid state is different from its gas phase structure or its solid crystal structure due to the presence of intermolecular interactions and, at the same time, their flexibility. Therefore, such direct comparison is not very meaningful. It was noted in the calculations that for both diastereoisomers, only one conformer contributed significantly to the calculated values of solubility. The two important conformers are shown in Fig. S1 (ESI†).

The calculated COSMO-RS parameters, the screening charge density distribution profile and surface chemical potential distribution, as functions of screening charge density, are shown in Fig. 2a. A phenomenological analysis of the resultant data can be given following a similar analysis of common solvents given earlier.¹⁸ The large peak of $P_s(\sigma)$ near $\sigma = 0$ corresponds to a non-polarised area of the molecule, mostly carbon and hydrogen atoms, whereas the complex peak at 1.25 e nm⁻² corresponds to the peroxide oxygen atoms (at *ca.* 1 e nm⁻²) and to the lactone oxygen (at *ca.* 1.25 e nm⁻²). Complementary profiles for the two liquids, *i.e.* matching the maxima of one component at a sigma value $-\sigma$ with the maxima of another at $+\sigma$, would indicate their miscibility. A similar analysis for a solvent and solute pair would indicate mutual affinity and hence indicate potentially good solubility.

The surface chemical potentials at positive and negative polarisations correspond to capacities towards hydrogen bond accepting and donating behaviour, see Fig. 2b. This analysis is normally done for solvents, rather than solutes. However, the phenomenological analysis should also be valid for solutes. For interpretation, it is necessary to keep in mind that the sign of polarity in Fig. 2b corresponds to the screening charge and, hence, is opposite to the polarity of the molecule. Negative polarity corresponds to interactions with hydrogen donors, which shows that artemisinin will interact with hydrogen donors through its exposed lone pairs in oxygen atoms. However, it would not interact with hydrogen bonding acceptors, since it does not have considerable exposed area of polarised hydrogen donors. Solvents with a large number of strong hydrogen bond acceptors should not have high solvation power for artemisinin. In the positive polarity range, artemisinin would behave as

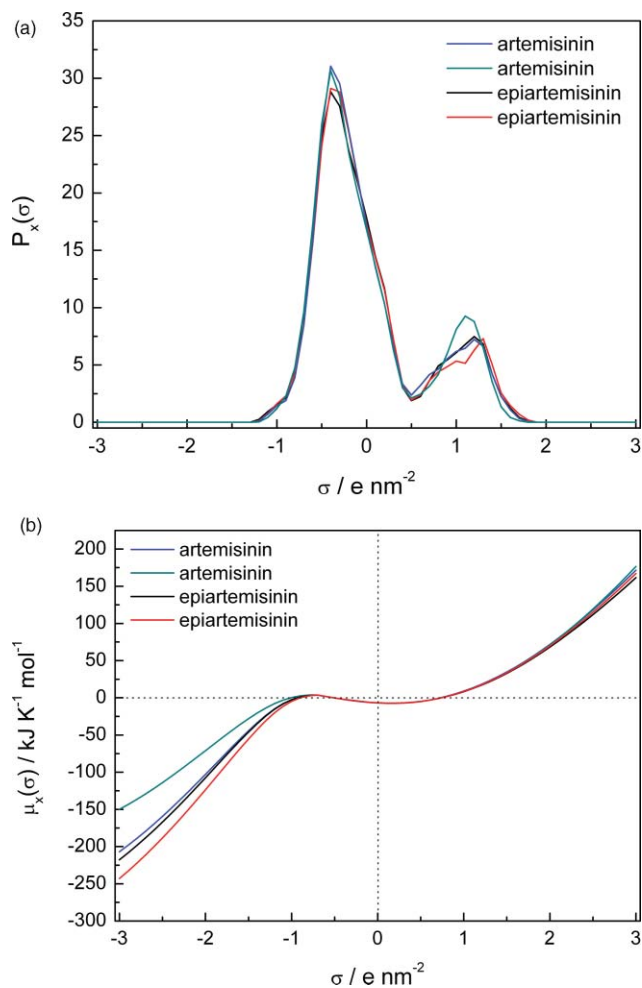


Fig. 2 Profile of (a) screening charge density distribution and (b) surface chemical potential at 298 K for two artemisinin diastereoisomers and all conformers.

hexane or acetone. Thus, it is expected that artemisinin should interact strongly with polar solvents containing few or weak hydrogen bonding donors, for example trichloromethane.

The clear difference between artemisinin diastereoisomers in the surface potential at negative polarity is noteworthy; there is a clear difference between the potentials even if averaged over the two conformers for each isomer. Epiartemisinin (**2**) shows a stronger tendency to hydrogen bond donor interactions. Thus, the two isomers should behave differently in solvents with hydrogen bonding donor functions, epiartemisinin always interacting the stronger.

Validation and fine-tuning of the solubility calculations

Calculation of solubility of artemisinin based on QSPR estimated free energy of fusion gives significantly over-estimated values for all solvents, see Table 1. When the value of ΔG_{fus} , calculated on the basis of experimental solubility of ethanol and the computed LLE data was used ($= 11.39 \text{ kJ mol}^{-1}$, see Experimental section), then the estimated value of solubility in ethanol matched the experimental value within 2%. The calculated data hint at inaccuracies in previously reported experimental data. Thus, the earlier reported figures of solubilities in

n-hexane and ethyl acetate² differ markedly from the calculated data, see Table 1. However, our own recent measurements are in agreement with calculations and with other literature data.³⁴

Prediction of solubility in the mixed water–ethanol solvent with the optimised value of ΔG_{fus} shows a reasonably good match, the calculated solubility being systematically higher than the experimental values, see Fig. 3. Only for pure water is the calculated value of solubility lower than the reported experimental value.³⁵

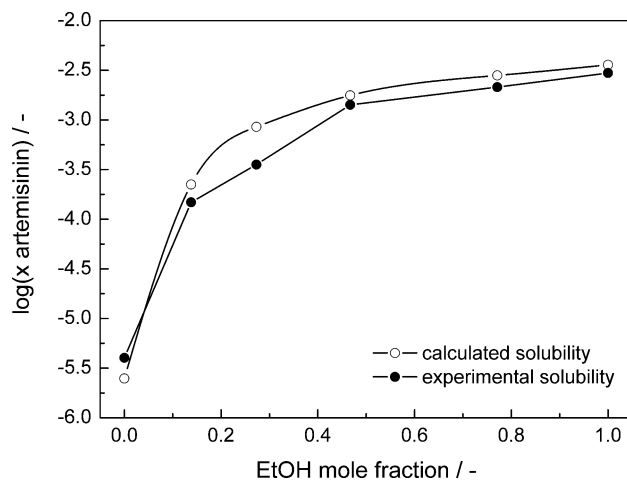


Fig. 3 Comparison of calculated and experimental solubilities of artemisinin in ethanol–water at 303 K. Data for EtOH–H₂O system are from ref. 36. Data for artemisinin solubility in pure water are from ref. 35. ΔG_{fus} (artemisinin, 303 K) = $11.28 \text{ kJ mol}^{-1}$.

Using the published experimental data on the temperature dependence of artemisinin solubility in ethanol³⁶ the temperature dependence of the Gibbs free energy of fusion of artemisinin was calculated. This was done by obtaining a linear fit to the experimental data of solubility plotted as $\log(x)$ vs T , and finding the best value of ΔG_{fus} at each temperature point that gave the closest calculated solubility value. The resultant data are shown in Fig. 4.

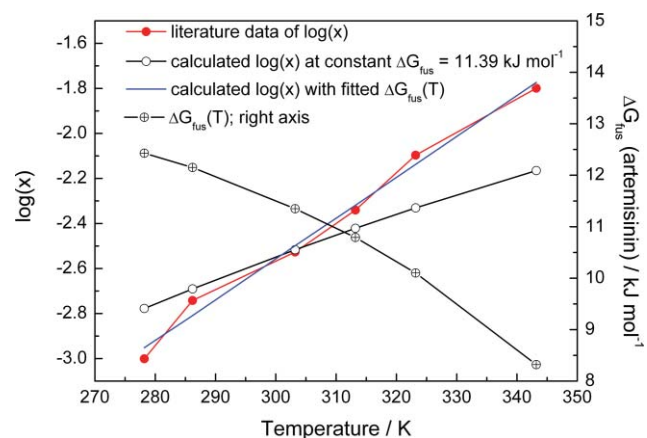


Fig. 4 Temperature dependence of the solubility of artemisinin in dry ethanol. Solid lines are for the convenience of viewing.

It is apparent that without a temperature dependence of the free energy of fusion, estimation of the solubility of artemisinin is

correct only within a very narrow range of temperatures around the reference temperature $T_{\text{ref}} = 294 \text{ K}$ at which ΔG_{fus} was determined. More accurate calculations could be obtained by fitting the calculated solubility values to the experimental data by adjusting ΔG_{fus} . The interpolated values for the temperature dependence of the Gibbs energy of fusion for **1** and **2** were used in all consecutive calculations. The temperature dependence of ΔG_{fus} is computed within COSMOtherm using the following equation:²⁹

$$\Delta G_{\text{fus}}(T) = -\Delta H_{\text{fus}} \left(1 - \frac{T}{T_{\text{melt}}} \right) + \Delta C p_{\text{fus}} (T_{\text{melt}} - T) - \Delta C p_{\text{fus}} T \ln \left(\frac{T_{\text{melt}}}{T} \right) \quad (2)$$

where T_{melt} is melting temperature of artemisinin, *ca.* $153 \text{ }^\circ\text{C}$,³⁷ ΔH_{fus} is the heat of fusion and $\Delta C p_{\text{fus}}$ is the heat capacity of fusion. The latter two parameters are also unknown for artemisinin. This equation does not describe the obtained temperature dependence for ΔG_{fus} for artemisinin and therefore this parameter was adjusted manually for each given temperature.

There are several outlying values of solubilities in Table 1 where there is a considerable difference between experiment and calculations, particularly in the case of toluene and acetonitrile. On one hand it is expected that the accuracy of calculation for very high solubilities would not be particularly high. On the other hand, such significant discrepancies may invalidate the method of calculation and should be examined more closely. These are discussed below within the discussion of specific groups of solvents.

Two conclusions can be drawn from these initial results: (1) the accuracy and quality of experimental data can be verified by the calculated data, allowing to identify non-linear behaviour and allowing further experimental planning and (2) the presence of water in mixed solvents, even in such highly complex polar systems as ethanol–water, can be described accurately by the model; thus, the solubility of artemisinin in wet solvents could also be estimated.

Screening of solubility of artemisinin in different solvents

Solubility calculations were performed for artemisinin and epiartemisinin. However, more detailed calculations with dry and wet solvents were only performed for artemisinin. The value of ΔG_{fus} of artemisinin at 293 K was estimated to be $11.83 \text{ kJ mol}^{-1}$ on the basis of the temperature dependence shown in Fig. 4. This value was used in all subsequent calculations at this temperature.

Results of the computational screening of a number of solvents that have not previously been considered for extraction of artemisinin, as well as some more common solvents, are shown in Table 2. The only solvents included in the analysis that score very badly in the GSK solvent selection guide³⁸ are chloroform, dichloromethane and acetonitrile.

There appears to be little difference between the n-alkanes of C_5 – C_7 chain length. Calculations predict a 30% lower solubility in n-heptane compared to n-hexane, which is somewhat unfortunate, due to its 10-fold lower toxicity.³ The parity with experimental data is also very good for linear alkanes. However, pure linear alkanes are rarely used in practical applications. The more common solvents, being the particular grades of petroleum

ether (PE), characterised by the range of boiling temperatures PE 60–90 with the density range 0.67 – 0.698 g ml^{-1} and consisting of n-pentane, 2-methylpentane, n-hexane, n-heptane and isopentane (0.25 : 0.25 : 0.25 : 0.23 : 0.02), were used in the calculations of artemisinin solubility. As expected solubility in PE ranked between that of n-pentane and n-heptane. The presence of aromatic impurities in PE would increase the solubility of artemisinin, according to both calculations and experimental data.

The move to aromatic solvents such as toluene results in a marked increase in the predicted and experimental solubilities of artemisinin. The screening charge density of toluene is higher in both polarity ranges than that of linear alkanes. The recently reported value of artemisinin solubility in toluene (145.6 g L^{-1} , ref. 34) is 10-fold higher than the predicted value. This value was obtained by light scattering measurements, based on the disappearance of artemisinin crystallites from solution upon gradual addition of solvent.³⁴

We attempted to measure several solubilities by using a gravimetric method and verified the results by diluting samples and using a UV-DAD detector in the HPLC instrument; the obtained data are reported in Tables 1 and 2. The accuracy of gravimetric measurements is not very high due to the errors in determining the mass of rapidly evaporating solvents. However, there was a good agreement between gravimetric measurements and HPLC-UV concentration measurements for the solubilities of artemisinin in toluene, acetonitrile and dimethylformamide.

The value of solubility obtained in toluene is significantly lower than that reported in ref. 34. In contrast, the value of solubility in acetonitrile is much higher. Our measured values correlate much better with the trend in the calculated values. Therefore, we have much more confidence in the order of experimental solubilities obtained in our own measurements. There is a concern that the light scattering method of determining solubilities introduces a systematic error due to an incorrect interpretation of the signal, since this is an indirect method. This error can be different for different solvent systems. It would therefore be necessary to validate experimental values of solubilities of artemisinin in toluene and several other solvents showing apparently high solubilities by a different, direct, reliable and independently validated method.

The large underprediction of the artemisinin solubility in toluene may arise from the inability of the theory to correctly account for the interactions of π -electrons of the aromatic ring of toluene with the unpaired spins of oxygens in artemisinin. Some of these interactions appear to be accounted for. This is evident in comparison of the homologous order of solvents from toluene to trifluorotoluene, perfluorotoluene and perfluoromethyl cyclohexane. There is a strong correlation between the decrease in the number of protons, the decrease in the π electron density, and the reduced solubility of artemisinin. Fig. S2 in the ESI† illustrates the differences in the screening charge densities of toluene and perfluorotoluene.

Amongst all screened solvents, the highest solubilities of artemisinin were predicted for chloroform and dichloromethane—two orders of magnitude higher than those for the standard extraction solvents n-hexane or PE. The experimental value of solubility in chloroform is 8% higher than the calculated value (Table 1). In our opinion this is

Table 2 Comparison of experimental and computed solubilities of artemisinin in novel solvents at $T = 293$ K

Solvent	Vapour pressure @ 20 °C/kPa	Boiling point/°C	Density/ g cm ⁻³	Solubility/g L ⁻¹				Artemisinin activity coefficient, ln(γ)
				Artemisinin dry	Epiartemisinin dry	Artemisinin (water concentration)	Artemisinin experimental	
High boiling point solvents								
3 Di-methyl carbonate	2.7	90.5	1.069	24.31	23.70	26.17 (245.2)	9.97	0.268
4 Propylene carbonate	0.002	242	1.2057	11.83	9.3	11.31 (250.7)	7.8	0.873
5 Butylene carbonate	0.007	251	1.141	17.23	16.0	16.9 (76.4)	8.11	0.484
6 Glycerine carbonate	0.016	110-115 at 0.1 mm Hg	1.462	3.77	2.28	2.2 (387)	8.23	4.017
7 1,3-dimethyl-2-imidazolidinone (DMI)	0.006 ^a	225	1.056	28.5	28.3	—	16.20	-0.372
8 1,3-dimethyl-3,4,5,6-tetrahydro-2(1H)-pyrimidinone (DMPU)	0.002 ^a	302 ^a	1.06	26.3	26.6	—	15.96	-0.413
9 γ -valerolactone (dihydro-5-methyl-2(3 h)-furanone	0.018 ^a	207	1.07	23.1	22.7	—	—	-0.002
10 1,8-Cineol	0.043 ^a	176-177	0.9515	6.6	7.2	—	—	0.619
14 Glycerol formal (1,3-dioxan-5-ol)	0.016 ^a	194	1.210	12.1	9.3	9.3 (12 ^b)	—	0.996
15 Glycerol isobutylal (2-isobutyl-1,3-dioxan-5-ol)	0.0002 ^a	280 ^a	1.086 ^a	22.7	15.8	16.2 (69.5)	—	-0.023
16 DMEA oct	—	—	0.90	—	1.6	—	82 ²	—
17 BMOEA bst	—	—	1.40	—	16.8	—	110 ²	0.564 ^d
18 EMIM OAc	—	—	1.1027	8.4	7.8	—	5.45	1.277
Tetradecanoic acid (myristic acid)	8.4×10^{-7}	78	0.888 ^a	36.0	21.2	21.3 (23.4)	—	-0.885
Dodecanoic acid (lauric acid)	1.7×10^{-5}	—	0.895 ^a	43.9	26.0	26.2 (28.8)	—	-0.951
19 Ethyl lactate	0.106	154	1.030	19.1	17.4	17.4	—	0.072
Methyl lactate	0.393	145	1.096	23.4	19.9	—	—	0.117
22 2-Butoxyethanol	0.08	171	0.90	9.0	8.3	8.3 (99)	—	1.263
20 Diacetone alcohol	0.04	167.9	0.94	15.4	14.8	13.2 (167)	—	1.281
26 Carvacrol	0.003 ^a	237.1	0.976	—	24.5	—	298	-2.652
Conventional low boiling point hydrocarbon solvents								
Chloroform (CHCl ₃)	21.2	61	1.489	318.5	280.1	—	304	-2.197
Dichloromethane (CH ₂ Cl ₂)	46.9	40	1.3	351.6	319	—	—	-2.100
Dimethylformamide, DMF (CH ₃) ₂ NCOH	0.36	153	0.949	35.6	34.4	34.4 (0)	113.2	-0.288
Bromoforn (CHBr ₃)	0.7	149.5	2.89	12.4	9.2	9.2 (3.8)	—	1.014
Acetonitrile (CH ₃ CN)	9.7	80	0.784	18.0	15.6	—	1.92/157.7	-0.083
Methyl isobutyl ketone, MIBK	2.0	116	0.804	18.3	19.1	19.4 (80.4)	—	-0.083
n-Pentane	57.1	35-36	0.63	1.9	2.3	2.3 (0.2)	—	2.111
n-Heptane	17.6	69	0.68	1.2	1.5	1.6 (0.1)	—	2.278
Petroleum ether (PE) 60-90 °C ^c	—	60-90	0.649 ^a	1.7	1.9	—	—	2.216
Toluene	2.9	110.6	0.867	13.1	14.7	15.0 (0.6)	145.6	0.340
Trifluorotoluene	2.1	100-103	1.19	8.4	8.8	—	—	0.691
Perfluorotoluene	1.4	104	1.584 ^a	0.12	0.13	—	—	4.673
Perfluoromethylcyclohexane	4.3	76.3	1.762 ^a	0.005	0.006	—	—	7.524
Pressurised gaseous solvents (in the liquid state)								
Dimethylether ((CH ₃) ₂ O)	515.1	-24.8	0.73	71.4	73.9	27.7 (285.4)	—	-0.746
NH ₃	888	-33.4	0.68	46.9	43.5	38.8 (44.9)	—	-0.137
CO ₂	5850	-78.5	0.9 ^a	134.0	135.0	141.7 (21.5)	2.79 ³⁹	-1.994
Fluoroform (CHF ₃)	4378	-84	1.156 ^a	321.4	275.1	289 (20.8)	0	-1.884
1,1,2,2-tetrafluoroethane	—	—	1.212	153.68	130.65	136.3 (15.9)	—	-1.472
1,1,1,2-tetrafluoroethane (R134a)	570	-26.6	1.212	66.8	57.2	61.3 (8.2)	—	-0.794
1,1,1,2,3,3,3-heptafluoropropane (R227)	400	-16.5	1.41	102.8	79.0	80.6 (9.6)	—	-1.297

^a Estimated by COSMOtherm for 293 K. ^b Water concentration was assumed to be 1 wt%. ^c Composition of petroleum ether was taken as: 25% n-pentane, 25% 2-methylpentane, 25% n-hexane, 23% n-heptane and 2% isopentane. ^d Calculated considering an equimolar mixture of neutral components, rather than ions.

a very good correlation, since the accuracy of calculations generally decreases at high solubilities. A very high solubility was calculated and experimentally verified for carvacrol, 245–298 g L⁻¹.

The next best solvents according to the predicted values are liquid tetrafluoromethane, liquid CO₂ and the symmetrical 1,1,2,2-tetrafluoroethane. There are no experimental data on the solubility of artemisinin in liquid CO₂ but there are data on its solubility in scCO₂.³⁹ Some experimental conditions reported are close to the density of liquid CO₂ at 293 K. Using the empirical relationship for solubility as a function of density and temperature developed in ref. 38, the experimental solubility of artemisinin at 293 K and density 770 g L⁻¹ is estimated as $y = 5.65 \times 10^{-4}$ or 2.79 g L⁻¹. There is a very large discrepancy between the calculated solubility of artemisinin in liquid CO₂ and the experimental solubility at close temperature and pressure, but in scCO₂. At this stage we cannot present an adequate explanation for this difference.

The predicted solubility in liquid ammonia is quite high. This is an expected result since ammonia is known to be a very good solvent. However, its practical use as a solvent is unlikely due to safety considerations and its basic character, which would promote undesirable decomposition reactions of the compounds of interest in the extracts. The inert hydrofluorocarbon refrigerants may potentially be good solvents. The commercially available unsymmetrical 1,1,1,2-tetrafluoroethane is already being used as a solvent for bio-extraction processes and was earlier shown to be economically and environmentally competitive against other extraction processes.²

The difference in the predicted solubility of artemisinin in the symmetrical 1,1,2,2-tetrafluoroethane and unsymmetrical 1,1,1,2-tetrafluoroethane is nearly 100%. Intuitively, the unsymmetrical isomer of tetrafluoroethane would be assigned as more polar. However, the σ profiles of the molecules suggest that the symmetrical isomer is the more polar of the two, with more negative and more positive surface charge areas, see Fig. 5. There is a better match for both the positive and the negative polarity peaks of artemisinin and 1,1,2,2-tetrafluoroethane on

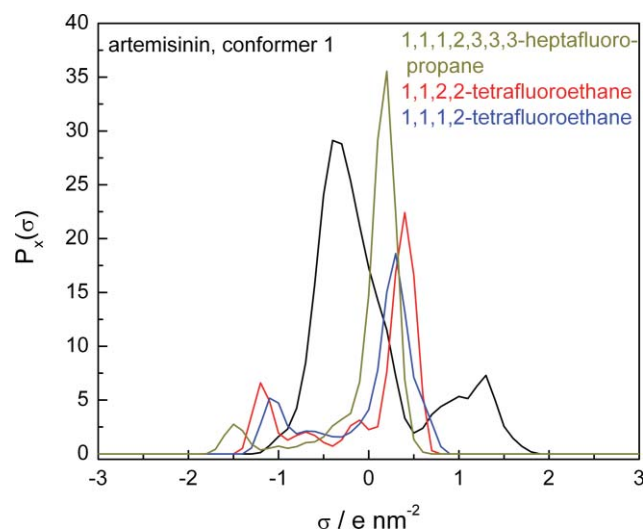


Fig. 5 Comparison of screening charge densities of the hydrofluorocarbon solvents and artemisinin.

the surface charge density scale (x axis). Unfortunately, the symmetrical tetrafluoroethane is not available commercially. The other symmetrical molecule of the same class which is commercially available is heptafluoropropane (**13**, ESI†), but even though its hydrogen carries a higher charge density than 1,1,2,2-tetrafluoroethane, the predicted solubility is only 28% higher, as only one polarised hydrogen is available.

In the class of solvents with high boiling points, a number of possible solvents were considered from the classes of carbonates, cyclic ethers, urea-based solvents, fatty acid-based solvents and naturally abundant terpenes. Here, we also considered several co-metabolites of artemisinin, which may act as co-solvents or solubility enhancement agents and thus could influence the process of extraction and also consecutive recovery of artemisinin from primary extracts. For a number of components, the optimised screening charge density files were not available in the COSMOTherm library and were computed in this study (structures of numbered compounds given in the ESI†): butylene carbonate (**5**), glycerine carbonate (**6**), DMI (**7**), DMPU (**8**), 1,3-dioxane-5-ol (**14**), 2-isobutyl-1,3-dioxane-5-ol (**15**), artemisia ketone (**21**), flavone casticin and a C₃₀ paraffin.

Table 2 and Fig. 6 show a reasonable correlation in the trend of solubilities between the experimental and predicted values, allowing a ranking of solvents. However, the errors in the absolute values in some cases are considerable, requiring experimental verification. The most interesting solvents are dimethyl carbonate, dimethylformamide, DMI, DMPU and γ -valerolactone. From these solvents, dimethyl carbonate and DMF have an appreciable vapour pressure and can still be used as conventional solvents with vacuum solvent distillation. All other solvents have very low vapour pressures and therefore a secondary extraction is needed to recover the desired compounds from the raw extracts. Furthermore, some low vapour pressure solvents are too viscous to be used as pure solvents, and could be considered as potential solvent additives.

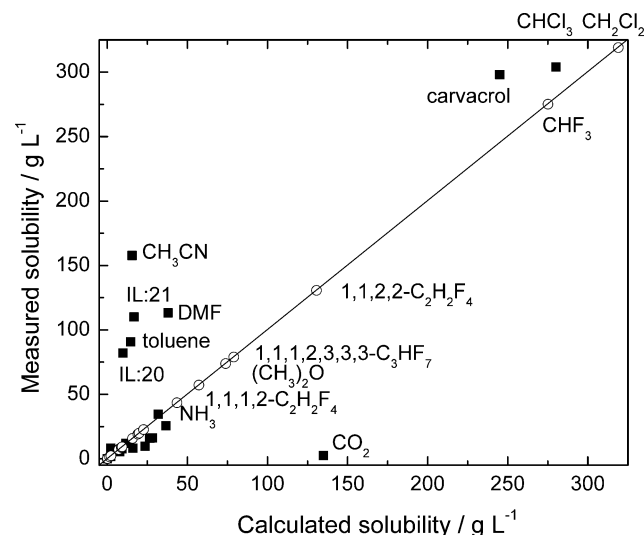


Fig. 6 Parity plot for all calculated solvents. Open symbols are for the calculated data only; closed symbols are for the parity data where experimental solubilities are available.

The predicted solubility values for the ionic liquids [DMEA] octanoate and [BMOEA][bst] (**16** and **17**, ESI†) are considerably

lower than the reported experimental values,^{2,40} but for the ionic liquid [EMIM] acetate (**18**, ESI⁺) the match is very close, see Table 2. In the case of [DMEA][oct] the two ion pairs are in equilibrium with the corresponding acid base pair. The calculated solubility for the equimolar mixture of the corresponding pair of DMEA and octanoic acid predicted a much higher value for solubility of artemisinin, although still not as high as the reported experimental value.

In the order of solubilities the novel green solvents came between the conventional hydrocarbon solvents, such as n-hexane and petroleum ether at the low end, and the compressed gases and chlorinated solvents at the high end of solubility values. Amongst the new solvents, diacetone alcohol is being used as an acetone replacement in cleaning applications; DMPU, DMI and carbonates are dipolar solvents with low volatility and toxicity. Some of the solvents could be obtained from renewable feedstocks e.g., DMPU, glyceryl carbonate, ethyl lactate, glycerol isobutyral.⁴¹

The predicted solubility of artemisinin in 1,8-cineol is reasonably high in comparison to conventional hydrocarbon solvents—7.2 g L⁻¹, see Table 2. It is also a major component of essential oil of *A. annua*.⁴² It is therefore possible that the presence of cineol and other secondary metabolites in the plant would affect solubilisation of artemisinin and its subsequent crystallisation in the work-up procedure. This also opens a new possibility of using natural products, such as light terpenes and some fatty acids, even as mixtures, as solvents for natural products extraction.

Influence of secondary metabolites on the solubility of artemisinin

Extraction from biomass is a highly unselective process: the main component is usually co-extracted with a number of secondary metabolites. Thus, PE extraction of *A. annua* produces a dark brown-green solution containing waxes, light terpenes and chlorophylls, as well as different artemisinin related compounds. Extraction with EtOH produces a solution containing more sugars and other polar compounds. Some of the extracted co-metabolites will influence the consecutive purification steps

and can also influence the primary extraction of artemisinin. It has been hypothesised that in the PE-based extraction of artemisinin, the actual extraction agent is not the PE solvent, but the higher polarity compounds that are extracted by PE first, such as terpenes, flavones, small phenolics, fatty acids, waxes, etc.

There exists a reasonable amount of data on the secondary metabolites of *A. annua*.⁴²⁻⁴⁵ The calculated solubilities of artemisinin in n-hexane–ethyl acetate mixed solvent in the presence of a number of co-metabolites are given in Table 3. The relative quantities of different metabolites vary strongly with the seed origin, growth conditions and the growing region. Therefore, the estimate of the potential influence of the co-metabolites on the solubility of artemisinin in the modified solvent system is based on the maximum amount of the particular compound reported in the literature. Thus, in the case of 1,8-cineol, the maximum reported content in the essential oil of *A. annua* is up to 30% (w/w), with the yield of the oil varying between ca. 0.4% w/w and 4.0% v/w.⁴² Similarly, the maximum reported quantity of camphor in the essential oil is 21.8%. Based on these data, and assuming that all available co-metabolite is extracted into the solvent mixture, the molar fractions of 1,8-cineol and camphor in the solvent mixture were estimated to be within the range 2.5×10^{-4} – 25×10^{-4} and 1.9×10^{-4} – 19×10^{-4} , respectively. In several cases, the major component of essential oil was reported to be artemisia ketone (**21**, ESI⁺)—up to 80%. The major fatty acids reported in the *A. annua* are 16:0, 18:1, 18:2 and 18:3, however free fatty acids comprise only ca. 4% of the total lipid content, the major components being C₃₈–C₂₀ saturated and unsaturated linear hydrocarbons.⁴⁶ In our own studies we identified 16:0 hexadecanoic (palmitic), 14:0 tetradecanoic (myristic) and 12:0 dodecanoic (lauric) acids as the main fatty acid compounds; dodecanoic acid was used in a representative simulation. The class of flavones is represented by casticin (**23**, ESI⁺), which is often found in *A. annua* extracts. Flavones, however, are found in extracts free and also with the glycoside function (**24**, ESI⁺), the latter being considerably more polar.

At such low concentrations of the co-extracted secondary metabolites, their effect on the solubility of artemisinin is

Table 3 Solubility of artemisinin in n-hexane–ethyl acetate solvent in the presence of co-metabolites at 293 K. Solvent comprises n-hexane–ethyl acetate (95 : 5% v/v) unless stated otherwise

Co-metabolite	Molar fraction co-metabolite in extract, $\times 10^{-4}$	Molar fraction artemisinin in extract, $\times 10^{-4}$	% Increase
—	—	8.6 ^a	—
—	—	12.4	0
Camphor	19	12.6	2.2
	1.9	12.6	1.6
Dodecanoic acid	2.6	12.4	0.6
1,8-Cineol	25	12.4	0.5
	2.5	12.6	2.0
aArtemisinin ketone	68	12.7	2.7
Casticin	12	12.7	2.7
Casticin monoglycoside	12	13.3	7.5
C ₃₀ paraffin	6.7	12.5	0.8
Deoxyartemisinin	12	12.5	1.1
	24	12.6	2.2
	48	12.9	4.4

^a Solvent: pure n-hexane without EtOAc additive

insignificant, only increasing solubility by up to 2.7%. This implies that consecutive crystallisation would not be considerably affected by the presence of these co-extractants. However, both deoxyartemisinin and the glycoside form of flavone casticin (**25** and **24**, ESI[†]) influence the solubility of artemisinin to a higher degree, up to 7.5% in the case of the flavone. Deoxyartemisinin is one of the stable products of degradation of artemisinin and is frequently found in some *A. annua* plant materials. The flavone glycoside appears to be a very significant modifier of artemisinin properties in the solvent matrix. It should be expected that other glycosides would have a similar effect. This is a possible reason for difficult crystallisation of artemisinin from ethanol extracts,⁴⁷ since ethanol extracts more sugars and other polar compounds.

Extraction of artemisinin using carbonates

In order to validate the possibility of using alternative greener solvents that were predicted to have high solubility of artemisinin as practical extraction solvents, exhaustive extraction of *A. annua* dry material was performed with propylene and butylene carbonate solvents, see Fig. 7. Both solvents gave a high efficiency of extraction, leaving a very small amount of artemisinin in the biomass. Moreover, the obtained extracts were lightly coloured solutions in contrast to darker brown-green hydrocarbon extracts, indicating that very small amounts of heavy compounds and chlorophylls are being extracted. Thus, consecutive separation of artemisinin from such extracts by *e.g.*, scCO₂ or liquid–liquid or liquid–solid fractionation with an affinity sorbent would yield a high purity product. Integration of extraction of biopharmaceuticals by high boiling point solvents with consecutive downstream processes is a topic of continuing investigation.

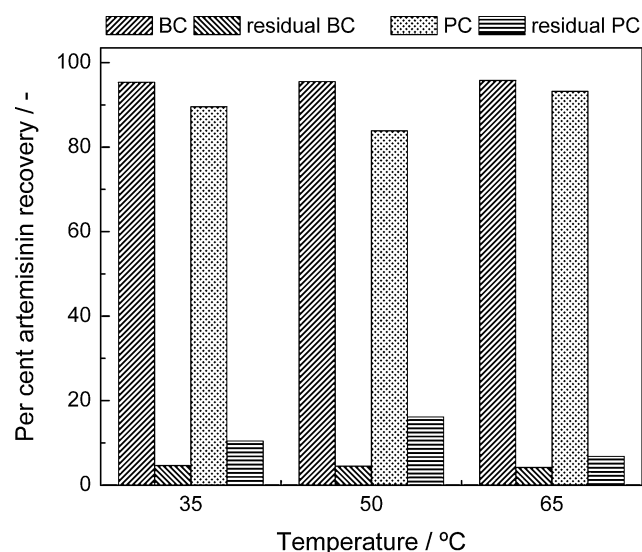


Fig. 7 Efficiency of extraction of artemisinin from *Artemisia annua* by carbonate solvents and hexane–ethyl acetate (95:5 v/v). Percent extracted and remaining in the biomass at different temperatures. BC: butylene carbonate, PC: propylene carbonate, residual BC: extract from the remaining biomass after butylene carbonate extraction, residual PC: extract from the remaining biomass after propylene carbonate extraction.

Conclusions

COSMO-RS was applied to the screening of solvents for the process of extraction of the valuable biopharmaceutical substance artemisinin. The method of calculation was improved by establishing a calibration procedure against a limited number of experimental data points to obtain an accurate value of the Gibbs energy of fusion for the solid substance of interest. Comparison with experimental values shows good accuracy of calculations for most types of molecules, although there are a number of compounds for which the deviation between the calculation and the experimental result is significant. Some experimental data are questioned, since both calculations and alternative experimental procedures yield markedly different results.

The computational method was shown to be effective in determining the behaviour of mixed solvent systems and in screening the effects of impurities on the solubilisation process. This should allow further development of the method for optimisation of biopharmaceutical separation processes. Several new green solvents were screened, for which no experimental data were available. This allowed us to identify the most promising solvents. Experimental validation of exhaustive extraction by carbonates shows the potential applicability of the new solvents for developing practical extraction processes for biopharmaceuticals.

Acknowledgements

This work was funded in part by the Engineering and Physical Sciences Research Council, project “Adaptive Processing of Natural Feedstocks”, EP/F016182/1, and the Cluster of Excellence EXC236 “Tailor Made Fuels from Biomass” at RWTH Aachen University. A.L. is grateful to the cluster for hosting his sabbatical and for financial assistance. Several colleagues have suggested new solvents to test in calculations: Prof. István Horváth, Prof. Matthew G. Davidson, Dr Carles Estévez, Dr Bhupinder Khambay. HPLC instrument was purchased with the help of Medicines for Malaria Ventures (MMV).

References

- D. J. Newman and G. M. Cragg, *J. Nat. Prod.*, 2007, **70**, 461–477.
- A. Lapkin, P. K. Plucinski and M. Cutler, *J. Nat. Prod.*, 2006, **69**, 1653–1664.
- M. S. Hutchenson, D. Pedersen, N. D. Anastas, J. Fitzgerald and D. Silverman, *Regul. Toxicol. Pharmacol.*, 1996, **24**, 85–101.
- P. F. Wilde, *US Patent* 5,512,285, 1996.
- P. F. Wilde, R. E. Skinner and R. F. Ablett, *WO* 03/090520 A2, 2002.
- Iodotrifluoromethane: toxicity review, <http://www.nap.edu/catalog/11090.html> Accessed 09.07.2006.
- W. C. McCain and J. Macko, Toxicity review for iodotrifluoromethane (CF₃I), <http://www.bfrl.nist.gov/866/HOTWC/HOTWC2006/pubs/R9902725.pdf>, Accessed 09.07.2006.
- D. Reinhardt, F. Ilgen, D. Kralisch, B. König and G. Kreisel, *Green Chem.*, 2008, **10**, 1170–1181.
- W. H. Laarhoven and T. J. H. M. Cuppen, *J. Chem. Soc., Perkin Trans. 2*, 1978, 315–318.
- J. Dupont, G. S. Fonseca, A. P. Umpierre, P. F. F. Fichtner and S. R. Teixeira, *J. Am. Chem. Soc.*, 2002, **124**, 4228–4229.
- V. Cimpeanu, M. Kočevár, V. I. Parvulescu and W. Leitner, *Angew. Chem., Int. Ed.*, 2009, **48**, 1085–1088.
- R. A. Sheldon, *Green Chem.*, 2005, **7**, 267–278.

- 13 P. G. Jessop, D. J. Heldebrant, X. Li, C. A. Eckert and C. L. Liotta, *Nature*, 2005, **436**, 1102.
- 14 G. Altshuller, *Creativity as an exact science*, Gordon & Breach Scientific Pub, 1984.
- 15 A. Lapkin, L. Joyce and B. Crittenden, *Environ. Sci. Technol.*, 2004, **38**, 5815–5823.
- 16 A. Lapkin, in *Renewables-Based Technology: Sustainability Assessment*, eds. J. Dewulf and I. H. v. Langenhove, John Wiley & Sons, 2006, pp. 39–53.
- 17 D. J. C. Constable, C. Jimenez-Gonzalez and A. Lapkin, in *Green chemistry metrics: measuring and monitoring sustainable processes*, eds. A. Lapkin and D. J. C. Constable, Wiley-Blackwell, Oxford, 2008, pp. 228–247.
- 18 A. Klamt and F. Eckert, *Fluid Phase Equilib.*, 2000, **172**, 43–72.
- 19 A. Klamt, F. Eckert, M. Hornig, M. E. Beck and T. Bürger, *J. Comput. Chem.*, 2002, **23**, 275–281.
- 20 C. A. Eckert, D. Bush, J. S. Brown and C. L. Liotta, *Ind. Eng. Chem. Res.*, 2000, **39**, 4615–4621.
- 21 Z. Lei, B. Chen, C. Li and H. Liu, *Chem. Rev.*, 2008, **108**, 1419–1455.
- 22 Z. Lei, B. Chen and C. Li, *Chem. Eng. Sci.*, 2007, **62**, 3940–3950.
- 23 W. Arlt, O. Spuhl and A. Klamt, *Chem. Eng. Process.*, 2004, **43**, 221–238.
- 24 M. Peters, M. Zavrel, J. Kahlen, T. Schmidt, M. Ansorge-Schumacher, W. Leitner, J. Büchs, L. Greiner and A. C. Spiess, *Eng. Life Sci.*, 2008, **8**, 546–552.
- 25 R. Gani, C. Jimenez-Gonzalez, A. t. Kate, P. A. Crafts, M. Jones, L. Powell, J. H. Atherton and J. L. Cordiner, *Chemical Engineering*, 2006, **113**, 30–43.
- 26 Z. Guo, B.-M. Lue, K. Thomasen, A. S. Meyer and X. Xu, *Green Chem.*, 2007, **9**, 1362–1373.
- 27 P. Kolář, J.-W. Shen, A. Tsuboi and T. Ishikawa, *Fluid Phase Equilib.*, 2002, **194–197**, 771–782.
- 28 H. Modarresi, E. Conte, J. Abildskov, R. Gani and P. Crafts, *Ind. Eng. Chem. Res.*, 2008, **47**, 5234–5242.
- 29 F. Eckert, *COSMOTerm Users Manual*, COSMOLogic GmbH & Co KG, 2007.
- 30 A. A. Lapkin, A. Walker, N. Sullivan, B. Khambay, B. Mlambo and S. Chemat, *J. Pharm. Biomed. Anal.*, 2009, **49**, 908–915.
- 31 J. N. Lisgarten, B. S. Potter, C. Bantuzeko and R. A. Palmer, *J. Chem. Crystallogr.*, 1998, **28**, 539–543.
- 32 V. Galasso, B. Kova and A. Modelli, *Chem. Phys.*, 2007, **335**, 141–154.
- 33 S. N. Sabarinath, O. P. Asthana, S. K. Puri, K. Srivastava, K. P. Madhusudan and R. C. Gupta, *Clin. Pharmacokinet.*, 2005, **44**, 1191–1203.
- 34 Y. Liu, H. Lu and F. Pang, *J. Chem. Eng. Data*, 2009, **54**, 762–764.
- 35 R. K. Haynes, B. Fugmann, J. Stetter, K. Riekmann, H.-D. Heilmann, H.-W. Chan, M.-K. Cheung, W.-L. Lam, H.-N. Wong, S. L. Croft, L. Vivas, L. Rattray, L. Stewart, W. Peters, B. L. Robinson, M. D. Edstein, B. Kotecka, D. E. Kyle, B. Beckermann, M. Gerisch, M. Radtke, G. Schmuck, W. Steinke, U. Wollborn, K. Schmeer and A. Römer, *Angew. Chem., Int. Ed.*, 2006, **45**, 2082–2088.
- 36 L.-H. Wang, Y.-T. Song, Y. Chen and Y.-Y. Cheng, *J. Chem. Eng. Data*, 2007, **52**, 757–758.
- 37 *The International Pharmacopeia*, WHO, Geneva, 2003, pp. 185–233.
- 38 A. D. Curzons, D. C. Constable and V. L. Cunningham, *Clean Products and Processes*, 1999, **1**, 82–90.
- 39 H. Xing, Y. Yang, B. Su, M. Huang and Q. Ren, *J. Chem. Eng. Data*, 2003, **48**, 330–334.
- 40 Bioniqs, Extraction of artemisinin using ionic liquids, Report by Bioniqs Ltd (UK) commissioned by the Medicines for Malaria Ventures (MMV), 2006.
- 41 C. Esteves, in *Sustainable Solutions for Modern Economies*, ed. R. Höfer, Royal Society of Chemistry, Cambridge, 2009, pp. 403–420.
- 42 R. S. Bhakuni, D. C. Jain, R. P. Sharma and S. Kumar, *Curr. Sci.*, 2001, **80**, 35–48.
- 43 R. S. Bhakuni, D. C. Jain and R. P. Sharma, in *Artemisia*, ed. C. W. Wright, Taylor & Francis, London and New York, 2002, pp. 211–248.
- 44 A. R. Bilia, P. M. d. M. Malgalhaes, M. C. Bergonzi and F. F. Vincieri, *Phytomedicine*, 2006, **13**, 487–493.
- 45 T. Kuhn and Y. Wang, in *Natural compounds as drugs. Vol 2*, eds. F. Petersen and R. Amstutz, Birkhäuser, Basel, 2008, pp. 383–422.
- 46 N. T. Ul'chenko, Z. A. Khushbaktova, N. P. Bekker, E. N. Kidisyuk, V. N. Syrov and A. I. Glushenkova, *Chem. Nat. Compd.*, 2005, **41**, 280–284.
- 47 A. Fleming and M. v. Freyhold, Assessing the technical and economic viability of the ethanolic extraction of *Artemisia annua*, http://www.mmv.org/IMG/pdf/3_ethanolic-extraction-december-2007.pdf Accessed 14.06.2009.

Environmentally benign metal-free decarboxylative aldol and Mannich reactions

Jérôme Baudoux, Pierre Lefebvre, Rémi Legay, Marie-Claire Lasne and Jacques Rouden*

Received 31st July 2009, Accepted 15th October 2009

First published as an Advance Article on the web 18th November 2009

DOI: 10.1039/b915681j

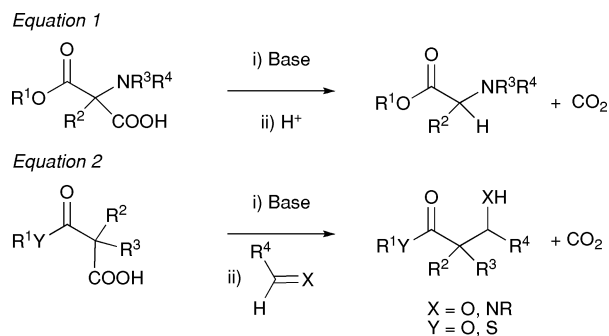
Aiming at the development of green and efficient C–C bond formations (aldol and Mannich reactions), the decarboxylative nucleophilic addition of malonic acid half ester to imines or aldehydes under mild metal-free conditions was studied. A careful control of the temperature and the appropriate choice of the organic base allowed us to obtain β -amino esters or β -hydroxy esters including α -substituted and α,α -disubstituted ones in moderate to excellent yields. $^1\text{H NMR}$ monitoring of the reaction unveiled two distinct mechanisms depending on the hemimalonate used. With the unsubstituted substrate, a carboxylic acid intermediate was isolated upon acid quench resulting from the nucleophilic addition of the putative enol carboxylate anion of the hemimalonate to imines/aldehydes before CO_2 loss. With substituted hemimalonates, the reaction likely involved an enolate which then added to imines/aldehydes or was competitively protonated. According to the base used, the reaction can be carried out either under solvent free-conditions or in an ionic liquid under mild conditions.

Introduction

The development of organic reactions based on the twelve principles of Green Chemistry is one of the most important issues in today's scientific community.¹ In recent years, much attention has been paid to the development of organocatalysis,² an eco-friendly and cost-effective concept well-suited for industrial applications, especially when metal traces is of real concern (pharmaceutical industry). Organocatalyzed aldol³ and Mannich⁴ reactions based on enamine reactive intermediates, two organic economical-atom transformations, have been widely studied. With the exception of a direct aldol reaction mediated by silyl trifluoromethanesulfonate in the presence of diisopropylethylamine,⁵ the available methods for a direct metal-free aldol reaction of esters are nearly non-existent because of the lower enolization ability of esters compared with that of ketones. Organocatalytic routes using ester and aldehyde partners involved ketene (thio)acetals as ester equivalents and chiral phosphoramides or pyridine *N*-oxides,⁶ oxazaborolidinone derivatives⁷ or triarylcarbenium ions⁸ as catalysts. An aldol reaction was also observed in DMSO.⁹ The formation of β -amino esters in organocatalyzed Mannich type reactions has been studied much more.⁴ Usually a protected imine (or an equivalent of imine) reacts with a dialkyl malonate,¹⁰ or a ketene acetal. Although efficient, these approaches require more than one step. Given their valuable roles as versatile building blocks in the synthesis of natural products or compounds of biological interest,¹¹ the development of an eco-friendly synthesis of β -

hydroxy esters and to a lesser extent to β -amino esters is rather desirable.

Recently, we showed¹² that enantioselective decarboxylative protonation¹³ of α -amino substituted malonic acid half esters is an attractive route to enantioenriched α -amino acids due to the mild conditions and the general applicability of the reaction. As part of an ongoing project concerning the metal-free synthesis of functionalized carbonyl compounds¹⁴ we envisaged the use of the organic base-catalyzed decarboxylation of malonic acid half esters (or "hemimalonates") as a mild and convenient procedure to generate an enolate of ester with its subsequent reaction with an electrophile (imines or aldehydes) (Scheme 1). The simple malonic acid half ethyl ester **1a** is a commercially available stable β -acid ester which can be easily made quantitatively from the very cheap diethyl malonate or the potassium salt of ethyl hemimalonate. Recently published work¹⁵ prompted us to describe thereafter our results focused on the following practical issues: (i) high conversion of the reagents under stoichiometric ratios, (ii) metal-free conditions, (iii) eco-friendly medium, (iv) cost-effectiveness, (v) low energy demand, (vi) easy work-up.



Scheme 1 Decarboxylative C–C bond forming reaction.

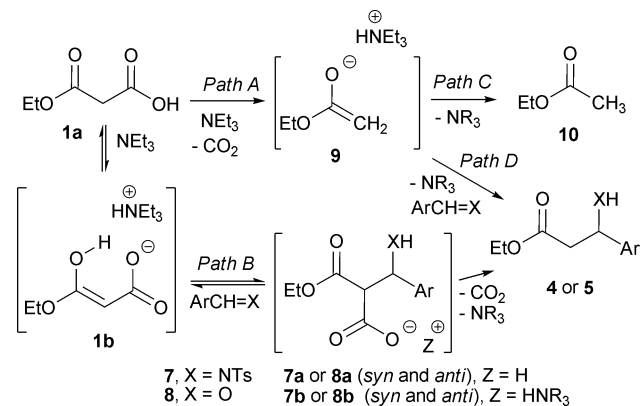
Laboratoire de Chimie Moléculaire et Thioorganique, UMR CNRS 6507, INC3M, FR 3038, ENSICAEN, Université de Caen Basse Normandie, 6, Bd Maréchal Juin, 14050 Caen, France.
E-mail: jacques.rouden@ensicaen.fr; Fax: +33 23145 2877; Tel: +33 23145 2893

Results and discussion

Decarboxylative C–C bond forming reactions from malonic acid half esters usually required the generation of a magnesium salt^{16,17} or the formation of a lithium enolate.¹⁸ Under basic conditions, *N*-acetyl serine esters were successfully prepared from acetamido hemimalonate¹⁹ whereas a decarboxylative Claisen reaction was observed²⁰ with activated malonic acid half esters. The related Doebner–Knoevenagel reaction was studied both from the mechanistic²¹ and practical²² points of view. Using a well-designed malonic acid half ester,²³ Ohta *et al.*²⁴ demonstrated that arylmalonate decarboxylase catalyzed an intramolecular decarboxylative aldol reaction.²⁵

While transition metal catalyzed decarboxylation of β -keto acids and esters is well known, particularly in aldol and Michael additions or in allylic substitutions,²⁶ only a few involve hemimalonates. Based on a biomimetic approach and on the enhanced acidity of a thioester function relative to simple esters, the groups of Cozzi²⁷ and Shair²⁸ developed the aldol-decarboxylation reaction of aldehydes and malonic- or methylmalonic acid half thioesters in the presence of a copper (II) complex. Ricci *et al.*²⁹ described the first organocatalytic asymmetric decarboxylative nucleophilic addition of malonic acid half thioesters to imines. This work led us to test the feasibility of a decarboxylative C–C bond forming reaction using hemimalonate **1a** as a straightforward available substrate.

Based on literature precedents, the mechanism of the reaction (Scheme 2) can involve the formation of enolate **9** (path A)²⁹ prior to protonation (path C) or reaction with imine **2a** (path D). Direct addition of imine **2a** to malonic acid half ester salt **1b** (path B)^{15,22,28} can also be envisaged prior to decarboxylation of salt **7** (or **8**).



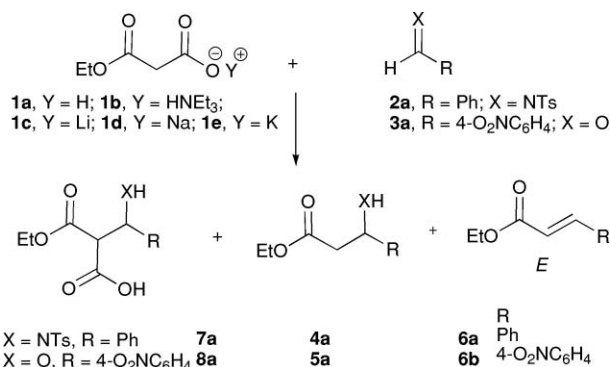
Scheme 2 Mechanistic hypothesis for the formation of the products.

When **1a** was mixed with imine **2a** in THF at 65 °C for 15 h but without any base, no reaction occurred. Adding a tertiary amine (NEt₃)³⁰ in a 1:1:2 imine/organic base/hemimalonate **1a** molar ratio, imine **2a** was completely transformed at room temperature affording β -amino ester **4a** in 68% yield (Scheme 3). The same reaction was performed with the preformed ammonium salt **1b** or with the salts **1c–1e**. The results, presented in Table 1, clearly show the benefits of using an organic ammonium counterion in these reactions. A mixture of the expected product **4a** was formed beside the non-decarboxylated compound **7a** (characterized in-situ as its ammonium salt **7b**) and the Knoevenagel–

Table 1 Influence of the cation on the outcome of the reaction of imine **2a** and hemimalonates **1b–e**

Entry ^a	Y	Compound 1	Products, ratio ^b		
			7a	4a	6a (<i>E</i>)
1	HNEt ₃	b	0	100	0
2	Li	c	43	22	35
3	Na	d	57	21	22
4	K	e	39	46	15

^a Conditions: salt **1** (1.55 mmol, 200 mg), imine **2a** (1 equiv), THF (0.1 M), room temperature, 24 h. Conversion: 100%. ^b From ¹H NMR after work-up.



Scheme 3 Reaction of hemimalonates with electrophiles.

Doebner product **6a** with the inorganic salts **1c–1e**, whereas the ammonium salt **1b** afforded exclusively the β -amino derivative **4a** (Table 1, comparison of entry 1 with entries 2–4).

In the following experiments, NEt₃ was chosen as the organic base for the optimization of the parameters. Several solvents were screened in the reaction carried out at 45 °C for 48 h. In dichloromethane, carbon tetrachloride, toluene or dioxane, the conversion was low (less than 50%) whereas the expected product **4a** was formed in satisfactory yields in THF, DMF or acetonitrile (Table 2). Decreasing the amount of hemimalonate **1a** had no significant influence (comparisons between entry 4).

Increasing the concentration of the imine **2a** to 1.8 mol.L⁻¹ improved the yields for the reaction carried out in DMF (comparison of entries 4 and 5) and allowed the reaction to be complete in 3 h in THF at 45 °C. The highest yield (66%) with the lowest amounts of solvent and substrate **1a** were thus obtained

Table 2 Reaction of ethyl hemimalonate **1a** with imine **2a**

Entry	2a ^a conc.	1a equiv	NEt ₃ equiv	Solvent	t (h)	4 yield ^b /%
1	0.1	1	1	THF	24	52–57
2	0.1	1.3	0.5	THF	24	49
3	0.1	1.3	0.25	THF	24	33
4	1.8	2 or 1	1	DMF	24	60–66
5	0.1	2	0.20	DMF	48	47
6	1.8	1.3	0.20	DMF	48	57
7	0.1	2	1	CH ₃ CN	15	67
8	1.8	1	1	CH ₃ CN	48	56

^a Conditions: hemimalonate **1a**, imine **2a** (100 mg, 0.386 mmol), molecular sieves (4 Å) and NEt₃ were stirred at 45 °C. ^b Isolated yields. Conversion of imine **2a**: 100%.

in DMF (entry 4). Working under solvent-free conditions gave only degradation products.

The reaction was attempted under catalytic conditions (Table 2, entries 2, 3, 5, 6). In THF (0.1 M), the yield of **4a** decreased with the amine loading (entries 2 and 3). However in DMF, under the standard conditions (1.8 M, entry 4) but with a longer reaction time (48 h) and 0.2 equiv of base, reaction of imine **2a** with hemimalonate **1a** (entry 6) afforded β -amino ester **4a** in just slightly lower yield than that obtained under stoichiometric conditions.

Next, ^1H NMR monitoring of the reaction at room temperature of malonic acid half ester **1a** with imine **2a** as a function of time clearly demonstrated the formation of carboxylic acid intermediate **7** as a 2/1 mixture of diastereoisomers **A** (*anti* or *syn*) and **B** (*syn* or *anti*) (Fig. 1). The experiments showed the rapid disappearance of imine **2a** concomitant with the dual formation of **A** and **B**, then product **4a** appeared after 90 min upon the slow decarboxylation of these intermediates. Whatever the conditions and all along the progress of the reaction, the ratio of both diastereoisomers stayed constant. This could be explained by the reversibility¹⁵ of the malonate nucleophilic addition on imines, reflecting thus the relative stability of intermediates **A** and **B**.

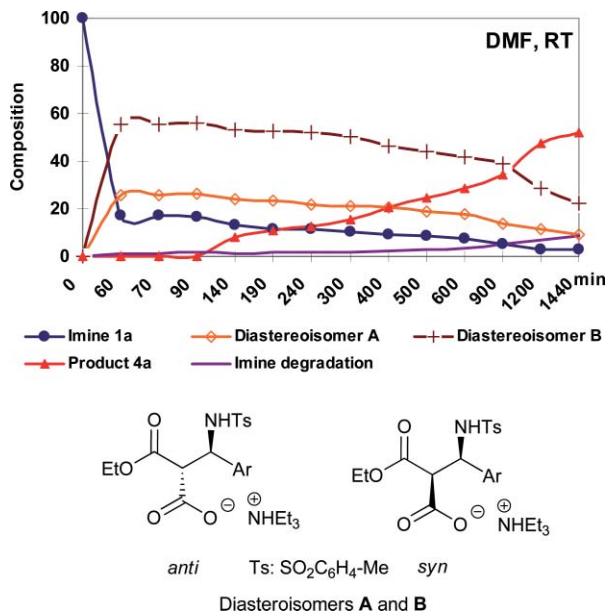


Fig. 1 Monitoring of the reaction mixture **1a**, imine **2a**, NEt_3 in DMF-d_7 , as a function of time at room temperature.

Having demonstrated the feasibility of forming a C–C bond from decarboxylative Mannich type reaction of malonic acid half ester **1a**, we attempted a decarboxylative aldol reaction using 4-nitrobenzaldehyde **3a** and hemimalonate **1a** (Table 3). In the presence of NEt_3 or DMAP (1 equiv) in DMF or acetonitrile (entries 1–4), the reaction of aldehyde **3a** with hemimalonate **1a** led exclusively to the expected aldol product **5a** in satisfactory yields. Similar results were obtained when 1,8-bis(dimethylamino)naphthalene (proton sponge “PS”) was used in acetonitrile (entry 6) whereas the Knoevenagel–Doebner

Table 3 Reaction of hemimalonate **1a** with 4-nitrobenzaldehyde **3a**

Entry	Base ^a	Solvent	Ratio 5a/6b/3a	5a Yield ^{b,c} %
1	NEt_3	DMF^c	100/0/0	78
2	NEt_3	MeCN^d	100/0/0	85
3	DMAP	DMF^c	100/0/0	70
4	DMAP	MeCN^d	100/0/0	70
5	PS ^e	DMF^c	76/24/0	50
6	PS	MeCN^d	90/0/10	82
7	NEt_3	[BMIM][PF ₆]	100/0/0	72 ^g
8	NEt_3	no ^f	100/0/0	85
9	NEt_3	no ^f	87/0/13	72 ^g

^a Reagents: hemimalonate **1a** (90 mg, 0.66 mmol), aldehyde **3a** (100 mg, 0.66 mmol, 1.8 M in the solvent), base (1 equiv). ^b Isolated yields with 100% conversion. ^c 24 h at 20 °C then 15 h at 60 °C. ^d 15 h at 80 °C. ^e PS: 1,8-bis(dimethylamino)naphthalene (Proton Sponge). ^f 2 h at 20 °C then 15 h at 60 °C. ^g Reaction carried out on a gram scale.

product **6b** was a side product in the reaction carried out in DMF (entry 5). Polar solvents being required for the reaction, we attempted the decarboxylative aldol reaction in the hydrophobic butyl methyl imidazolium hexafluorophosphate [BMIM][PF₆], a room temperature ionic liquid (RTIL). Indeed, due to their properties (high polarity, no vapor pressure, high thermal stability), RTILs are environmentally friendly substitutes for conventional organic solvents. Under the conditions described in entry 7, compound **5a** was isolated in 72% yield.

It is worth noting that the reaction proceeded in high yield in the absence of solvent. The isolation of the pure product required only an acid–base work-up (entry 8). The same reaction performed on a gram scale afforded product **5a** in a slightly lower yield due to the incomplete conversion of the starting material (entry 9).

Attempts to carry out the reaction under catalytic conditions of base gave no satisfactory results. A mixture of aldol **5a**, unsaturated ester **6b** and unreacted aldehyde **3a** was formed.

From the products observed in those reactions, Path B of the mechanism was mainly operating with unsubstituted hemimalonate at room temperature. The unstable carboxylic acid **8a**, as a mixture of two diastereoisomers, was isolated and characterized. Such an intermediate was postulated in the condensation of β -ketoacid salts with aldehydes.³¹

The scope of the reaction was then examined changing the electrophilic partner of hemimalonate **1a**. The reactions of **1a** with various aldehydes and imines were carried out in DMF or acetonitrile in the presence of NEt_3 . The results are shown in Table 4. Due to the instability of the imines used, average yields were obtained for the corresponding Mannich products (entries 1–4). Aldehydes bearing an electron-withdrawing group led to the aldol products with good yields (entries 6–9). Yields from halogenated aldehydes were slightly lower (entries 8–13). Benzaldehyde, pyridine carboxaldehyde, diphenylethanal gave moderate results, due to an incomplete conversion (entries 5, 14, 15). No reaction was observed with 4-methoxybenzaldehyde and *n*-hexanal (data not shown).

Finally, the reaction was examined with α -substituted malonic acid half esters **11a–c**, disubstituted α -methyl- α -phenyl hemimalonate **11d** and α -acetamido- α -benzyl hemimalonate **11e**. The first attempts to carry out the reaction of α -phenylmalonate

Table 4 Reaction of hemimalonate **1a** with imines and aldehydes

Entry	Electrophile	Product	Yields A ^a	(%) B ^b
1			4a 77	84
2			4b 47	52
3			4c 55	59
4			4d 51	49
5			5a nr	26
6			5b 78	85
7			5c 81	86
8			5e 81	81
9			5f 79	73
10			5g 70	67
11			5h 72	66
12			5i 57	68
13			5j 80	75
14			5k 39	52
15			5l 38	48
16	EtO ₂ C-CHO		5n 62	63

^a Reaction carried out in DMF (imine or aldehyde: 1.8 M), NEt₃ (1 equiv), room temperature for 24 h then 60 °C for 15 h. ^b Reaction carried out in acetonitrile (imine or aldehyde: 1.8 M), NEt₃ (1 equiv), 80 °C, 15 h.

11a with 4-nitrobenzaldehyde in the presence of NEt₃ in acetonitrile were unsuccessful. The sole product of the reaction was ethyl phenylacetate, resulting from the competitive protonation of the intermediate enolate (path A then C of the mechanistic hypothesis, Scheme 2).

Such an enhanced reactivity of ethyl α -phenylmalonic acid half ester towards the decarboxylation was observed in the sulfenylation of the hemiester **1a**.³² In order to avoid the fast protonation of the enolate, NEt₃ was substituted by proton sponge [1,8-bis(dimethylamino)naphthalene] as a better proton scavenger. Gratifyingly, this base allowed the decarboxylative aldolisation reaction at 0 °C in acetonitrile and **12a** was isolated in 76% yield (Table 5, entry 1). In DMF, the reaction was less efficient (entry 2). The reaction attempted in [BMIM][PF₆] did not improve the yield of **12a**, and 10% of the side-product ethyl phenylacetate was formed (entry 3).

The reaction involving the less reactive substituted derivatives **11b** and **11c** required heating in DMF to achieve the decarboxylation and afforded the hydroxy esters **12b** and **12c** in 68% and 77% yields respectively (entries 4, 5). Hemimalonates **11d** and **11e** bearing a quaternary carbon were subjected to the decarboxylative aldol reaction under different conditions of bases and solvents. Whereas the reaction of hemimalonate **11d** and 4-nitrobenzaldehyde **3a** in the presence of NEt₃ led only to the protonated side product (ethyl 2-phenylpropanoate, data not shown), the proton sponge mediated reaction of **3a** with **11d** or **11e** in DMF, afforded compound **12d** or **12e** in 39% or 78% yields respectively (entries 6, 9). Working in [BMIM][PF₆] at room temperature improved significantly the yield of **12d** (entry 7) whereas **12e** was formed in 51% yield in this solvent. Although these yields seem moderate, the reaction allowed the formation of a quaternary carbon and of two consecutive stereogenic centers under very mild conditions. Due to the disubstituted nature of the starting material, only the mechanistic hypothesis described by Path A then C on Scheme 2 is operating, *i.e.* the decarboxylation occurred first generating the enolate which was then trapped by the aldehyde before the protonation took place.

Conclusion

We have demonstrated that, using a metal-free procedure, the simple commercially available malonic acid half ethyl ester **1a** was an efficient reagent for the formation of β -hydroxy esters and β -amino esters from aryl aldehydes and arylimines *via* decarboxylative aldol and Mannich type reactions respectively. This one-step organic base-mediated procedure, possible under catalytic conditions in some cases, can replace favourably the well-known two-reaction sequence involving nucleophilic addition of malonate diester followed by a subsequent decarboxylation reaction. The simplicity of this synthetic approach which can be carried out in an open flask, even under solvent-free conditions or in ionic liquids, may render it applicable on a large scale. Depending on the malonyl starting material used (substituted or not), two different mechanisms can be involved which may dictate the choice of the organic base used. With α -substituted and α,α -disubstituted hemimalonates, two consecutive stereogenic centers are created, including a quaternary carbon with the later substrates.

Table 5 Decarboxylative aldolisation of α -substituted and disubstituted malonic acid hemi esters

Entry	Acid ^a	Base	Conditions: Solvent, Temp Time	Product 12 yield ^b %	<i>syn/anti</i> ^c ratio%
1	11a	PS	MeCN, 0 °C 18 h	12a , 76	44/56
2	11a	PS	DMF, 0 °C 60 h	12a , 43	45/55
3	11a	PS	[BMIM][PF ₆], 20 °C 48 h	12a , 65	50/50
4	11b	NEt ₃	DMF, 0 °C 60 h, then 60 °C 5 h	12b , 68	50/50
5	11c	NEt ₃	DMF, 0 °C 60 h, then 60 °C 5 h	12c , 77	34/66
6	11d	PS	DMF, 20 °C 48 h	12d , 39	50/50
7	11d	PS	[BMIM][PF ₆] 20 °C 48 h	12d , 56	50/50
8	11e	PS	[BMIM][PF ₆] 20 °C 48 h	12e , 51	50/50
9	11e	PS	DMF, 20 °C 48 h	12e , 78	50/50

^a Acid **11** (1.1 equiv), base (1 equiv), aldehyde **3a** (1 equiv). ^b Isolated yield. ^c Ratio in the crude product, from ¹H NMR spectra.

Experimental

General

Acetonitrile (MeCN), tetrahydrofuran (THF), toluene and dichloromethane were dried with a Pure-Solv™ 400 Solvent Purification System. Dimethylformamide (DMF) and triethylamine (Et₃N) were distilled from CaH₂ under a stream of nitrogen prior to use. Commercially available compounds (aldehydes, tosylamine, *p*-methoxybenzylamine, benzyl chloride, methyl iodide, 1,8-bis(dimethylamino)naphthalene, diethyl malonate, diethyl α -phenylmalonate, and diethyl α -acetamidomalonic acid) were used as received. *N*-Tosylimines and *N*-4-methoxybenzylimine precursor of compound **4b** were prepared according Kim *et al.*³³ Diethyl phenacylmalonate,³⁴ diethyl 2-methyl, 2-phenylmalonate,³⁵ and diethyl 2-(*N*-acetamido)-2-benzylmalonate³⁶ were prepared by alkylation of diethyl malonate, diethyl α -phenylmalonate, and diethyl α -acetamidomalonic acid respectively. Ethyl hemimalonates were obtained by selective hydrolysis³⁷ of the corresponding dialkylmalonates and their spectroscopic properties were in good agreement with those reported for **1a**,³⁷ **11a**,³⁷ **11b**,³⁸ **11c**,³⁹ **11d**,^{40,41} The spectral data of the known products **4a**,⁴² **5a**,⁴³ **5b**,⁴⁴ **5c**,⁴⁴ **5e**,⁴⁵ **5f-5i**,⁴⁴ **5l**,⁴⁶ **5n**,⁴⁷ were in agreement with literature data.

Characterization of the intermediates, ammonium salt **7b** and carboxylic acid **8a**

Reaction between malonate **1a and imine **2a**.** Freshly distilled triethylamine (28 μ L, 0.2 mmol) was added to a solution of malonic acid half ethyl ester **1a** (32 mg, 0.2 mmol) in dried DMF-d₇ (1 mL). In a NMR tube, imine **2a** (31 mg, 0.12 mmol) was weighed then 0.6 mL of the previous solution was added to start the reaction. The ammonium salt **7b** of carboxylic acid intermediate was characterized in-situ by ¹H NMR (–20 °C) after a few minutes in the form of two diastereomers. **First**

diastereomer: ¹H NMR (500 MHz, DMF-d₇) δ 1.18 [t, 3 H, ³J_{HH} = 7.5 Hz, CH₃(Et)], 1.19 (t, 9 H, ³J_{HH} = 7.5 Hz, CH₃), 2.30 [s, 3 H, CH₃(Ar)], 3.01 (q, 6 H, ³J_{HH} = 7.5 Hz, CH₂), 3.62 (d, 1 H, ³J_{HH} = 10.0 Hz, CH), 4.04 [q, 2 H, ³J_{HH} = 7.5 Hz, CH₂(Et)], 5.06 (t, 1 H, ³J_{HH} = 9.5 Hz, CH), 7.06 (m, 3 H, H_{Ar}), 7.12 (d, 2 H, ³J_{HH} = 8.0 Hz, H_{Ar}), 7.28 (m, 2 H, H_{Ar}), 7.43 (d, 2 H, ³J_{HH} = 8.0 Hz, H_{Ar}), 8.10 (d, 1 H, ³J_{HH} = 9.5 Hz, NH). ¹³C NMR (125 MHz, DMF-d₇) δ 8.5 (CH₃), 13.9 [CH₃(Et)], 20.6 (CH₃), 45.0 (CH₂), 58.5 (CH), 60.0 (CH₂), 62.5 (CH), 126.6, 127.4, 128.2, 128.9, 139.5, 140.6, 142.0 (C_{Ar}), 169.1 (C=O), 169.5 (C=O). **Second diastereomer:** ¹H NMR (500 MHz, DMF-d₇) δ 0.95 [t, 3 H, ³J_{HH} = 7.0 Hz, CH₃(Et)], 1.19 (t, 9 H, ³J_{HH} = 7.5 Hz, CH₃), 2.39 [s, 3 H, CH₃(Ar)], 3.01 (q, 6 H, ³J_{HH} = 7.5 Hz, CH₂), 3.45 (d, 1 H, ³J_{HH} = 9.5 Hz, CH), 3.81 [ABX₃ syst., 2 H, CH₂(Et)], 4.62 (s, 1 H, ³J_{HH} = 9.5 Hz, CH), 7.19 (m, 3 H, H_{Ar}), 7.29 (m, 2 H, H_{Ar}), 7.31 (d, 2 H, ³J_{HH} = 8.0 Hz, H_{Ar}), 7.57 (d, 2 H, ³J_{HH} = 8.0 Hz, H_{Ar}). ¹³C NMR (125 MHz, DMF-d₇) δ 8.5 (CH₃), 13.5 [CH₃(Et)], 20.6 (CH₃), 45.0 (CH₂), 58.0 (CH), 59.8 (CH), 59.9 (CH₂), 127.1, 127.2, 127.8, 128.1, 129.4, 138.1, 140.6, 142.7 (C_{Ar}), 168.9 (C=O), 171.0 (C=O).

Reaction between malonate **1a and aldehyde **3a**.** Freshly distilled triethylamine (1.06 mL, 7.6 mmol) was added to a solution of malonic acid half ethylester **1a** (1 g, 7.6 mmol) in CH₂Cl₂ (11 mL). Para-nitrobenzaldehyde **3a** (1.37 g, 9.1 mmol) was added to the solution and the reaction was stirred at room temperature for 20 h. The mixture was quenched with HCl (1 N) and extracted with CH₂Cl₂ to afford 0.95 g of the unstable carboxylic acid intermediate **8a** (49% yield) which was rapidly characterized by ¹H and ¹³C NMR shortly after as a mixture of two diastereomers.

First diastereomer: ¹H NMR (500 MHz, CDCl₃) δ 1.08 [t, 3 H, *J* = 7.2 Hz, CH₃(Et)], 3.74 (d, 1 H, *J* = 7.6 Hz, CH), 3.99–4.07 [m, 2 H, CH₂(Et)], 5.35 (d, 1 H, *J* = 7.6 Hz, CH), 7.55 (d, 2 H, *J* = 8.5 Hz, H_{Ar}), 8.14 (d, 2 H, *J* = 8.5 Hz, H_{Ar}). ¹³C NMR (125 MHz, CDCl₃) δ 13.7 [CH₃(Et)], 59.3 (CH), 62.0 [CH₂(Et)],

71.9 (CH), 123.5, 127.6, 147.5, 147.8 (C_{Ar}), 167.3 (C=O), 170.8 (C=O). **Second diastereomer:** ¹H NMR (500 MHz, CDCl₃) δ 1.12 [t, 3 H, *J* = 7.2 Hz, CH₃(Et)], 3.79 (d, 1 H, *J* = 5.8 Hz, CH), 4.07-4.14 [m, 2 H, CH₂(Et)], 5.41 (d, 1 H, *J* = 5.8 Hz, CH), 7.55 (d, 2 H, *J* = 8.5 Hz, H_{Ar}), 8.14 (d, 2 H, *J* = 8.5 Hz, H_{Ar}). ¹³C NMR (125 MHz, CDCl₃) δ 13.8 [CH₃(Et)], 58.7 (CH), 62.2 [CH₂(Et)], 71.7 (CH), 123.5, 127.3, 147.5, 147.9 (C_{Ar}), 168.3 (C=O), 169.9 (C=O).

Typical procedures

The organic base (1 equiv) was added to a stirred mixture of the aldehyde or imine (1 equiv), the malonic acid half ethylester (1.1 equiv) and the solvent. This mixture was stirred for a given time at a chosen temperature. In procedures **A-D**, the volatile compounds were removed under vacuum. The residue was diluted in ether/dichloromethane (1:1), washed with aqueous saturated NaHCO₃, then with HCl (1 N) and dried over MgSO₄. The solvents were removed under vacuum, and the residue was purified by silica-gel column chromatography to give the expected product.

Procedure	Base	Solvent	Temperature and time
A	NEt ₃	DMF	<i>cf.</i> Table 4 and Table 5 (entries 4-5).
B	NEt ₃	MeCN	80 °C, 15 h
C	PS	DMF MeCN	<i>cf.</i> Table 3 entries 5, 6 and Table 5, entries 1-3, 6-9.
D	NEt ₃	no	20 °C, 2 h then 60 °C, 15 h
E	PS	[BMIM][PF ₆]	20 °C, 48 h

In Procedure **E**, The reaction mixture was extracted with Et₂O. The organic layer was washed with H₂O, dried over MgSO₄, filtered and concentrated under reduced pressure. The residue was purified by silica-gel column chromatography.

Ethyl 3-*N*-[(4-methoxyphenyl)methyl]-3-(4-nitrophenyl)propanoate 4b (Procedure B). Under nitrogen and in the presence of molecular sieves (4Å). [69 mg, 52% yield from imine (99 mg)]. R_f 0.29 (Cyclohexane/AcOEt = 85:15). White solid (mp 105 °C). ¹H NMR (400 MHz, CDCl₃) δ 1.21 [t, 3 H, *J* = 7.2 Hz, CH₃(Et)], 2.77 [δ_{A(ABX)}, 1 H, *J*_{AB} = 15.2, *J*_{AX} = 7.6 Hz, CH₂(H_a)], 2.82 [δ_{A(ABX)}, 1 H, *J*_{AB} = 15.2, *J*_{BX} = 7.6 Hz, CH₂(H_b)], 3.70 (s, 3 H, OMe), 4.12 [q, 2 H, *J* = 7.2 Hz, CH₂(Et)], 4.83 (dd, 1 H, *J* = 5.6, 7.6 Hz, CH), 6.46 (d, 2 H, *J* = 9.2 Hz, H_{Ar}), 6.69 (d, 2 H, *J* = 9.2 Hz, H_{Ar}), 7.56 (d, 2 H, *J* = 8.8 Hz, H_{Ar}), 8.18 (d, 2 H, *J* = 8.8 Hz, H_{Ar}). ¹³C NMR (100 MHz, CDCl₃) δ 14.1 [CH₃(Et)], 26.9 (CH₂), 43.3 (MeO), 55.5 (CH), 61.1 [CH₂(Et)], 114.8, 115.2, 124.0, 127.4, 140.1, 147.3, 150.2, 153.7 (C_{Ar}), 170.6 (CO). IR (neat) 3385 (N-H), 1726 (C=O), 1605, 1509, 1342, 1234, 1177, 1031 cm⁻¹. HRMS (ESI) Calcd for C₁₈H₂₁N₂O₅ (MH⁺): 345.1450, Found: 345.1445; MS (ESI) *m/z* 345 (M + H)⁺, 299, 257, 124, 123.

Ethyl 3-(4-methylphenylsulfonamido)-3-(2-methoxyphenyl)propanoate 4c (Procedure B). Under nitrogen and in the presence of molecular sieves (4Å). [200 mg, 59% yield from imine (112 mg)]. White solid (mp 148 °C). R_f 0.28 (Cyclohexane/AcOEt = 80:20). ¹H NMR (400 MHz, CDCl₃) δ 1.13 [t, 3 H, *J* = 7.2 Hz, CH₃(Et)], 2.30 [s, 3 H, CH₃(Ts)], 2.76 [δ_{A(ABX)}, 1 H, *J*_{AB} = 15.2, *J*_{AX} = 7.2 Hz, H_a(CH₂)], 2.88

[δ_{A(ABX)}, 1 H, *J*_{AB} = 15.2, *J*_{BX} = 6.4 Hz, H_b(CH₂)], 3.75 [s, 3 H, CH₃(OMe)], 4.01 [m, 2 H, CH₂(Et)], 4.85 (m, 1 H, CH), 5.83 (dd, 1 H, *J* = 10.0 Hz, NH), 6.63 (dd, 1 H, *J* = 8.4, 0.8 Hz, H_{Ar}), 6.70 (dt, 1 H, *J* = 8.4 Hz, 0.8 Hz, H_{Ar}), 6.95 (dd, 1 H, *J* = 8.4 Hz, 0.8 Hz, H_{Ar}), 7.03 (d, 2 H, *J* = 8.3 Hz, H_{Ts}), 7.10 (dt, 1 H, *J* = 8.4 Hz, 0.8 Hz, H_{Ar}), 7.49 (d, 2 H, *J* = 8.3 Hz, H_{Ts}). ¹³C NMR (100 MHz, CDCl₃) δ 14.1 [CH₃(Et)], 31.4 [CH₃(Ts)], 40.4 (CH₂), 53.3 (CH), 55.2 [CH₃(OMe)], 60.7 [CH₂(Et)], 110.5, 120.5, 126.9, 128.9, 129.9, 129.3, 142.8, 156.3 (C_{Ar}), 170.5 (C=O). IR (neat) 3265 (N-H), 1733 (C=O), 1325, 1248, 1160 cm⁻¹. HRMS (ESI) Calcd for C₁₉H₂₄NO₅S (MH⁺): 378.1375, Found: 378.1367; MS (ESI) *m/z* 378 (M + H)⁺, 207.

Ethyl 3-(4-methylphenylsulfonamido)-3-(4-cyanophenyl)propanoate 4d (Procedure A). Under nitrogen and in the presence of molecular sieves (4Å). [70 mg, 51% yield from imine (110 mg)]. R_f 0.11 (Cyclohexane/AcOEt = 70:30). Yellow oil. ¹H NMR (400 MHz, CDCl₃) δ 1.12 [t, 3 H, *J* = 7.2 Hz, CH₃(Et)], 2.38 [s, 3 H, CH₃(Ts)], 2.70 [δ_{A(ABX)}, 1 H, *J*_{AB} = 16.0, *J*_{AX} = 5.6 Hz, H_a(CH₂)], 2.76 [δ_{A(ABX)}, 1 H, *J*_{AB} = 16.0, *J*_{BX} = 6.4 Hz, H_b(CH₂)], 4.00 [q, 2 H, *J* = 7.2 Hz, CH₂(Et)], 4.77 (m, 1 H, CH), 6.16 (d, 1 H, *J* = 8.0 Hz, NH), 7.17 (d, 2 H, *J* = 8.0 Hz, H_{Ar}), 7.26 (d, 2 H, *J* = 8.0 Hz, H_{Ar}), 7.47 (d, 2 H, *J* = 8.4 Hz, H_{Ar}), 7.57 (d, 2 H, *J* = 8.4 Hz, H_{Ar}). ¹³C NMR (100 MHz, CDCl₃) δ 14.0 [CH₃(Et)], 21.5 [CH₃(Ts)], 40.6 (CH₂), 53.8 (CH), 61.3 [CH₂(Et)], 111.6 (C_{Ar}), 118.4 (CN), 127.1, 127.4, 129.6, 132.3, 137.2, 143.8, 144.8 (C_{Ar}), 170.3 (C=O). IR (neat) 3164 (N-H), 2227 (CN), 1712 (C=O), 1270, 1160 cm⁻¹. HRMS (ESI) Calcd for C₁₉H₂₁N₂O₄S (MH⁺): 373.1222, Found: 373.1231 MS (ESI) *m/z* 373 (M + H)⁺, 202, 172.

Ethyl 3-hydroxy 3-(2-trifluoromethylphenyl)propanoate 5j (Procedure A). [190 mg, 80% yield from aldehyde (157 mg)]. R_f 0.31 (Cyclohexane/AcOEt = 90:10). Colorless oil. ¹H NMR (400 MHz, CDCl₃) δ 1.27 [t, 3 H, *J* = 7.2 Hz, CH₃(Et)], 2.56-2.71 (m, 2 H, CH₂), 3.64 (d, 1 H, *J* = 2.9 Hz, OH), 4.19 [q, 2 H, *J* = 7.2 Hz, CH₂(Et)], 5.52-5.55 (m, 1 H, CH), 7.38 (t, 1 H, *J* = 7.5 Hz, H_{Ar}), 7.55-7.63 (m, 2 H, H_{Ar}), 7.82 (d, 1 H, *J* = 7.5 Hz, H_{Ar}). ¹³C NMR (100 MHz, CDCl₃) δ 14.1 [CH₃(Et)], 43.4 (CH₂), 61.0 [CH₂(Et)], 65.9 (CH), 122.1, 125.4 (q, *J* = 5.8 Hz, CF₃), 126.6 (q, *J* = 22.9 Hz, CF₃), 127.6, 127.7, 132.4, 141.4 (C_{Ar}), 172.2 (C=O). ¹⁹F NMR (376 MHz, CDCl₃) δ -58.47. IR (neat) 3473 (O-H), 1717 (C=O), 1310, 1157, 1109 cm⁻¹. HRMS (ESI) Calcd for C₁₂H₁₄O₃F₃ (MH⁺): 263.0895, Found: 263.0901. MS (ESI) *m/z* 263 (M + H)⁺, 245, 203; Anal Calcd: C 54.96, H 5.00; Found: C 54.76; H 5.13.

Ethyl 3-hydroxy 3-(2-pyridinyl)propanoate 5k (Procedure B). [90 mg, 52% yield from aldehyde (96 mg)]. R_f 0.25 (Cyclohexane/AcOEt = 70:30). Light brown oil. ¹H NMR (400 MHz, CDCl₃) δ 1.25 [t, 3 H, *J* = 7.2 Hz, CH₃(Et)], 2.79 [δ_{A(ABX)}, 1 H, *J*_{AB} = 16.0, *J*_{AX} = 8.0 Hz, CH₂(H_a)], 2.94 [δ_{B(ABX)}, 1 H, *J*_{AB} = 16.0, *J*_{BX} = 4.4 Hz, CH₂(H_b)], 4.17 [q, 2 H, *J* = 7.2 Hz, CH₂(Et)], 5.21 [δ_{X(ABX)}, 1 H, *J*_{AX} = 8.0, *J*_{BX} = 4.4 Hz, CH], 7.26-7.29 (m, 1 H, H_{Ar}), 7.48 (d, 1 H, *J* = 8.0 Hz, H_{Ar}), 7.77 (dt, 1 H, *J* = 8.0 Hz, 2.0 Hz, H_{Ar}), 8.56 (d, 1 H, *J* = 4.0 Hz, H_{Ar}). ¹³C NMR (100 MHz, CDCl₃) δ 14.1 [CH₃(Et)], 42.5 (CH₂), 60.7 [CH₂(Et)], 70.1 (CH), 120.3, 122.6, 136.9, 148.5, 160.8 (C_{Ar}), 171.9 (C=O). IR (neat) 3365 (O-H), 1718 (C=O), 1596, 1163, 1024 cm⁻¹. HRMS (ESI)

Calcd for $C_{11}H_{14}NO_3$ (MH^+): 196.0974, Found: 196.0975. MS (ESI) m/z 196 ($M + H^+$), 178, 150, 132.

Ethyl 2-phenyl-3-hydroxy-3-(4-nitrophenyl)propanoate 12a (Procedure C). [50 mg, 77% yield from aldehyde (32 mg)]. R_f 0.29 (Cyclohexane/AcOEt = 80:20). Light brown oil. **First diastereomer:** 1H NMR (400 MHz, $CDCl_3$) δ 1.11 (t, 3 H, $J = 7.2$ Hz, CH_3), 3.20 (bs, 1 H, OH), 3.81 (d, H, $J = 6.0$ Hz, CHPh), 4.02-4.13 (m, 2 H, CH_2), 5.42 (d, 1 H, $J = 6.0$ Hz, CHOH), 7.19-7.22 (m, 2 H, H_{Ar}), 7.28-7.41 (m, 3 H, H_{Ar}), 7.41 (d, 2 H, $J = 8.8$ Hz, H_{Ar}), 8.12 (d, 2 H, $J = 8.8$ Hz, H_{Ar}). ^{13}C NMR (100 MHz, $CDCl_3$) δ 13.9 (CH_3), 58.8 (CPh), 61.4 (CH_2), 73.8 (COH), 123.3, 127.5, 128.2, 128.7, 129.2, 133.4, 147.5, 148.0 (C_{Ar}), 172.6 (C=O). **Second diastereomer:** 1H NMR (400 MHz, $CDCl_3$) δ 1.22 (t, 3 H, $J = 6.8$ Hz, CH_3), 3.49 (d, 1 H, $J = 4.0$ Hz, OH), 3.78 (d, 1 H, $J = 9.2$ Hz, CHPh), 4.14-4.27 (m, 2 H, CH_2), 5.27 (dd, 1 H, $J = 9.2$ Hz, $J = 4.0$ Hz, CHOH), 7.02-7.05 (m, 2 H, H_{Ar}), 7.20-7.23 (m, 5 H, H_{Ar}), 8.03 (d, 2 H, $J = 8.4$ Hz, H_{Ar}). ^{13}C NMR (100 MHz, $CDCl_3$) δ 14.0 (CH_3), 59.9 (CPh), 61.6 (CH_2), 75.7 (COH), 123.2, 127.5, 128.0, 128.4, 128.8, 134.5, 147.4, 148.0 (C_{Ar}), 173.1 (C=O). IR (neat) 3526 (O-H), 2984, 1705 (C=O), 1517, 1345 cm^{-1} . HRMS (ESI): Calcd. for $C_{18}H_{20}NO_5$ (MH^+): 330.1341. Found: 330.1330.

Ethyl 2-(phenylmethyl)-3-hydroxy-3-(4-nitrophenyl)propanoate 12b (Procedure A). [147 mg, 68% yield from **3a** (100 mg)]. R_f 0.28 (Cyclohexane/AcOEt = 80:20). Colorless oil. **First diastereomer:** 1H NMR (400 MHz, $CDCl_3$) δ 0.94 (t, 3 H, $^3J_{HH} = 6.8$ Hz, CH_3), 2.81-2.86 (m, 1 H, CHBn), 2.97-3.02 (m, 2 H, CH_2 Ph), 3.44 (br.s, 1 H, OH), 3.89-3.96 [m, 2 H, CH_2 (Et)], 5.16 [d, 1 H, $^3J_{HH} = 3.8$ Hz, CH(OH)], 7.04 (d, 2 H, $^3J_{HH} = 8.7$ Hz, H_{Ar}), 7.13-7.25 (m, 3 H, H_{Ar}), 7.58 (d, 2 H, $^3J_{HH} = 8.7$ Hz, H_{Ar}), 8.20 (d, 2 H, $^3J_{HH} = 8.7$ Hz, H_{Ar}). ^{13}C NMR (100 MHz, $CDCl_3$) δ 13.8 (CH_3), 32.8 (CH_2 Ph), 54.4 (CHBn), 60.9 [CH_2 (Et)], 72.9 (CHOH), 123.6, 126.5, 127.1, 128.4, 128.8, 138.3, 147.5, 148.6 (C_{Ar}), 174.2 (C=O). IR (neat) 3481 (O-H); 1722 (C=O); 1603; 1519; 1344 cm^{-1} . **Second diastereomer:** 1H NMR (400 MHz, $CDCl_3$) δ 0.90 (t, 3 H, $^3J_{HH} = 7.2$ Hz, CH_3), 2.84-3.00 (m, 3 H, CHBn), 3.68 (d, 1 H, $^3J_{HH} = 8.0$ Hz, OH), 3.82-3.95 [m, 2 H, CH_2 (Et)], 4.79 [dd, 1 H, $^3J_{HH} = 8.0$ Hz, $^3J_{HH} = 4.3$ Hz, CH(OH)], 7.11-7.24 (m, 5 H, H_{Ar}), 7.41 (d, 2 H, $^3J_{HH} = 8.5$ Hz, H_{Ar}), 8.11 (d, 2 H, $^3J_{HH} = 8.5$ Hz, H_{Ar}). ^{13}C NMR (100 MHz, $CDCl_3$) δ 13.9 (CH_3), 35.8 (CH_2 Ph), 53.9 (CHBn), 61.0 [CH_2 (Et)], 72.9 (CHOH), 123.6, 126.8, 126.9, 128.6, 129.0, 137.7, 147.4, 149.7 (C_{Ar}), 174.2 (C=O). IR (neat) 3531 (O-H), 1732 (C=O), 1604, 1516, 1351 cm^{-1} . HRMS (ESI): Calcd. for $C_{18}H_{20}NO_5$ (MH^+): 330.1341. Found: 330.1330.

Ethyl 2-[hydroxy(4-nitrophenyl)methyl]-4-oxo-4-phenylbutanoate 12c (Procedure A). [55 mg, 77% yield from **3b** (50 mg)]. R_f 0.2 (Cyclohexane/AcOEt = 70:30). Colorless oil. **Major diastereomer:** 1H NMR (400 MHz, $CDCl_3$) δ 1.06 (t, 3 H, $^3J_{HH} = 7.2$ Hz, CH_3), 3.20-3.43 (m, 3 H), 3.77 (d, 1 H, $^3J_{HH} = 6.2$ Hz, OH), 3.98-4.06 [m, 2 H, CH_2 (Et)], 5.09 [t, 1 H, $^3J_{HH} = 6.2$ Hz, CH(OH)], 7.25-7.56 (m, 5 H, H_{Ar}), 7.84 (d, 2 H, $^3J_{HH} = 8.4$ Hz, H_{Ar}), 8.12 (d, 2 H, $^3J_{HH} = 8.4$ Hz, H_{Ar}). ^{13}C NMR (100 MHz, $CDCl_3$) δ 14.0 (CH_3), 37.4 (CH_2), 47.3 (CH), 61.4 [CH_2 (Et)], 73.0 (CH), 123.6, 127.0, 128.1, 128.7, 133.7, 136.2, 147.5, 149.0, 173.6 (C=O), 197.4 (C=O). **Minor diastereomer:** 1H NMR (400 MHz, $CDCl_3$) δ 1.12 (t, 3 H, $^3J_{HH} = 7.2$ Hz,

CH_3), 2.97 [$\delta_{A(BX)}$, 1 H, $J_{AB} = 20.8$, $J_{AX} = 7.2$ Hz, $CH_2(H_a)$], 3.17-3.43 (m, 3 H), 4.06-4.15 [m, 2 H, CH_2 (Et)], 5.31 [br.s, 1 H, CH(OH)], 7.25-7.56 (m, 5 H, H_{Ar}), 7.79 (d, 2 H, $^3J_{HH} = 8.4$ Hz, H_{Ar}), 8.12 (d, 2 H, $^3J_{HH} = 8.4$ Hz, H_{Ar}). ^{13}C NMR (100 MHz, $CDCl_3$) δ 14.0 (CH_3), 34.7 (CH_2), 47.8 (CH), 61.4 [CH_2 (Et)], 72.6 (CH), 123.7, 126.9, 128.0, 128.6, 133.5, 136.3, 147.4, 148.6, 173.2 (C=O), 198.1 (C=O). IR (neat) 3475 (O-H), 1725 (C=O), 1683 (C=O), 1517, 1343 cm^{-1} . HRMS (ESI): Calcd. for $C_{19}H_{19}NO_6$ (MH^+): 358.1291. Found: 358.1293.

Ethyl 2-phenyl-2-methyl-3-hydroxy-3-(4-nitrophenyl) propanoate 12d (Procedure E or Procedure C). Purification on silica-gel column chromatography (cyclohexane/ Et_2O = 90:10). [54 mg, 39% yield from **3a** (100 mg)]. Two diastereoisomers. Colorless oil. **First diastereomer:** 1H NMR (400 MHz, $CDCl_3$) δ 1.13 (t, 3 H, $^3J_{HH} = 7.2$ Hz, CH_3), 1.44 (s, 3 H, CH_3), 3.70 (d, 1 H, $^3J_{HH} = 2.6$ Hz, OH), 4.14 (ABX₃, 2 H, CH_2O), 5.30 [d, 1 H, $^3J_{HH} = 2.6$ Hz, CH(OH)], 6.80-7.23 (m, 7 H, H_{Ar}), 7.97 (d, 2 H, $^3J_{HH} = 8.8$ Hz, H_{Ar}). ^{13}C NMR (400 MHz, $CDCl_3$) δ 13.9 (CH_3), 19.2 (CH_3), 55.5 (CH), 61.7 (ArCH), 77.9, 122.4, 127.8, 128.0, 129.2, 137.0, 146.2, 147.4 (C_{Ar}), 176.5 (C=O). **Second diastereomer:** 1H NMR (400 MHz, $CDCl_3$) δ 1.13 (t, 3 H, $^3J_{HH} = 7.2$ Hz, CH_3), 1.42 (s, 3 H, CH_3), 3.91 (d, 1 H, $^3J_{HH} = 3.0$ Hz, OH), 4.14 (ABX₃, 2 H, CH_2O), 5.43 [d, 1 H, $^3J_{HH} = 3.0$ Hz, CH(OH)], 6.78-7.23 (m, 7 H, H_{Ar}), 7.83 (d, 2 H, $^3J_{HH} = 8.8$ Hz, H_{Ar}). ^{13}C NMR (400 MHz, $CDCl_3$) δ 14.1 (CH_3), 19.2 (CH_3), 56.3 (CH), 61.8 (ArCH), 77.9, 122.1, 126.6, 127.9 (CH_{Ar}), 128.4, 128.7, 139.0, 145.9, 147.1 (C_{Ar}), 177.1 (C=O). HRMS (ESI) Calcd for $C_{18}H_{20}NO_5$ (MH^+): 330.1341, Found: 313.1330.

2-(N-acetylamino)-2-carboethoxy-3-(phenylmethyl)propionic acid 11e⁴⁸. [1.7 g, 89% yield from malonate (2 g)]. White solid (mp 135 °C). 1H NMR ($CDCl_3$) δ 1.24 [t, 3 H, $J = 7.2$ Hz, CH_3 (Et)], 1.92 [s, 3 H, CH_3], 3.39 [$\delta_{A(AB)}$, 1 H, $J_{AB} = 13.6$ Hz, CH_2], 3.45 [$\delta_{B(AB)}$, 1 H, $J_{AB} = 13.6$ Hz, CH_2], 4.12 [q, 2 H, $J = 7.2$ Hz, CH_2 (Et)], 6.99-7.29 (m, 5 H, H_{Ar}), 13.74 (bs, 1 H, CO_2H). ^{13}C NMR ($CDCl_3$) δ 13.8, 22.2, 37.3, 61.3, 66.8, 126.7, 128.1, 129.8, 135.6, 167.5, 168.3, 169.2. IR (neat) 3324 (O-H), 1721 (C=O), 1598, 1525, 1201 cm^{-1} . HRMS (ESI) Calcd for $C_{14}H_{17}NO_5$ (MH^+): 280.1172, Found: 280.1185.

Ethyl 2-(N-acetylamino)-2-(phenylmethyl)-3-hydroxy-3-(4-nitrophenyl) propanoate 12e (Procedure C). [144 mg, 77% yield from **11e** (134 mg)]. **First diastereomer:** Light brown solid (mp 125 °C). R_f 0.25 (Cyclohexane/AcOEt = 70:30). 1H NMR (400 MHz, $CDCl_3$) δ 1.21 [t, 3 H, $J = 7.2$ Hz, CH_3 (Et)], 1.98 (s, 3 H, $COCH_3$), 3.05-3.10 (m, 2 H, CH_2 Ph), 4.05-4.21 [m, 2 H, CH_2 (Et)], 5.60 (s, 1 H, CHOH), 5.85 (bs, 1 H, OH), 5.99 (s, 1 H, NH), 7.02 (m, 2 H, H_{Ar}), 7.26 (m, 2 H, H_{Ar}), 7.48 (d, 2 H, $J = 6.8$ Hz, H_{Ar}), 8.19 (d, 2 H, $J = 6.8$ Hz, H_{Ar}), 8.26-8.33 (m, 1 H, H_{Ar}). ^{13}C NMR (100 MHz, $CDCl_3$) δ 13.9 [CH_3 (Et)], 24.1 ($COCH_3$), 37.6 (CH_2 Ph), 62.8 [CH_2 (Et)], 70.7, 77.0 (COH), 123.3, 127.6, 128.1, 128.8, 129.7, 131.3, 134.7, 147.4, 170.4, 172.3 (C=O). IR (neat) 3260 (OH), 1728, 1645 (C=O), 1510, 1345 cm^{-1} . HRMS (ESI) Calcd for $C_{20}H_{23}N_2O_6$ (MH^+): 387.1556, found: 378.1567. **Second diastereomer:** Light brown solid (mp 123 °C). R_f 0.1 (Cyclohexane/AcOEt = 70:30). 1H NMR (400 MHz, $CDCl_3$) δ 1.43 [t, 3 H, $J = 7.2$ Hz, CH_3 (Et)], 1.98 (s, 3 H, $COCH_3$), 3.46 [d, 1 H, $J = 14.0$ Hz, CH_2 Ph (H_a)], 4.07 [d, 1 H, $J = 14.0$ Hz, CH_2 Ph (H_b)], 4.23-4.32

[m, 2 H, CH₂(Et)], 5.47 [d, 1 H, *J* = 10.4 Hz, CHO], 6.36 (s, 1 H, NH), 7.02 (m, 2 H, H_{Ar}), 7.25-7.33 (m, 5 H, H_{Ar}), 8.14 [d, 2 H, *J* = 6.8 Hz, H_{Ar}]. ¹³C NMR (100 MHz, CDCl₃) δ 14.1 [CH₃(Et)], 23.6 (COCH₃), 38.0 (CH₂Ph), 63.3 [CH₂(Et)], 72.2, 77.9 (COH), 123.4, 126.9, 127.5, 128.6, 129.6, 135.2, 147.5, 148.2, 170.6, 172.9 (C=O). IR (neat) 3286 (OH), 1713, 1641 (C=O), 1519, 1347 cm⁻¹. HRMS (ESI) Calcd for C₂₀H₂₃N₂O₆ (MH⁺): 387.1556, found: 378.1563.

Acknowledgements

We gratefully acknowledge Ministère de l'Enseignement Supérieur et de la Recherche for a fellowship to PL, ANR "Mesocat", CNRS and its program "Chimie pour le Développement Durable", Région Basse-Normandie, and the European Union (FEDER funding) for financial supports.

References

- 1 P. Tundo, and P. T. Anastas, *Green Chemistry: Challenging Perspectives*, Oxford Sciences, Oxford, 1999.
- 2 (a) For recent comprehensive reviews on the subject: P. I. Dalko, *Enantioselective Organocatalysis*, Wiley-VCH, Weinheim, 2007; (b) A. Berkessel, H. Gröger, *Asymmetric Organocatalysis – From Biomimetic Concepts to Application in Asymmetric Synthesis*, Wiley-VCH, Weinheim, 2005.
- 3 (a) R. Mestres, *Green Chem.*, 2004, **6**, 583 and references therein; (b) S. Adachi and T. Harada, *Eur. J. Org. Chem.*, 2009, 3661.
- 4 (a) J. M. M. Verkade, L. J. C. van Hemert, P. J. L. M. Quaedflieg and P. J. T. Rutjes, *Chem. Soc. Rev.*, 2008, **37**, 29 and references therein; (b) A. Ting and S. E. Schaus, *Eur. J. Org. Chem.*, 2007, 5797.
- 5 C. W. Downey and M. W. Johnson, *Tetrahedron Lett.*, 2007, **48**, 3559.
- 6 (a) S. E. Denmark, S. B. D. Winter, X. Su and K.-T. Wong, *J. Am. Chem. Soc.*, 1996, **118**, 7404; (b) S. E. Denmark and Y. Fan, *J. Am. Chem. Soc.*, 2002, **124**, 4233; (c) S. E. Denmark, Y. Fan and M. D. Eastgate, *J. Org. Chem.*, 2005, **70**, 5235.
- 7 S. Adachi and T. Harada, *Org. Lett.*, 2008, **10**, 4999.
- 8 C.-T. Chen, S.-D. Chao, K.-C. Yen, C.-H. Chen, I.-C. Chou and S.-W. Hon, *J. Am. Chem. Soc.*, 1997, **119**, 11341.
- 9 Y. Genisson and L. Gorrichon, *Tetrahedron Lett.*, 2000, **41**, 4881.
- 10 C. M. Bode, A. Ting and S. E. Schaus, *Tetrahedron*, 2006, **62**, 11499.
- 11 For examples: (a) R. Shen, C. T. Lin, E. J. Bowman, B. J. Bowman and J. A. Porco, *J. Am. Chem. Soc.*, 2003, **125**, 7889; (b) C. Aïssa, R. Riveiros, J. Ragot and A. Fürstner, *J. Am. Chem. Soc.*, 2003, **125**, 15512; (c) A. K. Ghosh and S. Kulkarni, *Org. Lett.*, 2008, **10**, 3907; (d) J. F. Bower, T. Riis-Johannessen, P. Szeto, A. J. Whitehead and T. Gallagher, *Chem. Commun.*, 2007, 728; (e) W. Seitz, H. Geneste, G. Backfisch, J. Delzer, C. Graef, W. Hornberger, A. Kling, T. Subkowski and N. Zimmermann, *Bioorg. Med. Chem. Lett.*, 2008, **18**, 527; (f) J. Jamison, S. Levy, X. Sun, D. Zeckner, W. Current, M. Zweifel, M. Rodriguez, W. Turner and S.-H. Chen, *Bioorg. Med. Chem. Lett.*, 2000, **10**, 2101.
- 12 M. Amere, M.-C. Lasne and J. Rouden, *Org. Lett.*, 2007, **9**, 2621.
- 13 For a review on asymmetric decarboxylative protonations, see: J. Blanchet, J. Baudoux, M. Amere, M.-C. Lasne and J. Rouden, *Eur. J. Org. Chem.*, 2008, 5493.
- 14 M. Pouliquen, J. Blanchet, M.-C. Lasne and J. Rouden, *Org. Lett.*, 2008, **10**, 1029.
- 15 N. Blaquiere, D. G. Shore, S. Rousseaux and K. Fagnou, *J. Org. Chem.*, 2009, **74**, 6190.
- 16 (a) R. E. Ireland and J. A. Marshall, *J. Am. Chem. Soc.*, 1959, **81**, 2907; (b) A. I. Scott, C. J. Wiesner, S. Yoo and S.-K. Chung, *J. Am. Chem. Soc.*, 1975, **97**, 6277; (c) Y. Kobuke and J.-I. Yoshida, *Tetrahedron Lett.*, 1978, **4**, 367; (d) D. W. Brooks, L. D.-L. Lu and S. Masamune, *Angew. Chem. Int. Ed. Engl.*, 1979, **18**, 72; (e) D. J. Krysan, *Tetrahedron Lett.*, 1996, **37**, 3303.
- 17 (a) M. Banwell, D. Hockless, B. Jarrott, B. Kelly, A. Knill, R. Longmore and G. Simpson, *J. Chem. Soc., Perkin 1*, 2000, 3555; (b) J. E. McMurry, W. A. Andrus and J. H. Musser, *Synth. Commun.*, 1978, **8**, 53.
- 18 M. Ihara, M. Takahashi, H. Niitsuma, N. Taniguchi, K. Yasui and K. Fukumoto, *J. Org. Chem.*, 1989, **54**, 5413.
- 19 H. Hellmann and H. Piechota, *Liebigs Ann. Chem.*, 1960, **631**, 175.
- 20 Y. Ryu and A. I. Scott, *Tetrahedron Lett.*, 2003, **44**, 7499.
- 21 (a) B. List, A. Doehring, M. T. Hechavarría Fonseca, K. Wobser, H. van Thienen, R. Rios Torres and P. L. Galilea, *Adv. Synth. & Cat.*, 2005, **347**, 1558; (b) B. List, A. Doehring, M. T. Hechavarría Fonseca, A. Job and R. Rios Torres, *Tetrahedron*, 2006, **62**, 476.
- 22 M. Tanaka, O. Oota, H. Hiramatsu and K. Fujiwara, *Bull. Chem. Soc. Jpn*, 1988, **61**, 2473.
- 23 [2-(3-oxopropyl)phenyl]malonic acid.
- 24 Y. Terao, K. Miyamoto and H. Ohta, *Chem. Lett.*, 2007, **36**, 420.
- 25 J. Nokami, T. Mandai, H. Watanabe, H. Ohyama and J. Tsuji, *J. Am. Chem. Soc.*, 1989, **111**, 4126.
- 26 (a) J. A. Tunge and E. C. Burger, *Eur. J. Org. Chem.*, 2005, 1715 and references therein; (b) S. C. Marinescu, T. Nishimata, J. T. Mohr and B. M. Stoltz, *Org. Lett.*, 2008, **10**, 1039.
- 27 S. Orlandi, M. Benaglia and F. Cozzi, *Tetrahedron Lett.*, 2004, **45**, 1747.
- 28 (a) G. Lalic, A. D. Aloise and M. D. Shair, *J. Am. Chem. Soc.*, 2003, **125**, 2852; (b) D. Magdziak, G. Lalic, H. M. Lee, K. C. Fortner, A. D. Aloise and M. D. Shair, *J. Am. Chem. Soc.*, 2005, **127**, 7284; (c) K. C. Fortner and M. D. Shair, *J. Am. Chem. Soc.*, 2007, **129**, 1032.
- 29 A. Ricci, D. Pettersen, L. Bernardi, F. Fini, M. Fochi, R. P. Herrera and V. Sgarzani, *Adv. Synth. & Cat.*, 2007, **349**, 1037.
- 30 DABCO and 3-quinuclidinol gave the same results than NEt₃. Unhindered secondary amines (piperidine, pyrrolidine) led exclusively to the unsaturated esters **6a** of *E* configuration. Pyridine did not catalyze the reaction even in a prolonged reaction time. The less nucleophilic secondary amines (diisopropylamine and 2,2,6,6-tetramethylpiperidine) gave a mixture of adduct **4a** and ester **6a** (*E*) (ratio 86/14 and 74/16 respectively).
- 31 T. Kourouli, P. Kefalas, N. Ragoussis and V. Ragoussis, *J. Org. Chem.*, 2002, **67**, 4615.
- 32 B. Wladislaw, L. Marzorati and C. L. Donnici, *J. Chem. Soc., Perkin Trans. 1*, 1993, 3167.
- 33 K. Y. Lee, C. G. Lee and J. N. Kim, *Tetrahedron Lett.*, 2003, **44**, 1231.
- 34 Y. Cai and B. P. Roberts, *Tetrahedron Lett.*, 2003, **44**, 4645.
- 35 J. M. Domagala and R. D. Bach, *J. Org. Chem.*, 1979, **44**, 2429.
- 36 R. Kuwano, Y. Kondo and Y. Matsuyama, *J. Am. Chem. Soc.*, 2003, **125**, 12104.
- 37 S. Niwayama, H. Cho and C. Lin, *Tetrahedron Lett.*, 2008, **49**, 4434.
- 38 M. Flipo, T. Beghyn, J. Charton, V. A. Leroux, B. P. Deprez and R. F. Deprez-Poulain, *Bioorg. Med. Chem.*, 2007, **15**, 63.
- 39 (a) J. Fuentes, J. L. Molina and M. A. Pradera, *Tetrahedron: Asymmetry*, 1998, **9**, 2517; (b) Y. Cai, B. P. Roberts, D. A. Tocher and S. A. Barnett, *Org. Biomol. Chem.*, 2004, **2**, 2517.
- 40 A. Vecchi and G. Melone, *J. Org. Chem.*, 1959, **24**, 109.
- 41 P. Dominguez de Maria, B. Kossmann, N. Potgrave, S. Buchholz, H. Trauthwein, O. May and H. Gröger, *Synlett*, 2005, 1746.
- 42 G. A. Molander and P. J. Stengel, *Tetrahedron*, 1997, **53**, 8887.
- 43 K. Y.-K. Chow and J. W. Bode, *J. Am. Chem. Soc.*, 2004, **126**, 8126.
- 44 A. I. Ayi, T. N. Condom, T. N. Wade and R. Guedj, *J. Fluorine Chem.*, 1979, **14**, 437.
- 45 Y. S. Suh and R. D. Rieke, *Tetrahedron Lett.*, 2004, **45**, 1807.
- 46 S. Kiyooka and M. Shirouchi, *J. Org. Chem.*, 1992, **57**, 1.
- 47 M. Miyashita, T. Suzuki, M. Hoshino and A. Yoshikoshi, *Tetrahedron*, 1997, **53**, 12469.
- 48 L. Berlinguet, *Can. J. Chem.*, 1954, **32**, 51.

Liquid phase oxidation of *p*-xylene to terephthalic acid at medium-high temperatures: multiple benefits of CO₂-expanded liquids

Xiaobin Zuo,^{a,b} Fenghui Niu,^a Kirk Snavely,^{a,c} Bala Subramaniam^{*a,c} and Daryle H. Busch^{*a,b}

Received 29th September 2009, Accepted 18th November 2009

First published as an Advance Article on the web 15th January 2010

DOI: 10.1039/b920262e

The Co/Mn/Br catalyzed oxidation of *p*-xylene to terephthalic acid (TPA) is demonstrated in CO₂-expanded solvents at temperatures lower than those of the traditional Mid-Century (MC) process. As compared with the traditional air (N₂/O₂) oxidation system, the reaction with CO₂/O₂ mixture at 160 °C and using an additional inert gas (N₂ or CO₂) pressure of 100 bar increases both the yield of TPA and the purity of solid TPA via a more efficient conversion of the intermediates, 4-carboxybenzaldehyde and *p*-toluic acid. At the same time, the amount of yellow colored by-products in the solid TPA product is also lessened, as determined by spectroscopic analysis. Equally important, the decomposition or burning of the solvent, acetic acid, monitored in terms of the yield of the gaseous products, CO and CO₂, is reduced by *ca.* 20% based on labeled CO₂ experiments. These findings broaden the versatility of this new class of reaction media in homogeneous catalytic oxidations by maximizing the utilization of feedstock carbon for desired products while simultaneously reducing carbon emissions.

1. Introduction

The Mid-Century (MC) process is well known for the production of terephthalic acid (TPA), a very important intermediate in the synthesis of polyethylene terephthalate and related polymers that can be fabricated into excellent fibers, resins and films.^{1,2} In this process, *p*-xylene is oxidized on a large scale by air at 180–225 °C and 15–30 bar in the presence of a catalyst composed of cobalt acetate, manganese acetate and hydrogen bromide. The optimized yield of TPA is greater than 95%, along with excellent product purity as shown by various analytical techniques.³ This process, despite successful on-stream operation for over 50 years, has the following distinct disadvantages. (1) High temperature operation decreases the solubility of O₂, while increasing solvent and product destruction and causing safety concerns. (2) Air is used as the primary oxidant instead of pure O₂ for safety reasons. This produces large amounts of contaminated vent gas and the abundant unreacted N₂ must be cleansed before venting into the environment. (3) The combination of corrosive bromide as a catalyst component and a high operating temperature requires the use of highly resistant but expensive titanium reactors. A recent breakthrough made by Poliakoff *et al.*,⁴ Savage *et al.*⁵ and Fulton *et al.*⁶ has shown that this reaction can be effectively catalyzed by MnBr₂ with pure O₂ in a new reaction medium—high temperature and supercritical water, thus circumventing the use of acetic acid. However, the scope of such reaction systems is

limited by the even harsher reaction conditions ($T = 300\text{--}400\text{ }^{\circ}\text{C}$, $P > 200\text{ bar}$).

CO₂-based media have attracted much attention in recent years because they provide the possibility of using pure O₂ under safe conditions while overcoming most of the aforementioned limitations of air oxidation systems, as follows.^{7–10} (1) The use of CO₂ in a mixed solvent increases both the O₂ solubility and the mass transport of the reactants in the liquid phase, the former because of the significant solubility of O₂ in liquid CO₂ and the latter because of improved diffusivities in CO₂ media.¹¹ This is especially the case in carbon dioxide expanded liquids (CXLs). A rule of thumb is the nearly ten fold increase in oxygen solubility when the volume of solvent is expanded by a factor of two, depending on the properties of solvent. (2) The presence of CO₂ in the vapor phase reduces flammability hazards because of the great abundance of inert CO₂ and its large heat capacity. (3) Replacing the N₂ from air with a much greater amount of CO₂ eliminates the contaminated vent gas because the CO₂ is more easily separated and recycled in the oxidation process. However, this is counterbalanced by the required separation of O₂ from N₂.

The first successful application of CXLs in oxidation reactions was reported in 2002.^{12,13} The Co(salen) catalyzed oxidation of 2,6-di-*tert*-butyl phenol to 2,6-di-*tert*-butyl-1,4-benzoquinone in CO₂-expanded acetonitrile was 1–2 orders of magnitude more active than in either the neat organic solvent or supercritical CO₂. We recently described the synergistic effect of co-catalyst zirconium and promoter ketone in the oxidation of toluene from 50 to 100 °C.¹⁴ It was found that CO₂ has a strong activation effect on the reaction, especially by shortening the induction period. Under certain conditions, the Co/Zr(acac)₄ catalyzed oxidation did not work at all with N₂/O₂ but proceeded effectively with CO₂/O₂, affording high yields of benzoic acid. In

^aCenter for Environmentally Beneficial Catalysis, University of Kansas, Lawrence, KS 66047, USA. E-mail: bsubramaniam@ku.edu; Fax: 785-864-6051; Tel: 785-864-2903

^bDepartment of Chemistry, University of Kansas, Lawrence, KS, 66047, USA. E-mail: busch@ku.edu; Fax: 785-864-6051; Tel: 785-864-1644

^cDepartment of Chemical and Petroleum Engineering, University of Kansas, Lawrence, KS 66045, USA

this work, we extend the CO₂ effect to this important industrial TPA process, which is extremely challenging because of much higher temperatures and the complexity of intermediates. More specifically, the TPA precipitates during the reaction, occluding with it 4-carboxybenzaldehyde and other by-products. In addition, the decomposition, or burning of solvent, is more significant at higher temperatures. To this end, in the present work, we first measured the expansion of acetic acid, containing dissolved catalysts and substrate, by dense CO₂. Then, based on these results, we investigated the semi-continuous oxidation of *p*-xylene at lower temperatures as compared with the MC process for a more significant CO₂ effect, with the expectation that CXLs could bring about some specific advantages for product selectivity and purity in this complex reaction system.

2. Experimental

2.1 Materials

All the catalysts, additives, substrates and solvents were commercially available and used without further treatment. Industrial grade ($\geq 99.9\%$ purity, < 32 ppm H₂O, < 20 ppm THC) liquid CO₂ and ultra high purity grade oxygen were purchased from Linweld. Isotopic gas ¹³CO₂ (99.5 atom% ¹³C) was purchased from Aldrich Chemical Co., Inc.

2.2 Volumetric expansion of acetic acid + catalyst mixtures by dense CO₂

The volumetric expansion by CO₂ of acetic acid containing dissolved catalysts was measured in a high-pressure Jerguson view cell that was placed in a high temperature oven (Yamato DKN-400, part of a Cambridge Viscosity ViscoPro 2000 system, Fig. 1). For these expansion studies, a measured volume of acetic acid containing a known amount of catalysts was loaded into the view cell and heated to the experimental temperature, which was followed by the addition of 20 bar N₂ as the substitute for O₂. Then CO₂ was gradually introduced into the cell until an expansion ratio ($\Delta V/V_o$, eqn 1) of *ca.* 1.0 was obtained.

$$\frac{\Delta V}{V_o} = \frac{V(P) - V_o(P_o)}{V_o(P_o)} \quad (1)$$

where P_o refers to ambient pressure from which the solution is expanded; and P refers to cell pressure at CO₂ expansion conditions.

2.3 Oxidation experiments and product analysis

2.3.1 Oxidation experiments. The semi-continuous oxidation of *p*-xylene to terephthalic acid was studied in a 50 mL, stirred, titanium Parr reactor (Fig. 2). Typically, N₂ or CO₂ was first added to the reactor containing the solvent and catalysts and heated to the reaction temperature; then O₂ was added until the selected final pressure was reached. *p*-Xylene was subsequently pumped into the reactor at a pre-defined rate (0.08 mL/min) to initiate the reaction. The total reactor pressure was maintained constant by continuously supplying fresh O₂ to compensate for the oxygen consumed in the reaction.



Fig. 1 Jerguson cell in oven for high temperature studies of CXLs.

2.3.2 Product analysis. After the reaction, the reaction mixture was cooled to room temperature and then treated as follows:

The gas mixture was analyzed by GC (Shin Carbon ST 100/120 mesh) to determine the yield of CO and CO₂ produced by solvent burning. For isotopic experiments, the ¹²CO₂/¹³CO₂ ratio was measured by mass spectrometry.

The insoluble terephthalic acid was separated from the liquid mixture by filtration and the solid was washed with methanol to remove most of the soluble impurities. The resulting white solid was dried at 100 °C for 2 hrs to remove absorbed solvent, after which a 10 mg sample was dissolved in 50 mL of methanol by sonication and analyzed by HPLC (C18 ODS-2 column). The reactor was washed with methanol and DMF to scavenge the residual TPA solid, which was combined with the filtrate that was retained after isolation of the solid TPA and analyzed by HPLC to determine the composition of liquids. The yields of products were based on the sums of those determined for the solid and liquid components.

The presence of yellow colored by-products in solid TPA was determined from optical density measurements using a UV-Vis spectrometer at 340 nm.¹⁵ Typically, 0.3 g solid sample was dissolved in 5 mL 4N NH₄OH. The optical density was calculated as in eqn 2:

$$OD_\lambda = A_\lambda / L \quad (2)$$

where A_λ refers to the absorbance at wavelength λ (nm); and L refers to the distance (cm) that light travels through the sample.

2.4 Safety

The amount of substrate used in the reaction studies was such that the maximum adiabatic temperature rise for total

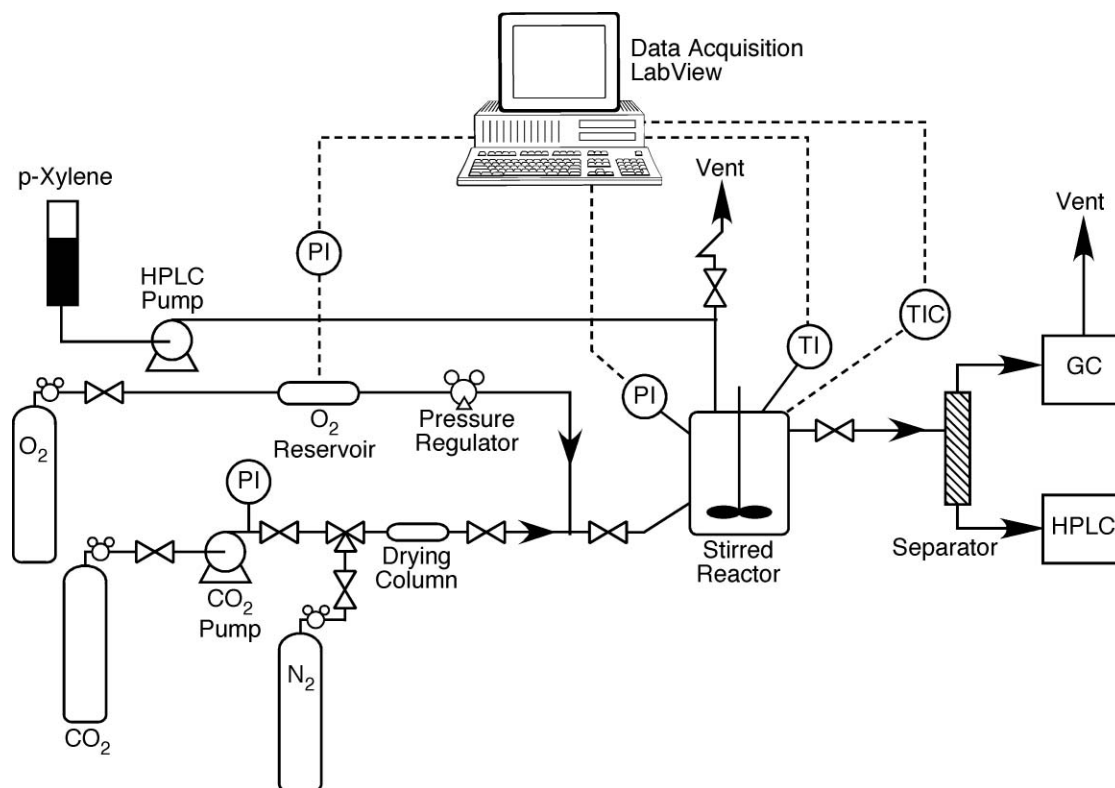


Fig. 2 Schematic diagram of semi-continuous oxidation *p*-xylene to terephthalic acid.

combustion of the substrate (taking into account the heat capacities of the reaction mixture and the solid reactor) was 25 °C. The actual temperature rise observed during reactions was a few °C, at most. In addition, the reactor was equipped with a safety release valve that exhausts the reactor contents safely to the building vent by means of a rupture disk in the event the set safe pressure (200 bar) is exceeded.

3. Results and discussion

3.1 CO₂ expansion measurements at 80 and 120 °C

Since supercritical CO₂ ($T_c = 31$ °C) expands liquids most effectively at temperatures up to 1.2 times the absolute critical temperature, our previous work was focused on reactions performed at 60 °C or less wherein it was possible to measure the solvent expansion in a water bath.^{12,16,17} Here, to measure the catalyst solubility in CO₂-expanded solvent at much higher temperatures, in experiments that are the first of their kind for *p*-xylene oxidation, we placed the high pressure Jerguson view cell in a high temperature oven that was originally designed for viscosity measurement (Fig. 1). Though the oven temperature can be maintained as high as 200 °C, these studies did not go beyond 120 °C because of the corroding capability of acetic acid and hydrogen bromide toward the stainless steel Jerguson cell.

The catalyst solution, containing 60 mM cobalt acetate, 1.8 mM manganese acetate and 60 mM hydrogen bromide in acetic acid, has a slight pink tint at room temperature (Fig. 3a) which turns blue when heated to 120 °C (Fig. 3b). The solution

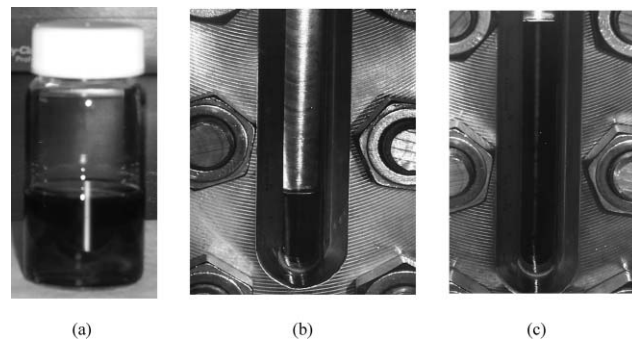


Fig. 3 Catalyst solution and its expansion with increasing CO₂ pressure. (a) room temperature, (b) 120 °C with 20 bar N₂ and 18 bar CO₂, (c) 120 °C with 20 bar N₂ and 159 bar CO₂; [Co] = 60 mM, [Mn] = 1.8 mM, [Br] = 60 mM prior to the expansion.

is expanded significantly at the much higher CO₂ pressure of *ca.* 160 bar (Fig. 3c).

Fig. 4a shows the dependence of the expansion ratio on CO₂ pressure at 120 °C. The expansion ratio increases gradually and reaches a value of 0.85 when CO₂ partial pressure is elevated to 160 bar (total pressure 180 bar). Accordingly, the concentrations of cobalt, manganese and bromide are diluted to 33 mM, 1.0 mM and 33 mM, respectively. It is noteworthy that no catalyst precipitates during the CO₂ expansion. This implies the possibility of replacing up to at least 50 vol% of the organic solvent by CO₂ while maintaining the catalyst in solution.

Fig. 4b shows the expansion result at 80 °C. As compared with 120 °C, the expansion ratio at 80 °C is much higher,

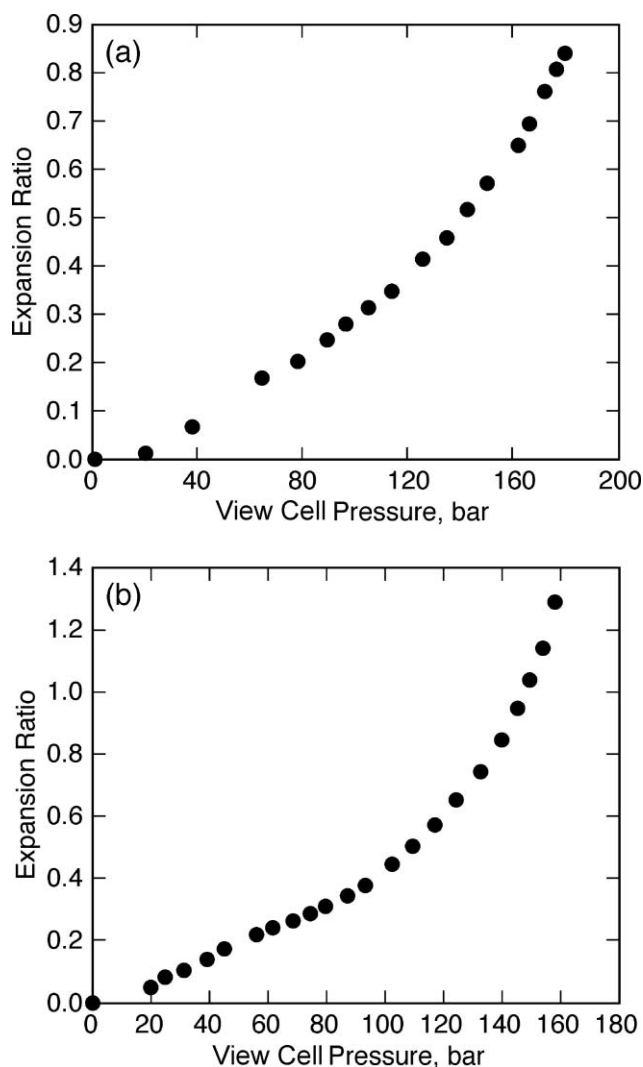


Fig. 4 Volumetric expansion of acetic acid by CO₂ with Co/Mn/Br catalysts. (a) $T = 120\text{ }^{\circ}\text{C}$, (b) $T = 80\text{ }^{\circ}\text{C}$; [Co] = 60 mM, [Mn] = 1.8 mM, [Br] = 60 mM prior to the expansion.

reaching an approximate value of one (1) when the CO₂ partial pressure is 130 bar. However, the catalysts precipitate upon further increases in CO₂ pressure; *e.g.*, approaching 140 bar.

Table 1 Oxidation of *p*-xylene in CO₂ expanded acetic acid^a

Entry	Inert gas	P inert (bar)	PO ₂ (bar)	T (°C)	Expansion Ratio ($\Delta V/V_0$)	Reaction Time (h)	Y _{TPA} (%)	Y _{4-CBA} (%)	Y _{PTA} (%)	TPA (s) ^b (wt%)	4-CBA (s) ^c ppm	OD ₃₄₀	CO/ <i>p</i> -x (mol/mol)
1	CO ₂	111	28	80	0.75	22	1.0	0.5	15.5	—	—	—	—
2	N ₂	45	45	120	0	0.5	78.6	10.5	4.7	85.7	104000	0.69	0.011
3	CO ₂	45	45	120	0.17	0.5	79.0	10.0	4.3	86.2	101000	0.58	0.0065
4	CO ₂	107	45	120	0.42	2.0	77.6	6.9	4.2	89.1	72000	0.66	0
5	CO ₂	145	20	120	0.69	2.0	73.4	8.6	5.7	85.4	94000	1.30	0
6	N ₂	30	30	160	0	0.5	94.6	1.3	0.7	98.4	11700	0.086	0.040
7	CO ₂	30	30	160	0	0.5	94.6	1.3	0.7	98.4	11500	0.087	0.038
8	N ₂	100	30	160	0	0.5	93.8	1.2	0.7	98.5	10500	0.069	0.035
9	CO ₂	100	30	160	0.15	0.5	95.1	0.8	0.6	99.1	6400	0.063	0.019

^a Reaction conditions: [Co] = 33 mM, [Mn] = 1.0 mM, [Br] = 33 mM, V_L (volume of liquid phase) = 35 mL (with or without CO₂ expansion), 1.6 mL *p*-xylene added at 0.08 mL/min, n (stirrer speed) = 1200 rpm. ^b TPA in dry isolated solid. ^c 4-CBA in dry isolated solid. The conversion of *p*-xylene is above 99% in all the reactions except entry 1. In addition to 4-CBA and PTA, a few other byproducts were detected in small amounts during the HPLC analysis. These compounds were not identified.

Further, the expansion behavior is different from that at 120 °C, displaying a sharp enhancement when CO₂ pressure exceeds 100 bar. This is attributed to the higher compressibility of the CO₂ with pressure at the lower temperature resulting in enhanced dissolution into and volumetric expansion of the liquid phase.

3.2 Semi-continuous oxidation of *p*-xylene

3.2.1 Reactions in CO₂-expanded acetic acid: CO₂ vs. N₂ as inert gas. The CO₂ effect on oxidation of *p*-xylene has been reported by Yoo *et al.*^{18,19,20} However, only a modest increase in the yield of TPA was achieved because of the high reaction temperature (> 190 °C) and low CO₂ partial pressure (< 14 bar). In these reactions, the solvents were not expanded; *i.e.*, CO₂ was not a significant component of the solvent.

We started the reaction at 80 °C, much lower than the temperature used in the *p*-xylene oxidation process, to ensure a substantial expansion at relatively low CO₂ pressure. Accordingly, a preliminary reaction was performed at a CO₂ pressure of 111 bar, where the expansion ratio was 0.75. However, as shown in Table 1, the process was very sluggish, generating only 1% TPA after 22 h (Entry 1). We rationalize this result on the basis of our understanding that the temperature was too low to overcome the activation energy of the reaction.

In the next reaction, the temperature was raised to 120 °C to accelerate the oxidation. As shown in Table 1, under a low inert gas pressure of 45 bar, there is no obvious difference between N₂ and CO₂ in the yield of TPA (*ca.* 80% in 0.5 h) as well as those of the by-products 4-carboxybenzaldehyde (4-CBA) and *p*-toluic acid (PTA) (Entries 2 and 3). HPLC analysis of the solid TPA quantified the expected major impurities, 4-CBA and PTA. As compared with *p*-xylene, PTA is much less reactive than the starting material due to the deactivating effect of the electron withdrawing carboxyl group. During the reaction, 4-CBA tends to co-precipitate with TPA and is very difficult to remove. Since 4-CBA is an inhibitor in the subsequent polymerization reaction, its concentration should be kept as low as possible. In addition, the solid also contains trace amounts of yellow colored by-products such as the derivatives of fluorenone and anthraquinone that can affect the quality of polymers.²¹ The presence of these compounds is detected by the optical density at 340 nm.¹⁵ The lower that optical density, the lesser the amounts

of these yellow colored by-products. As shown in Table 1, when the inert gas pressure is 45 bar, the amount of 4-CBA in the TPA solid is quite similar for N₂ and CO₂, whereas the optical density is lower for CO₂. As CO₂ pressure is increased to 107 bar, the corresponding expansion ratio is 0.42, and the yield of TPA approaches 80% (Entry 4), however, a relatively long reaction time of 2 h is required. Further increase of CO₂ pressure to 145 bar (expansion ratio = 0.69) and decrease of O₂ pressure to 21 bar produces a lower yield of TPA (Entry 5). On the other hand, the optical density is much higher, which indicates higher concentrations of yellow colored by-products. The reason for this phenomenon remains unclear. Based on HPLC analysis, the yields of TPA and the common by-products (4-CBA and PTA) at a CO₂ pressure of 145 bar are 73.4%, 8.6% and 5.7% respectively (Table 1, entry 5). Since the *p*-xylene conversion is above 99%, the unknown by-products (peaks seen in the HPLC but not positively identified) account for more than 10% of the *p*-xylene converted. The TPA precipitate recovered from the reaction mixture has a very dense yellow color (the optical density is much higher as compared with that of the TPA solid produced at lower CO₂ pressure), which indicates significant formation of derivatives of fluorenone and anthraquinone. Based on these results, it is reasonable to assume that at 120 °C, regardless of the use of CXLs at various O₂ partial pressures, the kinetic rates of the consecutive oxidation reactions of *p*-xylene to yield TPA are not fast enough to avoid the intermediate oxidation products and the other byproducts that adversely affect the TPA purity.

At 120 °C, the only positive effect of CO₂-based media is therefore the lower yield of the gaseous product CO, which falls to zero when CO₂ pressure is above 100 bar. This suggests that CO₂ might inhibit solvent burning. However, at this point we have not determined the yield of the second gaseous product, CO₂ produced by burning, although such a differentiation should be possible using labeled CO₂ (vide infra).

The catalytic performance is greatly improved as the temperature is further increased to 160 °C, where two sets of reactions were carried out to provide additional comparisons between the behaviors in N₂ and CO₂ at even higher yields of TPA. As shown in Table 1, under a low inert gas (N₂ or CO₂) pressure of 30 bar, the reaction results are almost identical for N₂ and CO₂ (Entries 6 and 7). When N₂ pressure is increased to 100 bar, there is little difference in the reaction results except a modest decrease of optical density (Entries 6 and 8). The results are completely different, however, when CO₂ pressure is increased to 100 bar. The expansion ratio is estimated to be 0.15, as extrapolated from the expansion data for 80–120 °C. In addition to a minor enhancement in TPA yield as compared to that for 100 bar of N₂, the oxidation process in CXL benefits a great deal in several aspects (Entries 6–9). (1) The yield of by-products, especially that of 4-CBA, is markedly decreased. This indicates the more complete oxidation of the intermediates to TPA in CO₂-expanded solvent that is possibly associated with increased oxygen availability. (2) The purity of solid TPA is enhanced by the reduction of 4-CBA concentration from 11000 ppm to 6400 ppm. (3) The optical density is the lowest among the four sets of reaction conditions. (4) The yield of CO is significantly decreased; *i.e.*, by about 50%. In general, the concentration of 4-CBA in TPA solid is inversely related to the burning of solvent, *i.e.* lower 4-CBA concentrations are always

accompanied by higher burning rate.²² In sharp contrast, our finding demonstrates that it is possible to reduce the production of both these solid and gaseous by-products simultaneously by employing high pressure CO₂. In conclusion, a multi-beneficial effect of CXL has been exhibited in the Co/Mn/Br catalyzed oxidation of *p*-xylene to terephthalic acid.

3.2.2 Reaction optimization at temperatures less than 180 °C.

As reported in the literature, two methods have commonly been used to adjust the catalyst to reduced reaction temperatures while maintaining TPA yields that are close to those of the current optimized industrial process: (1) The considerable increase of cobalt and bromide concentrations while decreasing the manganese concentration.²³ The mole ratio of cobalt to manganese can be as high as 100 to avoid the precipitation of manganese in order to avoid grey or black TPA products.²⁴ (2) The addition of other transition metals as co-catalysts,^{25–28} among which zirconium is the most efficient one that can further lower the reaction temperature to about 100 °C. Due to the lack of systematic data in these related systems, we have optimized the reactions in the temperature range 120–170 °C, with emphasis placed on the influence of cobalt and manganese concentrations and effect of zirconium on the yield of TPA, solid TPA purity, optical density at 340 nm and yield of CO. For ease of operation and comparison purposes, the pressure of CO₂ was chosen as 30 bar. As a superior flame inhibitor to nitrogen, the use of CO₂ makes it possible to run the reactions safely with an equimolar amount of oxygen in the gas phase.²⁹ Thus, 30 bar O₂ was introduced to ensure a large excess of oxygen over *p*-xylene.

As shown in Fig. 5a, the yield of TPA is significantly elevated by doubling the concentration of cobalt from 33 mM to 66 mM and adding zirconium, in the form of the acetate (Zr/Co = 1/6) at lower temperatures. However, this promoting effect diminishes when the temperature is above 150 °C. The highest TPA yield of 97.5% is achieved with the combination of cobalt and zirconium at 170 °C.

The effect on the purity of solid TPA parallels that on TPA yield. As shown in Fig. 5b, increasing the cobalt concentration and the use of zirconium enhances the purity of solid TPA, an effect that is more pronounced at lower temperatures. Also the highest purity is achieved with the combination of cobalt and zirconium at 170 °C. This is not surprising because the more complete conversion of the dissolved intermediates will definitely decrease their concentration in solid TPA.

The effect on the optical density at 340 nm is somewhat intriguing. As shown in Fig. 5c, an increase in cobalt concentration always helps lower the yield of yellow colored by-products within the studied temperature ranges. However, the incorporation of zirconium works well only at lower temperatures. The quality of the optical density no longer benefits from zirconium when the temperature is greater than 160 °C.

The effect on the yield of CO is more complicated. As shown in Fig. 5d, the production of CO can be inhibited by doubling the cobalt concentration and adding zirconium at temperatures below 135 °C. This might be unexpected since higher cobalt concentrations are considered to favor solvent burning.³⁰ In contrast, there is a surge in CO yield when the temperature rises above 150 °C, especially with the use of zirconium.

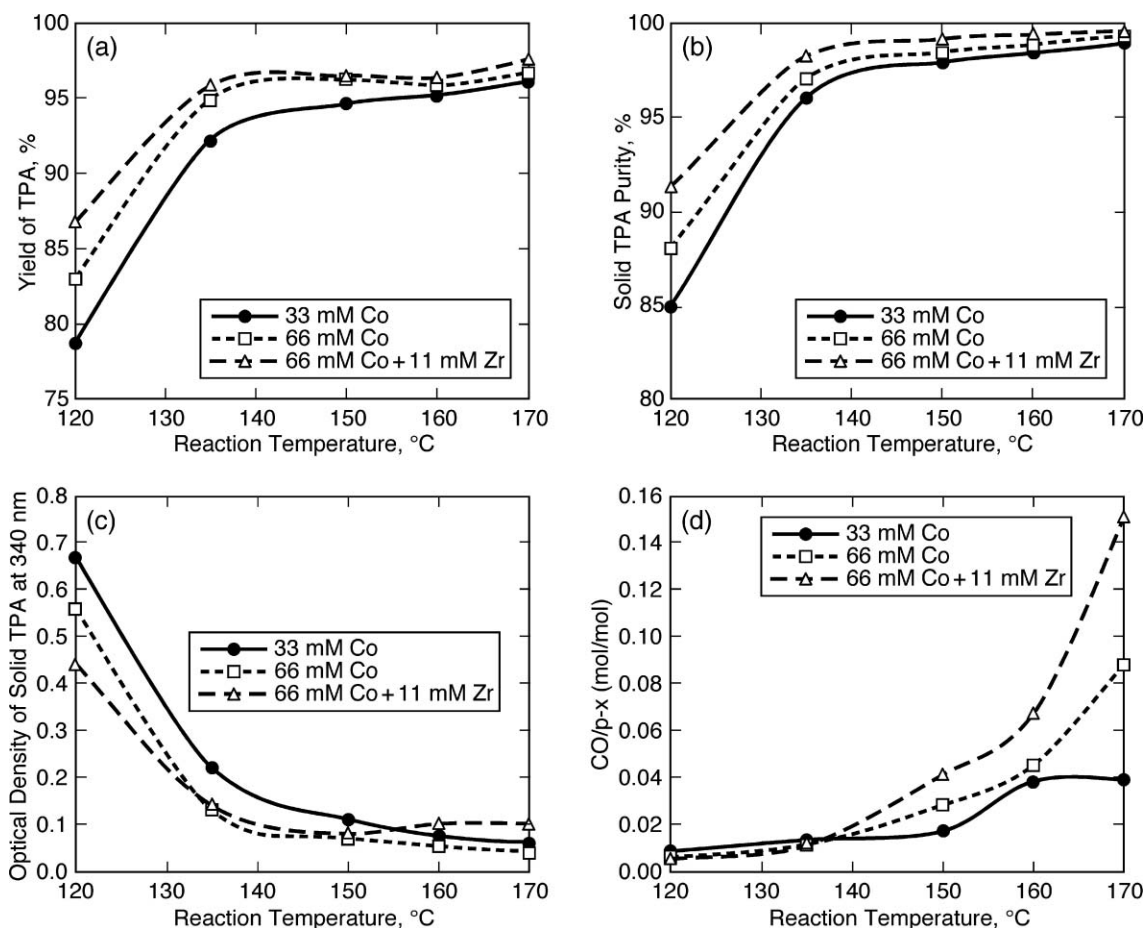


Fig. 5 Effects of cobalt concentration and zirconium on *p*-xylene oxidation. Reaction conditions: $\text{PCO}_2 = \text{PO}_2 = 30$ bar, $[\text{Mn}] = 1.0$ mM, $[\text{Br}] = 33$ mM, $V_L = 35$ mL, 1.6 mL *p*-xylene added at 0.08 mL/min, $t = 0.5$ hr, $n = 1200$ rpm.

Fig. 6 shows the effect of manganese. The reactions were carried out with a higher cobalt concentration of 66 mM at 170 °C. No zirconium was used because of the much higher solvent burning at this temperature.

As shown in Fig. 6a and 6b, the yield of TPA and solid TPA purity decrease monotonically with the increase of manganese concentration. In the absence of manganese, the yield and purity can be as high as 96.9% and 99.5%, and these are decreased to 93.3% and 98.5% respectively when the manganese concentration is increased to 8.0 mM.

Too much manganese is also disadvantageous from the standpoint of the optical density. As shown in Fig. 6c, in the complete absence of manganese, the TPA solid has a very low optical density of 0.025. In comparison, this value quadruples to *ca.* 0.1 when the manganese concentration is 8.0 mM.

In spite of all these negative effects, manganese still plays a crucial role. As shown in Fig. 6d, the yield of CO is decreased by *ca.* 30% at a very low manganese concentration of 1.0 mM. At the same time, the yield of TPA is only slightly decreased from 96.9% to 96.6%. Thus, manganese is very effective in reducing solvent burning.

From the results described above, the optimized parameters for the medium-high temperature oxidation of *p*-xylene are: $[\text{Co}] \geq 60$ mM, $[\text{Mn}] \leq 1.0$ mM, $[\text{Zr}] = 0$ mM, $T = 150$ – 160 °C.

3.2.3 Effect of CO₂ on solvent burning—*isotopic study.*

Solvent burning is a very important side reaction in *p*-xylene oxidation, which accounts for a significant loss of acetic acid each year. It is estimated that 70% of acetic acid produced worldwide is used to manufacture TPA, and about 5% of this solvent is destroyed by burning.^{22,31} Therefore, solvent burning is a significant factor in the economics of the MC process. The burn rate is reported as the mole ratio of gaseous products, CO and CO₂, produced to the moles of *p*-xylene added. Our previous work on the Shell catalyst (Co/Zr) suggests that CO₂ might reduce solvent burning by inhibiting the Co(III)-catalyzed decarboxylation of acetic acid.¹⁴ The compelling issue is expressed in the question “is it possible to reduce solvent burning in the Co/Mn/Br catalyzed oxidation of *p*-xylene by using CO₂-based media?”

For this purpose, we chose the labeled compound ¹³CO₂ as the inert gas. By mass spectrometry, the CO₂ produced by burning can be differentiated from the CO₂ added to the system by chemical reaction(s). To compare the different behavior of N₂ and CO₂ in solvent burning, three sets of reactions have been carried out, among which two sets are based on a lower temperature of 160 °C and a higher inert gas pressure of 45 bar, while the other set is based on a higher temperature of 191 °C and a lower inert gas pressure of 23 bar. The O₂ pressure for the latter case is controlled at 7 bar to mimic an MC process as

Table 2 Effect of CO₂ on solvent burning

Inert gas	T (°C)	P inert (bar)	PO ₂ (bar)	Y _{TPA} (%)	¹² CO (mmol)	¹² CO ₂ (mmol)	(¹² CO ₂ + ¹² CO)/ <i>p</i> -x (mol/mol)
N ₂	160	45	45	94.6	0.52	1.30	0.14
¹³ CO ₂	160	45	45	95.1	0.32	1.11	0.11
N ₂	160	45	12	94.1	0.37	0.89	0.095
¹³ CO ₂	160	45	12	94.3	0.23	0.76	0.075
N ₂	191	23	7	84.7	0.45	0.68	0.085
¹³ CO ₂	191	23	7	94.1	0.46	1.13	0.12

Reaction conditions: for 160 °C reaction [Co] = 33 mM, [Mn] = 1.0 mM, [Br] = 33 mM; for 191 °C reaction [Co] = [Mn] = [Br] = 5.5 mM; *V*_L = 35 mL, 1.6 mL *p*-xylene added at 0.08 mL/min, *t* = 0.5 hr, *n* = 1200 rpm. The conversion of *p*-xylene is above 99% in all the reactions. In addition to 4-CBA and PTA, a few other byproducts were detected in small amounts during the HPLC analysis. These compounds were not identified.

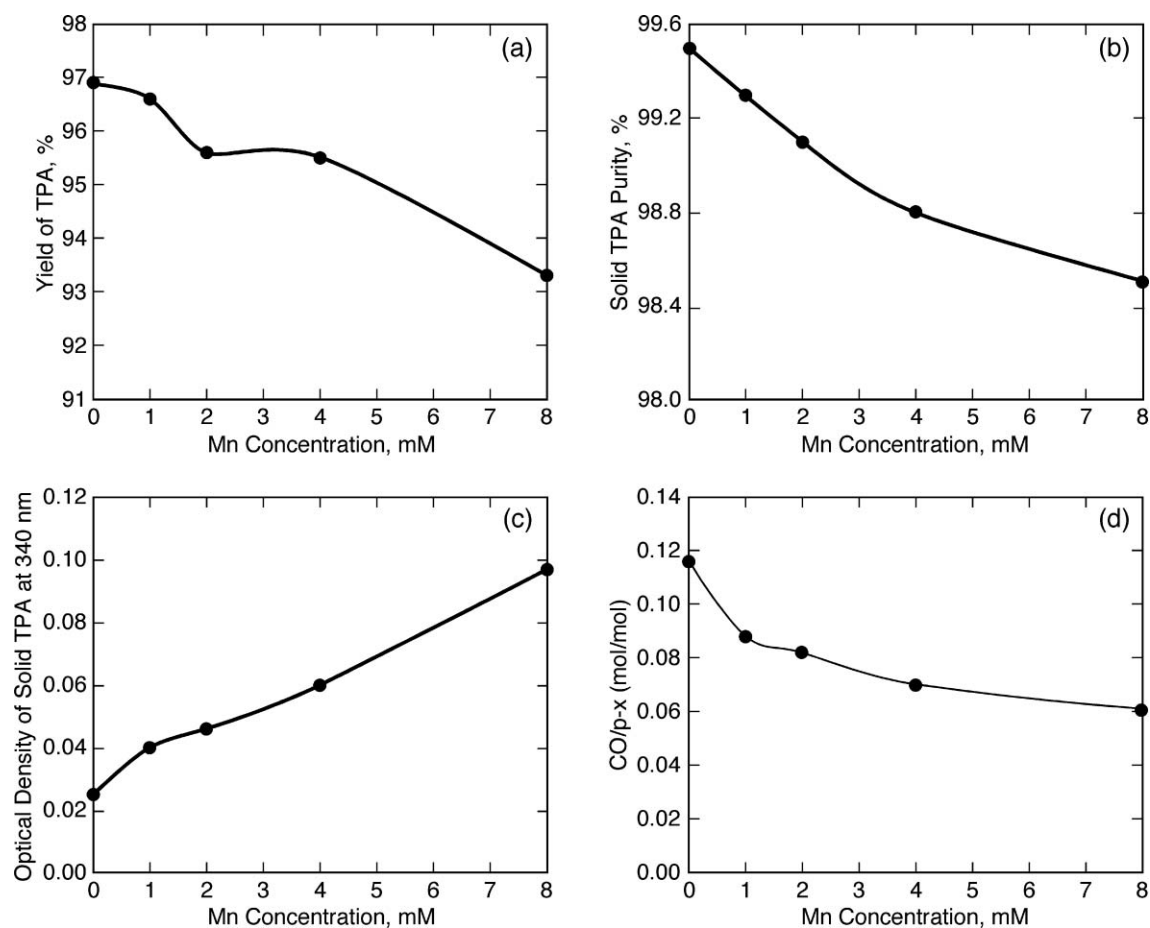


Fig. 6 Effects of manganese concentration on *p*-xylene oxidation. Reaction conditions: PCO₂ = PO₂ = 30 bar, *T* = 170 °C, [Co] = 66 mM, [Br] = 33 mM, *V*_L = 35 mL, 1.6 mL *p*-xylene added at 0.08 mL/min, *t* = 0.5 hr, *n* = 1200 rpm.

operated by industry. As the data in Table 2 reveal, the reactions yield 2–3 times as much CO₂ as CO, regardless of the kind of inert gas present during reaction. This is in good agreement with the previous report that the CO₂/CO mole ratio is around 3.³² Remarkably, the use of CO₂ can suppress not only the production of CO, but also the production of CO₂ at 160 °C, and it is interesting to note that the yield of CO is reduced to a larger extent. As a result, the burn rate is 0.14 for N₂ and 0.11 for CO₂ when O₂ pressure is 45 bar, and 0.095 for N₂ and 0.075 for CO₂ when O₂ pressure is 12 bar. In both cases, the burning is reduced by *ca.* 20% when compared to N₂ with similar yields (*ca.* 95%) of TPA. Also, the yield of TPA is much better with CO₂ at 191 °C,

suggesting the positive effect of overcoming the kinetic barrier. While the yield of CO is nearly indistinguishable, the yield of CO₂ is increased markedly at the higher temperature. Consequently, the reactions should be performed at lower temperature and higher CO₂ pressure to inhibit solvent burning.

The formation of CO_x (CO plus CO₂) during the MC process involves a very complicated reaction mechanism. Apart from the solvent burning that is the major source of CO_x, CO_x can also be produced by the over-oxidation of *p*-xylene and the decomposition of the TPA product. These mechanisms are currently under investigation. From the point of view of thermodynamics, it seems plausible that the equilibrium shifts

to the left upon the addition of a large excess of CO₂. In addition, we also observed that the CO₂ yield is decreased by adding an appropriate amount of water, another by-product of burning. This also suggests the leftward shift of the equilibrium.

4. Conclusion

In summary, we have studied the Co/Mn/Br catalyzed medium-high temperature oxidation of *p*-xylene to terephthalic acid in CO₂-expanded acetic acid based on the measurement of solvent expansion in a Jerguson cell that is equipped with a high temperature oven. The reactions have been optimized by varying the reaction temperature, the concentration of cobalt and manganese and the use of co-catalyst zirconium. As compared with N₂/O₂, the use of CO₂/O₂ at sufficiently high inert gas pressure and 160 °C significantly improved the catalytic performance by decreasing the yield of 4-carboxybenzaldehyde, *p*-toluic acid and other sources of yellow colored by-products. In addition, the quality of solid TPA is also greatly increased due to the reduction of the concentration of the by-products, especially 4-carboxybenzaldehyde. More worthy of mention is that solvent decomposition can also be effectively inhibited with CO₂, as confirmed by isotopic experiments, which adds greater value to the CO₂-expanded solvents. These results, as an extension of our previous work on the remarkable CO₂ effect on Co/Zr catalytic system, further support the feasible and promising industrial application of CXLs in this kind of important oxidation reaction. The use of high pressure CO₂ as reaction medium requires compression power and this could nullify the energy gain made by operating at lower temperatures. However, with the ever-growing global sentiment towards reduction of carbon emissions, novel solutions such as the one discussed here would be needed to meet government regulations on such emissions and thereby make carbon-emitting processes economically viable.

Acknowledgements

This work was supported by the National Science Foundation Engineering Research Centers Program, Grant EEC-0310689. We are particularly grateful for the valuable discussions with Drs. Peter Metelski, Wayne Schammel and David Sikkenga of BP, Naperville, IL. We would also like to thank Dr. Todd Williams of the University of Kansas for his kind help with MS analysis.

Notes and references

1 W. Parteneimer, *Catal. Today*, 1995, **23**, 69–158.

- 2 P. Raghavendrachar and S. Ramachandran, *Ind. Eng. Chem. Res.*, 1992, **31**, 453–462.
- 3 H. Milan, A. G. Hussain and R. Roberto, *US Pat.*, 20080293964.
- 4 P. A. Hamley, T. Ilkenhans, J. M. Webster, E. Garcia-Verdugo, E. Vernardou, M. J. Clarke, R. Auerbach, W. B. Thomas, K. Whiston and M. Poliakoff, *Green Chem.*, 2002, **4**, 235–238.
- 5 J. B. Dunn and P. E. Savage, *Environ. Sci. Technol.*, 2005, **39**, 5427–5435.
- 6 Y. S. Chen, J. L. Fulton and W. Parteneimer, *J. Am. Chem. Soc.*, 2005, **127**, 14085–14093.
- 7 P. Jessop and B. Subramaniam, *Chem. Rev.*, 2006, **107**, 2666–2694.
- 8 T. Seki and A. Baiker, *Chem. Rev.*, 2009, **109**, 2409–2454.
- 9 C. A. Eckert, D. Bush, J. S. Brown and C. L. Liotta, *Ind. Eng. Chem. Res.*, 2000, **39**, 4615–4621.
- 10 C. A. Eckert, C. L. Liotta, D. Bush, J. S. Brown and J. P. Hallett, *J. Phys. Chem. B*, 2004, **108**, 18108–18118.
- 11 G. T. Musie, M. Wei, B. Subramaniam and D. H. Busch, *Coord. Chem. Rev.*, 2001, **219**, 789–820.
- 12 M. Wei, G. T. Musie, D. H. Busch and B. Subramaniam, *J. Am. Chem. Soc.*, 2002, **124**, 2513–2517.
- 13 M. Wei, G. T. Musie, D. H. Busch and B. Subramaniam, *Green Chem.*, 2004, **6**, 387–394.
- 14 X. Zuo, B. Subramaniam and D. H. Busch, *Ind. Eng. Chem. Res.*, 2008, **47**, 546–552.
- 15 M. A. Zeitlin and D. Wilger-Nowicki, *US Pat.*, 5 095 146, 1992.
- 16 H. Jin, B. Subramaniam, A. Ghosh and J. Tunge, *AIChE J.*, 2006, **52**, 2575–2581.
- 17 B. Rajagopalan, M. Wei, G. T. Musie, B. Subramaniam and D. H. Busch, *Ind. Eng. Chem. Res.*, 2003, **42**, 6505–6510.
- 18 D. R. Burri, K. W. Jun, J. S. Yoo, C. W. Lee and S. E. Park, *Catal. Lett.*, 2002, **81**, 169–173.
- 19 J. S. Yoo, S. H. Jhung, K. H. Lee and Y. S. Park, *Appl. Catal. A-Gen.*, 2002, **223**, 239–251.
- 20 S. E. Park, J. S. Chang and K. W. Lee, *Stud. Surf. Sci. Catal.*, 2004, **153**, 303–314.
- 21 P. Roffia, P. Calini and L. Motta, *Ind. Eng. Chem. Prod. Res. Dev.*, 1984, **23**, 629–634.
- 22 Personal Communication, BP Personnel (names provided in the acknowledgement section), 2007.
- 23 G. G. Lavoie, R. T. Hembre, C. E. J. Sumner, J. N. Bays, D. B. Compton, B. A. Tennant, B. W. Davenport, D. Lange and T. R. Floyd, *PCT Int. Appl.* 2006, WO 2006096312.
- 24 S. H. Jhung and Y. S. Park, *Bull. Korean Chem. Soc.*, 2002, **23**, 369–373.
- 25 A. W. Chester, E. J. Y. Scott and P. S. Landis, *J. Catal.*, 1977, **46**, 308–319.
- 26 R. L. June, M. W. Potter, E. J. Simpson and C. L. Edwards, *US Pat.*, 6 153 790, 2000.
- 27 W. Parteneimer, *J. Mol. Catal. A-Chem.*, 2003, **206**, 105–119.
- 28 W. Parteneimer, *US Pat.*, 4 992 580, 1991.
- 29 B. Rajagopalan, *Ph.D. Thesis*, University of Kansas, 2007.
- 30 W. Parteneimer, in *Catalysis of Organic Reactions*, ed. D. W. Blackburn, Marcel Dekker, New York, 1990, pp. 321–346.
- 31 P. D. Metelski and J. H. Espenson, *PCT Int. Appl.* 2005, WO 2005000779.
- 32 Y. Cheng, L. Zhang, G. Xie and X. Li, *Chem. React. Eng. Technol. (China)*, 2003, **19**, 182–187.

Effects of anionic structure and lithium salts addition on the dissolution of cellulose in 1-butyl-3-methylimidazolium-based ionic liquid solvent systems†

Airong Xu,^a Jianji Wang^{*b} and Huiyong Wang^b

Received 17th August 2009, Accepted 30th September 2009

First published as an Advance Article on the web 4th November 2009

DOI: 10.1039/b916882f

Cellulose is the most abundant biorenewable and biodegradable resource on the earth. However, the extent of its application is limited due to its inefficient dissolution in solvents. Thus, the development of new cellulose solvents continues to be an active area of investigation. In this work, a series of ionic liquids (ILs) have been synthesized by coupling the 1-*N*-butyl-3-methylimidazolium cation [C₄mim]⁺ with the Brønsted basic anions [CH₃COO]⁻, [HSCH₂COO]⁻, [HCOO]⁻, [(C₆H₅)COO]⁻, [H₂NCH₂COO]⁻, [HOCH₂COO]⁻, [CH₃CHOHCOO]⁻ and [N(CN)₂]⁻. The solubilities of microcrystalline cellulose (MCC) in these ionic liquids were determined as a function of temperature. The effect of the anion structure on the solubility of cellulose has been estimated, and investigated by ¹H NMR and a solvatochromic UV/vis probe. It was found that the solubility of cellulose increases almost linearly with increasing hydrogen bond accepting ability of anions in the ionic liquids. At the same time, novel [C₄mim][CH₃COO]/lithium salt (LiCl, LiBr, LiAc, LiNO₃, or LiClO₄) solvent systems have been developed by adding 1.0 wt% of lithium salt into [C₄mim][CH₃COO]. It was shown that the addition of lithium salts significantly increased the solubility of the cellulose. This observation was studied by ¹³C NMR spectra, and the results suggested that the enhanced solubility of cellulose originated from the disruption of the intermolecular hydrogen bond, O(6)H...O(3) owing to the interaction of Li⁺ with the hydroxyl oxygen O(3) of cellulose. Furthermore, the cellulose materials regenerated from the ionic liquids were characterized by scanning electron micrograph, thermogravimetric analysis and Fourier transform infrared spectroscopy, and the degree of polymerization of the original and regenerated cellulose materials was also determined. Good thermal stability was found for the regenerated cellulose. It is expected that the above information is useful for the design of novel ionic liquids and ionic liquid-based solvent systems for cellulose.

Introduction

Cellulose is the most abundant biorenewable and biodegradable resource in the world, with an annual yield of over 1.0 × 10¹⁰ ton.¹ Cellulose can be derived from cellulose-rich starting materials like trees, cotton, and crop wastes. Cellulose and its derivatives have been widely used in our society in fibers, tissues, paper, membranes, polymers, paints and medicines.^{2,3} However, due to its close packing by numerous inter- and intramolecular hydrogen bonds, cellulose is extremely difficult to dissolve in water and most of the conventional organic solvents. Therefore, the main obstacle to the further application of cellulose is the lack of powerful solvent systems. Until now, only a limited number of solvent systems have been industrialized. However,

the dissolution processes using these solvent systems suffer from environmental, energy, safety, and other problems. For example, the viscose process, which is a traditional technology used in industry, sometimes causes serious environmental pollution and involves derivatization of cellulose products.⁴ Although the *N*-methylmorpholine-*N*-oxide (NMMO) process is a direct dissolution process commercialized for the manufacture of so-called lyocell fibres,⁴ this process also has some problems, such as the severe fibrillation of the manufactured fibres, a high dissolution temperature (130 °C), and the requirement of a major investment in safety technology because of its thermal instability. Other solvent systems investigated include DMAc/LiCl, DMSO/TBAF, DMF/N₂O₄, LiClO₄·3H₂O, and LiSCN·2H₂O,⁵⁻⁸ where DMAc, DMSO, TBAF, DMF, and N₂O₄ stand for *N,N*-dimethylacetamide, dimethyl sulfoxide, tetrabutyl ammonium fluoride, *N,N*-dimethylformamide and nitrous tetroxide, respectively. Such solvent systems still retain certain drawbacks such as high cost, toxicity, difficulty in solvent recovery or harsh processing conditions. Therefore, it is highly desirable to develop less energy consuming, more environmentally friendly, and highly efficient solvent systems for cellulose.

^aCollege of Chemistry and Chemical Engineering, Lanzhou University, Lanzhou, Gansu, 730000, P. R. China

^bSchool of Chemistry and Environmental Science, Henan Key Laboratory of Environmental Pollution Control, Henan Normal University, Xinxiang, Henan, 453007, P. R. China

† Electronic supplementary information (ESI) available: ¹H NMR data of the ILs and FTIR spectra of cellulose before and after dissolution. See DOI: 10.1039/b916882f

Ionic liquids (ILs) are a novel class of green solvents. They have many distinct advantages such as chemical and thermal stability, non-flammability, non-detectable vapor pressures and chemical tunabilities,^{9–11} and promise widespread application in industry. In 2002, Rogers and coworkers¹² reported, for the first time, that cellulose could be efficiently dissolved in 1-*N*-butyl-3-methylimidazolium chloride [C₄mim]Cl, whereas the ILs containing [BF₄]⁻ and [PF₆]⁻ anions were poor solvents. ¹³C and ^{35/37}Cl NMR relaxation measurements demonstrated that the high solubility of cellulose in [C₄mim]Cl was attributable to the formation of hydrogen bonding between the hydroxyl protons of cellulose and the chloride anion of the IL.^{13,14} Since then, a series of researches has been conducted in this field. Zhang *et al.*¹⁵ reported that 1-*N*-allyl-3-methylimidazolium chloride [Amim]Cl was a powerful solvent for cellulose, in which microcrystalline cellulose could be dissolved quickly without activation or pretreatment. They also indicated that 1-*N*-ethyl-3-methylimidazolium acetate [C₂mim][CH₃COO], which has a lower melting point and viscosity, showed a much higher ability to dissolve cellulose.¹⁶ Ohno *et al.*^{17,18} found that *N,N'*-dialkylimidazolium formates, [RR'im][HCOO], and *N*-ethyl-*N'*-methylimidazolium alkylphosphates, [C₂mim][(MeO)₂PO₂], displayed superior solubility for a variety of polysaccharides, including cellulose. In the extended dissolution studies of Schubert *et al.*¹⁹ for cellulose in imidazolium-based ionic liquids, an odd–even effect was found for different alkyl side-chain lengths of the imidazolium chlorides, and 1-ethyl-3-methylimidazolium diethyl phosphate was found to be best suited to the dissolution of cellulose. It was also reported that wood and other biomasses such as bagasse and straw can be dissolved, at least partially, in ILs such as [Amim]Cl, [C₄mim]Cl and [C₂mim][CH₃COO].^{20–24} These encouraging results provide possibilities for the dissolution of cellulose and biomass by ILs instead of conventional organic solvents, as well as for solutions to the problems described above in the solvent systems of cellulose.

Although previous investigations revealed some important aspects for the dissolution of cellulose in ILs, very few studies have been conducted to explore the influence of the structure of ILs on the dissolution performance of cellulose. Considering the fact that the dissolution of cellulose is significantly determined by the nature of the anions in ILs,^{13,14} we prepared a series of ionic liquids with a fixed cationic backbone and a fixed alkyl chain length, *i.e.* the 1-butyl-3-methylimidazolium cation [C₄mim]⁺, but with varied anion structures. This allowed us to examine the effect of the ILs' anion structure on the solubility of cellulose, as well as the related dissolution mechanism. In order to further enhance the dissolution of cellulose, several novel solvent systems have been developed by the addition of 1.0 wt% of a lithium salt (LiAc, LiCl, LiBr, LiClO₄, or LiNO₃) into [C₄mim][CH₃COO]. The dissolution of cellulose in the ILs and the [C₄mim][CH₃COO]/lithium salt solvent systems was studied by ¹H and ¹³C NMR spectroscopies and solvatochromic UV/vis probe. In addition, the regenerated cellulose materials were investigated by means of scanning electron microscopy (SEM), thermogravimetric analysis (TGA), and Fourier transform infrared (FT-IR), and the dissolution temperature and dissolution time effects on the degree of polymerization of the regenerated cellulose were also discussed.

Table 1 Solubility of microcrystalline cellulose in the ILs at different temperatures

Entry	IL	Solubility/wt%			
		40 °C	50 °C	60 °C	70 °C
1	[C ₄ mim][CH ₃ COO]	11.5	12.5	13.0	15.5
2	[C ₄ mim][HSCH ₂ COO]	<1.0	9.5	12.5	13.5
3	[C ₄ mim][HCOO]	7.5	8.5	9.0	12.5
4	[C ₄ mim][(C ₆ H ₅)COO]	<1.0	<1.0	<1.0	12.0
5	[C ₄ mim][H ₂ NCH ₂ COO]	<1.0	2.0	8.0	12.0
6	[C ₄ mim][HOCH ₂ COO]	— ^a	7.5	9.0	10.5
7	[C ₄ mim][CH ₃ CHOHCOO]	— ^a	— ^a	8.0	9.5
8	[C ₄ mim][N(CN) ₂]	— ^a	— ^a	— ^a	— ^a

^a Insoluble at the given temperature.

Results and discussion

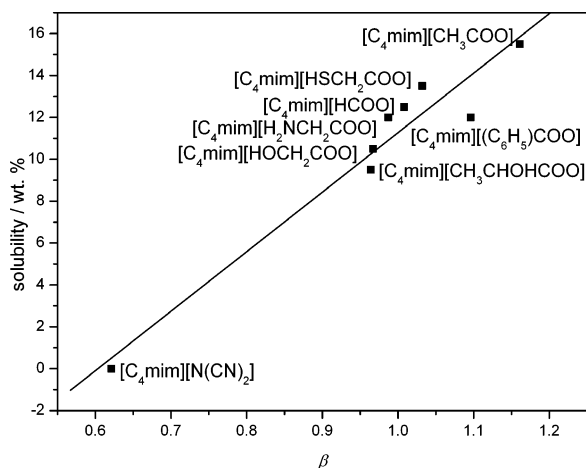
Influence of the ionic liquids' anion structure on the solubility of cellulose

The solubility values of microcrystalline cellulose in the studied ILs are shown in Table 1 as a function of temperature. It can be seen that the structure of the anions significantly affects the solubility of the cellulose. Among the investigated ILs, [C₄mim][CH₃COO] is the most efficient ionic liquid for the dissolution of cellulose. In contrast, cellulose is insoluble in [C₄mim][N(CN)₂]. This indicates that the anions of the ILs play a key role in the disruption of the inter- and intramolecular hydrogen bonds of cellulose. Generally, the solubility of cellulose in these ILs decreases in the order: [C₄mim][CH₃COO] > [C₄mim][HSCH₂COO] > [C₄mim][HCOO] > [C₄mim][(C₆H₅)COO] > [C₄mim][H₂NCH₂COO] > [C₄mim][HOCH₂COO] > [C₄mim][CH₃CHOHCOO] > [C₄mim][N(CN)₂]. It is interesting to note that replacing H in the CH₃COO⁻ anion of the ionic liquid [C₄mim][CH₃COO] with electron-withdrawing groups such as OH, SH, NH₂ or CH₃OH leads to decreased solubility. Considering the fact that replacement of H in the CH₃COO⁻ anion by an electron-withdrawing group would decrease the ability of CH₂XCOO⁻ (X = OH, SH, NH₂ and CH₃OH) to form hydrogen bonds with the hydroxyl protons of cellulose, the decreased solubility observed is not difficult to understand. This suggests that the hydrogen bond accepting ability of the anions strongly dominates the ILs' capacity for the dissolution of cellulose. In addition, it is noted from Table 1 that the solubility of cellulose in these ILs is enhanced with increasing temperature. In the case of [C₄mim][CH₃COO], the solubility of cellulose at 70 °C (15.5 wt%) is higher than that at 40 °C (11.5 wt%) by about 35%. This is an indication that hydrogen bonds of the cellulose were also partially disrupted by the increased temperature.

The β parameter, introduced by Kamlet and Taft, has been established as a measure of the hydrogen bond accepting ability of anions of ionic liquids.^{25–27} Unfortunately, most of the β parameters for the ILs investigated in the present work are not available in the literature. Therefore, we determined these parameters and the results are given in Table 2. It is evident that the ILs with different anion structures exhibit a marked variation in the β parameter. As shown in Fig. 1, the solubility values of cellulose increase almost linearly with increasing β parameter of the ILs. This indicates that the solubility of the cellulose strongly depends on the hydrogen bond-accepting ability of the

Table 2 The β parameter values for the ILs investigated

Entry	IL	β
1	[C ₄ mim][CH ₃ COO]	1.161
2	[C ₄ mim][HSCH ₂ COO]	1.032
3	[C ₄ mim][HCOO]	1.008
4	[C ₄ mim][(C ₆ H ₅)COO]	0.987
5	[C ₄ mim][H ₂ NCH ₂ COO]	1.096
6	[C ₄ mim][HOCH ₂ COO]	0.967
7	[C ₄ mim][CH ₃ CHOHCOO]	0.964
8	[C ₄ mim][N(CN) ₂]	0.621

**Fig. 1** Linear correlation between solubility of microcrystalline cellulose at 70 °C and β Parameter of the ILs investigated.

anions of the ILs. The stronger the hydrogen bond accepting ability of the anions, the higher the solubility of cellulose in the IL. For example, the anion of [C₄mim][CH₃COO] has the strongest hydrogen bond accepting ability (highest β value) of the ILs investigated, and solubility of the cellulose is found to be the highest in [C₄mim][CH₃COO].

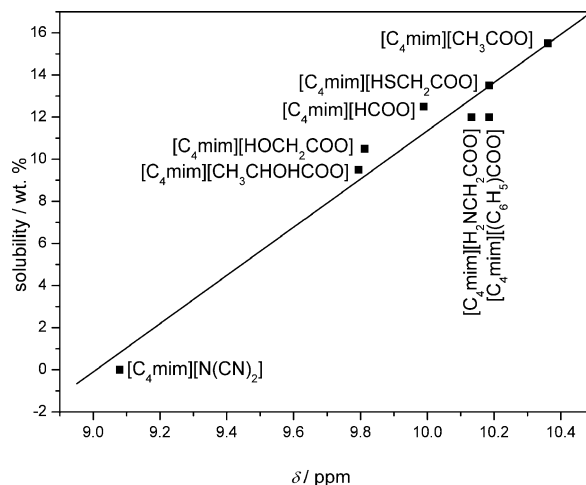
It is known that the ¹H NMR chemical shift (δ) of the proton in the 2-position of the imidazolium ring can be used as a measure of the capacity of the anion of an IL to form hydrogen bonds,²⁸ which is crucial to the breaking of the inter- and intramolecular hydrogen bonds of the cellulose chains,^{17,18} and thus to the dissolution of cellulose. Therefore, ¹H NMR chemical shifts of the proton in the 2-position of the imidazolium ring have been determined for the ILs under study, and the correlation between the solubility of cellulose and the chemical shift of this proton is shown in Fig. 2. As expected, the solubility of cellulose increases almost linearly with the chemical shift of the proton in the 2-position of the imidazolium ring. Hence, the solubility of cellulose in a certain IL can be predicted by using this linear correlation. According to our result, the ILs with a δ value smaller than 9.5 are not suitable solvents for the dissolution of cellulose.

Lithium salt-promoted dissolution of cellulose in [C₄mim][CH₃COO]

The solubility of cellulose in various [C₄mim][CH₃COO]/lithium salt solvent systems was investigated at different temperatures. Table 3 summarizes the results obtained for microcrystalline cellulose. It can be seen that solubility of

Table 3 Solubility of microcrystalline cellulose in [C₄mim][CH₃COO]/lithium salt solvent systems

Solvent system	Solubility (wt%) at different temperatures				
	40 °C	50 °C	60 °C	70 °C	80 °C
[C ₄ mim][CH ₃ COO]	11.5	12.5	13.0	15.5	19.0
[C ₄ mim][CH ₃ COO]/LiAc	12.0	16.0	17.5	19.0	20.0
[C ₄ mim][CH ₃ COO]/LiCl	12.0	14.5	16.0	18.5	20.0
[C ₄ mim][CH ₃ COO]/LiBr	11.5	13.5	15.0	18.0	19.5
[C ₄ mim][CH ₃ COO]/LiClO ₄	12.0	15.0	17.5	20.0	21.0
[C ₄ mim][CH ₃ COO]/LiNO ₃	12.0	15.0	18.5	19.5	21.0

**Fig. 2** Linear correlation between solubility of microcrystalline cellulose at 70 °C and the ¹H NMR chemical shifts of the proton in the 2-position of the imidazolium ring measured in DMSO-d₆ at a concentration of 1.0 mol kg⁻¹.

the cellulose is enhanced significantly after the addition of a small amount of lithium salt into [C₄mim][CH₃COO]. As reported in the literature,²⁹ some lithium salt hydrates have the capacity to dissolve cellulose through the hydroxyl groups of the cellulose taking part in the coordination of Li⁺. Compared to LiX·*n*H₂O, the lack of water molecules in LiX leads to more free coordination sites at the lithium cation. These sites can be occupied by other coordinating groups, e.g. the hydroxyl groups of cellulose, resulting in the breaking of some inter- and intramolecular hydrogen bonds of cellulose. This is a possible reason why higher solubility was observed for cellulose in [C₄mim][CH₃COO]/lithium salt solvent systems than in [C₄mim][CH₃COO] alone.

In order to further examine how the addition of lithium salts increases the solubility of cellulose, ¹³C NMR measurements of cellulose were carried out in solutions of [C₄mim][CH₃COO]/cellulose (9.0 wt%) and [C₄mim][CH₃COO]/LiCl (1.0 wt%)/cellulose (9.0 wt%) at 90 °C. The ¹³C NMR spectra are shown in Fig. 3, and the ¹³C NMR chemical shift data are presented in Table 4. It can be seen from Table 4 that the addition of LiCl produces a downfield shift (an increase in chemical shift) for C3 and upfield shifts (decrease in chemical shift) for the other C atoms. Based on the results reported in literature,^{30,31} the hydrogen bonds of cellulose are mainly the intramolecular hydrogen bonds, O(3)H...O(5) and O(2)H...O(6), present on both sides of the cellulose chain,

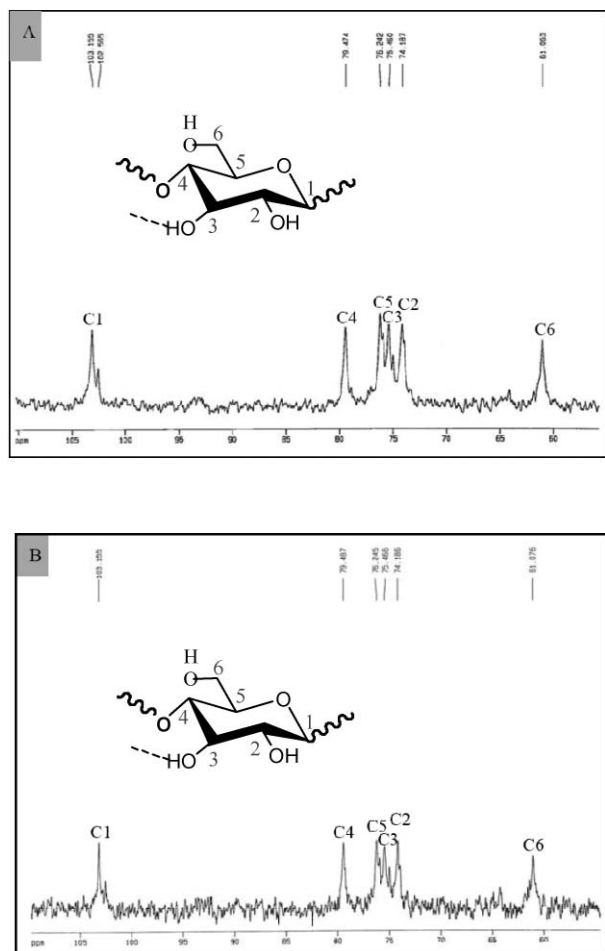


Fig. 3 ^{13}C NMR spectra of microcrystalline cellulose in IL and IL/lithium salt systems at 90 °C: (A) $[\text{C}_4\text{mim}][\text{CH}_3\text{COO}]$; (B) $[\text{C}_4\text{mim}][\text{CH}_3\text{COO}]/\text{LiCl}$.

and the intermolecular hydrogen bond, $\text{O}(6)\text{H}\cdots\text{O}(3)$, which builds a bridge between two neighboring molecules (Fig. 4). After the addition of LiCl into the $[\text{C}_4\text{mim}][\text{CH}_3\text{COO}]/\text{cellulose}$ system, the intermolecular hydrogen bond, $\text{O}(6)\text{H}\cdots\text{O}(3)$, was broken owing to the interaction of Li^+ with the hydroxyl oxygen $\text{O}(3)$ of cellulose, and thus the electron cloud density of $\text{C}3$ bonded to the hydroxyl oxygen $\text{O}(3)$ of cellulose decreased. Consequently, the ^{13}C NMR signal of $\text{C}3$ shifts downfield, and the chemical shift of $\text{C}3$ increases correspondingly. At

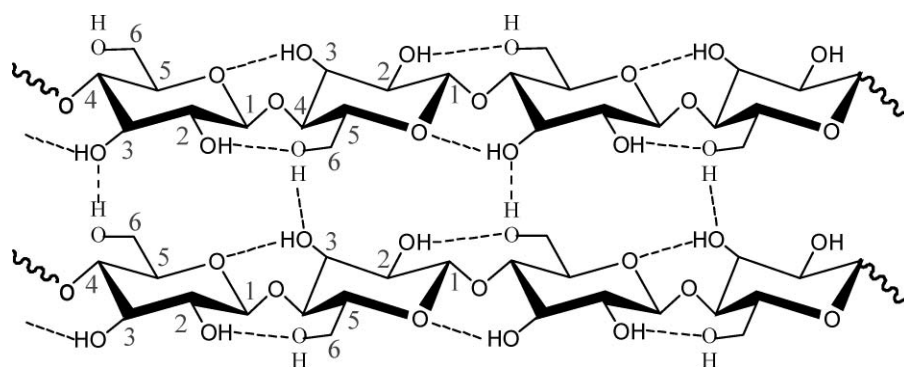


Fig. 4 Schematic structure and numbering of cellulose.

Table 4 ^{13}C NMR chemical shifts (δ (ppm) relative to TMS) of cellulose in $[\text{C}_4\text{mim}][\text{CH}_3\text{COO}]/\text{cellulose}$ (9.0 wt%) and $[\text{C}_4\text{mim}][\text{CH}_3\text{COO}]/\text{LiCl}$ (1.0 wt%)/cellulose (9.0 wt%) systems

Solvent system	δ (ppm)					
	C(1)	C(2)	C(3)	C(4)	C(5)	C(6)
$[\text{C}_4\text{mim}][\text{CH}_3\text{COO}]$	103.165	74.188	75.468	79.488	76.242	61.063
$[\text{C}_4\text{mim}][\text{CH}_3\text{COO}]/\text{LiCl}$	103.146	74.182	75.478	79.467	76.189	61.034

the same time, disruption of this intermolecular hydrogen bond prompts further dissolution of the cellulose. However, the chemical shifts for the other C atoms of cellulose behave differently. This may be interpreted as the interactions of the Cl^- anion of LiCl with the hydroxyl proton of cellulose in the $[\text{C}_4\text{mim}][\text{CH}_3\text{COO}]/\text{LiCl}/\text{cellulose}$ system, which leads to an increase of electron cloud density of the C atoms and an upfield shift of their ^{13}C NMR signals. The dissolution mechanism of cellulose in $[\text{C}_4\text{mim}][\text{CH}_3\text{COO}]/\text{LiCl}$ reported here is somewhat similar to that in N,N -dimethylacetamide/ LiCl , and the breaking of intermolecular hydrogen bonds results from the direct interaction of lithium with the cellulosic hydroxyl oxygen.³² The difference is that $[\text{C}_4\text{mim}][\text{CH}_3\text{COO}]$ in the $[\text{C}_4\text{mim}][\text{CH}_3\text{COO}]/\text{LiCl}$ solvent system can dissolve cellulose, but N,N -dimethylacetamide in N,N -dimethylacetamide/ LiCl cannot.

Compared to other solvent systems for cellulose, the $[\text{C}_4\text{mim}][\text{CH}_3\text{COO}]/\text{lithium salt}$ solvent systems reported in the present work have the advantages of higher solubility and lower dissolution temperature. For example, at 40 °C, the solubility of cellulose in $[\text{C}_4\text{mim}][\text{CH}_3\text{COO}]/\text{LiX}$ ($\text{X} = \text{Cl}, \text{NO}_3, \text{ClO}_4, \text{Ac}$) systems could be as high as 12.0 wt%, whereas only 8.0 wt% of cellulose was dissolved in $[\text{C}_2\text{mim}][(\text{MeO})\text{HPO}_2]$.¹⁸ At 60 °C, 18.5 wt% of cellulose can be dissolved in $[\text{C}_4\text{mim}][\text{CH}_3\text{COO}]/\text{LiNO}_3$, but only 10.0 wt% of cellulose has been dissolved in $[\text{C}_2\text{mim}][\text{HCOO}]$.¹⁷ On the other hand, cellulose cannot be dissolved in $[\text{Amim}]\text{Cl}$ at temperatures below 70 °C,¹⁵ and the temperature needs to be maintained at 130 °C for the dissolution of 10–15 wt% of cellulose in the NMMO system. In addition, our ILs and $[\text{C}_4\text{mim}][\text{CH}_3\text{COO}]/\text{lithium salt}$ solvent systems can be used for the direct dissolution of cellulose without any pretreatment or activation. In contrast, in most of the conventional solvent systems for cellulose such

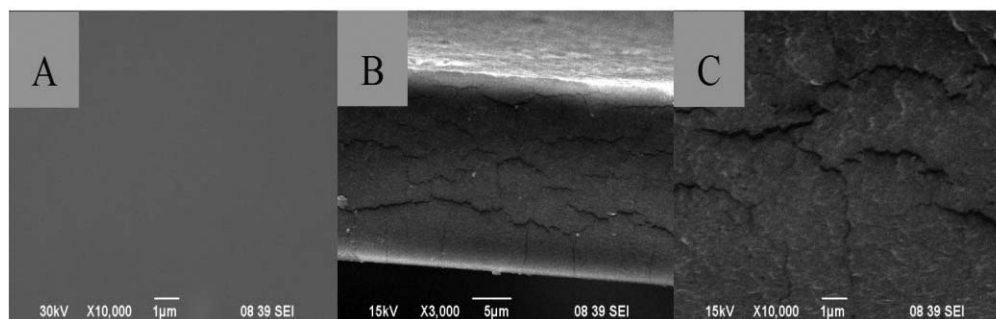


Fig. 5 SEM images of the free and fracture surfaces for the regenerated cellulose films from $[C_4mim][CH_3COO]/LiCl$ /cellulose solution: (A) free surface at 10 000 \times magnification; (B), (C) fracture surface at 3000 \times magnification and 10 000 \times magnification, respectively.

as DMAc/LiCl and NaOH/H₂O, pretreatment or activation of the original cellulose is often necessary.^{33,34}

Encouragingly, it is also found that absorbent cotton with a degree of polymerization as high as 1586 could be dissolved in the $[C_4mim][CH_3COO]/LiCl$ system in high concentrations (up to 21 wt%) at 90 °C. We have tried to increase the content of the lithium salts in $[C_4mim][CH_3COO]$ to enhance the cellulose solubility further. However, we failed to do this because of the limited solubility of the lithium salts in the ILs.

Structure and properties of the regenerated cellulose

The cellulose regenerated from $[C_4mim][CH_3COO]$ /lithium salt solvent systems (see Experimental section) was characterized by SEM, TGA, and FTIR spectroscopy. The degree of polymerization of the original and the regenerated cellulose materials was also determined, and the dissolution temperature and the dissolution time effects were examined.

SEM images of the regenerated cellulose films from $[C_4mim][CH_3COO]/LiCl$ solution are shown in Fig. 5. It can be seen that the free surface and fracture surface of the dried films display homogeneous structures from the interior to the surface, indicating a dense architecture, in which no undissolved original cellulose can be detected. The structure of the regenerated cellulose is quite similar to that reported by Zhang *et al.*¹⁵ and Zhang *et al.*,³⁵ but different from the porous structure regenerated from aqueous NaOH/thiourea solution.³⁶

FTIR spectra of the original and the regenerated cellulose materials are shown in Fig. S1 (see ESI†). It can be seen that all the spectra are quite similar and no new peaks are observed in the regenerated sample. This indicates that no chemical reaction takes place during the cellulose dissolution and regeneration processes. The absorption band at 1427 cm⁻¹ in the regenerated cellulose was assigned to the CH₂ scissoring vibration. This band was weakened and shifted to a lower wavenumber compared to the peak at 1431 cm⁻¹ for the original cellulose, suggesting the destruction of an intra-molecular hydrogen bond involving O6.³⁵ A new shoulder at 990 cm⁻¹ was observed in the regenerated cellulose, which could be assigned to a C–O stretching vibration in the amorphous region.³⁷ The O–H vibration in the regenerated cellulose shifts to a higher wavenumber (3427 cm⁻¹), indicating the breaking of hydrogen bonds to some extent.^{38,39} The absorption bands in the range of 1164–1061 cm⁻¹ are assigned to the C–O–C stretching of the original cellulose.⁴⁰ The presence of such bands in the absorption of the regenerated cellulose

suggests that the macromolecular structure of cellulose has not been destroyed.

TGA curves for both the original cellulose and the regenerated cellulose are shown in Fig. 6. It is noted that the two TGA curves nearly overlapped at lower temperatures, and rapid decomposition occurred in the temperature range from 313 to 351 °C for the original cellulose and from 301 to 341 °C for the regenerated cellulose. The regenerated sample exhibits a slightly lower onset temperature (301 °C) for the decomposition compared to the original cellulose (313 °C), and gives a slightly higher char yield (nonvolatile carbonaceous material) on pyrolysis, indicated by the slightly higher residual mass after the decomposition step. This result indicates that the cellulose regenerated from the $[C_4mim][CH_3COO]$ /lithium salts solvent systems has good thermal stability. This is significantly different from the cellulose regenerated from the reported solvent systems^{12,15} in which a large difference in the decomposition temperature was observed between the regenerated and the original materials.

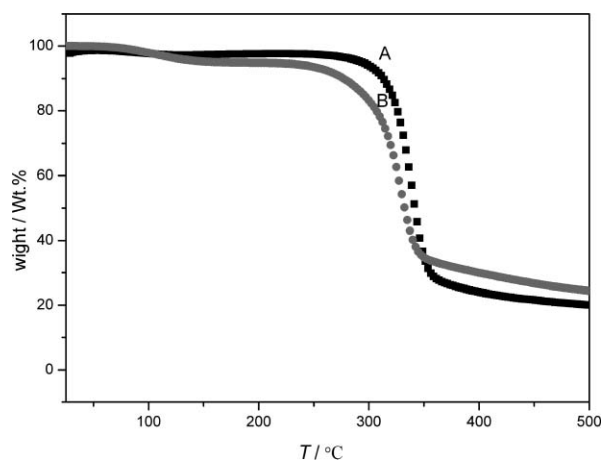


Fig. 6 Thermal decomposition profiles of the original cellulose and the regenerated cellulose materials: (A) the original cellulose; (B) the cellulose regenerated from $[C_4mim][CH_3COO]/LiCl$ /cellulose after 1 h of dissolution at 60 °C.

The effects of the dissolution temperature and dissolution time on the degree of polymerization (DP) of the regenerated cellulose are shown in Fig. 7 and 8, respectively. In the temperature range from 40 to 80 °C, the DP values (from 215 to 209) of the regenerated cellulose are slightly smaller than that of the original cellulose (DP = 229). Only at 100 °C was a slight degradation of

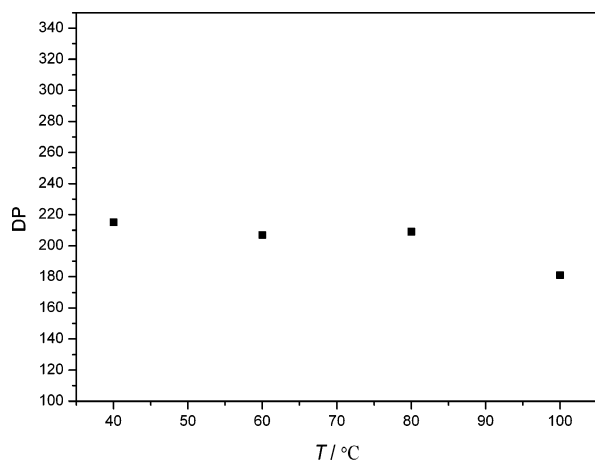


Fig. 7 Degree of polymerization for the cellulose regenerated from $[C_4mim][CH_3COO]/LiCl/cellulose$ after 1 h of dissolution at different temperatures.

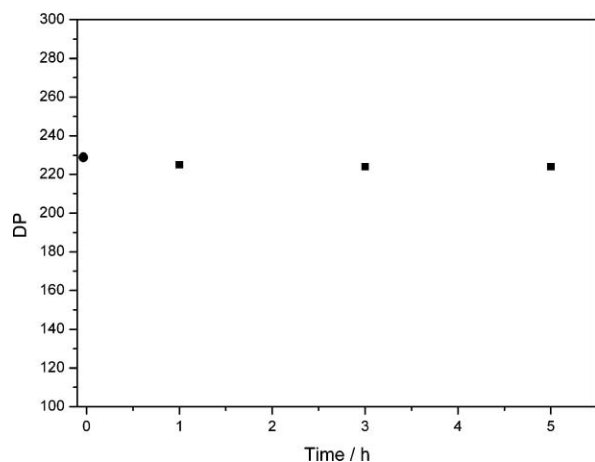


Fig. 8 Degree of polymerization for the original cellulose and the cellulose regenerated from $[C_4mim][CH_3COO]/LiCl/cellulose$ at 40 °C as a function of the dissolution times: (●) the original cellulose; (■) the regenerated cellulose.

cellulose observed, with the DP value of the regenerated cellulose being 181. It is worth noting that at 40 °C, the DP value of the regenerated cellulose hardly changed, even if the dissolution time was prolonged to as much as 5 h. This result indicates that no cellulose degradation took place at 40 °C during 5 h of dissolution in the $[C_4mim][CH_3COO]/lithium$ salt solvent systems. Obviously, the $[C_4mim][CH_3COO]/lithium$ salt solvent systems of cellulose are superior to some of the reported systems in which cellulose degradation definitely occurred.^{15,41} All of these facts suggest that our new solvent systems are excellent solvents for cellulose, and they could provide a new platform for the homogeneous processing of cellulose and the production of advanced cellulose materials under mild conditions.

Conclusions

In this work, solubility, 1H and ^{13}C NMR and solvatochromic UV/vis probe measurements have been performed to study the effects of the structure of the anion in selected ILs and the effect of adding lithium salts to $[C_4mim][CH_3COO]$ on the solubility of microcrystalline cellulose. It was shown that the structure of

the anion and the addition of lithium salts significantly affected the solubility of cellulose. The hydrogen bond accepting ability of the anions of the ILs, as characterized by the chemical shift values of the proton in the 2-position of the imidazolium ring, and the β parameter of the ILs, are closely linked to the solubility of cellulose. Thus, replacement of H in the CH_3COO^- anion of $[C_4mim][CH_3COO]$ by an electron-withdrawing group such as OH, SH, NH_2 or CH_3OH leads to decreased solubility. The nature the enhanced dissolution achieved with lithium salts is suggested to result from the interaction of Li^+ with the hydroxyl oxygen O(3) of the cellulose, which disrupts the intermolecular hydrogen bond $O(6)H \cdots O(3)$. Such information is expected to be useful for the design of novel ILs and IL-based solvent systems for cellulose.

Cellulose can be regenerated from the ILs and the $[C_4mim][CH_3COO]/lithium$ salt solvent systems by precipitation with water. The regenerated cellulose was studied by SEM, TGA, FTIR and degree of polymerization measurements. It was found that no chemical reaction took place between cellulose and the ILs or the $[C_4mim][CH_3COO]/lithium$ salt systems during the dissolution and precipitation processes. The regenerated cellulose exhibited a quite similar thermal stability to the original cellulose. Therefore, the $[C_4mim][CH_3COO]/Li$ salt solvent systems reported here are expected to provide a possible platform for the homogeneous processing of cellulose and the production of advanced cellulose materials under mild conditions. However, it should be pointed out that the recovery and reuse of the ILs and the lithium salts are the key issue for the practical application of the new solvent systems mentioned above. Although both of them can be recovered by simple evaporation from their aqueous solutions and then dried under vacuum, this method is energy consuming and thus expensive. Therefore, alternative low-cost methods for the recovery of the ILs and the lithium salts from the aqueous solutions need to be developed.

Experimental

Materials

Absorbent cotton and 1-methylimidazole (99%) were purchased from Shanghai Chem. Co.; 1-chlorobutane (>99.0%), 1-bromobutane (98.0%), mercaptoacetic acid (>97.0%), glycolic acid (98.0%), glycine (>99.0%), microcrystalline cellulose (MCC) and anion exchange resin (Ambersep 900 OH) were from Alfa Aesar; acetic acid (>99.5%), formic acid (>88.0%), benzoic acid (>99.5%) and lactic acid (85.0–90.0%) were obtained from Shanghai Shiyi Chem. Reagent Co. Ltd.; *N,N*-diethyl-4-nitroaniline (97.0%) was purchased from Nanjing Chemlin Chemical Industrial Co. Ltd.; deuterated DMSO ($DMSO-d_6$) used for NMR samples was purchased from Qingdao Weibo Tenglong Technol. Co. Ltd. The above materials were used as received. 1,1,1-Trichloroethane (95.0%) was obtained from Shanghai Shanpu Chem. Co. Ltd., and distilled before use. 4-Nitroaniline (98.0%) from Alfa Aesar was dissolved in methanol, and the mixture was stirred and then filtered to remove insoluble impurities. The methanol in the filtrate was evaporated, and 4-nitroaniline was dried under vacuum for 12 h at 40 °C. $LiCl \cdot 3H_2O$, $LiBr \cdot 2H_2O$, $LiAc \cdot 2H_2O$, $LiClO_4 \cdot 3H_2O$ and $LiNO_3 \cdot 3H_2O$ were obtained from Shanghai Chem. Co. and dried under vacuum before use to remove the crystallization water.

Synthesis of 1-butyl-3-methylimidazolium bromide [C₄mim]Br and 1-butyl-3-methylimidazolium chloride [C₄mim]Cl

[C₄mim]Br was prepared and purified by using the procedure described in the literature.⁴² Briefly, the reaction of 1-methylimidazole with an excess of 1-bromobutane was performed in 1,1,1-trichloroethane at 70 °C for 48 h. The solid product of [C₄mim]Br was washed with 1,1,1-trichloroethane and then filtered. The residual solvent was removed by rotary evaporation, and the resulting product was dried under vacuum for 24 h. [C₄mim]Cl was prepared similarly, but ethyl acetate was used instead of 1,1,1-trichloroethane.⁴³

Synthesis of 1-butyl-3-methylimidazolium acetate [C₄mim][CH₃COO], 1-butyl-3-methylimidazolium formate [C₄mim][HCOO], 1-butyl-3-methylimidazolium lactate [C₄mim][CH₃CHOHCOO], 1-butyl-3-methylimidazolium glycolate [C₄mim][HOCH₂COO], 1-butyl-3-methylimidazolium thioglycolate [C₄mim][HSCH₂COO], and 1-butyl-3-methylimidazolium benzoate [C₄mim][(C₆H₅)COO]

An aqueous solution of [C₄mim]Br was allowed to pass through a column filled with anion exchange resin to obtain [C₄mim][OH].¹⁷ The aqueous [C₄mim][OH] solution was then neutralized with equal molar acetic acid. After removing water by evaporation under reduced pressure, the viscous liquid [C₄mim][CH₃COO] was thoroughly washed with diethyl ether, and finally dried under vacuum for 72 h at 70 °C. The other ionic liquids were prepared by a similar process.

Synthesis of 1-butyl-3-methylimidazolium aminoethanoic acid salt [C₄mim][H₂NCH₂COO]

This IL was prepared by a similar procedure to that reported by Ohno *et al.*⁴⁴ Aqueous [C₄mim][OH] solution was thoroughly mixed with a slight excess of aqueous amino acid solution. After 12 h of reaction under cooling, water in the mixture was evaporated at 50 °C, and a slightly viscous liquid was obtained. After addition of acetonitrile–methanol (9 : 1, v/v), the mixture was stirred and then filtered to remove the excess amino acid. The organic solvents in the filtrate were evaporated and the product was dried under vacuum for 72 h at 80 °C.

Synthesis of 1-butyl-3-methylimidazolium dicyanamide [C₄mim][N(CN)₂]

This IL was synthesized and purified by using the procedure described by Sheldon and coworkers.⁴⁵ Briefly, to a solution of [C₄mim]Cl in acetone, Na[N(CN)₂] was added. The mixture was stirred for 24 h and the solid NaCl was removed by filtration. After removing acetone by evaporation under reduced pressure, the viscous liquid [C₄mim][N(CN)₂] was washed with dichloromethane, and dried under vacuum for 24 h at 60 °C.

The ¹H NMR data of the above ILs are summarized in the supporting information. They were in good agreement with those available in literature.^{42,43,45}

Preparation of [C₄mim][CH₃COO]/lithium salt solvent systems

1.0% (w/w) of LiCl, LiBr, LiAc, LiNO₃ or LiClO₄ was dissolved in [C₄mim][CH₃COO] to prepared the [C₄mim][CH₃COO]/

lithium salt solvent systems. These solvent mixtures were prepared immediately before use to minimize moisture uptake.

Dissolution of cellulose in the ILs and [C₄mim][CH₃COO]/lithium salt solvent systems

In a typical dissolution experiment, microcrystalline cellulose or absorbent cotton sample was added into a 20 mL colorimetric tube which contained 2.0 g of the dried IL or the IL/lithium salt, and the tube was sealed with parafilm. The tube was then immersed in an oil bath (DF-101S, Gongyi Yingyu Instrument Factory); the instability of the bath temperature was estimated to be ± 0.5 °C. The mixture was heated at a given temperature and stirred under argon atmosphere. Additional cellulose was added until the solution became optically clear under a polarization microscope (Nanjing Jiangnan Novel Optics Co. Ltd.). When cellulose became saturated, judged to be the point where cellulose could not be dissolved further within 1 h, its solubility (expressed in g per 100 g of IL) at the given temperature could be calculated from the amount of solvent and cellulose added. For each IL or [C₄mim][CH₃COO]/lithium salt solvent, the solubility values of cellulose were measured at different temperatures with 10 °C intervals.

Measurements of ¹H NMR and ¹³C NMR spectra

¹H NMR spectra of the ILs were collected at room temperature on a Bruker Avance-400 NMR spectrometer operating at 400.13 MHz. Measurements of ¹³C NMR spectra for the cellulose in [C₄mim][CH₃COO]/cellulose (9.0 wt%) and [C₄mim][CH₃COO]/LiCl (1.0 wt%)/cellulose (9.0 wt%) were performed on a Bruker DMX 300 spectrometer at 90 °C. Chemical shifts were given in ppm downfield from TMS.

Measurements of the β parameter for the ILs

The β parameter of the ILs, introduced as a measure of the hydrogen bond accepting ability of a solvent, was determined by following the procedure reported by Ohno *et al.*¹⁸ To calculate the β parameter, two different dyes, 4-nitroaniline (NA) and *N,N*-diethyl-4-nitroaniline (DENA) were employed. In a dry box, a given amount of the dried IL and a concentrated solution of NA or DENA in dry methanol were added into a vial and mixed homogeneously. The methanol was then carefully removed by drying under vacuum at 40 °C for 12 h. To avoid aggregation of the dyes, concentrations of NA or DENA in the ILs were selected to give an absorbance between 0.15 and 0.30. The IL containing NA or DENA was added into a quartz cell in a dry box and the cell was capped and sealed. The visible spectra of the ILs containing NA or DENA were recorded on a TU-1810 ultraviolet-visible spectrophotometer at 25.0 ± 0.1 °C. The wavelength at the maximum absorption (λ_{max}) was determined and used to calculate the β values by the following equations:¹⁸

$$v_{(\text{NA})} = 1/(\lambda_{\text{max}(\text{NA})} \times 10^{-4}) \quad (1)$$

$$v_{(\text{DENA})} = 1/(\lambda_{\text{max}(\text{DENA})} \times 10^{-4}) \quad (2)$$

$$\beta = (1.035v_{(\text{NA})} + 2.64 - v_{(\text{DENA})})/2.80 \quad (3)$$

Recovery and recycling of [C₄mim][CH₃COO]/Li salt solvent systems

After the complete dissolution of cellulose in the [C₄mim][CH₃COO]/Li salt solvent systems, cellulose can be regenerated and the [C₄mim][CH₃COO]/Li salt solvent mixtures can be recovered by addition of water or ethanol. In a typical recovery trial, 2.0 g of [C₄mim][CH₃COO]/LiCl solvent and 5.0 wt% cellulose solution were used. The cellulose solution was poured into a 100 mL beaker containing 10 mL of water. The beaker was sealed with preservative film and the mixture was stirred for 30 min at ambient temperature. The precipitated cellulose was separated by filtration through a ceramic funnel with Nylon filter paper on a Büchner flask under vacuum. The cellulose was washed four times to ensure that all the [C₄mim][CH₃COO]/LiCl solvent had been washed out. The filtrates were combined in a round bottomed flask, and water was removed by rotatory evaporation under reduced pressure. The resulting [C₄mim][CH₃COO]/LiCl solvent mixture was dried under vacuum for 24 h at 70 °C, and then could be used in the next dissolution process. In each dissolution–recovery cycle, the recovery percentage of [C₄mim][CH₃COO]/LiCl solvent is approximately 99.2 wt%, and the dissolving capacity of the recovered solvent for cellulose is equivalent to the original solvent.

Characterization of the regenerated cellulose

Fourier transform infrared (FTIR) spectra were recorded on a Nicolet Nexus spectrometer with KBr pellets. A total of 16 scans were taken for each sample at a resolution of 2 cm⁻¹. Scanning electron micrographs were taken with a JEOL JSM-6390LV scanning electron microscope. The regenerated cellulose films in the dry state were frozen in liquid nitrogen, immediately snapped, and then dried under vacuum. The free surface (side in direct contact with the coagulant) and the fracture surface of the films were sputtered with gold, and then photographed. TGA was carried out with a NETZSCH STA 449 C thermal analyser using alumina crucibles. The sample mass was ca. 10–15 mg per measurement. The measurements were carried out under flowing N₂ at a heating rate of 10 °C min⁻¹. The viscosity-average degree of polymerization (DP) for the original and regenerated cellulose materials was determined by using an Ubbelohde viscometer in cupriethylenediamine hydroxide solutions.

Acknowledgements

This work was supported financially by the National High Technology Research and Development Program (863 Program, No.2007AA05Z454), the National Natural Science Foundation of China (No.20873036) and the Innovation Scientists and Technicians Troop Construction Projects of Henan Province (No.084200510015).

References

- 1 D. Klemm, B. Heublein, H. P. Fink and A. Bohn, *Angew. Chem., Int. Ed.*, 2005, **44**, 3358.
- 2 K. J. Edgar, C. M. Buchanan, J. S. Debenham, P. A. Rundquist, B. D. Seiler, M. C. Shelton and D. Tindall, *Prog. Polym. Sci.*, 2001, **26**, 1605.
- 3 F. T. Moutos, L. E. Freed and F. Guilak, *Nat. Mater.*, 2007, **6**, 162.
- 4 F. Hermanutz, F. Gähr, E. Uerdingen, F. Meister and B. Kosan, *Macromol. Symp.*, 2008, **262**, 23.
- 5 C. L. McCormick and T. R. Dawsey, *Macromolecules*, 1990, **23**, 3606.
- 6 S. Fischer, W. Voigt and K. Fischer, *Cellulose*, 1999, **6**, 213.
- 7 T. Heinze and T. Liebert, *Prog. Polym. Sci.*, 2001, **26**, 1689.
- 8 Z. Wang, T. Yokoyama, H. M. Chang and Y. Matsumoto, *J. Agric. Food Chem.*, 2009, **57**, 6167.
- 9 T. Welton, *Chem. Rev.*, 1999, **99**, 2071.
- 10 P. Wasserscheid and W. Keim, *Angew. Chem., Int. Ed.*, 2000, **39**, 3772.
- 11 J. Dupont, R. F. de Souza and P. A. Z. Suarez, *Chem. Rev.*, 2002, **102**, 3667.
- 12 R. P. Swatloski, S. K. Spear, D. John, J. D. Holbrey and R. D. Rogers, *J. Am. Chem. Soc.*, 2002, **124**, 4974.
- 13 J. S. Moulthrop, R. P. Swatloski, G. Moyna and R. D. Rogers, *Chem. Commun.*, 2005, 1557.
- 14 R. C. Remsing, R. P. Swatloski, R. D. Rogers and G. Moyna, *Chem. Commun.*, 2006, 1271.
- 15 H. Zhang, J. Wu, J. Zhang and J. S. He, *Macromolecules*, 2005, **38**, 8272.
- 16 Y. Cao, J. Wu, J. Zhang, H. Q. Li, Y. Zhang and J. S. He, *Chem. Eng. J.*, 2009, **147**, 13.
- 17 Y. Fukaya, A. Sugimoto and H. Ohno, *Biomacromolecules*, 2006, **7**, 3295.
- 18 Y. Fukaya, K. Hayashi, M. Wadab and H. Ohno, *Green Chem.*, 2008, **10**, 44.
- 19 J. Vitz, T. Erdmenger, C. Haensch and U. S. Schubert, *Green Chem.*, 2009, **11**, 417.
- 20 D. A. Fort, R. C. Remsing, R. P. Swatloski, P. Moyna, G. Moyna and R. D. Rogers, *Green Chem.*, 2007, **9**, 63.
- 21 I. Kilpeläinen, H. Xie, A. King, M. Granstrom, S. Heikkinen and D. S. Argyropoulos, *J. Agric. Food Chem.*, 2007, **55**, 9142.
- 22 M. Zavrel, D. Bross, M. Funke, J. Büchs and A. C. Spiess, *Bioresour. Technol.*, 2009, **100**, 2580.
- 23 N. Sun, M. Rahman, Y. Qin, M. L. Maxim, H. Rodríguez and R. D. Rogers, *Green Chem.*, 2009, **11**, 646.
- 24 S. D. Zhu, *J. Chem. Technol. Biotechnol.*, 2008, **83**, 777.
- 25 A. Oehlke, K. Hofmann and S. Spange, *New J. Chem.*, 2006, **30**, 533.
- 26 C. Chiappe and D. J. Pieraccini, *J. Phys. Org. Chem.*, 2005, **18**, 275.
- 27 J. G. Huddleston, G. A. Broker, H. D. Willauer and R. D. Rogers, *ACS Symp. Ser.*, 2002, **818**, 270.
- 28 R. Lungwitz and S. Spange, *New J. Chem.*, 2008, **32**, 392.
- 29 E. Brendler, S. Fischer and H. Leipner, *Cellulose*, 2001, **8**, 283.
- 30 B. Hinterstoisser, M. Åkerholm and L. Salmén, *Biomacromolecules*, 2003, **4**, 1232.
- 31 Y. Sun, L. Lin, C. S. Pang, H. B. Deng, H. Peng, J. Z. Li, B. H. He and S. J. Liu, *Energy Fuels*, 2007, **21**, 2386.
- 32 B. Morgensrern, H. W. Kammer and W. Berger, *Acta Polym.*, 1992, **43**, 356.
- 33 C. L. McCormick, P. A. Callais and B. H. Hutchinson Jr., *Macromolecules*, 1985, **18**, 2394.
- 34 D. Ishii, D. Tatsumi and T. Matsumoto, *Biomacromolecules*, 2003, **4**, 1238.
- 35 L. N. Zhang, D. Ruan and J. P. Zhou, *Ind. Eng. Chem. Res.*, 2001, **40**, 5923.
- 36 L. N. Zhang, D. Ruan and S. J. Gao, *J. Polym. Sci., Part B: Polym. Phys.*, 2002, **40**, 1521.
- 37 H. G. Higgins, C. M. Stewart and K. J. Harrington, *J. Polym. Sci.*, 1961, **51**, 59.
- 38 S. M. Zhou, K. Tashiro, T. Hongo, H. Shirataki, C. Yamane and T. Ii, *Macromolecules*, 2001, **34**, 1274.
- 39 Y. Kataoka and T. Kondo, *Macromolecules*, 1998, **31**, 760.
- 40 L. J. Qu, Y. Zhang, J. Q. Wang and D. L. Chi, *J. Qingdao University*, 2008, **23**, 44.
- 41 A. Potthast, T. Rosenau, H. Sixta and P. Kosmaa, *Tetrahedron Lett.*, 2002, **43**, 7757.
- 42 P. Bonhote, D. Ana-Paula, N. Papageorgiou, K. Kalyanasundaram and M. Gratzel, *Inorg. Chem.*, 1996, **35**, 1168.
- 43 J. G. Huddleston, H. D. Willauer, R. P. Swatloski, A. E. Visser and R. D. Rogers, *Chem. Commun.*, 1998, 1765.
- 44 K. Fukumoto, M. Yoshizawa and H. Ohno, *J. Am. Chem. Soc.*, 2005, **127**, 2398.
- 45 Q. B. Liu, M. H. A. Janssen, F. V. Rantwijk and R. A. Sheldon, *Green Chem.*, 2005, **7**, 39.

Ligand-free iron/copper cocatalyzed *N*-arylations of aryl halides with amines under microwave irradiation†

Diliang Guo,^{a,b} He Huang,^b Yu Zhou,^b Jinyi Xu,^a Hualiang Jiang,^b Kaixian Chen^{a,b} and Hong Liu^{*a,b}

Received 18th August 2009, Accepted 19th October 2009

First published as an Advance Article on the web 11th November 2009

DOI: 10.1039/b917010c

Ligand-free iron/copper cocatalyzed cross-coupling reactions of aryl halides with amines were carried out to provide the corresponding coupling products in good yields. It is worth noting that the method displays a broad substrate scope, and is convenient, rapid, low-cost and environmentally friendly.

Introduction

Transition metal-catalyzed carbon–nitrogen bond formation with aryl halides and aliphatic or aromatic amines is considered to be an important strategy that finds wide applications in the synthesis of many substances such as natural products, agrochemicals, materials, dyes, and pharmaceuticals.¹ In particular, the majority of the existing protocols for performing the *N*-arylation of amines with aryl halides have been mediated by palladium,² copper³ and, more recently, environmentally benign iron⁴ catalysts. Although significant progress has been made in this field, there are still some drawbacks of these methods that include the need for (1) specially designed ligands or stoichiometric amounts of catalysts/reagents, (2) anhydrous solvents and an inert atmosphere, and (3) long reaction time. Recently, Norrby, Bolm and their co-workers reported copper-catalyzed cross-couplings with parts-per-million catalyst loadings; they lowered the catalyst loading to 0.01 mol%. And they found that it was crucial that the ligand-to-metal ratio was high (with 20 mol% of DMEDA).⁵ Therefore, it is a highly challenging and desired endeavor to find a readily available, inexpensive and ligand-free^{6,7} catalytic system for cross-coupling reactions. Taillefer and co-workers reported the first ligand-free iron/copper cooperative catalysis for *N*-arylation of nitrogen heterocycles.⁸ Although these results are encouraging, there is much room for improvement. For example, the methods require long reaction times and are limited in terms of the substrates for which they can be used. So room for exploration of an efficient ligand-free catalytic system, especially proceeding in short reaction times, still remains.

In continuation of our endeavors devoted to the development of copper and iron catalyzed cross coupling reactions,⁹ herein we wish to report the first ligand-free iron/copper cocatalyzed¹⁰ C–N cross coupling reaction in the presence of water¹¹ under

microwave (MW) irradiation. This method is attractive for several reasons: (i) it employs an economically competitive and environmentally-friendly catalytic system that is a combination of readily available iron and copper salts, without ligands or other additives; (ii) it offers experimental simplicity, and does not require an inert atmosphere and anhydrous solvents; (iii) it is applicable to a broad scope of substrates, both aliphatic and aromatic amines and various substituted aryl halides; (iv) it proceeds quickly and affords moderate to good yields within minutes under microwave irradiation,¹² which proved to be a green and rapid route in organic synthesis. At the same time, water is abundant, cheap and an environmentally benign solvent. In recent years the combination of these two prominent green chemistry principles, “microwaves” and “water”, has become very popular and has received substantial interest.^{12c}

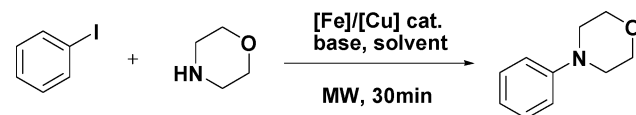
Results and discussion

Initially, we screened typical reaction parameters including catalysts, solvents, base and temperature, using iodobenzene (1.5 equiv) and morpholine (1.0 equiv) as model substrates, and the results are summarized in Table 1. The preliminary investigation was carried out in water under microwave irradiation at 135 °C for 30 min using caesium carbonate as base. The coupling reaction provided promising products in the presence of catalytic amounts of both Fe₂O₃ (having a purity of 99.9995+%, from Alfa Aesar) and Cu(acac)₂ (23% yield; Table 1, entry 1; acac = acetylacetonate). To our pleasure, switching pure H₂O to H₂O:DMSO = 1:1 promoted the yield to 75% (Table 1, entry 2), while it was not able to increase the yield in DMSO (Table 1, entry 3). Comparing the microwave-assisted reaction conditions with conventional thermal conditions, the former manifested a significant boost in terms of shorter reaction time and higher yields (Table 1, entries 2 and 6). When we raised the temperature to 150 °C, the yields were improved (Table 1, entries 7–9). In the absence of an iron source, catalytic amounts of Cu(acac)₂ afforded a moderate yield of the coupling product (Table 1, entries 5 and 11), and it indicated that the iron source also had a pronounced impact on the efficient cocatalysis (compare entries 2 and 9 with 5 and 11, Table 1). However, a catalytic amount of Fe₂O₃ alone was unable to promote the reaction (Table 1, entries 4 and 10), indicating that the copper

^aDepartment of Medicinal Chemistry, China Pharmaceutical University, 24 TongjiaXiang, Nanjing, 210009, P. R. China

^bThe Center for Drug Discovery and Design, State Key Laboratory of Drug Research, Shanghai Institute of Materia Medica, Shanghai Institutes for Biological Sciences, Chinese Academy of Sciences, Shanghai, 201203, P. R. China. E-mail: hliu@mail.shnc.ac.cn

† Electronic supplementary information (ESI) available: ¹H and ¹³C NMR spectra.

Table 1 Optimization of the catalysis conditions


Entry	Iron (0.2 eq)	Copper (0.1 eq)	<i>T</i> /°C	Base (2.0 eq)	Solvent	Yield (%)
1	Fe ₂ O ₃	Cu(acac) ₂	135	Cs ₂ CO ₃	H ₂ O	23
2	Fe ₂ O ₃	Cu(acac) ₂	135	Cs ₂ CO ₃	DMSO:H ₂ O = 1:1	75
3	Fe ₂ O ₃	Cu(acac) ₂	135	Cs ₂ CO ₃	DMSO	10<
4	Fe ₂ O ₃	—	135	Cs ₂ CO ₃	DMSO:H ₂ O = 1:1	trace
5	—	Cu(acac) ₂	135	Cs ₂ CO ₃	DMSO:H ₂ O = 1:1	47
6 ^a	Fe ₂ O ₃	Cu(acac) ₂	135	Cs ₂ CO ₃	DMSO:H ₂ O = 1:1	56
7	Fe ₂ O ₃	Cu(acac) ₂	150	Cs ₂ CO ₃	H ₂ O	46
8	Fe ₂ O ₃	Cu(acac) ₂	150	Cs ₂ CO ₃	DMSO	31
9	Fe ₂ O ₃	Cu(acac) ₂	150	Cs ₂ CO ₃	DMSO:H ₂ O = 1:1	83
10	Fe ₂ O ₃	—	150	Cs ₂ CO ₃	DMSO:H ₂ O = 1:1	trace
11	—	Cu(acac) ₂	150	Cs ₂ CO ₃	DMSO:H ₂ O = 1:1	62
12	—	—	150	Cs ₂ CO ₃	DMSO:H ₂ O = 1:1	0
13	Fe ₂ O ₃	CuI	150	Cs ₂ CO ₃	DMSO:H ₂ O = 1:1	70
14	Fe ₂ O ₃	Cu(OAc) ₂	150	Cs ₂ CO ₃	DMSO:H ₂ O = 1:1	76
15	Fe ₂ O ₃	Cu ₂ O	150	Cs ₂ CO ₃	DMSO:H ₂ O = 1:1	67
16	FeCl ₃	Cu(acac) ₂	150	Cs ₂ CO ₃	DMSO:H ₂ O = 1:1	71
17	FeCl ₂	Cu(acac) ₂	150	Cs ₂ CO ₃	DMSO:H ₂ O = 1:1	61
18	Fe(acac) ₃	Cu(acac) ₂	150	Cs ₂ CO ₃	DMSO:H ₂ O = 1:1	75
19	Fe ₂ O ₃	Cu(acac) ₂	150	NaO <i>t</i> Bu	DMSO:H ₂ O = 1:1	16
20	Fe ₂ O ₃	Cu(acac) ₂	150	K ₂ CO ₃	DMSO:H ₂ O = 1:1	29
21	Fe ₂ O ₃	Cu(acac) ₂	150	K ₃ PO ₄	DMSO:H ₂ O = 1:1	trace
22	Fe ₂ O ₃	Cu(acac) ₂	150	Cs ₂ CO ₃	DMF:H ₂ O = 1:1	60
23	Fe ₂ O ₃	Cu(acac) ₂	150	Cs ₂ CO ₃	NMP:H ₂ O = 1:1	63

^a Performed under conventional thermal conditions, 24h. ^b Yield of isolated product.

source is essential for this process (Table 1, entries 2, 4, 5 and 9-12). Combined with Fe₂O₃ as cocatalyst, copper salts such as CuI, Cu(OAc)₂ and Cu₂O were also effective (Table 1, entries 13-15). When we screened the iron sources, preliminary results showed that the yield afforded by Fe₂O₃ was better than that afforded by FeCl₃ (having a purity of 98+%, from Alfa Aesar), FeCl₂ (having a purity of 99.5+%, from Alfa Aesar) and Fe(acac)₃ (having a purity of 99.9+%, from Aldrich) (Table 1, entries 16-18). Furthermore, we found that the nature of bases was crucial for the reaction. NaO*t*Bu, K₂CO₃ and K₃PO₄ were all ineffective (Table 1, entries 19-21). Among the solvents used, H₂O:DMSO = 1:1 was superior to other solvents (Table 1, entries 22 and 23). In summary, the optimum results were obtained when amine (1.0 equiv) and aryl halide (1.5 equiv) were allowed to react with Fe₂O₃ (0.2 equiv), Cu(acac)₂ (0.1 equiv), Cs₂CO₃ (2.0 equiv) stirred in H₂O:DMSO = 1:1 at 150 °C for 30 min.

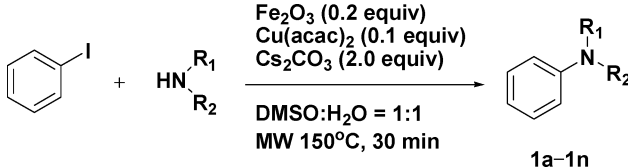
With the optimized conditions in hand, we investigated the scope of this methodology among a variety of nitrogen-containing compounds, including aliphatic primary amines, aliphatic secondary amines, benzylamine, phenethylamine, anilines and nitrogen heterocycles. In general, the corresponding *N*-arylation products were obtained in moderate to good yields (Table 2). All the aliphatic primary amines and benzylamine, phenethylamine were effective in the formation of C–N bonds (Table 2, entries 1-5, 8 and 9). Although the steric hindrance of secondary amines often makes them more sluggish than primary amines to couple with aryl halides, it was a delight to find that the coupling of aliphatic secondary amines with iodobenzene was also quite successful (Table 2, entries 6 and 7). Low yields

were observed for nitrogen heterocycles, such as pyrazole and indole, but elevating the reaction temperature could lead to an improvement in reaction yields (Table 2, entries 10 and 11). As shown, anilines containing an electron-withdrawing group typically gave lower yields than anilines and those containing an electron-donating group (Table 2, entries 12-14).

The scope of the process with respect to aryl halides was then investigated (Table 3). The coupling reactions of morpholine as the model amine with aryl halides containing various substituents were carried out under the optimal reaction conditions. As expected, the desired products were obtained in moderate to good yields. The results indicated that aryl iodides were more reactive than aryl bromides and aryl chlorides (Table 3, entries 1, 5 and 8). This protocol was tolerant to electron-donating functional groups (Table 3, entries 2 and 5); a good yield was obtained even in the presence of a strongly electron-donating functional group (Table 3, entry 2). Although a satisfactory result was obtained for 4-chloriodobenzene (Table 3, entry 12), the protocol didn't exhibit good tolerance with aryl halides bearing the strongly electron-withdrawing functional groups, such as CF₃ or NO₂ (Table 3, entries 8 and 11). The steric effect was significant, the reactions of *para*- or *meta*-substituted aryl halides afforded higher yields than steric *ortho*-substituted aryl halides. The results indicated the reactivity order of substituted aryl halides: *para*- > *meta*- > *ortho*- (Table 3, entries 2-7, 9 and 10).

In an endeavor to expand the scope of the methodology, we attempted to apply the iron/copper cocatalytic system to some important compounds that occur in many natural and synthetic products, such as indoline,¹³ *N*-alkylanthranilic acid¹⁴

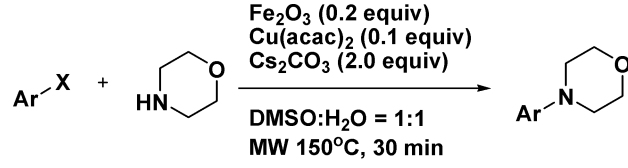
Table 2 Iron/copper cocatalyzed *N*-arylation of aryl iodide with various nitrogen derivatives



Entry	Amines	Product	Yield (%)
1			1a 76
2			1b 90
3			1c 93
4			1d 76
5			1e 75
6			1f 73
7			1g 83
8			1h 77
9			1i 66
10			1j 35 57 ^a
11			1k 22
12			1l 51
13			1m 35
14			1n trace

^a MW 165 °C, 30 min. ^b Yield of isolated product.

Table 3 Iron/copper cocatalyzed *N*-arylation of morpholine with different substituted aryl halides



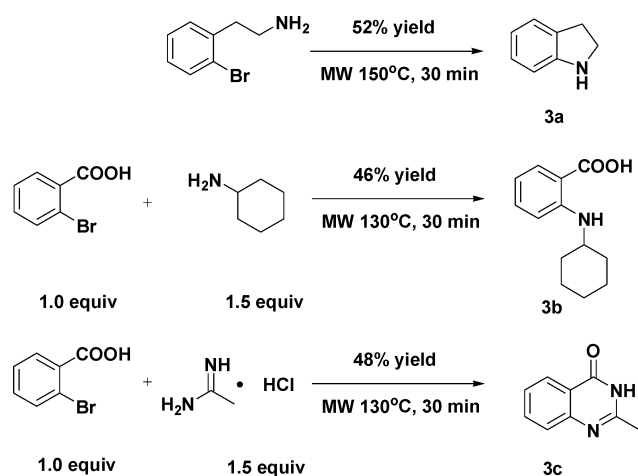
Entry	Aryl halides	Product	Yield (%)
1			1g 85 (X = I) 22 (X = Br) 0 (X = Cl)
2			2a 80
3			2b 54
4			2c 36
5			2d 83 (X = I) 20 (X = Br) 0 (X = Cl)
6			2e 45
7			2f trace
8			2g 25 (X = I) 11 (X = Br)
9			2h 62
10			2i trace
11			2j 39
12			2k 78

^aYield of isolated product.

and quinazolinone.¹⁵ The synthesis of their derivatives has attracted much attention because of their importance as drug molecules and key core blocks. Generally, it was encouraging to reveal that the desired products were obtained in moderate yields (Scheme 1). Further work is underway in our laboratory.

Conclusion

In summary, we have developed a convenient, rapid, economical, and environmentally friendly protocol for the *N*-arylation of



Scheme 1 Iron/copper cocatalyzed synthesis of indoline, 2-(cyclohexylamino)benzoic acid and 2-methylquinazolin-4(3H)-one.

various amines with differently substituted aryl halides promoted by a ligand-free iron/copper cocatalyst under microwave irradiation. In addition, the short reaction times and simple reaction conditions coupled with a broad substrate scope make this method viable for use both in the efficient preparation of biologically and medicinally interesting molecules, and library synthesis in drug discovery.

Experimental

General experimental procedures

The reagents were purchased from a commercial chemical reagent company, and used without further purification unless otherwise stated. All of the microwave-assisted reactions were performed in an Initiator™ EXP microwave system (Biotage, Inc.) at the specified temperature using the standard mode of operation. Analytical thin-layer chromatography (TLC) was HSGF 254. Proton and carbon magnetic resonance spectra (¹H NMR and ¹³C NMR) were recorded using tetramethylsilane (TMS) in CDCl₃ or DMSO-*d*₆ as the internal standard (¹H NMR: TMS at 0.00 ppm, CDCl₃ at 7.24 ppm, DMSO at 2.50 ppm; ¹³C NMR: CDCl₃ at 77.0 ppm, DMSO at 40.0 ppm).

General procedure for the coupling reaction

A mixture of Fe₂O₃ (32 mg, 0.2 mmol), Cu(acac)₂ (26 mg, 0.1 mmol), and Cs₂CO₃ (650 mg, 2.0 mmol) was dissolved in DMSO (3 mL). Subsequently, iodobenzene (160 μL, 1.5 mmol), morpholine (88 μL, 1.0 mmol) and H₂O (3 mL) were added to this mixture. The vial was sealed and the mixture was then irradiated for 30 min at 150 °C. The mixture was then cooled to room temperature, and diluted with dichloromethane, washed with brine, dried using anhydrous Na₂SO₄, and concentrated in vacuum. The residue was purified by flash column chromatography (petroleum ether/ethyl acetate = 10:1) to yield the expected product.

Spectroscopic and analytical data

***N*-butylbenzenamine (1a).** ¹H NMR (300 MHz, CDCl₃): δ 7.19-7.14 (m, 2H), 6.70-6.66 (m, 1H), 6.61-6.58 (m, 2H), 3.12-

3.07 (m, 2H), 1.61-1.54 (m, 2H), 1.46-1.38 (m, 2H), 0.98-0.93 (m, 3H). ¹³C NMR (100 MHz, CDCl₃): δ 148.4, 129.1, 117.0, 112.6, 43.6, 31.6, 20.2, 13.8. MS (EI, *m/z*): 149 [M]⁺; HRMS (EI): Calcd. for C₁₀H₁₅N [M]⁺: 149.1204; Found: 149.1208.

***N*-(2-methoxyethyl)benzenamine (1b).** ¹H NMR (300 MHz, CDCl₃): δ 7.20-7.15 (m, 2H), 6.74-6.69 (m, 1H), 6.64-6.61 (m, 2H), 3.58 (t, *J* = 5.1 Hz, 2H), 3.37 (s, 3H), 3.27 (t, *J* = 5.1 Hz, 2H). ¹³C NMR (100 MHz, CDCl₃): δ 148.1, 129.1, 117.5, 113.0, 70.9, 58.6, 43.3. MS (EI, *m/z*): 151 [M]⁺; HRMS (EI): Calcd. for C₉H₁₃NO [M]⁺: 151.0997; Found: 151.0990.

***N*-(3-methoxypropyl)benzenamine (1c).** ¹H NMR (300 MHz, CDCl₃): δ 7.19-7.14 (m, 2H), 6.71-6.66 (m, 1H), 6.62-6.59 (m, 2H), 3.50 (t, *J* = 6.0 Hz, 2H), 3.35 (s, 3H), 3.21 (t, *J* = 6.0 Hz, 2H), 1.91-1.83 (m, 2H). ¹³C NMR (100 MHz, CDCl₃): δ 148.4, 129.1, 117.0, 112.6, 71.1, 58.6, 41.6, 29.2. MS (EI, *m/z*): 165 [M]⁺; HRMS (EI): Calcd. for C₁₀H₁₅NO [M]⁺: 165.1154; Found: 165.1149.

***N*-(cyclopropylmethyl)benzenamine (1d).** ¹H NMR (300 MHz, CDCl₃): δ 7.19-7.14 (m, 2H), 6.71-6.66 (m, 1H), 6.61-6.58 (m, 2H), 2.94 (d, *J* = 6.3 Hz, 2H), 1.11-1.06 (m, 1H), 0.57-0.51 (m, 2H), 0.25-0.20 (m, 2H). ¹³C NMR (100 MHz, CDCl₃): δ 148.4, 129.2, 117.2, 112.7, 49.0, 10.8, 3.4. MS (EI, *m/z*): 147 [M]⁺; HRMS (EI): Calcd. for C₁₀H₁₃N [M]⁺: 147.1048; Found: 147.1044.

***N*-cyclohexylbenzenamine (1e).** ¹H NMR (300 MHz, CDCl₃): δ 7.18-7.12 (m, 2H), 6.68-6.63 (m, 1H), 6.59-6.56 (m, 2H), 3.29-3.21 (m, 1H), 2.08-2.03 (m, 2H), 1.79-1.72 (m, 2H), 1.68-1.62 (m, 1H), 1.44-1.08 (m, 5H). ¹³C NMR (100 MHz, CDCl₃): δ 147.3, 129.2, 116.8, 113.1, 51.6, 33.4, 25.9, 25.0. MS (EI, *m/z*): 175 [M]⁺; HRMS (EI): Calcd. for C₁₂H₁₇N [M]⁺: 175.1361; Found: 175.1362.

***N*-phenylpiperidine (1f).** ¹H NMR (300 MHz, CDCl₃): δ 7.26-7.21 (m, 2H), 6.94-6.92 (m, 2H), 6.83-6.78 (m, 1H), 3.14 (t, *J* = 5.7 Hz, 4H), 1.74-1.66 (m, 4H), 1.59-1.54 (m, 2H). ¹³C NMR (100 MHz, CDCl₃): δ 152.2, 128.9, 119.2, 116.5, 50.6, 25.8, 24.2. MS (EI, *m/z*): 161 [M]⁺; HRMS (EI): Calcd. for C₁₁H₁₅N [M]⁺: 161.1204; Found: 161.1201.

4-phenylmorpholine (1g). ¹H NMR (300 MHz, CDCl₃): δ 7.30-7.25 (m, 2H), 6.92-6.85 (m, 3H), 3.85 (t, *J* = 4.8 Hz, 4H), 3.14 (t, *J* = 4.8 Hz, 4H). ¹³C NMR (100 MHz, CDCl₃): δ 151.2, 129.1, 120.0, 115.6, 66.9, 49.3. MS (EI, *m/z*): 163 [M]⁺; HRMS (EI): Calcd. for C₁₀H₁₃NO [M]⁺: 163.0997; Found: 163.0995.

***N*-benzylbenzenamine (1h).** ¹H NMR (300 MHz, CDCl₃): δ 7.34-7.24 (m, 5H), 7.18-7.12 (m, 2H), 6.73-6.68 (m, 1H), 6.61-6.58 (m, 2H), 4.27 (s, 2H). ¹³C NMR (100 MHz, CDCl₃): δ 148.0, 139.3, 129.2, 128.6, 127.4, 127.1, 117.5, 112.8, 48.2. MS (EI, *m/z*): 183 [M]⁺; HRMS (EI): Calcd. for C₁₃H₁₃N [M]⁺: 183.1048; Found: 183.1090.

***N*-phenethylbenzenamine (1i).** ¹H NMR (300 MHz, CDCl₃): δ 7.35-7.30 (m, 2H), 7.26-7.15 (m, 5H), 6.75-6.69 (m, 1H), 6.61-6.59 (m, 2H), 3.40 (t, *J* = 6.9 Hz, 2H), 2.91 (t, *J* = 6.9 Hz, 2H). ¹³C NMR (100 MHz, CDCl₃): δ 147.9, 139.2, 129.2, 128.7, 128.5, 126.4, 117.4, 112.9, 45.0, 35.4. MS (EI, *m/z*): 197 [M]⁺; HRMS (EI): Calcd. for C₁₄H₁₅N [M]⁺: 197.1204; Found: 197.1218.

1-phenyl-1H-pyrazole (1j). ^1H NMR (300 MHz, CDCl_3): δ 7.92-7.91 (m, 1H), 7.74-7.69 (m, 3H), 7.48-7.42 (m, 2H), 7.31-7.26 (m, 1H), 6.47-6.45 (m, 1H). ^{13}C NMR (100 MHz, CDCl_3): δ 141.0, 140.0, 129.3, 126.6, 126.3, 119.0, 107.4. MS (EI, m/z): 144 $[\text{M}]^+$; HRMS (EI): Calcd. for $\text{C}_9\text{H}_8\text{N}_2$ $[\text{M}]^+$: 144.0687; Found: 144.0691.

1-phenyl-1H-indole (1k). ^1H NMR (300 MHz, CDCl_3): δ 7.70-7.67 (m, 1H), 7.57-7.54 (m, 1H), 7.49-7.46 (m, 4H), 7.34-7.30 (m, 2H), 7.24-7.14 (m, 2H), 6.67-6.66 (m, 1H). ^{13}C NMR (100 MHz, CDCl_3): δ 139.8, 135.8, 129.5, 129.3, 127.9, 126.4, 124.3, 122.3, 121.1, 120.3, 110.4, 103.5. MS (EI, m/z): 193 $[\text{M}]^+$; HRMS (EI): Calcd. for $\text{C}_{14}\text{H}_{11}\text{N}$ $[\text{M}]^+$: 193.0891; Found: 193.0886.

4-methoxy-N-phenylaniline (1l). ^1H NMR (300 MHz, CDCl_3): δ 7.23-7.19 (m, 2H), 7.08-7.06 (m, 2H), 6.91-6.81 (m, 5H), 5.49 (s, br, 1H), 3.70 (s, 3H). ^{13}C NMR (100 MHz, CDCl_3): δ 155.2, 145.1, 135.7, 129.3, 122.1, 119.5, 115.6, 114.6, 55.5. MS (EI, m/z): 199 $[\text{M}]^+$; HRMS (EI): Calcd. for $\text{C}_{13}\text{H}_{13}\text{NO}$ $[\text{M}]^+$: 199.0997; Found: 199.0999.

Diphenylamine (1m). ^1H NMR (300 MHz, CDCl_3): δ 7.29-7.25 (m, 4H), 7.08-7.06 (m, 4H), 6.96-6.91 (m, 2H). ^{13}C NMR (100 MHz, CDCl_3): δ 143.0, 129.3, 121.0, 117.8. MS (EI, m/z): 169 $[\text{M}]^+$; HRMS (EI): Calcd. for $\text{C}_{12}\text{H}_{11}\text{N}$ $[\text{M}]^+$: 169.0891; Found: 169.0886.

4-(4-methoxyphenyl)morpholine (2a). ^1H NMR (300 MHz, CDCl_3): δ 6.91-6.83 (m, 4H), 3.87-3.84 (m, 4H), 3.77 (s, 3H), 3.07-3.04 (m, 4H). ^{13}C NMR (100 MHz, CDCl_3): δ 153.9, 145.5, 117.8, 114.5, 67.0, 55.5, 50.8. MS (EI, m/z): 193 $[\text{M}]^+$; HRMS (EI): Calcd. for $\text{C}_{11}\text{H}_{15}\text{NO}_2$ $[\text{M}]^+$: 193.1103; Found: 193.1108.

4-(3-methoxyphenyl)morpholine (2b). ^1H NMR (300 MHz, CDCl_3): δ 7.23-7.17 (m, 1H), 6.56-6.52 (m, 1H), 6.47-6.44 (m, 2H), 3.85 (t, $J = 4.8$ Hz, 4H), 3.80 (s, 3H), 3.15 (t, $J = 4.8$ Hz, 4H). ^{13}C NMR (100 MHz, CDCl_3): δ 160.5, 152.6, 129.8, 108.3, 104.6, 102.1, 66.7, 55.0, 49.1. MS (EI, m/z): 193 $[\text{M}]^+$; HRMS (EI): Calcd. for $\text{C}_{11}\text{H}_{15}\text{NO}_2$ $[\text{M}]^+$: 193.1103; Found: 193.1105.

4-(2-methoxyphenyl)morpholine (2c). ^1H NMR (300 MHz, CDCl_3): δ 7.03-6.99 (m, 1H), 6.94-6.92 (m, 2H), 6.89-6.86 (m, 1H), 3.89 (t, $J = 4.8$ Hz, 4H), 3.86 (s, 3H), 3.07 (t, $J = 4.8$ Hz, 4H). ^{13}C NMR (100 MHz, CDCl_3): δ 152.1, 141.0, 123.1, 120.9, 117.9, 111.1, 67.1, 55.2, 51.1. MS (EI, m/z): 193 $[\text{M}]^+$; HRMS (EI): Calcd. for $\text{C}_{11}\text{H}_{15}\text{NO}_2$ $[\text{M}]^+$: 193.1103; Found: 193.1110.

4-p-tolylmorpholine (2d). ^1H NMR (300 MHz, CDCl_3): δ 7.21-7.19 (m, 2H), 7.05-7.02 (m, 2H), 3.87 (t, $J = 4.5$ Hz, 4H), 2.93 (t, $J = 4.5$ Hz, 4H), 2.33 (s, 3H). ^{13}C NMR (100 MHz, CDCl_3): δ 153.4, 148.8, 130.0, 129.6, 116.3, 115.1, 66.8, 50.1, 20.4. MS (EI, m/z): 177 $[\text{M}]^+$; HRMS (EI): Calcd. for $\text{C}_{11}\text{H}_{15}\text{NO}$ $[\text{M}]^+$: 177.1154; Found: 177.1158.

4-m-tolylmorpholine (2e). ^1H NMR (300 MHz, CDCl_3): δ 7.20-7.17 (m, 1H), 6.77-6.73 (m, 3H), 3.89-3.86 (m, 4H), 3.19-3.16 (m, 4H), 2.35 (s, 3H). ^{13}C NMR (100 MHz, CDCl_3): δ 151.2, 138.8, 128.9, 120.9, 116.5, 112.8, 66.8, 49.4, 21.7. MS (EI, m/z): 177 $[\text{M}]^+$; HRMS (EI): Calcd. for $\text{C}_{11}\text{H}_{15}\text{NO}$ $[\text{M}]^+$: 177.1154; Found: 177.1151.

4-(4-(trifluoromethyl)phenyl)morpholine (2g). ^1H NMR (300 MHz, CDCl_3): δ 7.50 (d, $J = 6.6$ Hz, 2H), 6.92 (d, $J =$

6.6 Hz, 2H), 3.87 (t, $J = 3.6$ Hz, 4H), 3.24 (t, $J = 3.6$ Hz, 4H). ^{13}C NMR (100 MHz, CDCl_3): δ 153.3, 126.5, 126.4, 114.3, 66.6, 48.1. MS (EI, m/z): 231 $[\text{M}]^+$; HRMS (EI): Calcd. for $\text{C}_{11}\text{H}_{12}\text{F}_3\text{NO}$ $[\text{M}]^+$: 231.0871; Found: 231.0871.

4-(3-(trifluoromethyl)phenyl)morpholine (2h). ^1H NMR (300 MHz, CDCl_3): δ 7.39-7.33 (m, 1H), 7.17-7.11 (m, 2H), 7.08-7.05 (m, 1H), 3.91-3.88 (m, 4H), 3.22-3.20 (m, 4H). ^{13}C NMR (100 MHz, CDCl_3): δ 151.4, 129.6, 118.4, 116.3, 116.2, 111.9, 111.8, 66.7, 48.8. MS (EI, m/z): 231 $[\text{M}]^+$; HRMS (EI): Calcd. for $\text{C}_{11}\text{H}_{12}\text{F}_3\text{NO}$ $[\text{M}]^+$: 231.0871; Found: 231.0873.

4-(4-chlorophenyl)morpholine (2j). ^1H NMR (300 MHz, CDCl_3): δ 8.16-8.12 (m, 2H), 6.93-6.90 (m, 1H), 6.84-6.81 (m, 1H), 3.87 (t, $J = 5.1$ Hz, 4H), 2.93 (t, $J = 5.1$ Hz, 4H). ^{13}C NMR (100 MHz, CDCl_3): δ 155.0, 138.9, 126.2, 125.9, 115.6, 112.6, 66.3, 47.1. MS (EI, m/z): 208 $[\text{M}]^+$; HRMS (EI): Calcd. for $\text{C}_{10}\text{H}_{12}\text{N}_2\text{O}_3$ $[\text{M}]^+$: 208.0848; Found: 208.0855.

4-(4-chlorophenyl)morpholine (2k). ^1H NMR (300 MHz, CDCl_3): δ 7.23-7.20 (m, 2H), 6.84-6.81 (m, 2H), 3.86-3.83 (m, 4H), 3.13-3.09 (m, 4H). ^{13}C NMR (100 MHz, CDCl_3): δ 149.8, 129.0, 124.8, 116.8, 66.7, 49.3. MS (EI, m/z): 197 $[\text{M}]^+$; HRMS (EI): Calcd. for $\text{C}_{10}\text{H}_{12}\text{ClNO}$ $[\text{M}]^+$: 197.0607; Found: 197.0610.

Indoline (3a). ^1H NMR (300 MHz, CDCl_3): δ 7.13-7.10 (m, 1H), 7.04-6.98 (m, 1H), 6.73-6.70 (m, 1H), 6.68-6.62 (m, 1H), 3.64 (s, br, 1H), 3.52 (t, $J = 8.1$ Hz, 2H), 3.01 (t, $J = 8.1$ Hz, 2H). ^{13}C NMR (100 MHz, CDCl_3): δ 151.4, 129.3, 127.1, 124.5, 118.6, 109.4, 47.2, 29.7. MS (EI, m/z): 119 $[\text{M}]^+$; HRMS (EI): Calcd. for $\text{C}_8\text{H}_9\text{N}$ $[\text{M}]^+$: 119.0735; Found: 119.0730.

2-(cyclohexylamino)benzoic acid (3b). ^1H NMR (300 MHz, CDCl_3): δ 7.99-7.96 (m, 1H), 7.38-7.33 (m, 1H), 6.73-6.70 (m, 1H), 6.58-6.53 (m, 1H), 3.43-3.42 (d, br, 1H), 2.07-2.02 (m, 3H), 1.80-1.77 (m, 2H), 1.43 (s, 1H), 1.40-1.28 (m, 5H). ^{13}C NMR (100 MHz, CDCl_3): δ 174.8, 151.0, 135.4, 132.8, 114.0, 111.8, 108.3, 50.6, 32.8, 25.8, 24.7. MS (EI, m/z): 219 $[\text{M}]^+$; HRMS (EI): Calcd. for $\text{C}_{13}\text{H}_{17}\text{NO}_2$ $[\text{M}]^+$: 219.1259; Found: 219.1264.

2-methylquinazolin-4(3H)-one (3c). ^1H NMR (300 MHz, DMSO-d_6): δ 12.2 (s, br, 1H), 8.07 (d, 1H, $J = 7.8$ Hz), 7.76 (t, 1H, $J = 7.2$ Hz), 7.56 (d, 1H, $J = 7.8$ Hz), 7.44 (t, 1H, $J = 7.2$ Hz), 2.35 (s, 3H). ^{13}C NMR (100 MHz, DMSO-d_6): δ 161.7, 154.3, 149.0, 134.2, 126.6, 125.8, 125.7, 120.6, 21.4. MS (EI, m/z): 160 $[\text{M}]^+$; HRMS (EI): Calcd. for $\text{C}_9\text{H}_8\text{N}_2\text{O}$ $[\text{M}]^+$: 160.0637; Found: 160.0641.

Acknowledgements

We gratefully acknowledge financial support from the National Natural Science Foundation of China (Grant 20721003 and 20872153), International Collaboration Projects (Grant 2007DFB30370 and 20720102040) and the 863 Hi-Tech Program of China (Grants 2006AA020602).

References

- For general reviews, see: (a) I. P. Beletskaya and A. V. Cheprakov, *Coord. Chem. Rev.*, 2004, **248**, 2337; (b) S. V. Ley and A. W. Thomas, *Angew. Chem., Int. Ed.*, 2003, **42**, 5400; (c) C. Bolm, J. Legros, J. Le Pailh and L. Zani, *Chem. Rev.*, 2004, **104**, 6217; (d) G. Evano,

- N. Blanchard and M. Toumi, *Chem. Rev.*, 2008, **108**, 3054; (e) J.-P. Corbet and G. Mignani, *Chem. Rev.*, 2006, **106**, 2651; (f) S. L. Buchwald, *Acc. Chem. Res.*, 2008, **41**, 1439; (g) D. S. Surry and S. L. Buchwald, *Angew. Chem., Int. Ed.*, 2008, **47**, 6338; (h) J. F. Hartwig, *Nature*, 2008, **455**, 314.
- 2 For representative papers on the palladium-catalyzed C–N cross coupling reactions, see: (a) N. Kataoka, Q. Shelby, J. P. Stambuli and J. F. Hartwig, *J. Org. Chem.*, 2002, **67**, 5553; (b) J. Barluenga, F. Aznar and C. Valés, *Angew. Chem., Int. Ed.*, 2004, **43**, 343; (c) S. L. Buchwald, C. Mauger, G. Mignani and U. Scholz, *Adv. Synth. Catal.*, 2006, **348**, 23; (d) K. W. Anderson, R. E. Tundel, T. Ikawa, R. A. Altman and S. L. Buchwald, *Angew. Chem., Int. Ed.*, 2006, **45**, 6523; (e) Q. Shen and J. F. Hartwig, *J. Am. Chem. Soc.*, 2007, **129**, 7734.
- 3 For representative papers on the copper mediated C–N cross coupling reactions, see: (a) H. Zhang, Q. Cai and D. Ma, *J. Org. Chem.*, 2005, **70**, 5164; (b) D. Ma and Q. Cai, *Acc. Chem. Res.*, 2008, **41**, 1450; (c) N. Xia and M. Taillefer, *Angew. Chem., Int. Ed.*, 2009, **48**, 337; (d) S. L. Buchwald and C. Bolm, *Angew. Chem., Int. Ed.*, 2009, **48**, 5586; (e) E. R. Strieter, B. Bhayana and S. L. Buchwald, *J. Am. Chem. Soc.*, 2009, **131**, 78.
- 4 For representative papers on the iron catalyzed mediated C–N cross coupling reactions, see: (a) A. Correa, O. Garcia Mancheno and C. Bolm, *Chem. Soc. Rev.*, 2008, **37**, 1108; (b) A. Correa and C. Bolm, *Angew. Chem., Int. Ed.*, 2007, **46**, 8862; (c) A. Correa, S. Elmore and C. Bolm, *Chem.-Eur. J.*, 2008, **14**, 3527; (d) A. Correa, M. Carril and C. Bolm, *Chem.-Eur. J.*, 2008, **14**, 10919; (e) M. Nakanishi, A.-F. Salit and C. Bolm, *Adv. Synth. Catal.*, 2008, **350**, 1835; (f) A. Correa and C. Bolm, *Adv. Synth. Catal.*, 2008, **350**, 391; (g) Y.-C. Teo, *Adv. Synth. Catal.*, 2009, **351**, 720; (h) B. Yao, Z. Liang, T. Niu and Y. Zhang, *J. Org. Chem.*, 2009, **74**, 4630.
- 5 P. F. Larsson, A. Correa, M. Carril, P. O. Norrby and C. Bolm, *Angew. Chem. Int. Ed.*, 2009, **48**, 5691.
- 6 For representative papers on the ligand-free transition metal-catalyzed cross-coupling reactions, see: (a) S. Uk Son, I. Kyu Park, J. Park and T. Hyeon, *Chem. Commun.*, 2004, 778; (b) A. Correa and C. Bolm, *Adv. Synth. Catal.*, 2007, **349**, 2673; (c) T. Kubo, C. Katoh, K. Yamada, K. Okano, H. Tokuyama and T. Fukuyama, *Tetrahedron*, 2008, **64**, 11230; (d) E. Sperotto, G. P. van Klink, J. G. de Vries and G. van Koten, *J. Org. Chem.*, 2008, **73**, 5625; (e) H. Xu and C. Wolf, *Chem. Commun.*, 2009, 1715; (f) M. Wang, K. Ren and L. Wang, *Adv. Synth. Catal.*, 2009, **351**, 1586.
- 7 For metal-free amination of aryl halides *via* the benzyne mechanism in the presence of a strong base in refluxing DMSO, see: L. Shi, M. Wang, C.-A. Fan, F.-M. Zhang and Y.-Q. Tu, *Org. Lett.*, 2003, **5**, 3515.
- 8 M. Taillefer, N. Xia and A. Ouali, *Angew. Chem. Int. Ed.*, 2007, **46**, 934.
- 9 (a) Z. Li, H. Sun, H. Jiang and H. Liu, *Org. Lett.*, 2008, **10**, 3263; (b) H. Huang, X. Yan, W. Zhu, H. Liu, H. Jiang and K. Chen, *J. Comb. Chem.*, 2008, **10**, 617; (c) D. Guo, H. Huang, J. Xu, H. Jiang and H. Liu, *Org. Lett.*, 2008, **10**, 4513; (d) E. Feng, H. Huang, Y. Zhou, D. Ye, H. Jiang and H. Liu, *J. Org. Chem.*, 2009, **74**, 2846.
- 10 For recent examples on iron/copper cocatalyzed cross-coupling reactions, see: (a) V. H. Jadhav, D. K. Dumbre, V. B. Phapale, H. B. Borate and R. D. Wakharkar, *Catal. Commun.*, 2007, **8**, 65; (b) H. Huang, H. Jiang, K. Chen and H. Liu, *J. Org. Chem.*, 2008, **73**, 9061; (c) Z. Wang, H. Fu, Y. Jiang and Y. Zhao, *Synlett*, 2008, 2540; (d) C. M. Rao Volla and P. Vogel, *Tetrahedron Lett.*, 2008, **49**, 5961; (e) J. Mao, G. Xie, M. Wu, J. Guo and S. Ji, *Adv. Synth. Catal.*, 2008, **350**, 2477; (f) X. Ku, H. Huang, H. Jiang and H. Liu, *J. Comb. Chem.*, 2009, **11**, 338; (g) S. Li, W. Jia and N. Jiao, *Adv. Synth. Catal.*, 2009, **351**, 569.
- 11 For recent examples on transition metal-catalyzed cross-coupling reactions with the participation of water or in water, see: (a) Y. Ju and R. S. Varma, *Green Chem.*, 2004, **6**, 219; (b) Liu, Y. Zhang and B. Xin, *J. Org. Chem.*, 2006, **71**, 3994; (c) H. Xu and C. Wolf, *Chem. Commun.*, 2009, 3035; (d) L. Liang, Z. Li and X. Zhou, *Org. Lett.*, 2009, **11**, 3294; (e) Y.-C. Teo and G.-L. Chua, *Chem.-Eur. J.*, 2009, **15**, 3072; (f) G. Marzaro, A. Guiotto and A. Chilin, *Green Chem.*, 2009, **11**, 774.
- 12 For representative papers on the microwave irradiation, see: (a) C. O. Kappe, *Angew. Chem. Int. Ed.*, 2004, **43**, 6250; (b) B. A. Roberts and C. R. Strauss, *Acc. Chem. Res.*, 2005, **38**, 653; (c) D. Dallinger and C. O. Kappe, *Chem. Rev.*, 2007, **107**, 2563; (d) P. Appukkuttan and E. Van der Eycken, *Eur. J. Org. Chem.*, 2008, 1133; (e) V. Polshettiwar and R. S. Varma, *Chem.-Eur. J.*, 2009, **15**, 1582; (f) C. O. Kappe, *Chem. Soc. Rev.*, 2008, **37**, 1127; (g) V. Polshettiwar and R. S. Varma, *Acc. Chem. Res.*, 2008, **41**, 629; (h) V. Polshettiwar and R. S. Varma, *Chem. Soc. Rev.*, 2008, **37**, 1546.
- 13 For representative papers on the synthesis of indoline, see: (a) R. Viswanathan, E. N. Prabhakaran, M. A. Plotkin and J. N. Johnston, *J. Am. Chem. Soc.*, 2003, **125**, 163; (b) A. Correa, I. Tellitu, E. Domínguez and R. SanMartin, *J. Org. Chem.*, 2006, **71**, 8316; (c) R. Viswanathan, C. R. Smith, E. N. Prabhakaran and J. N. Johnston, *J. Org. Chem.*, 2008, **73**, 3040; (d) T. Watanabe, S. Oishi, N. Fujii and H. Ohno, *Org. Lett.*, 2008, **10**, 1759.
- 14 For representative papers on the synthesis of *N*-alkylanthranilic acids, see: (a) X. Mei, A. T. August and C. Wolf, *J. Org. Chem.*, 2006, **71**, 142; (b) C. Wolf, S. Liu, X. Mei, A. T. August and M. D. Casimir, *J. Org. Chem.*, 2006, **71**, 3270; (c) L. Zeng, H. Fu, R. Qiao, Y. Jiang and Y. Zhao, *Adv. Synth. Catal.*, 2009, **351**, 1671.
- 15 For representative papers on the synthesis of quinazolinone, see: (a) C. L. Yoo, J. C. Fettinger and M. J. Kurth, *J. Org. Chem.*, 2005, **70**, 6941; (b) D. J. Connolly, D. Cusack, T. P. O'Sullivan and P. J. Guiry, *Tetrahedron*, 2005, **61**, 10153; (c) D. Yang, H. Fu, L. Hu, Y. Jiang and Y. Zhao, *J. Comb. Chem.*, 2009, **11**, 653; (d) X. Liu, H. Fu, Y. Jiang and Y. Zhao, *Angew. Chem. Int. Ed.*, 2009, **48**, 348.

Direct synthesis of hydrogen peroxide in methanol and water using scCO_2 and N_2 as diluents

Teresa Moreno, Juan García-Serna* and María José Cocero

Received 21st August 2009, Accepted 6th October 2009

First published as an Advance Article on the web 24th November 2009

DOI: 10.1039/b916788a

Direct synthesis of hydrogen peroxide is of high importance nowadays due to its improvement over the traditional anthraquinone hydrogenation-oxidation process. In this work we show how H_2O_2 can be obtained from H_2 and O_2 in water pressurised with CO_2 under supercritical conditions or with N_2 at similar conditions without using organic solvents. Pressures up to 16.7 MPa and mild temperatures from 10 to 45 °C using a commercial 5 wt.% Pd/C catalyst lead to yields from 10.8% to 82.6%, concentrations from 0.22 to 4.01 wt.% of H_2O_2 and Turn Over Frequency at 30 minutes values, TOF_{30} , from 6.0 to 1538 $\text{mol}\cdot\text{h}^{-1}\cdot\text{kg}_{\text{cat}}^{-1}$. The effect of several variables on H_2O_2 yield has been examined: amount of catalyst, promoters/Pd ratio, amount and nature of solvent and inert gas, reaction temperature, and O_2/H_2 ratio. Results for methanol and water are compared.

Introduction

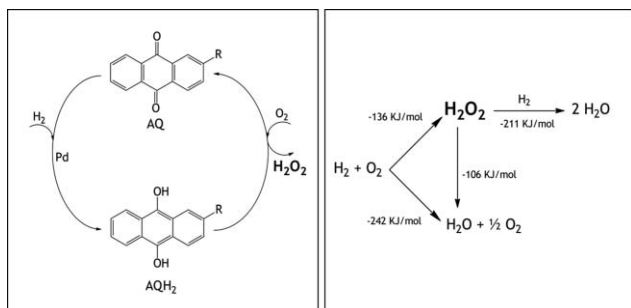
Hydrogen peroxide (H_2O_2) is a strong oxidising agent used in applications as varied as chemical synthesis, bleaching in the pulp and paper industry, wastewater treatment and electronics. Since H_2O is its only by-product in oxidation reactions, it is considered a very attractive selective oxidant to be used in green oxidations. Over 95% of the current industrial production of hydrogen peroxide is carried out *via* the anthraquinone route (see Scheme 1), which involves hydrogenation of a 2-alkyl-anthraquinone using Ni or Pd catalyst followed by an extremely rapid oxidation with air. The hydrogen peroxide stream is then purified and concentrated.^{1,2} This process has the advantage of avoiding direct contact between H_2 and O_2 , and offers a continuous production at moderate temperatures. Nevertheless, large amounts of by-products (mainly over-reduced anthraquinone) are produced, and the process requires several steps of separation

and concentration, consequently requiring a rather large energy input.

Several alternatives have been investigated over the last few years, as Campos-Martin *et al.*³ have thoroughly analysed in their extensive review of hydrogen peroxide synthesis. Among these, **direct synthesis** of hydrogen peroxide has become a promising alternative to the anthraquinone route.⁴ In theory, the direct reaction between hydrogen and oxygen would be the simplest way to produce H_2O_2 . In practice, the actual reaction scheme is more complex due to the occurrence of simultaneous and consecutive reactions, all of which are thermodynamically favoured and highly exothermic, including the formation of water, the decomposition of hydrogen peroxide, and the reduction of hydrogen peroxide (see Scheme 1). Furthermore, the process is highly complicated owing to the existence of three phases: gases (H_2 and O_2), liquid (solvent) and solid (catalyst), which usually involves important mass transfer limitations.

One of the issues that traditionally have promoted the use of the anthraquinone process instead of direct synthesis is that H_2/O_2 mixtures are explosive over a wide range, flammability limits for H_2 in O_2 and air (at 25 °C and atmospheric pressure) are 4.0 mol% H_2 (Lower Flammability Limit, LFL) to 94 mol% H_2 (Upper Flammability Limit, UFL).⁵ In the former process H_2 and O_2 are not in contact. For direct synthesis operation under the LFL is preferred for safety reasons but also in order to minimise the hydrogenation of H_2O_2 . This forces the use of large amounts of diluents, usually nitrogen. Due to the hazardous nature of the gas mixture, the choice of solvent is decisive. All these issues associated with the direct synthesis process have made it a challenge for scientists over the last century; the anthraquinone process extended worldwide due to its high tonnage scalability and the absence of effective catalysts for direct synthesis at the moment of the first industrial plant commissioned by DuPont in 1953.⁶

The most desirable **solvent** and the first option for a liquid reaction medium is water, since it provides the safest



Scheme 1 Reactions involved in the anthraquinone route (left) and direct synthesis of H_2O_2 (right).

High Pressure Processes Group, Department of Chemical Engineering and Environ. Tech., Facultad de Ciencias, Universidad de Valladolid, c/ Prado de la Magdalena s/n, 47011, Valladolid, Spain.
E-mail: jgserna@iq.uva.es; Fax: +34 983423013; Tel: +34 983184934

conditions, is non toxic, non flammable, and highly miscible with hydrogen peroxide. In fact, aqueous reaction media are found in literature;⁷⁻¹⁰ however, their main drawback is the low solubility of the reacting gases, which strongly limits mass transfer and thus the rate of peroxide production, and therefore results using water have been rather poor this far. To minimise this limitation, organic co-solvents (*i.e.* alcohols) are usually added to the reaction medium,¹¹ and even pure ethanol¹² and methanol¹³ are found as solvents in literature. For instance, Degussa/Headwaters recently announced the construction of the first pilot plant for direct synthesis of organic or aqueous organic H₂O₂ to be used as an in situ source integrated into a propylene oxide plant disclosing that methanol is used as solvent.^{14,15} An interesting alternative as cosolvent is **supercritical CO₂**, which is considered a “green solvent” and presents total miscibility with the reagent gases and low solubility of the product, thus facilitating its separation from the solvent and minimising the chances for product degradation due to prolonged contact with the catalyst.¹⁶ Moreover, the acidic character of CO₂ also helps in the stabilisation of aqueous hydrogen peroxide reducing the need for acidic promoters.¹⁷ Beckman and his co-workers¹⁸ first achieved the direct synthesis of H₂O₂ in liquid CO₂ following a Pd-catalysed hydrogenation and a subsequent oxidation process of fluorinated and therefore CO₂-philic anthraquinones. Later, they developed CO₂ soluble Pd catalysts¹⁹ and also obtained good results using regular Pd-based catalysts.^{17,20}

The substitution of organic solvents by water is a breakthrough in the synthesis that will certainly reduce fire risks, avoiding possible oxidations of the solvent by O₂. Nevertheless, note that explosion hazards associated to H₂ still remain and operation under flammability limits is indispensable.²¹ Following this argument, several authors stated that the use of CO₂ as inert diluent in a H₂/air mixture increases the LFL up to 9.5% for H₂ at atmospheric pressure.²² Other groups and our group have found in a previous study that at higher pressures, however, the flammability region of systems containing H₂, O₂ and CO₂ becomes wider as pressure increases. Thus, the LFL is reduced to *ca.* 3.5% at 10.0 MPa.²³ The use of pure oxygen will put up the price of the final product; therefore, the preferred raw material is air or enriched air mixtures. In this work we show results that assure that water works well as a solvent for both CO₂ and N₂ as diluents.

The choice of an active and highly selective **catalyst** is one of the most important variables in the direct synthesis of H₂O₂.

Most catalysts described in literature are supported on carbon, zeolites, Al₂O₃ or SiO₂²⁴ and the active metals are usually palladium,^{25,26} gold^{9,27} or combinations of Pd+Au^{13,28,29} or Pd+Pt.^{12,29} It must be noted that the major drawback of the active metals for H₂O₂ production is the fact that they are also active for the combustion of hydrogen to water and the decomposition of hydrogen peroxide. To minimise this effect, promoters—namely acids (H₂SO₄, HBr, H₃PO₄) and halides (Cl⁻, Br⁻)—are added³⁰⁻³³ or the support³⁴ is modified.

Many of the published results present very low H₂O₂ concentrations in the final product or low conversions of H₂, although selectivities reach values as high as 80%.¹¹ This cannot be accepted for an industrial process, where economics require concentrations of H₂O₂ at least between 10 and 20 wt.% and

yields above 80-85%, inasmuch as in the anthraquinone process the hydrogen peroxide is stripped from the organic working solution producing solutions of *ca.* 30% by weight H₂O₂. Further distillations remove impurities and can increase the concentration up to a maximum of 70 wt.%.³

This work is included in a project dedicated to the direct synthesis of H₂O₂ in a mixture of methanol and CO₂ at supercritical conditions aimed at producing H₂O₂ in a greener way compared to the traditional synthesis. There are two main improvements identified: change of the synthesis route and substitution of the solvent by a benign pressurised solvent (methanol, water and CO₂). The efficient use of water as a solvent for the direct synthesis opens a novel alternative avoiding the use of organic solvents, thus reducing the risks associated and minimising the number of separation steps.

Materials and methods

The catalyst used in this study was made up of fine particles with an average of 5 wt.% palladium over carbon support purchased from Aldrich and used fresh for each experiment. It has been selected because it is well known, commercially available and monometallic, so the influence of the catalyst (which is critical) is not studied here, and this study is focussed on the use of methanol or water together with scCO₂. Industrial grade oxygen and carbon dioxide and premier grade hydrogen and argon were purchased from Carburros Metálicos (Spain) and used without further modification. Methanol with a purity of 99.8% was used as solvent (Panreac). KI, H₂SO₄ and Na₂S₂O₃·5H₂O (Panreac) were used for iodometric titration of hydrogen peroxide.³⁵ A method for analysing H₂ and O₂ by Micro Gas Chromatography (Varian CP 4900 with a 5A molecular sieve column operating at 90 °C and equipped with a TCD detector, injector initial temperature was 110 °C and pressure 20 psi) was also developed. (Note: since the micro-GC is intended to be used in a continuous system these results are not included in this work.)

Experimental section

Experimental apparatus

A flow diagram of the system is shown in Fig. 1. H₂ and O₂ were stored in high pressure cylinders, outlet pressure was fixed using self-regulating valves (V1 and V4 respectively). The flow of H₂ and O₂ was controlled by Bronkhorst EL-FLOW mass flow meter controllers (E1 and E3) before entering the reactor. CO₂ from a cylinder was pumped as a liquid by a refrigerated Jasco 2080 HPLC pump (E2). Reactions were performed in a 0.350 L AISI 316 SS agitated reactor (E4). A magnetic stirrer lined with DuPont™ Teflon® and a magnetic stirrer operating at 1000 rpm were used. The reactor has an internal coil used for cooling down the reaction and it has an external heating jacket as well. Temperature was controlled by modifying both cooling/heating as per requirement. The effluent of the reactor is depressurised using a back-pressure valve, the product is separated in a flash vessel (E7) into the off-gas (CO₂, N₂, O₂, H₂ mainly) and the liquid product (H₂O₂, H₂O and CH₃OH). Liquid samples were taken every 10 to 30 mins and analysed off-line by iodometric titration.

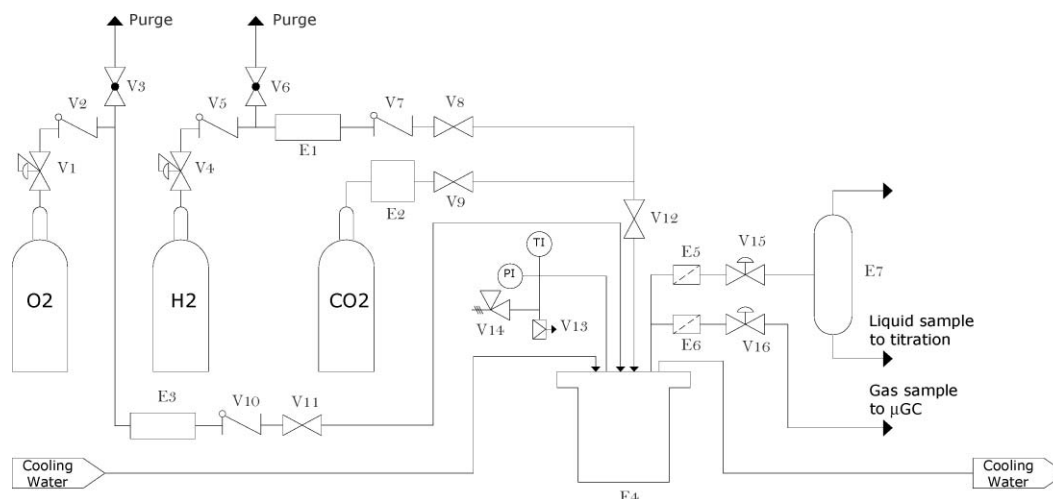


Fig. 1 Experimental set-up for direct synthesis of H_2O_2 . Equipment, E1: mass flow controller, E2: HPLC pump, E3: mass flow controller, E4: Reactor, E5: $1\ \mu\text{m}$ online filter, E6: $5\ \mu\text{m}$ online filter, E7: flash separator, V1, V4: pressure regulators, V2, V5, V7, V10: check valves, V3, V6: globe valves, V8, V9, V11, V12: ball valves, V13: rupture disc, V14: pressure safety valve, V15 and V16: back pressure regulators.

From the point of view of transport phenomena, the process is carried out in a stirred slurry batch reactor where three phases are present. The catalyst (solid phase) contains the metal active sites and is dispersed in water or methanol (liquid phase), the gas reagents H_2 and O_2 (gas phase) are dissolved in the liquid phase and react on the surface of the catalyst. To increase mass transfer between the gas and liquid phases, the system is pressurised using an inert gas (that also permits us to operate under safe conditions, away from the explosive range). To increase mass transfer between the liquid and the catalyst, the system is vigorously stirred. The reaction step is affected by the type of catalyst, solvent, inert gas, temperature and O_2 : H_2 ratio.

Experimental procedure

The reactor was initially passivated with 35% HNO_3 for 4 h and 30% H_2O_2 for 10 h to minimise H_2O_2 decomposition. All tests were carried out in methanol or water under high pressure (4.6–16.7 MPa). Temperature was measured *via* an internal thermocouple and datalogged automatically. The calculated amounts of solvent and promoters (H_3PO_4 and NaBr) were introduced in the reactor together with the catalyst before each run. The reactor was first flushed with CO_2 , and then CO_2 was introduced using the HPLC pump until the calculated pressure was reached, according to a simulation using Aspen Plus software. O_2 and H_2 were introduced afterwards in this order, using the counters of their mass flow controllers. During runs, small aliquots of the liquid phase ($2.5 \cdot 10^{-3}$ L) were sampled and used for hydrogen peroxide iodometric determination. At the end of each run, gas samples were injected in the μGC without any dilution. H_2O_2 yield is defined in eq. 1:

$$\text{H}_2\text{O}_2 \text{ Yield (\%)} = 100 \times \frac{\text{H}_2\text{O}_2 \text{ generated (mol)}}{\text{H}_2 \text{ added to reactor (mol)}} \quad (1)$$

Results and discussion

Two sets of 14 experiments in methanol and 15 in water were carried out to determine the influence of catalyst, solvent,

temperature, O_2 : H_2 ratio and inert gas. The main results and experimental conditions of these experiments are summarised in Tables 1 and 2. These experiments have been designed in order to identify the complex influences of the variables in the synthesis of H_2O_2 ; the maximum values for yield and concentration are included as well as the Turn Over Frequency at 30 minutes (TOF_{30}) giving the idea of initial rate of reaction and Turn Over Number at 120 min (TON_{120}) indicating productivity after 2 hours. The transient state is included in the figures.

Effect of the amount of catalyst and Br^-/Pd ratio

Different amounts of Pd/C catalyst ranging from $50 \cdot 10^{-6}$ to $400 \cdot 10^{-6}$ kg were tested under the same conditions in methanol in runs M1 to M6 ($35\ ^\circ\text{C}$, 25 wt.% methanol, 0.142 mol of hydrogen and oxygen/hydrogen ratio 2:1) and from $75 \cdot 10^{-6}$ to $750 \cdot 10^{-6}$ kg of catalyst in water in runs W1 to W5 ($35\ ^\circ\text{C}$, 25 wt.% methanol, 0.174 mol of hydrogen and oxygen/hydrogen ratio 2:1). Since the experiments were carried out in batch mode, pressure is not constant and varies between experiments. For safety reasons, the initial composition of the gas mixture was kept to CO_2 : O_2 : H_2 92.3:5.1:2.6.

For the case of using methanol as solvent, the optimum amount of catalyst to maximise H_2O_2 production was $75 \cdot 10^{-6}$ kg, reaching a 37.4% yield after 90 minutes (1.87 wt.%) in these initial experiments. At this point, the amount of peroxide in the reaction medium slowly decreases due to its decomposition and hydrogenation, as most of the initial H_2 has been consumed. Using $50 \cdot 10^{-6}$ kg led to a slightly lower maximum yield of 34.9% but higher TOF_{30} ($1538\ \text{mol}\cdot\text{h}^{-1}\cdot\text{kg}_{\text{cat}}^{-1}$) and TON_{120} ($950\ \text{mol}\cdot\text{kg}_{\text{cat}}^{-1}$) were obtained. In the case of H_2O as a solvent, the optimum amount of catalyst seems to be higher, *ca.* $150 \cdot 10^{-6}$ kg, achieving yields of 45.6% after 120 minutes (3.02 wt.%), as plotted in Fig. 3. The influence of side reactions is higher as can be observed comparing Fig. 2 and Fig. 3.

Although the yields in methanol are slightly lower than in water, note that the initial observed reaction rates expressed as TOF_{30} are considerable higher as shown in Table 1. For

Table 1 Experiment summary for H₂O₂ batch production. Reaction conditions: 5.0 wt.% Pd/C catalyst, overall promoter concentrations were maintained at 0.018 mol·L⁻¹ H₃PO₄ and 3·10⁻³ mol·L⁻¹ NaBr, solvents methanol (M) and water (W)

Run	Catalyst (10 ⁶ ·kg)	Solvent (wt.%)	T (°C)	O ₂ :H ₂ ratio	Initial H ₂ (mol)	TOF ₃₀ (mol·h ⁻¹ ·kg _{cat} ⁻¹)	TON ₁₂₀ (mol·kg _{cat} ⁻¹)	H ₂ O ₂ yield (%)	Max. Conc. H ₂ O ₂ wt.% (time, min.)
M1	50	25	35	2:1	0.142	1538	950	34.9	1.82 (165)
M2	75	25	35	2:1	0.142	1279	664	37.4	1.87 (90)
M3	100	25	35	2:1	0.142	692	485	35.0	1.81 (165)
M4	150	25	35	2:1	0.142	451	278	30.4	1.54 (165)
M5	250	25	35	2:1	0.142	141	84.8	15.5	0.78 (165)
M6	400	25	35	2:1	0.142	103	50.1	14.4	0.71 (30)
M7	75	10	35	2:1	0.142	513	458 ^c	24.2	3.79 (90)
M8	75	35	35	2:1	0.142	1152	602	35.6	1.07 (120)
M9	75	25	25	2:1	0.142	982	670	36.5	1.91 (165)
M10	75	25	45	2:1	0.142	983	567	30.8	1.55 (165)
M11	75	25	35	1:1	0.142	290	216	11.6	0.62 (165)
M12	75	25	35	4:1	0.142	942	753	40.4	2.01 (165)
M13	150	45	25	2:1	0.0659	59.6	113	25.8	0.43 (120)
M14 ^a	150	71	25	2:1	0.0659	69.3	61.5	14.0	0.22 (120)
W1	75	25	35	2:1	0.173	616	620	31.6	2.54 (210)
W2	150	25	35	2:1	0.173	413	528	45.6	3.02 (120)
W3	250	25	35	2:1	0.173	147	309	45.2	3.01 (140)
W4	500	25	35	2:1	0.173	52.4	95.4	27.4	1.76 (120)
W5	750	25	35	2:1	0.173	5.96	24.4	10.8	0.88 (165)
W6	250	10	35	2:1	0.200	61.0 ^b	50.4 ^c	12.0	2.12 (180)
W7	250	50	35	2:1	0.109	73.6	191	43.5	0.91 (120)
W8	150	25	10	2:1	0.173	543	636	54.6	3.90 (165)
W9	150	25	25	2:1	0.173	253	683	57.4	4.01 (120)
W10	150	25	45	2:1	0.173	217	276	23.9	1.78 (120)
W11	150	25	25	1:1	0.173	126 ^b	141	11.9	0.79 (120)
W12	150	25	25	4:1	0.173	746	648	53.6	3.95 (120)
W13 ^a	150	81	25	2:1	0.0659	406	352	82.6	1.38 (165)
W14	150	36	25	2:1	0.0659	127	291	66.3	1.09 (120)
W15	150	60	25	2:1	0.0659	118	199	45.2	0.74 (120)

^a M14 and W13 with N₂. ^b Data at 30 min N/A, W6 at 45 min, W11 at 60 min. ^c Data at 120 min N/A, M7 and W6 at 90 min.

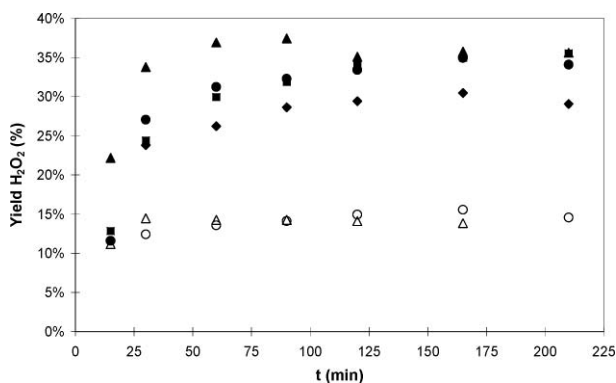


Fig. 2 H₂O₂ yield for different amounts of Pd/C catalyst in MeOH, 35 °C, 25 w% H₂O, O₂:H₂ = 2. Series: ● 50·10⁻⁶ kg, ▲ 75·10⁻⁶ kg, ■ 100·10⁻⁶ kg, ◆ 150·10⁻⁶ kg, ○ 250·10⁻⁶ kg, △ 400·10⁻⁶ kg.

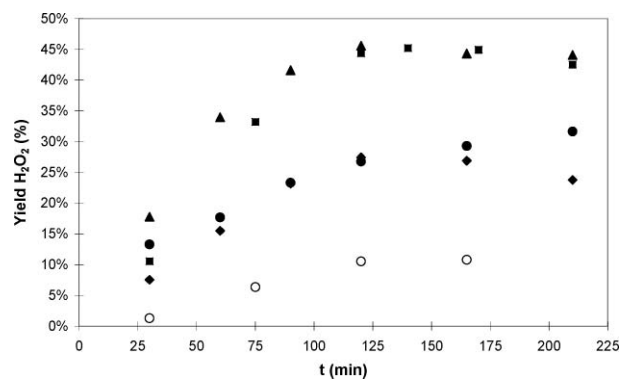


Fig. 3 H₂O₂ yield for different amounts of Pd/C catalyst in H₂O, 35 °C, 25 w% H₂O, O₂:H₂ = 2. Series: ● 75·10⁻⁶ kg, ▲ 150·10⁻⁶ kg, ■ 250·10⁻⁶ kg, ◆ 500·10⁻⁶ kg, ○ 750·10⁻⁶ kg.

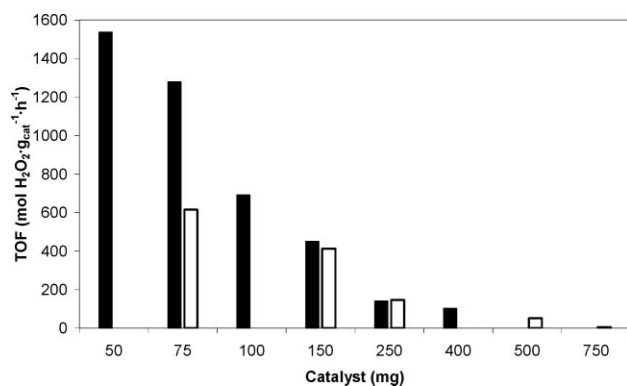
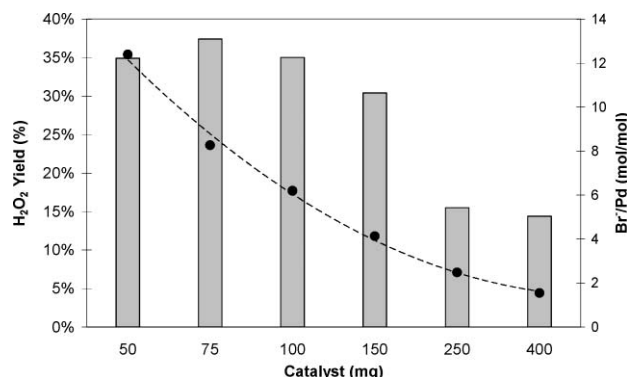
methanol, the maximum TOF₃₀ was 1538 mol·h⁻¹·kg_{cat}⁻¹ using 50·10⁻⁶ kg of catalyst (run M1), and for water 746 mol·h⁻¹·kg_{cat}⁻¹ using 150·10⁻⁶ kg of catalyst (run W12). The stability of the catalyst is currently being studied in order to evaluate a possible reutilization of the catalyst.

Interestingly, in both cases higher amounts of catalyst lead to lower productivities (see Fig. 4), indicating that an excessive amount of catalyst causes decomposition or less probable hydrogenation. Nevertheless, we are interested in increasing the amount of catalyst to the maximum to enhance the reaction rate (reducing reactor volume), which we can achieve using

promoters. The role of halide anions has been thoroughly studied in literature. It has been proposed²⁵ that the basic role of halide anions is the inhibition in the cleavage of O–O bonds in both H₂O₂ and O₂ during their adsorption on the catalytic sites, resulting in a higher selectivity towards hydrogen peroxide, but an acidic medium is also necessary since the role of protons is to facilitate the adsorption of halide anions on the catalyst.³⁶ Furthermore, the acidic medium decreases peroxide decomposition by decreasing its adsorption on decomposition sites. However, an excess of halide ions results in catalyst poisoning, with the consequent decrease in activity. Most

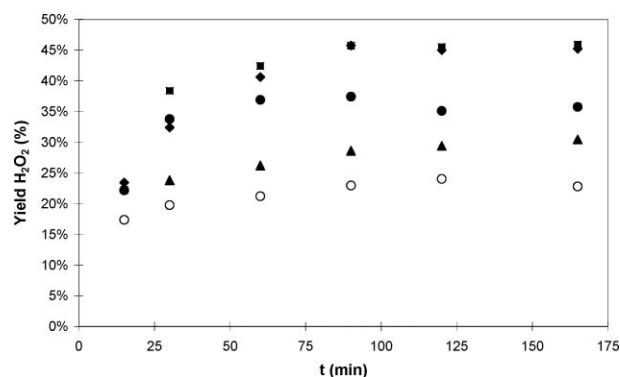
Table 2 Effect of halide and acid to Pd molar ratios on direct synthesis of H₂O₂ in scCO₂. Reaction conditions: 5 wt.% Pd/C catalyst, 35 °C, 25 wt.% methanol

Run	Catalyst (10 ⁶ -kg)	Br ⁻ /Pd (mol/mol)	H ⁺ /Pd (mol/mol)	Initial H ₂ (mol)	H ₂ O ₂ yield (%)	TOF ₃₀ (mol·h ⁻¹ ·kg _{cat} ⁻¹)	TON ₁₂₀ (mol·kg _{cat} ⁻¹)	Max. Conc. H ₂ O ₂ wt.% (time, min.)
M2	75	8.26	52.15	0.142	37.4	1279	664	1.87 (90)
M4	150	4.13	26.07	0.142	30.4	451	278	1.54 (165)
M15	150	8.26	26.07	0.142	45.9	727	431	2.30 (165)
M16	150	4.13	52.15	0.142	45.7	613	426	2.26 (90)
M17	150	8.26	52.15	0.142	24.0	748	455	1.19 (120)

**Fig. 4** Turn Over Frequency of the Pd/C catalyst in methanol (filled bars) and water (empty bars).**Fig. 5** H₂O₂ yield for different amounts of Pd/C catalyst and effect of Br⁻/Pd ratio in methanol, bars = H₂O₂ yield (%), ● molar ratio Br⁻/Pd.

of the authors focus on determining the optimum promoter concentration, but we believe that the halide and acid required is a function of the amount of active sites of the catalyst. As shown in Fig. 5, the optimum amount of catalyst in the case of methanol corresponds to a Br⁻/Pd molar ratio of 8.26. Therefore, we have studied the influence of the promoter/Pd ratio carrying out an additional set of 3 experiments taking experiments M2 and M4 as starting point for comparison purposes (M2 yielded more than M4 having less catalyst), using 50·10⁻⁶ kg of catalyst and different halide/Pd and H⁺/Pd ratios; the main results are summarised in Table 2 and Fig. 6.

In run M15, the Br⁻/Pd ratio was raised from 4.13 to 8.26, which had been found to be optimal in experiments M1 to M6, increasing the yield from 30.4% to 45.9%. In run M16, the Br⁻/Pd ratio was not changed and the H⁺/Pd ratio was doubled, increasing the yield from 30.4% to 45.7%. Interestingly, when both acid and halide to palladium ratios were doubled

**Fig. 6** Effect of Br⁻/Pd and H⁺/Pd molar ratios on H₂O₂ yield in methanol. Series (see Table 1 and Table 2): ● M2, ▲ M4, ■ M15, ◆ M16, ○ M17.

in the same experiment (run M17), the yield was reduced by 21% in respect to experiment M4. Therefore, comparing runs M2 and M17, where Br⁻/Pd and H⁺/Pd ratios were identical but the amount of catalyst was increased from 75·10⁻⁶ kg (M2) to 150·10⁻⁶ kg (M17), the yield decreased from 37.4% to 24.0%.

To sum up, increasing the halide (M15) achieves faster reaction rates compared to increasing the acid (M16), exhibiting TOF₃₀ of 727 vs. 471 mol·h⁻¹·kg_{cat}⁻¹ respectively. This result corroborates the interaction between halide ions and protons and the necessity of an optimisation of the trinomial catalyst-halide-acid. Further research into the role of these ions in hydrogen peroxide decomposition and hydrogenation is currently being carried out.

Effect of the amount of solvent

The concentration of H₂O₂ produced is one of the variables to consider, and the simplest way to increase its value (keeping initial H₂ and reaction time constant) is by reducing the amount of solvent. However, this will also decrease the quantity of gases dissolved, therefore reducing productivity. Fig. 7 represents the results obtained using different volumes of solvent, expressed as wt.% in relation to the total reaction mixture. The maximum yield using methanol (37.4%) was reached using 25 wt.%, while the maximum H₂O₂ concentration of 3.79 wt.% was obtained for 10 wt.% solvent. In the case of water, the effect is slightly different, obtaining the maximum concentration (3.01 wt.% H₂O₂), yield (45.2%) and TOF₃₀ (147 mol·h⁻¹·kg_{cat}⁻¹) with 25 wt.% of H₂O.

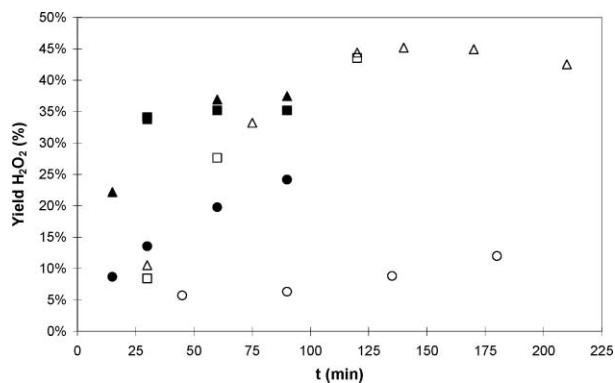


Fig. 7 H_2O_2 yield for different amounts of solvent, in methanol: 35 °C, $75 \cdot 10^{-6}$ kg Pd/C, $\text{O}_2:\text{H}_2 = 2$. Series: ● 10 wt.%, ▲ 25 wt.%, ■ 35 wt.%; in water: 35 °C, $250 \cdot 10^{-6}$ kg Pd/C, $\text{O}_2:\text{H}_2 = 2$. Series: ○ 10 wt.%, △ 25 wt.%, □ 50 wt.%.

Effect of reaction temperature

From an industrial point of view, the use of energy in terms of quality (temperature level) and quantity (kilowatts consumed) has to be considered, especially for these types of exothermic reactions. Several researchers claim to obtain the best results at low temperatures^{12,28} while others have worked at temperatures close to room temperature.^{7,37,38} It is generally accepted that H_2O_2 formation rate decreases by increasing reaction temperature^{9,39} due to the enhancement of decomposition reaction over H_2O_2 production. As indicated above, reduction of energy consumption is one of the aims of this work, therefore 35 °C has been chosen as a desired operational temperature for three main reasons: firstly, the reaction will occur above the supercritical point of CO_2 enhancing mass transfer, secondly, at industrial scale 35 °C can be reached easily by only using cooling water and thirdly, it minimises energy losses to ambient. Nonetheless, tests at higher (45 °C) and lower (10, 25 °C) temperature have also been carried out in order to study the effect of temperature.

Fig. 8 shows that for methanol, temperatures of 45 °C lead to lower production of peroxide, probably due to an increase of side reactions (decomposition/hydrogenation) coupled with a decrease of the solubility of reagents. Although there is not a

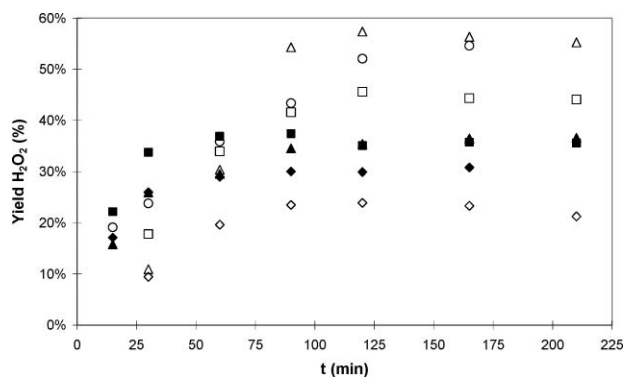


Fig. 8 Effect of reaction temperature on H_2O_2 yield in methanol solvent, $75 \cdot 10^{-6}$ kg Pd/C, 25 w% MeOH, $\text{O}_2:\text{H}_2 = 2$. Series: ▲ 25 °C, ■ 35 °C, ◆ 45 °C and in water of reaction temperature on H_2O_2 yield, $150 \cdot 10^{-6}$ kg Pd/C, 25 w% H_2O , $\text{O}_2:\text{H}_2 = 2.0$. Series: ○ 10 °C, △ 25 °C, □ 35 °C, ◇ 45 °C.

large difference, the maximum yields of 36.6% and 35.6% were obtained at 25 and 35 °C respectively, reaction at 35 °C reached its maximum after 90 minutes (TOF_{30} of $1279 \text{ mol} \cdot \text{h}^{-1} \cdot \text{kg}_{\text{cat}}^{-1}$), whereas reaction at 25 °C was slightly slower (TOF_{30} of $982 \text{ mol} \cdot \text{h}^{-1} \cdot \text{kg}_{\text{cat}}^{-1}$). Therefore, the optimum reaction temperature was found to be 35 °C, which is, interestingly, right above the critical temperature of CO_2 . This confirms previously reported results³² which showed that the yield of H_2O_2 increases as the temperature passes through the critical temperature of CO_2 . For the case of water, yields are considerably higher and the maximum yield of 57.4% was obtained at 25 °C with a TOF_{30} of $253 \text{ mol} \cdot \text{h}^{-1} \cdot \text{kg}_{\text{cat}}^{-1}$. Note that a similar good result was obtained at 10 °C (54.6% yield, TOF_{30} of $543 \text{ mol} \cdot \text{h}^{-1} \cdot \text{kg}_{\text{cat}}^{-1}$, 3.90 wt.% H_2O_2), but such a low temperature requires a cryogenic system and therefore is a less attractive alternative at industrial scale.

Effect of the $\text{O}_2:\text{H}_2$ ratio

For safety reasons the concentration of H_2 needs to be below the LFL, but the concentration of O_2 is a variable that will affect the reaction and must be optimised. For economic reasons H_2 must react to the maximum (over 99% if possible). Considering the reaction pathway for H_2O_2 , low partial pressure of O_2 may benefit the formation of water, decomposition of H_2O_2 and hydrogenation over oxidation; therefore, $\text{O}_2:\text{H}_2$ ratios over the unity are recommended at a glance. This prediction has been demonstrated in runs M11 and M12 for methanol and W11 and W12 for water (see Fig. 9), in which ratios of 1 and 4 were tested. Results using a stoichiometric ratio were similarly poor in both solvents: yields of 11.6 and 11.9% and H_2O_2 concentration 0.62 and 0.79 wt.% (in methanol and water, respectively). On the other hand, a ratio $\text{O}_2:\text{H}_2 = 4$ in methanol provided the best results (yield 40.4%, H_2O_2 concentration 2.01 wt.%, TOF_{30} of $942 \text{ mol} \cdot \text{h}^{-1} \cdot \text{kg}_{\text{cat}}^{-1}$), although the reaction rate was slower than using a ratio $\text{O}_2:\text{H}_2 = 2$ (TOF_{30} of $1279 \text{ mol} \cdot \text{h}^{-1} \cdot \text{kg}_{\text{cat}}^{-1}$). For water, the ratios $\text{O}_2:\text{H}_2 = 2$ and 4 provide similar yields and concentrations but the reaction rates were faster for the higher ratio tested (TOF_{30} of $253 \text{ mol} \cdot \text{h}^{-1} \cdot \text{kg}_{\text{cat}}^{-1}$ and $746 \text{ mol} \cdot \text{h}^{-1} \cdot \text{kg}_{\text{cat}}^{-1}$ respectively).

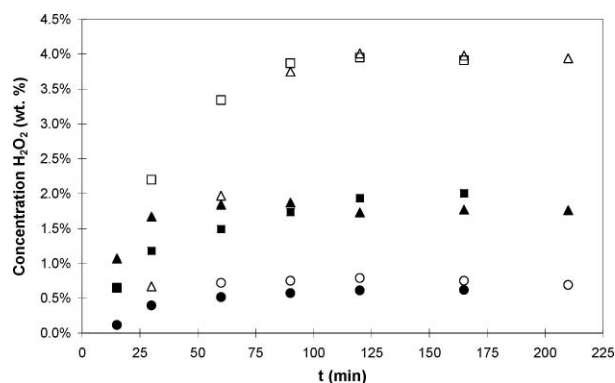


Fig. 9 Effect of $\text{O}_2:\text{H}_2$ ratio on H_2O_2 concentration in methanol solvent, $75 \cdot 10^{-6}$ kg Pd/C, 25 w% MeOH, 35 °C. Series: ● $\text{O}_2:\text{H}_2 = 1.0$, ▲ $\text{O}_2:\text{H}_2 = 2.0$, ■ $\text{O}_2:\text{H}_2 = 4.0$ and in water: $150 \cdot 10^{-6}$ kg Pd/C, 25 w% H_2O , 25 °C. Series: ○ $\text{O}_2:\text{H}_2 = 1.0$, △ $\text{O}_2:\text{H}_2 = 2.0$, □ $\text{O}_2:\text{H}_2 = 4.0$.

Inert gas: CO₂ vs. N₂

The reduction of H₂ concentration to avoid explosive mixtures is normally achieved by adding an inert gas. Traditionally, N₂ has been used, as air is a cheaper choice compared to pure oxygen. However, the use of CO₂ is a good alternative for reaction in a number of processes. For this synthesis, CO₂ has good affinity with both O₂ and H₂ increasing the solubility in methanol and to a lesser extent in water. Results for methanol and H₂O are plotted in Fig. 10. In the case of methanol, after 90 minutes reaction time, the amount of peroxide formed in the CO₂-compressed system is 136% higher than in the N₂-compressed system. This could be explained to some extent by two effects: an increased solubility of the reactant gases and the acidification effect of CO₂. Due to the latter effect, CO₂ can be considered an acid promoter itself helping in the minimization of H₂O₂ decomposition. In the case of water, two different pressures for CO₂ were tested in order to either maintain similar high pressure conditions to those in the experiment with N₂ (P = 16.7 MPa) or to maintain equal numbers of mols of CO₂ and N₂ (P = 4.6 MPa). The best result was obtained using N₂ achieving a yield of 82.6% and 1.38 wt.% H₂O₂ after 165 minutes, compared to the results in CO₂. We consider this a striking result, since a high yield is obtained using water as solvent, nitrogen as a diluent and ambient temperature, making it very attractive from an industrial point of view. For CO₂ higher pressures gave better results, as expected due to an increase in H₂ and O₂ solubility.

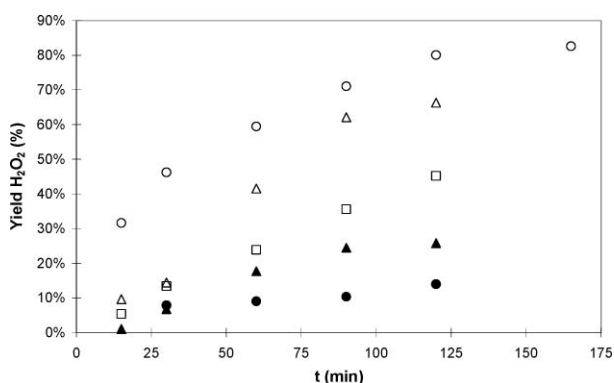


Fig. 10 H₂O₂ formation in N₂ and CO₂ in both solvents, methanol: 25 °C, 150·10⁻⁶ kg Pd/C, O₂:H₂ = 2, Series: ● N₂ (initial P 12.2 MPa), ▲ CO₂ (initial P 9.8 MPa); water: 25 °C, 150·10⁻⁶ kg Pd/C, O₂:H₂ = 2, Series: ○ N₂ (initial P 11.5 MPa), △ CO₂ (initial P 16.7 MPa), □ CO₂ (initial P 4.6 MPa).

Conclusions

In this work, a commercial 5 wt.% Pd/C catalyst has been successfully used for direct synthesis of hydrogen peroxide in CO₂ expanded methanol (obtaining yields from 11.6 to 45.9% and H₂O₂ concentrations between 0.22 and 3.79 wt.%) and in water using CO₂ and N₂ as pressurising gas at nearly ambient temperature (with yields from 11.9 to 82.6% and H₂O₂ concentrations between 0.74 and 4.01 wt.%). It is the first time that H₂O₂ has been produced *via* direct synthesis at high yields and medium concentrations in water without using organic solvents. The possibility of synthesising H₂O₂ in H₂O without the

use of organic solvents is a breakthrough that must be considered for the future development of this process.

In order to study in depth this reaction system, **future work** includes testing of different catalysts and also different solvent solutions (*i.e.* water-methanol mixtures), as well as the study of the effect of catalyst reuse. A mathematical model of the system that can predict the experimental results obtained is also under development. As mentioned previously, extensive research on hydrogen peroxide decomposition and hydrogenation is currently being carried out. Also, a novel technique for hydrogen peroxide determination using Raman technology is under investigation. Ultimately, one of the main objectives of this research is to design a continuous system for hydrogen peroxide production.

Acknowledgements

The authors wish to thank the Spanish Education and Science Ministry, Project Reference: CTQ 2006-0299/PPQ for funding and for the FPI fellowship granted; the Emerging Technologies Group at REPSOL Technology Center in Móstoles (Spain) for scientific advice; the Department of Physics of Condensed Matter, Crystallography and Mineralogy at University of Valladolid; and Eduardo García-Verdugo and the Sustainable Chemistry Group at Jaume I University (Castellón) also for scientific advice and help.

Notes and references

- H.-J. Rledl and G. Pfeleiderer, *US Pat.*, 2158525, 1939.
- W. Eul, M. A. and N. Steiner, in *Kirk-Othmer Encyclopedia of Chemical Technology*, Wiley, 4th edn., 2001.
- J. M. Campos-Martin, G. Blanco-Brieva and J. L. G. Fierro, *Angew. Chem., Int. Ed.*, 2006, **45**, 6962–6984.
- C. Samanta, *Appl. Catal., A*, 2008, **350**, 133–149.
- M. G. Zabetakis, *Bureau of Mines Bulletin*, 1965, 627.
- K. Weissermel, and H.-J. Arpe, in *Industrial Organic Chemistry*, Wiley-VCH, Weinheim, 2003.
- R. Burch and P. R. Ellis, *Appl. Catal., B*, 2003, **42**, 203–211.
- D. P. Dissanayake and J. H. Lunsford, *J. Catal.*, 2002, **206**, 173–176.
- T. Ishihara, Y. Ohura, S. Yoshida, Y. Hata, H. Nishiguchi and Y. Takita, *Appl. Catal., A*, 2005, **291**, 215–221.
- S.-E. Park, L. Huang, C. W. Lee and J.-S. Chang, *Catal. Today*, 2000, **61**, 117–122.
- J. K. Edwards, A. Thomas, B. E. Solsona, P. Landon, A. F. Carley and G. J. Hutchings, *Catal. Today*, 2007, **122**, 397–402.
- Q. Liu, J. C. Bauer, R. E. Schaak and J. H. Lunsford, *Appl. Catal., A*, 2008, **339**, 130–136.
- F. Menegazzo, P. Burti, M. Signoreto, M. Manzoli, S. Vankova, F. Boccuzzi, F. Pinna and G. Strukul, *J. Catal.*, 2008, **257**, 369–381.
- T. Haas, G. Stochniol and R. Jahn, *US Pat.*, 7241908, 2007.
- Headwaters-Incorporated, Degussa/Headwaters Incorporated building demonstration plant for direct synthesis of hydrogen peroxide, <http://www.headwaters.com/data/upimages/press/Degussa%20PR.pdf>, Accessed March 2nd, 2009.
- E. J. Beckman, *J. Supercrit. Fluids*, 2004, **28**, 121–191.
- E. J. Beckman, *Green Chem.*, 2003, **5**, 332–336.
- D. Hâncu, J. Green and E. J. Beckman, *Acc. Chem. Res.*, 2002, **35**, 757–764.
- D. Hâncu and E. J. Beckman, *Green Chem.*, 2001, **3**, 80–86.
- Q. Chen and E. J. Beckman, *Green Chem.*, 2007, **9**, 802–808.
- Y.-F. Han and J. H. Lunsford, *Catal. Lett.*, 2005, **99**, 13–19.
- J. O. Pande and J. Tonheim, *Process Saf. Prog.*, 2001, **20**, 37–39.
- J. B. Sierra, M. T. Parra-Santos, J. García-Serna and M. J. Cocero, *Proceedings of the 2nd International Congress on Green Process Engineering and 2nd European Process Intensification Conference, Venice*, 2009.

- 24 E. Ntainjua, J. K. Edwards, A. F. Carley, J. A. Lopez-Sanchez, J. A. Moulijn, A. A. Herzing, C. J. Kiely and G. J. Hutchings, *Green Chem.*, 2008, **10**, 1162–1169.
- 25 C. Samanta and V. R. Choudhary, *Appl. Catal., A*, 2007, **330**, 23–32.
- 26 S. Park, S. H. Lee, S. H. Song, D. R. Park, S.-H. Baeck, T. J. Kim, Y.-M. Chung, S.-H. Oh and I. K. Song, *Catal. Commun.*, 2009, **10**, 391–394.
- 27 G. Li, J. Edwards, A. F. Carley and G. J. Hutchings, *Catal. Today*, 2006, **114**, 369–371.
- 28 J. K. Edwards, A. Thomas, A. F. Carley, A. A. Herzing, C. J. Kiely and G. J. Hutchings, *Green Chem.*, 2008, **10**, 388–394.
- 29 G. Bernardotto, F. Menegazzo, F. Pinna, M. Signoreto, G. Cruciani and G. Strukul, *Appl. Catal., A*, 2009, **358**, 129–135.
- 30 V. R. Choudhary, C. Samanta and P. Jana, *Ind. Eng. Chem. Res.*, 2007, **46**, 3237–3242.
- 31 Y.-F. Han and J. H. Lunsford, *J. Catal.*, 2005, **230**, 313–316.
- 32 P. Landon, P. J. Collier, A. F. Carley, D. Chadwick, A. J. Papworth, A. Burrows, C. J. Kiely and G. J. Hutchings, *Phys. Chem. Chem. Phys.*, 2003, **5**, 1917–1923.
- 33 Q. Liu and J. H. Lunsford, *Journal of Catalysis*, 2006, **239**, 237–243.
- 34 J. K. Edwards, B. Solsona, E. N. Ntainjua, A. F. Carley, A. A. Herzing, C. J. Kiely and G. J. Hutchings, *Science*, 2009, **323**, 1037–1041.
- 35 I. R. Cohen, T. C. Purcell and A. P. Altshuller, *Environmental Science and Technology*, 1967, **1**, 247–252.
- 36 V. R. Choudhary, C. Samanta and P. Jana, *Applied Catalysis A: General*, 2007, **317**, 234–243.
- 37 V. V. Krishnan, A. G. Dokoutchaev and M. E. Thompson, *Journal of Catalysis*, 2000, **196**, 366–374.
- 38 S. Melada, R. Rioda, F. Menegazzo, F. Pinna and G. Strukul, *Journal of Catalysis*, 2006, **239**, 422–430.
- 39 G. Li, J. Edwards, A. F. Carley and G. J. Hutchings, *Catalysis Today*, 2007, **122**, 361–364.

Hydrogenolysis of glycerol over a highly active CuO/ZnO catalyst prepared by an oxalate gel method: influence of solvent and reaction temperature on catalyst deactivation

Arne Bienholz, Frederick Schwab and Peter Claus*

Received 20th July 2009, Accepted 20th October 2009

First published as an Advance Article on the web 26th November 2009

DOI: 10.1039/b914523k

The hydrogenolysis of glycerol was performed in an autoclave at temperatures between 190 and 225 °C and at a H₂ pressure of 5 MPa over a CuO/ZnO catalyst prepared by an oxalate gel (OG) method. Compared to a CuO/ZnO catalyst prepared by coprecipitation, much higher conversions of glycerol and space–time yields up to 9.8 g_{propylene glycol} g_{Cu}⁻¹ h⁻¹ are achieved with CuO/ZnO-OG, whereas both catalysts produced propylene glycol with selectivities of about 90%. Additionally, the influence of the temperature and the solvent was examined. Compared to a conversion of glycerol of only 5% in an aqueous glycerol solution, the use of 1,2-butanediol as a solvent leads to a high conversion of 55%. Moreover, experiments were carried out in pure glycerol and from transmission electron microscopy images of fresh and spent catalysts, it was obvious that the morphology of the catalyst changed during the reaction. By X-ray diffraction and N₂O chemisorption, it was proved that a tremendous loss of copper surface area occurred during the hydrogenolysis of glycerol. Taking together the influence of the solvent on the conversion of glycerol and the results of the catalyst characterization, it can be concluded that water, as an unavoidable by-product of the reaction, is responsible for a strong deactivation of the catalyst.

1. Introduction

As a byproduct of biodiesel production, glycerol is a highly-functionalized platform chemical available in large amounts and, thus, at low costs. Therefore, the development of new catalytic processes to convert glycerol to value-added products, *e. g.* dihydroxyacetone or hydrogen,¹ is the subject of an increasing number of investigations. One of the promising approaches is the hydrogenolysis of glycerol, leading to 1,2-propanediol (propylene glycol). Propylene glycol has a wide range of practical applications, like its use as a heat transfer fluid or its polymerisation to polyesters and polyurethanes. Supported Pt, Rh, Co, Ru and Cu catalysts are used for the hydrogenolysis of glycerol at temperatures between 170 and 220 °C under elevated hydrogen pressures and in dilute aqueous solutions of glycerol.^{2–8} Several attempts were made to enhance glycerol conversion by the addition of solid acids like ion-exchange resins^{9,10} or zeolites and sulfated zirconia¹¹ to supported noble metal catalysts, suggesting that the hydrogenolysis of glycerol occurs in two steps. Initially, glycerol is dehydrated to acetol over acid sites followed by hydrogenation over metal catalysts. Indeed, acetol was detected by several groups,⁶ particularly when the hydrogenolysis of glycerol is carried out in the vapour phase and, thus, under rather low hydrogen pressures.^{12,13}

Among the different noble metal catalysts, Cu catalysts turned out to combine high selectivities for propylene glycol with satisfying conversion levels of glycerol.^{5,6,14–17}

However, the reaction times needed to achieve high glycerol conversions are rather long. Additionally, Cu catalysts suffer from deactivation in the hydrogenolysis of glycerol. It is observed in the literature that a strong decrease in glycerol conversion occurs if a Cu/Zn/Al catalyst is used in a second run, regardless of whether the spent catalyst was dried or calcinated before it was reused.¹⁷ Moreover, Montassier *et al.* reported the deactivation of Cu/C because of the sintering of copper particles in the hydrogenolysis of glycerol in a tube reactor.¹⁵

Besides the preparation of copper catalysts by precipitation,^{5,14,17} different preparation methods like the template preparation of Cu–Cr catalysts¹⁸ and the precipitation–gel method for a Cu/SiO₂ catalyst¹⁹ have been applied. However, the Cu/ZnO catalysts used in the hydrogenolysis of glycerol have usually been prepared by precipitation and the effect of the Cu/ZnO catalyst synthesis procedure was not investigated, although the properties of Cu/ZnO catalysts, and, thus, their performance in the methanol synthesis from CO and H₂, have been shown to be strongly dependent on the preparation method.^{20–22} Here, we report the preparation of a copper catalyst by an oxalate gel method, its characterization and its use in the hydrogenolysis of glycerol. Additionally, the deactivation of the catalyst was examined with regard to the reaction temperature and the generation of water as a by-product of the hydrogenolysis of glycerol.

Department of Chemistry, Ernst-Berl-Institute/Chemical Technology II, Technical University Darmstadt, Petersenstr. 20, 64287, Darmstadt, Germany. E-mail: claus@ct.chemie.tu-darmstadt.de; Fax: +49 6151 16 4788; Tel: +49 6151 16 5369

2. Experimental

2.1 Preparation of the catalysts

The preparation of the CuO/ZnO catalyst was carried out by an oxalate gel coprecipitation method.²³ Cu(NO₃)₂·2.5H₂O (4.87 g, 20.9 mmol) and Zn(NO₃)₂·6 H₂O (12.2 g, 41 mmol) were dissolved in 65 ml ethanol. Then, oxalic acid (6.68 g, 74.3 mmol) in 40 ml ethanol was added to form a light blue precipitate. After one hour, the precipitate was separated by filtration, washed with 500 ml deionised water and finally dried overnight at 70 °C. Afterwards, the precipitate was calcined at 150, 200 and 300 °C for one hour at each temperature, followed by a final step at 360 °C for four hours. Hereafter, this catalyst will be referred to as the CuO/ZnO-OG catalyst.

As a reference, a CuO/ZnO catalyst was prepared by coprecipitation. Copper acetate (3.8 g, 20.9 mmol) and Zn(NO₃)₂·6H₂O (12.2 g, 41 mmol) were dissolved in 300 ml deionised water. Precipitation was achieved by the dropwise addition of 140 ml of a 1 M NaOH solution at 80 °C. The precipitate was aged for 2 h at a constant pH value of 9 at the same temperature. Finally, the precipitate was separated by filtration, washed with one litre of deionised water and dried overnight at 70 °C. The calcination of this catalyst was the same as that for the CuO/ZnO-OG catalyst. This catalyst will be referred to as the CuO/ZnO-CP catalyst. The copper oxide content of both catalysts was 33 wt%.

2.2 Catalyst characterisation

Copper surface areas were determined by N₂O chemisorption followed by temperature-programmed reduction (TPR) of the formed Cu₂O species in a stream of H₂ (Cu₂O-TPR). All these treatments of the catalyst were carried out by means of a TPDR 1100 device (Porotec). Before the analysis, *in situ* pre-reduction of the catalysts in a stream of 4.95% H₂ in Ar (20 ml min⁻¹), at a heating rate of 10 °C min⁻¹, to a temperature of 330 °C was performed. This temperature was held for 60 min. The catalyst was cooled down in a stream of He in order to oxidize Cu to Cu₂O with 1% N₂O in He (10 ml min⁻¹) at 20 °C. Finally, Cu₂O-TPR was carried out in 4.95% H₂ in Ar (20 ml min⁻¹) at a heating rate of 10 °C min⁻¹, to a temperature of 330 °C. From the amount of H₂ needed to completely reduce Cu₂O, the specific copper surface area, the dispersion and the mean particle diameter were calculated.

Additionally, the morphology of the catalysts was examined by transmission electron microscopy (HRTEM JEOL, JEM 3010, 300 kV). Powder X-ray diffraction (XRD) patterns of the catalysts were recorded using Co K α 1 radiation ($\lambda = 1.78896 \text{ \AA}$).

2.3 Hydrogenolysis of glycerol

In a standard experiment, 140 mL pure glycerol and 3 g catalyst were loaded into a stainless steel reactor (Parr). The reactor was pressurized with hydrogen to a pressure of 5 MPa and heated to a temperature of 200 °C. The samples were taken at desired time intervals and analyzed with a Hewlett-Packard 6890 gas chromatograph equipped with a DB-WAX GC column and a flame ionization detector. The selectivity of the products was calculated on a carbon basis.

In order to investigate the role of water (section 3.4) in the deactivation of the catalyst, 1,2-butanediol was used as a solvent. Glycerol and the reaction products, including several alcohols, have to be dissolved easily in the solvent making the use of an alcohol desirable. Furthermore, no C₁ to C₃ components were chosen as solvent due to their possible formation during the hydrogenolysis of glycerol. Therefore, this C₄ polyol was used as the solvent.

3. Results and discussion

3.1 Preparation method of the catalyst

Initially, the CuO/ZnO catalysts prepared by the two different preparation methods were tested in the hydrogenolysis of glycerol. According to Table 1, no differences between the two catalysts in terms of the selectivities are observed. Both CuO/ZnO-OG and CuO/ZnO-CP catalysts exhibited high selectivities towards propylene glycol of 90 and 87%, respectively. Moreover, the selectivities towards undesired side products like ethylene glycol and acetol were low. Concerning the activity of the two catalysts, a much higher conversion of glycerol was achieved in the case of the CuO/ZnO-OG catalyst compared to CuO/ZnO-CP. Using the CuO/ZnO-OG catalyst, a conversion of 46% is achieved, whereas the conversion at the CuO/ZnO-CP catalyst is only 17%. With the CuO/ZnO-OG catalyst, the space–time yield amounts to 9.8 g_{propylene glycol} g_{Cu}⁻¹ h⁻¹. Compared to other copper-based catalysts like Cu/SiO₂¹⁹ and CuO/ZnO, prepared by coprecipitation,¹⁴ which produce propylene glycol with space–time yields of 3.2 and 0.8 g_{propylene glycol} g_{Cu}⁻¹ h⁻¹, respectively, the CuO/ZnO-OG catalyst is extremely active. Therefore, the CuO/ZnO-OG catalyst was chosen for further investigations.

In order to determine the reason for the different conversions of glycerol, N₂O chemisorption was carried out with both catalysts which were reduced in 4.95% H₂ in Ar at 330 °C (heating rate = 10 °C min⁻¹) for 60 min prior to N₂O chemisorption. The resulting copper surface areas, dispersions and mean copper particle diameters are listed in Table 2. The copper surface area of the CuO/ZnO-CP catalyst amounts to 16.8 m² g⁻¹, and

Table 1 Hydrogenolysis of glycerol over the CuO/ZnO-OG and CuO/ZnO-CP catalysts, both with a copper oxide content of 33 wt%

Catalyst	Conversion (%)	Selectivity(%)			
		Propylene glycol	Ethylene glycol	Acetol	Others ^b
CuO/ZnO-OG ^a	46	90	1	1	8
CuO/ZnO-CP ^a	17	87	0	1	12

^a Reaction conditions: 140 mL pure glycerol, 3 g catalyst, 5 MPa H₂, 200 °C, 7 h. ^b Unidentified side products.

Table 2 Comparison of the structural properties of the CuO/ZnO-OG and CuO/ZnO-CP catalysts determined by N₂O chemisorption

Catalyst	$S_{\text{Cu}}^a / \text{m}^2 \text{g}^{-1}$	$D^b / \%$	$d_{\text{Cu}}^c / \text{nm}$
CuO/ZnO-OG	30.1	16.8	6.3
CuO/ZnO-CP	16.7	9.1	12.1

^a Copper surface area. ^b Dispersion. ^c Mean copper particle size.

the mean copper particle diameter is 12.1 nm. Agrell *et al.*²⁴ prepared a CuO/ZnO catalyst by coprecipitation of an aqueous Zn(NO₃)₂ and Cu(NO₃)₂ solution and obtained a catalyst with a copper surface area of 21.5 m² g⁻¹. Taking into account the higher copper oxide loading of 39 wt% in the study of Agrell compared to 33 wt% of the CuO/ZnO-CP catalyst, the results are in good agreement. In comparison, the copper surface area of the CuO/ZnO-OG catalyst is twice as high, which indicates the reason for the improved activity of this catalyst compared to the CuO/ZnO-CP catalyst.

3.2 Recycling of the catalyst

The CuO/ZnO-OG catalyst was recovered and used in a second experiment under the same reaction conditions. However, a glycerol conversion of just 10% was achieved, although the high selectivity for propylene glycol was preserved (97%). In order to examine the reason for the loss of activity, the catalyst was recovered after the first experiment and analysed by XRD and N₂O chemisorption. The XRD pattern of the spent catalyst, along with the pattern of the fresh catalyst, is shown in Fig. 1.

The fresh CuO/ZnO-OG catalyst contained merely CuO and ZnO crystallites. After the hydrogenolysis of glycerol at 200 °C and at a hydrogen pressure of 5 MPa, the CuO phase was completely reduced to metallic copper. The crystallite sizes of the CuO, Cu and ZnO were calculated using the Scherrer equation. The resulting crystallite sizes, together with the copper surface areas and copper particle sizes obtained from N₂O chemisorption, are listed in Table 3. Before the reaction, the mean diameters of the CuO and ZnO crystallites were determined to be 15 and 10 nm, respectively. After the reaction, the mean crystallite diameters obtained from XRD of both the Cu and ZnO crystallites were calculated to be 40 nm. Therefore, a strong increase in the copper crystallite size during the reaction was observed, leading to a decrease in the active surface area and, thus, to a loss of activity. These results were confirmed by N₂O chemisorption as the copper surface area decreases during the reaction from 30.1 m² g⁻¹ to 5.3 m² g⁻¹. Moreover, a strong increase in the ZnO crystallite size is also observed. A loss of activity may occur as well because of the agglomeration of the ZnO crystallites, as glycerol may be dehydrated to acetol and glycidol at the ZnO surface.⁵ The loss of active copper surface area is also known for methanol synthesis. Muhler *et al.*²⁵ reported the growth of copper particles in a Cu/ZnO methanol catalyst with increasing time on stream.

To further investigate the deactivation of the CuO/ZnO-OG catalyst, TEM images of the catalyst were recorded before and after the reaction (Fig. 2). From the TEM images, a change in morphology is clearly observed. Before the catalyst was used in the hydrogenolysis of glycerol, almost spherical particles with

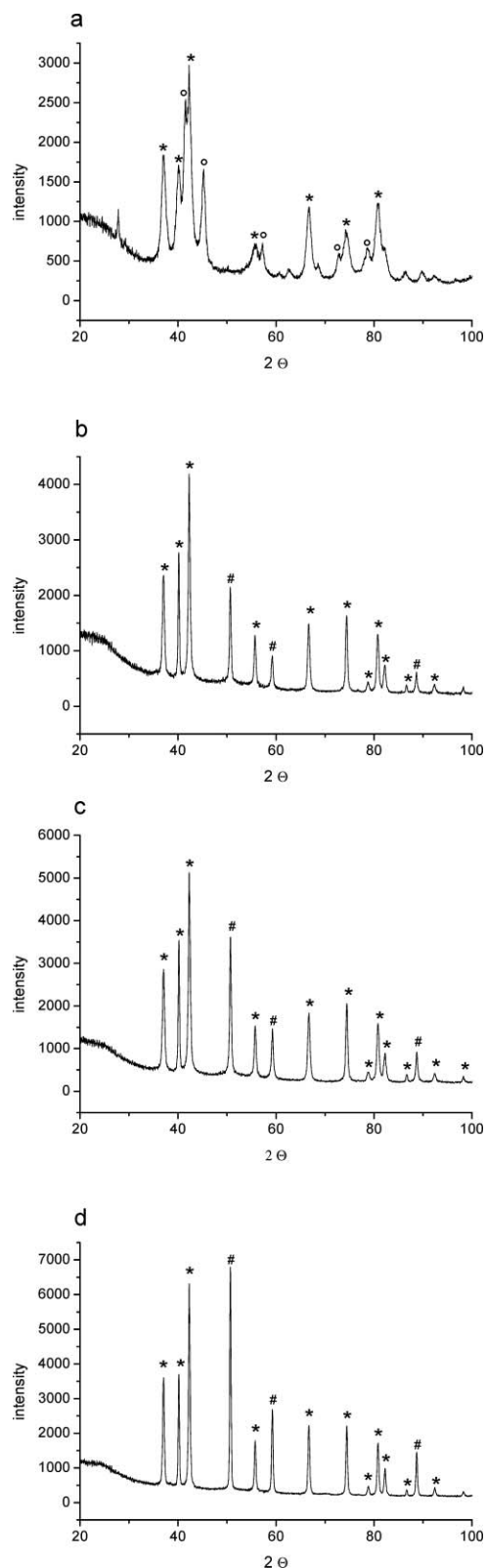


Fig. 1 XRD patterns of the CuO/ZnO-OG catalyst before (a) and after (b) use in the hydrogenolysis of pure glycerol or of glycerol with 1,2-butanediol (c) or water (d) as a solvent. Reaction conditions: 140 mL pure glycerol (b) or 140 mL 50 wt% glycerol in 1,2-butanediol (c) or water (d), 3 g catalyst, 5 MPa H₂, 200 °C, 7 h. * ZnO, ○ CuO, # Cu.

Table 3 Comparison of the structural properties of fresh and spent CuO/ZnO-OG catalysts

Catalyst	$d_{\text{CuO}}^d/\text{nm}$	$d_{\text{ZnO}}^d/\text{nm}$	$d_{\text{Cu}}^e/\text{nm}$	$S_{\text{Cu}}^e/\text{m}^2 \text{g}^{-1}$	$d_{\text{Cu}}^e/\text{nm}$
Fresh CuO/ZnO-OG	15	10	—	30.1	6.3
Spent Cu/ZnO OG ^a	—	40	40	5.3	38.2
Spent Cu/ZnO OG ^b	—	40	40	4.2	47.5
Spent Cu/ZnO OG ^c	—	40	80	2.7	75.6

^a Reaction conditions: 140 ml pure glycerol, 3 g catalyst, 5 MPa H₂, 200 °C, 7 h. ^b Reaction conditions: 140 ml 50 wt% glycerol in 1,2-butanediol, 3 g catalyst, 5 MPa H₂, 200 °C, 7 h. ^c Reaction conditions: 140 ml 50 wt% glycerol in water, 3 g catalyst, 5 MPa H₂, 200 °C, 7 h. ^d Mean CuO, Cu and ZnO crystallite sizes determined by XRD. ^e Copper surface area and mean copper particle size determined by N₂O chemisorption.

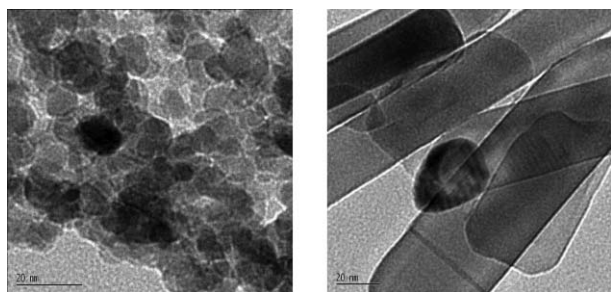


Fig. 2 TEM images of the CuO/ZnO-OG catalyst before (left) and after (right) use in the hydrogenolysis of glycerol. Reaction conditions: 140 ml pure glycerol, 3 g catalyst, 5 MPa H₂, 200 °C, 7 h.

a mean diameter of about 10 nm are visible, while after the reaction, the catalyst consists of rod-shaped particles with a considerably larger size.

3.4 The effect of the solvent

Montassier *et al.* proved that the size of copper particles in a Cu/C catalyst increased if the catalyst is stirred in water at elevated temperatures.¹⁵ As no water is loaded into the reactor at the beginning of the reaction, the deactivation of the CuO/ZnO-OG catalyst might be due to formation of water as an unavoidable by-product during the hydrogenolysis of glycerol. Because of this, the deactivation of the catalyst should occur much faster if the hydrogenolysis of glycerol is carried out with an aqueous glycerol solution.

Therefore, a 50 wt% aqueous solution of glycerol was loaded into the reactor. As a reference, the same experiment was repeated but now with a solution of glycerol in 1,2-butanediol. The results of these experiments are shown in Table 4. It is obvious that the conversion of glycerol is strongly affected by the choice of solvent. Compared to a conversion of glycerol of only 5% in an aqueous glycerol solution after 7 h, the use of 1,2-butanediol as a solvent leads to a higher conversion of 55%.

In order to determine the reason for the poor conversion of an aqueous solution of glycerol compared to 1,2-butanediol, the catalysts were recovered after the reaction and characterised by XRD and N₂O chemisorption. The XRD patterns of the two recovered catalysts are shown in Fig. 1. From the XRD patterns, the CuO, Cu and ZnO crystallite sizes were calculated and are shown in Table 3, together with the copper surface areas determined after the reaction. Before the catalyst CuO/ZnO-OG was used in the hydrogenolysis of glycerol, the mean crystallite size of the CuO and ZnO crystallites was determined to be 15 and 10 nm, respectively (Table 3). Regarding the ZnO crystallite size, a strong increase ($d = 40$ nm) is observed, which is not affected by the choice of solvent (Table 3). However, the calculated size of the Cu crystallites after the reaction strongly depends on the solvent. In comparison to 1,2-butanediol as a solvent, the size of the Cu crystallites is, in the case of water, twice the size. This increase in the copper particle size can be confirmed by N₂O chemisorption as the copper surface is also influenced by the choice of solvent. The copper surface area strongly decreased in the case of water as a solvent, from 30.1 m² g⁻¹ before to 2.7 m² g⁻¹ after the reaction, while in the case of 1,2-butanediol the copper surface area diminished to 4.2 m² g⁻¹.

3.5 Reaction temperature

As well as the solvent, the reaction temperature might also play an important role in the deactivation process of the Cu/ZnO-OG catalyst. Thus, the hydrogenolysis of glycerol was performed in the temperature range between 190 and 225 °C. The effect of the reaction temperature on the conversion of glycerol and the selectivity for propylene glycol are shown in Fig. 3. While there was no significant influence of the reaction temperature on the selectivity for propylene glycol ($S = 84\text{--}92\%$), the conversion of glycerol was strongly affected when raising the temperature. However, there is no consistent dependence of the conversion on the reaction temperature as would be expected according to Arrhenius behaviour: the conversion first strongly increases

Table 4 Effect of the solvent on the conversion of glycerol and the selectivities towards propylene glycol, ethylene glycol and acetol of the CuO/ZnO-OG catalyst

Solvent	Conversion ^a (%)	Selectivity (%)			
		Propylene glycol	Ethylene glycol	Acetol	Others ^b
1,2-Butanediol	55	86	1	1	12
Water	5	87	9	2	2

^a Reaction conditions: 140 ml 50 wt% glycerol dissolved in 1,2-butanediol or water, 3 g catalyst, 5 MPa H₂, 200 °C, 7 h. ^b Unidentified side products.

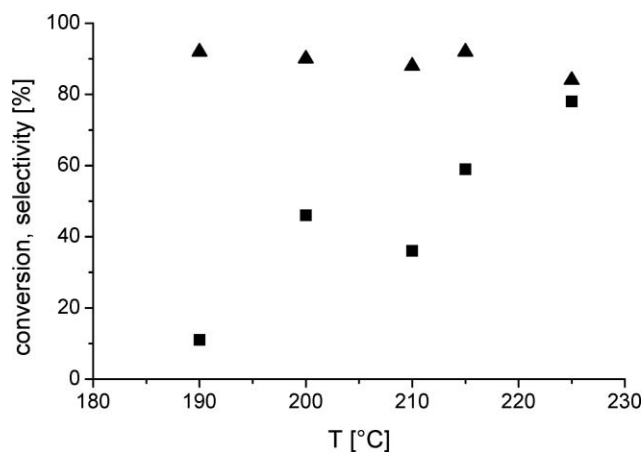


Fig. 3 Dependence of the conversion (▲) and the selectivity for propylene glycol (■) on the reaction temperature. Reaction conditions: 140 ml glycerol, 3 g CuO/ZnO-OG catalyst, 5 MPa H₂, 7 h.

with an increase in temperature from 190 to 200 °C, but then, if the temperature is further increased to 210 °C, the conversion decreases. Raising the temperature further to 215 °C and, finally, to 225 °C then gives the expected increase in conversion again. The reason for this relationship between the reaction temperature and the conversion during glycerol hydrogenolysis may be an interference between the acceleration of the reaction rate due to elevated temperatures and the stronger deactivation of the catalyst at higher reaction temperatures. Furthermore, an interplay between the temperature dependence of the adsorption constants determining the individual adsorption enthalpy of one or more reactants and the temperature dependence of the rate constant dictating the activation energy may cause the observed decrease in conversion with rising temperature. According to the copper surface areas determined by N₂O chemisorption for the CuO/ZnO-OG catalyst after being used in the hydrogenolysis of glycerol at different temperatures (Fig. 4), the temperature seems to influence the growth of the copper particles. It is expected that the decrease in the copper surface area correlates with the amount of water produced during the reaction. However, at a reaction temperature of 210 °C, the

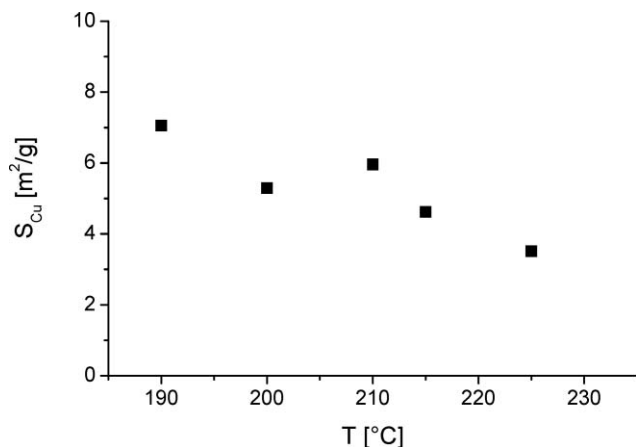


Fig. 4 Copper surface areas determined by N₂O chemisorption of the CuO/ZnO-OG catalyst after the reaction at temperatures between 190 and 225 °C. Reaction conditions: 140 ml glycerol, 3 g CuO/ZnO-OG catalyst, 5 MPa H₂, 7 h.

glycerol conversion, which proved to be reproducible with a standard deviation of $\pm 3\%$, is only 36% compared to 46% at 200 °C, suggesting that less water is formed at a reaction temperature of 210 °C. From that, an increase of the copper surface area can be assumed and Fig. 4 shows that this is indeed the case ($6.0 \text{ m}^2 \text{ g}^{-1}$ vs. $5.2 \text{ m}^2 \text{ g}^{-1}$). Therefore, it is worth mentioning that by an increase of reaction temperature from 200 to 210 °C, the conversion of glycerol decreased (Fig. 3) although the copper surface area increased (Fig. 4). Thus, the decrease in glycerol conversion between 200 to 210 °C cannot be attributed to a growth of copper particles. Keeping in mind that the product distribution remained unchanged during the course of glycerol hydrogenolysis between 190 and 225 °C (1,2-propanediol is always produced with high selectivity, Fig. 3), a change of the reaction mechanism should be ruled out, and the unusual behavior is likely to be due to a difference in the temperature dependence of the rate constant and the reactants' adsorption constants.

4. Conclusions

A CuO/ZnO catalyst prepared by an oxalate gel method was proven to be highly active in the hydrogenolysis of glycerol compared to a CuO/ZnO catalyst prepared by the standard coprecipitation method. The higher activity can be attributed to the copper surface area, which was as high as $30.1 \text{ m}^2 \text{ g}^{-1}$ in the case of the CuO/ZnO-OG catalyst, whereas the copper surface area of the CuO/ZnO-CP catalyst amounted to only $16.7 \text{ m}^2 \text{ g}^{-1}$. With both catalysts, a selectivity for propylene glycol of about 90% is achieved.

In the presence of water, the size of the copper crystallites of the CuO/ZnO catalyst increases tremendously, leading to a decrease in active surface area and, thus, to a loss of activity. Even if no water is loaded into the reactor, the water formed during the hydrogenolysis of glycerol causes the deactivation of the catalyst. Increasing the reaction temperature has no significant influence on the loss of active surface area and cannot, therefore, be the reason for the deactivation of the catalyst.

Acknowledgements

The authors are grateful to the FAUDI-Stiftung (project 73) for financial support of this work.

References

- 1 A. Brandner, K. Lehnert, A. Bienholz, M. Lucas and P. Claus, *Top. Catal.*, 2009, **52**, 278–287.
- 2 E. Maris and R. Davis, *J. Catal.*, 2007, **249**, 328–337.
- 3 D. Lahr and B. Shanks, *J. Catal.*, 2005, **232**, 386–394.
- 4 I. Furikado, T. Miyazawa, S. Koso, A. Shima, K. Kunimori and K. Tomishige, *Green Chem.*, 2007, **9**, 582–588.
- 5 S. Wang and H. Liu, *Catal. Lett.*, 2007, **117**, 62–67.
- 6 M. Dasari, P. Kiatsimkul, W. Sutterlin and G. Suppes, *Appl. Catal., A*, 2005, **281**, 225–231.
- 7 Q. Liu, X. Guo, Y. Li and W. Shen, *J. Phys. Chem. C*, 2009, **113**, 3436–3441.
- 8 M. Balaraju, V. Rekha, P. S. Sai Prasad, B. L. A. Prabhavathi Devi, R. B. N. Prasad and N. Lingaiah, *Appl. Catal., A*, 2009, **354**, 82–87.
- 9 T. Miyazawa, S. Koso, K. Kunimori and K. Tomishige, *Appl. Catal., A*, 2007, **329**, 30–35.
- 10 T. Miyazawa, S. Koso, K. Kunimori and K. Tomishige, *Appl. Catal., A*, 2007, **318**, 244–251.

- 11 Y. Kusunoki, T. Miyazawa, K. Kunimori and K. Tomoshige, *Catal. Commun.*, 2005, **6**, 645–649.
- 12 L. Huang, Y. Zhu, H. Zheng, Y. Li and Z. Zheng, *J. Chem. Technol. Biotechnol.*, 2008, **83**, 1670–1675.
- 13 C. Chiu, A. Tekeci, W. Sutterlin, J. Ronco and G. Suppes, *AIChE J.*, 2008, **54**, 2456–2463.
- 14 M. Balaraju, V. Rekha, P. S. Sai Prasad, R. B. N. Prasad and N. Lingaiah, *Catal. Lett.*, 2008, **126**, 119–124.
- 15 C. Montassier, J. Dumas, P. Granger and J. Barbier, *Appl. Catal., A*, 1995, **121**, 231–244.
- 16 J. Chaminand, L. Djakovitch, P. Gallezot, P. Marion, C. Pinel and C. Rosier, *Green Chem.*, 2004, **6**, 359–361.
- 17 L. Meher, R. Gopinath, S. Naik and A. Dalai, *Ind. Eng. Chem. Res.*, 2009, **48**(4), 1840–1846.
- 18 C. Liang, Z. Ma, L. Ding and J. Qiu, *Catal. Lett.*, 2009, **130**, 169–176.
- 19 Z. Huang, F. Cui, H. Kang, J. Chen, X. Zhang and C. Xia, *Chem. Mater.*, 2008, **20**(15), 5090–5099.
- 20 M. Kurtz, n Bauer, C. Büscher, H. Wilmer, O. Hinrichsen, R. Becker, S. Rabe, K. Merz, M. Driess, R. Fischer and M. Muhler, *Catal. Lett.*, 2004, **92**, 49–52.
- 21 Y. Guo, W. Meyer-Zaika, M. Muhler, S. Vukojević and M. Epple, *Eur. J. Inorg. Chem.*, 2006, 4774–4781.
- 22 T. Shishido, Y. Yamamoto, H. Morioka, K. Takaki and K. Takehira, *Appl. Catal., A*, 2004, **263**, 249–253.
- 23 Q. Sun, Y.-L. Zhang, H.-Y. Chen, J.-F. Deng, D. Wu and S.-Y. Chen, *J. Catal.*, 1997, **167**, 92–105.
- 24 J. Agrell, M. Boutonnet, I. Melián-Cabrera and J. Fierro, *Appl. Catal., A*, 2003, **253**, 201–211.
- 25 M. C. Carroll, B. Skrotzki, M. Kurtz, M. Muhler and G. Eggeler, *Scr. Mater.*, 2003, **49**, 527–532.

Hierarchical macroporous–mesoporous SBA-15 sulfonic acid catalysts for biodiesel synthesis†

Jérémy Dhainaut, Jean-Philippe Dacquin, Adam F. Lee* and Karen Wilson*

Received 17th September 2009, Accepted 10th November 2009

First published as an Advance Article on the web 16th December 2009

DOI: 10.1039/b919341c

Hierarchical macroporous–mesoporous SBA-15 silicas have been synthesised *via* dual-templating routes employing liquid crystalline surfactants and polystyrene beads. These offer high surface areas and well-defined, interconnecting macro- and mesopore networks with respective narrow size distributions around 300 nm and 3–5 nm for polystyrene:tetraethoxysilane ratios $\geq 2:1$. Subsequent functionalisation with propylsulfonic acid yields the first organized, macro-mesoporous solid acid catalyst. The enhanced mass transport properties of these new bi-modal solid acid architectures confer significant rate enhancements in the transesterification of bulky glyceryl trioctanoate, and esterification of long chain palmitic acid, over pure mesoporous analogues. This paves the way to the wider application of hierarchical catalysts in biofuel synthesis and biomass conversion.

Introduction

The International Energy Agency predicts a 55% increase in global fuel consumption by the year 2030,¹ principally the result of the growing needs of emerging nations. The combination of dwindling oil reserves and growing concerns over carbon dioxide emissions and associated climate change is driving the urgent development of clean, sustainable energy supplies. Biomass offers a partial solution to the replacement of fossil fuels for the production of key chemical feedstocks and transportation fuels such as ethanol and biodiesel. First generation alternative biofuels have proven controversial due to their synthesis from important food crops including corn, sugarcane and palm or rapeseed oils, and consequent impact on global food prices. Recent focus has therefore shifted towards so-called second generation non-food biomass sources like cellulose, algae or non-edible plant oils from the Euphorbiaceae family² (notably *Jatropha* or *Castor* oil), which do not compete with traditional agronomies.

Biodiesel sourced from renewable second generation crops is non-toxic and biodegradable, with the potential for closed CO₂ cycles³ and thus vastly reduced carbon footprints compared with petroleum fuels.^{3,4} It comprises long chain fatty acid methyl esters (FAMES), typically derived from vegetable oils or animal fats rich in triacyl glycerides (TAGs) and free fatty acids (FFAs).⁵ The transesterification of oil seed TAGs to methyl (or ethyl) esters can be catalyzed by acids or bases, and the vast majority of biodiesel is currently produced *via* homogeneous catalysis, using soluble bases such as NaOH/NaOMe or KOH.^{6,7} Although liquid base catalysts offer high transesterification rates, they

are sensitive to water and FFA impurities which are always present in trace amounts even in refined plant oils. FFA removal from biodiesel is essential in order to prevent corrosion of vehicle fuel tanks and engine blocks, and is currently achieved through an acid catalyzed esterification pretreatment step prior to transesterification. Simultaneous FFA esterification and TAG transesterification using acid catalysts provides an alternative single step (albeit high temperature) process for poor quality oils containing high FFA levels.^{5,6,8–10} However, in both scenarios reactor corrosion and removal of soluble catalyst species from the resulting biofuel mixture is particularly problematic, requiring aqueous quench and neutralisation steps which themselves generate undesired emulsions and soap formation.^{6,11} The resultant *E*-factor (defined as the [total waste]/[product] ratio) is concomitantly poor due to catalyst losses after each reaction and the production of copious contaminated water. Furthermore, the major by-product of biodiesel synthesis, glycerol, is heavily contaminated by homogeneous catalyst residues and/or water and therefore of little re-sale value to potential consumers in the cosmetic, food and pharmaceutical industries.

Non-corrosive heterogeneous catalysts that are easily recovered and recyclable could greatly improve the environmental impact of commercial biodiesel processing, eliminating the need for aqueous quench cycles while offering the opportunity for continuous operation in flow reactors.^{5,6,11,12} Diverse solid acids and bases including zeolites,¹³ resins,¹⁴ alkali earth oxides,^{15–17} hydrotalcites¹⁸ and calcined dolomitic rock¹⁹ have been investigated for TAG transesterification and their application recently reviewed.^{4,5,6,12} Unfortunately, the micro and mesoporous catalyst systems investigated to date are not optimal for the bulky and viscous C₁₆–C₁₈ TAGs typical of plant oils.²⁰ Even tailored, large pore (>4–15 nm) mesoporous catalysts based upon SBA-15²¹ that are active for esterification and transesterification,^{9,22–25} often possess long, isolated parallel channels resulting in slow in-pore diffusion and correspondingly slow turnover. Current material syntheses have focused solely on generating and tuning mesoporosity, largely

School of Chemistry, Cardiff University, Cardiff, UK CF10 3AT.
E-mail: leeaf@cardiff.ac.uk, wilsonk5@cardiff.ac.uk; Fax: 44 2920 870827; Tel: 44 2920 874030

† Electronic supplementary information (ESI) available: PS bead characterization and comparative textural properties of pre- and post-functionalized silicas. See DOI: 10.1039/b919341c

ignoring the benefits of hierarchical porous networks containing macropores to act as rapid transport conduits to the active sites. Simulations show that in the Knudsen diffusion regime,²⁶ where reactants/products are able to enter/exit mesopores but experience attendant diffusion limitations, such bi-modal pore structures could significantly improve catalyst activity. Catalytically active materials possessing such interconnecting macropore–mesopore networks²⁷ with well-defined dimensions would be particularly suited to boosting mass-transport in viscous liquid phase reactions such as biodiesel synthesis. They can be prepared using microemulsion,²⁸ colloidal polystyrene microspheres²⁹ or co-surfactants³⁰ routes in conjunction with mesoporous templates, and are particularly attractive for application in liquid continuous flow reactors wherein rapid pore diffusion is required. Polystyrene microspheres allow great control over the final macropore properties. SBA-15 silicas have been recently synthesised incorporating macropores of a few hundred nanometres by the use of these templating polymers,^{31–33} offering high specific surface areas and improved diffusion characteristics, but to our knowledge have yet to be applied in heterogeneous catalysis.

Surface grafting of alkoxy silanes offers a convenient method to covalently attach organic functional groups to porous silica frameworks without the risk of pore blockage or leaching of the grafted component.³⁴ Sulfonic acid silicas are a class of solid Brønsted acid catalyst comprising tethered organo-sulfonic acid groups^{35–37} that provide alternatives to commercially available sulfonated polymer resins, such as Amberlyst-15 and Nafion-H. In this paper we explore the use of grafting to attach pure Brønsted acid sites to macroporous–mesoporous SBA-15 supports and thereby generate a new class of ordered, hierarchical sulfonic acid functionalised silicas, designed specifically for bulky plant oils. Macropore inclusion significantly enhances the rate of both C₈ TAG transesterification to FAME and C₁₆ FFA esterification with methanol.

Experimental

Polystyrene bead synthesis

The emulsion polymerisation approach of Vaudreuil and co-workers was adopted to generate monodisperse polystyrene (PS) beads.³⁸ 0.083 g of potassium persulfate (99%, Sigma-Aldrich) was dissolved in 6 ml of deionized water and dried at 70 °C. Separately, 239.5 ml of deionized water was added to a 500 ml three-neck round-bottom flask and heated to 70 °C under N₂. 25 ml of styrene (99%, Sigma-Aldrich) and 4.75 ml of divinylbenzene (80%, Sigma-Aldrich) was washed three times in a separating funnel with a 0.1 M NaOH solution (pellets, Sigma-Aldrich) and deionized water to remove polymerization inhibitors. The styrene and divinylbenzene were transferred to the 500 ml temperature stabilized flask, along with 26 ml of deionized water used to wash out the funnel. The potassium persulfate was then added to initiate styrene polymerization, and 15 h later the resultant white solution was filtered, then washed three times with deionized water and three times with ethanol. The final beads possessed a narrow size distribution of ~320 nm diameter (Figures S1 and 2†), while thermo-gravimetric analysis

(TGA) revealed their complete decomposition in air at 550 °C (Figure S3†).

SBA-15 synthesis

Macroporous–mesoporous SBA-15 silicas were synthesized following the approach of Zhao *et al.*,³⁹ with the addition of polystyrene beads during the synthesis to create macropores.^{31,32,33} Typically, 1.0 g of Pluronic P123 triblock copolymer was dissolved in 7.5 ml of water and 25 ml of 2 M HCl solution (Fisher) while stirring at 35 °C. The required amount of polystyrene beads for the appropriate PS:tetraethoxysilane (TEOS 98%, Sigma-Aldrich) mass ratio were then added to the solution and stirred for an hour. Once a good dispersion of PS beads was achieved, 2.3 ml of TEOS were added to the solution, which was maintained at 35 °C for 24 h while stirring. The mixture was then aged at 80 °C for 24 h and the solid product filtered, washed 3 times with deionised water, and calcined statically in air at 550 °C (ramp rate of 0.5 °C min⁻¹) for 6 h. The final solids are termed MM-SBA15-X, where X = PS:TEOS weight ratio.

Sulfonic acid functionalization

Sulfonic acid functionalization was performed by post-synthesis grafting as described previously.^{9,40,41} A mixture of 0.5 g of MM-SBA15-X and 0.50 ml of 3-mercaptopropyl trimethoxysilane (MPTMS 95%, Alfa Aesar) in 15 ml of toluene (Fisher) was refluxed at 130 °C for 24 h, and the resulting thiol-functionalized solid filtered, washed 3 times with methanol (Fisher) and dried at 80 °C overnight. Thiol groups were converted to –SO₃H by mild oxidation with 10 ml of 30% hydrogen peroxide (Sigma-Aldrich) by continuous stirring at room temperature for 24 h. Sulfonated MM-SBA15-X solid was subsequently filtered, washed 3 times with methanol, and dried at 80 °C overnight.

Glyceryl trioctanoate transesterification

Transesterification was performed at 60 °C under stirring using 0.05 g of catalyst, 4.92 ml of glyceryl trioctanoate (commercial name tricaprylin 99%, Sigma-Aldrich), 0.59 ml of dihexylether (Fisher) as an internal standard, and 12.50 ml of methanol, giving a MeOH:TAG ratio of 30:1. Aliquots of 0.1 ml were regularly sampled and analyzed by gas chromatography using a Varian 450-GC equipped with a VF-1ms 25 m × 0.25 mm capillary column. Product yields were calculated using response factors derived for methyl octanoate (99%, Fluka).

Palmitic acid esterification

Esterification was performed at 60 °C under stirring using 0.05 g of catalyst, 2.564 g (10 mmol) of palmitic acid (Sigma-Aldrich), 0.59 ml (2.5 mmol) of dihexylether and 12.50 ml (300 mmol) of methanol. Aliquots of 0.1 ml were regularly sampled and analyzed using a Varian 3900 GC equipped with a CP-Sil 5CB, 15 m × 0.25 mm capillary column. Product yields were calculated using response factors derived for methyl palmitate (99%, Sigma-Aldrich).

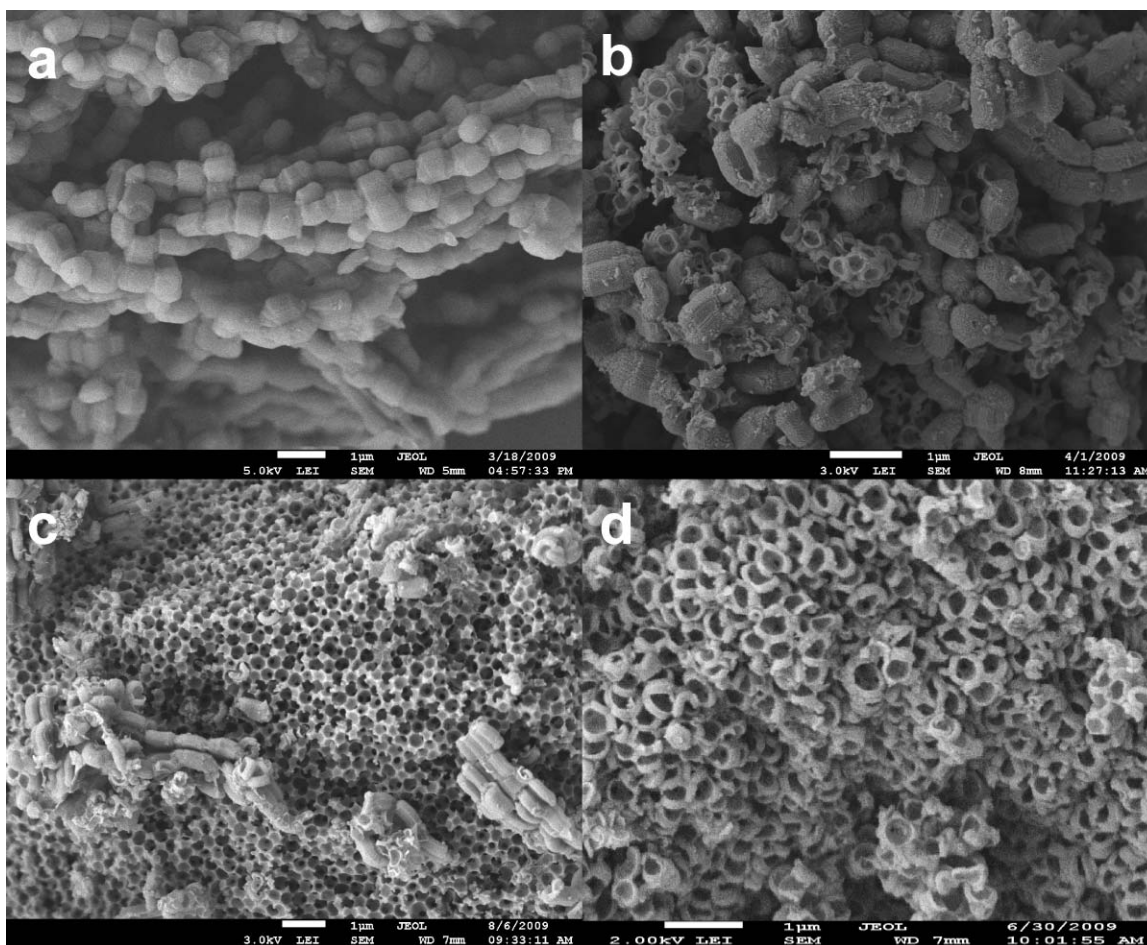


Fig. 1 SEM images of: a) SBA-15; b) MM-SBA15-1; c) MM-SBA15-2 and d) MM-SBA15-4 hierarchical macroporous-mesoporous silicas.

Material characterization

Powder X-ray diffraction patterns were collected on a Bruker D8 Advance diffractometer fitted with a Lynx eye high-speed strip detector and Cu-K α radiation source. Small-angle patterns were recorded from 0.65° to 3° with 0.02° steps at 10 s per point. Sulfur content was determined using an Horiba XGT-7000 X-Ray Fluorescence spectrometer. Nitrogen porosimetry was performed on a Quantasorb Nova 1200 instrument, after sample evacuation at 200 °C for 4 h. Surface areas were calculated using the Brunauer-Emmet-Teller (BET) method over the range $P/P_0 = 0.075-0.35$, where a linear relationship is maintained. Pore size distributions were calculated using the Barrett-Joyner-Halenda (BJH) model applied to the desorption isotherm branch. Mesopore volumes were evaluated at $P/P_0 = 0.98$. SEM was conducted on a JEOL JSM 7500F system; samples were gold coated prior to analysis. High-resolution TEM was carried out on a JEOL 2011 operating at 200 kV; samples were deposited from ethanolic solution onto holey-carbon copper grids. XPS measurements were performed using a Kratos AXIS HSi instrument equipped with a charge neutraliser and Mg-K α X-ray source. TGA was performed using a Stanton Redcroft STA 780 thermal analyser at 10 °C min⁻¹ under flowing He/O₂ (80:20 v/v) or He (20 ml min⁻¹ total) for template removal and sulfonic acid decomposition studies respectively.

Results and discussion

Materials characterization

A series of macro-mesostructured derived silicas were first prepared using different PS:TEOS ratios to incorporate macropores within the conventional SBA-15 mesopore framework. These are denoted MM-SBA15-1, MM-SBA15-2 and MM-SBA15-4 corresponding to 1:1, 2:1 and 4:1 weight ratios of PS beads to TEOS. A pure mesoporous SBA-15 silica was also synthesised for comparison. The morphology and porosity of these materials were explored *via* electron microscopy to confirm successful macropore incorporation. SEM of the undoped SBA-15 reveals a bead-like morphology characteristic of this class of material (Fig. 1).⁴² The addition of PS beads progressively modifies the SBA-15-like organization, creating a new morphology comprising two distinct structures for the intermediate MM-SBA15-1 and MM-SBA15-2 samples, which evolve into a more uniform macroporous network for MM-SBA15-4. The macropores in MM-SBA15-2 and MM-SBA15-4 are very regular, with average diameters around 300 nm, close to the parent PS bead dimensions. This contrasts with previous reports³³ wherein notable macropore shrinkage was observed after calcination, and likely reflects the slower heating rate used in the present study. It is also interesting to note that the

macropores are open and interconnected and thus well-suited to promote rapid through particle diffusion.

Mesopore character was evaluated by TEM which shows that the typical 2D periodic hexagonal structure of SBA-15 was retained in all cases, while the introduction of macropores, as anticipated (and desired) breaks up extended mesoporous channels. Fig. 2a demonstrates how the macropore framework silica is composed of highly-organized concentric mesoporous channels, resulting from self-assembly of the block copolymer solution around polystyrene beads. Hexagonal ordering of the mesopore channels is also clearly visible at higher magnification (Fig. 2b and 2c), with a mean lattice parameter (a_0) of 11.2 nm measured for the purely mesoporous SBA-15, and a slight decrease to 10.0 nm observed as the degree of macroporosity increases.† The high curvature of mesoporous channels in MM-SBA-4 suggests that strong electrostatic and hydrogen-bonding interactions³¹ between polystyrene beads, the block co-polymer and silica precursor promote self assembly of templated, mesostructured channels around the physical PS bead template. This curvature, presumably arising from strain on the block co-polymer layers of the liquid crystal template phase in conforming to the PS bead morphology, may account

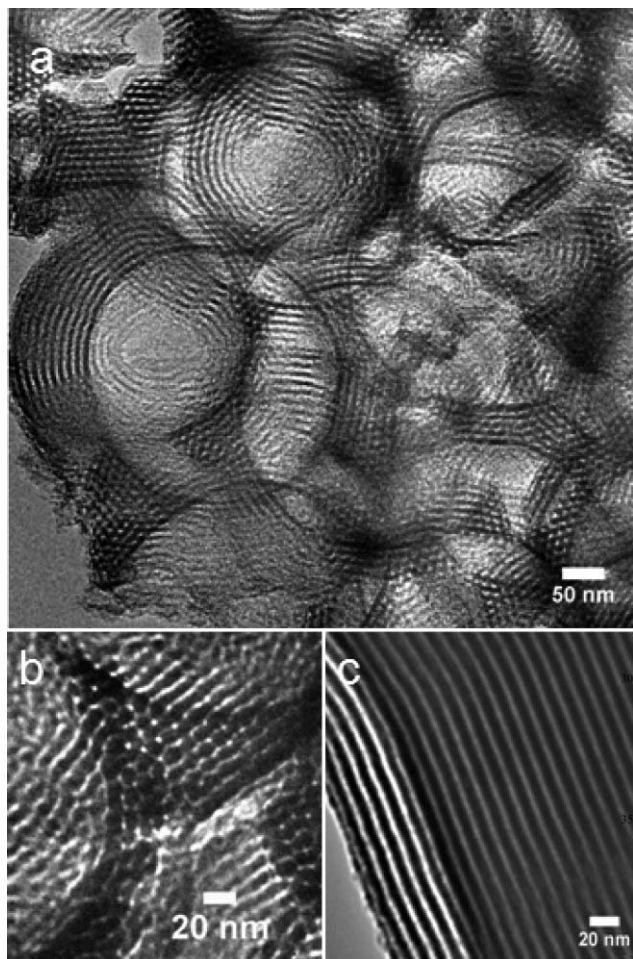


Fig. 2 HRTEM of: a) hierarchical macro and mesopore structures in MM-SBA15-4; b) high resolution image of hexagonal mesoporous arrays in MM-SBA15-4 and c) mesoporous channels in MM-SBA15-2.

for the slightly contracted mesoporous channels observed in the hierarchical materials (Figure S4†).

Long range ordering and porosity were subsequently investigated by XRD and N_2 porosimetry. Fig. 3 presents low angle diffraction patterns which evidence a major reflection at $2\theta \sim 0.9^\circ$ for all samples, characteristic of a periodic mesopore framework. Calcined SBA-15 material exhibits well defined peaks at 0.98 , 1.57 and 1.81° , associated with the (100), (110) and (200) planes of the P6mm space group for the hexagonal arrangement of mesoporous channels.^{39,43,44} Macropore incorporation slightly shifts diffraction peaks to higher angles, corresponding to a contraction in the mesopore lattice parameter from 11.2 to 10 nm. Increasing PS loading is also accompanied by attenuation and broadening of the d_{100} peak; line broadening analysis (Table 1) indicates a progressive decrease in the average mesopore domain size from 98 to 35 nm upon macropore inclusion, consistent with localisation of mesopore domains solely in the walls of the macropore framework as observed by HRTEM (Fig. 2a). Porosimetry shows all materials exhibit Type IV adsorption isotherms with type-H1 hysteresis loops characteristic of bottlenecked pore openings evident in Fig. 4. The loop size decreases with increasing macropore character, which may be accounted for by disruption of extended mesopore networks⁴⁵ that typically limit diffusion and impart hysteresis in the desorption isotherm branch. Additional prominent hysteresis observed above $P/P_0 = 0.9$ for MM-SBA15-4 is attributed to the high concentration of

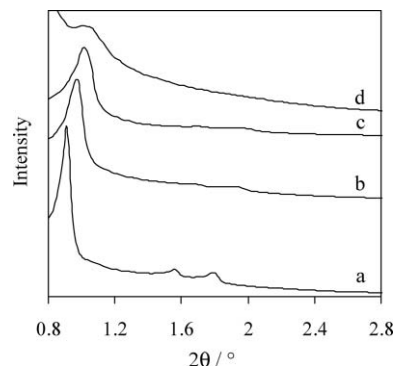


Fig. 3 Low angle powder XRD patterns of: a) SBA-15; b) MM-SBA15-1; c) MM-SBA15-2 and d) MM-SBA15-4 hierarchical macroporous-mesoporous silicas.

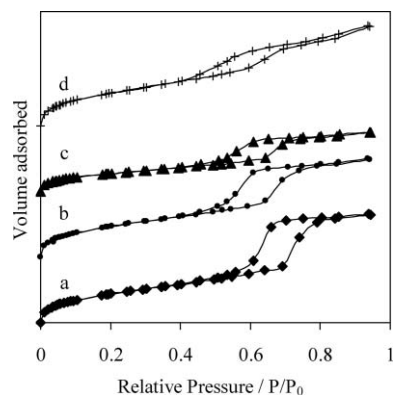


Fig. 4 Nitrogen adsorption-desorption isotherms of a) SBA-15; b) MM-SBA15-1; c) MM-SBA15-2 and d) MM-SBA15-4 hierarchical macroporous-mesoporous silicas.

Table 1 Physical and structural properties of selected *meso* and macro-mesoporous silica

Sample	Surface area ^a /m ² g ⁻¹	Mesopore volume ^b /cm ³ g ⁻¹	BJH pore diameter ^c /nm	d ₁₀₀ ^d /nm	Wall thickness ^e /nm	Mesopore domain size ^f /nm
SBA-15	974	1.08 (1.18)	5.8	9.73	5.4	98.2
MM-SBA15-1	976	0.82 (1.07)	5.0	9.17	5.6	74.3
MM-SBA15-2	971	0.87 (0.99)	4.5	8.68	5.0	55.2
MM-SBA15-4	938	0.84 (1.15)	3.9	8.68	6.1	34.6

^a Evaluated by multi-point BET method. ^b BJH mesopore volumes from the desorption isotherm, and total pore volume shown in brackets. ^c BJH average pore diameters from desorption isotherm. ^d Interlayer spacing derived from Bragg's Law. ^e Wall thickness = $(2d_{100}/\sqrt{3}) - \text{pore diameter}$. ^f Calculated from Scherrer equation.

macropores interconnected *via* bottlenecks.⁴⁵ Porosimetry also confirms shrinkage of the mesopore diameter with increased macropore character, shown in Fig. 5.

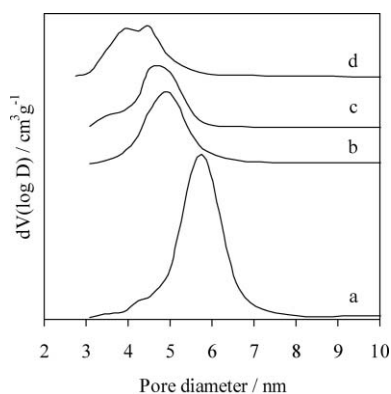


Fig. 5 BJH pore size distributions of a) SBA-15; b) MM-SBA15-1; c) MM-SBA15-2 and d) MM-SBA15-4 hierarchical macroporous-mesoporous silicas.

These textural properties are summarized in Table 1. Conventional mesoporous SBA-15 has a high specific surface area of 974 m²g⁻¹ and pore volume of 1 cm³g⁻¹, in good agreement with the literature.^{9,39,40} Comparable high surface areas are achieved for all the bi-modal MM-SBA15 materials, although the relative mesopore volume decreases from 92 to 73% with increasing macropore density, in line with expectations. The mesopore walls thicken slightly following co-templating with PS beads, demonstrating that the mesostructure is not degraded during removal of the macropore template, and may even possess greater mechanical stability than their pure mesoporous SBA-15 counterpart.

Sulfonic acid functionalization

Successful grafting of mercaptopropyl thiol groups on these macroporous-mesoporous SBA-15 analogues, and their subsequent oxidation to yield tethered sulfonic acid centres, was subsequently assessed *via* XRF, TGA and XPS (Table 2). Elemental analysis reveals the bulk S content ranges between 1.2 and 1.8 wt% across the series, increasing with total surface area. These values are typical for grafted sulfonic acid silicas,^{40,46} and equate to a sulfonic acid surface site density of ~0.24–0.35 nm⁻². In every case, surface sensitive S 2p XP spectra reveal the presence of a single sulfur chemical environment with a binding

Table 2 Sulfur and sulfonic acid content of functionalized materials evaluated by different techniques

Sample	S content ^a wt %	RSO ₃ H site density ^b /nm ²
RSO3-SBA-15	1.8 (1.90)	0.35
RSO3-MM-SBA15-1	1.2 (1.14)	0.22
RSO3-MM-SBA15-2	1.0 (0.98)	0.20
RSO3-MM-SBA15-4	1.2 (1.12)	0.24

^a TGA values shown in brackets. ^b Based on mean S content from TGA and XRF.

energy of 169.9 eV following peroxide treatment, indicative of complete thiol oxidation to sulfonic acid (Figure S5†).

TGA was also performed to quantify the sulfonic acid loading and thermal stability of untreated and functionalized silicas (Fig. 6). SBA-15 tethered mercaptopropyl groups are known to decompose by 350 °C,⁴⁷ whereas propylsulfonic acid moieties are stable until 450 °C,⁴³ at which point they decompose evolving C₃H₆, SO₂ and H₂O.⁴⁸ No major weight loss occurred below 450 °C for any of the functionalized materials, confirming complete conversion of grafted thiols into the desired sulfonic acid groups. The loss between 400 and 500 °C, and corresponding calculated total S content shown in Table 2, is in good agreement with the degree of sulfonation predicted by XRF. Although the absolute S content is expected to reflect changes in the total surface area across these different porous solids, if the inherent properties of the exposed silica surface remain identical then one would anticipate a constant surface density of grafted groups. The fall in sulfonic acid group surface density on transition from mesoporous to dual-templated SBA-15 silicas is therefore likely associated with the longer

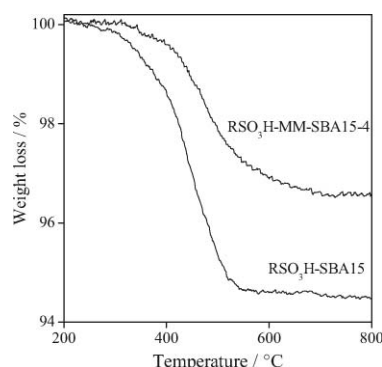


Fig. 6 TGA profiles of sulfonic acid functionalized SBA-15 and MM-SBA15-4 hierarchical macroporous-mesoporous silicas.

calcination protocol required to synthesise the MM-SBA-15 family, and concomitant lower surface hydroxyl density for subsequent thiol grafting.

It is important to note that the SBA-15 and MM-SBA15 materials retained their structural integrity post-functionalization. Porosimetry and XRD (Figures S6 and S7†) demonstrate the mesopore network is essentially unchanged by sulfonic acid grafting, while SEM confirms no impact on the longer range macroporosity (Fig. 7).

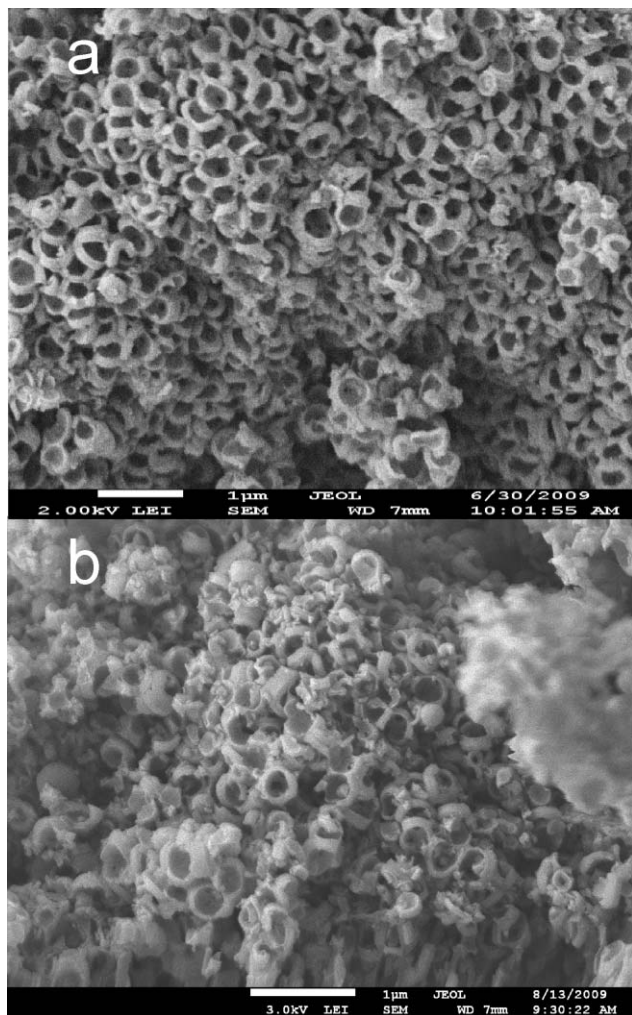
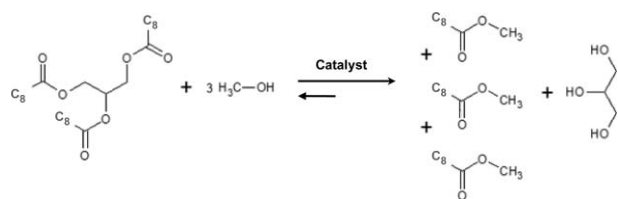


Fig. 7 SEM images of (a) as-prepared and (b) sulfonic acid functionalized MM-SBA15-4 hierarchical macroporous-mesoporous silicas.

Catalytic reactivity

The efficacy of SBA-15 and MM-SBA15 sulfonic acid silicas was subsequently evaluated towards the transesterification of tricaprylin, a bulky C_8 TAG, and separate esterification of palmitic acid (a C_{16} saturated FFA), with methanol (Scheme 1). These chemistries represent the two key steps necessary for the development of a heterogeneous biodiesel manufacturing process, namely the removal of FFA impurities and subsequent transformation of remaining TAGs through to fatty acid methyl esters.



Scheme 1 Transesterification of tricaprylin to fatty acid methyl esters and glycerol using methanol.

Steric factors render tricaprylin difficult to transesterify using conventional solid acid catalysts,^{10,49} wherein diffusion-limited kinetics are observed, making it an ideal model TAG with which to assess potential benefits of the hierarchical solid acids designed in this work. All samples proved active for tricaprylin transesterification, albeit at a low level under these mild conditions with only ~0.2 mmol converted after 6 h. Similar low conversions are common in solid acid catalysed transesterification at low temperature.^{50,51} Higher conversions were attained at elevated temperature (which necessitated autoclave operation under autogeneous conditions to prevent solvent loss), however the primary goal of this work was not to optimise FAME yields, hence of greater interest is the impact of macropores upon the initial reaction rate and concomitant turnover frequency (TOF, calculated on a per SO_3H site basis). Fig. 8 reveals a striking enhancement in the rate of transesterification as a function of increasing macropore density. The sulfonated MM-SBA15-4 material is more than twice as active as the corresponding sulfonated mesoporous SBA-15, despite its lower total surface area and pore volume. We attribute this enhanced reactivity to the greater accessibility of sulfonic acid sites within the mesopores of MM-SBA15-X materials. This improved mass-transport throughout the pore network could arise in two different ways. First, the interpenetrating macropores could simply act as large conduits to boost tricaprylin bulk diffusion throughout catalyst particles. Alternatively, by breaking up the mesopore domain size, macropore incorporation may increase the density of *accessible* sulfonic acid active sites which are likely located at the entrances to these mesopores. Smaller mesopore domains arising in the latter scenario would result in a higher *local density* of such accessible active sites per mesopore volume. In light of the strong interdependence between macropore content and mesopore domain size (the latter accounting for the majority of active surface acid sites) we cannot easily discriminate these two possible mechanisms and are therefore

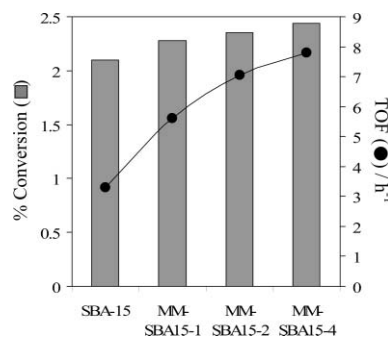


Fig. 8 Tricaprylin transesterification with MeOH over hierarchical macro-mesoporous SBA-15 sulfonic acid silicas. Conversions after 6 h at 60 °C.

currently undertaking molecular dynamics simulations to better understand and optimise TAG diffusion *via* tuning the relative macropore *versus* mesopore diameters.

Similar benefits were conferred by macropores in the esterification of palmitic acid over these hierarchical sulfonic acid silicas (Fig. 9). For all materials, conversions were far superior to those observed during the transesterification, as is well established in the literature, reaching 55% after 6 h using the sulfonated MM-SBA15-4 catalyst. The associated TOFs reveal a similar progressive increase with rising macroporosity, with esterification proceeding 50% faster over the acid modified MM-SBA15-4 than its SBA-15 counterpart.

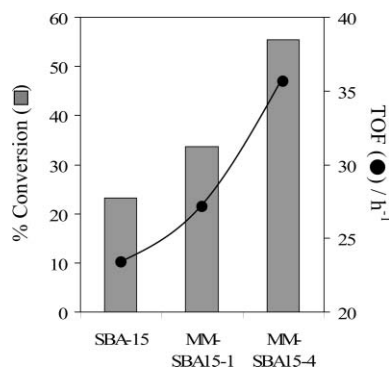


Fig. 9 Palmitic acid esterification with MeOH over hierarchical macroporous SBA-15 sulfonic acid silicas. Conversions shown after 6 h at 60 °C.

We are also investigating functionalization of this macroporous–mesoporous SBA-15 family with more active surface acid and base species to further promote plant oil transesterification and esterification.

Conclusions

Macroporous SBA-15 were synthesized *via* a simple protocol, using polystyrene bead templates, in order to improve diffusion of bulk molecules such as long-chain triglycerides and free fatty acids. PS/TEOS ratios of 2/1 and 4/1 lead to a meso-macroporous interconnected network of high specific surface area. TOFs evaluated from tricaprylin methanolysis catalysed by these sulfonic-acid functionalized silicas show that macropores enhance reactivity. These materials could provide a solution to mass-transport limitations encountered in industry when producing biodiesel from bulky plant oils *via* heterogeneous catalysis. Our preliminary study provides a new illustration of how tailoring the physical properties of solids can improve their catalytic application.

Acknowledgements

We thank the Engineering and Physical Sciences Research Council for financial support (EP/F063423/1; EP/G007594/1) and the award of a Leadership Fellowship (A.F.L.).

Notes and references

1 International Energy Agency, *World Energy Outlook 2007 - Executive Summary*, IEA publications, 2007.

- S. Pinzi, I. L. Garcia, F. J. Lopez-Gimenez, M. D. Luque de Castro, G. Dorado and M. P. Dorado, *Energy Fuels*, 2009, **23**, 2325.
- M. Lapuerta, O. Armas and J. Rodríguez-Fernández, *Prog. Energy Combust. Sci.*, 2008, **34**, 198.
- A. Demirbas, *Energy Convers. Manage.*, 2009, **50**, 14.
- K. Narasimharao, A. F. Lee and K. Wilson, *J. Bio. Mater. Bioenergy*, 2007, **1**, 19.
- A. Sivasamy, K. Y. Cheah, P. Fornasiero, F. Kemausuor, S. Zinoviev and S. Miertus, *ChemSusChem*, 2009, **2**, 278.
- Z. X. Wang, J. Zhuge, H. Fang and B. A. Prior, *Biotechnol. Adv.*, 2001, **19**, 201.
- N. R. Soriano Jr, R. Venditti and D. S. Argyropoulos, *Fuel*, 2009, **88**, 560.
- S. Miao and B. H. Shanks, *Appl. Catal., A*, 2009, **359**, 113.
- E. Lotero, Y. Liu, D. E. López, K. Suwannakarn, D. A. Bruce and J. G. Jr Goodwin, *Ind. Eng. Chem. Res.*, 2005, **44**, 5353.
- M. Di Serio, R. Tesser, L. Pengmei and E. Santacesaria, *Energy Fuels*, 2008, **22**, 207.
- M. Zabeti, W. M. A. W. Daud and M. K. Aroua, *Fuel Process. Technol.*, 2009, **90**, 770.
- E. Leclercq, A. Finiels and C. Moreau, *J. Am. Oil Chem. Soc.*, 2001, **78**, 1161.
- Y. Liu, E. Lotero, J. G. Jr Goodwin and C. Lu, *J. Catal.*, 2007, **246**, 428.
- M. Kouzu, T. Kasuno, M. Tajika, S. Yamanaka and J. Hidaka, *Appl. Catal., A*, 2008, **334**, 357; M. Verziu, B. Cojocaru, J. Hu, R. Richards, C. Ciuculescu, P. Filip and V. I. Parvulescu, *Green Chem.*, 2008, **10**, 373.
- R. S. Watkins, A. F. Lee and K. Wilson, *Green Chem.*, 2004, **6**, 335.
- J. M. Montero, P. L. Gai, K. Wilson and A. F. Lee, *Green Chem.*, 2009, **11**, 265.
- Y. Liu, E. Lotero, J. G. Jr Goodwin and X. Mo, *Appl. Catal., A*, 2007, **331**, 138; D. G. Cantrell, L. J. Gillie, A. F. Lee and K. Wilson, *Appl. Catal., A*, 2005, **287**, 183.
- K. Wilson, C. Hardacre, A. F. Lee, J. M. Montero and L. Shellard, *Green Chem.*, 2008, **10**, 654.
- D. E. De Vos and P. A. Jacobs, *Microporous Mesoporous Mater.*, 2005, **82**, 293.
- D. Zhao, Q. Huo, J. Feng, B. F. Chmelka and G. D. Stucky, *J. Am. Chem. Soc.*, 1998, **120**, 6024.
- Y. Chen, J. Han and H. Zhang, *Appl. Surf. Sci.*, 2007, **253**, 9400.
- S. Garg, K. Soni, G. M. Kumaran, R. Bal, K. Gora-Marek, J. K. Gupta, L. D. Sharma and G. M. Dhar, *Catal. Today*, 2009, **141**, 125.
- I. K. Mbaraka, D. R. Radu, V. S. Y. Lin and B. H. Shanks, *J. Catal.*, 2003, **219**, 329.
- E. Li and V. Rudolph, *Energy Fuels*, 2008, **22**, 145.
- S. Gheorghiu and M. O. Coppens, *AIChE J.*, 2004, **50**, 812.
- A. Imhof and D. J. Pine, *Nature*, 1997, **389**, 948; W. Deng, M. W. Toepke and B. H. Shanks, *Adv. Funct. Mater.*, 2003, **13**, 61; Z. Y. Yuan and B. L. Su, *J. Mater. Chem.*, 2006, **16**, 663.
- X. Zhang, F. Zhang and K. Y. Chan, *Mater. Lett.*, 2004, **58**, 2872.
- O. Sel, D. Kuang, M. Thommes and B. Smarsly, *Langmuir*, 2006, **22**, 2311.
- J. H. Sun, Z. Shan, T. Maschmeyer and M. O. Coppens, *Langmuir*, 2003, **19**, 8395.
- J. S. Yun and S. K. Ihm, *J. Phys. Chem. Sol.*, 2008, **69**, 1133.
- C. G. Oh, Y. Baek and S. K. Ihm, *Adv. Mater.*, 2005, **17**, 270.
- T. Sen, G. J. T. Tiddy, J. L. Casci and M. W. Anderson, *Chem. Mater.*, 2004, **16**, 2044.
- J. P. Blitz, and C. P. Little, *Fundamentals and Applied Aspects of Chemically Modified Surfaces*, Royal Society of Chemistry, 1999, 235.
- W. M. Van Rhijn, D. E. De Vos, B. F. Sels, W. D. Bossaert and P. A. Jacobs, *Chem. Comm.*, 1998, 317.
- W. D. Bossaert, D. E. De Vos, W. M. Van Rhijn, J. Bullen, P. J. Grobet and P. A. Jacobs, *J. Catal.*, 1999, **182**, 156.
- I. Diaz, C. Marquez-Alvarez, F. Mohino, K. Prez-Pariente and E. Sastre, *J. Catal.*, 2000, **193**, 283.
- S. Vaudreuil, M. Bousmina, S. Kaliaguine and L. Bonnevot, *Adv. Mater.*, 2001, **13**, 1311.
- D. Zhao, J. Feng, Q. Huo, N. Melosh, G. H. Fredrickson, B. F. Chmelka and G. D. Stucky, *Science*, 1998, **279**, 548.
- P. F. Siril, N. R. Shiju, D. R. Brown and K. Wilson, *Appl. Catal. A*, 2009, **364**, 95.

- 41 R. I. Kureshy, I. Ahmad, K. Pathak, N. H. Khan, S. H. R. Abdi and R. V. Jasra, *Catal. Commun.*, 2009, **10**, 572.
- 42 P. Lanzafame, S. Perathoner and G. Centi, *J. Porous Mater.*, 2007, **14**, 305.
- 43 D. Margolese, J. A. Melero, S. C. Christiansen, B. F. Chmelka and G. D. Stucky, *Chem. Mater.*, 2000, **12**, 2448.
- 44 J. J. Chiu, D. J. Pine, S. T. Bishop and B. F. Chmelka, *J. Catal.*, 2004, **221**, 400.
- 45 I. Nowak, *Col. Surfa. A*, 2004, **241**, 103.
- 46 A. F. Lee, and K. Wilson, 'Chapter 2: Sol-gel sulfonic acid silicas as catalysts' in *Handbook of Green Chemistry - Green Catalysis*, Edited by P. T. Anastas & R. H. Crabtree, Wiley-VCH, 2009, **2**.
- 47 D. Das, J. F. Lee and S. Cheng, *J. Catal.*, 2004, **223**, 152.
- 48 K. Wilson, A. F. Lee, D. J. Macquarrie and J. H. Clark, *Appl. Catal. A*, 2001, **5913**, 1.
- 49 X. Mo, D. E. López, K. Suwannakarn, Y. Liu, E. Lotero, J. G. Jr Goodwin and C. Lu, *J. Catal.*, 2008, **254**, 332.
- 50 L. Guerreiro, J. E. Castanheiro, I. M. Fonseca, R. M. Martin-Aranda, A. M. Ramos and J. Vital, *Catal. Today*, 2006, **118**, 166.
- 51 D. E. López, J. G. Jr Goodwin, D. A. Bruce and E. Lotero, *Appl. Catal. A*, 2005, **295**, 97.

Fischer indole synthesis in water: simple, efficient preparation of naltrindole, naltriben and analogs†

Romain A. Duval^{a,b} and John R. Lever^{*a,b,c}

Received 6th October 2009, Accepted 17th November 2009

First published as an Advance Article on the web 7th January 2010

DOI: 10.1039/b920864j

Naltrindole, naltrindole analogs and the benzofuran congener naltriben have been prepared by Fischer syntheses using mildly acidic, purely aqueous conditions. The preparation of naltrindole and several analogs was accomplished under almost neutral conditions using just the hydrochloride salts of naltrexone and various electron-rich and electron-poor phenylhydrazines in boiling water. The products were obtained by simple filtration in good to excellent yields and with high purities in the majority of cases. The route is suited to gram-scale synthesis, does not require the use of organic solvents, minimizes the use of corrosive acids, and is simple, efficient and environmentally friendly. Naltriben was prepared efficiently from the hydrochloride salts of naltrexone and *O*-phenylhydroxylamine but more forcing conditions, 6.0 N HCl, were required. A limitation to the method is the failure of Fischer cyclization between naltrexone and nitro-substituted phenylhydrazines under aqueous conditions.

Introduction

Since their development by the Portuguese group, naltrindole¹ (NTI, **1**) and its benzofuran congener naltriben² (NTB, **2**) have become valuable tools for studies of opioid receptor pharmacology (Fig. 1). These potent and selective δ opioid receptor antagonists were designed from the peptide enkephalin using the message-address concept.^{1,2} Tritiated NTI is routinely used for δ opioid receptor binding assays *in vitro*,³ while tritiated NTI analogs and tritiated NTB have been used for *in vivo* studies of cerebral δ opioid receptors in rodents.⁴ Moreover, a number of NTI analogs have been labeled with positron- and single photon-emitting radionuclides for non-invasive imaging.⁵ In fact, carbon-11 labeled *N*1'-methyl-NTI⁶ (Fig. 1) is in use for clinical positron emission tomography (PET) imaging studies of the δ opioid receptors expressed by normal brain^{7a} and heart,^{7b} as well as the δ sites expressed by the primary tumors of certain breast^{8a} and lung cancer patients.^{8b} In our laboratories, an area of current interest is the development of radiometal-labeled, macrocyclic conjugates of NTI (Fig. 1) for studies of the peripheral δ opioid receptors expressed by some normal organs and certain cancers.⁹ Although small samples of NTI and NTB for pharmacology studies are commercially available, continued advances in the field would be facilitated by simple, scalable

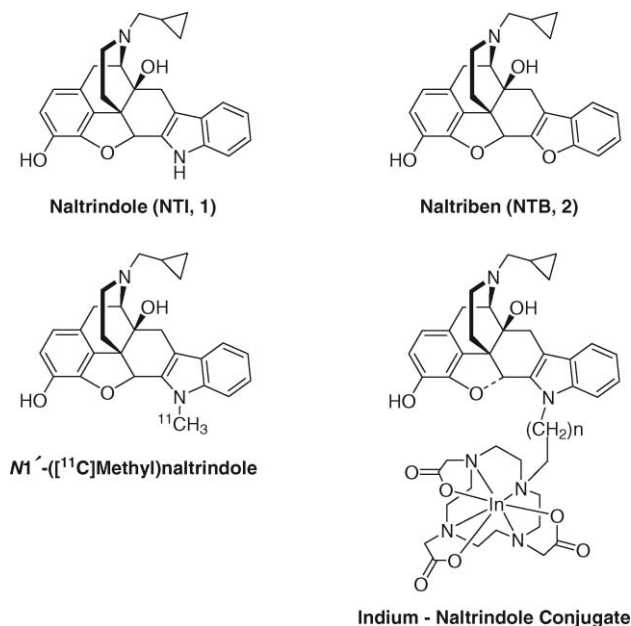


Fig. 1 Naltrindole, naltriben and selected analogs.

and environmentally friendly methods for preparation of gram quantities of NTI, NTB and analogs for synthetic elaborations and pharmacological evaluations.¹⁰

NTI and derivatives having a variety of substituents have been obtained in moderate to good yields by Fischer cyclizations between naltrexone (NTX), a ketonic 4,5 α -epoxymorphinan, and various phenylhydrazines as exemplified in Scheme 1.^{1,4a,10} Similarly, NTB and analogs have been obtained by using NTX and *O*-phenylhydroxylamines.^{2,10} These reactions use strongly acidic conditions, such as concentrated HCl or methanesulfonic acid, and take place at elevated temperatures in organic solvents, such as refluxing ethanol or acetic acid. A milder variant using

^aDepartment of Radiology and the Radiopharmaceutical Sciences Institute, University of Missouri, Columbia, Missouri, 65212.

E-mail: leverj@health.missouri.edu; Fax: (573) 814-6551; Tel: (573) 814-6000 ext. 53686

^bResearch Service, Harry S. Truman Veterans Administration Medical Center, Columbia, Missouri, 65201

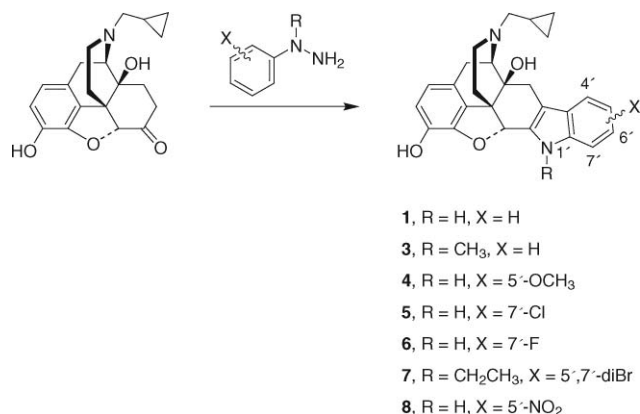
^cDepartment of Medical Pharmacology and Physiology, University of Missouri, Columbia, Missouri, 65212

† Electronic supplementary information (ESI) available: Further experimental details, spectroscopic analyses, and reversed-phase HPLC conditions, retention times and capacity factors. See DOI: 10.1039/b920864j

Table 1 Exploratory screening of conditions for Fischer synthesis of NTI (**1**)

^a Reactants	^b Conditions	^c Product(s)	^c Conversion (%)
NTX·HCl, Phenylhydrazine·HCl	Amberlyst-15 [®] , toluene	^d NTX-phenylhydrazone	~100
NTX·HCl, Phenylhydrazine·HCl	Amberlyst-15 [®] , CH ₃ OH	NTI	~100
NTX·HCl, Phenylhydrazine·HCl	0.01 - 6 N HCl	NTI	~100
NTX·HCl, Phenylhydrazine·HCl	H ₂ O	NTI	~100
NTX base, Phenylhydrazine·HCl	H ₂ O	NTI	~ 50
		^d NTX-phenylhydrazone	~ 50

^a NTX·HCl (10 mg, 25 μmol) and phenylhydrazine·HCl (1.2 equiv). ^b Reflux, 1.5 h. ^c Product assignments and estimates of conversion are from visual inspection of analytical silica gel TLC of reaction mixtures as compared to standard samples of reactants and products. TLC used cyclohexane/EtOAc (25/75) containing 1% triethylamine: *R_f* 0.41, NTX; *R_f* 0.29, NTI; *R_f* 0.51, NTX-phenylhydrazone. ^d NTX-phenylhydrazone was identified in the crude mixtures by HRMS (ESI): calcd for C₂₆H₃₀N₃O₃ [M+H]⁺ 432.2287; found 432.2271.

**Scheme 1** Fischer synthesis of naltrindole and analogs from naltrexone.

just 2 equivalents of *p*-toluenesulfonic acid in ethanol at reflux has been reported for the Fischer synthesis of several NTI analogs.^{10c,d} Overall, fairly harsh conditions are typical for the classical Fischer indole synthesis.¹¹

Recently, a variety of synthetic modifications have been introduced to increase the practicality, and to lessen the environmental impact, of the Fischer cyclization. This is particularly important from the process chemistry viewpoint.¹² Hazardous materials have been reduced by use of Brønsted or Lewis acids in ionic liquids, followed by filtration or sublimation for product isolation.¹³ Mild solid acids, including zeolites^{14a} and montmorillonite clays,^{14b,c} have been used as catalysts for some Fischer reactions, although organic solvents, such as acetic acid, dihydropyran and aqueous dimethylacetamide, are employed. Zinc chloride has been used successfully in truly catalytic quantities during microwave-assisted Fischer reactions conducted in biodegradable triethyleneglycol.^{15a} The reusable catalysts, Amberlyst-15[®]^{15b} and bismuth nitrate,^{15c} have also been used to promote Fischer indole synthesis in organic solvents.

Here we report “green” Fischer syntheses of NTI and several analogs using essentially neutral and purely aqueous media at reflux. Aqueous mineral acids, however, were required for efficient synthesis of NTB. The majority of reactions led to the targets in good to excellent yields, and furnished compounds of high purity after simple filtration or centrifugation. These economical and efficient methods do not require the use of organic solvents, minimize the use of corrosive acids, and

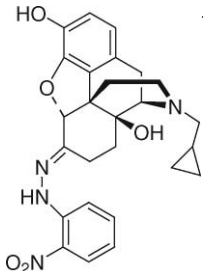
provide an environmentally friendly synthetic approach to this important class of opioid receptor ligands.

Results and discussion

We explored several conditions on a small scale for Fischer synthesis of NTI (**1**) from NTX·HCl and phenylhydrazine·HCl using various acids and solvents at reflux for 1.5 h (Table 1, Scheme 1). Initial studies using the strongly acidic resin Amberlyst-15[®] in refluxing toluene led quantitatively to a non-polar compound that remained stable even during extended reaction times (ca. 10 h). This material was isolated by filtration, and characterized as the phenylhydrazone of NTX by mass spectroscopy. Interestingly, the use of Amberlyst-15[®] in refluxing methanol for 1.5 h gave quantitative conversion to NTI·HCl. Although Amberlyst-15[®] has some advantages as a reusable heterogeneous catalyst, the use of water alone and dilute mineral acids proved simpler and just as efficient. In model reactions, treating NTX·HCl with phenylhydrazine·HCl in aqueous HCl ranging from 0.01 to 6.0 N at reflux for 1.5 h led quantitatively to NTI·HCl by TLC. A 90% yield of NTI·HCl, pure by reversed-phase HPLC, was obtained on a 1.3 mmol scale by using 0.1 N HCl followed by filtration. Similar aqueous conditions, 4% H₂SO₄ at reflux, have previously been employed for Fischer synthesis of various pharmacologically active tryptamines,^{16a,b} and indole analogs of the antipsychotic butyrophenones.^{16c} Next, we investigated the degree of acidity required for NTI synthesis in water. The minimum amount of HCl necessary was found to be just two molar equivalents, corresponding to that provided by the hydrochloride salts of the reactants. Quantitative conversion of NTX·HCl and phenylhydrazine·HCl to NTI·HCl in boiling water was observed by TLC over 1.5 h. By contrast, treating the free base of NTX with phenylhydrazine·HCl under the same conditions for 2.5 h led to a roughly equimolar mixture of NTI and a compound tentatively assigned by mass spectroscopy of the crude mixture as the phenylhydrazone of NTX. Presumably, the phenylhydrazone is formed quantitatively, but one equivalent of HCl is not sufficient to promote isomerization to the ene-hydrazine tautomer necessary for [3,3]-sigmatropic rearrangement to the indole.¹¹

The novel synthesis of NTI using just the hydrochloride salts of the reactants in boiling water is particularly mild, pH ~ 5, and proved efficient and convenient on a preparative scale. We obtained 3.6 g (96%) of pure NTI·HCl (8 mmol) after bringing an equimolar mixture of the salts to reflux and stirring for

Table 2 Preparation of NTI, NTI congeners and NTB in aqueous media at reflux

Reactants	Product	Conditions	% Purity	% Yield Aqueous Conditions	% Yield Classical Conditions
NTX·HCl, Phenylhydrazine·HCl	NTI NTI·HCl 1	H ₂ O, precipitation	99	97	71 ^a
NTX·HCl, 1-Methyl-1-phenylhydrazine	<i>N</i> 1'-Me-NTI·HCl 3	H ₂ O, filtration, 4 °C HCl 0.1 N, centrifugation, 4 °C	99 99	96 73	58 ^a
NTX·HCl, <i>O</i> -Phenylhydroxylamine·HCl	NTB·HCl 2	HCl 0.1 N, evaporation HCl 6.0 N, filtration, 4 °C	98 98	97 93	80 ^e
NTX·HCl, <i>p</i> -Methoxyphenylhydrazine·HCl	5'-OMe-NTI·HCl 4	H ₂ O, centrifugation, 4 °C	95	61	56 ^a
NTX·HCl, <i>o</i> -Chlorophenylhydrazine·HCl	7'-Cl-NTI·HCl 5	HCl 0.1 N, filtration, 4 °C	90	78 ^c	77 ^b
NTX·HCl, <i>o</i> -Fluorophenylhydrazine·HCl	7'-F-NTI·HCl 6	H ₂ O, centrifugation, 4 °C	71	53 ^c	50 ^a
NTX·HCl, <i>N</i> -Ethyl-2,4-dibromophenylhydrazine·HCl	<i>N</i> 1'-Et-5',7'-dibromo-NTI·HCl 7	H ₂ O, extraction and chromatography	98	27	13 ^d
NTX·HCl, <i>o</i> -Nitrophenylhydrazine	 ·HCl 9	HCl 0.1 N, filtration	96	75	---

^a Ref. 1. ^b Present work. ^c Molar yield calculated based on HPLC data as if purification to homogeneity were performed. Isolated yields of stated purity reported for other cases. ^d Ref. 4a. ^e Ref. 2.

45 min, followed by cooling and simple filtration of the product that has low solubility in water (Table 2). Alternatively, the free base of NTI could be prepared, with similar results, by careful addition of solid potassium carbonate to precipitate the product from the hot reaction medium. The method can also be applied to *N*-substituted phenylhydrazines as long as sufficient acid is available. Treatment of NTX·HCl with 1-methyl-1-phenylhydrazine in refluxing HCl (0.1 N) for 90 min, followed by chilling and centrifugation at 4 °C, gave *N*1'-methyl-NTI (**3**) in 73% yield with high purity (Table 2, Scheme 1). Alternatively, **3** was obtained in nearly quantitative yield and with high purity after evaporation of the reaction medium (Table 2). In marked contrast, reaction of NTX·HCl with the free base of 1-methyl-1-phenylhydrazine in plain water was not complete even after extended times. Next, we attempted to obtain NTB (**2**, Fig. 1) from NTX·HCl and phenylhydroxylamine·HCl under aqueous conditions. NTB synthesis in water or dilute HCl proved sluggish. However, NTB·HCl was obtained in 90% yield with 98% purity by using boiling 6.0 N HCl followed by cooling and filtration. This procedure proved more convenient than the use of refluxing methanesulfonic acid for NTB synthesis as previously described.²

To gain insight into the scope and limitations of such aqueous Fischer syntheses, we treated various aryl-substituted phenylhydrazines with NTX·HCl (Table 2, Scheme 1). Treatment of electron-rich *p*-methoxyphenylhydrazine·HCl with NTX·HCl in boiling water gave 5'-OMe-NTI·HCl (**4**) in 61% isolated yield with 95% purity. The yield proved similar to the 56% reported when boiling acetic acid was used,¹ but

without the need for organic solvents or a discrete purification step.

We then examined the reactivity of electron-deficient phenylhydrazines (Table 2). In the halogen series, *o*-chlorophenylhydrazine·HCl reacted with NTX·HCl in boiling water to give 7'-Cl-NTI·HCl (**5**) in 74% yield with 90% purity after filtration. This derivative has not been described previously to our knowledge, so we also used typical Fischer conditions for synthesis. Refluxing NTX·HCl and *o*-chlorophenylhydrazine·HCl in methanol/HCl (g) for 4.5 h, followed by workup and flash chromatography, provided **5** in 54% yield. Thus, synthesis in water and isolation by filtration provides a simpler alternative that gives fairly comparable results. 7'-F-NTI (**6**) was formed as the major product resulting from refluxing NTX·HCl and *o*-fluorophenylhydrazine·HCl in water. However, evaporation followed by HPLC analysis showed only 42% purity and a calculated yield of 49%. Purity was increased to a more acceptable 71% by chilling the mixture and isolating the product by centrifugation in 53% yield. Using methanol/HCl (g) at reflux, **6** was obtained previously in 50% yield after recrystallization.¹

We then explored Fischer cyclization between NTX·HCl and *N*-ethyl-2,4-dibromophenylhydrazine·HCl. This synthesis was best conducted under dilute conditions, and the poorly reactive dihalophenylhydrazine had to be used in two-fold excess to achieve significant conversion. Nonetheless, *N*1'-ethyl-5',7'-dibromo-NTI·HCl (**7**) was obtained after chromatography in 27% yield with >98% purity. Although rigorous purification was required and the isolated yield was low, the results still compare

favorably to the 13% yield reported for preparation of **7** under harsher, classical conditions (concentrated HCl/glacial HOAc) for use as the precursor to [³H]-N1'-Et-NTI·HCl.^{4a}

Fischer synthesis of even simple nitroindoles is difficult, and requires forcing conditions such as polyphosphoric acid or 85% phosphoric acid/toluene at elevated temperatures.¹⁷ Notably, Portoghesi and colleagues were able to prepare 5'-NO₂-NTI (**8**) in 55% yield using concentrated HCl/glacial HOAc at reflux.¹ Treatment of NTX·HCl with *p*-nitrophenylhydrazine failed to provide **8** under a variety of aqueous conditions (0.1 - 12 N HCl, reflux). We then tested the reactivity of NTX·HCl with *o*-nitrophenylhydrazine in boiling 0.1 N HCl and observed a clean reaction by TLC and HPLC. However, the product obtained by filtration and drying was not 7'-NO₂-NTI (R = H, X = 7'-NO₂; Scheme 1), but *o*-nitrophenylhydrazone **9** which was obtained in 71% yield with 96% purity (Table 2). Although phenylhydrazones are intermediates in the Fischer cyclization, this compound could not be forced to cyclize after extended reaction times in aqueous acid. Apparently, reactivity is diminished predominantly by electronic rather than steric effects under aqueous conditions since neither *p*- nor *o*-nitro groups permitted cyclization. Thus, nitro-substituted NTI analogs are best prepared under the classical, harsher conditions.

Conclusion

We have described novel Fischer indole syntheses of NTI, indole ring-substituted NTI analogs, and the benzofuran congener NTB under mildly acidic, purely aqueous conditions. Two equivalents of HCl were required to promote the condensation and rearrangement steps of the Fischer reaction, allowing synthesis of NTI and analogs using just the hydrochloride salts of NTX and the various phenylhydrazines in boiling water. In one case where the HCl salt of the phenylhydrazine was not available, the reaction took place efficiently in dilute HCl (0.1 N). Notably, these mild conditions sufficed for both electron-rich and electron-poor phenylhydrazines, but failed to furnish the corresponding indoles when the phenylhydrazine was substituted with strongly electron-withdrawing nitro groups. With the exception of poorly reactive *N*-ethyl-2,4-dibromophenylhydrazine·HCl, the phenylhydrazines were used in only 2 - 10% molar excess relative to NTX·HCl. Thus, convergent synthesis of more elaborate NTI analogs from NTX using only a slight excess of complex phenylhydrazines from custom synthesis seems feasible. The aqueous Fischer reaction between NTX·HCl and phenylhydroxylamine·HCl to produce NTB·HCl was best accomplished using boiling 6.0 N HCl. The synthesis of NTB analogs from substituted phenylhydroxylamines may also be possible, but was not explored in our study. The Fischer products were easily obtained by filtration or centrifugation due to their insolubility in water with respect to the reactants and byproducts (e.g., NH₄Cl). In the majority of cases, product yields and purities were good to excellent. These mild aqueous conditions provide a simple, efficient, scalable and environmentally friendly alternative to the harsher Fischer conditions typically used for the preparation of NTI, NTB and analogs. Moreover, the use of only the acid salts of Fischer reaction components in water may have a degree of general applicability, and could circumvent

problems encountered under the standard conditions when the product proves acid-sensitive.¹⁸

Experimental

General information

Reagents and solvents were the best grades available, and were used as received. Naltrexone·HCl was obtained from Mallinckrodt, Inc. Naltrindole hydrochloride and naltriben methanesulfonate were purchased as reference standards from Sigma-Aldrich, Inc. Known, but commercially unavailable, naltrindole derivatives were synthesized for reference as described previously.^{1,4a} TLC was done on Macherey-Nagel silica gel 60 UV254 (250 μm) plates. Flash chromatography was conducted with EM Science 9385 silica gel 60 (230 - 400 mesh) under N₂ pressure. Reversed-phase column chromatography was performed under N₂ pressure using C18 (35-75 μm) from Analtech. High resolution mass spectroscopy (HRMS) using electrospray (ESI) mode was done at the University of Minnesota.¹ ¹H NMR spectra were obtained on Bruker spectrometers at 300 MHz. Chemical shifts are parts per million (δ) relative to residual solvent (CHCl₃, 7.24 ppm), or to TMS (0.00 ppm) as an internal standard. Elemental analyses were performed by Atlantic Microlab, Inc.

17-(Cyclopropylmethyl)-6,7-didehydro-4,5α-epoxy-3,14-dihydroxy-indolo[6,7:2',3'] morphinan (naltrindole, NTI, **1). Procedure A (NTI free base).** NTX·HCl (3.00 g, 7.94 mmol) and phenylhydrazine·HCl (1.18 g, 8.08 mmol, 1.02 equiv) were dissolved in water (60 mL) with stirring at ambient temperature. After approximately 5 min a heavy precipitate, presumably the phenylhydrazone, was formed. The mixture was then brought to boiling and a clear yellow solution was obtained. After reflux for 45 min, solid K₂CO₃ (2.00 g, 14.5 mmol) was added cautiously and in small portions. The mixture was then cooled to ambient temperature, and a yellow paste was obtained by filtration. Trituration with water followed by drying *in vacuo* at 45 °C gave NTI·0.7 H₂O (3.32 g, 98%) as a beige powder of 99% purity by reversed-phase HPLC. Characteristic ¹H NMR signals¹ (CDCl₃, 300 MHz): δ 8.15 (s, 1H), 7.39 (d, *J* = 7.8 Hz, 1H), 7.25 (d, *J* = 7.8 Hz, 1H), 7.12 (dd, *J* = 7.2 Hz, *J* = 7.8 Hz, 1H), 7.0 (dd, *J* = 7.2 Hz, *J* = 7.8 Hz, 1H). HRMS (ESI) calcd for C₂₆H₂₇N₂O₃ [M+H]⁺ 415.2022; found: 415.2002. Anal. Calcd for C₂₆H₂₆N₂O₃ · 0.7 H₂O: C, 73.11; H, 6.47; N, 6.56. Found: C, 73.15; H, 6.19; N, 6.63.

Procedure B (NTI·HCl). As described above, NTX·HCl (3.00 g, 7.94 mmol) and phenylhydrazine·HCl (1.18 g, 8.08 mmol) in water (60 mL) were brought to reflux for 45 min. The mixture was cooled to ambient temperature, and then chilled at 4 °C for 1 h. The resulting pale yellow solid was filtered, triturated with ice-cold water, and then dried *in vacuo* at 45 °C to give NTI·HCl·1.8 H₂O (3.57 g, 93%) as a pale beige powder of > 99% purity by reversed-phase HPLC. Anal. Calcd for C₂₆H₂₇ClN₂O₃ + 1.8 H₂O: C, 64.60; H, 6.38; N, 5.80. Found: C, 64.58; H, 6.26; N, 6.17.

17-(Cyclopropylmethyl)-6,7-dehydro-4,5α-epoxy-3,14-dihydroxy-1'-methyl-indolo [6,7:2',3'] morphinan hydrochloride (N1'-methylNTI·HCl, **3). Procedure A (isolation by centrifugation).**

A mixture of NTX·HCl (0.15 g, 0.40 mmol) and 1-methyl-1-phenylhydrazine (50 μ L, 0.052 g, 0.42 mmol) was dissolved in 0.1 N HCl (3 mL) using a 15 mL plastic centrifuge tube as the reaction vessel. After heating in a boiling water bath for 1.5 h, the mixture was cooled to ambient temperature and then chilled at 4 °C for 30 min. After centrifugation (10,000 rpm, 4 °C; 5 min), the supernatant was discarded and the precipitate dried *in vacuo* at 45 °C to furnish *N*1'-Me-NTI·HCl (0.14 g, 73%) as a beige powder of 99% purity by reversed-phase HPLC. Characteristic ¹H NMR signals¹ for the free base (CDCl₃, 300 MHz): δ 7.40 (d, *J* = 7.8 Hz, 1H), 7.23 (d, *J* = 8.2 Hz, 1H), 7.17 (ddd, *J* = 1.0 Hz, *J* = 6.9 Hz, *J* = 8.2 Hz, 1H), 7.0 (ddd, *J* = 1.0 Hz, *J* = 6.9 Hz, *J* = 7.8 Hz, 1H), 3.80 (s, 3H). HRMS (ESI) calcd for C₂₇H₂₉N₂O₃ [M+H]⁺ 429.2173; found: 429.2162. **Procedure B (isolation by evaporation).** As described above, NTX·HCl (0.15 g, 0.40 mmol) and 1-methyl-1-phenylhydrazine (50 μ L, 0.052 g, 0.42 mmol) in 0.1 N HCl (3 mL) were heated in a boiling water bath for 1.5 h, and then cooled to ambient temperature. The entire reaction mixture was evaporated to dryness under reduced pressure, and then dried *in vacuo* at 45 °C to furnish *N*1'-Me-NTI·HCl (0.20 g, 97%) as a beige powder of 98% purity by reversed-phase HPLC.

17-(Cyclopropylmethyl)-6,7-didehydro-4,5 α -epoxy-3,14-dihydroxy-benzo[*b*]furano [6,7:2',3'] morphinan hydrochloride (naltrexen hydrochloride, NTB·HCl, 2). A mixture of NTX·HCl (1.13 g, 3.00 mmol) and *O*-phenylhydroxylamine·HCl (0.46 g, 3.16 mmol, 1.05 equiv) in 6.0 N HCl (30 mL) was refluxed for 4 h. The reaction was cooled to ambient temperature, and then refrigerated at 4 °C overnight. The precipitate was collected by filtration, and washed with ice-cold 6.0 N HCl until the filtrate was colorless. The solid was dried *in vacuo* at 45 °C to furnish NTB·HCl (1.26 g, 93%) as a pale brown powder of 98% purity by reversed-phase HPLC. Characteristic ¹H NMR signals² for the free base (CDCl₃, 300 MHz): δ 7.42 (d, *J* = 8.1 Hz, 1H), 7.37 (d, *J* = 7.4 Hz, 1H), 7.25 (ddd, *J* = 1.3 Hz, *J* = 7.2 Hz, *J* = 8.1 Hz, 1H), 7.15 (ddd, *J* = 0.9 Hz, *J* = 7.2 Hz, *J* = 7.4 Hz, 1H). HRMS (ESI) calcd for C₂₆H₂₆NO₄ [M+H]⁺ 416.1862; found: 416.1869.

17-(Cyclopropylmethyl)-6,7-didehydro-4,5 α -epoxy-3,14-dihydroxy-7'-chloro-indolo[6,7:2',3'] morphinan (7'-chloronaltrexone, 7'-Cl-NTI, 5). **Procedure A (classical Fischer conditions, free base).** A mixture of NTX·HCl (0.75 g, 2.0 mmol) and 2-chlorophenylhydrazine·HCl (0.54 g, 3.0 mmol) was dissolved in MeOH (20 mL) that had been treated with HCl (g) to 10% by weight. After reflux under nitrogen for 4.5 h, the reaction mixture was cooled, and solvent removed under reduced pressure. The residue was dissolved in MeOH, and then partitioned between EtOAc and saturated Na₂CO₃. The combined organic extracts were dried (Na₂SO₄), filtered and concentrated under reduced pressure. The residue was purified by flash chromatography using a gradient of hexane/EtOAc (70/30) containing 2 - 10% MeOH and 2% triethylamine to give 0.72 g (77%) of 7'-Cl-NTI monohydrate as a yellow powder (mp 240 °C, dec). ¹H NMR (CDCl₃, 300 MHz): δ 8.52 (s, 1H), 7.27 (d, *J* = 9.0 Hz, 1H), 7.09 (d, *J* = 7.5 Hz, 1H), 6.91 (t, *J* = 7.7 Hz, 1H), 6.62 (d, *J* = 8.1 Hz, 1H), 6.54 (d, *J* = 8.1 Hz, 1H), 5.67 (s, 1H), 5.23 (br. s, 1H), 3.37 (d, *J* = 6.1 Hz), 3.13 (d, *J* = 18.5 Hz, 1H), 2.86 (d, *J* = 15.5 Hz, 1H), 2.81 - 2.73 (m, 2H), 2.63 (d, *J* = 15.5 Hz, 1H), 2.49 - 2.25 (m, 4H), 1.77 (d, *J* = 11.8 Hz, 1H) 1.26 (br s, 1H), 0.89 (m, 1H), 0.57 (d, *J* = 7.3 Hz, 2H), 0.17 (d, *J* = 4.6 Hz, 2H). Anal. Calcd

for C₂₆H₂₅ClN₂O₃ · H₂O: C, 66.88; H, 5.82; N, 6.00. Found: C, 67.29; H, 5.54; N, 5.93. **Procedure B (aqueous Fischer conditions, HCl salt):** A mixture of NTX·HCl (0.15 g, 0.40 mmol) and 2-chlorophenylhydrazine·HCl (0.080 g, 0.44 mmol) was dissolved in water (3.0 mL) using a 15 mL plastic centrifuge tube as the reaction vessel. After heating in a boiling water bath for 1.5 h, the mixture was cooled to ambient temperature and then chilled at 4 °C for 30 min to give a brown precipitate. After centrifugation (10,000 rpm, 4 °C; 5 min), the supernatant was discarded and the precipitate suspended in ice-cold 0.1 N HCl (2 mL), vortexed thoroughly, and then centrifuged again. This process was repeated three times, and the solid was then dried *in vacuo* at 45 °C to furnish 7'-Cl-NTI·HCl·0.4 H₂O (0.16 g) as a brown powder of 90% purity by reversed phase HPLC in an effective 78% molar yield when adjusted for purity. ¹H NMR data obtained for the free base as reported in Procedure A above. HRMS (ESI) calcd for C₂₆H₂₆ClN₂O₃ [M+H]⁺ 449.1626; found: 449.1618. Anal. Calcd for C₂₆H₂₅ClN₂O₃ · 0.4 H₂O: C, 68.46; H, 5.70; N, 6.14, Cl, 7.77. Found: C, 68.43; H, 6.25; N, 6.46, Cl, 7.92.

17-(Cyclopropylmethyl)-4,5 α -epoxy-3,14-dihydroxymorphinan-6-one, (E)-2-nitrophenylhydrazone hydrochloride (naltrexone *o*-nitrophenylhydrazone·HCl, 9). A mixture of NTX·HCl (0.15 g, 0.40 mmol) and *o*-nitrophenylhydrazine (0.065 g, 0.41 mmol, 1.03 equiv) in 0.1 N HCl (3 mL) was refluxed for 1.5 h, and then cooled to ambient temperature. The bright orange paste was collected by filtration, and washed with 0.1 N HCl until the filtrate was pale yellow. The solid was dried *in vacuo* at 45 °C to furnish the monohydrate of the title compound (0.16 g, 75%) as a yellow powder of 96% purity by reversed-phase HPLC. ¹H NMR (free base, CDCl₃, 300 MHz): δ 12.74 (s, 1H), 8.11 (dd, *J* = 1.2 Hz, *J* = 7.6 Hz, 1H), 7.77 (dd, *J* = 1.2 Hz, *J* = 8.5 Hz, 1H), 7.47 (ddd, *J* = 1.2 Hz, *J* = 7.0 Hz, *J* = 7.6 Hz, 1H), 6.77 (ddd, *J* = 1.2 Hz, *J* = 7.0 Hz, *J* = 8.5 Hz, 1H), 6.69 (d, *J* = 8.1 Hz, 1H), 6.59 (d, *J* = 8.1 Hz, 1H), 5.49 (bs, 1H), 5.36 (s, 1H), 5.13 (bs, 1H), 3.15 (d, *J* = 6.1 Hz, 1H), 3.03 (d, *J* = 18.5 Hz, 1H), 2.94 (m, 1H), 2.70 (dd, *J* = 4.3 Hz, *J* = 11.9 Hz, 1H), 2.58 (dd, *J* = 6.1 Hz, *J* = 18.5 Hz, 1H), 2.46 (m, 1H), 2.39 (d, *J* = 6.6 Hz, 2H), 2.33 (dd, *J* = 4.9 Hz, *J* = 11.9 Hz, 1H), 2.16 (m, 1H), 1.71 (m, 1H), 1.56 (m, 2H), 0.85 (m, 1H), 0.54 (m, 2H), 0.13 (m, 2H). HRMS (ESI) calcd for C₂₆H₂₉N₄O₅ [M+H]⁺ 477.2138; found: 477.2154. Anal. Calcd for C₂₆H₂₈ClN₄O₅ · H₂O: C, 58.92; H, 5.71; N, 10.57. Found: C, 58.78; H, 5.68; N, 10.51.

Acknowledgements

We thank Dr. Yong-de Lu for preparation of 7'-Cl-NTI using classical Fischer conditions. We thank the National Cancer Institute (P50 CA 103130: Center for Single Photon-Emitting Cancer Imaging Agents) for support of this research, and for a postdoctoral fellowship (RAD) through the Career Development Core. We also acknowledge resources provided by Harry S. Truman Memorial Veterans' Hospital, the University of Missouri Life Sciences Mission Enhancement Program, and NSF CHE-95-31247 and NIH 1S10RR11962-01 awards for NMR instrumentation.

References

- 1 P. S. Portoghese, M. Sultana and A. E. Takemori, *J. Med. Chem.*, 1990, **33**, 1714–1720.
- 2 P. S. Portoghese, H. Nagase, K. E. Maloney-Huss, C.-E. Lin and A. E. Takemori, *J. Med. Chem.*, 1991, **34**, 1715–1720.
- 3 (a) C. R. Dorn, C. S. Markos, M. S. Dappen and B. S. Pitzele, *J. Labelled Compd. Radiopharm.*, 1992, **31**, 375–380; (b) M. S. Yamamura, R. Horvath, G. Tóth, F. Ötvös, E. Malatynska, R. J. Knapp, F. Porreca and V. J. Hruby, *Life Sci.*, 1992, **50**, PL119–124; (c) G. Tóth, F. Ötvös and S. Hosztafi, *Helv. Chim. Acta*, 1993, **76**, 2274–2278; (d) P. C. Contreras, L. Tam, E. Drower and M. F. Rafferty, *Brain Res.*, 1993, **604**, 160–164.
- 4 (a) J. R. Lever and S. M. Johnson, *J. Labelled Compd. Radiopharm.*, 1997, **39**, 115–122; (b) J. R. Lever and U. Scheffel, *Eur. J. Pharmacol.*, 1998, **350**, 335–344; (c) J. R. Lever, S. L. McCallister, S. A. Chapman, P. A. Rauser, R. L. Allmon, W. B. Mathews and U. Scheffel, *Soc. Neurosci. Abstr.*, 2003, **33**, 802.1.
- 5 For a review on opioid receptor radioligands for imaging, see: J. R. Lever, *Curr. Pharm. Des.*, 2007, **13**, 33–49.
- 6 J. R. Lever, C. M. Kinter, H. T. Ravert, J. L. Musachio, W. B. Mathews and R. F. Dannals, *J. Labelled Compd. Radiopharm.*, 1995, **36**, 137–145.
- 7 (a) I. Madar, J. R. Lever, C. M. Kinter, U. Scheffel, H. T. Ravert, J. L. Musachio, W. B. Mathews, R. F. Dannals and J. J. Frost, *Synapse*, 1996, **24**, 19–28; (b) P. S. R. Villemagne, R. F. Dannals, H. T. Ravert and J. J. Frost, *Eur. J. Nucl. Med. Mol. Imaging*, 2002, **29**, 1385–1388.
- 8 (a) P. M. Villemagne, D. A. Bluemke, R. F. Dannals, H. T. Ravert and J. J. Frost, *J. Nucl. Med.*, 2002, **43S**, 280P; (b) I. Madar, B. Bencherif, J. Lever, R. F. Heitmiller, S. C. Yang, M. Brock, J. Brahmer, H. Ravert, R. Dannals and J. J. Frost, *J. Nucl. Med.*, 2007, **48**, 207–213.
- 9 R. A. Duval, R. L. Allmon and J. R. Lever, *J. Med. Chem.*, 2007, **50**, 2144–2156.
- 10 For examples of NTI and NTB analog synthesis and pharmacological studies, see: (a) M. Spetea, S. T. Nevin, S. Hosztafi, A. Z. Rónai, G. Tóth and A. Borsodi, *Neurochem. Res.*, 1998, **23**, 1211–1216; (b) S. Ananthan, C. A. Johnson, R. L. Carter, S. D. Clayton, K. C. Rice, H. Xu, P. Davis, F. Porreca and R. B. Rothman, *J. Med. Chem.*, 1998, **41**, 2872–2881; (c) A. Coop, J. Pinto, L. Wang, K. McCullough, R. B. Rothman, C. Dersch, A. E. Jacobson and K. C. Rice, *Bioorg. Med. Chem. Lett.*, 1999, **9**, 3435–3438; (d) A. Coop, A. E. Jacobson, M. D. Aceto, L. S. Harris, J. R. Traynor, J. H. Woods and K. C. Rice, *Bioorg. Med. Chem. Lett.*, 2000, **10**, 2449–2451; (e) J. Schütz, C. M. Dersch, R. Horel, R., M. Spetea, M. Koch, R. Meditz, E. Greiner, R. B. Rothman and H. Schmidhammer, *J. Med. Chem.*, 2002, **45**, 5378–5383; (f) S. Sakami, M. Maeda, K. Kawai, T. Aoki, K. Kawamura, H. Fujii, K. Hasebe, M. Nakajima, T. Endo, S. Ueno, T. Ito, J. Kamei and H. Nagase, *J. Med. Chem.*, 2008, **51**, 4404–4411.
- 11 For reviews of the Fischer indole synthesis, see: (a) B. Robinson, *The Fischer Indole Synthesis*, John Wiley and Sons, New York, NY, 1982; (b) G. W. Gribble, *Contemp. Org. Synth.*, 1994, **1**, 145–172.
- 12 G. R. Humphrey and J. T. Kuethe, *Chem. Rev.*, 2006, **106**, 2875–2911.
- 13 (a) R. Calderon-Morales, V. Tambyrajah, P. R. Jenkins, D. L. Davies and A. P. Abbott, *Chem. Commun.*, 2004, 158–159; (b) D.-Q. Xu, W.-Y. Yang, S.-P. Luo, B.-T. Wang, J. Wu and Z.-Y. Xu, *Eur. J. Org. Chem.*, 2007, 1007–1012; (c) D.-Q. Xu, J. Wu, S.-P. Luo, J.-X. Zhang, J.-Y. Wu, X.-H. Du and Z.-Y. Xu, *Green Chem.*, 2009, **11**, 1239–1246.
- 14 (a) S. B. Mhaske and N. P. Argade, *Tetrahedron*, 2004, **60**, 3417–3420; (b) A. Dhakshinamoorthy and K. Pitchumani, *Appl. Catal., A*, 2005, **292**, 305–311; (c) P. R. Singh, M. P. Surpur and S. B. Patil, *Tetrahedron Lett.*, 2008, **49**, 3335–3340.
- 15 (a) T. M. Lipińska and S. J. Czarnocki, *Org. Lett.*, 2006, **8**, 367–370; (b) L. Martarello, D. Joseph and G. Kirsch, *J. Chem. Soc. Perkin Trans. I*, 1995, 2941–2944; (c) A. Sudhakara, H. Jayadevappa, H. N. H. Kumar and K. M. Mahadevan, *Lett. Org. Chem.*, 2009, **6**, 159–164.
- 16 (a) C.-Y. Chen, C. H. Senanayake, T. J. Bill, R. D. Larsen, T. R. Verhoeven and P. J. Reider, *J. Org. Chem.*, 1994, **59**, 3738–3741; (b) C. F. Masaguer, E. Formoso, E. Raviña, H. Tristán, M. I. Loza, E. Rivas and J. A. Fontenla, *Bioorg. Med. Chem. Lett.*, 1998, **8**, 3571–3576; (c) A. M. Schmidt and P. Eilbracht, *J. Org. Chem.*, 2005, **70**, 5528–5535.
- 17 (a) S. M. Parmerter, A. G. Cook and W. B. Dixon, *J. Am. Chem. Soc.*, 1958, **80**, 4621–4622; (b) A. R. Katritzky, S. Rachwal and S. Bayyuk, *Org. Prep. Proc. Int.*, 1991, **23**, 357–363.
- 18 (a) P. R. Brodfuehrer, B.-C. Chen, T. R. Sattelberg, P. R. Smith, J. P. Reddy, D. R. Stark, S. L. Quinlan, J. G. Reid, J. K. Thottathil and S. Wang, *J. Org. Chem.*, 1997, **62**, 9192–9202; (b) K. R. Campos, J. C. S. Woo, S. Lee and R. D. Tillyer, *Org. Lett.*, 2004, **6**, 79–82.

Continuous heterogeneous catalytic oxidation of primary and secondary alcohols in scCO₂

Adrian O. Chapman, Geoffrey R. Akien, Nicholas J. Arrowsmith, Peter Licence and Martyn Poliakoff*

Received 7th July 2009, Accepted 17th November 2009

First published as an Advance Article on the web 7th January 2010

DOI: 10.1039/b913434d

A miniature catalytic reactor has been developed for the oxidation of alcohols with O₂ in supercritical CO₂. Particular attention has been given to ensuring good mixing of O₂ and CO₂ prior to contact with the substrate. The reactor was optimised using the oxidation of 2-octanol over 5% Pt + 1% Bi on Al₂O₃ and the mass balance was measured. The reactor was then evaluated for the oxidation of a series of secondary alcohols, and also the primary alcohol, 1-octanol.

Introduction

Devising cleaner and more efficient oxidation reactions is still a major challenge for green chemistry. Supercritical CO₂ (scCO₂) is an appealing solvent in this context because it is already fully oxidised and cannot react with O₂. scCO₂ has an excellent heat capacity, and is also completely miscible with O₂. The use of O₂ as an oxidant in scCO₂ has been reported by numerous authors, for example Wang *et al.*,¹ He *et al.*,² and Kimmerle *et al.*,³ and a comprehensive review of these reactions has been recently published by Seki and Baiker.⁴ In addition, we have demonstrated⁵ that O₂ can be combined with a CO₂-soluble photosensitiser to perform reactions of singlet O₂ in scCO₂ as efficiently as in CCl₄.

Most relevant to this paper has been the elegant work by Baiker on the continuous oxidation of 2-octanol.⁶ He and his co-workers were able to achieve good selectivities for the formation of 2-octanone combined with a long catalyst lifetime. However, this was with relatively low conversions because of difficulties in dissipating the heat produced by the reaction. They also oxidised 1-octanol, but with lower selectivity than with 2-octanol.

The aim of the work reported here was to build on Baiker's experiments by increasing both the yield and the selectivity to 2-octanone, while also achieving a high mass balance. As we show later, a significant amount of organic material can be lost through total oxidation. We have examined the reactions of other secondary alcohols, and the oxidation of 1-octanol, a more challenging substrate, because the intermediate aldehyde can be oxidised further to form the corresponding carboxylic acid.

The apparatus and its development

Safety warning: High pressure experiments are potentially dangerous and high pressure oxidations have the additional possibility of runaway reactions leading to explosive failure of the equipment.

It is the responsibility of researchers to ensure the suitability of their own equipment.

The apparatus which we have developed for continuous flow oxidations in scCO₂ differs from previous continuous flow equipment in a number of ways, all aimed at enabling O₂ to be used safely at high pressures. The apparatus also differs from that of Baiker in that it is much smaller, because miniaturisation reduces the risks even further. Our initial objective was to demonstrate that the apparatus could be used safely, reliably and predictably before any further studies could take place.

The final apparatus design, shown in Fig. 1, is a substantially modified version of that previously used in our group for continuous hydrogenations in scCO₂.⁷ As with the hydrogenations, a Rheodyne 7000L switching valve was used to dose O₂ (rather than H₂) into the CO₂ stream. The higher the rate of valve switching, the higher the concentration of O₂ in the scCO₂.

An initial series of experiments was conducted to ensure that the concentration of O₂ was both accurately controllable and reproducible using this particular gas dosing method. For increased safety, these first tests were carried out using N₂ rather than O₂ because, under these conditions, the physical properties of N₂ and O₂ are very similar. Thus, N₂ in CO₂ was tested with gas dosing frequencies calculated to deliver concentrations of 5 or 10 mol% N₂, comparable to those of O₂ used elsewhere.^{6,8} The mixture of N₂ and CO₂ was passed through a heated, sand-filled reactor and the concentration of N₂ was monitored at the BPR outlet by a microGC fitted with a Thermal Conductivity Detector (TCD).

The traces in Fig. 2(a) clearly demonstrate that the concentration of N₂ fluctuated substantially over time, despite maintaining a mean concentration close to the calculated value. Therefore, both the gas dosing volume and the gas over-pressure were reduced so that the gas dosage frequency could be increased, while still delivering the same amount of gas at the reactor outlet. Fig. 2(b) shows the effectiveness of these modifications, now using O₂ for the same target concentrations as previously. It is clear that the large fluctuations in gas concentration have been smoothed out, resulting in a more uniform concentration. A model liquid substrate was also introduced in a further set of experiments (not shown here) to demonstrate that the control over the gas concentration was maintained under near-reaction

School of Chemistry, University of Nottingham, University Park, Nottingham, UK NG7 2RD.
E-mail: martyn.poliakoff@nottingham.ac.uk; Fax: +44 (0)115 951 3058; Tel: +44 (0)115 951 3520

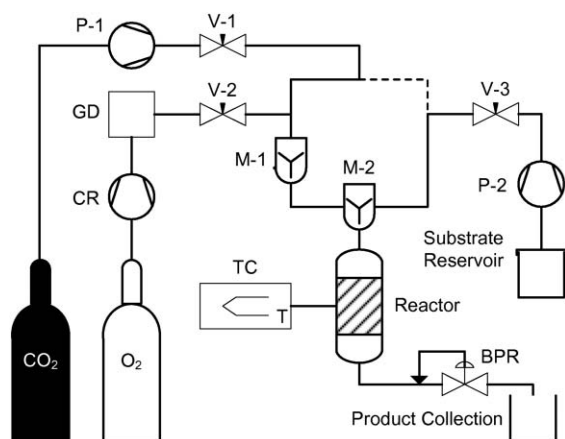


Fig. 1 Schematic of the scCO_2 oxidation reaction system. The CO_2 is pressurised and delivered by a Peltier-cooled piston pump P-1 (Jasco PU-1580- CO_2) in constant flow mode. O_2 is dosed in at a known pressure (set by a cylinder regulator CR) into the system by a 6-port HPLC switching valve GD (Rheodyne 7000L) fitted with small gas reservoirs (50–200 μL), the supply being isolable using the needle valve (V-2). Organic substrates are delivered at a constant flow rate *via* an HPLC pump, P-1 (Jasco PU-980). The CO_2 stream is divided into two, and then each stream mixed separately with O_2 and substrate. The O_2 is mixed with CO_2 in a static mixer M-1 (a sand-filled reactor) heated to 60 $^\circ\text{C}$, before being combined with the CO_2 + substrate stream in another static mixer M-2 (a Y-piece). The mixed stream is then passed through a packed catalyst bed with an internal thermocouple. Products are collected after depressurisation of the fluid mixture with an electronically-controlled backpressure regulator, BPR (Jasco BP-1580-81). Since the commissioning of the equipment, it was realised that safer operation could be realised by eliminating the pipework shown with a dashed line, as, if there is a blockage, it is possible for the flow to be reversed. However, most of the experiments in this work were conducted with this pipe in place.

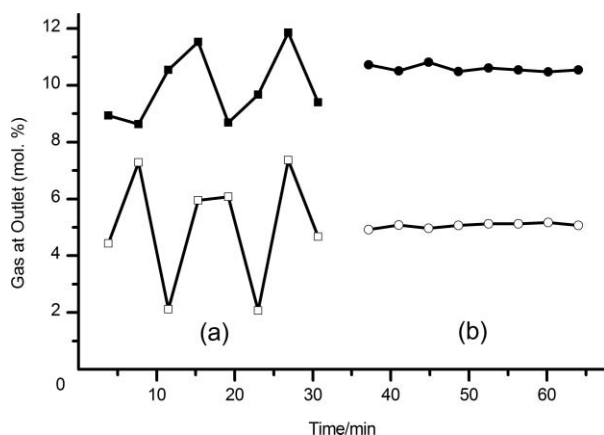


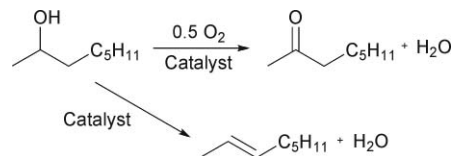
Fig. 2 Traces showing the results of the gas dosing experiments with a nominal 5 and 10 mol% of gas. (a) shows the large variation in N_2 concentration in the original apparatus and (b) shows the results for the equivalent experiments for O_2 after alteration of the apparatus, showing the improvement in homogeneity. Conditions: pressure: 100 bar; temperature: 50 $^\circ\text{C}$; CO_2 flow rate: 1 mL min^{-1} , with (a) gas reservoir volume: 500 μL , N_2 over-pressure: 50 bar; and (b) gas reservoir size: 100 μL , O_2 over-pressure: 50 bar.

conditions. However, our test oxidation reaction showed that further modification of the apparatus was required.

Oxidation of 2-octanol

Test reaction

The oxidation of 2-octanol was chosen as the test reaction as both the starting material and products are liquids and the reaction is relatively simple, with octenes being the only significant by-product, as in Scheme 1.



Scheme 1 Oxidation of 2-octanol with O_2 and a catalyst, including the possible dehydration side-reaction.

Previous investigations by Baiker *et al.*^{6,8} had shown that this reaction works well in scCO_2 . However, we found supported Pt catalysts to be more active than Pd catalysts similar to those used by Baiker. In particular, a supported platinum and bismuth catalyst was chosen as further studies by ourselves and others have shown this to be less susceptible to deactivation than Pt alone.^{9–11}

A 0.5 mm diameter thermocouple was carefully pushed upwards through the centre of the reactor, so that the tip was situated half-way up the catalyst bed. This thermocouple was connected to a data logger to provide continuous recording of the internal temperature of the catalyst bed. The small size of this thermocouple and its direct contact with the catalyst meant it was able to respond rapidly to any temperature changes occurring in the reactor. The oxidation of 2-octanol was then performed under conditions similar to those used by Baiker *et al.* The temperature data produced from this experiment are shown in Fig. 3(a), where it can be seen that large, regular exotherms occurred within the catalyst bed, with temperature spikes of >300 $^\circ\text{C}$. This can easily be explained by the fact that an inhomogeneous O_2 concentration will lead to higher

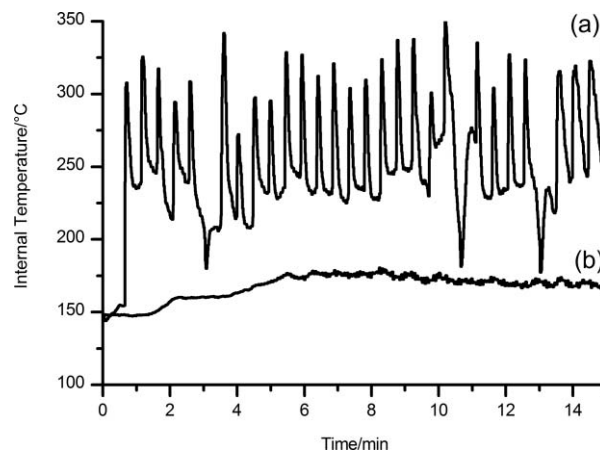


Fig. 3 Traces of the temperature at the centre of the catalyst bed during the oxidation of 2-octanol (a) before and (b) after further reducing the gas reservoir volume from 100 μL to 20 μL , and adding an additional heated mixer to the CO_2 + O_2 stream. Conditions: pressure: 100 bar, temperature: 150 $^\circ\text{C}$, CO_2 flow rate: 0.5 mL min^{-1} , 2-octanol: 2.50 mol%, O_2 :2-octanol ratio: 1.5.

local O₂ concentrations. This will increase the rate of reaction in these regions, which, since the reaction is exothermic, would increase the temperature, causing a further increase in the rate *etc.*, leading to a “hot-spot”.

The frequency of these exotherms was identical to the O₂ dosing rate, indicating that the O₂ concentration was still inhomogeneous within the reactor, with variations large enough to cause substantial over-oxidation, probably to CO₂ and H₂O, because no other species were detected by offline GC. The temperatures reached were also high enough to rapidly deactivate the catalyst, presumably by sintering of the metal component. When the experiment was continued further, the measured temperature inside the reactor returned to 150 °C, indicating that the reaction had ceased in the region around the thermocouple. Approximately 30 minutes later, no more 2-octanone was detected at the BPR outlet, demonstrating that the whole catalyst bed was now inactive. Fig. 3(b) shows that the exotherm problem could be completely removed when the mixing of O₂ and CO₂ upstream of the reactor was improved even further by 1) reducing the gas reservoir volume again from 100 μL down to 20 μL, and 2), adding an additional static mixer heated to 60 °C in the CO₂ + O₂ flow path (labelled M-1 in Fig. 1).

Once the apparatus had been completely modified, the reaction gave a steady yield of 2-octanone of 75% for 5 hours with no evidence for catalyst deactivation or the formation of octenes.

Mass balance

The real test of this reaction is to establish an accurate mass balance. This is complicated in oxidation reactions by the fact that over-oxidation can lead to the formation of CO₂, which would be masked by the large excess of CO₂ used here as the solvent. Nevertheless, a series of experiments were conducted to determine the mass balance of the reaction.

Two different reactor designs were tested, as shown in Fig. 4; one was the original tubular reactor, and the second was a catalyst-filled tee-piece. Experiments were conducted using each reactor with varying O₂:2-octanol ratios. The quantities of 2-octanol and 2-octanone recovered at the outlet were accurately measured and compared to the quantity of 2-octanol pumped into the apparatus.

Although some material was lost in both reactor designs (there is enough O₂ remaining to totally oxidise the unaccounted-for material), the tee-piece reactor performed better, with >90% mass balance at a 75% yield of 2-octanone. In both cases, the “missing” mass may well be due to total oxidation of some of the substrate leading to the formation of CO₂ and H₂O. The tee-piece possibly performed better because the concentrations of reactants at the mixing point were lower than in the tubular reactor. However, many other factors are also changing between the two reactor designs, *e.g.* the residence time distribution or the fluid dynamics.

As far as we are aware, this is the first time such an in-depth study of the mass balance of oxidation reactions has been conducted in sCO₂. It demonstrates that these reactions can be performed with both high efficiency and acceptable recovery, at least on a small scale.

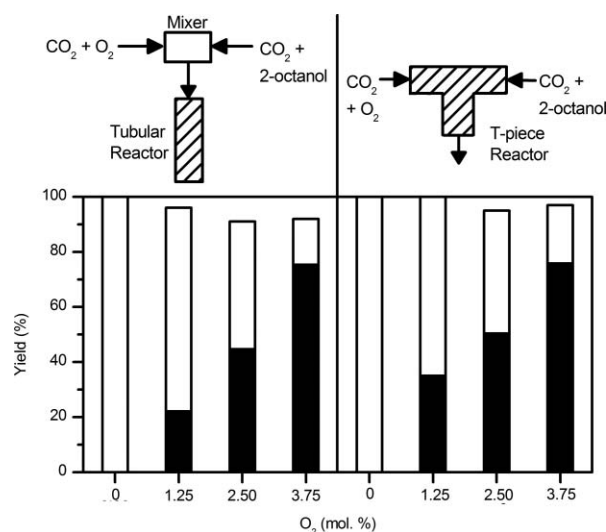


Fig. 4 The results from the mass balance experiments for the two reactor designs, 2-octanol represented by white bars, and 2-octanone with black bars. Each bar shows the fraction of material recovered, calibrated to the result without O₂. No octenes were observed during any of these experiments. Conditions: pressure: 100 bar, temperature: 150 °C, CO₂ flow rate: 0.5 mL min⁻¹, 2-octanol: 2.50 mol%.

Variation of experimental conditions

A range of experiments were then performed to investigate the impact on the reaction of changing the conditions. Due to the small volume of the apparatus, steady state was usually reached in under 5 minutes, allowing rapid study of the reaction. One of the most important parameters turned out to be the temperature, as shown in Fig. 5.

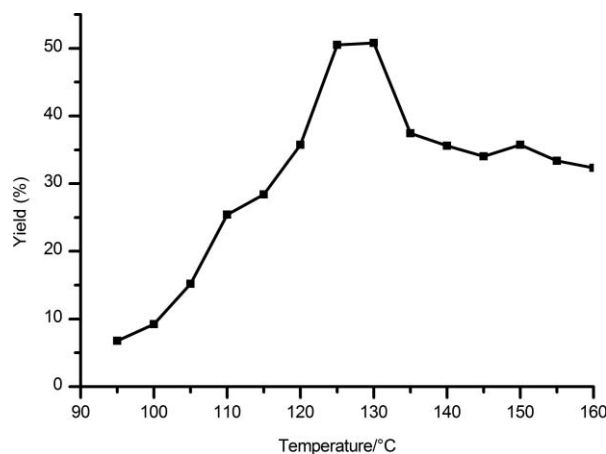


Fig. 5 Variation in the yield of 2-octanone with temperature, using a 5% Pt + 1% Bi/Al₂O₃ catalyst. No octenes are formed with this catalyst, unlike with a similar undoped catalyst. Conditions: pressure: 100 bar, CO₂ flow rate: 0.5 mL min⁻¹, 2-octanol: 2.5 mol%, O₂:2-octanol ratio: 1.5.

As the temperature was increased, the yield increased correspondingly as might be expected. However, above 130 °C, the yield decreased, perhaps because of a change to single phase conditions where the concentrations of reactants could be lower. Although the concentrations are lower than in the work of Baiker,⁶ we believe that their phase behaviour measurements

at the very least indicate that a phase transition to a single phase would be possible under these conditions. It does not seem plausible that the catalyst was sintering, since this usually takes place at higher temperatures ($>300\text{ }^\circ\text{C}$). In general, octenes were produced at higher temperatures (higher than shown here), which other experiments have shown were mainly due to dehydration promoted by the catalyst support.¹¹ The Bi-doped catalyst also required higher temperatures than the undoped Pt catalyst to catalyse the formation of octenes.¹¹

Another key parameter was the O_2 :substrate ratio, as shown in Fig. 6. The 2-octanone yield increased with increasing O_2 concentration as expected, and correlated well with previous literature data,⁶ although Baiker *et al.* have also reported a decrease in the yield with more than 2 equivalents of O_2 . The effect of increasing the O_2 concentration is less marked at higher ratios, presumably because mass transfer limitations are overcome.

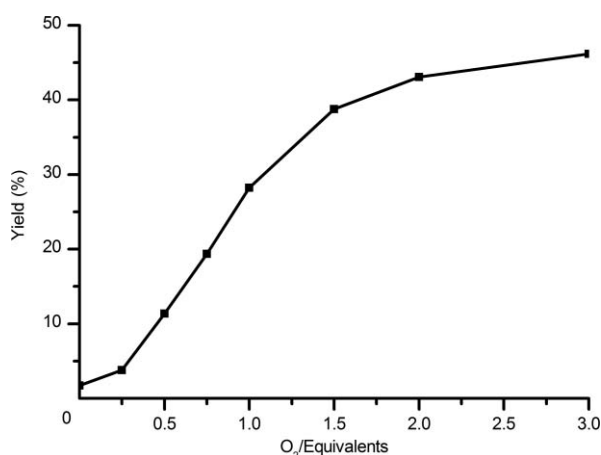


Fig. 6 Variation in the yield of 2-octanone with O_2 concentration. The 2-octanone yield increases with increasing O_2 concentration. Conditions: pressure: 100 bar, temperature: $125\text{ }^\circ\text{C}$; 2-octanol: 1.94 mol%.

Oxidation of other secondary alcohols

To investigate how widely the same approach could be applied, a range of other secondary alcohols was oxidised, as shown in Table 1. Standard conditions were chosen only to give a partial conversion of 2-octanol so that one could easily establish whether any particular alcohol behaved better or worse than 2-octanol.

In general, most of the secondary alcohols gave 33–46% yield, with the exception of 2-pentanol, which was much higher. Phenyl-substituted alcohols gave much lower yields, perhaps due to increased steric demands, but despite the expectation of increased product stability from delocalisation of the $\text{C}=\text{O}$ bond of the product into the aromatic ring.

We encountered issues with reproducibility when using 3-pentanol; it sometimes deactivated to zero activity within an hour of start-up. However, subsequent re-injection of 2-octanol showed that the catalyst was still functioning normally when compared to routine use with 2-octanol alone, and a satisfactory reason for the lack of reproducibility could not be found, despite several experiments with mixed alcohol feeds to investigate this further. This decay in activity was also observed

Table 1 Oxidation of different secondary alcohols

Entry	Alcohol	Yield (%)
1	2-propanol	37.7
2	2-butanol	43.6
3	2-pentanol	70.0
4	2-heptanol	45.8
5	2-octanol	33.7
6	2-decanol	43.2
7	3-pentanol	deactivates ^b
8	2-heptanol	45.8
9	3-heptanol	deactivates ^b
10	4-heptanol	21.0
11	1-phenylethanol	10 ^c
12	1-phenyl-1-propanol	10

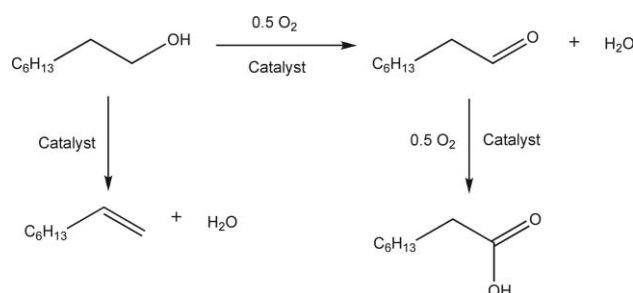
^a Conditions: pressure: 100 bar, temperature, $130\text{ }^\circ\text{C}$, alcohol: 1.93 mol%, O_2 :alcohol ratio 0.5. ^b See text for more details. ^c Selectivity was also poor, with five unidentified by-products being observed by GC with an approximate total yield of 5% by peak area.

for 3-heptanol, although the deactivation occurred over twice as long a timescale. Both the 3-pentanol and the 3-heptanol were pure by GC, apart from traces of the corresponding ketone.

We thought that the reaction transferred well to other substrates, so the logical continuation was on to the oxidation of primary alcohols.

Primary alcohols—1-octanol

The reaction of 1-octanol to form octanal is a more challenging prospect than the oxidation of 2-octanol, because the aldehyde could easily react further to form the acid, as shown in Scheme 2.



Scheme 2 Oxidation of 1-octanol with O_2 and a catalyst, including the possible dehydration side-reaction. Note that H_2O also catalyses the transformation of the aldehyde into the acid.⁶

As with 2-octanol, the reactor temperature was varied for the oxidation of 1-octanol. As can be seen in Fig. 7, the conversion did not change much with increasing temperature, perhaps because all of the O_2 was being consumed at all of the temperatures tested. Interestingly, above $100\text{ }^\circ\text{C}$, the yield of octanoic acid decreases with increasing temperature. As was noted by Baiker *et al.*,⁶ biphasic conditions occurred over the majority of the conditions they tested in the oxidation of 2-octanol (5 mol% 2-octanol in sCCO_2). 1-Octanol is known to have substantially higher miscibility pressures and temperatures than the other isomers of octanol,¹² suggesting that the reaction mixture may well be biphasic here too, despite the lower substrate concentrations (2 mol% *versus* 5 mol%). For the acid to form at an appreciable rate, the aldehyde must be hydrated before it can be dehydrogenated. Increasing the temperature

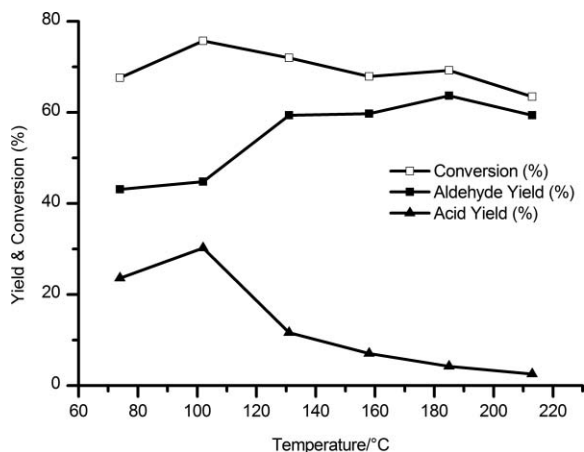


Fig. 7 Variation in yields in the oxidation of 1-octanol with varying temperature, using a 5% Pt + 1.5% Bi/ Al_2O_3 catalyst. Trace quantities of the ester octyl octanoate were observed, but no octenes were detected by GC. Conditions: pressure: 100 bar, CO_2 flow rate: 1 mL min^{-1} , 1-octanol: 1.96 mol%, O_2 :1-octanol ratio: 0.5.

could possibly increase the partitioning of the aldehyde and/or water into the vapour phase, thereby decreasing the likelihood of the aldehyde being hydrated by a water-rich liquid phase covering the catalyst surface. Although challenging because of the high temperatures, investigations into the phase behaviour of this system would prove interesting.

The behaviour of 1-octanol with increasing O_2 concentration largely echoes that of 2-octanol, although the maximum conversion is shifted to significantly lower O_2 concentrations, as shown in Fig. 8.

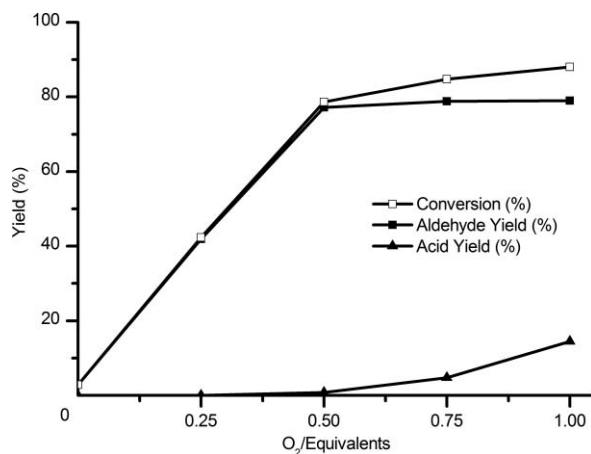


Fig. 8 Variation in the yield of octanal; with O_2 concentration. Conditions: pressure: 100 bar, temperature: 135°C , CO_2 flow rate: 1 mL min^{-1} , 1-octanol: 1.96 mol%.

Conclusions

In this paper we have described a miniature reactor which can be successfully used for the continuous oxidation of primary and secondary alcohols with O_2 in scCO_2 . In the case of 2-octanol, we have shown that a 75% yield of 2-octanone can be achieved with a >90% mass balance. The oxidation of a series of other secondary alcohols was also investigated. High selectivity to

octanal was obtained during the oxidation of 1-octanol. We are now investigating this methodology for the oxidation of more complex substrates.

Experimental

The following materials were used without purification: CO_2 (SFC grade, >99.99%, BOC Gases), O_2 (BOC), He (CP Grade, 99.999%, BOC Gases), H_2 (99.995%, BOC Gases), air (BOC Gases), Ar (BOC Gases), 2-octanol (97%, Alfa Aesar), 1-octanol (>99%, Aldrich), 2-propanol (reagent grade, Fisher), acetone (reagent grade, Fisher), \pm -2-pentanol (99%, Alfa Aesar), 3-pentanol (98+%, Alfa Aesar), 2-butanol (99%, Alfa Aesar), 2-decanol (98%, Aldrich), \pm -1-phenylethanol (96%, Fluka), 1-phenyl-1-propanol, 3-heptanol, 2-heptanol, 5 wt% Pt + 1 wt% Bi on Al_2O_3 (batches M01620C/D, Johnson Matthey), 5 wt% Pt + 1.5 wt% Bi on Al_2O_3 (batch M04432, Johnson Matthey), sodium borohydride (Fisher), ethanol (reagent grade, Fisher), 40–60 petroleum ether (reagent grade, Fisher), sodium sulfate (Fisher). Water was obtained from an in-house deionisation and purification system (Elga PureLab Option S). 4-Heptanol was not readily available commercially so was synthesised according to a modified literature preparation, and its identity confirmed by ^1H and ^{13}C NMR (Jeol EX-270).

The 2-octanol experiments used the 5% Pt + 1% Bi/ Al_2O_3 catalyst, and the 1-octanol experiments the 1.5% Bi analogue. In a typical reaction, the tubular reactor (78 mm long, 3.05 mm I.D., volume 0.57 mL) was filled with catalyst (typically ~300 mg), and then pressurised and heated with CO_2 at the desired flow rate. The substrate and O_2 were then introduced, and this was defined to be the beginning of the experiment.

Gas analysis was performed with a Varian CP 4900 Micro-Gas Chromatograph (microGC), fitted with 20 m M5A molecular sieve and 0.4 m HSA porous polymer columns for analysing low molecular weight gases and heavier components, respectively. The carrier gas was Ar and detection was with a Thermal Conductivity Detector (TCD).

Reactions were analysed by Gas Chromatography (GC) using a Shimadzu GC-2010 fitted with RTX-5 (Restek, $10 \text{ m} \times 0.1 \text{ mm}$ I.D. \times $0.20 \mu\text{m}$ film thickness) or BETADDEX 110 (Supelco, $30 \text{ m} \times 0.25 \text{ mm}$ I.D. \times $0.25 \mu\text{m}$ film thickness) columns. He was used as the carrier gas, and appropriate temperature programming was used to separate the components before detection with a Flame Ionisation Detector (FID). Samples were prepared by dilution of the BPR effluent in acetone or methanol, and compared with external standards to determine concentrations. Analysis was quantitative for the mass balance experiments, but qualitative for others.

Acknowledgements

We are grateful to the EPSRC and DICE for support (grant no. EP/FO15275/1), and Johnson Matthey for the kind donation of catalysts. We thank Xue Han for her assistance and M. Guyler, P. Fields and R. Wilson for technical support.

Notes and references

- X. G. Wang, H. Kawanami, S. E. Dapurkar, N. S. Venkataramanan, M. Chatterjee, T. Yokoyama and Y. Ikushima, *Appl. Catal., A*, 2008, **349**, 86–90.

- 2 J. L. He, T. B. Wu, T. Jiang, X. S. Zhou, B. J. Hu and B. X. Han, *Catal. Commun.*, 2008, **9**, 2239–2243.
- 3 B. Kimmerle, J.-D. Grunwaldt and A. Baiker, *Top. Catal.*, 2007, **44**, 285–292.
- 4 T. Seki and A. Baiker, *Chem. Rev.*, 2009, **109**, 2409–2454.
- 5 R. A. Bourne, X. Han, A. O. Chapman, N. J. Arrowsmith, H. Kawanami, M. Poliakoff and M. W. George, *Chem. Commun.*, 2008, 4457–4459.
- 6 G. Jenzer, M. S. Schneider, R. Wandeler, T. Mallat and A. Baiker, *J. Catal.*, 2001, **199**, 141–148.
- 7 P. Stephenson, P. Licence, S. K. Ross and M. Poliakoff, *Green Chem.*, 2004, **6**, 521–523.
- 8 G. Jenzer, D. Sueur, T. Mallat and A. Baiker, *Chem. Commun.*, 2000, 2247–2248.
- 9 R. Anderson, K. Griffin, P. Johnston and P. L. Alsters, *Adv. Synth. Catal.*, 2003, **345**, 517–523.
- 10 M. Besson and P. Gallezot, *Catal. Today*, 2000, **57**, 127–141.
- 11 A. O. Chapman, Ph.D., University of Nottingham, 2007.
- 12 F. Fourie, C. E. Schwarz and J. H. Knoetze, *J. Supercrit. Fluids*, 2008, **47**, 161–167.

Moringa stenopetala seed oil as a potential feedstock for biodiesel production in Ethiopia

Andinet Ejigu,^a Araya Asfaw,^a Nigist Asfaw^b and Peter Licence*^c

Received 11th August 2009, Accepted 25th November 2009

First published as an Advance Article on the web 7th January 2010

DOI: 10.1039/b916500b

Moringa stenopetala seed oil was evaluated as a potential sustainable feedstock for biodiesel production in Ethiopia. Base catalyzed transesterification of *M. stenopetala* seed oil was carried out with methanol, ethanol and a mixture of methanol and ethanol (1:1 molar ratios) with an alcohol to oil molar ratio of 6:1. The physicochemical characteristics of the esters were assessed to evaluate their suitability for use in standard diesel engines. The study indicated that *M. stenopetala* seeds yield 45% w/w of oil. The oil contains 78% mono-unsaturated fatty acid and 22% saturated fatty acid. Oleic is the dominant fatty acid, about 76%. When mixtures of alcohols were used, the amount of ethyl ester formed was 30% that of methyl ester. The physicochemical properties of *M. stenopetala* oil methyl ester and mixture of esters (methyl and ethyl) were found to comply with both the American ASTM D6751 and the European standard EN 14214. Overall, the physicochemical properties of the ester mixture of *M. stenopetala* oil were better than that of methyl ester. The recommended way to use the oil as a fuel is as a mixture of esters. The study indicates that compared to biodiesel fuels derived from other vegetable oils, *M. stenopetala* has a number of advantages. Furthermore, the use of *M. stenopetala* seed oil for the production of biodiesel will not compete with food as neither the seeds nor the oil are used for food in Ethiopia.

Introduction

Ethiopia belongs to the non-oil exporting less developed countries (LED) of Africa. Ethiopia imports all of its petroleum products and the demand for petroleum fuel is rising rapidly due to the growing economy of about 10% GDP growth¹ and infrastructure development. In the second quarter of 2007/08, petroleum imports exceeded export earnings by 30%.¹ With the recent trends and volatility of oil prices, the country has been forced to develop a biofuel strategy to mitigate the impacts of imported oil on its economy. The strategy encourages the diversification of energy supplies in the transport sector; therefore, biodiesel offers significant opportunities.⁷

Biodiesel is defined as a fuel comprised of mono-alkyl esters of long chain fatty acids derived from vegetable oils or animal fats. It can be used in diesel engines and heating systems.² Biodiesel is a preferred fuel because it has a lower emission profile than petro diesel and also it can be derived from renewable sources. Biodiesel can be produced from a variety of renewable lipid sources by a transesterification process. Transesterification is a common and well-established chemical reaction in which linear monohydroxy alcohols react with vegetable oils, which are triglycerides of fatty acids, in the presence of a catalyst.

Among alcohols commonly used for the transesterification process are methanol, ethanol, propanol and butanol. Methanol and ethanol are used most frequently, but methanol is preferred because of its low cost and its physical and chemical properties (polar and shortest chain alcohol).³ The methods of preparation of biodiesel can be classified into: chemical catalytic (base- or acid catalysis), biocatalytic (enzyme catalysis) and non-catalytic supercritical alcohol processes—a very good overview of such methods has recently been published by Luque *et al.*³⁰ However, alkali catalysts are the most commonly used in the biodiesel industry, since the process is faster and the reaction conditions are moderated.⁴ It was reported that base catalysts performed better than the acid catalysts.⁵ The reaction can be performed at lower temperature, as low as at 25 °C, with the base catalysts, whereas acid catalysis requires a higher temperature (100 °C) and longer reaction time.⁵ However, if a glyceride has a higher free fatty acid content and more water, acid-catalyzed transesterification is suitable. The acids could be sulfuric acid, phosphoric acid, hydrochloric acid or organic sulfonic acid.^{4,31} The cheapest and the best known homogeneous acid catalyst used for the esterification reaction is H₂SO₄. The main disadvantages of this catalyst are the possibility that at the high temperature the more unsaturated fatty acids would undergo polymerization and that side products like dark colored oxidized compounds or other decomposition products could be formed. Furthermore, the use of strong acids implies the need for special equipment (*e.g.*, stainless steel) and care for handling.³¹

The stoichiometry of the transesterification reaction requires 3 mol of methanol and 1 mol of triglyceride to give 3 mol of fatty acid methyl ester and 1 mol of glycerol. This reaction,

^aAddis Ababa University, Environmental science program, P.O. Box 1176, Addis Ababa, Ethiopia

^bAddis Ababa University, Chemistry department, P.O. Box 1176, Addis Ababa, Ethiopia

^cSchool of Chemistry, University of Nottingham, NG7 2RD, UK.
E-mail: pete.licence@nottingham.ac.uk

in turn, consists of three consecutive reversible reactions with intermediate formation of diglycerides and monoglycerides. After the reaction, the glycerol is separated by settling or centrifuging. In practice, the ratio needs to be higher (6:1) to drive the equilibrium to a maximum ester yield.³

In this study, biodiesel was produced by base catalyzed transesterification of *M. stenopetala* seed oil which was carried out using methanol, ethanol and a mixture of methanol and ethanol (1:1 molar ratios). The purpose of using a mixture of methanol and ethanol was to take the advantage of the better solubility of oil in ethanol than methanol and better reactivity of methoxide ion than ethoxide to attain the desired equilibrium.⁶ In addition, Ethiopia plans to produce 1 billion litres of ethanol from molasses which is a by product of the sugar industry. Therefore, part of the ethanol could be used for biodiesel processing.⁷

Moringa stenopetala belongs to the family *Moringaceae* and is often referred to as the African 'Moringa Tree' because it is native only to Ethiopia and northern Kenya.^{8,9} Though it does grow in many other parts of the old- and new-world tropics, it is not as widely known as its close relative, *Moringa oleifera*.¹⁰ The *M. stenopetala* tree, locally called *shiferaw* or *aleko*, grows widely in southern Ethiopia, mainly in the Keffa, Gamo Gofa, Bale, Sidamo, Borana and Debub Omo zones, and in Konso and Dherashe areas. In the Arba Minch and Wollayta areas, the local people cook the leaves of the *M. stenopetala* tree and eat them with their traditional *kurkufa* (a cereal dish made with maize and sorghom).¹¹ The people of Konso use the tree not only for food but also as a medicine and they cultivate it in large areas around their villages.¹² The leaves and roots of *M. stenopetala* are used as a cure for malaria, stomach problems and diabetes¹³ and the seeds are used in some areas to clear muddy water. There are no reports on the uses of the seeds or the oil of *M. stenopetala* in Ethiopia. This would make it a potential feedstock for the production of biodiesel since it does not compete with food production.

In this paper, the evaluation of *M. stenopetala* seeds as a potential feedstock for biodiesel production is presented. There are no studies on biodiesel derived from *M. stenopetala* seed oil prior to this work.

Results and discussion

M. stenopetala oil

The yield of oil obtained by hexane extraction of *M. stenopetala* seeds was found to be 45% w/w which is in agreement with previous work.¹⁰ The high oil yield allows the possibility of economical exploitation which results in lower operating costs compared to some other oilseeds, such as soybean and cottonseed, which have average oil contents of only 20% and 14%, respectively.¹⁴

The titrated acidities of the *M. stenopetala* seed oil was 1.42 mg KOH/g of oil. The maximum acid value for alkaline transesterification is 2 mg [KOH]/g [oil] recommended by Canakci and Van Gerpen.¹⁵ Based on the acid value, the free fatty acid (FFA) content of *M. stenopetala* oil was 0.71% and thus, the oil does not need acid pre-treatment for transesterification. The iodine value of *M. stenopetala* oil was found

to be 69 g I₂/100 g of oil. In this regard, *M. stenopetala* oil is relatively stable to oxidation when compared to canola,¹⁶ sunflower,¹⁷ linseed¹⁸ and soybean oils¹⁹ which have higher iodine values.

Fatty acid composition of *M. stenopetala* oil

The fatty acid composition of *M. stenopetala* seed oil was determined by gas chromatography. The oil contains a high level of mono-unsaturated fatty acids (78%), while the saturated fatty acid accounts for the remaining 22% (Table 1). The dominant fatty acid is oleic (76%) and therefore the oil belongs to the oleic acid category.²⁰

These results agree well with those reported for *M. stenopetala* samples collected in Kenya.¹⁰ *M. stenopetala* oil is more highly saturated than soybean, sunflower and rapeseed oils, but less saturated than palm oil (Table 1). The absence of polyunsaturated fatty acids (C18:2 and C18:3) and the relatively high content of C22:0 fatty acid (behenic acid)¹⁰ in *M. stenopetala* oil when compared to other common vegetable oils, makes it a preferred oil in terms of the oxidative stability. The fatty acid composition of *M. stenopetala* oil was found to be similar to that of the *M. oleifera*²¹ although there are some differences regarding C18:0, C18:1 and C22:0 (Table 1).

Transesterification of *M. stenopetala* oil

Base catalyzed transesterification of *M. stenopetala* seed oil was carried out using methanol, ethanol and a mixture of methanol and ethanol (1:1 molar ratios). After the purification step, 96% (wt) of methyl ester and 94% (wt) of a mixture of methyl-ethyl esters were recovered at 25 °C. But the biodiesel yields of both esters at 45 °C and 60 °C reaction temperatures were lower at 25 °C (Fig. 1). Therefore, the optimized temperature for transesterification was 25 °C. Studies indicate that if there are no side reactions, the biodiesel weight yields, relative to the initial amount of oil, should be nearly 99–100 wt%. In this sense, two possible side reactions could occur: the saponification of triglycerides or neutralization of the FFAs of the vegetable oil. Both of them produce soaps and, therefore, decrease the biodiesel yield.¹⁴

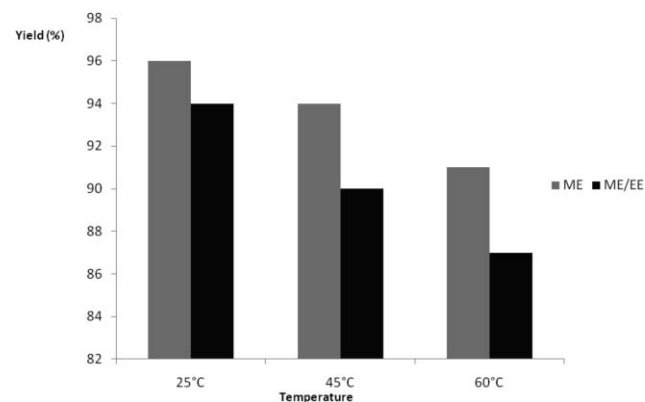


Fig. 1 Effect of temperature on the yield of *M. stenopetala* derived biodiesel.

Table 1 Fatty acid composition of the oils of *M. stenopetala*, soybean, *M. oleifera*, sunflower, rapeseed and palm

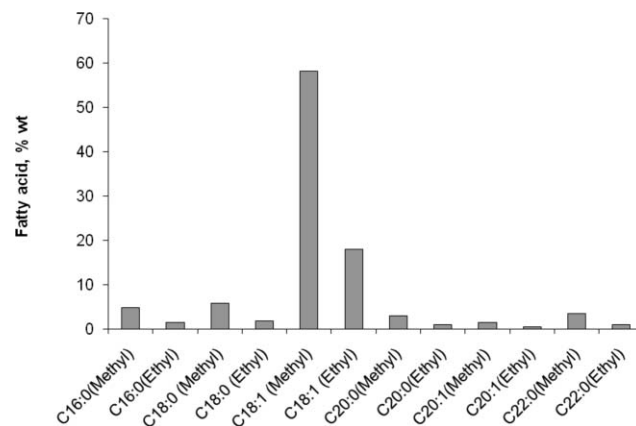
Fatty acid	<i>M. stenopetala</i>	<i>M. oleifera</i> ^a	Soybean ^a	Sunflower ^a	Rapeseed ^a	Palm ^a
C16:0	6.1	6.5	11	6.4	3.6	44.1
C18:0	7.5	6.0	4	4.5	1.5	4.4
C18:1	76.0	72.2	23.4	24.9	61.6	39.0
C18:2	-	1.0	53.2	63.8	21.7	10.6
C18:3	-	-	7.8	<1(trace)	9.6	0.3
C20:0	3.8	4.0	-	-	-	0.2
C20:1	1.7	2.0	-	-	1.4	-
C22:0	4.4	7.1	-	-	-	-

^a Data.²¹**Table 2** Summary of properties of *M. stenopetala* esters in comparison with the standards of ASTM and EN Limit

Fuel properties	Units	ME	ME/EE	ASTM D6751	EN 14214
Density@15 °C	g/ml	0.885	0.8872	-	0.86-0.9
Viscosity@40 °C	mm ² /s	4.58	4.69	1.9-6	3.5-5
Flash point	°C	185	197	Min 120	Min 130
Acid number	mgKOH/g	0.126	0.212	Max 0.5	Max 0.5
Iodine value	g I ₂ /100g of oil	69	69	-	Max 120
Ash content	Wt, %	0.0098	0.0067	0.01	-
Conradson carbon residue (10%)	Wt, %	0.075	0.0778	-	Max 0.3
Caloric value	MJ/KG	38.23	39.5	-	-
Water content	Wt, %	Nil	Nil	0.05 vol-%	Max 500mg/l
Cloud point	°C	15	15	-	**
Pour point	°C	12	12	-	**
Na + K	mg/Kg	3.734	3.972	5 µg/g	5
Ca + Mg	mg/Kg	4.365	4.635	-	5

However, at a 6:1 ethanol to oil molar ratio using 1% of KOH as a catalyst at 70 °C and 25 °C, after 2 hours reaction time, phase separation does not occur which could be due to the type of catalyst used. Lang *et al.*²² have reported that KOH was less effective than ethoxide as a catalyst for ethyl ester synthesis from vegetable oils. This is because ethanol ($pK_a = 15.9$) and other primary alcohols are somewhat weaker acids compared to water ($pK_a = 15.7$), while methanol ($pK_a = 15.5$) is a slightly stronger acid. Hence, the reaction of KOH with methanol favours the formation of methoxide ion, and the reactivity between KOH and another alcohol to form the respective alkoxide anion is very low. Although KOH is an excellent base catalyst for methyl esters, it is less effective for ethyl ester synthesis.²² However, phase separation takes place when a small amount of NaCl powder is added (to increase the density of glycerol in *M. stenopetala* oil) in the presence of KOH as a catalyst. But the biodiesel yield was significantly very low (< 50% wt). This was due to the formation of emulsions and gelatinous matter during purification. Although ethanol has better solvent properties than methanol for the solubility of oil, formation of emulsion after the transesterification reaction makes ethanolysis more complicated and impractical.²³

When using ethanol and methanol mixtures, ethyl esters also formed alongside methyl esters. The amount of ethyl esters was 30% that of the methyl esters (Fig. 2). Even though the molar ratio of methanol to ethanol was 1:1 the formation of ethyl esters was much lower than the methyl esters. The slower reaction rate of ethanol when compared with methanol can be explained by the reaction mechanisms of alkaline catalyzed transesterification.⁶

**Fig. 2** Composition of methyl and ethyl ester of *M. stenopetala* oil using a mixture of methanol and ethanol in a 1:1 molar ratio.

Physicochemical properties of *M. stenopetala* oil esters (Table 2)

The density of *M. stenopetala* oil, *M. stenopetala* methyl ester and mixture of (methyl and ethyl) esters at 15 °C were 0.903, 0.885 and 0.8872 g/ml, respectively. The kinematic viscosity of *M. stenopetala* oil was 28.4 mm²/s at 40 °C. Kinematic viscosity is significantly influenced by compound structure, chain length, position, number, and nature of double bonds, as well as the nature of oxygenated moieties.²⁴ In addition, there are high regressions between density and viscosity values of vegetable oil methyl esters. An increase in density from 0.860 to 0.885 g/ml for vegetable oil methyl esters or biodiesel increases the viscosity from 3.59 to 4.63 mm²/s and the increases are

highly regular.²⁹ The kinematic viscosity of *Moringa oleifera* seed oil is 29.63 mm²/s²¹ which is slightly higher than the viscosity of *M. stenopetala* oil. This is due to the fact that the content of the longest saturated fatty acid, behenic acid (C22:0), in *M. oleifera* is relatively higher (7%) than *M. stenopetala* (4%). After transesterification of *M. stenopetala* oil, the viscosity was significantly reduced. The viscosities of methyl and mixture of (methyl and ethyl) esters were 4.58 and 4.69 mm²/s respectively. The kinematic viscosities of methyl esters are slightly lower than that of the mixture of esters. This is in agreement with canola oil methyl ester and a mixture of esters with a 1:1 methanol and ethanol molar ratio. The viscosity of canola oil methyl esters was 3.9 mm²/s and the viscosity of mixtures of esters is 4.1 mm²/s.⁶ *M. stenopetala* esters meet the requirements of both ASTM D6751 and EN 14214 biodiesel standards, which require viscosity ranges of 1.9–6.0 and 3.5–5.0 mm²/s, respectively.

The cloud and pour point for both the methyl and the mixture of (methyl and ethyl) esters of *M. stenopetala* oil were similar, 15 °C and 12 °C, respectively. These results are higher when compared to other biodiesels derived from vegetable oils, but less than biodiesel from palm oil and *M. oleifera* oil.²¹ The key fatty acids limiting the cold flow quality of biodiesel are palmitic (16:0) and stearic acids (18:0) since the melting points of the fatty acid esters are higher.²⁵ The relatively high content of C22:0 (behenic acid), which demands a higher melting point than C16:0 or C18:0 contributes to the poor cold flow properties of *M. stenopetala* oils. The reason is that the cold flow properties of biodiesel are determined by the amounts of higher-melting components (usually the saturated esters) and not their nature.²¹ Polyunsaturated fatty acids improve cold flow properties but the disadvantage is they are most susceptible to oxidation.²⁵ In this respect biodiesel from *M. stenopetala* oil is less susceptible to oxidation. However, when 80% of petro diesels was blended with 20% of both esters (*Moringa* biodiesels) the cloud and pour point were +4 and –5 °C respectively. B20 derived from *M. stenopetala* therefore can be used in all Ethiopian geographies.

The presence of water in biodiesel enhances corrosion, promotes growth of microorganisms and increases the probability that oxidation products may be formed during storage. Water cleaves the ester bond of the FAMES *via* hydrolytic degradation.¹⁴ Therefore, EN 14214 and ASTM D6751 require a maximum water concentration of 500 mg/l in biodiesel. In this study, the methyl as well as the mixture of (methyl and ethyl) esters was dried with anhydrous sodium sulfate until the water content of *Moringa* esters was less than the specification. The flashpoint of *M. stenopetala* methyl ester and mixture of (methyl and ethyl) esters were 185 °C and 197 °C, respectively. *M. stenopetala* derived biodiesels are consequently safer when compared to traditional diesels with lower flash points. *M. stenopetala* esters thus meet the requirements of the ASTM D6751 biodiesel standards, which demands a minimum flash point of 130 °C. The heat of combustion of *M. stenopetala* methyl ester and mixture of (methyl and ethyl) esters were 38.23 and 39.5 MJ/Kg respectively. They have 15% and 12% less heat energy on a mass basis, respectively, when compared to a diesel fuel which has about 45 MJ/Kg.⁶

The cetane numbers of the esters were not determined experimentally during the course of this work. However, the cetane numbers of methyl oleate, methyl palmitate and methyl stearate

are 59.3, 85.9 and 101, respectively, using an Ignition Quality Tester.²⁶ The methyl oleate composition of *M. stenopetala* is 76% and thus the cetane number of *M. stenopetala* derived biodiesel will be over the minimum cetane number requirements of both the ASTM D6751 and EN 14214 biodiesel standards, which are 47 and 51, respectively. The ash content of methyl and mixture of (methyl and ethyl) esters were 0.0098 and 0.0067%, respectively. It has been demonstrated that heating values are inversely related to ash content, with every 1% increase in ash concentration decreasing the heating value by 0.2 MJ/kg.²⁷ The ash content of *Moringa stenopetala* biodiesel meets the requirements of the ASTM D6751 biodiesel standards, which prescribe a maximum of 0.01%.

Experimental

Materials

The *M. stenopetala* seed used in this process was purchased from Podo PLC, Addis Ababa, Ethiopia. All the chemicals used were analytical grade and purchased from Sigma-Aldrich Chemie GmbH (Germany).

Extraction of *M. stenopetala* oil

350 g of crushed *M. stenopetala* seeds were extracted with 1 L of hexane at 60 °C for 6 hours in a Soxhlet apparatus. The solvent was removed at 65 °C under vacuum using a rotary evaporator to obtain crude *M. stenopetala* oil.

Transesterification of *M. stenopetala* oil

Transesterification with methanol. Methyl ester from the oil was prepared using a two-stage process as per the method described by Lang.²⁸ The amount of *M. stenopetala* oil used in the reaction was 300 g. A 6:1 molar ratio of methanol to oil was used in order to utilize 100% stoichiometric excess of methanol. Therefore, 68 g of methanol was used for the entire procedure, and 34 g was used per stage. The amount of potassium hydroxide (3 g) used was 1.0 wt% of the vegetable oil. The reaction was carried out at 25 °C, 45 °C and 60 °C to see the effect of temperature on yield. 30 minutes of reaction time per stage was used. Afterwards the mixture was added to a separatory funnel and allowed to separate overnight. Traces of moisture and unreacted methanol were removed by Rota-evaporator. A layer of anhydrous sodium sulfate crystals was added to a vacuum filtration funnel, and the ester was filtered through it to remove any traces of water present.

Transesterification with ethanol. The ethyl ester of *M. stenopetala* oil was prepared in a similar way to the methyl ester. The transesterification reaction was carried out at 25 °C and 70 °C with stirring for 2 hours. To avoid the emulsion after the transesterification reaction, 0.1% aqueous tannic acid was used as a washing solution to remove catalyst.⁶

Transesterification with a mixture of methanol and ethanol in 1:1 molar ratios. A mixture of methanol and ethanol in 1:1 molar ratios was used for the transesterification reaction, keeping the molar ratio of oil to alcohol 1:6. *M. stenopetala* oil (100 g) was placed in a dry Erlenmeyer flask equipped with

a magnetic stirrer. In another dry Erlenmeyer flask 1.0 g of potassium hydroxide was mixed with a mixture of methanol and ethanol (11.25 g of methanol and 15.5 g of ethanol). This mixture was then added to the oil and stirred for 50 minutes at 25 °C. The mixtures were poured into a separatory funnel and allowed to separate overnight. The ester layer was washed 3–4 times with 0.1% tannic acid solution to reduce emulsification. Finally, the ester was dried over anhydrous sodium sulfate crystals.

Characterization of biodiesel fuels

To determine suitability for use in diesel engines, methyl and methyl-ethyl esters were then characterized by determining their diesel properties following standard methods. The fatty acid compositions of the methyl and mixture of methyl and ethyl esters were measured by gas chromatography using a Dani GC 1000. Standards of the methyl esters of the fatty acids (products of Aldrich Chem. Co.) were obtained from the Essential Oils Research Center, Addis Ababa, Ethiopia. The GC was calibrated by injecting standards at varying concentrations. Then, samples were injected (0.5 µL) on the GC equipped with a capillary column of EC TM-5 (25 m × 0.53 mm × 1 µm). The GC oven was primarily kept at 50 °C for 2 minutes, and then heated at 4 °C/min up to 250 °C, where it was kept for 15 minutes. The flame ionization detector (FID) was at 260 °C while the injector temperature was kept at 210 °C, and the carrier gas was nitrogen at (1 mL/min). The viscosities of the esters were determined at 40 °C using a Cannon-Fenske glass capillary viscometer tube in accordance with ASTM D445. The properties of the biodiesels were measured using accepted standards. Cloud point (ASTM D2500), pour point (ASTM D97), acid value (ASTM D974), gross heat of combustion (ASTM D240), density (ASTM D1298), water content (ASTM D95), iodine value (AOCS Cd 1c-85) and carbon residue (ASTM D189) were used. Alkali and alkaline earth metals were determined by Flame Atomic Absorption Spectrophotometer (FAAS), BUCK SCIENTIFIC MODEL 210 VGP.

Conclusion

The study revealed that *M. stenopetala* seeds yield a high content of oil (45% w/w). The biodiesels (methyl ester and mixture of methyl and ethyl esters) derived from the oil meet the international standards. The fuel properties of the mixed (methyl and ethyl) esters were found to be better than that of the methyl ester alone. B20 is the preferred blend for use in Ethiopia. The biodiesel derived from *M. stenopetala* seed oil is an acceptable substitute for petro diesel. Its use will address two of the major global as well as national issues: climate change and energy security. Furthermore, the uses of *M. stenopetala* seed oil for the production of biodiesel will not compete with food since the oil is non-edible and the tree is used for other purposes such as food.

Acknowledgements

Financial support from the Horn of Africa Regional Environmental Centre, DelPHE and University of Nottingham is gratefully acknowledged. Andinet Ejigu is grateful to Dr Gerhard Knothe and the Ethiopian Petroleum Enterprise for technical support.

References

- 1 National Bank of Ethiopia, June 2007. www.nbe.gov.et.
- 2 S. Al-Zuhair *et al.*, *Biofuels, Bioprod. Biorefin.*, 2007, **1**, 57–663.
- 3 F. Ma and M. A. Hanna, *Bioresour. Technol.*, 1999, **70**, 1–15.
- 4 B. Freedman, E. H. Pryde and T. L. Mounts, *J. Am. Oil Chem. Soc.*, 1984, **61**, 1638–1643.
- 5 S. L. Dmytryshyn, A. K. Dalai, S. T. Chaudhari, H. K. Mishra and M. J. Reaney, *Bioresour. Technol.*, 2004, **92**, 55–64.
- 6 M. G. Kulkarni and A. K. Dalai, *Bioresour. Technol.*, 2007, **98**, 2027–2033.
- 7 *Ministry of Mines and Energy of Ethiopia report*, Addis Ababa, 2007, volume 2, pp 1–54.
- 8 J. F. Morton, *Econ. Bot.*, 1991, **45**, 318–333.
- 9 S. L alas and J. Tsaknis, *J. Food Compos. Anal.*, 2002, **15**, 65–77.
- 10 S. L. L alas, J. Tsaknis and K. Sfimos, *Eur. J. Lipid Sci. Technol.*, 2003, **105**, 23–31.
- 11 Y. Mekonnen, *Phytother. Res.*, 1999, **13**, 442–444.
- 12 S. A. A. Jahn, *GTZ*, No 191, 541, 1986.
- 13 E. Makonnen, A. Hunde and G. Damecha, *Phytother. Res.*, 1997, **11**, 147–148.
- 14 P. Schinas, G. Karavalakis, C. Davaris, G. Anastopoulos, D. Karonis, F. Zannikos, S. Stournas and E. Lois, *Biomass Bioenergy*, 2008, **33**, 44–49.
- 15 M. Canakci and J. Van Gerpen, *Trans. Am. Soc. Agr. Eng.*, 2001b, **44**, 1429–1436.
- 16 S. L. Dmytryshyn, A. K. Dalai, S. T. Chaudhari, H. K. Mishra and M. J. Reaney, *Bioresour. Technol.*, 2004, **92**, 55–64.
- 17 Olivera S. Stamenković, Zoran B. Todorović, Miodrag L. Lazić, Vlada B. Veljković and Dejan U. Skala, *Bioresour. Technol.*, 2007, **99**, 1131–1140.
- 18 A. Demirbas, *Biomass Bioenergy*, 2008, **33**, 113–118.
- 19 R. A. Ferrari, V. S. Oliveira and A. Scabio, *Scientia Agricola*, 2005, **62**, 291–295.
- 20 N. O. V. Sonntag, Ed. D. E. Swern, John Wiley and Sons, New York (USA), 4th edition, 1982, Vol. 2, pp. 407–527.
- 21 U. Rashid, F. Anwar, R. B. Moser and G. Knothe, *Bioresour. Technol.*, 2008, **99**, 8175–8179.
- 22 X. Lang, A. K. Dalai, N. N. Bakhshi, M. J. Reaney and P. B. Hertz, *Bioresour. Technol.*, 2001b, **80**, 53–62.
- 23 L. C. Meher, D. V. Sager and S. N. Naik, *Renewable Sustainable Energy Rev.*, 2006b, **10**, 248–268.
- 24 G. Knothe and K. R. Steidley, *Fuel*, 2005, **84**, 1059–1065.
- 25 G. Knothe, J. Krahl and J. Van Gerpen, *Am. Oil Chem. Soc.*, Press, Champaign, IL (USA), 2005, pp. 98–114.
- 26 G. Knothe, A. C. Matheaus and T. W. Ryan III, *Fuel*, 2003, **82**, 971–975.
- 27 K. A. Cassida, J. P. Muir, M. A. Hussey, J. C. Read, B. C. Venuto and W. R. Ocumpaugh, *Crop Sci.*, 2005, **45**, 682–92.
- 28 X. Lang, A. K. Dalai, M. J. Reaney and P. B. Hertz, *Tribotest J.*, 2001a, **8**, 131–150.
- 29 B. K. Bala, *Ener. Edu. Sci. and Technol*, 2005, **15**, 1–45.
- 30 R. Luque, L. Herrero-Davila, J. M. Campelo, J. H. Clark, J. M. Hidalgo, D. Luna, J. M. Marinasa and A. A. Romero, *Energy Environ. Sci.*, 2008, **1**, 542–564.
- 31 C. Echim, R. Verhe, W. De Greyt and C. Stevens, *Energy Environ. Sci.*, 2009, **2**, 1131–1141.

Direct conversion of glucose to 5-(hydroxymethyl)furfural in ionic liquids with lanthanide catalysts

Tim Ståhlberg, Mathilde Grau Sørensen and Anders Riisager*

Received 10th August 2009, Accepted 20th November 2009

First published as an Advance Article on the web 12th January 2010

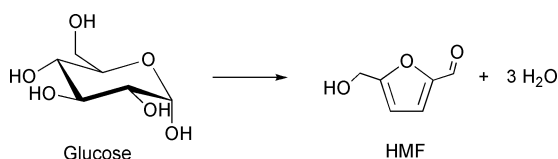
DOI: 10.1039/b916354a

The direct conversion of glucose to 5-(hydroxymethyl)furfural (HMF) in ionic liquids with lanthanide catalysts was examined in search of a possibly more environmentally feasible process not involving chromium. The highest HMF yield was obtained with ytterbium chloride or triflate together with alkyimidazolium chlorides. Notably, a higher reactivity was observed when the hydrophobicity of the imidazolium cation was increased, in contrast to analogous chromium catalyst systems. This indicates a different reaction mechanism for the lanthanides than for the chromium catalyst systems.

Introduction

In recent years, the search for alternatives to today's platform chemicals derived from fossil sources has intensified. One molecule under particular scrutiny has been 5-(hydroxymethyl)furfural (HMF), which is expected to become an important precursor to fuels, solvents and polymers in the chemical infrastructure.¹⁻³

HMF is formed by dehydration of hexoses under elevated temperature (Scheme 1, exemplified for glucose). The mechanism of the dehydration of hexoses has been subject of some debate, and proposals include both a mechanism consisting of only cyclic intermediates⁴⁻⁸ as well as an open-chain mechanism.⁹⁻¹³



Scheme 1 Dehydration of glucose to HMF.

The dehydration of fructose is quite facile – even in the absence of catalyst – in high-boiling solvents such as DMSO, DMF and DMA,^{14,15} whereas glucose requires a special catalyst for the formation of HMF.¹⁶⁻¹⁹ However, fructose is derived from glucose in a process that only yields about 50% of fructose and involves a chromatographic step in order to be purified.²⁰ Consequently, in order to find an economical and environmentally feasible industrial process for the production of HMF, an efficient direct conversion from glucose would be most beneficial.

In the last five years or so, interesting results have been presented on the dehydration of hexoses by the use of ionic liquids. As in the case of high-boiling organic solvents, ionic liquids have proven to be efficient media for converting fructose

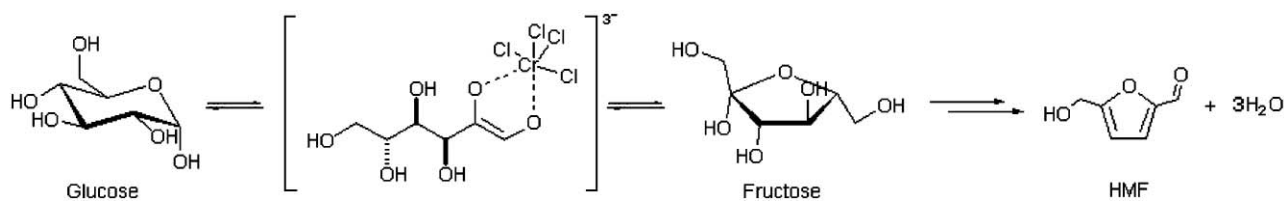
to HMF.²¹⁻²⁵ More importantly, very good results have been shown for the direct conversion of glucose to HMF (up to 70% yield) in 1-ethyl-3-methylimidazolium chloride ([EMIm]Cl) with a catalytic amount of chromium(II) chloride.¹⁶ In the proposed mechanism, a complex between ionic liquid and CrCl₂ interacts with the open chain of glucose, leading both to isomerization to fructose and direct conversion to HMF (Scheme 2).

An even higher yield of HMF was obtained when using chromium(II) or chromium(III) chloride complexed with sterically hindered carbenes.¹⁷ Comparable yields were also shown using a large surplus of metal halides in DMA together with chromium(II/III) chloride.¹⁸ Here a detailed mechanism of the actual role of the halide in the dehydration was also proposed. In this mechanism, fructose initially loses one water molecule, and the nucleophilic halide is then added to the anomeric carbon. The intermediate formed is then deprotonated to an enolic species, which is subsequently dehydrated twice to form HMF. Alternatively, the halide acts as a base in the second step and generates the enolic intermediate by deprotonation (Scheme 3).

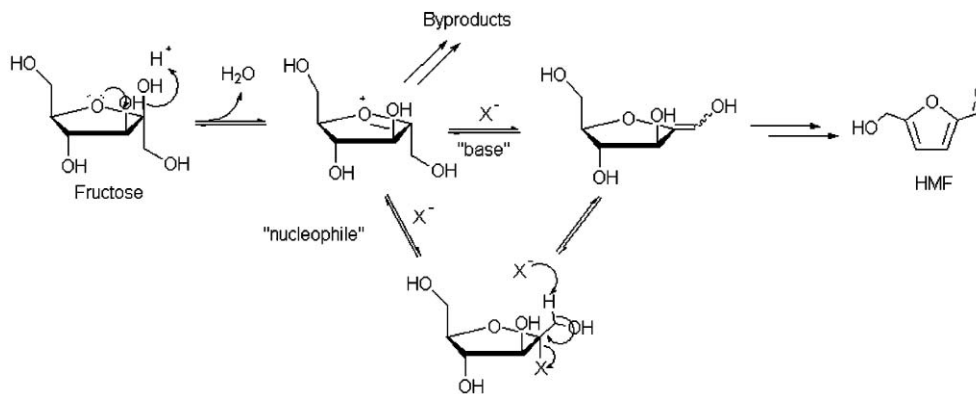
Apart from chromium chloride, there are no reports of equally efficient catalysts for the direct conversion of glucose to HMF. A very recent publication showed, however, that a dual-function catalyst composed of sulfated zirconia on alumina support could convert glucose directly to HMF with a moderate yield, presumably *via* glucose isomerization to fructose followed by dehydration.¹⁹ Furthermore, lanthanide chlorides have been shown to have a catalytic effect on glucose dehydration in supercritical water.²⁶ Notably, no levulinic acid or formic acid was observed here, as is normally the case when exposing HMF to aqueous acidic conditions.²⁷ In the study, kinetic and spectroscopic experiments suggested weak interaction between lanthanide and saccharide, resulting in higher reaction rates for smaller, less hydrated and heavier lanthanide ions.^{28,29}

Our objective in this work was to combine in particular the heavier lanthanide catalysts with ionic liquids and to investigate its catalytic effect on the direct conversion of glucose to HMF. Thus, imidazolium-based ionic liquids were used as solvents together with various lanthanide chloride catalysts in

Centre for Catalysis and Sustainable Chemistry, Department of Chemistry, Building 207, Technical University of Denmark, DK-2800, Kgs. Lyngby, Denmark. E-mail: ar@kemi.dtu.dk; Tel: +45 45252233



Scheme 2 Possible mechanism for the chromium-catalyzed dehydration of glucose to HMF in ionic liquids.¹⁶



Scheme 3 Proposed mechanism for the dehydration of fructose to HMF with halides.¹⁸

Table 1 HMF degradation in ionic liquids^a

Ionic liquid	Conversion of HMF (%)
[MIm]Cl	9
[EMIm]Cl	3
[BMIm]Cl	29
[HMIm]Cl	9
[OMIm]Cl	11
[EMIm]OAc	> 99
[BMIm]OAc	> 99
[Choline][dmp] ^b	6
[MIm][HSO ₄]	69
[EMIm][N(CN) ₂]	59
[EMIm][C ₂ H ₅ OSO ₃]	9
[EMIm][AlCl ₄]	77

^a Reaction conditions: 1.0 g ionic liquid, 100 mg (0.56 mmol) glucose, 100 °C, 8 h. ^b dmp = dimethyl phosphate.

the temperature range 120–200 °C. Additionally, the investigation was expanded to include even stronger Lewis acids such as ytterbium triflate.

Results and discussion

We initially screened the stability of HMF in several ionic liquids at elevated temperature to make sure that the ionic liquid used was not detrimental to the desired product. As seen from the data in Table 1, all ionic liquids induced some degradation of HMF during the stability tests. The acidic and basic ionic liquids proved to promote highest degree of degradation, whereas the imidazolium chlorides, [EMIm][C₂H₅OSO₃] and [Choline][dmp] were the most benign.

On the basis of the initial experiments, we further discovered that there was no HMF formed from glucose in ionic liquids that did not have chloride or other halides as anion. This is in agreement with the mechanism proposed by Binder and

Raines,¹⁸ where the chloride acts as a nucleophile and promotes the dehydration of the furanose fructose. Consequently, our study focused on the alkylimidazolium chlorides as solvents. [BMIm]Cl or [EMIm]Cl converted only fructose to HMF without additives (as also reported by Zhao *et al.*¹⁶) and not glucose. The addition of lanthanide chlorides, on the other hand, revealed a catalytic effect on glucose conversion (but not on fructose conversion), even though temperatures above 140 °C were required to avoid slow reactions and negligible yields. Furthermore, methylimidazolium chloride, which previously has given an excellent conversion of fructose to HMF,²³ gave less than one percent HMF from glucose with any lanthanide.

In the experiments with lanthanides (Table 2), cerium had very little catalytic effect in both [BMIm]Cl and [EMIm]Cl, whereas the other lanthanides showed quite different behaviours depending on the liquid. In the case of [EMIm]Cl, the reactivity for the lanthanide chlorides was the highest for promethium and then decreased almost linearly through the heavy lanthanides to YbCl₃. Moreover, when using the more Lewis-acidic ytterbium

Table 2 Lanthanide-catalyzed dehydration of glucose in [EMIm]Cl and [BMIm]Cl^a

Catalyst	[EMIm]Cl		[BMIm]Cl	
	Yield (%)	Selectivity (%)	Yield (%)	Selectivity (%)
CeCl ₃	3	3	3	4
PrCl ₃	13	27	7	22
NdCl ₃	12	24	8	23
DyCl ₃	10	19	10	23
YbCl ₃	5	7	12	15
Yb(OTf) ₃	10	16	24	37

^a Reaction conditions: 1.0 g ionic liquid, 100 mg (0.56 mmol) glucose, 0.056 mmol catalyst, 140 °C, 6 h.

triflate, a comparable yield to that of dysprosium chloride was obtained.

In [BMIm]Cl a completely different pattern was observed. Here the yield increased gradually from CeCl₃ to YbCl₃. This is consistent with the earlier relative catalytic effect found in supercritical water.^{26,28,29} Furthermore, ytterbium chloride and ytterbium triflate gave significantly higher yields in [BMIm]Cl than in [EMIm]Cl. This is the opposite of what has been shown earlier using chromium catalysts, where the yields were markedly better in [EMIm]Cl,¹⁶ thus clearly suggesting different catalyst–ionic liquid interaction in the systems.

Increasing the catalyst concentration of YbCl₃ in [EMIm]Cl, up to as much as 30 mol%, did not reveal any improvement in HMF yield. In contrast, the amount of catalyst had a significant effect on the HMF yield in [BMIm]Cl, thus further signifying differences between the catalytic systems (Fig. 1).

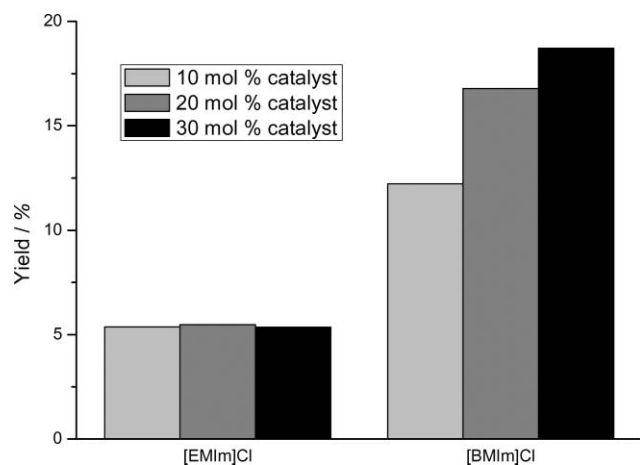


Fig. 1 Dehydration of glucose in [EMIm]Cl and [BMIm]Cl at 140 °C for 6 h with different amount of YbCl₃ catalyst. The reaction contained 1.0 g ionic liquid, 100 mg (0.56 mmol) glucose and 16 mg (0.056 mmol), 32 mg (0.112 mmol) and 48 mg (0.168 mmol) YbCl₃, respectively.

During dehydration in [BMIm]Cl, the selectivity towards HMF reached a maximum already after 10 min and a maximum yield after 30 min. The HMF was then slowly degraded due to the high temperature (Fig. 2). At an even higher temperature of 200 °C the yield was slightly increased, but at the expense of an even faster degradation of the product. In this case maximum yield was obtained after five minutes, and HMF was completely degraded after two hours (Fig. 3). All reactions formed substantial amounts of humins, but no other by-products were detected, as the essential anhydrous conditions (small amount of water is formed upon dehydration) prevented rehydration of HMF into levulinic acid and formic acid.

When it comes to finding an explanation why a longer alkyl chain on the imidazolium ring gave higher reaction rates for YbCl₃ and Yb(OTf)₃ catalysts, a possible reason could be related to ion pairing in the solvent. Cations with more hydrophobic character would be expected to have a weaker association with the chloride ion, which in turn would become more reactive. Earlier work has already shown that rates of reactions in ionic liquids involving halides are highly dependent on the nature of the cation.³⁰ This was also one of the rationales in the work of

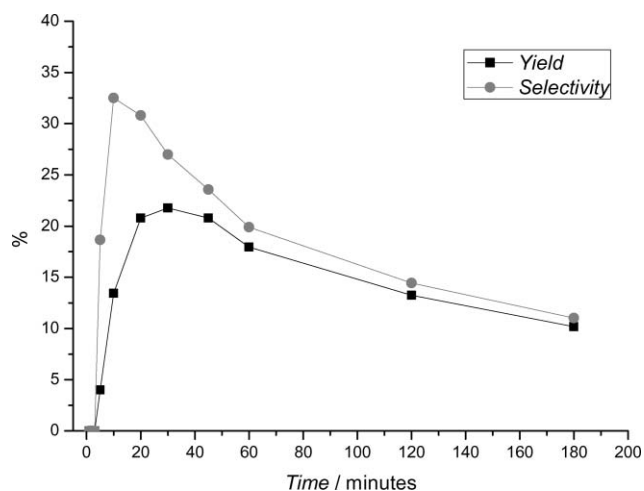


Fig. 2 Dehydration of glucose in [BMIm]Cl catalyzed by YbCl₃ at 160 °C as a function of the reaction time. The reaction contained 1.0 g ionic liquid, 100 mg (0.56 mmol) glucose and 16 mg (0.056 mmol) YbCl₃.

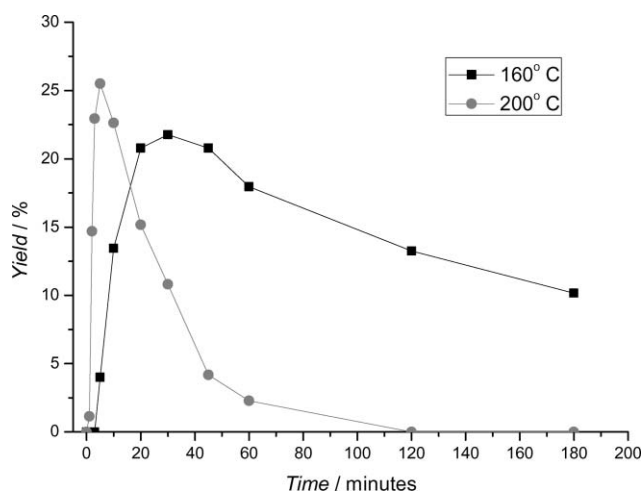


Fig. 3 Dehydration of glucose in [BMIm]Cl catalyzed by YbCl₃ at 160 °C and 200 °C as a function of time. Both reactions contained 1.0 g ionic liquid, 100 mg (0.56 mmol) glucose and 16 mg (0.056 mmol) YbCl₃.

Binder and Raines,¹⁸ who combined LiCl with DMA in order to produce weakly ion-paired chloride ions for sugar dehydration. In order to examine the effect of ion-pairing more closely, additional experiments with even longer alkyl chains, such as 1-hexyl-3-methylimidazolium chloride ([HMIm]Cl) and 1-octyl-3-methylimidazolium chloride ([OMIm]Cl), were performed. In these experiments, a faster conversion and a small increase in yield could actually be seen when using [HMIm]Cl or [OMIm]Cl as solvents (Fig. 4), even though it was less pronounced than the difference between [EMIm]Cl and [BMIm]Cl. The decrease in selectivity for [HMIm]Cl and [OMIm]Cl compared to [BMIm]Cl could be a result of the faster formation of humins.

Conclusions

We have shown that lanthanides catalyze the conversion of glucose to HMF in dialkylimidazolium chlorides. The strongest Lewis acids, YbCl₃ and Yb(OTf)₃, gave the highest yields, even

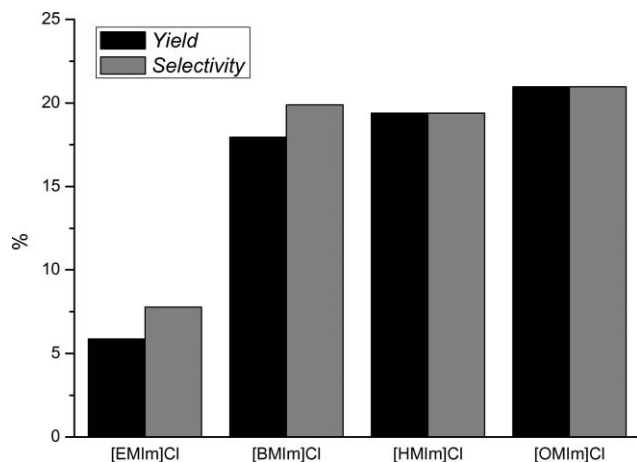


Fig. 4 Dehydration of glucose in [EMIm]Cl, [BMIm]Cl, [HMIm]Cl and [OMIm]Cl at 160 °C for 1 h. All reactions contained 1.0 g ionic liquid, 100 mg (0.56 mmol) glucose and 16 mg (0.056 mmol) YbCl₃.

though these were moderate (24%) compared to CrCl₂ (70%).¹⁶ Our results also suggest that the mechanism of the reaction might be different to that of chromium-catalyzed dehydration of glucose.

In the chromium system, highest yields are obtained with [EMIm]Cl, whereas the yield decreases with more hydrophobic imidazolium cations.¹⁶ In this reaction, chromium(II) chloride is believed to form a complex with the ionic liquid and then associate with the open chain form of glucose.¹⁶ Ytterbium showed a different reaction pattern, whereby the yield increased as the hydrophobic character of the imidazolium ring increased. We believe that the increase in reaction rates are due to weaker ion pairing between the chloride and imidazolium cation, making this more reactive in the dehydration mechanism. Furthermore, ytterbium could be less prone to form complexes with the imidazolium chlorides, which would explain the difference in reactivity compared to chromium.

Further studies on the actual complexation between lanthanide chlorides and imidazolium chlorides are needed to clarify the exact reaction pattern with glucose. Modeling of the various structures and intermediates together with the metals could also give new insights into the mechanism. Combined, this information could provide valuable directions on how to improve the lanthanide–ionic liquid systems to become competitive with present chromium systems.

Experimental

Materials and apparatus

Glucose (99.5%), 1-hexyl-3-methylimidazolium chloride (98%), 1-octyl-3-methylimidazolium chloride (98%) and ytterbium triflate (99%) were purchased from Aldrich. [EMIm][N(CN)₂] (98%), [Choline][dmp] (98%) and [EMIm][C₂H₅OSO₃] (98%) were purchased from Solvent Innovation. All other ionic liquids were obtained from BASF (>95%). Lanthanide chlorides (p.a.) were purchased from Rare Earth Ltd. All experiments were performed under nitrogen atmosphere using a Radley Carousel 12 Plus Basic System.

Dehydration reactions

A 40 mL reaction tube was charged with ionic liquid (1 g) and lanthanide(III) chloride (0.056 mmol) and heated at 100 °C for 1 h. Glucose (100 mg, 0.56 mmol) was then added and the solution stirred for 3 h at 140 °C. After reaction the reaction tube was cooled in an ice bath and water (5 mL) added. The solids were filtered off and the filtrate analyzed by HPLC (Agilent 1200 series, Bio-Rad Aminex HPX-87H, 300 mm × 7.8 mm pre-packed column, 0.005 M H₂SO₄ mobile phase, 60 °C, 0.6 mL min⁻¹).

Definitions of yield and selectivity

The yields and selectivities were based on conversion of glucose and confirmed by calibration of standard solutions of the products and reactants involved. With a known molar amount of all components, the conversion, yield and selectivity were calculated from the equations below:

$$\text{Glucose conversion} = \left(1 - \frac{\text{Amount of glucose}}{\text{Starting amount of glucose}} \right) \times 100\% \quad (1)$$

$$\text{Yield of HMF} = \frac{\text{Amount of HMF}}{\text{Starting amount of glucose}} \times 100\% \quad (2)$$

$$\text{Selectivity of HMF} = \frac{\text{Yield of HMF}}{\text{Glucose conversion}} \times 100\% \quad (3)$$

Acknowledgements

The reported work was supported by the Danish National Advanced Technology Foundation in cooperation with Novozymes A/S. Special gratitude is due to BASF for providing the ionic liquids.

References

- 1 T. Werpy and G. Petersen, *US DOE*, 2004, No. DOE/GO-102004-1992, <http://www.nrel.gov/docs/fy04osti/35523.pdf>.
- 2 A. Corma, S. Iborra and A. Velty, *Chem. Rev.*, 2007, **107**(2411), 2502.
- 3 J. N. Chheda, Y. Roman-Leshkov and J. A. Dumesic, *Green Chem.*, 2007, **9**, 342–350.
- 4 J. U. Nef, *Justus Liebigs Ann. Chem.*, 1910, **376**, 1–119.
- 5 W. N. Haworth, E. L. Hirst and V. S. Nicholson, *J. Chem. Soc.*, 1927, 1513–1526.
- 6 W. N. Haworth and W. G. M. Jones, *J. Chem. Soc.*, 1944, 667.
- 7 M. J. Antal, W. S. L. Mok and G. N. Richards, *Carbohydr. Res.*, 1990, **199**, 91–109.
- 8 A. S. Amarasekara, L. D. Williams and C. C. Ebede, *Carbohydr. Res.*, 2008, **343**, 3021–3024.
- 9 M. L. Wolfrom, E. G. Wallace and E. A. Metcalf, *J. Am. Chem. Soc.*, 1942, **64**, 265–269.
- 10 M. L. Wolfrom, R. D. Schuetz and L. F. Cavalieri, *J. Am. Chem. Soc.*, 1948, **70**, 514–517.
- 11 M. L. Wolfrom, R. D. Schuetz and L. F. Cavalieri, *J. Am. Chem. Soc.*, 1949, **71**, 3518–3523.
- 12 E. F. L. J. Anet, *J. Am. Chem. Soc.*, 1960, **82**, 1502–1502.
- 13 E. Anet, *Aust. J. Chem.*, 1961, **14**, 295–301.
- 14 Y. Nakamura and S. Morikawa, *Bull. Chem. Soc. Jpn.*, 1980, **53**, 3705–3706.
- 15 R. M. Musau and R. M. Munavu, *Biomass*, 1987, **13**, 67–74.
- 16 H. Zhao, J. E. Holladay, H. Brown and Z. C. Zhang, *Science*, 2007, **316**, 1597–1600.

- 17 G. Yong, Y. Zhang and J. Y. Ying, *Angew. Chem., Int. Ed.*, 2008, **47**, 9345–9348.
- 18 J. B. Binder and R. T. Raines, *J. Am. Chem. Soc.*, 2009, **131**, 1979–1985.
- 19 H. Yan, Y. Yang, D. Tong, X. Xiang and C. Hu, *Catal. Commun.*, 2009, **10**, 1558–1563.
- 20 S. Bhosale, M. Rao and V. Deshpande, *Microbiol. Rev.*, 1996, **60**, 280–300.
- 21 C. Fayet and J. Gelas, *Carbohydr. Res.*, 1983, **122**, 59–68.
- 22 C. Lansalot-Matras and C. Moreau, *Catal. Commun.*, 2003, **4**, 517–520.
- 23 C. Moreau, A. Finiels and L. Vanoye, *J. Mol. Catal. A: Chem.*, 2006, **253**, 165–169.
- 24 S. Hu, Z. Zhang, Y. Zhou, B. Han, H. Fan, W. Li, J. Song and Y. Xie, *Green Chem.*, 2008, **10**, 1280–1283.
- 25 Q. Bao, K. Qiao, D. Tomida and C. Yokoyama, *Catal. Commun.*, 2008, **9**, 1383–1388.
- 26 H. Ishida and K.-i. Seri, *J. Mol. Catal. A: Chem.*, 1996, **112**, L163–L165.
- 27 H. P. Teunissen, *Recl. Trav. Chim. Pays Bas*, 1930, **49**, 784–826.
- 28 K.-i. Seri, Y. Inoue and H. Ishida, *Bull. Chem. Soc. Jpn.*, 2001, **74**, 1145–1150.
- 29 K.-i. Seri, T. Sakaki, M. Shibata, Y. Inoue and H. Ishida, *Bioresour. Technol.*, 2002, **81**, 257–260.
- 30 N. L. Lancaster, P. A. Salter, T. Welton and G. B. Young, *J. Org. Chem.*, 2002, **67**, 8855–8861.

A straightforward synthesis of unsymmetrical secondary phosphine boranes†

Christelle Petit,^a Alain Favre-Réguillon,^{*a,b} Gérard Mignani^c and Marc Lemaire^{*a}

Received 29th September 2009, Accepted 11th November 2009

First published as an Advance Article on the web 14th January 2010

DOI: 10.1039/b920324a

A one-pot procedure for the synthesis of unsymmetrical alkyl-substituted secondary phosphine oxides is described. The sequential addition of *N*-benzylaniline to a solution of dichlorophenylphosphine and 1-methylimidazole in methylcyclohexane, separating of the protic ionic liquid formed, addition of Grignard reagent followed by hydrolysis gave unsymmetrical secondary phosphine oxides (SPOs) in high yield. The use of ionic liquids in the first step is essential and streamlined the synthesis. Unsymmetrical SPOs could be quantitatively reduced to secondary phosphine using a catalytic amount of Ti(O*i*Pr)₄ and tetramethyldisiloxane (TMDS) under mild reaction conditions.

Introduction

As the price of petrochemicals and the cost of waste disposal increases, the chemical industry is striving to minimize waste and negative environmental impact.^{1–2} A key objective is to eliminate the adverse environmental effects of chemical synthesis. Toward this end, progress has been made using safer reagents, eliminating the generation of dangerous and toxic byproducts and reducing the amount of waste produced. To minimize waste, several options should be considered: working under more concentrated conditions, selecting different starting materials and designing new routes that require fewer steps. For the latter, smaller quantities of starting materials, solvent and reagents will be used and thus reduce the cost for waste disposal.

Recent interest in air and moisture-stable SPOs has led to the identification of efficient transition metal catalyzed C–C, C–N and C–S bond forming reactions.^{3–5} Furthermore, SPOs are effective building blocks for the preparation of tertiary phosphines³ and P-chirogenic tertiary phosphines.^{6–9} The synthesis of unsymmetrical SPOs *via* substitution of organolithium or Grignard reagents with H-phosphinate according to the methods of Emmick^{10–13} is well-known, and recently the conversion of optically pure H-phosphinates to optically-active P-stereogenic SPOs has been described.^{14–15} However, a limited number of H-phosphinates has been described and alternative starting material and methods have to be studied.

Dichloro- and dibromoarylphosphine are easily accessible^{7,16–18} and the one-pot synthesis of unsymmetrical SPOs by reaction of Grignard reagents with dichlorophenylphosphine followed by hydrolysis has been studied.^{19–20} However, due to the highly electrophilic character of the chlorophosphine, the yields are often low, with the exception of the bulky *t*Bu.^{19–20} Thus, a two-step procedure^{21–22} and solid phase synthesis have been studied.^{23–25}

The development of an efficient strategy to synthesize unsymmetrical alkyl-substituted SPOs is in high demand. In this paper, we report a very efficient and versatile one-pot, homogeneous liquid phase synthesis of unsymmetrical secondary phosphine oxides (SPOs). Furthermore, we have found that these SPOs could be quantitatively reduced at 60 °C using tetramethyldisiloxane (TMDS) in the presence of 10% of titanium tetraisopropoxide (Ti(O*i*Pr)₄).²⁶

Results and discussion

Synthesis of unsymmetrical alkyl-substituted SPOs

When *N*-benzylaniline was reacted with PhPCl₂ in THF at 0 °C in the presence of Et₃N (Scheme 1), the ³¹P NMR showed that aminophosphine **1** was obtained in high purity. However, the separation of triethylamine hydrochloride from the reaction mixture was not straightforward. The ease of formation of aminophosphine **1** prompted us to further optimize this step. Neither the change of base (2,6 lutidine, DIPEA, pyridine) or solvent (toluene, THF, methylcyclohexane (MCH)) improved the separation or the selectivity.

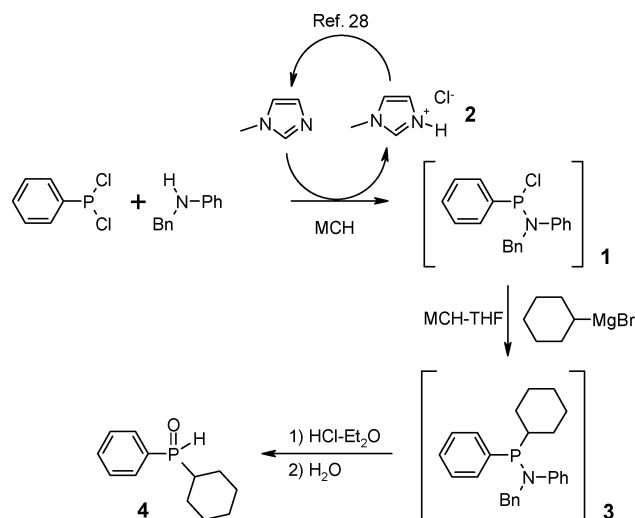
Recently, the BASIL process was developed and is operated by BASF. This process, which involves ionic liquids (ILs), uses 1-methylimidazole as an acid scavenger of the HCl produced during the synthesis of alkoxyphenylphosphine.²⁷ The protic ILs (PILs)²⁸ formed could be easily separated from the product and the Brønsted base 1-methylimidazole is easily regenerated by distillation.^{27–28} These results prompted us to examine whether

^aLaboratoire de Catalyse et de Synthèse Organique, UMR 5246, ICBMS, Université Claude Bernard Lyon 1, CPE Bat. 308, 43, bd du 11 Novembre 1918, 69622, Villeurbanne, Cedex, France. E-mail: marc.lemaire@univ-lyon1.fr

^bLaboratoire de Transformations Chimiques et Pharmaceutiques, Conservatoire National des Arts et Métiers, 2 rue Conté, 75003, Paris, France. E-mail: alain.favre-reguillon@univ-lyon1.fr

^cRhodia, Lyon Research Center, 85, avenue des Frères Perret, BP 62, 69192, Saint-Fons, Cedex, France

† Electronic supplementary information (ESI) available: Copies of ¹H, ¹³C and ³¹P NMR of the compounds listed in Tables 1 and 2. See DOI: 10.1039/b920324a



Scheme 1 One-pot synthesis of cyclohexylphenylphosphine oxide **4** with protic ILs.

PILs could be used to synthesize unsymmetrical secondary phosphine oxides (Scheme 1).

The addition of *N*-benzylaniline to a mixture of dichlorophenylphosphine and 1-methylimidazole at 0 °C in THF gave aminophosphine **1** but the problem of the separation of the ammonium salt remained. However, using MCH as solvent, the reaction mixture gave a biphasic reaction media. The lower phase consists of protic ILs, *i.e.* 1-methylimidazolium hydrochloride **2**, and the upper phase of aminochlorophosphine **1** in MCH. The use of MCH is essential to minimize the solubility of the PILs in the upper phase. The lower phase was discarded and the crude upper phase was diluted with THF (1 : 3, v/v). Then, a stoichiometric amount of cyclohexylmagnesium chloride solution in THF was added at 0 °C. A single product, **3**, was detected by ³¹P NMR.

After 1 h at room temperature, the mixture was quenched with HCl in diethylether at 0 °C and then with water. The reaction mixture was then extracted with ethyl acetate and cyclohexylphenylphosphine oxide **4** was obtained with a ³¹P NMR purity of 95%. The pure compound, as ascertained by ¹H, ¹³C and ³¹P NMR spectroscopy, could be obtained after chromatography on neutral alumina using cyclohexane/ethyl acetate as eluent.

The procedure was straightforward and reaction of the aminophosphine **1** with a stoichiometric amount of a variety of organomagnesium chlorides led to complete substitution of the P–Cl bonds. After hydrolysis, unsymmetrical SPOs could be obtained in good yield and the results are summarized in Table 1.

Entries 1–5 in Table 1 illustrate substitutions with Grignard compounds in order to obtain electron-rich SPOs. However, a low yield was obtained with methylmagnesium chloride (Entry 1). The substitution of aminophosphine **1** by methylmagnesium chloride gave the methylphenylphosphinamide with ³¹P NMR purity higher than 98%. However, during hydrolysis, several by-products are formed. Under those conditions, only 65% of methylphenylphosphinamide is transformed into methylphenylphosphine oxide as ascertained by ³¹P NMR (Table 1). Thus, alternative hydrolysis procedures were evaluated,²¹ but in that particular case, we were not able to limit

Table 1 One-pot synthesis of unsymmetrical SPOs

Entry	R-MgCl	SPOs	Isolated yield ^a (%)
1	CH ₃ –		40 ^b
2	C ₂ H ₅ –		71
3	<i>n</i> C ₅ H ₁₁ –		85
4	Cyclohexane–		73
5	<i>i</i> Pr–		80
6	4-MeO-Ph–		72

^a All compounds were isolated after chromatography on alumina. ^b The conversion was 65% as determined by ³¹P NMR of the crude.

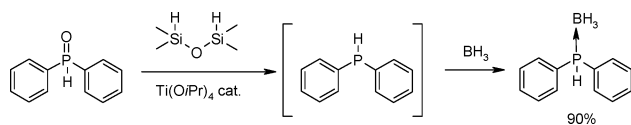
the formation of by-products. The methylphenylphosphine oxide was isolated in moderate yield (40%, entry 1) when compared to the yield obtained with two-step synthetic procedure starting from methyl- or phenylphosphinate ethyl esters.^{13,29} However, for ethyl- and other alkylmagnesium chlorides (entries 2–5), the hydrolysis reaction proceeded well and SPOs were obtained in good yield. Entry 6 shows a clean and complete substitution of the chloride by an aryl group. Thus, we can conclude that this methodology represents a versatile and general protocol for the synthesis of unsymmetrical SPOs, which can be prepared in one-pot starting from dichlorophenylphosphine using PILs.

Reduction of unsymmetrical SPOs to unsymmetrical secondary phosphines

The reduction of these unsymmetrical SPOs to unsymmetrical secondary phosphines was then studied. The reduction of SPOs is generally obtained using silanes such as diphenylsilane³⁰ or trichlorosilane in the presence of an amine base.³¹ However, reductions using silane are performed at temperature far from their boiling point.^{30,31} Thus, alternative process have been studied using borane³² or DIBAL-H.³³ Industries involved in phosphorus chemistry have successfully developed processes using these reagents. Nevertheless, due to new regulations and safety requirements, new, safer and cleaner reduction reagents compatible with sustainable chemistry are needed for the reduction of phosphine oxides on a large scale. Recently, we have shown that using a catalytic amount of Ti(O*i*Pr)₄ and tetramethyldisiloxane (TMDS), as the hydride source, various tertiary phosphine oxides and secondary phosphine oxides could be effectively reduced.²⁶ However, a temperature of 100 °C was needed to quantitatively reduce tertiary phosphine oxides in 5 h

using 10 mol% catalyst and a Si–H:P=O ratio of 2.5. As the boiling point of TMDS is 70 °C, the reaction has to be done in a sealed tube.

However, there are several advantages in using TMDS/Ti(O*i*Pr)₄ system as an alternative reduction system. TMDS is a liquid compound soluble in most organic solvents and inert to air and moisture. Furthermore, the work up was straightforward and the by-products are inert TiO₂ and oligomeric siloxanes. Thus, we decided to further investigate this catalytic system for the reduction of SPOs using diphenylphosphine oxide (Scheme 2).



Scheme 2 Reduction of diphenylphosphine oxide using the TMDS/Ti(O*i*Pr)₄ system.

We began our investigation with the reduction of diphenylphosphine oxide in toluene at 60 °C with 2.5 mol of TMDS and a stoichiometric amount of Ti(O*i*Pr)₄. The reaction was monitored by ³¹P NMR and we were pleased to see that diphenylphosphine oxide was reduced under those conditions even though the reaction proceeded slowly: 24 h at 60 °C are necessary for complete conversion. We next looked at making the reaction catalytic in Ti(O*i*Pr)₄. Again the reaction with 10 mol% Ti(O*i*Pr)₄ worked nearly as well as the stoichiometric variant. However, no conversion was observed for lower amounts of Ti(O*i*Pr)₄. The amount of TMDS was also decreased down to 1.25 mol and under those conditions the reduction was quantitative.

Thus, we have studied the reduction with the unsymmetrical alkyl-substituted secondary phosphine oxides previously synthesized (Table 1) under those conditions. In these experiments, the products were isolated as air-stable borane adducts by treatment of the reaction mixture with BH₃/THF complex. The results are summarized in Table 2. Various secondary phosphine oxides including electron-rich ones were effectively reduced in high yield. Aromatic SPOs (entries 1 and 2) were reduced in high isolated yield under the standard conditions. Electron-rich alkyl(phenyl)phosphine oxides were also effectively reduced. Table 2 illustrates the wide substrate scope of this process and these mild reduction conditions offer several advantages compared to previously methods of reduction.^{30–33} Moreover, given that TMDS is a hydride source inert to air and moisture and Ti(O*i*Pr)₄ was used as an activating agent, these conditions may be attractive as a general way to reduce SPOs.

Conclusion

In conclusion, we have developed a mild, one-pot synthesis of unsymmetrical secondary phosphine oxides (SPOs) using protic ionic liquids (PILs). The use of methylcyclohexane, that effectively separates the protic ionic liquid formed and the product, allows the one-pot synthesis of these SPOs. The use of methylcyclohexane as solvent is essential to minimize the solubility of the PILs. Furthermore, we have shown that these SPOs could be readily converted into the corresponding secondary

Table 2 SPOs reduction and protection as borane complex

Entry	SPOs	SPs-BH ₃	Isolated yield (%)
1			90
2			88
3			99
4			85
5			90
6			89

phosphine borane in high yield by the use of catalytic amount of air-stable Ti(O*i*Pr)₄ and tetramethyldisiloxane (TMDS) as an hydride source inert to air and moisture. The reaction can be performed at temperature below the boiling point of TMDS and provides secondary phosphines in high yields.

Experimental

General

Tetramethyldisiloxane (TMDS), Ti(O*i*Pr)₄ were obtained from Alfa Aesar, 1-methylimidazole and methylcyclohexane from Acros and dichlorophenylphosphine, HCl in Et₂O and organomagnesium were obtained from Aldrich. All compounds were used without further purification. NMR spectra were recorded on a Bruker DRX 300 and ALS 300. Chemical shifts are given in ppm using tetramethylsilane as the external standard for ¹H and ¹³C NMR spectra, and ³¹P NMR from 85% H₃PO₄.

General procedure A: synthesis of secondary phosphine oxide

An oven-dried three-necked round-bottomed flask under an argon atmosphere was charged with *N*-benzylphenylamine (0.9 mg, 5 mmol) and 1-methylimidazole (0.50 mL, 6 mmol) followed by methylcyclohexane (35 mL). Dichlorophenylphosphine (0.75 mL, 5 mmol) was added at room temperature. After 1 h, a biphasic solution was obtained. The crude methylcyclohexane upper phase was removed by syringe through the septum and added to an oven-dried three-necked round-bottomed flask under an argon atmosphere. 10 mL of anhydrous THF was added with a syringe and the homogenous reaction mixture was

cooled to 0 °C. Alkyl magnesium bromide (6 mmol, solution in THF) was then added and the reaction mixture is stirred at room temperature. After 1 h, ³¹P NMR analysis of an aliquot indicates the formation of a single product. The flask was then cooled to 0 °C and the reaction mixture was quenched with HCl 1M in diethylether. The reaction mixture was diluted by ethyl acetate then washed with NaHCO₃ and brine. The organic phase was dried over MgSO₄, filtered and concentrated under reduced pressure. The crude residue was dissolved in cyclohexane and deposited on a neutral aluminium oxide column. Cyclohexane was first used as eluent to removed *N*-benzylphenylamine hydrochloride. The desired secondary phosphine oxide was then obtained ethyl acetate–methanol as eluent (100 : 0 to 90 : 10, v/v).

Methyl(phenyl)phosphine oxide. Prepared by general procedure A to give the product (40%) as a colourless oil. ¹H NMR (300 MHz, CDCl₃): 7.55 (1 H, d, *J* = 567 Hz) 7.78–7.52 (2 H, m), 7.47–7.32 (3 H, m), 4.16–1.55 (3 H, m). ³¹P NMR (81 MHz, CDCl₃) 23.

Ethyl(phenyl)phosphine oxide. Prepared by general procedure A to give the product (71%) as colourless oil. ¹H NMR (300 MHz, CDCl₃) 7.68–7.61 (2 H, m), 7.52–7.46 (3 H, m), 7.39 (1 H, dt, *J* = 463, 7.4 Hz) 2.01–1.94 (2 H, m), 1.09 (3 H, dt, *J* = 20, 7.7 Hz). ¹³C NMR (75 MHz, CDCl₃) 132.8 (d, *J* = 2.5 Hz), 131.0 (d, *J* = 96.1 Hz), 130.3 (2C, d, *J* = 10.6 Hz), 129.3 (2C, d, *J* = 12.4 Hz), 23.6 (d, *J* = 68.2 Hz), 5.8 (d, *J* = 3.7 Hz). ³¹P NMR (81 MHz, CDCl₃) 32.

Pentyl(phenyl)phosphine oxide. Prepared by general procedure A to give the product (85%) as a colourless oil. ¹H-NMR (300 MHz, CDCl₃) 7.64–7.50 (2 H, m), 7.48–7.29 (3 H, m), 7.35 (1 H, d, *J* = 464 Hz) 1.88–1.8 (2 H, m), 1.59–1.40 (2 H, m), 1.34–1.15 (4 H, m), 0.8–0.64 (3 H, m). ¹³C-NMR (75 MHz, CDCl₃) δ 132.2 (d, *J* = 2.9 Hz), 130.9 (d, *J* = 96.2 Hz), 129.7 (2C, d, *J* = 10.7 Hz), 128.7 (2C, d, *J* = 12.4 Hz), 32.5 (d, *J* = 14.3 Hz), 30.0 (d, *J* = 67.9 Hz), 21.0 (d, *J* = 3.7 Hz), 20.78, 12.6. ³¹P-NMR (81 MHz, CDCl₃) 29.

Cyclohexyl(phenyl)phosphine oxide. Prepared by general procedure A to give the product (73%) as a colourless oil. ¹H NMR (300 MHz, CDCl₃): δ = 7.65–7.45 (5 H, m), 7.91 (1 H, d, *J* = 456 Hz), 1.87–1.66 (6 H, m), 1.20–1.17 (5 H, m). ¹³C NMR (75 MHz, CDCl₃): δ = 132.68 (d, *J* = 1.9 Hz), 130.64 (2C, d, *J* = 10.3 Hz), 130.0 (d, *J* = 92.7 Hz), 129.05 (2C, d, *J* = 11.9 Hz), 38.87 (d, *J* = 70.1 Hz), 26.37 (d, *J* = 3.0 Hz), 26.18 (d, *J* = 2.6 Hz), 26.1 (d, *J* = 1.2 Hz), 25.6 (d, *J* = 1.1 Hz), 24.9 (d, *J* = 2.3 Hz). ³¹P NMR (81 MHz, CDCl₃) 38.

Isopropyl(phenyl)phosphine oxide. Prepared by general procedure A to give the product (80%) as a yellow oil. ¹H NMR (300 MHz, CDCl₃): δ = 7.4 (1 H, dd, *J* = 458, 2.4 Hz), 7.65–7.53 (2 H, ddd, *J* = 12.6, 6.9, 1.3 Hz), 7.53–7.34 (3 H, m), 2.14–1.97 (1 H, m), 1.19–1.00 (6 H, m). ¹³C NMR (75 MHz, CDCl₃) δ = 132.66 (d, *J* = 3.0 Hz), 130.47 (2 CH, d, *J* = 10.1 Hz), 129.38 (2 CH, d, *J* = 93.2 Hz), 128.90 (d, *J* = 12.2 Hz), 28.64 (d, *J* = 69.0 Hz), 14.94 (2 CH₃, dd, *J* = 38.1, 1.4 Hz). ³¹P NMR (81 MHz, CDCl₃) 41.

(2-methoxyphenyl)(phenyl)phosphine oxide. Prepared by general procedure A to give the product (72%) as a yellow oil. ¹H

NMR (300 MHz, CDCl₃) 8.20 (1 H, d, *J* = 519 Hz), 7.85–7.66 (3 H, m), 7.57–7.38 (4 H, m), 7.14–7.06 (1 H, m), 6.90 (1 H, dd, *J* = 8.3, 5.7 Hz), 3.77 (s, 3 H). ¹³C NMR (75 MHz, CDCl₃): δ = 160.82 (d, *J* = 2.7 Hz), 134.62 (d, *J* = 1.9 Hz), 133.22 (d, *J* = 7.0 Hz), 132.32 (d, *J* = 78.0 Hz), 132.21 (d, *J* = 2.9 Hz), 131.68, 130.65 (2 C, d, *J* = 11.8 Hz), 128.71 (2 C, d, *J* = 13.1 Hz), 121.32 (d, *J* = 12.1 Hz), 119.56 (d, *J* = 75.2 Hz), 110.99 (d, *J* = 6.0 Hz), 55.72. ³¹P NMR (81 MHz, CDCl₃) 15.7.

General procedure B: reduction of secondary phosphine oxides

At room temperature and under an argon atmosphere was added Ti(O^{*i*}Pr)₄ (0.05 mL, 0.14 mmol) and TMDS (0.38 mL, 2.0 mmol) to a stirred solution of secondary phosphine oxide (1.4 mmol) with toluene (3 mL). The reaction mixture was then heated to 60 °C. After cooling for 24 h, ³¹P NMR analysis of an aliquot indicates that conversion was complete. The reaction mixture was then cooled to 0 °C and BH₃/THF (3 mmol) was added. After 1 h at room temperature, ³¹P NMR analysis of an aliquot indicates complete conversion to phosphine borane adduct. Silica gel was then carefully added to the flask and the reaction mixture was filtered through a Buchner funnel and then washed with ethyl acetate. The resulting mixture was concentrated under reduced pressure. The residue was purified by flash chromatography on silica gel with cyclohexane/ethyl acetate as eluent (100 : 0 to 80 : 20, v/v) to give secondary phosphine borane.

Diphenylphosphine borane. Prepared by general procedure B to give the product (90%) as a colourless oil. ¹H NMR (300 MHz, CDCl₃) 7.50–7.47 (m, 4 H), 7.14–7.12 (m, 6 H), 5.32 (d, *J* = 215 Hz, 1 H). ¹³C NMR (75 MHz, CDCl₃) 133.1 (d, *J* = 9.2 Hz), 131.7 (d, *J* = 2.5 Hz), 129.2 (d, *J* = 9.8 Hz), 127.2 (d, *J* = 177 Hz). ³¹P NMR (81 MHz, CDCl₃) 2.4 (m).

Ethyl(phenyl)phosphine borane. Prepared by general procedure B to give the product (99%) as a colourless oil. ¹H NMR (300 MHz, CDCl₃) 7.79–7.59 (2 H, m), 7.57–7.36 (3 H, m), 5.38 (1 H, ddd, *J* = 367.9, 12.3, 6.1 Hz), 2.06–1.81 (2 H, m), 1.13 (3 H, dtd, *J* = 8.0, 7.5, 2.3 Hz), 0.17–0.04 (m, 3 H). ¹³C NMR (75 MHz, CDCl₃): 132.9 (2 CH, d, *J* = 8.6 Hz), 131.8 (d, *J* = 2.6 Hz), 129.1 (2 CH, d, *J* = 9.9 Hz), 125.4 (d, *J* = 55.2 Hz), 17.0 (d, *J* = 36.6 Hz), 8.6 (d, *J* = 3.6 Hz). ³¹P NMR (81 MHz, CDCl₃): 2.32 (dd, *J* = 95.9, 41.6 Hz).

Pentyl(phenyl)phosphine borane. Prepared by general procedure B to give the product (85%) as a colourless oil. ¹H NMR (300 MHz, CDCl₃) 7.72–7.66 (2 H, m), 7.53–7.46 (3 H, m), 5.42 (dm, 1 H, *J* = 368 Hz), 1.98–1.79 (3 H, m), 1.50–1.57 (2 H, m), 1.36–1.29 (3 H, m), 0.88–0.85 (6 H, m). ¹³C NMR (75 MHz, CDCl₃) 132.9 (2 CH, d, *J* = 8.1 Hz), 131.7 (d, *J* = 2.2 Hz), 129.13 (2 CH, d, *J* = 10 Hz), 129.08 (d, *J* = 63 Hz), 33.4 (d, *J* = 13.2 Hz), 32.8 (d, *J* = 12.5 Hz), 25.7 (d, *J* = 35.9 Hz), 24.0 (d, *J* = 27.9 Hz), 23.1 (d, *J* = 86.5 Hz). ³¹P NMR (81 MHz, CDCl₃): –1.87 (d, *J* = 41.3 Hz).

Cyclohexyl(phenyl)phosphine borane. Prepared by general procedure B to give the product (90%) as a colourless oil. ¹H NMR (300 MHz, CDCl₃): δ = 7.70–7.57 (2 H, m), 7.56–7.39 (3 H, m), 5.23 (1 H, dm, *J* = 367 Hz) 2.00–1.54 (7 H, m), 1.41 (5 H, s). ¹³C NMR (75 MHz, CDCl₃) 133.80 (2 CH, d,

$J = 7.9$ Hz), 131.90 (d, $J = 2.4$ Hz), 129.20 (2 CH, d, $J = 9.6$ Hz), 125 (d, $J = 50$ Hz), 33.4 (d, $J = 25.8$ Hz), 28.3 (d, $J = 1.4$ Hz), 27.2 (d, $J = 92$ Hz), 26.47 (d, $J = 5.5$ Hz), 26.39, 25.68 (d, $J = 1.1$ Hz). ^{31}P NMR (81 MHz, CDCl_3) 13.6–11.8 (dd, $J = 57.4, 5.4$).

Isopropyl(phenyl)phosphine borane. Prepared by general procedure B to give the product (83%) as a colourless oil. ^1H NMR (300 MHz, CDCl_3) 7.68–7.45 (5 H, m), 5.86–4.63 (1 H, dm, $J = 363$ Hz), 6.67–3.63 (1 H, m), 1.22–1.15 (6 H, m). ^{13}C NMR (75 MHz, CDCl_3) 133.6 (2 CH, d, $J = 8.0$ Hz), 131.8 (d, $J = 2.5$ Hz), 129.0 (2 CH, d, $J = 9.9$ Hz), 125.0 (d, $J = 53.0$ Hz), 23.9 (d, $J = 35.1$ Hz), 17.9 (2CH₃, d, $J = 17.9$ Hz). ^{31}P NMR (81 MHz, CDCl_3) 16.65 (d, $J = 50.9$ Hz).

(2-Methoxyphenyl)(phenyl)phosphine borane. Prepared by general procedure B to give the product (88%) as a colourless oil. ^1H NMR (300 MHz, CDCl_3) 7.62 (3 H, dddd, $J = 21.7, 11.9, 7.8, 1.7$ Hz), 7.49–7.20 (4 H, m), 6.98 (1 H, ddd, $J = 14.9, 7.4, 1.3$ Hz), 6.84 (1 H, dd, $J = 8.2, 3.4$ Hz), 6.44 (1 H, qd, $J = 395, 6.9$ Hz), 3.74 (3 H, s). ^{13}C NMR (75 MHz, CDCl_3) 160.63 (d, $J = 1.2$ Hz), 134.94 (d, $J = 13.7$ Hz), 133.92, 132.83 (2 CH, d, $J = 9.8$ Hz), 131.13 (d, $J = 2.5$ Hz), 128.72 (2 CH, d, $J = 10.4$ Hz), 126.96 (d, $J = 57.9$ Hz), 121.38 (d, $J = 12.3$ Hz), 114.63 (d, $J = 55.5$ Hz), 110.81 (d, $J = 4.2$ Hz), 55.79. ^{31}P NMR (81 MHz, CDCl_3) –15.28 (d, $J = 65.1$ Hz).

References

- P. T. Anastas and J. B. Zimmerman, *Environ. Sci. Technol.*, 2003, **37**, 94A–101A.
- N. G. Anderson, *Org. Process Res. Dev.*, 2008, **12**, 1019–1020.
- G. Y. Li, *Angew. Chem., Int. Ed.*, 2001, **40**, 1513–1516.
- L. Ackermann, *Synthesis*, 2006, 1557–1571.
- N. V. Dubrovina and A. Boerner, *Angew. Chem., Int. Ed.*, 2004, **43**, 5883–5886.
- H. Lebel, S. Morin and V. Paquet, *Org. Lett.*, 2003, **5**, 2347–2349.
- D. Mimeau, O. Delacroix and A.-C. Gaumont, *Chem. Commun.*, 2003, 2928–2929.
- V. S. Chan, M. Chiu, R. G. Bergman and F. D. Toste, *J. Am. Chem. Soc.*, 2009, **131**, 6021–6032.
- N. F. Blank, J. R. Moncarz, T. J. Brunker, C. Scriban, B. J. Anderson, O. Amir, D. S. Glueck, L. N. Zakharov, J. A. Golen, C. D. Incarvito and A. L. Rheingold, *J. Am. Chem. Soc.*, 2007, **129**, 6847–6858.
- T. L. Emmick and R. L. Letsinger, *J. Am. Chem. Soc.*, 1968, **90**, 3459–3465.
- R. L. Wife, A. B. Van Oort, J. A. Van Doorn and P. W. N. M. Van Leeuwen, *Synthesis*, 1983, 71–73.
- C. A. Busacca, J. C. Lorenz, P. Sabila, N. Haddad and C. H. Senanayake, *Org. Synth.*, 2007, **84**, 242–261.
- T. K. Olszewski, B. Boduszek, S. Sobek and H. Kozłowski, *Tetrahedron*, 2006, **62**, 2183–2189.
- A. Leyris, J. Bigeault, D. Nuel, L. Giordano and G. Buono, *Tetrahedron Lett.*, 2007, **48**, 5247–5250.
- Q. Xu, C.-Q. Zhao and L.-B. Han, *J. Am. Chem. Soc.*, 2008, **130**, 12648–12655.
- Z.-W. Wang and L.-S. Wang, *Green Chem.*, 2003, **5**, 737–739.
- T. J. Clark, J. M. Rodezno, S. B. Clendenning, S. Aouba, P. M. Brodersen, A. J. Lough, H. E. Ruda and I. Manners, *Chem.–Eur. J.*, 2005, **11**, 4526–4534.
- V. Chandrasekhar, P. Sasikumar, R. Boomishankar and G. Anantharaman, *Inorg. Chem.*, 2006, **45**, 3344–3351.
- H. Hoffmann and P. Schellenberg, *Chem. Ber.*, 1966, **99**, 1134–1142.
- X. Cheng, P. N. Horton, M. B. Hursthouse and K. K. Hii, *Tetrahedron: Asymmetry*, 2004, **15**, 2241–2246.
- G. Baba, J.-F. Pilard, K. Tantaoui, A.-C. Gaumont and J.-M. Denis, *Tetrahedron Lett.*, 1995, **36**, 4421–4424.
- C.-H. Wei, C.-E. Wu, Y.-L. Huang, R. G. Kultyshev and F.-E. Hong, *Chem.–Eur. J.*, 2007, **13**, 1583–1593.
- G. Y. Li and P. J. F. P. L. Watson, *Angew. Chem., Int. Ed.*, 2001, **40**, 1106–1109.
- G. Y. Li, *Patent PCT WO 01/79213*, 2001.
- G. Y. Li, *Patent PCT WO 02/00574*, 2002.
- M. Berthod, A. Favre-Reguillon, J. Mohamad, G. Mignani, G. Docherty and M. Lemaire, *Synlett*, 2007, 1545–1548.
- M. Volland, V. Seitz, M. Maase, M. Flores, R. Papp, K. Massonne, V. Stegmann, K. Halbritter, R. Noe, M. Bartsch, W. Siegel, O. M. Becker, and *Huttenloch Patent PCT WO 03/06225*, 2003.
- T. L. Greaves and C. J. Drummond, *Chem. Rev.*, 2008, **108**, 206–237.
- S. P. Collingwood and R. J. Taylor, *Synlett*, 1998, 283–285.
- L. McKinstry and T. Livinghouse, *Tetrahedron Lett.*, 1994, **35**, 9319–9322.
- X. Dong and C. Erkey, *J. Mol. Catal. A: Chem.*, 2004, **211**, 73–81.
- M. Stankevicius and K. M. Pietrusiewicz, *Synlett*, 2003, 1012–1016.
- C. A. Busacca, J. C. Lorenz, N. Grinberg, N. Haddad, M. Hrapchak, B. Latli, H. Lee, P. Sabila, A. Saha, M. Sarvestani, S. Shen, R. Varsolona, X. Wei and C. H. Senanayake, *Org. Lett.*, 2005, **7**, 4277–4280.

Microreactor with mesoporous silica support layer for lipase catalyzed enantioselective transesterification†

Sho Kataoka, Yasutaka Takeuchi, Atsuhiko Harada, Mitsuhiro Yamada and Akira Endo*

Received 22nd August 2009, Accepted 21st November 2009

First published as an Advance Article on the web 18th January 2010

DOI: 10.1039/b917374a

Lipase PS was immobilized in mesoporous silica (MPS) thin films inside a borosilicate tube microreactor for use in the enantioselective transesterification of vinyl acetate with (±)-1-phenylethanol. The immobilization was tested for 3D cubic and 2D hexagonal MPS thin films inside microreactors with and without hydrophobic treatment. The hydrophobic treatment enhanced the adsorption amount and the lipase activity for both 3D cubic and 2D hexagonal films. Of these treated films, the 3D cubic structure film exhibited the highest yield (64%) with an enantioselectivity higher than 99% in a continuous flow experiment. The activity of the immobilized lipase PS was well maintained for 36-hour continuous operation. A Ping-Pong Bi Bi kinetic model was employed to interpret the activity of the immobilized lipase PS. The ratios of the maximum velocity to the Ping-Pong constant (*i.e.*, specificity constants) were measured for lipase PS immobilized inside the microreactor and for native lipase PS. The value inside the microreactor was 800 times greater than that of the native lipase PS.

Introduction

Enzymatic reactions have acquired increasing importance as tools for fine chemical syntheses. Lipase exhibits an excellent stereoselectivity and enantioselectivity in hydrolysis and acylation reactions, and has been widely investigated over recent decades.^{1–3} Lipase-catalyzed acylations are of great importance for optical resolution in chemical syntheses; however, native lipase is not uniformly dispersed in organic solvents because of its poor solubility, which results in low enzymatic activity. It is reported that the activity and enantioselectivity in the acylation of chiral alcohols catalyzed by lipase PS can be altered in various solvent systems.^{4,5} Many attempts have been made to improve the lipase activity and enantioselectivity,^{4–9} and a common solution is to immobilize it in support matrices, such as metal oxides, sol-gel materials, and polymers.^{10–12} Lipase is uniformly dispersed in a matrix by the immobilization, and can be used effectively in organic solvent systems.

Enzyme immobilization has commonly been employed for large scale synthesis in both aqueous and organic solvents.¹³ Since immobilization simplifies the separation and reuse of enzymes reducing chemical wastes, it is a valuable tool in food, pharmaceutical, and chemical industries.¹⁴ However, by comparison with native enzymes homogeneously dissolved in an aqueous solution, the activity of enzymes in support matrices is generally reduced. This is mainly attributed to the denaturation of the enzymes and to the diffusion limitation of the reactants.

As regards diffusion limitation in particular, if enzymes are immobilized deep inside a matrix, the probability of the reactant molecules encountering enzymes is limited because of the slow molecular diffusion inside the support matrix. It is inferred that enzymes immobilized near the matrix surface are mainly exploited in the reactions. Therefore, if the diffusion limitation in the support matrix is diminished, the apparent lipase activity would be enhanced.

A microreactor with a small reaction space in the range from 100 μm to 1 mm is a useful tool for fine chemical synthesis.^{15–17} One characteristic feature is that it has a large interfacial area per unit volume. If a catalyst is coated on its wall, reactant molecules can easily encounter the catalyst because of the short diffusion distance inside the microreactor. Such a system can be expected to be an efficient tool for heterogeneous catalytic reactions.¹⁸ Microreactors have increasingly been employed for enzymatic reactions as high throughput analytical and synthetic tools.^{14,19} In these applications, enzymes were immobilized inside microreactors with elegant techniques including biotin–avidin labeling techniques,^{20–22} cross-linking enzyme aggregation,^{23,24} and use of metal oxide monolith/beads.^{25–28} A simple and robust enzyme immobilization method is desired for further use of microreactors.

Recently, we have developed a microreactor that has a mesoporous silica (MPS) thin film on its inner walls.^{29,30} MPS, which is typically synthesized with a silica precursor and surfactant micelle templates, and possesses a highly ordered pore structure.^{31–34} Because of its uniform pores (about 7.5 nm in diameter), MPS is suitable for use as a catalyst support, and has recently been used as an enzyme support matrix.³⁵ Several types of MPS powder exhibited high enzyme loading capacities for horseradish peroxidase,³⁶ catalase,³⁷ and lipase.^{38–43} It is also reported that this immobilization technique often enhanced the thermal and chemical stabilities of enzymes.^{36,37}

National Institute of Advanced Industrial Science and Technology (AIST), 1-1-1 Higashi, Tsukuba, Ibaraki, 305-8565, Japan.
E-mail: endo-akira@aist.go.jp; Fax: +81-29-861-4660;
Tel: +81-29-861-4653

† Electronic supplementary information (ESI) available: Estimation of effective diffusivity inside mesoporous silica films. See DOI: 10.1039/b917374a

Therefore, the MPS film was provided inside the microreactor as a support matrix. Importantly, the thin MPS film (less than 150 nm) could minimize the diffusion limitation within the MPS support matrix, and enhance the apparent activity of immobilized enzymes. In this context, a microreactor containing MPS films is better adapted to enzymatic reactions in fine chemical syntheses.

This study describes the immobilization of lipase PS in MPS thin films inside a microreactor for use in the acylation of (\pm)-1-phenylethanol with vinyl acetate. This paper has two main parts. The first part describes the testing of several types of MPS film appropriate for lipase immobilization, and the second part evaluates the immobilized enzyme activity by comparison with native lipase PS. The surface hydrophilicity and porous structure of MPS films are discussed in the first part with a view to achieving effective lipase immobilization. It is known that the hydrophilicity of SiO₂ considerably alters the adsorption property of lipase.^{12,44} The porous structure of MPS film affects the access of reactant molecules to the immobilized lipase. These two factors would play an important role in lipase activity. In the second part, the activity of the immobilized lipase is quantified by fitting to a Ping-Pong Bi Bi kinetic model for comparison with native lipase.¹³

Experimental

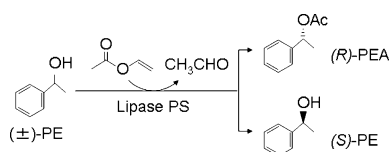
All chemicals were used as received. For the MPS preparation, ethanol, tetraethyl orthosilicate (TEOS), and hydrochloric acid were obtained from Junsei Chemical Co. (Tokyo, Japan). F127 block copolymer supplied by BASF (Mount Olive, NJ, USA) was used as a structure-directing agent. A borosilicate tube (Vitrocom, Mountain Lakes, NJ, USA) containing six bores 0.20 mm in inner diameter and 30 cm long (3 mm outer diameter) was used as a microreactor. Lipase PS SD and lipase PS IM are products of Amano Pharmaceutical Co. Note that lipase PS IM is a commercial formulation of lipase PS immobilized on SiO₂ (diatomaceous earth). For a buffer solution, 2-(*N*-morpholino)ethanesulfonic acid (MES) was obtained from Dojin Chemical (Kumamoto, Japan). For the transesterification, (\pm)-1-phenylethanol (PE) and (*S*)-(-)-1-phenylethanol ((*S*)-PE) were purchased from Wako Pure Chemical Industries Ltd. (Osaka, Japan); (\pm)-1-phenylethylacetate (PEA) was purchased from Merck Schuchardt OHG (Hohenbrunn, Germany); vinyl acetate (VA) and diisopropyl ether (*i*Pr₂O) were obtained from Kishida Chemical Co. (Osaka, Japan); 1,1,1,3,3,3-hexamethyldisilazane (HMDS) was purchased from Aldrich (Milwaukee, WI, USA).

The preparation of MPS thin films inside microreactors has been detailed elsewhere.^{29,30} Two different MPS structures were formed in the present study. The molar ratios of TEOS, H₂O, HCl, EtOH, and F127 in precursor solutions were 1:9.2:0.042:51:0.0041 for 3D cubic MPS film and 1:9.2:0.021:40:0.0072 for 2D hexagonal film. The inner walls of micro-capillary tubes were coated with these precursor solutions. In fact, it is difficult to measure the amount of adsorption inside microreactors directly. Accordingly, a quartz microbalance system (QCM: Q-Sense D300, Göteborg, Sweden) was used for measuring the amount of lipase adsorbed on the MPS films. The same precursor solutions were used to form

MPS thin films on QCM oscillators by dip coating with a 3.6 cm min⁻¹ withdrawing speed. The hydrophobic surfaces were prepared with HMDS. The prepared MPS thin films were exposed to HMDS vapor at room temperature for 2 h. After this exposure, the films were dried at 70 °C to remove excess adsorbed HMDS. In this process, the surface Si-OH groups of MPS were converted into methyl terminals and became hydrophobic.⁴⁵ Surface and cross-sectional images of the prepared MPS films were acquired with a scanning electron microscope (SEM) at an acceleration voltage of 0.8–1.5 kV (S-4800 FE-SEM: Hitachi High-Technologies, Japan). For this observation, the micro-capillary tubes were broken to reveal the MPS films coated on their inner walls.

In the lipase immobilization process, the developed microreactor was filled with a 10 mg mL⁻¹ lipase PS solution and kept at 5 °C for 12 h to reach adsorption equilibrium. The lipase solution was prepared by dissolving lipase PS SD in 20 mM MES buffer solution controlled at pH 7. Prior to the experiment, the microreactor was rinsed with the buffer solution for more than 30 min to remove excess lipase. Subsequently, N₂ gas was fed through the microreactor to remove any remaining buffer solution because the reactant solution is not soluble in water. In the QCM analyses used to measure the amount of adsorbed lipase, 10 mg mL⁻¹ lipase solution was fed into the system where it remained for 2 h. After flowing the buffer solution to remove excess lipase near the surface, the mass change of the QCM oscillator was monitored.

Transesterification was carried out with lipase immobilized inside the microreactor. All the experiments using the microreactor were performed at 40 °C in a continuous flow manner. The reaction is expressed as follows: This model reaction catalyzed



by lipase PS is known as a route to enantiomerically pure compounds under mild conditions.³ Because of its high activity and selectivity, the reaction is frequently discussed in the field of green chemistry.^{4,46} A mixture of (\pm)-PE and VA dissolved in *i*Pr₂O was fed at a rate ranging from 0.3 to 24 μ L min⁻¹ by using a syringe pump (PHD2000, Harvard Apparatus, Holliston, MA, USA). The initial concentration was ranging from 5 to 26 mM for PE and from 5 to 50 mM for VA, respectively. The effluent was collected to measure its concentration with an HPLC (Shimadzu LC-10A, Kyoto, Japan) equipped with a Chiralcel OD column (Daicel Chemical Industries, Tokyo, Japan). The UV detector was set at 254 nm, and the column temperature was held at 30 °C. The mobile phase was hexane/2-propanol (6/1), and the flow rate was 1 mL min⁻¹. Reference compounds including (\pm)-1-phenylethanol, (*S*)-(-)-1-phenylethanol, and (\pm)-1-phenylethylacetate were used to identify the retention time of the products.

Additional batch experiments were conducted using lipase PS SD and lipase PS IM to evaluate enzyme activity. The mixture of PE and VA dissolved in *i*Pr₂O (3 mL) was added to a 13.5 mL glass vial containing lipase PS SD (30 mg) or lipase PS IM (5 mg), and was then stirred (600 rpm) at 40 °C. The initial concentration

of PE tested in these batch experiments was ranging from 6 to 26 mM; the initial concentration of VA was ranging from 5.7 to 57 mM. After completion of the reaction time, the suspension was quickly filtered through a cellulose acetate filter (0.5 μm , Advantec DISMIC-13, Tokyo, Japan) and then was injected into the HPLC system.

Results and discussion

MPS films for lipase PS immobilization

The first part of this study focuses on the influence of the porous structure and hydrophilicity of MPS thin films on the amount and activity of adsorbed lipase. Fig. 1 shows SEM images of MPS thin films that were formed on the inner wall of the microreactor. Two forms of MPS were prepared for the investigation: 3D-cubic (Fig. 1a and b) and 2D-hexagonal (Fig. 1c and d). A major difference between two structures was the existence of open mesopores on the surface. Uniform open pores about 7.5 nm in diameter are aligned in an orderly way with 3-fold symmetry on the surface (Fig. 1a). This is a typical feature of a 3D cubic structure.^{30,34} As shown in Fig. 1b, the film thickness is about 45 nm. With the 2D hexagonal film shown in Fig. 1c, the pore channels are aligned parallel to the surface forming a swirling pattern with few open pores (dark spots in the figure) on the surface. Fig. 1d shows that the film

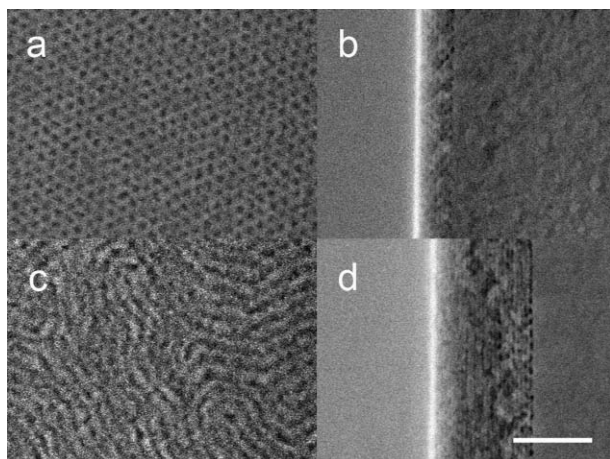


Fig. 1 Structures of mesoporous thin films on the inner wall of microreactors: (a) Surface image of 3D cubic; (b) cross-sectional image of 3D cubic; (c) surface image of 2D hexagonal, (d) cross section of 2D hexagonal. Scale bar: 100 nm.

thickness is about 125 nm and that the pore channel size is about 7.5 nm, which is almost the same as the pore size of 3D cubic film. We confirmed that ordered pore structures were present inside the microreactor. We also confirmed that the films on the QCM oscillators had the same structures as those inside the microreactor.

The amount of lipase adsorbed on the MPS films on QCM oscillators was measured in order to understand the properties of support matrices suitable for lipase immobilization. We investigated MPS films with and without HMDS hydrophobic treatment. Hereafter, we refer to HMDS-treated 3D cubic and 2D hexagonal films as H-cubic and H-hexagonal films, respectively. The mass change (ΔM) of QCM oscillators coated with MPS films was monitored after they were exposed to lipase solution (Fig. 2). Fig. 2 shows that lipase adsorption increased rapidly and reached equilibrium after exposure to lipase solution. Importantly, ΔM remained constant after it was rinsed with buffer solution, which indicates that little lipase leached from the MPS films. Although several reports mention that a strong interaction between enzyme and silica is required in the immobilization process to minimize the amount of enzyme leaching out from silica,^{40,47} the MPS films exhibited excellent affinity to lipase PS. The final values of ΔM are also listed in Table 1. A comparison of the final ΔM values for MPS films showed that lipase adsorbed more on HMDS-treated films than on untreated films. The lipase adsorption on H-cubic film (1.55 $\mu\text{g cm}^{-2}$) was about 9 times that on the untreated film (0.173 $\mu\text{g cm}^{-2}$), while the adsorption on H-hexagonal film (2.12 $\mu\text{g cm}^{-2}$) was about 20 times that on the untreated film

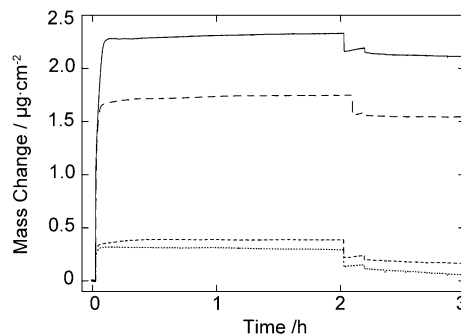


Fig. 2 Amount of lipase adsorbed in MPS films on QCM oscillators: (from top to bottom) solid line: H-hexagonal, long-dashed line: H-cubic, short-dashed line: cubic, dotted line: hexagonal. At 2 min, lipase solution was supplied to the QCM system. Every 10 min after 122 min, the buffer solution was supplied to remove excess lipase.

Table 1 Amount and activity of lipase adsorbed on 4 types of MPS thin film

Type of MPS	$\Delta M / \mu\text{g cm}^{-2a}$	(R)-PEA/mM ^b	(R)-PE/mM ^b	(S)-PE/mM ^b	i-(R)-PE/mM ^c	i-(S)-PE/mM ^c	Yield [%] ^d
Cubic	0.173	0.272	12.9	12.9	13.0	12.9	2.10
Hexagonal	0.102	0.202	13.1	12.4	13.0	12.9	1.56
H-Cubic	1.55	9.53	5.44	14.9	14.9	14.9	63.9
H-Hexagonal	2.12	6.64	8.31	14.8	14.9	14.9	44.7
H-Cubic ^e	—	11.2	1.17	12.5	12.1	12.1	92.5

^a Mass change (ΔM) was calculated from frequency shift (Δf) of QCM based on Sauerbrey equation. ^b The concentration in the effluent. ^c The concentration in the influent. ^d Ratio of the concentration of (R)-PEA in the effluent and the initial concentration of (R)-PE. ^e Microreactor experiment was at a flow rate of 0.3 $\mu\text{L min}^{-1}$. Other experiments were at 1.2 $\mu\text{L min}^{-1}$. When the flow rate is small in this system, the reaction proceeds further because of long contacting time.

($0.102 \mu\text{g cm}^{-2}$). It is clear that lipase was preferentially adsorbed on the hydrophobic films. This agrees with other reports on silica and MPS.^{12,39,44} While several types of interaction including electrostatics, hydrogen bonding, hydrophobic interactions, and van der Waals interactions govern protein adsorptions,⁴⁸ the hydrophobic interaction dominates in the lipase adsorption in MPS. Furthermore, the QCM results showed that more lipase was adsorbed on H-hexagonal film than on H-cubic film. It is simply because the thickness of H-hexagonal film is greater than that of H-cubic film. As shown in Fig. 1b and d, the hexagonal film (125 nm) was thicker than the cubic film (45 nm). Because thicker films should have a larger pore volume, the H-hexagonal film had a greater lipase adsorption capacity than the H-cubic film. From the ΔM values and the size of lipase, we calculated the total volume of adsorbed lipase and compared it with the size of the pore volume. From this estimation, lipase was adsorbed on almost the entire H-cubic film from top to bottom, while an open space still remained in the H-hexagonal film. Therefore, lipase was adsorbed more on the H-hexagonal film because it even migrated inside the narrow pore channels of the H-hexagonal film during the long immobilization process.

The activity of the adsorbed lipase was also compared with four types of MPS film coated inside the microreactors. Transesterification was carried out in a continuous flow manner at a rate of $1.2 \mu\text{L min}^{-1}$.⁴⁹ The measured concentration of the effluent flow is summarized in Table 1. The product concentrations, (*R*)-PEA, for the HMDS-treated films (9.53 mM for H-cubic and 6.64 mM for H-hexagonal) were about 35 times greater than that for the bare films (0.272 mM for cubic and 0.202 mM for hexagonal). This supports the QCM results showing that more lipase was adsorbed on the hydrophobic surface than on the hydrophilic surface. The result also suggests that lipase immobilized on the hydrophobic surface maintained good enzymatic activity and that denaturation *via* the adsorption process was not significant in the current system. Furthermore, it should be noted that while H-cubic film had only 9 times more lipase adsorption than the untreated cubic film, it exhibited a 35-fold increment in the product concentration. In other words, lipase adsorbed on H-cubic film was more active than that on the untreated cubic film. It is reported that the lipase active site is covered by a lid domain and that the lid moves away when lipase is exposed to hydrophobic environments.⁵⁰ An open form of lipase is thought to exhibit good activity. The hydrophobic treatment in the present study also had a similar effect on the transesterification catalyzed by lipase. Indeed, both H-cubic and H-hexagonal films had similar acceleration effects on the reaction. The results indicate that the hydrophobic treatment of MPS thin film enhanced the catalytic activity of immobilized lipase as well as the amount of adsorption.

We discuss the effect of MPS structure on the activity of immobilized lipase by comparing H-cubic and H-hexagonal films. As shown in Table 1, the (*R*)-PEA concentration of the H-hexagonal film (6.64 mM) was 30% less than that of the H-cubic film (9.53 mM), whereas the lipase adsorption of the H-hexagonal film ($2.12 \mu\text{g cm}^{-2}$) was 70% more than that of the H-cubic film ($1.55 \mu\text{g cm}^{-2}$). Interestingly, the reaction rate of lipase immobilized in the H-hexagonal film was slower than that in the H-cubic film. We speculate that the slow reaction rate was due to reactant molecules' access to the lipase inside H-

hexagonal film. The H-hexagonal film has a limited number of open pores on the surface and appears to provide poor accessibility to its pores through its surface compared with H-cubic film (see Fig. 1c).^{30,34} In some cases, there are micropores (smaller than 2 nm) on the walls of mesopore channels. However, the diffusion of reactant molecules through such micropores is presumably small compared with the diffusion through the open mesopores in Fig. 1a. Unlike the H-hexagonal film, the H-cubic film has many open mesopores on its surface, and the reactant molecules have good accessibility to the lipase immobilized inside the mesopores. Since the reaction was conducted in a continuous flow manner, its reaction rate was greatly affected by diffusion limitation. Hence, the reaction rate of immobilized lipase is correlated with the MPS film structure in terms of reactant molecules' accessibility to lipase inside the pores. Of the MPS films tested in this study, the H-cubic film is the most suitable for transesterification with immobilized lipase.

In our preliminary experiments, lipase PS SD and lipase PS IM showed good enantioselectivity in batch reactions. However, it should be noted that the enantioselectivity of lipase PS is dependent on its solvent environment and is sometimes altered by the addition of ionic liquids.¹⁴ In this context, the enantioselectivity in the experiments was judged from the (*S*)-PEA and (*S*)-PE concentrations in Table 1. In fact, the concentration of (*S*)-PEA was lower than the detection limit; the change in the (*S*)-PE concentration was negligible. Hence, in all cases, the enantiomeric excess values were higher than 99%. For the H-cubic film, the enantioselectivity was high even at a yield of 92.5% in an additional experiment with a flow rate of $0.3 \mu\text{L min}^{-1}$. Thus, the lipase immobilized in the MPS films maintains good enantioselectivity.

Evaluation of immobilized lipase PS

The H-cubic film exhibited a good capacity for lipase immobilization based on an activity test for four types of MPS film. The second part of this study focuses on the characteristics of lipase immobilized in the H-cubic film. The reactant solution was continuously fed into a microreactor containing lipase PS at a rate of $3 \mu\text{L min}^{-1}$ for 36 h, and the product concentration in the effluent solution was monitored to determine its stability (Fig. 3). The concentration after the first hour was 6.21 mM, which corresponds to a yield of 51% in a contact time of 18.8 min. The

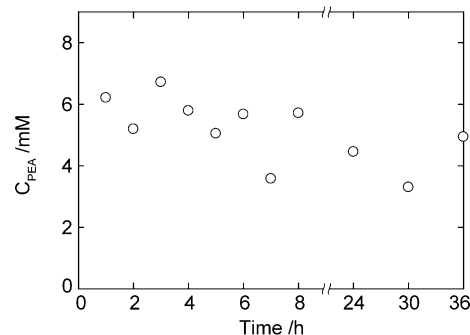


Fig. 3 Changes in the product concentration in the effluent solution with time in long-term continuous test. The reactant solution ($C_{(R)\text{-PE}} = 12.1 \text{ mM}$, $C_{(S)\text{-PE}} = 12.1 \text{ mM}$, $C_{\text{VA}} = 50 \text{ mM}$) was continuously fed at $3 \mu\text{L min}^{-1}$ over 36 h. The temperature of the reactor was kept at 40°C .

concentration at 8 h was 5.71 mM and the final concentration at 36 h was 4.94 mM, which was about 80% of the original value.⁵¹ The results indicate that the reaction rate slowly decreased with time. Since a small amount of lipase was leached out in the QCM experiments, the decrease in the reaction rate was largely due to the natural decay of lipase activity. It is well known that lipase loses its activity in organic solvents.^{41,52} Amano Pharmaceutical Co. also reported that lipase PS IM loses about 20% of its activity after being stirred in *i*Pr₂O at 25 °C for 24 h. Therefore, the lipase immobilized in the H-cubic film provided fairly good stability, based on the result showing that it maintained about 80% of its original activity after 36 h of continuous reaction at 40 °C.

The enzymatic activity of lipase immobilized in MPS films was quantified for evaluation through a comparison with native lipase and a commercial immobilized lipase PS. Since the MPS film coated inside the microreactor was designed for continuous operation, we conducted tests with various reactant concentrations at a flow rate of 24 μL min⁻¹, and calculated the reaction rates from the product concentrations. Compared with the flow rate in the previously described activity test (1.2 μL min⁻¹), the rate in this experiment is fast (24 μL min⁻¹). Under this condition, the change in the reactant concentration is very small because of the short contact time. This allows us to assume that the reactant concentration is constant across the microreactor and then to calculate the reaction rates directly from product concentrations and flow rates.²⁹ It should be noted that the rates obtained with this method are equivalent to the initial rates in the batch experiments.

Fig. 4a shows the reaction rates as a function of VA concentration at (R)-PE concentrations, $C_{(R)\text{-PE}}$ of 2.5, 5, 6, and 13 mM. The reaction rates gradually increase with VA concentration and reach a plateau at high VA concentrations. This feature is observed for all PE concentrations. For further analysis, the results were re-plotted in Lineweaver–Burk form, where the reciprocals of the reaction rates were plotted against the reciprocal of the VA concentration, C_{VA} (Fig. 4b). Data sets at a constant $C_{(R)\text{-PE}}$ form straight parallel lines. We also confirmed that the y -intercepts of the straight lines are proportional to the reciprocal of $C_{(R)\text{-PE}}$. These are typical features representing the Ping-Pong Bi Bi mechanism.¹³ In this transesterification, VA first binds to lipase to give an intermediate form that then reacts with PE to yield the product, PEA. It is known that PE sometimes acts as a competitive inhibitor in the first step of this reaction.^{53–55} The current results show that the rate increased with the PE concentration (Fig. 4a), and suggest that PE inhibition was minimal under these conditions. This is because we set the initial reactant concentrations at relatively low values in order to quantify the initial activity of lipase immobilized in MPS films in the absence of competitive inhibition. While many kinetic forms have been proposed for the interpretation of transesterification,^{56–58} the Ping-Pong Bi Bi mechanism in the absence of competitive inhibition was suitable for acquiring kinetic parameters in this study and is expressed as follow:

$$r_{(C_{\text{VA}}, C_{(R)\text{-PE}})} = \frac{V_{\text{max}} C_{\text{VA}} C_{(R)\text{-PE}}}{C_{\text{VA}} C_{(R)\text{-PE}} + K_{\text{PE}} C_{\text{VA}} + K_{\text{VA}} C_{(R)\text{-PE}}} \quad (1)$$

where V_{max} is the maximum velocity (mol s⁻¹ g_{lipase}⁻¹); K_{VA} and K_{PE} are the Ping-Pong constants for VA and PE (M). Since the

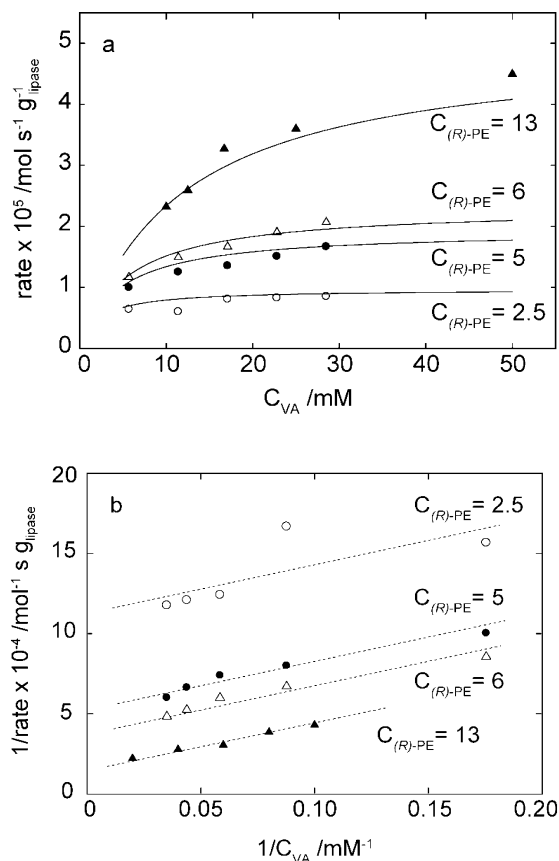


Fig. 4 (a) Transesterification experiments as a function of VA concentration. The solid lines are the fitted results based on the Ping-Pong Bi Bi mechanism. In the graph, $C_{(R)\text{-PE}}$ is the concentration of (R)-PE in mM. \blacktriangle : $C_{(R)\text{-PE}} = 13$ mM, \triangle : $C_{(R)\text{-PE}} = 6$ mM, \bullet : $C_{(R)\text{-PE}} = 5$ mM, \diamond : $C_{(R)\text{-PE}} = 2.5$ mM. (b) Lineweaver–Burk plot of the transesterification experiments in Fig. 4a. Dotted lines are guides to the eye.

substrate concentrations (C_{VA} and $C_{(R)\text{-PE}}$) were set at very low values, eqn (1) can be simplified as follows:^{54,55}

$$r_{(C_{\text{VA}}, C_{(R)\text{-PE}})} = \frac{1}{\frac{K_{\text{VA}}}{V_{\text{max}} C_{\text{VA}}} + \frac{K_{\text{PE}}}{V_{\text{max}} C_{(R)\text{-PE}}} + 1} \quad (2)$$

In eqn (2), it is estimated that $1/V_{\text{max}}$ is far smaller than $K_{\text{VA}}/V_{\text{max}} C_{\text{VA}}$ and $K_{\text{PE}}/V_{\text{max}} C_{(R)\text{-PE}}$. The specificity constants, which correspond to $V_{\text{max}}/K_{\text{VA}}$ and $V_{\text{max}}/K_{\text{PE}}$, indicate the efficiency of an enzyme that converts a substrate into a product. Hence, instead of estimating the individual parameters of V_{max} , K_{PE} , and K_{VA} , the specificity constants were obtained by fitting the results to eqn (2) to evaluate the immobilized lipase activity. In addition, the slope of the straight lines in the Lineweaver–Burk plot corresponds to $K_{\text{VA}}/V_{\text{max}}$, which is the reciprocal of the specificity constant (Fig. 4b). To estimate commercial lipase activity, the initial reaction rates were measured in batch experiments using lipase PS SD and lipase PS IM. The results of the batch experiments were also fitted to eqn (2) in the same manner. The obtained specificity constants of immobilized lipase, lipase PS SD, and lipase PS IM are summarized in Table 2.

The values of $V_{\text{max}}/K_{\text{VA}}$ and $V_{\text{max}}/K_{\text{PE}}$ for lipase immobilized in the MPS film are roughly the same, which indicates that the Ping-Pong constants, K_{VA} and K_{PE} are not very different

Table 2 Specificity constants of lipase PS

Type of lipase	V_{\max}/K_{VA} [$\text{L s}^{-1} \text{g}_{\text{lipase}}^{-1}$]	V_{\max}/K_{PE} [$\text{L s}^{-1} \text{g}_{\text{lipase}}^{-1}$]
Immobilized	4.50×10^{-3}	3.86×10^{-3}
Lipase PS SD	5.71×10^{-6}	6.85×10^{-6}
Lipase PS IM	1.17×10^{-4}	3.08×10^{-4}

from each other. The specificity constant V_{\max}/K_{VA} for lipase immobilized in the MPS film is greater than that for native lipase PS SD by a factor of nearly 800. As described in the introduction, lipase PS was not dissolved in organic solvents and was not equally dispersed in the solution. This low solubility caused the native lipase activity to be low in organic solutions. Hence, the results suggest that the lipase immobilized in the MPS film encountered reactant molecules with an increased frequency, which led to excellent enzymatic activity in the transesterification. The specificity constant of lipase PS IM in Table 2 was estimated for the total weight which includes diatomaceous earth and lipase because the immobilization percentage was not provided. Although the specificity constant of lipase PS IM is not directly comparable, the specificity constant for the lipase immobilized in the MPS film ($4.50 \times 10^{-3} \text{ L s}^{-1} \text{g}^{-1}$) is about 40 times that for lipase PS IM ($1.17 \times 10^{-4} \text{ L s}^{-1} \text{g}^{-1}$). We also estimated the amount of lipase immobilized in lipase PS IM by measuring the protein concentrations of lipase PS IM and lipase PS SD using standard BCA protein assays (Pierce BCA Protein Assay Kit, Rockford, IL, USA). The estimated immobilization percentage of lipase PS IM was 34%. If this immobilization percentage (34%) is included in the values for lipase PS IM, the specificity constants were $3.44 \times 10^{-4} \text{ L s}^{-1} \text{g}^{-1}$ for V_{\max}/K_{VA} and $9.06 \times 10^{-4} \text{ L s}^{-1} \text{g}^{-1}$ for V_{\max}/K_{PE} . The V_{\max}/K_{VA} value of lipase PS IM is smaller than that for lipase PS immobilized in the MPS films by a factor of 13. Hence, the activity of lipase PS immobilized in the MPS film was much greater than that of commercial immobilized lipase PS.

Conclusion

Microreactors with MPS thin films were employed for enantioselective transesterification catalyzed by immobilized lipase. The porous structure and surface hydrophilicity of the MPS film affected the adsorption amount and the activity of lipase PS. Hydrophobic treatment enhanced both the adsorption amount of lipase PS in the MPS films and its enzymatic activity. MPS film with open pores on the surface, which possessed good reactant accessibility, exhibited an increased reaction rate. Of the films tested in this study, lipase PS immobilized in the 3D cubic film with hydrophobic treatment exhibited the highest activity while maintaining enantioselectivity higher than 99%. The immobilized lipase also showed good stability during 36-hour continuous operation. The activity of lipase immobilized in the MPS film was quantified by fitting the results to the Ping-Pong Bi Bi mechanism. The specificity constant of immobilized lipase was 800 times greater than that of native lipase PS and was 13 times greater than that of lipase PS IM. The immobilized lipase PS in the MPS film inside the microreactor exhibited the enzymatic activity higher than the native lipase PS and lipase PS IM. A microreactor containing MPS film showed good

applicability to enantioselective chemical reactions catalyzed by immobilized enzymes.

Acknowledgements

This study was funded by “Development of Microspace and Nanospace Reaction Environment Technology for Functional Materials” project (NEDO, Japan). We thank Dr Toshiyuki Kanamori for use of the QCM system and Dr Toshiyuki Takagi, Dr Yasumasa Takenaka and Dr Katsuyuki Iwanami at AIST (Tsukuba, Japan) for fruitful discussion.

References

- 1 F. Theil, *Chem. Rev.*, 1995, **95**, 2203–2227.
- 2 M. T. Reetz, *Curr. Opin. Chem. Biol.*, 2002, **6**, 145–150.
- 3 E. Garcia-Urdiales, I. Alfonso and V. Gotor, *Chem. Rev.*, 2005, **105**, 313–354.
- 4 T. Itoh, S. H. Han, Y. Matsushita and S. Hayase, *Green Chem.*, 2004, **6**, 437–439.
- 5 T. Itoh, Y. Matsushita, Y. Abe, S. H. Han, S. Wada, S. Hayase, M. Kawatsura, S. Takai, M. Morimoto and Y. Hirose, *Chem.–Eur. J.*, 2006, **12**, 9228–9237.
- 6 I. J. Colton, S. N. Ahmed and R. J. Kazlauskas, *J. Org. Chem.*, 1995, **60**, 212–217.
- 7 Y. Okahata and T. Mori, *Trends Biotechnol.*, 1997, **15**, 50–54.
- 8 L. Iskandar, T. Ono, N. Kamiya, M. Goto, F. Nakashio and S. Furusaki, *Biochem. Eng. J.*, 1998, **2**, 29–33.
- 9 S. Shah and M. N. Gupta, *Bioorg. Med. Chem. Lett.*, 2007, **17**, 921–924.
- 10 I. Gill and A. Ballesteros, *Trends Biotechnol.*, 2000, **18**, 469–479.
- 11 I. Gill and A. Ballesteros, *Trends Biotechnol.*, 2000, **18**, 282–296.
- 12 M. T. Reetz, P. Tielmann, W. Wiesenhofer, W. Konen and A. Zonta, *Adv. Synth. Catal.*, 2003, **345**, 717–728.
- 13 H. W. Blanch and D. S. Clark, *Biochemical Engineering*, M. Dekker, New York, 1996.
- 14 R. A. Sheldon, *Adv. Synth. Catal.*, 2007, **349**, 1289–1307.
- 15 R. F. Ismagilov, *Angew. Chem., Int. Ed.*, 2003, **42**, 4130–4132.
- 16 K. Jahnisch, V. Hessel, H. Lowe and M. Baerns, *Angew. Chem., Int. Ed.*, 2004, **43**, 406–446.
- 17 T. Kawaguchi, H. Miyata, K. Ataka, K. Mae and J. Yoshida, *Angew. Chem., Int. Ed.*, 2005, **44**, 2413–2416.
- 18 J. Kobayashi, Y. Mori, K. Okamoto, R. Akiyama, M. Ueno, T. Kitamori and S. Kobayashi, *Science*, 2004, **304**, 1305–1308.
- 19 M. Miyazaki and H. Maeda, *Trends Biotechnol.*, 2006, **24**, 463–470.
- 20 H. B. Mao, T. L. Yang and P. S. Cremer, *Anal. Chem.*, 2002, **74**, 379–385.
- 21 G. H. Seong and R. M. Crooks, *J. Am. Chem. Soc.*, 2002, **124**, 13360–13361.
- 22 N. J. Gleason and J. D. Carbeck, *Langmuir*, 2004, **20**, 6374–6381.
- 23 T. Honda, M. Miyazaki, H. Nakamura and H. Maeda, *Adv. Synth. Catal.*, 2006, **348**, 2163–2171.
- 24 H. Y. Qu, H. T. Wang, Y. Huang, W. Zhong, H. J. Lu, J. L. Kong, P. Y. Yang and B. H. Liu, *Anal. Chem.*, 2004, **76**, 6426–6433.
- 25 M. Miyazaki, J. Kaneno, M. Uehara, M. Fujii, H. Shimizu and H. Maeda, *Chem. Commun.*, 2003, 648–649.
- 26 M. Heule, K. Rezwan, L. Cavalli and L. J. Gauckler, *Adv. Mater.*, 2003, **15**, 1191.
- 27 K. M. de Lathouder, T. M. Flo, E. Kapteijn and J. A. Moulijn, in *2nd International Conference on Structured Catalysts and Reactors (ICOSCAR-2)*, Delft, Netherlands, 2005, pp. 443–447.
- 28 K. Kawakami, D. Abe, T. Urakawa, A. Kawashima, Y. Oda, R. Takahashi and S. Sakai, *J. Sep. Sci.*, 2007, **30**, 3077–3084.
- 29 S. Kataoka, A. Endo, M. Oyama and T. Ohmori, *Appl. Catal., A*, 2009, **359**, 108–112.
- 30 S. Kataoka, A. Endo, A. Harada, Y. Inagi and T. Ohmori, *Appl. Catal., A*, 2008, **342**, 107–112.
- 31 C. T. Kresge, M. E. Leonowicz, W. J. Roth, J. C. Vartuli and J. S. Beck, *Nature*, 1992, **359**, 710–712.
- 32 U. Ciesla and F. Schuth, *Microporous Mesoporous Mater.*, 1999, **27**, 131–149.

- 33 K. J. Edler and S. J. Roser, *Int. Rev. Phys. Chem.*, 2001, **20**, 387–466.
- 34 S. Kataoka, A. Endo, A. Harada and T. Ohmori, *Mater. Lett.*, 2008, **62**, 723–726.
- 35 S. Hudson, J. Cooney and E. Magner, *Angew. Chem., Int. Ed.*, 2008, **47**, 8582–8594.
- 36 H. Takahashi, B. Li, T. Sasaki, C. Miyazaki, T. Kajino and S. Inagaki, *Chem. Mater.*, 2000, **12**, 3301–3305.
- 37 T. Itoh, R. Ishii, S. Matsuura, S. Hamakawa, T. Hanaoka, T. Tsunoda, J. Mizuguchi and F. Mizukami, *Biochem. Eng. J.*, 2009, **44**, 167–173.
- 38 T. Itoh, N. Ouchi, Y. Nishimura, H. S. Hui, N. Katada, M. Niwa and M. Onaka, *Green Chem.*, 2003, **5**, 494–496.
- 39 A. Salis, M. S. Bhattacharyya, M. Monduzzi and V. Solinas, *J. Mol. Catal. B: Enzym.*, 2009, **57**, 262–269.
- 40 A. Salis, D. Meloni, S. Ligas, M. F. Casula, M. Monduzzi, V. Solinas and E. Dumitriu, *Langmuir*, 2005, **21**, 5511–5516.
- 41 G. D. Yadav and S. R. Jadhav, *Microporous Mesoporous Mater.*, 2005, **86**, 215–222.
- 42 A. Galarneau, M. Mureseanu, S. Atger, G. Renard and F. Fajula, *New J. Chem.*, 2006, **30**, 562–571.
- 43 H. Jaladi, A. Katiyar, S. W. Thiel, V. V. Gulians and N. G. Pinto, *Chem. Eng. Sci.*, 2009, **64**, 1474–1479.
- 44 R. M. Blanco, P. Terreros, M. Fernandez-Perez, C. Otero and G. Diaz-Gonzalez, *J. Mol. Catal. B: Enzym.*, 2004, **30**, 83–93.
- 45 J. J. Shi, T. L. Yang, S. Kataoka, Y. J. Zhang, A. J. Diaz and P. S. Cremer, *J. Am. Chem. Soc.*, 2007, **129**, 5954–5961.
- 46 H. R. Hobbs, B. Kondor, P. Stephenson, R. A. Sheldon, N. R. Thomas and M. Poliakoff, *Green Chem.*, 2006, **8**, 816–821.
- 47 H. H. P. Yiu, P. A. Wright and N. P. Botting, in *2nd International Symposium on Mesoporous Molecular Sieves (ISMMS)*, Quebec City, Canada, 2000, pp. 763–768.
- 48 G. M. L. Messina, C. Satriano and G. Marletta, *Colloids Surf., B*, 2009, **70**, 76–83.
- 49 The flow rate ($1.2 \mu\text{L min}^{-1}$) is relatively low in the present experiment, which results in the small production rate. We used this condition only to emphasize the difference in the yields among four types of mesoporous silica. High productivity can be achieved with a longer reactor which can be operated at higher flow rates.
- 50 K. E. Jaeger and M. T. Reetz, *Trends Biotechnol.*, 1998, **16**, 396–403.
- 51 The product concentration was slightly fluctuated in Fig. 3. We believe that it is an experimental error in our sampling process because we needed to collect a small amount of effluent solution by using connecting parts containing a relatively large dead volume between the microreactor and a sampling syringe.
- 52 I. Gill and A. Ballesteros, *J. Am. Chem. Soc.*, 1998, **120**, 8587–8598.
- 53 J. W. Swarts, P. Vossenbergh, M. H. Meerman, A. E. M. Janssen and R. M. Boom, *Biotechnol. Bioeng.*, 2008, **99**, 855–861.
- 54 A. E. M. Janssen, B. J. Sijnsnes, A. V. Vakurov and P. J. Halling, *Enzyme Microb. Technol.*, 1999, **24**, 463–470.
- 55 A. E. M. Janssen, A. M. Vaidya and P. J. Halling, *Enzyme Microb. Technol.*, 1996, **18**, 340–346.
- 56 G. D. Yadav and P. S. Lathi, *J. Mol. Catal. B: Enzym.*, 2005, **32**, 107–113.
- 57 S. Al-Zuhair, *Biotechnol. Prog.*, 2005, **21**, 1442–1448.
- 58 S. Al-Zuhair, *J. Chem. Technol. Biotechnol.*, 2006, **81**, 299–305.

Ionic liquid tolerant hyperthermophilic cellulases for biomass pretreatment and hydrolysis†

Supratim Datta,^{a,b} Bradley Holmes,^{a,b} Joshua I. Park,^{a,b} Zhiwei Chen,^{a,b} Dean C. Dibble,^{a,b} Masood Hadi,^{a,b} Harvey W. Blanch,^{a,c} Blake A. Simmons^{a,b} and Rajat Saprana^{a,b}

Received 11th August 2009, Accepted 11th November 2009

First published as an Advance Article on the web 21st January 2010

DOI: 10.1039/b916564a

One of the main barriers to the enzymatic hydrolysis of cellulose results from its highly crystalline structure. Pretreating biomass with ionic liquids (IL) increases enzyme accessibility and cellulose recovery through precipitation with an anti-solvent. For an industrially feasible pretreatment and hydrolysis process, it is necessary to develop cellulases that are stable and active in the presence of small amounts of ILs co-precipitated with recovered cellulose. However, a significant decrease in cellulase activity in the presence of trace amounts of ILs has been reported in the literature, necessitating extensive processing to remove residual ILs from the regenerated cellulose. Towards that end, we have investigated the stability of hyperthermophilic enzymes in the presence of the IL 1-ethyl-3-methylimidazolium acetate ([C2mim][OAc]) and compared it to the industrial benchmark *Trichoderma viride* (*T. viride*) cellulase. The endoglucanase from a hyperthermophilic bacterium, *Thermatoga maritima*, and a hyperthermophilic archaeon, *Pyrococcus horikoshii*, were over expressed in *E. coli* and purified to homogeneity. Under their optimum conditions, both hyperthermophilic enzymes showed significantly higher [C2mim][OAc] tolerance than *T. viride* cellulase. Using differential scanning calorimetry we determined the effect of [C2mim][OAc] on protein stability and our data indicates that higher concentrations of IL correlated with lowered protein stability. Both hyperthermophilic enzymes were active on [C2mim][OAc] pretreated Avicel and corn stover. Furthermore, these enzymes can be recovered with little loss in activity after exposure to 15% [C2mim][OAc] for 15 h. These results demonstrate the potential of using IL-tolerant extremophilic cellulases for hydrolysis of IL-pretreated lignocellulosic biomass, for biofuel production.

Introduction

The use and depletion of fossil fuels are major environmental and energy security issues for the twenty-first century.¹ Renewable biofuels produced from biomass are an important alternative to petroleum use for transportation. Lignocellulosic (LC) biomass is an abundant and, potentially, carbon-neutral energy resource for the production of biofuels and chemicals.² However, there are scientific and technological challenges that need to be overcome before LC biomass-derived biofuels can be a significant and economically competitive alternative to petroleum.

The production of ethanol from corn grain represents the most convenient and technically advanced option for biofuels in the United States today. However, the increased displacement of available corn supplies for fuel has adverse effects on food

markets given the role of corn as a food commodity. LC biomass, on the other hand, is an abundant and potentially low cost resource that does not compete with human needs.³ It includes agricultural residues (corn stover, wheat straw and rice straw), deciduous and coniferous woods, agricultural processing by-products (corn fiber, rice hulls and sugar cane bagasse) and energy crops like switch grass and miscanthus.⁴

Lignocellulosic biomass is made of three major components—cellulose (35–50%), hemicellulose (20–35%) and lignin (10–25%)—the relative concentrations of which vary according to the source.⁵ For efficient utilization, the biomass has to undergo pretreatment before it can be enzymatically hydrolyzed to glucose and other constituent sugars. Cellulosic component of LC biomass is highly crystalline with polymeric cellulose chains held together by hydrogen bonds and van der Waals forces.⁶ The polymeric chains are made of anhydroglucose units joined together by glycosidic bonds with degree of polymerization (DP) ranging from 1000–20 000 units.⁷ Pretreatment is essential to reduce the DP of the cellulose and make it amorphous to facilitate access to the substrate for enzymatic cellulose hydrolysis.⁸ Current strategies in pretreatment and recovery of cellulose from biomass have been primarily derived from pulp and paper industry, where the downstream process of converting cellulose to glucose is not a consideration and are incompatible

^aDeconstruction Division, Joint BioEnergy Institute, 5885 Hollis St, 4th Floor, Emeryville, CA, USA. E-mail: rsaprana@lbl.gov; Fax: +1 510-486-4252; Tel: +1 510-508-9956

^bBiomass Science and Conversion Technology Department, Sandia National Laboratory, Livermore, CA, USA

^cDepartment of Chemical Engineering, University of California, Berkeley, CA, USA

† Electronic supplementary information (ESI) available: DSC, halotolerance and compositional analysis. See DOI: 10.1039/b916564a

with enzymatic hydrolysis; thereby requiring extensive cellulose processing for enzymatic hydrolysis and resulting in an increase in time and cost. It is therefore desirable and important to develop a biomass pretreatment process that is compatible with not only the enzymatic hydrolysis but also subsequent fermentation of glucose to biofuels.

Current pretreatment methods include mechanical reduction in biomass particulate size followed by dilute acid, flow-through ammonia fiber expansion, ammonia recycle percolation, lime, steam explosion, or organosolv (OS) pretreatment.⁹ The drawbacks of these methods include severe reaction conditions (high temperature and/or high pressure and extremes of pH), and high processing costs. A new pretreatment approach using ionic liquids (ILs) has been shown to be effective in solubilizing crystalline cellulose.¹⁰

Room temperature ILs are pure salts with melting points typically below 100 °C.^{10,11} While the properties of ILs are very diverse, high thermal stability and non-volatility make this class of compounds an attractive alternative to organic solvents in several existing industrial processes.¹² ILs depending on their chemistry, can dissolve a wide range of polar and non-polar organic and polymeric compounds, including cellulose, and make the polysaccharide chains more accessible to enzymatic hydrolysis.¹³ Of particular interest to the biofuels industry is the ability of several imidazolium based ionic liquids with weak conjugated-base anions to dissolve crystalline cellulose at moderate temperatures.^{13,14} The cellulose is subsequently recovered in the amorphous form upon the addition of anti-precipitants like water^{15–17} rendering it more accessible to enzymatic hydrolysis and subsequent rapid hydrolysis to glucose using cellulases.¹⁸ The dissolution of lignocellulosic materials such as corn stalks, rice straw, bagasse, pine wood, and spruce wood in ILs followed by cellulose hydrolysis with acid or enzymes has also been recently reported in literature.^{18–20}

Cost-effective enzymatic hydrolysis of cellulose to sugars would benefit from the development of enzymes that are effective under pretreatment conditions (which may be extreme pH or temperature). However, significant decreases in cellulase activity in the presence of trace amounts of ILs have been reported in literature.^{21,22} In order to avoid extensive processing and clean up of the regenerated cellulose, the cellulases that are used must be able to perform optimally in up to 15% concentrations of IL that is co-precipitated with cellulose. The amount of leftover IL would however depend on the cost of recovery of ILs. Towards the goal of discovering cellulases that are stable and active in the presence of trace amounts of ILs, we investigated the stability of hyperthermophilic enzymes, broadly categorized with extremophilic enzymes, as a function of IL concentration. Since extremophilic organisms grow in extremes of pH, temperature and/or salinity *etc.*, these are a promising source of enzymes for industrial processes. The enzymes derived from hyperthermophilic organisms may be capable of tolerating ionic liquids since the native growth condition of these organisms is greater than 80 °C in a strongly reducing environment.²³

A model extremophilic organism is the hyperthermophilic bacterium *Thermatoga maritima* (*Tma*), a member of the order thermotogales, which is an anaerobic heterotrophic hyperthermophile capable of fermenting both simple and complex sugars.²⁴ Roughly 7% of the predicted coding sequences in its

genome encode enzymes that are involved in the metabolism of monosaccharides and polysaccharides. *Tma* Cel5A is a free-acting endoglucanase containing only a catalytic domain.²⁵ *Pyrococcus horikoshii* (*Pho*), a hyperthermophilic archaeon found in deep-sea hydrothermal vents, is an anaerobic heterotroph, which utilizes peptides as its main carbon source at temperatures approaching 100 °C but has been shown to contain an endoglucanase (EG) that is functional at an optimum temperature of 97 °C.

Since cellulases from *Trichoderma* constitute an established cellulase hydrolysis process for benchmarking, here we present data comparing the efficiency of hydrolysis of *Tma* Cel5A and *Pho* EG with the *Trichoderma viride* cellulase. *Tma* Cel5A and *Pho* EG were purified to homogeneity and enzymatic hydrolysis activity was measured in the presence of varying concentrations of [C2mim][OAc]. Both enzymes showed significant specific activity at 15% (v/v) [C2mim][OAc] with specific activities decreasing at higher concentrations. Decreased specific activities at higher concentrations showed a direct correlation to enzyme stability as indicated by decreases in unfolding temperatures by DSC measurements. Both enzymes were very stable at high temperatures for extended periods of time and were tolerant to 2 M NaCl and KCl. These enzymes are also active on pretreated biomass. Long half-lives and a near 100% recovery of activity from ILs make them promising targets for further investigation for use in large-scale saccharification reactions employing this pretreatment technology.

Results

Hyperthermophilic enzymes and specific activity assays

Previous studies by Chhabra *et al.*²⁶ showed that the *Tma* Cel5A from *Tma* is intracellularly expressed in *T. maritima* and has an optimum temperature (T_{opt}) of 80 °C. The EG from *Pho* has a even higher T_{opt} of 97 °C and specific activity of 8.5 U mg⁻¹ (1 U = 1 μmole of reducing sugar produced min⁻¹ using CMC as substrate) at pH 5.6 and 85 °C.²⁷ Thus, both of these enzymes were attractive targets for our work. The enzymes were expressed in *E. coli* in autoinduction media and purified by nickel affinity chromatography to homogeneity as detected by SDS-PAGE. Maximal amounts of soluble *Tma* Cel5A were obtained following induction at 37 °C, yielding 30 mg L⁻¹. The yield of *Pho* EG was around 2 mg L⁻¹, under similar conditions except that an additional anion exchange chromatography step was added to obtain purer protein. Both cellulases were active on carboxymethyl cellulose (CMC). In our experiments, the specific activities of *Tma* Cel5A and *Pho* EG were 30 U mg⁻¹ and 1.9 U mg⁻¹, respectively (Table 1). The commercially available *T. viride* cellulase, has a specific activity of 10–12 U mg⁻¹ at 37 °C with CMC as the substrate, depending on the batch of enzyme used.

Specific activity in the presence of [C2mim][OAc]

The purified recombinant enzymes were assayed in the presence of [C2mim][OAc] and the specific activity results were compared with the cellulase from *T. viride*. [C2mim][OAc] was selected as the IL of choice. The assays were performed under optimum pH and temperatures for *T. maritima* and *T. viride* enzymes, as

Table 1 Biochemical properties of hyperthermophilic enzymes: optimum temperature and pH, specific activity, and stability in presence of [C2mim][OAc]. The % specific activities (last column) are reported as percentages of residual specific activity, taking the specific activity of IL free enzyme as 100% activity

Enzymes	Properties					
	$T_{\text{opt}}/^{\circ}\text{C}$	pH_{opt}	$T_{1/2}/\text{h}$ in 0% IL	$T_{1/2}/\text{h}$ in 15% IL	Specific activity ^a	% Activity recovered after incubation in 15% IL for 15 h
<i>T. viride</i> cellulase ^b	37	4.5	9	0	11 ± 2	0
<i>Tma</i> Cel5A ^b	80	4.8	20 ± 2	19 ± 3	30 ± 2	44
<i>Pho</i> EG ^c	>95	6.4	24 ± 4	23 ± 4	1.9 ± 0.3	79

^a Units is μmoles of reducing sugars $\text{min}^{-1} \text{mg}^{-1}$ with carboxymethylcellulose as substrate. ^b Assays were done at T_{opt} . ^c Assays were done at 80 °C.

shown in Table 1. The *Pho* EG was assayed at 80 °C where its specific activity is around 10% less than at 95 °C (data not shown). As seen in Fig. 1, the cellulase from *T. viride* rapidly lost activity with increasing concentration of [C2mim][OAc]. In the presence of 5% (v/v) [C2mim][OAc] the enzyme lost 60%

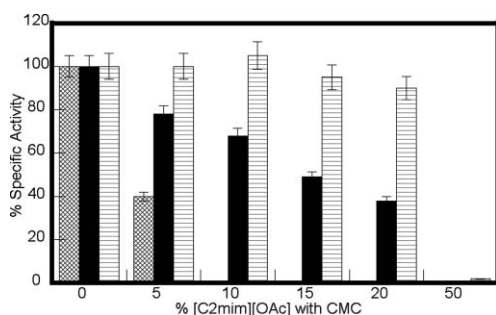


Fig. 1 Enzymatic hydrolysis of CMC by cellulase from *T. viride* (cross line), *Tma* Cel5A (solid) and *Pho* EG (horizontal line), in the presence of various [C2mim][OAc]: 2% CMC in and 0–50% of [C2mim][OAc] (v/v) were incubated at 37 °C (*T. viride*), 80 °C (*Tma* EG, *Pho* EG). The specific activities were calculated as μmoles of reducing sugars formed per min per mg of enzyme. The specific activities are reported as percentages of residual specific activity, taking the specific activity of IL free enzyme as 100% activity. Error bars indicate the standard deviation.

of its activity while it was undetectable in the presence of 10% (v/v) [C2mim][OAc]. Both the recombinant hyperthermophilic enzymes behaved very differently. *Tma* Cel5A in the presence of 5% [C2mim][OAc] loses 24% of its specific activity. At 15% IL (v/v), *Tma* Cel5A retains 50% of its specific activity. The highest residual activities were observed with *Pho* EG which retains 100% activity in 20% IL (v/v) (Fig. 1). Pre-incubation overnight (15 h) in 15% [C2mim][OAc] resulted in an almost complete loss of activity for the *T. viride* cellulases, as expected (Table 1) while the *Tma* Cel5A and *Pho* EG retained 44% and 70% respectively of their activity. The hyperthermophilic enzymes also exhibited longer half-lives, around 20–24 h, compared to the 9 h for the fungal *T. viride* cellulase, at their optimal pH and temperatures (Table 1).

Effect on enzyme stability

To understand the effect of ILs on protein stability, differential scanning calorimetry studies were done on the *T. viride* cellulase and compared to *Tma* Cel5A and *Pho* EG. The unfolding temperatures of the enzymes are listed in Table 2 and the thermograms for *Tma* Cel5A and *Pho* EG are shown in the ESI, Figure 1A and 1B.† The decrease in unfolding temperatures for *T. viride* cellulase between 0 and 5% [C2mim][OAc] is 7.2 °C

Table 2 Unfolding temperatures from differential scanning calorimetry thermograms of *Tma* Cel5A (5 mg mL⁻¹), *T. viride* cellulase (2.2 mg mL⁻¹) and *Pho* EG (1.8 mg mL⁻¹). The decrease in unfolding temperature of *Tma* Cel5A, *T. viride* cellulase and *Pho* EG is compared to the decrease in percent specific activity

Enzyme	% [C2mim][OAc] (v/v)	Unfolding $T/^{\circ}\text{C}$	Decrease in % specific activity	Decrease in unfolding $T/^{\circ}\text{C}$
<i>T. viride</i> cellulase	0	64.2	—	—
	5	57.0	60	7.2
	10	52.4	100	11.8
	15	49.4	100	14.8
	20	47.5	100	16.7
<i>T. maritima</i> endoglucanase (<i>Tma</i> Cel5A)	0	92.0	—	—
	5	89.8	23	2.2
	10	89.3	35	2.7
	15	88.5	52	3.5
	20	87.2	58	4.8
	50	67.0	98	25.0
<i>P. horikoshii</i> Endoglucanase (<i>Pho</i> EG)	0	102.3	—	—
	5	99.3	0	3
	10	97.5	0	4.8
	15	94.9	5	7.4
	20	91.8	10	10.5
	50	66.1	100	36.2

compared to a 2.2 °C drop in *Tma* Cel5A and a 3 °C drop in *Pho* EG (Table 2). This difference gets more pronounced at 10% [C2mim][OAc] (11.8 °C vs. 2.7 °C) when the *T. viride* cellulase is completely inactive. In the case of *Tma* Cel5A, there is a 25 °C drop in unfolding temperature at 50% [C2mim][OAc] (v/v) when the specific activity of *Tma* Cel5A is undetectable using the DNS assay. Similarly there is a 36.2 °C drop in unfolding temperature of *Pho* EG when the specific activity becomes undetectable. To understand the basis of tolerance to ILs we also looked at the effect of high concentrations of salt on the specific activity of the hyperthermophilic enzymes. To investigate whether the IL tolerance of the *Tma* Cel5A can be correlated with ionic strength of the buffer, *Tma* Cel5A was assayed in the presence of high salt concentration. As seen in the ESI, Figure 2A and 2B,† *Tma* Cel5A and *Pho* EG retained 65% and 85% of its activity respectively, in the presence of 2 M NaCl and 2 M KCl.

Effect on pretreated biomass

Corn stover refers to stalks, leaves and cobs that remain in the fields after the corn kernel harvest and is the largest quantity of biomass residue in the United States²⁸ and as such is also a LC-biomass source for producing cellulosic ethanol in the United States.²⁹ [C2mim][OAc] pretreated corn stover was used as a substrate to verify enzymatic efficiency on IL-pretreated biomass and a comparison made with [C2mim][OAc] pretreated Avicel. Avicel is a commercially available microcrystalline cellulose and a good model substrate for analysis. Similar assays were done in the presence of [C2mim][OAc] to simulate real biomass processing and saccharification scenarios. The assay products for the reactions in the presence of IL were detected by high performance anion exchange chromatography (HPAEC). The enzymatic hydrolysis reaction was carried out for 8 h for the *T. viride* cellulase and 15 h for the hyperthermophilic enzymes, taking into account the half-lives of these enzymes. To compare the amounts of total sugars formed between different reactions we chose to calculate the sum of glucose, xylose and cellobiose and report as μmoles of sugars formed per min per mg of enzyme used (Table 3). A comparison of assay results between pretreated and untreated substrate indicates a 2–6 fold increase in hydrolysis products after pretreatment irrespective of the enzyme used, thereby confirming that IL pretreatment can increase the efficiency of hydrolysis of cellulose recovered from biomass. The fungal enzyme was more active on untreated substrates compared to the hyperthermophilic enzymes probably due to the presence of cellobiohydrolases and xylanases in the enzyme mix (Table 3). The catalytic efficiency of the fungal enzyme however, decreases with increasing IL concentration in the reaction mix. After normalizing for the reaction time and enzyme amounts, the amount of sugars formed is undetectable at 15% [C2mim][OAc]. The catalytic efficiencies of the hyperthermophilic enzymes with insoluble substrates and in the presence of [C2mim][OAc] follow a similar trend as seen with the soluble substrate CMC. The yield of sugars from *Tma* Cel5A hydrolysis of pretreated Avicel in the presence of 15% IL decreases by 43% compared to 0% IL, while the decrease is only 10% in the case of *Pho* EG on the same substrate under similar conditions (Table 3). Cellobiose was the major product in the case of *Pho* EG, while a mixture of sugars were obtained for Cel5A.

Discussion

Hyperthermophilic proteins exhibit a remarkable balance between heat stability and functionality. This makes such proteins suitable for industrial applications like enzymatic hydrolysis of biomass for biofuels production. These enzymes generally owe their stability to a higher number of ion pairs and the polarity of exposed surfaces.³⁰ We started our present studies with two endoglucanase from hyperthermophilic organisms (one characterized representative each from bacterial and archaeal), to look into the effect of ILs with an eye on developing a large scale bioprocess.

Current processing conditions do not allow an *in situ* pretreatment and saccharification using an ionic liquid solvent, since ILs has been shown to affect the activity of cellulases. Turner *et al.*³¹ reported the inhibition of *T. reesei* cellulases by the IL 1-butyl-3-methylimidazolium chloride. A recent report by Pottkämper *et al.*³² reported the IL tolerance of a salt-tolerant cellulase from an uncultured microorganism³³ and discovered that a GH5 family cellulase that was active at IL concentrations of up to 30% (v/v). However the specific activity of these cellulases was very low, in the range of $0.014 \mu\text{moles min}^{-1} \text{mg}^{-1}$ with the assay performed with cell extracts.³²

We wanted to conduct an extensive study to look into the effect of ILs on hyperthermophilic cellulases with an eye on developing a large scale bioprocess with the hypothesis that hyperthermophilic enzymes would better tolerate ILs. Both *Tma* Cel5A and *Pho* EG were found to retain between 44% and 79% respectively of their activity in the presence of 15% [C2mim][OAc] unlike the *T. viride* cellulase with greater than 85% recovery of activity after exposure to 15% [C2mim][OAc] for 15 h. To verify enzymatic activity on biomass, we compared the efficiency of the recombinant cellulases to those from *T. viride* cellulase using both corn stover and Avicel as substrates and compared the results with assays on IL pretreated Avicel and corn stover. The pretreated substrates were more efficiently hydrolyzed compared to the untreated substrates. None of our recombinant proteins contain carbohydrate-binding domains, yet we detect the formation of sugars in the presence of untreated Avicel or corn stover. Further studies are needed to differentiate between the possibility of hydrolysis of amorphous cellulose in these samples or the possible effect of hyperthermophilic enzymes without carbohydrate-binding domains on insoluble substrates. However, as would be expected from reactions with insoluble substrates, enzymatic efficiency was less compared to results obtained using CMC. These results also show the importance of evaluating enzymatic efficiency with “real-world” insoluble substrates as opposed to synthetic soluble substrates that are easier to manipulate but cannot be used for translating analysis to actual substrates. The hyperthermophilic enzymes displayed higher activity compared to *T. viride* cellulase in the presence of [C2mim][OAc] (Table 3) for IL-pretreated cellulose, verifying our earlier results using a soluble substrate. The CMC activity results of the three cellulases are not indicative of the activity on non-pretreated biomass where the *T. viride* outperforms the extremophilic cellulases. However since IL pretreatment increases the amount of sugars released, it would thus be preferred to pretreat the biomass prior to enzymatic hydrolysis, thus underscoring the need for IL-tolerant cellulase.

Table 3 Activity assay on insoluble substrates in the absence of [C2mim][OAc] and presence of [C2mim][OAc]. The hydrolysis reactions were performed under pH and temperatures for each enzyme as listed in the Methods section. The reactions were run over a 14 h period with 5–10 μg of enzyme with 6% (w/v) enzyme loading in optimum buffer for each enzyme and run in duplicate. The reaction products were measured on a HPLC and HPAEC. The amounts of sugars detected are shown in μmoles and normalized with regards to amount of enzyme and time of reaction. Different reactions under each enzyme were run under exactly similar conditions

% [C2mim][OAc]	Enzyme	Substrate	Sugars produced ^a / $\mu\text{moles min}^{-1} \text{mg}^{-1}$
0	<i>T. viride</i> cellulase	Avicel	3 \pm 0.5
		pAvicel	5 \pm 0.9
		Corn stover	2.8 \pm 0.8
		pCorn stover	6 \pm 0.9
	<i>Tma</i> Cel5A	Avicel	1.1 \pm 0.1
		pAvicel	6.6 \pm 0.8
		Corn stover	3 \pm 0.9
		pCorn stover	9 \pm 1
	<i>Pho</i> EG	Avicel	0.54 \pm 0.1
pAvicel		3.2 \pm 0.2	
Corn stover		0.58 \pm 0.1	
pCorn stover		2.14 \pm 0.1	
5	<i>T. viride</i> cellulase	Avicel	2.1 \pm 0.6
		pAvicel	4 \pm 0.9
		Corn stover	2.3 \pm 0.5
		pCorn stover	3.6 \pm 0.6
	<i>Tma</i> Cel5A	Avicel	1.0 \pm 0.2
		pAvicel	6 \pm 0.5
		Corn stover	2 \pm 0.3
		pCorn stover	8 \pm 0.9
	<i>Pho</i> EG	Avicel	0.5 \pm 0.1
pAvicel		3.3 \pm 0.2	
Corn stover		0.59 \pm 0.1	
pCorn stover		2.2 \pm 0.14	
10	<i>T. viride</i> cellulase	Avicel	0.2 \pm 0.1
		pAvicel	1 \pm 0.1
		Corn stover	0.6 \pm 0.3
		pCorn stover	1.1 \pm 0.3
	<i>Tma</i> Cel5A	Avicel	0.9 \pm 0.1
		pAvicel	5.7 \pm 1
		Corn stover	2.4 \pm 0.8
		pCorn stover	7 \pm 1
	<i>Pho</i> EG	Avicel	0.52 \pm 0.1
pAvicel		3.1 \pm 0.2	
Corn stover		0.57 \pm 0.1	
pCorn stover		2.0 \pm 0.2	
15	<i>T. viride</i> cellulase	Avicel	<0.01
		pAvicel	<0.01
		Corn stover	<0.01
		pCorn stover	<0.01
	<i>Tma</i> Cel5A	Avicel	0.6 \pm 0.1
		pAvicel	4 \pm 0.5
		Corn stover	2.3 \pm 0.5
		pCorn stover	5.9 \pm 1
	<i>Pho</i> EG	Avicel	0.6 \pm 0.08
pAvicel		2.9 \pm 0.06	
Corn stover		0.59 \pm 0.1	
pCorn stover		1.9 \pm 0.1	

^a The sum of glucose, cellobiose and xylose obtained, normalized by enzyme amount and time. ^b The reactions were spiked with 0 to 15% (v/v) [C2mim][OAc], everything else being the same for all substrates for an enzyme. ^c The sum of glucose, cellobiose and xylose obtained, normalized by enzyme amount and time.

Future studies would focus on using optimum sized particles, solids loading during the saccharification reaction as well as enzyme loadings.

The DSC experiments indicate that at higher concentrations of [C2mim][OAc] the enzymes unfold and are less stable. Thus, the loss of activity could be accounted by the denaturation of the enzyme or a disruption of the tertiary structure of the protein. It has been speculated that halotolerant enzymes are more stable in ILs in comparison to non-halotolerant enzymes, because of the inherent ability of such organisms to live in high salt concentration environments.¹¹ However, we found that the recombinant proteins *Tma* Cel5A and *Pho* EG from non-halotolerant organisms maintained around 80% of their activity in 1.5 M sodium or potassium chloride (ESI, Fig. 2).[†] This is in contrast to general findings that non-halotolerant cellulases show reduced activity at high salt concentrations.²¹ This implies a different mechanism of denaturation depending on the identity of the cation and anion of the IL. Further studies are needed to better understand the differences in behaviour of *Tma* Cel5A and *Pho* EG at higher concentrations of ionic liquids to get a better understanding of the mechanisms of deactivation, and to investigate if other ILs used in biomass pretreatment would better stabilize the cellulases.

The recombinant enzymes studied here are members of the GH5 family, supporting the speculation that the higher resistance to ILs is due to a common structural motif.³² Based on saturation mutagenesis studies, J. Pottkämper *et al.*³² have suggested that motifs within the N-terminal part of the protein and within carbohydrate-binding domain are responsible for IL tolerance. We speculate that the hyperthermophilic properties of these enzymes may lead to stability of the enzymes in ionic liquids. Related studies with IL tolerance of other cellulases from hyperthermophilic organisms support a similar trend (S. Datta, J. I. Park and R. Saprà—unpublished results).

Conclusions

While there are a number of reports in literature on using ILs to deconstruct cellulosic biomass, the present work reports on the effects of ILs on purified and active recombinant cellulases. Our work suggests that hyperthermophilic cellulases can tolerate around 15% (v/v) of ILs, which reflects the IL content that may be present from a large-scale commercial IL pretreatment process. Fungal enzymes studied did not possess this tolerance to ILs. Further work is needed to discover, evolve and engineer cellulases with longer half-lives that are more stable and active in higher concentrations of IL, towards the ultimate goal of cheaper and efficient saccharification of biomass.

Experimental

Chemicals

All chemicals used were reagent grade. *Trichoderma viride* cellulase (Sigma Cat # C9422), sodium acetate, 3,5-dinitrosalicylic acid (DNS), sodium hydroxide, sodium potassium tartrate and carboxymethylcellulose (CMC) was obtained from Sigma (St. Louis, MO). 1-ethyl-3-methylimidazolium acetate ([C2mim][OAc]) was obtained from BASF, USA.

PCR and cloning of endoglucanase from *T. maritima* and *P. horikoshii*

The open reading frame of the endoglucanase from *Tma* Cel5A (NP_229549), and *Pho* EG (UniProt ID: O58925) was synthesized and codon optimized for protein expression in *E. coli* (GenScript Corporation, Piscataway, NJ). *Tma* Cel5A was cloned by ligation independent cloning method into the expression vector, pCDF2 LIC/Ek (Novagen/EMD Chemicals, Gibbstown, NJ), using the kit supplied by the manufacturer. The *Pho* EG amplicon was gel-purified, and then cloned into pDONR221 (Invitrogen, Carlsbad, CA) via BP recombination reaction to create an entry vector. The *Pho* EG gene was then inserted into pET DEST42 vector (Invitrogen, Carlsbad, CA) as a fusion to a C-terminal V5 epitope and His(×6) tags by LR recombination reaction to create pET DEST42-PhoEG plasmid. The DNA sequence of entry and expression vectors for *Pho* EG and expression vector containing *Tma* Cel5A was confirmed by DNA sequencing.

Protein expression and purification

Escherichia coli BL21(DE3) star transformed with the plasmid construct was grown in Luria–Bertani (LB) medium containing streptomycin (50 µg mL⁻¹) at 37 °C, induced with 0.5 mM IPTG (at $A_{600\text{ nm}} = 0.5\text{--}0.7$), and then grown overnight at 30 °C. *Tma* Cel5A with a C-terminal His tag was purified from cells (10 g wet weight) suspended in 100 mL of 10 mM potassium phosphate buffer (pH 7.2) and containing 0.15 mg mL⁻¹ lysozyme and one tablet of complete EDTA-free protease inhibitor (Roche). After sonication, NaCl (150 mM) and imidazole (10 mM) were added to achieve the specified final concentrations and loaded onto a Ni-nitrilotriacetic acid column (GE Healthcare, Piscataway, NJ) equilibrated with phosphate buffer containing 150 mM NaCl, and 10 mM imidazole. The column was washed extensively, and proteins were eluted with a 10–400 mM imidazole gradient. The protein eluted between 100 and 350 mM imidazole and were pooled and dialyzed against 100 mM Acetate buffer (pH 4.8). The *Pho* EG was purified under similar conditions with an additional purification step by Q Sepharose High Performance column (GE Healthcare, Piscataway, NJ) using manufacturer recommended protocol and dialyzed against 100 mM MES buffer (pH 6.4). The protein concentrations were measured by Bradford Assay for both recombinant and commercial enzymes used in this study. The recombinant protein purity was visually assessed using SDS-PAGE.

Avicel and corn stover pretreatment by [C2mim][OAc]

[C2mim][OAc] (1 kg, as received, < 0.2% moisture specified) was heated to 130 °C in a 1.5 L glass reaction vessel with mechanical stirring and 8% w/w (corn stover, 4.8% moisture) or 10% w/w (Avicel PH-101, 3% moisture). After around 3 h when the majority (corn stover) or all (Avicel) had dissolved, the dissolved corn stover or Avicel was allowed to cool to below 80 °C and was added to 2 L of 95% ethanol with rapid agitation to induce the precipitation of dissolved materials. The resulting slurry was filtered under pressure through polypropylene filter cloth and the solids redispersed in 2 L of additional ethanol. The filtration and redispersion steps were repeated twice to remove

most residual ionic liquid and the filter cake dried under vacuum at 40 °C to yield a free-flowing powder product. Residual free ionic liquid remaining in the dried biomass is estimated to be less than 4% (w/w).

Enzyme activity assays on soluble and insoluble polysaccharides

Enzymatic activity was measured on soluble polysaccharide substrates, CMC, using the 3,5-dinitrosalicylic acid (DNS) reducing sugar assay.³⁴ Briefly, 2% CMC (w/v) in 120 µL acetate buffer, (100 mM, pH 4.5 and pH 4.8 for *T. viride* and *Tma*, respectively, and 100 mM MES buffer, pH 6.4 for *P. hori* EG) was incubated at 80 °C for 30 min for *Tma* Cel5A and *Pho* enzymes and 37 °C and 10 min for *T. viride*. The solution was cooled down to 4 °C and 80 µL of DNS solution was added. The reactants were incubated at 95 °C for 5 min and cooled down to room temperature before the absorbance was read at 540 nm. The reducing sugar concentration in the sample was calculated from its absorbance using the standard curve of D-glucose and cellobiose. All experiments were run in triplicate. For hydrolysis reactions in the presence of [C2mim][OAc], control reactions with CMC in the presence of IL but without no enzyme was subtracted from each measurement.

The solid substrate (Avicel and corn stover) hydrolysis reactions were conducted at 80 °C for 15 h for the recombinant enzymes and at 37 °C for 8 h in the case of *T. viride* cellulase at the optimum pH for each enzyme. The reaction products were monitored using an Agilent 1200 HPLC equipped with Varian 380-LC Evaporative Light Scattering Detector. The total reaction volumes were 500 µL and shaken at 900 rpm at temperature controlled shakers. Enzyme loadings were 0.4 mg per g of glucan and each data point was measured in triplicate. Separation was achieved using a Varian/Polymer labs Hi-Plex Pb carbohydrate analytical column (300 × 7.7 mm) with a guard column (50 × 7.7 mm) at 85 °C (Polymer Laboratories, Varian Inc., Shropshire, UK). The mobile phase was deionized water with a flow rate of 0.6 mL min⁻¹. Hydrolysis reactions in the presence of [C2mim][OAc] were monitored by either by High Performance Anion Exchange Chromatography with Pulsed Amperometric Detection (HPAEC-PAD) on a Dionex DX600 equipped with a Dionex Carbopac PA-20 analytical column (3 × 150 mm) and a Carbopac PA-20 guard column (3 × 30 mm) (Dionex, Sunnyvale, CA). Eluent flow rate was 0.4 mL min⁻¹ and the temperature was 30 °C. A gradient consisting of a 12 min elution with 14 mM NaOH followed by a 5 min ramp to 450 mM NaOH for 20 min, then a return to the original NaOH concentration of 14 mM for 10 min prior to the next injection. Product concentrations were determined by the integrations of the appropriate peaks from the HPLC or HPAEC chromatograms.

Estimation of temperature dependence and thermostability

T. viride enzyme was assayed at 37 °C and pH 4.5 as suggested by the manufacturer. The pH dependence of the recombinant enzymes was determined by measuring specific activities of the enzyme on CMC in a series of pH values between 4 and 5 with 100 mM sodium acetate buffer, and between 5 and 8 with sodium phosphate buffer. The optimal temperature of *Tma* Cel5A was determined by measuring specific activity of the enzyme on

CMC in 100 mM sodium acetate buffer (pH 4.8) at various temperatures. Similar experiments in 50 mM MES buffer, pH 6.4 was done for *Pho* EG. Thermostability was determined by incubating the enzyme at 80 °C in 100 mM acetate buffer, pH 4.8 for Cel5A and 50 mM MES buffer, pH 6.4 for *Pho* EG and for 24 h prior to determining specific activity.

Differential scanning calorimetry

Unfolding temperatures of *Tma* Cel5A (5 mg mL⁻¹) in the absence and presence of 5–50% (v/v) of [C2mim][OAc] were determined with a multi-cell differential scanning calorimeter (Calorimetry Sciences Corporation, Lindon, UT, USA). The [C2mim][OAc] containing samples were dialyzed overnight against 100 mM sodium acetate buffer (pH 4.8) in the presence of similar amounts [C2mim][OAc] as in sample. The dialyzed enzyme was scanned between 25 and 100 °C using a scan rate of 0.5 °C min⁻¹. The enzyme scans were corrected with a buffer–buffer baseline. The *T. viride* cellulase (2 mg mL⁻¹) was run under similar conditions in the presence of 0–20% (v/v) [C2mim][OAc]. Unfolding temperatures of *Pho* EG (2.6 mg mL⁻¹) were determined similarly to the *Tma* but on a NanoDSC, Differential Scanning Calorimeter (TA Instruments—Waters LLC, New Castle, DE). The protein sample was dialyzed overnight against the presence of similar amounts of IL as in sample in the pH_{opt} buffer. A scan rate of 2 °C min⁻¹ was used and the data analyzed using the NanoAnalyze software supplied by the manufacturer.

Acknowledgements

The DSC experiments were performed in the laboratory of Prof. Francis C. Szoka, Jr., Department of Bioengineering and Therapeutic Sciences, University of California, San Francisco, with the help of Dr Zhaohua Huang and with the help of Dr Mara Bryan at Energy Biosciences Institute, Berkeley. This work was part of the DOE Joint BioEnergy Institute (<http://www.jbei.org>) supported by the U. S. Department of Energy, Office of Science, Office of Biological and Environmental Research, through contract DE-AC02-05SCH11231 between Lawrence Berkeley National Laboratory and the U. S. Department of Energy.

References

- 1 M. Klare, *Blood and Oil: The Dangers and Consequences of America's Growing Dependency on Imported Petroleum*, Macmillan, London, 2005.
- 2 J. Barnett, *Global Environ. Change*, 2003, **13**, 7–17.
- 3 B. Simmons, D. Loque and H. Blanch, *GenomeBiology*, 2008, **9**, 242–247.
- 4 J. D. Wright, *Energy Progress*, 1988, **8**, 71–80.
- 5 L. R. Lynd, P. J. Weimer, W. H. van Zyl and I. S. Pretorius, *Microbiol. Mol. Biol. Rev.*, 2002, **66**, 506–577.
- 6 R. Atalla and D. VanderHart, *Science*, 1984, **223**, 283–286.
- 7 D. Klemm, B. Philipp, T. Heinze, U. Heinze, and W. Wagenknecht, *Comprehensive Cellulose Chemistry*, Wiley–VCH Verlag GmbH, Berlin, 1998.
- 8 T. A. Hsu, M. R. Ladisch and G. T. Tsao, *Chem. Technol.*, 1980, **10**, 315–319.
- 9 N. Mosier, C. E. Wyman, B. Dale, R. Elander, Y. Lee, M. Holtzapple and M. Ladisch, *Bioresour. Technol.*, 2005, **96**, 673–686.
- 10 R. P. Swatloski, S. K. Spear, J. D. Holbrey and R. D. Rogers, *J. Am. Chem. Soc.*, 2002, **124**, 4974–4975.

- 11 F. Van Rantwijk and R. A. Sheldon, *Chem. Rev.*, 2007, **107**, 2757–2785.
- 12 R. A. Sheldon, R. M. Lau, M. J. Sorgedraeger and F. van Rantwijk, *Green Chem.*, 2002, **4**, 147–151.
- 13 S. Zhu, Y. Wu, Q. Chen, Z. Yu, C. Wang, S. Jin, Y. Ding and G. Wu, *Green Chem.*, 2006, **8**, 325–327.
- 14 Y. Fukaya, K. Hayashi, M. Wada and H. Ohno, *Green Chem.*, 2008, **10**, 44–46.
- 15 A. P. Dadi, S. Varanasi and C. A. Schall, *Biotechnol. Bioeng.*, 2006, **95**, 904–910.
- 16 A. P. Dadi, C. A. Schall and S. Varanasi, *Appl. Biochem. Biotechnol.*, 2007, **137–140**, 407–421.
- 17 M. J. Earle, J. M. Esperança, M. A. Gilea, J. N. Lopes, L. P. Rebelo, J. W. Magee, K. R. Seddon and J. A. Widegren, *Nature*, 2006, **439**, 831–834.
- 18 S. Singh and B. A. Simmons, *Biotechnol. Bioeng.*, 2009, **104**, 68–75.
- 19 I. Kilpeläinen, H. Xie, A. King, M. Granstrom, S. Heikkinen and D. S. Argyropoulos, *J. Agric. Food Chem.*, 2007, **55**, 9142–9148.
- 20 C. Li, Q. Wang and Z. Zhao, *Green Chem.*, 2008, **10**, 177–182.
- 21 M. B. Turner, S. K. Spear, J. G. Huddleston, J. D. Holbrey and R. D. Rogers, *Green Chem.*, 2003, **5**, 443–447.
- 22 H. Zhao, C. L. Jones, G. A. Baker, S. Xia, O. Olubajo and V. N. Person, *J. Biotechnol.*, 2009, **139**, 47–54.
- 23 P. Turner, M. Gashaw and Eva Nordberg Karlsson, *Microb. Cell Fact.*, 2007, **6**, 9.
- 24 K. Nelson, R. Clayton, S. Gill, M. Gwinn, R. Dodson, D. Haft, E. Hickey, J. Peterson, W. Nelson, K. Ketchum, L. McDonald, T. Utterback, J. Malek, K. Linher, M. Garrett, A. Stewart, M. Cotton, M. Pratt, C. Phillips, D. Richardson, J. Heidelberg, G. Sutton, R. Fleischmann, J. Eisen, O. White, S. Salzberg, H. Smith, J. Venter and C. Fraser, *Nature*, 1999, **399**, 323–329.
- 25 S. Arumugam Mahadevan, S. Gon Wi, D.-S. Lee and H.-J. Bae, *FEMS Microbiol. Lett.*, 2008, **287**, 205–211.
- 26 S. R. Chhabra, K. R. Shockley, D. E. Ward and R. M. Kelly, *Appl. Environ. Microbiol.*, 2002, **68**, 545–554.
- 27 S. Ando, H. Ishida, Y. Kosugi and K. Ishikawa, *Appl. Environ. Microbiol.*, 2002, **68**, 430–433.
- 28 Robert D. Perlack, Lynn L. Wright, Anthony F. Turhollow, Robin L. Graham, Bryce J. Stokes, and D. C. Erbach, (DOE/GO-102005-2135), Oak Ridge National Laboratory, Oak Ridge, TN, 2005.
- 29 R. L. Graham, R. Nelson, J. Sheehan, R. D. Perlack and L. L. Wright, *Adv. Agron.*, 2007, **92**, 1–11.
- 30 L. D. Unsworth, John van der Oost and Sotirios Koutsopoulos, *FEBS J.*, 2007, **274**, 4044–4056.
- 31 M. Turner, S. Spear, J. Huddleston, J. Holbrey and R. Rogers, *Green Chem.*, 2003, **5**, 443–447.
- 32 J. Pottkämper, P. Barthen, N. Llmberger, U. Schwaneberg, A. Schenk, M. Schulte, N. Ignatiev and W. Streit, *Green Chem.*, 2009, **11**, 957–965.
- 33 S. Voget, H. Steele and W. Streit, *J. Biotechnol.*, 2006, **126**, 26–36.
- 34 G. L. Miller, *Anal. Chem.*, 1959, **31**, 426–428.

Ionic liquids based on imidazolium tetrafluoroborate for the removal of aromatic sulfur-containing compounds from hydrocarbon mixtures

Marya Nefedieva,^a Olga Lebedeva,^{*a} Dmitry Kultin,^a Leonid Kustov,^a Svetlana Borisenkova^a and Vladimir Krasovskiy^b

Received 14th August 2009, Accepted 30th November 2009

First published as an Advance Article on the web 21st January 2010

DOI: 10.1039/b916789g

Two ionic liquids 1-methyl-3-butylimidazolium (BMImBF₄) tetrafluoroborate and 1-methyl-3-octylimidazolium (OMImBF₄) tetrafluoroborate were studied from the viewpoint of removing aromatic sulfur-containing compounds from hydrocarbon mixtures using transition metal ions as complexing centers. The values of distribution coefficients (*D*) indicate that OMImBF₄ absorbs benzothiophene (BT) and dibenzothiophene (DBT) better than BMImBF₄, which corresponds to the increasing absorption ability of the IL due to the presence of a longer hydrocarbon (octyl) chain in the third position of the imidazolium ring. The influence of additives of various complexes of cobalt(II) on the extraction of BT and DBT was studied in the system OMImBF₄–heptane. The planar complex of the Na-salt of 4,5-dicarboxyphthalocyanine of cobalt was found to be the most efficient for the extraction of both substances. The electrochemical approach enables one to purify the IL from BT and DBT by electrochemical oxidation or reduction. This result can be used for searching ways to increase the degree of extraction of BT and DBT in hydrocarbon–IL systems.

Introduction

The removal of sulfur-containing compounds has become an increasing technical challenge as oil refineries face growing environmental pressures and regulations.¹ Catalytic processes are conventionally used for desulfurization of transportation fuels through hydroprocessing,² but these processes fail to reach the sulfur level set by new requirements. Further removal of residual sulfur from fuels is expected to significantly increase the cost of hydroprocessing, that is why alternative methods of sulfur removal to below 10 ppm (part per million) are being of particular interest. The use of enzymes and novel catalytic and adsorption methods are among these alternative technologies, but ionic liquids (ILs) as extraction agents are most promising.^{3–6} ILs such as 1-methyl-3-butylimidazolium (BMIm) tetrafluoroborate, 1-methyl-3-butylimidazolium octyl- and ethyl-sulfates are moisture-stable and do not cause corrosion of the equipment which is why they could be used repeatedly in technological cycles. ILs are not miscible with gasoline or diesel oil.⁷ It is very important for preserving the optimal ratio of hydrocarbons in the fuel that substances with low polarity, such as thiophene, are being extracted much better than non-polar aromatic compounds, for example, toluene.⁸

The aim of the current research was to study the extraction of benzothiophene (BT) and dibenzothiophene (DBT) by 1-methyl-3-butylimidazolium (BMImBF₄) tetrafluoroborate

and 1-methyl-3-octylimidazolium (OMImBF₄) tetrafluoroborate. BT and DBT were selected as model sulfur-compounds that are difficult to remove from gasoline and diesel fuels, although it is known that methyl-substituted derivatives are even more difficult to remove.

Results and discussion

Extraction using metal salts in ionic liquids

The addition of transition metal ions into the extractant leads to an increase of its extractive power.⁸ To increase the degree of extraction (*R*, %) of BT from octane, we studied the addition of different salts of d-elements and their influence on the extraction of BT into BMImBF₄ from an octane–benzene mixture. The effect of cobalt(II), nickel(II), iron(III), iron(II) and copper(I) additives was investigated. The addition of cobalt(II) nitrate led to the most pronounced increase of the *R* value as compared to other salts. Since the nitrates are fixed in ILs, the salts were dissolved in water and aqueous solutions were introduced into the IL, which was followed by the removal of water in the IL by vacuum distillation. That was the reason why, for further investigations, complex compounds of cobalt(II) with organic ligands with better solubility in ILs were chosen. According to the literature,^{8,9} chlorides and water are the main impurities in ILs which strongly affect their properties. The presence of 1–3% water could dramatically change the properties of ILs.

The influence of additives of various complexes of cobalt(II) on the extraction of BT and DBT was studied in the system OMImBF₄–heptane at 20 °C. Hydrates of cobalt acetylacetonate (Co(AcAc)₂·2H₂O) [I], cobalt acetoacetate [II], cobalt

^aMoscow State University, Chemistry Department, 119991, Moscow, Russia. E-mail: lebedeva@general.chem.msu.ru

^bZelinsky Institute of Organic Chemistry, Leninsky prospect, 47, 119991, Moscow, Russia. E-mail: lmk@ioc.ru

Table 1 Distribution coefficient (D) and degree of extraction (R) of BT and DBT from heptane ($C_0 = 500$ ppm) into IL (I – BMImBF₄, II – OMImBF₄), C_b – residual concentration of BT and DBT

Substance	C_b /ppm		D		R (%)	
	I	II	I	II	I	II
BT	340	160	0.50	2.0	33	66
DBT	420	360	0.20	0.39	17	28
BT (electrochemically)	125	115	3.1	3.3	74	77
DBT (electrochemically)	380	360	0.35	0.39	24	28

Table 2 Distribution coefficient (D) and degree of extraction (R) of BT and DBT ($C_0 = 500$ ppm) from heptane into OMImBF₄ with the addition of complexes of cobalt(II), C_b – residual concentration of BT and DBT

Complex	C_b /ppm		D		R (%)	
	DBT	BT	DBT	BT	DBT	BT
I	360	345	0.40	0.45	28	31
II	320	—	0.56	—	35	—
III	420	>450	0.19	<0.11	16	<10
IV	>450	—	<0.11	—	<10	—
V	200	85	1.5	4.9	60	83
VI	160	—	2.2	—	68	—

acetylacetonate (Co(AcAc)₂) [III], cobalt pivalate [IV], Na-salt of 4,5-dicarboxyphthalocyanine of cobalt [V] and *N,N*-bis(salicyliden) ethylenediamine cobalt complex (Co-Salen)[VI] were studied.

The results are shown in Tables 1 and 2. As shown in Table 1, the degrees of extraction of aromatic sulfur-containing compounds are not very high. Also it follows from Table 1 that BT is extracted more efficiently in comparison with DBT. Besides, the values of the obtained distribution coefficients (D) show that OMImBF₄ absorbs BT and DBT better than BMImBF₄, which can be explained by the increasing absorption ability of the IL due to the presence of a longer hydrocarbon (octyl) chain in the third position of the imidazolium ring. The planar complex of the sodium form of 4,5-dicarboxyphthalocyanine of cobalt [V] was found to be the most efficient for the extraction of both substances (Table 2), as can be judged from the distribution coefficient and degree of extraction.

The extraction of thiophenes by ionic liquids has been studied (see ref. 6), but in most cases no work on the effect of additives of transition metal complexes has been investigated. Nevertheless, the extraction characteristics obtained in our work using pure ionic liquids are comparable with data reported so far. On the contrary, the introduction of transition metal complexes into ionic liquids, especially cobalt(II) moieties, results in a dramatic enhancement of the distribution coefficient and degree of extraction of thiophenes as compared to the case of pure ionic liquids.

Electrochemical approach to the removal of sulfur compounds using ionic liquids

ILs are unique, ecologically friendly solvents since they can behave as extractants and organic electrolytes. Therefore, it was of interest to investigate the electrochemical behavior of

extracted organic substances in the media of a conducting extractant (IL). It should be mentioned that literature data related to the electrochemical removal of BT are limited⁷ and relevant data on DBT are absent.

With the aim of determining the range of electrochemical stability of the ILs, the background cyclic voltammograms (CVA) of pure ILs – OMImBF₄ and BMImBF₄ – were studied. The “window” of the electrochemical stability of BMImBF₄ is found to be 4.2 V (–2.0 to +2.2 V) in agreement with literature data⁹ and the corresponding window for OMImBF₄ is 4.5 V (–2.2 to +2.3 V). The CVA curves of ILs with dissolved BT and DBT were measured to investigate their electrochemical behavior at an optimal scan rate, which was found to be 50 mV s^{–1}. This scan rate will be used in all further experiments. The CVA curves of BT in BMImBF₄ are presented in Fig. 1. They show that an increase of the current is observed in parallel with the scan rate of the anodic potential from the stationary value (E_s). The value of the anodic current increases in the second cycle and in all further cycles. This finding provides evidence for the oxidation of BT. No such oxidation peaks were observed in the anodic region of the first CVA cycle of DBT in BMImBF₄, but there was an area of reduction in the cathodic region (Fig. 2).

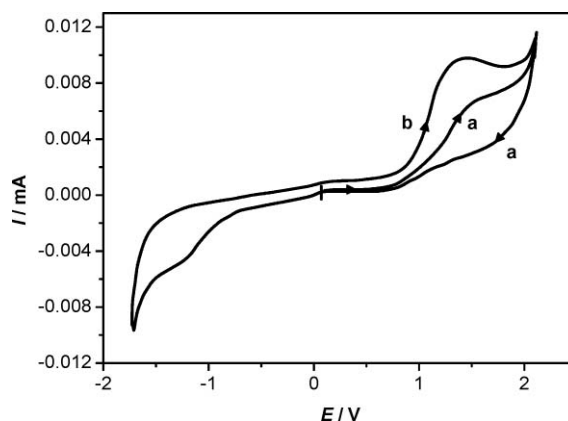


Fig. 1 CVA curve of BT in BMImBF₄. The scan rate is 50 mV s^{–1}; $C_0 = 2.72 \cdot 10^{-6}$ mol dm^{–3}; $E = [-1.9 \div +2.1]$; a – the first cycle; b – the second cycle. Arrows indicate the scan direction.

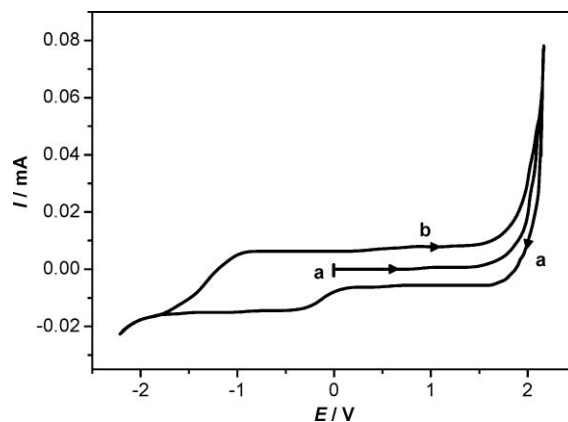
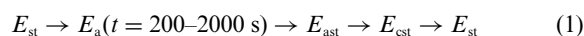


Fig. 2 CVA curve of DBT in BMImBF₄. The scan rate is 50 mV s^{–1}; $C_0 = 3.73 \cdot 10^{-6}$ mol dm^{–3}; $E = [-2.0 \div +2.1]$; a – the first cycle; b – the second cycle. Arrows indicate the scan direction.

The data obtained from voltammetric studies allow us to use the electrochemical effect as a means to shift the absorptive equilibrium. The volume of heptane (or the model mixture of octane–benzene with the volume ratio 80:20) equal to the volume of IL with a dissolved substance (BT or DBT) was placed into an electrochemical cell. The concentrations of BT and DBT were the same as in the studies of the influence of additives of cobalt(II) compounds and equal to $C_0 = 500$ ppm. As a factor for shifting the absorptive equilibrium we used the exposition of the oxidation potential for BT and the reduction potential for DBT.

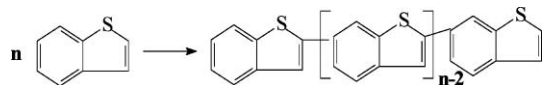
The CVA curves with exposition of the potential in OMImBF₄ were also measured in the case of studying the electrochemical behavior of the pure component of the model mixture heptane–IL. As it was established in preliminary experiments, heptane does not change the shape of the background CVA of IL. CVA curves were measured in the systems where the absorptive equilibrium had already been achieved by preliminary stirring. The exposition of the potential for BT was $E_c = 2.0$ V, the time of exposition was varied from 200 to 2000 s. The total cycling time was 3 h. The scheme of varying the potential while cycling could be described in the following way:



where E_{ast} and E_{cst} stand for the potential of the anodic and cathodic stability threshold of IL, respectively, E_{st} is the stationary potential.

The extraction of BT from heptane into BMImBF₄ was carried out in a similar manner. The potential of exposition was 1.8 V. Voltammetric curves in the system BT–BMImBF₄ after ten cycles performed according to eqn (1) are similar to the CVA curves presented in Fig. 1.

After consecutive scanning of the potential over BT, the peak attributed to the peak of the oxidation process increases at the CVA curve after exposition of the potential, and the black solid product was formed at the surface of the electrode. This solid was identified as polybenzothiothiophene by IR-spectroscopy. Thus, the possibility of the removal of BT from ILs by electrocatalytic polymerization was established (Scheme 1).



Scheme 1 Electropolymerization of BT.

The potential of exposition for DBT was $E_c = -1$ V, the time of exposition and the time of cycling were the same as in the case of BT. The value and position of peaks at the CVA curve for DBT after multiple scanning were the same as for the first CVA curve.

The obtained results can be used to increase the degree of extraction of BT and DBT in the hydrocarbon (octane, heptane)–IL system. This is due to a decrease in concentration of S-containing compounds in ILs caused by their electrochemical transformation into new substances and shift of equilibrium in the system that leads to an increase in the degree of extraction and the distribution coefficient of BT and DBT in ILs. After completing the experiments, the final concentration of DBT in

heptane was determined: $C_{b1} = 360$ ppm. This value is exactly the same as in the case of extraction without the effect of the electrochemical factors (see data in Table 1). The values $D_{eff} = 0.39$ and $R_{eff} = 28\%$ were calculated from the obtained data. Similar experiments were carried out for BT in both investigated ILs. The final concentration of BT in heptane was $C_b = 115$ ppm. Thus, $D_{eff} = 3.3$ and $R_{eff} = 77\%$. The comparison of D_{eff} and R_{eff} with data from Tables 1 and 2 indicates that D_{eff} and R_{eff} are higher than the values of D and R , obtained for pure IL and are comparable to the values found in the case of the addition of the Na-salt of 4,5-dicarboxyphthalocyanine of cobalt(II) into IL.

Experimental

Materials

Ionic liquids used in this work were from the kind donation from Merck KgaA, Germany. Heptane, octane, benzene, benzothiothiophene, dibenzothiothiophene (Fluka, 99%), cobalt(II), nickel(II), iron(III), iron(II) and copper(I) nitrates were purchased from Aldrich. Hydrates of cobalt acetylacetonate ($\text{Co}(\text{AcAc})_2 \cdot 2\text{H}_2\text{O}$), cobalt acetoacetate, cobalt acetylacetonate ($\text{Co}(\text{AcAc})_2$), cobalt pivalate, Na-salt of 4,5-dicarboxyphthalocyanine of cobalt and *N,N*-bis(salicyliden) ethylenediamine of cobalt (Co-Salen) were synthesized according to procedures described elsewhere.

Methods

The extraction of BT and DBT from heptane was performed by using BMImBF₄ and OMImBF₄ at 20 °C, the extraction time was one hour under stirring. The time of extraction was established in preliminary experiments as the time taken for liquid–liquid equilibrium. The volume of the phases of IL and heptane (or a model mixture) was varied from 0.5 to 2.0 ml and the volume ratio of the components was kept at 1:1. The residual concentrations (C_b) of BT and DBT were determined from the calibration curves obtained by measuring the band intensity at $\lambda_{max}(\text{DBT})/327$ nm and at $\lambda_{max}(\text{BT})/322$ nm for different concentrations.¹⁰

The concentration of salts dissolved in IL was $C = 1.27 \cdot 10^{-3}$ mol dm⁻³. The initial concentration of BT and DBT in heptane was 500 ppm. The concentration of BT in the octane–benzene mixture was 1000 ppm.

Electrocatalytic studies were carried out in the electrochemical cell with unseparated cathodic and anodic areas. The volume of the electrolyte was 3–5 ml. Platinum wire was used as auxiliary and quasi-irreversible reference electrodes. The scan rate of the potential was varied in the voltammetric investigations from 5 to 50 mV s⁻¹ depending on the composition and viscosity of the IL. The choice of the scan rate was determined by convective mixing of the liquid (lower than 5 mV s⁻¹) and by the absence of the resolution of peaks (more than 50 mV s⁻¹). In the chosen range of potentials the CVA curves were similar, so further experiments were carried out with the scan rate of 50 mV s⁻¹.

Conclusions

The obtained data demonstrate the feasibility of using ionic liquids with dissolved metal complexes and salts for the

extraction of S-containing compounds from hydrocarbon mixtures. The electrochemical approach enables one to purify the IL from BT and DBT by electrochemical oxidation or reduction, respectively. This result can be used for searching ways to increase the degree of extraction of BT and DBT in hydrocarbon-IL systems. The redox reactions of BT and DBT occurring with the formation of new products can decrease the concentration of these substances in ILs and as a consequence displace the equilibrium in the studied system towards the complete removal of S-containing compounds. Hence, further development of the method of simultaneous extraction under the electrochemical effect seems to provide a perspective technique for increasing the degree of extraction of S-containing compounds and as a simultaneous solution of the problem of regeneration of costly ILs.

Acknowledgements

The authors wish to express their thanks to Merck, KGaA, Germany and Merck employees, Dr Nikolai Ignatiev and Dr Urs Weltz-Biermann for the donation of ionic liquids.

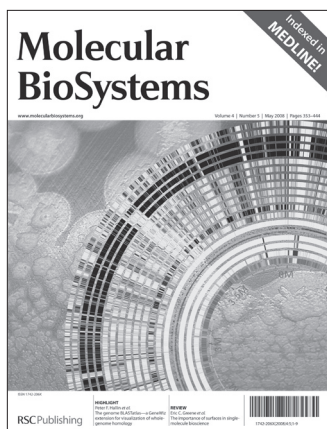
References

- 1 J. Esser, P. Wasserscheid and A. Jess, *Green Chem.*, 2004, **6**, 316–220.
- 2 R. S. Sokolov, in *Chemistry Technology*, M., Chemistry, 2000, vol. 1, p. 69–93.
- 3 I. V. Babich and J. A. Moulijn, *Fuel*, 2003, **82**, 607–631.
- 4 S. M. S. Chauhan, A. Kumar and K. A. Srinivas, *Chem. Commun.*, 2003, 2348–2349.
- 5 W.-H. Lo, H.-Y. Yang and G.-T. Wei, *Green Chem.*, 2003, **5**, 639–642.
- 6 S. Zhang, Z. C. Zhang, *224th ACS National Meeting*, Boston, MA, USA, 2002; S. Zhang and Z. C. Zhang, *Green Chem.*, 2002, **4**, 376–379; F.-T. Li, R.-H. Liu, J.-H. Wen, D.-S. Zhao, Z.-M. Sun and Y. Liu, *Green Chem.*, 2009, **11**, 883–888; H. Li, W. Zhu, Y. Wang, J. Zhang, J. Lu and Y. Yan, *Green Chem.*, 2009, **11**, 810–815; Y. Nie, C. Li, H. Meng and Z. Wang, *Fuel Process. Technol.*, 2008, **89**(10), 978–983; J. Wang, D. Zhao, E. Zhou and Z. Dong, *J. Fuel Chem. Technol.*, 2007, **35**(3), 293–296; X. Jiang, Y. Nie, C. Li and Z. Wang, *Fuel*, 2008, **87**(1), 79–84; L. Alonso, A. Arce, M. Francisco and A. Soto, *J. Chem. Thermodyn.*, 2008, **40**(6), 966–972; M. Haumann, M. Jakuttis, S. Werner and P. Wasserscheid, *J. Catal.*, 2009, **263**(2), 321–327.
- 7 R. C. Schucker, W. C. Baird, *Pat. US*, 6274026, 2001.
- 8 J. H. Davis, C. M. Gordon, C. Hilgers and P. Wasserscheid in *Ionic Liquids in synthesis*, ed. P. Wasserscheid and T. Welton, Wiley-VCH Verlag GmbH & Co. KGaA, Weinheim, Germany, 2002, 7–20.
- 9 O. K. Lebedeva, D. Yu. Kultin, L. M. Kustov and S. F. Dunaev, *Russ. Chem. J.*, 2004, **48**(6), 59–73.
- 10 U-V Atlas of Organic Compounds, 1991, **5**, H5/1, H11/1.

Research at the interface between chemistry, the –omic sciences and systems biology

IMPACT FACTOR
4.236*

0880777a



- High impact, high visibility
- Fast publication times (average 80 days from receipt)
- Enhanced HTML articles, including:
 - Hyperlinked compound information, including downloadable structures in text
 - Gene, Sequence and Cell Ontology terms linked to definitions and related articles
 - IUPAC Gold Book terms linked

*2008 Thomson Scientific (ISI) Journal Citation Reports ®

RSC Publishing

www.molecularbiosystems.org

Registered Charity Number 207890

For the highest impact – publish in Photochemical & Photobiological Sciences

The official journal of the European Photochemistry Association, the European Society for Photobiology, the Asia and Oceania Society for Photobiology and the Korean Society of Photoscience.

Photochemical & Photobiological Sciences (PPS) publishes high quality research on all aspects of photochemistry and photobiology, including elemental photochemical and photophysical processes, the interaction of light with living systems, environmental photochemistry, environmental photobiology, the use of light as a reagent, how light affects health, the use of light as a diagnostic tool and for curative purposes and areas in which light is a cost-effective catalyst.

PPS provides:

- High visibility with an impact factor of 2.144*
- Fast publication times
- RSC Manuscript Central submission system
- No page charges and free colour where it enhances the article

PPS has a strong themed issue programme, with contributions from key people in the relevant fields. Recent themed issues include:

- Microscopy beyond imaging: space-resolved photochemistry and photobiology
- Photosynthesis from molecular perspectives – towards future energy production
- Issue dedicated to Professor NJ Turro

PPS publishes high impact research, recent papers include:

- Triplet-relaxation microscopy with bunched pulsed excitation by G Donnert, C Eggeling and SW Hell
- Mimicking the antenna system of green plants by G Calzaferri and K Lutkouskaya
- Time-resolved fluorescence microscopy by K Suhling, PNW French and D Phillips
- Effects of solar UV radiation on aquatic ecosystems and interactions with climate change by DP Hader, HD Kumar, RC Smith *et al.*
- Milestones in the development of photodynamic therapy and fluorescence diagnosis by A Juzeniene, Q Peng and J Moan
- Combining intracellular and secreted bioluminescent reporter proteins for multicolor cell-based assays by E Micheli, L Cevenini, L Mezzanotte *et al.*

*2008 Thomas Scientific (ISI) Journal Citation Reports

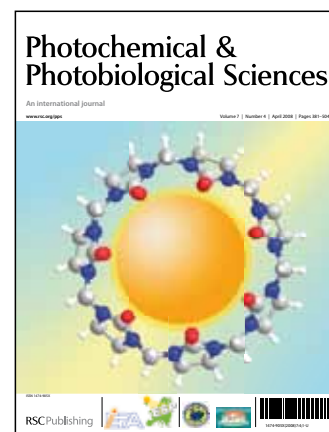
Editors-in-chief:



Rex Tyrrell
Bath, UK
Photobiology Editor



Frans De Schryver
Leuven, Belgium
Photochemistry Editor



060978

RSC Publishing



www.rsc.org/pps

Registered Charity Number 207890

Introducing....

a new integrated publishing platform



The RSC has launched a powerful new integrated content delivery platform, providing over 165 years of world-class RSC-hosted journal, book and database content – all from one simple search. The new online resource supports multiple content types and offers rich functionality, powerful searching, simple browsing and intuitive navigation.

search faster ○ **navigate smarter** ○ **connect more**

RSC Publishing

www.rsc.org/publishing

Registered Charity Number 207890